Title

Design and synthesis of extended aromatic systems toward applications in biological host—guest chemistry

ISBN

9798288858307

Author

Hartung, Kaitlin Marie

Publication Date

2025-07-16

Peer reviewed|Thesis/dissertation

UNIVERSITY OF CALIFORNIA

Los Angeles

Design and synthesis of extended aromatic systems toward applications in biological host–guest chemistry

A dissertation submitted in partial satisfaction of the

requirements for the degree Doctor of Philosophy

in Chemistry

by

Kaitlin Marie Hartung

2025

ABSTRACT OF THE DISSERTATION

Design and synthesis of extended aromatic systems toward applications in biological host–guest chemistry

by

Kaitlin Marie Hartung

Doctor of Philosophy in Chemistry

University of California, Los Angeles, 2025

Professor Ellen May Sletten, Chair

The ability to study biomolecules in their native environments using chemical tools drives much of the development and innovation in chemical biology. The bioorthogonal chemical reporter strategy has proven useful for labeling biomolecules to study natural processes with minimal perturbation. However, this approach suffers from drawbacks, including difficulty achieving fast reactivity in dilute cellular media. One potential strategy to overcome this limitation is to employ non-covalent bonding: namely, supramolecular host–guest chemistry. We aim to develop new host–guest systems that rely on rare-in-biology non-covalent interactions to

employ in the chemical reporter strategy; to do so, we need to develop and systematically study synthetic systems, with the ability to synthetically tune many key aspects.

The present work establishes important design principles for bioorthogonal host–guest systems. Two polycyclic aromatic hydrocarbon (PAH) scaffolds are featured: phenanthrene and olympicene. These motifs recognize perfluoroarenes, options for bioorthogonal, non-covalent chemical reporters. Earlier work in the lab established a phenanthrene-based host to recognize perfluoroaromatic guests, but the individual contributions of different non-covalent forces in different solvents were not dissected. Here, it is shown that the phenanthrene system displays strong binding with electron-deficient guests in organic solvent through a combination of preorganization and hydrogen bonding. These results are informing design choices for a cell-labeling platform. In exploring alternative aromatic systems to phenanthrene, it was found that chemistry off the olympicene PAH was poorly characterized, igniting a synthetic endeavor to probe both its potential uses and limitations. The work presented here begins to fill in the large methodology gap for achieving diverse functionality from this intriguing and understudied PAH. Both stories highlight new directions for chemical biology tool development and the use of different PAHs in organic synthesis for designing new materials.

Chapter One is a perspective on the field of bioorthogonal chemistry. It begins with exploration of the fundamental organic reactions that represent the first bioorthogonal reactions, then evaluates advances and new additions to these chemistries. Alternatives to covalent bond formation are also discussed, including applications of host–guest chemistry in biological labeling. Examples of using bioorthogonal chemistry to study biology and make new discoveries are then explored, followed by applications in medicine and implications for the future of disease treatments based on bioorthogonal chemistry.

Chapter Two is a perspective on the applications of perfluoroaromatics in chemical biology. The first section explores modifications to biomolecules and the reactivity of the perfluoroarene motif. The second half explores the non-covalent interactions of perfluroroarenes and applications therein. The chapter contains proposals of how both the reactivity and non-covalent interaction tendencies of perfluoroaromatics may be combined and used in future biological studies.

Chapter Three summarizes the characterization of a phenanthrene-based host platform and the principles that guide its binding with various phenolic guests in organic media. Through studies with both fluorinated and non-fluorinated guests, the roles of both cavity preorganization and hydrogen bonding in guest recognition are thoroughly examined. This work importantly establishes a foundation for future developments using this fully synthetic and tunable host–guest platform.

Chapter Four is a summary of the first attempts to create a nucleophile-functionalized version of the host described in Chapter Three. Here, binding of perfluoroaromatic guests, the interaction discussed in Chapter Three, is expected to promote reactivity with a nucleophile strategically placed in the host cavity. The synthesis of alternative linkers, including the various considerations for compatible chemistries, is discussed, ending with successful synthesis of a new host and preliminary screens for final nucleophile installation. This work highlights challenges and necessary future directions for establishing such a functionalized host.

Chapter Five summarizes the attempts to build a host platform based on the olympicene PAH as an alternative to phenanthrene, with a larger surface area expected to enhance non-covalent interactions with perfluoroarenes. The first half is a synthetic endeavor to access unprecedented substitution patterns on the symmetric olympicene ketone. The second half details

the challenges faced attempting to synthesize a simplified, more flexible host based on olympicene. Some of the synthetic and stability challenges here are addressed in more detail in Chapter Six.

Chapter Six classifies the distinct reactivities of three related olympicene starting materials. The most used olympicene synthon, a symmetric polycyclic aromatic ketone, is found to give many unstable products. The reduced form, base olympicene, had only been used synthetically once before; the chemistry here shows that this starting material is likely a more viable starting point for many functional olympicene syntheses. Finally, a separate ketone isomer with previously undocumented chemistry is explored. Preliminary work included at the end highlights a new class of olympicene compounds with potential for chiral material synthesis and new PAH-based fluorescent probes.

The dissertation of Kaitlin Marie Hartung is approved.

Robert Thompson Clubb

Neil Kamal Garg

Kendall N. Houk

Ellen May Sletten, Committee Chair

University of California, Los Angeles

2025

This dissertation is dedicated to the educators in my life.

TABLE OF CONTENTS

Abstract of the dissertation ii

Committee page vi

Dedication vii

Table of contents viii

List of figures xiii

List of schemes xvi

List of tables xviii

Acknowledgements xix

Biographical sketch xxii

Chapter 1. Bioorthogonal chemistry: A brief history and future directions

1.1 Abstract 1

1.2 Introduction 1

1.3 Development and improvement of foundational chemistries 4

1.3.1 Building on classic themes: Phosphine reactions and cycloadditions 5

1.3.2 Light-activated bioorthogonal reactions 7

1.3.3 Fluorogenic bioorthogonal reactions 8

1.3.4 Click-and-release reactions 9

1.3.5 Non-covalent chemistry 10

1.4 Biology in context 12

1.4.1 Characterizing glycans 12

1.4.2 Labeling lipids 16

1.4.3 Bioorthogonal chemistry and proteins 17

1.4.4 Interfacing with CRISPR 18

1.5 Biomedical applications 19

1.5.1 Diagnostic profiling 20

1.5.2 Therapeutic potential 20

1.5.3 First use in humans 24

1.6 Conclusion 24

1.7 References 25

Chapter 2. Perfluoroarenes in chemical biology: A perspective on biomolecule modification and host–guest chemistry

2.1 Abstract 36

2.2 Introduction 36

2.3 Biomolecule modifications with perfluoroaryl groups 39

2.3.1 Modified building blocks 39

2.3.2 Biomolecules reacting with perfluoroaromatic probes 42

2.4 Arene-perfluoroarene interactions in chemical biology 47

2.4.1 Background 47

2.4.2 Arene-perfluoroarene interactions in biological studies 49

2.4.3 Host–guest chemistry and arene-perfluoroarene interactions 50

2.5 Conclusion 53

2.6 Abbreviations and chemical formulas 54

2.7 References 54

Chapter 3. The interplay between preorganization and hydrogen bonding in perfluoroaromatic-binding cyclophane hosts

3.1 Abstract 64

3.2 Introduction 64

3.3 Results and discussion 67

3.3.1 The complementarity of H-bonding an a preorganized host cavity 67

3.3.2 Non-hydrogen bonding controls 70

3.3.3 Exploring an expanded scope of guests 72

3.3.4 Observations of 1:2 binding with fluorinated phenols 75

3.4 Conclusion 78

3.5 Experimental procedures 79

3.5.1 Synthetic abbreviations and chemical formulas 79

3.5.2 General host–guest titration/K_a determination procedures 80

3.5.3 Equations used 80

3.5.4 ^{1}H NMR titrations 81

3.5.5 All NMR titration trials with BindFit links 89

3.5.6 Selection of 1:2 binding model for tetrafluoronitrohenol and host (**3.3a•3.14**) 91

3.6 References 92

Chapter 4. Progress toward complexation-driven labeling of perfluoroaromatic-modified biomolecules via a modified phenanthrene-based host

4.1 Abstract 96

4.2 Introduction 96

4.3 Results and discussion 99

4.3.1 Attempted late-stage deprotection route to thiol host 99

4.3.2 Late-stage nucleophilic substitution route to thiol host 102

4.4 Conclusion 108

4.5 Experimental procedures 108

4.5.1 Synthetic abbreviations and chemical formulas 108

4.5.2 Materials and instrumentation.....109

4.5.3 Synthetic experimental procedures 110

4.5.4 ^{1}H NMR spectra 122

4.5.5 ^{13}C NMR spectra.....137

4.5.6 ^{19}F NMR spectra 146

4.6 References.....154

Chapter 5. Toward an olympicene-based host for perfluoroaromatics

5.1 Abstract.....156

5.2 Introduction.....156

5.3 Results and discussion 159

5.3.1 Attempts to synthesize a 3,8-substituted olympicene ketone 159

5.3.2 Synthesis of a flexible olympicene molecular tweezer.....167

5.4 Conclusion 173

5.5 Experimental procedures 174

5.5.1 Synthetic abbreviations and chemical formulas 174

5.5.2 Materials and instrumentation.....175

5.5.3 Note on observed masses 176

5.5.4 Synthetic experimental procedures 176

5.5.5 ^{1}H NMR spectra 199

5.5.6 ^{13}C NMR spectra.....222

5.5.7 ^{19}F NMR spectra 231

5.6 References 235

Chapter 6. Characterization of the chemistry of olympicene derivatives

6.1 Abstract 241

6.2 Introduction 241

6.3 Results and discussion 243

6.3.1 Chemistry of symmetric ketone 243

6.3.2 Chemistry of reduced olympicene 249

6.3.3 Chemistry of asymmetric ketone 251

6.4 Conclusion 255

6.5 Experimental procedures 256

6.5.1 Synthetic abbreviations and chemical formulas 256

6.5.2 Materials and instrumentation 256

6.5.3 Note on observed masses 258

6.5.4 Synthetic experimental procedures 258

6.5.5 ^{1}H NMR spectra 279

6.5.6 ^{13}C NMR spectra 298

6.5.7 2-D NMR spectra 316

6.5.8 Absorption spectra 320

6.5.9 Computational methods and data 321

6.5.10 Crystallographic information 325

6.6 References 329

LIST OF FIGURES

Chapter 1

Figure 1.1 The various roles of bioorthogonal chemistry in chemical biology 2

Figure 1.2 Expanding classic bioorthogonal chemical reactions 5

Figure 1.3 Moving beyond covalent bond formation 10

Figure 1.4 Bioorthogonal host–guest chemistry 11

Figure 1.5 Applying bioorthogonal chemistry to the study and manipulation of living systems 13

Figure 1.6 Host–guest chemistry employed in the chemical reporter strategy 15

Figure 1.7 Biomedical avenues of bioorthogonal chemical reactions 21

Chapter 2

Figure 2.1 Overview of perfluoroaromatics in the context of chemical biology tools 37

Figure 2.2 Perfluoroarene-containing synthetic metabolites 40

Figure 2.3 Peptide side-chain modifications using perfluoroaromatics 44

Figure 2.4 Engineering methods to promote S_NAr reactions in aqueous, biological settings 46

Figure 2.5 Non-covalent interactions and perfluoroaromatics 48

Figure 2.6 Impact of arene-perfluoroarene interactions on overall peptide dimer stability when one phenylalanine peptide is fluorinated 50

Figure 2.7 Examples of solution-phase host–guest chemistry with perfluoroaromatics 51

Chapter 3

Figure 3.1 Design principles for host–guest complexes in organic solutions 65

Figure 3.2 Comparison of different cavity sizes and binding to non-fluorinated versus fluorinated phenols 68

Figure 3.3 Non-hydrogen bonding control experiments 71

Figure 3.4 Summary of binding results....72

Figure 3.5 Evidence of 1:2 binding between **3.3a** and fluorinated phenols....76

Figure 3.6 Exploring potential trends between guest pK_a and binding affinity, K_a 78

Chapter 4

Figure 4.1 A general bimolecular reaction compared to a similar reaction with non-covalent or covalent bonds bringing reactants together to increase reactivity 97

Figure 4.2 Overview of thiol-functionalized host project....98

Figure 4.3 Formation of host with electrophilic site for late-stage thiol installation....106

Chapter 5

Figure 5.1 Target host structures: motivation and challenges 157

Figure 5.2 Molecular tweezers, an overview 159

Figure 5.3 Anthraquinone-based route to substituted olympicene ketone....160

Figure 5.4 Synthesis of aldehyde **5.12** and purification challenges....163

Figure 5.5 Approach to substituted ketone based on benzanthrone....164

Figure 5.6 Starting material syntheses and benzanthrone cyclization reaction 165

Figure 5.7 Synthesis of starting materials for tweezer host **5.5** 169

Figure 5.8 Attempted synthesis of tweezer **5.5** via alkyne addition 170

Figure 5.9 Attempt to access tweezer **5.5** via cross-coupling 171

Chapter 6

Figure 6.1 Olympicene and its derivatives....242

Figure 6.2 Olympicene propargyl alcohol instability 244

Figure 6.3 Further analysis of alcohol **6.1** 245

Figure 6.4 Evidence for formation of allene **6.5** 247

Figure 6.5 Exploring chemistry of **5.32** beyond alkyne additions 248

Figure 6.6 Chemistry of asymmetric ketone **5.40**.....252

Figure 6.7 Preliminary photophysical investigation of **6.17**.....254

LIST OF SCHEMES

Chapter 2

Scheme 2.1 Reactivity tuning of perfluoroaromatic probes 43

Chapter 3

Scheme 3.1 Crystal structure of complex **3.3a•3.16**.....73

Scheme 3.2 Crystal structure of host **3.3a** showing interactions with 2 molecules of guest **3.4**.....77

Chapter 4

Scheme 4.1 Retrosynthesis of thiol-functionalized host with late-stage deprotection step 99

Scheme 4.2 Synthesis of protected diol **4.9**.....100

Scheme 4.3 General C–S cross-coupling scheme for installing protected thiol.....101

Scheme 4.4 Retrosynthesis of thiol-functionalized host featuring late-stage S_NAr 102

Scheme 4.5 Amide coupling, then bromination attempts toward **4.13**.....104

Scheme 4.6 Bromination first, then amide coupling attempts toward **4.13**.....104

Scheme 4.7 Synthesis of ester linker **4.14** 105

Scheme 4.8 Attempts at late-stage thiol installation on mix of host isomers 107

Chapter 5

Scheme 5.1 Retrosynthesis of ketone **5.2** via pyrene-based route.....161

Scheme 5.2 Synthesis of methoxy- and bromine-substituted pyrene **5.13** 162

Scheme 5.3 Alternative conditions attempted for accessing benzanthrone **5.19a**.....166

Scheme 5.4 Attempted two-step, amide cyclization to access benzanthrone **5.19a**.....167

Scheme 5.5 Retrosynthetic analysis of tweezer host **5.5** via two routes 168

Chapter 6

Scheme 6.1 Transformations of **5.39** and derivatives.....249

Scheme 6.2 Proposed mechanism of decarbonylation to yield **6.8** from **6.11**.....250

Scheme 6.3 Crystal structure of **6.15**.....253

Scheme 6.4 Bromination of **5.40** and subsequent cross-coupling.....254

LIST OF TABLES

Chapter 3

Table 3.1 Summary of K_a values in $CDCl_3$ and calculated binding energies 73

Chapter 4

Table 4.1 Conditions for improving yield of **4.12** 101

Chapter 5

Table 5.1 Summary of olefination attempts on **5.9** to synthesize **5.8**.....161

Table 5.2 Optimization of substitution conditions to access pyrene **5.13** 162

Table 5.3 Attempts to access **5.19a** via cyclization of amide **5.31**.....167

Chapter 6

Table 6.1 Methods to synthesize olympicene synthons.....243

ACKNOWLEDGEMENTS

The first thank-yous go to my advisor, Ellen Sletten, my committee members, and my colleagues at UCLA. Ellen, I am grateful to have been advised these past five years by someone with the most impressive ability to think like an organic chemist, a biologist, and a materials scientist all at once. From you I learned new, creative ways of approaching problems and how to tell a compelling story, skills I know will serve me well. I'm grateful to Neil Garg, Ken Houk, and Rob Clubb for their encouragement as committee members. I additionally thank Neil for an impactful first-year lab rotation where I learned many fundamental chemistry skills, and for his helpful suggestions for my projects over the years.

Every member of the Sletten group I overlapped with helped me in my research at least once, and I am grateful for each instance. It was an honor to learn from this extremely talented group of scientists. I will also fondly remember ventures outside lab, from baseball games in the blazing sun to Barney's karaoke to Helen's wedding in the Bay Area. I need to especially thank members of 4210, past and present. Margeaux and Heidi, you were my original mentors in the lab and your early guidance helped shape my PhD. Paige and Eric, I appreciated that you were as quick to dish out words of encouragement as food and drink recommendations. Prairie, I enjoyed working together on our host–guest problems and trying to overcome a difference of opinion on the best baseball team (sorry, Dodgers > Giants), and you are the best cat-sitter ever. And Ethan, thank you for both introducing me to rock climbing and sharing wisdom while we traded vents about the stresses of grad school.

A thank you to the LA friends who reminded me that I was a person beyond a grad student and made me feel important and valued. Anthony and Irene, I learned so much from you, from not taking my chemistry failures too personally to not always taking life too seriously.

Cesar, you are that special friend who can go from a deep conversation about the meaning of life one second to trading jabs about our respective sports allegiances (boo Padres) in the next. Thank you for teaching me just about everything I know about baseball; I can't wait for our next game. Caitlyn, I can't imagine making it through grad school without you. How lucky were we to find another person from a small Oregon/Oregon-adjacent town willing to do anything from grocery shop to go on an hours-long road trip together for an adventure? Here's to many more to come.

To America, Ellie, and Ram, the best Cal Poly crew ever, I am so grateful that our struggles in biochemistry created a lasting friend group. If the pandemic did anything good, it was making Zoom normal – I don't know how I would have made it through grad school without our regular hangouts. I look forward to the virtual and in-person meetings in the years to come.

I am very grateful for the support of family and friends over these past five years: Uncle David, Aunt Eunyoung, and Annalee; Knox and Lynette; Ray and Brooke; Uncle Steve H.; Aunt Darlene, Uncle Steve A., Randi, Taylor, and the whole Ventura cousin crew. To Dr. Bailey and to Dr. K and the entire Kantorowski family, thank you for all of your advice and encouragement.

Getting close to home: D'Anna, our friendship looks very different from our high school days, but I always look forward to playing Trader Joe's Santa for Ellie, Evie, and Eamon every few months and catching up with you and Luke. Thank you to the TGIF families (Baker-Kings, Haupts, Fakhres, and Mahans) for reminding me to take time and celebrate every good thing.

Eric, thank you for your brotherly support throughout the years. We may be on different paths but I'm glad that at the end of the day, we can go to each other for advice, a laugh, or a good chat. Mom and Dad, there aren't words to express how grateful I am for your love and support. I am so lucky to have you both in my corner. And finally, thank you to June Bug for being the cutest, meanest, and best cat ever.

Chapter One is a version of a published perspective: Kaitlin M. Hartung, Ellen M. Sletten. “Bioorthogonal chemistry: Bridging chemistry, biology, and medicine.” *Chem* **2023**, *9*, 2095–2109. Hartung and Sletten contributed to writing.

Chapter Two is an unpublished perspective on perfluoroaromatics in chemical biology written by Hartung.

Chapter Three is a version of a manuscript in preparation. Kaitlin M. Hartung, Ga Young Lee, Margeaux M. Miller, Erika Aguiluz Ramirez, Prairie E. Hammer, Kendall N. Houk, Ellen M. Sletten. “The interplay between preorganization and hydrogen bonding in perfluoroaromatic-binding cyclophane hosts.” Experimental work was performed by Lee, Miller, Aguiluz-Ramirez, Hammer, and Hartung. X-ray crystallography was performed by Dr. Tyler Kerr. Hartung and Sletten contributed to writing.

Chapter Four is unpublished work written by Hartung. Experimental work was performed by Hartung.

Chapter Five is unpublished work written by Hartung. Experimental work was performed by Hartung.

Chapter Six is a version of a published manuscript: Kaitlin M. Hartung, Ellen M Sletten. “Achieving Olympicene Functionalization Three Ways.” *J. Org. Chem.* **2025**, *90*, 889–893. Experimental work was performed by Hartung. Hartung and Sletten contributed to writing. Additional unpublished experimental work by Hartung is included.

Throughout these studies, Kaitlin Hartung was supported by the NIH Chemistry-Biology Interface Training Program (T32 training grant, T32GM136614).

Additional funding sources include: UCLA, NIH (DP2GM13268), NIH NIBIB (2R01EB027172), and instrumentation grants provided by the NSF (CHE-1048804) and NIH (S10OD028644).

BIOGRAPHICAL SKETCH

EDUCATION

University of California, Los Angeles, Los Angeles, CA
MS in Chemistry 2022
GPA: 4.00/4.00

California Polytechnic State University, San Luis Obispo, CA 2016–2020
BS in Biological Sciences
Summa cum laude, GPA: 3.91/4.00
Senior thesis: "Cyclopropane kinetics: formation and electrophilic ring-opening and epoxide synthesis and rearrangement in the undergraduate teaching lab."

RESEARCH EXPERIENCE

Graduate Student Researcher, University of California, Los Angeles 2020–present
Advisor: Prof. Ellen M. Sletten

- Established synthetic routes to new aromatic hydrocarbon scaffolds after common starting materials did not work for initial goal; this work demonstrates first synthetic uses of previously unexplored materials; published in peer-reviewed journal.
- Lead author on a collaborative project designing, synthesizing, characterizing molecular recognition platform based on specific interactions, examining effects of structural modifications.
- Trained group members on multiple lab techniques (including hydrogenation reactions, NMR experiments, use of pyrophoric reagents) and use of specialized equipment; group operator of solvent purification system.
- Editing proposals, manuscripts, experimental documents, presentations; over 20 to date.
- Formally mentored 2 incoming PhD students.

Teaching & Research Intern, Scripps College, Claremont, CA Jan. 2024–Mar. 2024

- Held twice-weekly office hours regularly attended by 3–10 students from a general chemistry course; created weekly review materials.
- Prepared and delivered 2 lectures for general chemistry class.
- *Research*: purified, characterized, analyzed kinetics of 3 mutant luciferase enzymes toward bioimaging work.

Undergraduate Researcher, Cal Poly 2018–2020
Advisor: Prof. Eric Kantorowski

- Developed a new experiment that was incorporated into the organic chemistry teaching lab curriculum; conducted reactions and kinetics studies, helped develop written procedure.
- Led research on a structure-reactivity/physical organic chemistry project, training 5 other undergraduates who then contributed to this and another project.

FELLOWSHIPS AND AWARDS

Herbert Newby McCoy Commencement Award	2025
UCLA-Amgen Lectureship Poster Award	2024
UCLA Chemistry-Biology Interface (CBI) Trainee	2021–2024
John Stauffer Excellence in Second Year Academics and Research Award	2023
UCLA College of Letters and Science Alumni Fellowship	2021
UCLA Graduate Dean's Scholar Award	2020–2022
Cal Poly William & Linda Frost Merit-Based Scholarship	2016–2020
Cal Poly Dean's List	2016–2020
Brandon D. Huang Memorial Scholarship	2019
William & Linda Frost Summer Research Fellowship	2019
Research Award in Organic Chemistry	2019
William & Linda Frost Academic Year Research Grant	2019

PUBLICATIONS

1. **Hartung, K. M.**; Lee, G. Y.; Miller, M. A.; Aguiluz Ramirez, E.; Hammer, P. E.; Houk, K. N.; Sletten, E. M. *Manuscript in preparation.*
2. **Hartung, K. M.**; Sletten, E. M. Achieving Olympicene Functionalization Three Ways. *J. Org. Chem.* **2024**. DOI: 10.1021/acs.joc.4c02471.
3. **Hartung, K. M.**; Sletten, E. M. Bioorthogonal Chemistry: Bridging Chemistry, Biology, and Medicine. *Chem* **2023**, *9*, 2095–2109. DOI: 10.1016/j.chempr.2023.05.016.

CHAPTER ONE

Bioorthogonal chemistry: A brief history and future directions

Adapted from: Kaitlin M. Hartung, Ellen M. Sletten. Bioorthogonal chemistry: Bridging chemistry, biology, and medicine. *Chem* **2023**, *9*, 2095–2109. DOI: 10.1016/j.chempr.2023.05.016

1.1 Abstract

As chemical biologists sought methods to modify and study biomolecules in their native environments, the need for bioorthogonal chemical reactions emerged. These fast and selective reactions between otherwise inert, abiotic functional groups have enabled exploration of some of the most intriguing and challenging questions in chemical biology. Further, the ability to perform organic reactions in cells and organisms has led to important applications in clinical spaces, and one reaction is now an integral part of a phase 2 trial for treating solid tumors. Given that bioorthogonal chemistry was a recipient of the 2022 Nobel Prize, we expect this field to be even more energized. Here, we highlight some of the most recent studies in this sphere and how these set the stage for where bioorthogonal chemistry is headed.

1.2 Introduction

The foundation of chemical biology can be traced back centuries to the use of chemicals to perturb biological processes.[1] Today, it is an active field applying chemistry to study biological systems and using biology to enable new chemistries.[2] A distinction between chemical biology and biochemistry is the desire to characterize biomolecules in their native environments rather than *in vitro*, a challenging task due to the complexity of living cells and organisms.

A breakthrough towards studying biomolecules in living systems came with the advent of bioorthogonal chemistry: chemical reactions between abiotic functional groups that react

selectively with each other but are inert to biological functionalities. Bioorthogonal reactions must exhibit exquisite selectivity, be high yielding, require simple design and execution, feature non-toxic components, and proceed in physiological media and conditions.[3] The first three requirements overlap with those of click reactions, introduced to the synthetic chemistry community around the same time by Barry Sharpless;[4] however, the remaining conditions impose additional challenges. Despite this, bioorthogonal chemistry has quickly become a veritable wealth of tools used to probe biological questions once out of reach and has even expanded to technologies related to human health (Figure 1.1A). Its impact, intertwined with click chemistry, was recognized with the awarding of the 2022 Nobel Prize.

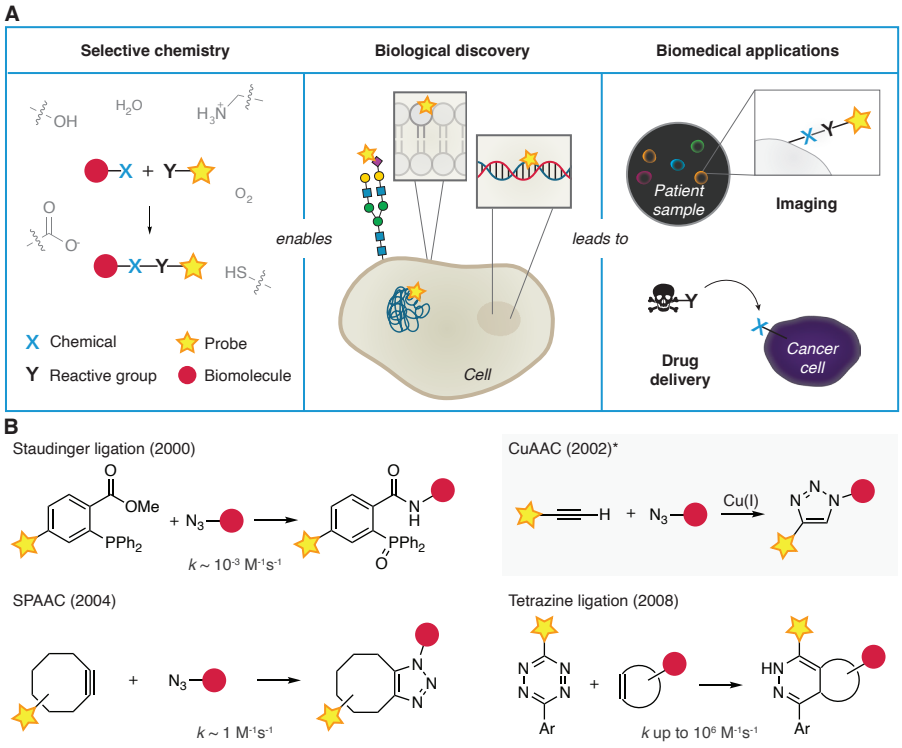

Figure 1.1 The various roles of bioorthogonal chemistry in chemical biology. (A) Selective reactions that take place in living systems without interacting with native functionalities have enabled detailed studies and discoveries in chemical biology and led to important biomedical advances. (B) The four standard bioorthogonal and click reactions: the Staudinger ligation, copper-catalyzed azide-alkyne click cycloaddition (CuAAC),* strain-promoted azide-alkyne cycloaddition (SPAAC), and the inverse electron-demand Diels-Alder (IEDDA) reaction between tetrazines and strained alkenes (tetrazine ligation). General second-order rate constants are listed

for bioorthogonal reactions. *CuAAC is generally not considered bioorthogonal due to the toxicity of copper.

An initial inspiration for the pursuit of bioorthogonal reactions was the need for new chemistries to study glycans, which were not amenable to molecular biology tools available at the time. Developing such reactions was the quest of Carolyn Bertozzi and her lab in the 1990s. At the turn of the century, Bertozzi and co-workers published the Staudinger ligation, the first of what would become a suite of bioorthogonal reactions (Figure 1.1B).[5] A modification of the classic Staudinger reduction of azides by phosphine reagents, this reaction includes a trap on the phosphine probe that allows for the generation of an amide-linked ligation product. This report also served as the introduction of the azide as an ideal bioorthogonal functional group for modifying biomolecules, as it is not found naturally in biology and is small and non-perturbing. This small but mighty three-atom arrangement has become a staple in chemical biology.

The azide is also a key component of the quintessential click reaction– a formal [3+2] cycloaddition between azides and terminal alkynes catalyzed by Cu(I), which was reported independently by Morten Meldal and Sharpless in 2002 (Figure 1.1B, CuAAC).[6,7] While not bioorthogonal due to the toxicity of Cu(I), CuAAC is a prominent method for labeling azides in fixed cells, lysates, and proteins. More recent advances in ligands have decreased the amount of Cu(I) necessary, allowing CuAAC to be used on live cells and organisms, though the need for three things to come together still limits *in vivo* applications.[8]

During the early 2000s, Bertozzi and co-workers were also focused on the 1,3-diploar cycloaddition between azides and alkynes, taking inspiration from physical organic chemists Huisgen, Wittig, and Krebs.[9] Instead of activating alkynes for reactivity with azides by Cu-catalysis, Bertozzi and co-workers looked to a fundamental chemistry concept: ring strain. The

strain-promoted azide-alkyne cycloaddition (SPAAC, or copper-free click chemistry), between a strained cyclooctyne and azide, was thus born (Figure 1.1B).[10] A variety of cyclooctynes for SPAAC have been discovered, enabling tagging of biomolecules in live cells, zebrafish, and mice.[3,8] A few years later, a faster reaction between strained alkenes and tetrazines, new bioorthogonal functional moieties, burst onto the scene (Figure 1.1B).[11,12] This inverse electron-demand Diels-Alder (IEDDA) reaction quickly became a staple in the bioorthogonal toolbox. With inherent strain energy now taking the place of a discrete catalyst, click and bioorthogonal chemistries converged in a partnership that would propel the field of chemical biology into a new era of development, discovery, and applications.

We begin this perspective broadly discussing the evolution of bioorthogonal chemistry, highlighting recent new directions likely to be applied in chemical biology. We then venture into the realm of biological inquiry and discovery made possible by bioorthogonal strategies, and finally, we highlight the potential bioorthogonal chemistry holds with regards to medical advances.

1.3 Development and improvement of foundational chemistries

While the four popular reactions introduced above remain standards in chemical biology applications, new and improved reactions are continuously in development, particularly for metal-free reactions. Improvements on old reactions often focus on increasing reaction rates without compromising the size and/or stability of reagents, a tradeoff commonly encountered in bioorthogonal reaction development. Other developments incorporate features for increased control over when or where a reaction occurs in living systems, including light-activated reagents and click-and-release technologies.

1.3.1 Building on classic themes: Phosphine reactions and cycloadditions

Widely regarded as the first bioorthogonal reaction, the Staudinger ligation has experienced many modifications. One of the first advancements was a traceless variant where the phosphine reagent is not attached to the amide bond-containing final product (Figure 1.2A).[13,14] This is a desirable reaction for modifying molecules in living systems, as the result is a naturally occurring linkage. Focusing on the final product linkage has not taken center stage in bioorthogonal reaction development but represents a subfield of bioorthogonal chemistry that is ripe for development. Reactions that yield natural linkages or known pharmacophores would have potential for in situ synthesis of (bio)therapeutics. Other modifications have featured phosphite or phosphonite reagents, introduced by Hackenberger and co-workers, in place of phosphines[15,16] and the formation of a stable iminophosphorane intermediate that is resistant to hydrolysis.[17]

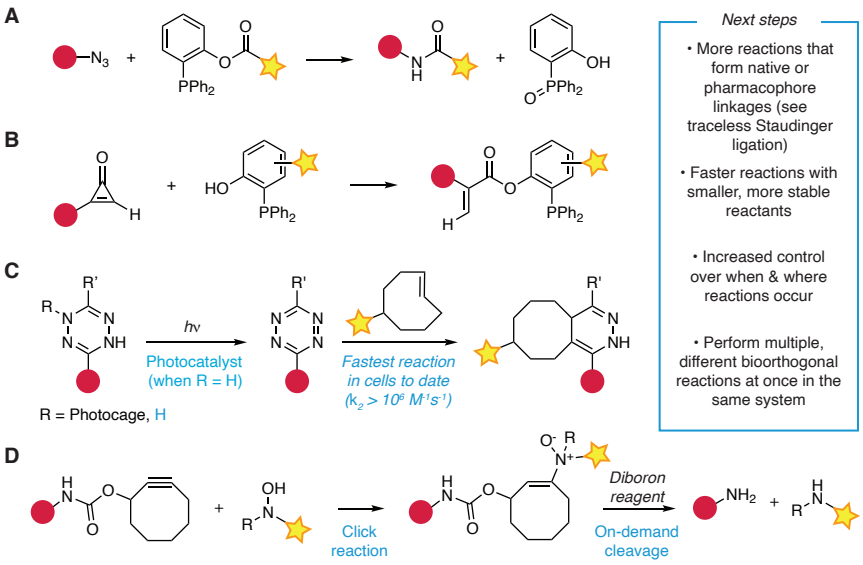

Figure 1.2 Expanding classic bioorthogonal chemical reactions. A sampling of the bioorthogonal reactions in use today, including variations on the classic Staudinger reactions such as a traceless variant (A) and using cyclopropenones (B), tetrazine ligations enabled by photocleavage of a

protecting group or dihydrotetrazine oxidation promoted by a photocatalyst (C), and cyclooctyne retro-Cope eliminations with hydroxylamines (D). The hydroamination product in (E) can be selectively cleaved with diboron reagents.

Inspired by the ideal properties of the Staudinger ligation – namely, its high selectivity and the small size of azides – the Prescher group developed alternative cyclopropenone chemical reporters that react with phosphines via conjugate additions (Figure 1.2B).[18] Variations on this reaction have enabled multiple applications, including reaction-promoted fluorophore synthesis and orthogonal bioorthogonal reactions.[19] While most of these applications are possible with other bioorthogonal reactions, the facile chemical adaptation of this new reaction showcases the opportunities when selectivity and size are key motivators during reaction development.

Bioorthogonal cycloadditions have also seen extensive optimization and derivation. Newer renditions improve in the areas of reactivity, stability, size, hydrophilicity, and orthogonality. Many iterations of alternative cyclooctyne and tetrazine reactive partners have been explored and are included in recent reviews.[8,20] Other variations of cycloaddition reactions have been added to the bioorthogonal toolbox, including those featuring alternative 1,3-dipoles: (imino)sydnones in the strain-promoted (imino)sydnone-alkyne cycloaddition (SPSAC or SPICC),[21,22] nitrones in the strain-promoted alkyne-nitrone cycloaddition (SPANC),[23,24] nitrile oxides,[25,26] nitrile imines,[27] and diazo compounds.[28] For IEDDA reactions, tetrazine substitutes have been explored, such as the more biologically stable triazines,[29] and cyclopentadienes have been adopted for a classic Diels-Alder bioorthogonal reaction.[30] Notably, some of these reactions are orthogonal to each other, enabling multiple bioorthogonal chemistries to be performed at once. We expect the development of orthogonal, bioorthogonal chemistries to be increasingly important as the complexity of systems that are studied using these chemistries increases.

Computation has played an increasingly important role in discovering and enhancing bioorthogonal cycloaddition reactions. For example, Houk, Murphy, and co-workers used computational methods to design cyclopentadienes to react with existing biocompatible dienophiles.[30] Experimental work confirmed the computed reactivities, with reaction rates on par with SPAAC. More recently, Stuyver and Coley used machine learning to screen thousands of cycloaddition partners for potential new bioorthogonal reactions.[31] Reactions were evaluated for "bioorthogonal potential," or the likelihood to react with theoretical partners over biological functional groups. As computation workflows are optimized and expanded to include other types of potential bioorthogonal reagents, we will likely see the design of entire new classes of reactions, rather than optimization of existing reaction partners.

1.3.2 Light-activated bioorthogonal reactions

The growing use of light to activate bioorthogonal reactions adds a degree of spatiotemporal control in chemical biology studies.[32] Early examples included "photoclick chemistry" pioneered by Lin, where irradiation of a tetrazole lead to in situ formation of nitrile-imine 1,3-dipole that rapidly reacted with alkenes.[33] In a similar timeframe, Boons and Popik reported a cyclopropenone-masked dibenzocyclooctyne, which upon irradiation with light released CO to reveal the alkyne for reaction with azide.[34] More recently, focus has switched to controlling the location and timing of tetrazine ligations with light. Devaraj and co-workers recently tackled the issue of tetrazine instability in biological settings by adding a photocage to a dihydrotetrazine (Figure 1.2C, R = photocage). Following UV light-activated deprotection, the unreactive dihydrotetrazine was oxidized to a reactive tetrazine, which underwent rapid IEDDA with a trans-cyclooctene probe.[35] The control this strategy provides, in addition to the stability of

the photocaged tetrazine, is likely to find use in future studies, especially as cages responding to longer wavelengths of light – which are more biocompatible – are incorporated. On the theme of using more red-shifted light to control bioorthogonal chemistry, Jia, Li, Fox, and co-workers employed silicon-rhodamine dyes as photocatalysts that promoted the oxidation of dihydrotetrazines to tetrazines (Figure 1.2C, R = H).[36] The photocatalyst is activated by far-red (660 nm) light. Besides control, this approach also benefits from low catalyst loadings and the observation that oxidation occurs much faster than singlet oxygen sensitization, which would otherwise damage cells. An elaborated version of this system with a more cell-permeable dihydrotetrazine led to the most reactive tetrazine used to-date in living cells, with an IEDDA rate constant over 10^6 $M^{-1}s^{-1}$.[37] This combination of control, speed, and biocompatibility promises future applications and further demonstrates the general utility light brings to the bioorthogonal table.

1.3.3 Fluorogenic bioorthogonal reactions

As many applications of bioorthogonal chemistry revolve around imaging, it is beneficial to have methods of reducing complicating background signal. One approach is to use fluorogenic bioorthogonal reactions, designed to produce a probe with signal only after the reaction has occurred. This was first demonstrated with the Staudinger ligation through fluorophore activation upon phosphine oxide formation.[38] A few iterations of bioorthogonal reactions have been co-opted to be fluorogenic, including coumarins activated by SPAAC[39,40] or SPSAC.[41] Prescher and co-workers have also designed a cyclopropenone where, following phosphine attack, the ketene-ylide intermediate undergoes an intramolecular reaction to generate a fluorescent coumarin dye.[19] The tetrazine ligation has enjoyed the most success with fluorogenic probes, as tetrazine

naturally quenches the fluorescence of red fluorophores.[42] Recent work has demonstrated impressive turn-on capabilities for fluorophores emitting at far-red and near infrared wavelengths.[43,44] This red-shifting has long been desired such that turn-on probes can be used for in vivo applications, and future fluorogenic reactions will continue the trek across the electromagnetic spectrum, moving to the near- and shortwave-infrared regions.

1.3.4 Click-and-release reactions

While a key focus of bioorthogonal reaction development is the selective formation of bonds to label biomolecules, there is parallel interest in selectively cleaving bonds in biological contexts through the development of click-and-release, or bioorthogonal cleavage, reactions.[45] Some click-and-release reactions arose through a redesign of existing reactions, such as the inclusion of a collapsible carbamate moiety in a trans-cyclooctene scaffold. Upon reaction with a tetrazine, an intermediate spontaneously collapses, releasing a molecule of CO_2 and an attached payload (Figure 1.3A).[46] This strategy has expanded over the years, and is employed in the first click chemistry performed in human patients (*vide infra*). Another recent example of click-and-release chemistry utilized the SPICC reaction, releasing two fluorescent products at once.[47] Kim and co-workers expanded their previously disclosed reaction between cyclooctynes and hydroxylamines to include an on-demand cleavage of the enamine *N*-oxide products (Figure 1.2D).[48] On-demand, as opposed to spontaneous, cleavage adds a new layer of control to reversible chemical modifications. Kim's work represents an adaptation of classic dynamic covalent chemistry to bioorthogonal chemistries, an area where there is significant potential for further expansion. Future advances will focus on improved yield and rate of cleavage and will likely also feature development of other click and on-demand release pairings.

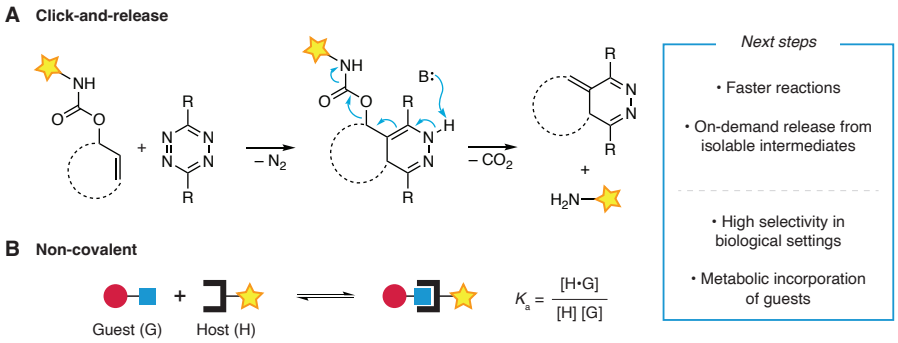

Figure 1.3 Moving beyond covalent bond formation. Bringing chemical partners together in living systems is not limited to irreversible covalent bonds. Several click-and-release reactions have been developed, where the formed intermediate is designed to spontaneously collapse and release two products (A). Non-covalent approaches using host–guest chemistry principles have seen increased use in labeling living cells (B).

1.3.5 Non-covalent chemistry

Non-covalent chemistry is growing in popularity as an alternative approach to covalency for forming unnatural associations in living systems (Figure 1.3B). This often involves the application of host–guest chemistry to cell labeling, which relies on the combined strength of multiple non-covalent interactions.[49] Besides the potential for reversibility, non-covalent chemistry benefits from not being reliant on second-order rate constants or highly activated reagents, two of the major challenges present in bioorthogonal reaction development. Instead, the focus is on achieving high binding affinities (K_a).

Our group used known host cucurbit[7]uril (CB[7]) to label modified cell-surface sialic acids and demonstrated significant labeling with nanomolar concentrations of host (Figure 1.4A).[50] CB[7] is a well-studied host with many known guests, whose binding affinities range from 10^6–10^{17} M^{-1}.[51,52] Through modifying cell-surface sialic acids with an oxidation, oxime ligation sequence, different known guest motifs were added to cells (Figure 1.4A). Addition of fluorophore-conjugated CB[7] led to significant labeling when guests with K_a's of 10^8 M^{-1} or higher were present, suggesting a threshold for labeling via 1:1 host–guest complexes.

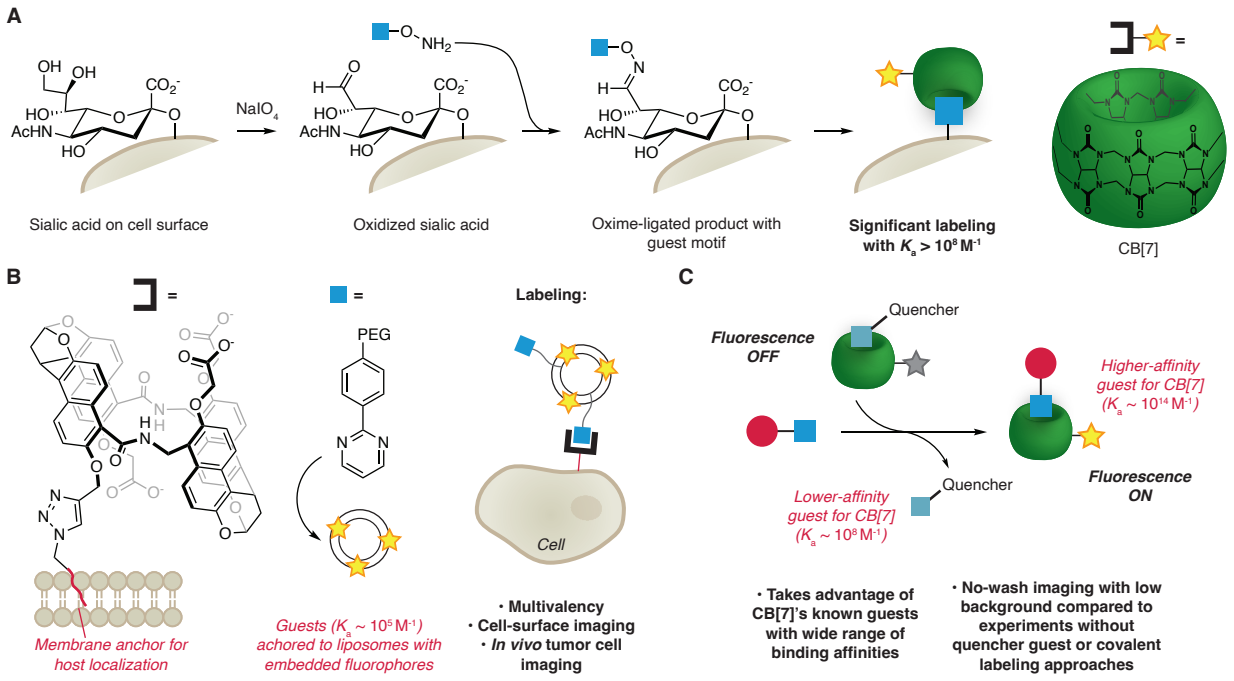

Figure 1.4 Bioorthogonal host–guest chemistry. (A) Cell-surface sialic acid oxidation followed by ligation of guest motifs leads to labeling by cucurbit[7]uril (CB[7]) (ref. 50). (B) Synthetic amide naphthotube hosts embedded in cell membranes are labeled by guest-modified liposomes (ref. 54). (C) CB[7] guest exchange strategy for low-background cell imaging (ref. 55).

Work from the groups of Papot and Jiang recently showed that host compounds cyclodextrin or amide naphthotubes, respectively, could be used to label living systems through recognition of appropriate guests.[53,54] In the latter case, synthetic naphthotube hosts were modified with hydrophobic anchoring groups to localize hosts to cell membranes (Figure 1.4B). Phenylpyrimidine guests were modified with water-solubilizing polyethylene glycol (PEG) groups and embedded in liposomes, which also contained fluorophores for imaging. Association of host and guest led to cell labeling, including in tumor cells in mice. The presence of multiple guests on a single liposome increased the opportunities for association, an approach known as multivalency. Given the lower K_a's of naphthotube guests (K_a ~10^5 M^{-1}), multivalency is a possible strategy for circumventing the 10^8 M^{-1} threshold our work suggests for surface labeling via monovalent associations.

A more recent example of using host–guest associations for efficient cell labeling from the Agasti group again takes advantage of the large range of binding affinities with CB[7].[55] Here, a lower-affinity guest is modified with a quencher moiety that quenches fluorescence from a fluorophore-conjugated CB[7] when bound (Figure 1.4C). Upon introduction of a second, higher-affinity guest, the quencher is displaced, leading to an increase in fluorescence. Higher-affinity guests were appended to different biological targets for fixed and live cell imaging. The fluorogenic nature of this work significantly improved imaging resolution when compared to just labeling with fluorescent host, as well as compared to labeling via bioorthogonal reactions. Future work using bioorthogonal host–guest chemistry will involve utilizing small guests that can be metabolically incorporated and the design of new hosts specifically for bioorthogonal labeling.

1.4 Biology in context

Since its inception, bioorthogonal chemistry has been applied to answering many biological questions that were previously daunting or fully unanswerable using existing tools. Here we highlight certain foundational applications and recent works that showcase the power and future promise of such studies.

1.4.1 Characterizing glycans

As mentioned, the study of glycans is not amendable to traditional molecular biology techniques. To address this, a two-step approach, referred to as the chemical reporter strategy (Figure 1.5A),[3] was introduced where an unnatural carbohydrate with a bioorthogonal functional group was incorporated into glycans using natural biosynthetic pathways. In a second step, a

probe was attached. The need to attach the probe to the unnatural functional group gave rise to the field of bioorthogonal chemistry. Today, the chemical reporter strategy has been applied to many different metabolites and biomolecules; however, glycans continue to be a popular target for advances in bioorthogonal chemistry.

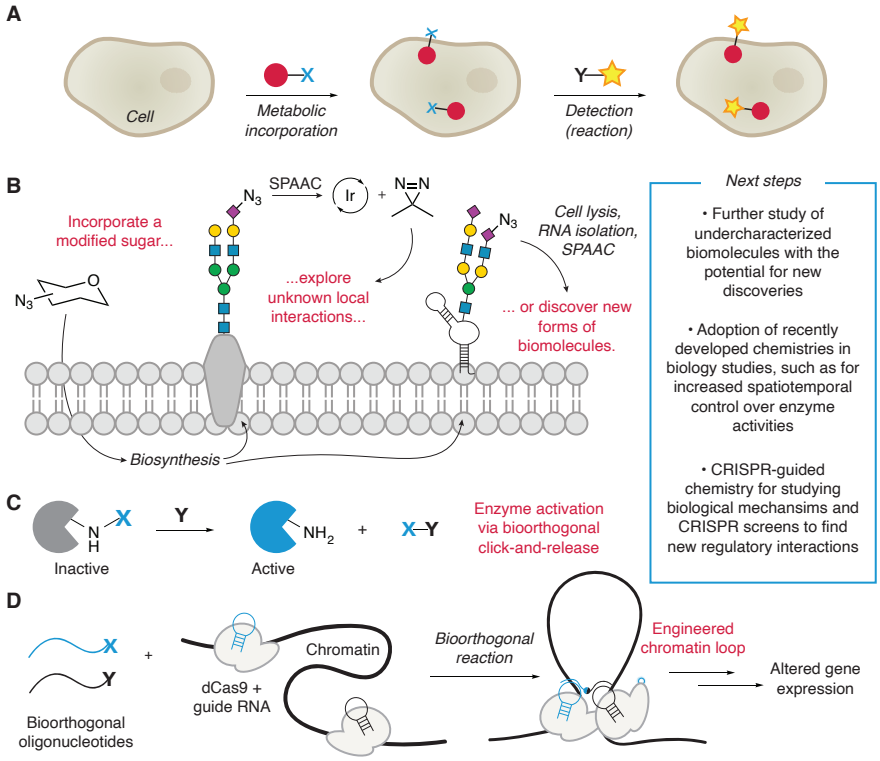

Figure 1.5 Applying bioorthogonal chemistry to the study and manipulation of living systems. (A) The bioorthogonal chemical reporter strategy. (B) Scheme of unnatural sugar modification and display. Specific examples of photolabeling and glycoRNA discovery are shown. (C) Bioorthogonal control over enzyme activation. (D) CRISPR-guided, SPAAC-enabled control over formation of chromatin loops.

A recent application using glycan-associated chemical reporters was the mapping of the local interactions of cell-surface sialic acids (Figure 1.5B).[56] In this work, an iridium photocatalyst was appended via a SPAAC reaction rather than attachment of a traditional probe (e.g. fluorophore or biotin). With the photocatalyst installed, the "microenvironment" of sialic acid-capped glycoproteins in cells was characterized through iridium-catalyzed proximity

labeling with diazarenes. The proximity labeling revealed a relationship between sialylation and regulation of expression of solute carrier proteins in cancerous cervical cells. This approach is amenable to further profiling of the consequences of sialic acid overexpression in various cancers and could be extended to characterizing other cell-surface interactions. More broadly, this report represents the expanding functionality of groups that are attached via the bioorthogonal reaction, a trend that will likely increase in the coming years.

Bioorthogonal chemistry and the chemical reporter strategy have also led to striking new discoveries regarding glycosylation in terms of localization, dynamics, and biomolecule modification. A marquee example is the recent finding that RNA can be glycosylated (Figure 1.5B).[57] RNA samples from cells grown in the presence of azide-containing sialic acid precursors were found to have high amounts of azides reacting with dibenzocyclooctyne probes. This study revealed a new dimension of RNA structure and function, and further investigations into glycoRNAs are sure to probe the mechanisms of transport and localization as well as other undiscovered functions.

Recently, bioorthogonal host–guest chemistry has been employed in the chemical reporter strategy using guest-labeled glycans (Figure 1.6A). With sufficiently high binding affinities, lower concentrations of host and guest are needed for labeling results comparable to bioorthogonal chemistry. This makes a non-covalent approach appealing for using the chemical reporter strategy in more dilute systems, such as larger organisms like mice, where the slow rates of some bioorthogonal reactions can cause issues. In our group's work using CB[7] to label cells, it was found that high-affinity guests were not amenable to metabolic incorporation, likely due to size and/or charge.[50] Instead, a lower-affinity, neutral guest, *ortho*-carborane, could be incorporated via modified sialic acid (Figure 1.6B). In sialic-acid deficient cells, the modified

sugar was successfully taken up and labeled with CB[7], though higher concentrations of host were needed compared to non-incorporated cell-surface guests. This was attributed to either background associated with the cell line and/or the lower affinity of ortho-carborane with CB[7] (K_a ~10^9 M^{-1}).

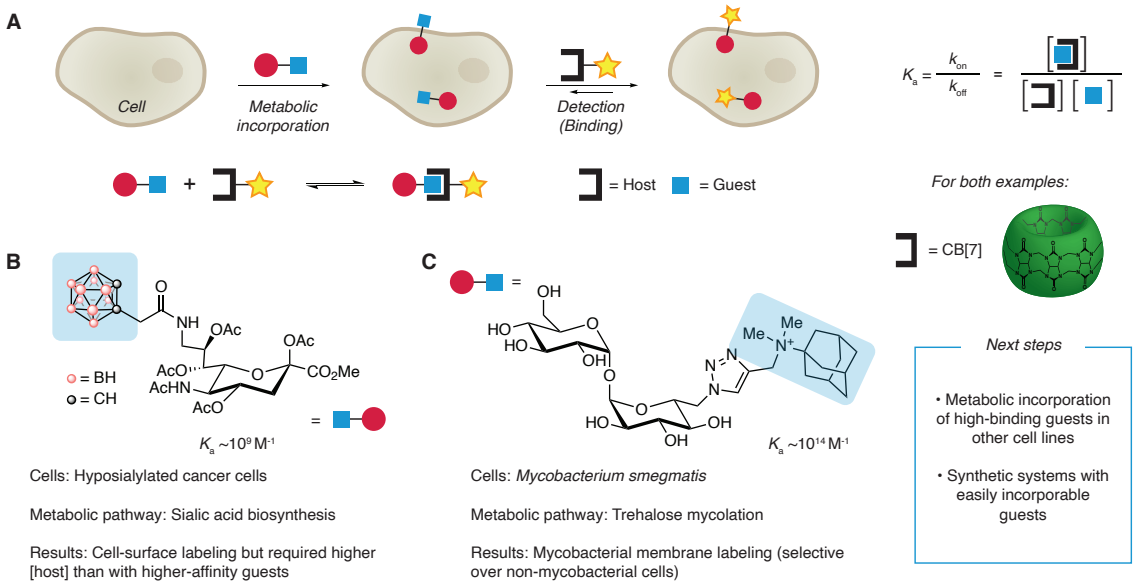

Figure 1.6 Host–guest chemistry employed in the chemical reporter strategy. (A) The non-covalent chemical reporter strategy. (B) A guest-modified sialic acid (guest = *ortho*-carborane) taken up by natural sialic acid biosynthesis, displayed on cell surfaces, and labeled with CB[7] (ref. 50). (C) A guest-modified trehalose (guest = adamantylamine) used in trehalose metabolism by *Mycobacterium* cells leads to membrane labeling by CB[7] (ref. 55).

One example where a higher-affinity guest for CB[7] was successfully incorporated is featured in the Agasti group's guest-exchange strategy for cell labeling (Figure 1.6C).[55] Here, trehalose is modified with a high-affinity adamantylamine motif and selectively processed by *Mycobacterium* cells for display on cell membranes, then successfully labeled with CB[7]. The ability for high-affinity CB[7] guests to be used in some metabolic pathways but not others, as our group observed, may be useful for orthogonal labeling studies. Otherwise, the future use of CB[7] systems in metabolic labeling will likely require optimization with lower-affinity, neutral guests or the exploration of turn-on approaches to overcome incorporation challenges with high-

affinity guests. Ultimately, our group aims to create synthetic, bioorthogonal hosts based on the recognition of small, neutral guests that are facilely incorporated and apply these in the chemical reporter strategy. This is the motivation for the work presented in Chapters 3–6.

As the analytical toolbox for detecting glycosylated biomolecules increases, we expect metabolic incorporation of chemical reporters followed by bioorthogonal chemistry to unveil many other unique roles of carbohydrates.

1.4.2 Labeling lipids

Lipids are another class of biomolecules whose in-depth exploration has been enhanced by bioorthogonal chemistry. Like glycans, there are no direct genetic techniques for systematically manipulating lipids. Initial applications of bioorthogonal chemistry to lipids included introduction of complete lipids containing a chemical reporter group for subsequent labeling with fluorophores using click or SPAAC chemistries.[58] Shortly after, metabolic approaches were pursued where alkyne-functionalized choline was employed as a precursor to phosphatidylcholine lipids,[59] the most abundant mammalian lipids, or alkynols were introduced to label phosphatidic acid.[60] Both of these studies employed click chemistry to image lipid synthesis. For the case of phosphatidic acid labeling, the scope of accepted chemical reporter groups has expanded for labeling with SPAAC[61] and the tetrazine ligation.[62] In the latter work, a fluorogenic tetrazine allowed for real-time imaging and revealed new subcellular information regarding the synthesis of phosphatidic acid. The work with phosphatidic acid comparing the utility of the click chemistry to the tetrazine ligation showcased the importance of rapid, fluorogenic bioorthogonal reactions. However, it was a significant challenge obtaining a system that accepted the *trans*-cyclooctene chemical reporter group required for the fast tetrazine

ligation, demonstrating the need for fast bioorthogonal reactions with small chemical reporter groups.

Imaging of biomolecules has been a primary application of bioorthogonal chemistry and the chemical reporter strategy. As more detailed subcellular information is desired, the limits of conventional optical microscopy are reached. One approach to overcome these limitations is to use super-resolution microscopy, but another is to make the cell bigger through expansion microscopy. The Baskin Group has utilized chemical reporter incorporation on lipids and click chemistry to create a variation on expansion microscopy deemed lipid expansion microscopy (LExM).[63] In LExM, metabolically labeled lipids are detected by a dual-purpose probe via click reaction. The probe functions as both a fluorescent reporter and a crosslinker with a hydrogel matrix that is expanded. The membranes of cells and organelles can be visualized in striking detail on a standard fluorescence microscope. This version of expansion microscopy completely removes the membrane permeabilization step that limited previous lipid microscopy endeavors. The unique approach to expansion microscopy based on chemical reporter groups is set for extension to other metabolically labeled biomolecules.

1.4.3 Bioorthogonal chemistry and proteins

Protein chemical biology has benefited greatly from bioorthogonal chemistry, both for tracking proteins in natural settings and improving chemical modifications in proteomics workflows. The introduction of chemical reporter-modified amino acids to living systems offers a powerful way to investigate protein synthesis. Bioorthogonal non-canonical amino-acid tagging (BONCAT) emerged as such a tool.[64] Here, modified amino acids are utilized by cells for protein synthesis, and following cell lysis, new proteins that used the unnatural building

blocks can be detected by bioorthogonal reaction. Commonly, an azide- or alkyne-tagged amino acid is used and detected by CuAAC or SPAAC. While this is no longer a new strategy, BONCAT's usefulness continues in characterizing protein dynamics under changing conditions, such as infection by microorganisms.[65] The technique can also be combined with other labeling strategies to identify protein exchange between host and microbe. Elsewhere, bioorthogonal reactions have offered solutions to challenges with older techniques, such as activity-based protein profiling (ABPP), a tool to identify active enzymes in samples using specially designed probes featuring an enzyme inhibitor conjugated to a detection tag.[66] Plagued in its original form by large tags that disrupted inhibitor function, ABPP was altered to introduce minimally disruptive chemical reporters that could be tagged in cell lysates or live cells, and has since seen routine use in diverse proteomics studies.[67]

Additionally, while proteins have the advantage of being able to be modified with genetic techniques, bioorthogonal chemistry will continue to be an important force for studying these biopolymers. For example, the convergence of genetic techniques and bioorthogonal cleavage reactions has allowed for the selective uncaging of active-site residues in enzymes to allow for controlled enzyme turn-on (Figure 1.5C).[68,69] As orthogonal, bioorthogonal cleavage reactions emerge, the control of multiple enzymes in a single cell could be on the horizon. Further, reversible bioorthogonal cleavage reactions could allow for temporal control.

1.4.4 Interfacing with CRISPR

Bioorthogonal chemistry is well-equipped to augment other powerful biological techniques. The pairing of bioorthogonal chemistry and CRISPR led to greater understanding of regulatory mechanisms at both genomic and enzymatic levels. Qu and co-workers developed a

system where CRISPR Cas9/sgRNA technology was utilized to bring bioorthogonal reaction partners to specific genomic loci, and their reaction caused a chromatin loop to form (Figure 1.5D).[70] Chromatin folding is a key epigenetic regulatory event, and the ability to control it with the formation of multiple loops at once, shown here for the first time, will improve studies on proper gene regulation. Baskin and co-workers also strengthened a CRISPR genome-wide screen by incorporating a bioorthogonal reaction for the phenotypic selection step.[71] The group's previously mentioned SPAAC-based approach to studying phosphatidic acid was enabled by the promiscuity of phospholipase (PLD), the enzyme that transforms phosphatidylcholine to the acid product. Employing the strategy in a CRISPR interference screen led to the identification of glycogen synthase 3 (GSK3) as a previously unknown regulator of PLD signaling. This application of bioorthogonally introduced tags in CRISPR screens holds potential for identifying regulatory genes in other pathways. Other work combining bioorthogonal chemistry and CRISPR may make use of small reporters on guide RNA for selectively delivering probes to specific genes. Overall, the combination of bioorthogonal chemistry and CRISPR will increase opportunities for discovery and control in biological settings.

1.5 Biomedical applications

Excitingly, we have recently seen the impact of bioorthogonal chemistry extend beyond fundamental science research. The same tools used to investigate biological systems are finding their way into the clinic to diagnosis and even treat diseases. Not only are the products of bioorthogonal chemistry part of clinical trials,[72] but an ongoing trial involves the tetrazine ligation occurring in humans. The current trials likely represent just the beginning of new medical applications.

1.5.1 Diagnostic profiling

In immunotherapy research, the ability to visualize several different biomarkers quickly in the same sample from a sick patient allows for detailed profiling of disease states, and similarly, biomarker profiling at different time points can paint a picture of disease progress. Toward this end, bioorthogonal chemistry has enabled documentation of changes in the tumor microenvironment over the course of cancer treatment. The Weissleder group developed a platform for single-cell cyclic imaging of samples taken from patients.[73] Antibodies for specific biomarkers were connected to different fluorophores via a *trans*-cyclooctene, allowed to bind, and imaged. A tetrazine reagent was then added to trigger a click-and-release reaction, resulting in free fluorophore that was washed away. New antibody-fluorophore conjugates for other biomarkers were then introduced and imaged, and the cycle was repeated. These "bioorthogonal recycling reagents" were applied to patient samples and demonstrated rapid destaining, allowing for the quick elaboration of the phenotypic profile of tumors with minimal residual background signal from each cycle. This diagnostic application shows the relevancy of not only classical bioorthogonal reactions but also the more contemporary advances such as click-and-release for clinical purposes. This work featured antibody-targeting for biomarkers, but it will be interesting to see similar technology applied using alternative targeting approaches in addition to applications to other cell populations and diseases.

1.5.2 Therapeutic potential

Metabolic incorporation of chemical reporter groups provides an opportunity to selectively tag specific cell types, which can be further elaborated via bioorthogonal chemistry.

An example of this is the incorporation of azide-containing D-amino acids into gut microbiota, designed to react with dibenzocyclooctyne-displaying probiotics (Figure 1.7A).[74] The SPAAC reaction between gut colonizers and delivered bacteria enhanced retention and demonstrated relief from induced colitis in mice. In the future, one could imagine similar strategies to target and treat drug-resistant infections, tuberculosis, or diseases with increased metabolism such as cancer.

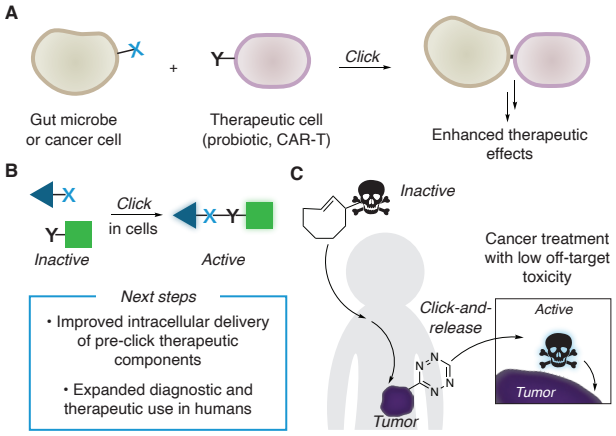

Figure 1.7 Biomedical avenues of bioorthogonal chemical reactions. (A) Bioorthogonal chemistry increases cell-cell interactions in cell-based therapies. (B) Bioorthogonal reactions allow for *in situ* formation of active drug molecules from delivered fragments. (C) Model of targeted drug delivery and activation via tetrazine ligation currently in clinical trials.

Bioorthogonal chemistry has also enabled improved theranostic approaches; namely, pretargeting of tumor cells with a reporter-labeled antibody that can then be modified with radiolabels through a reaction. Robillard and co-workers demonstrated the promise of this two-step approach utilizing the IEDDA reaction, which removed the issues of immunogenicity and lengthy engineering requirements of previous pretargeting systems.[75] Over the past decade, this approach has been greatly expanded upon and the process detailed, and we refer readers to recent reports.[76,77]

Cell therapy represents another avenue to introduce chemical reporter groups that can later be elaborated via bioorthogonal chemistry. This has indeed been applied to one of the most prominent types, chimeric antigen receptor T cell (CAR-T) therapy. For CAR-T therapy, primary patient-derived T-cells are genetically modified to target cancer cells, often using viral transduction. A combination of metabolic incorporation of azides into the T-cells followed by SPAAC with a dibenzocyclooctyne-polyethyleneimine resulted in enhanced lentiviral transduction and doubled the yield of CAR-T cells.[78] In other instances, the properties of the genetically engineered T-cells have been improved through surface modification by bioorthogonal chemistry. Yuan and co-workers used SPAAC to append an engineered hyaluronidase (HAse) and an α-PDL1 antibody to azide-decorated CAR-T cells.[79] The extracellular matrix-degrading activity of HAse improved the efficiency of CAR-T penetration into solid tumors, and the antibody was released in the low-pH environment of said tumors to reverse the suppression of the PD1-PDL1 pathway. Ultimately, the power of bioorthogonal chemistry is its ability to be performed *in vivo* and thus the above examples do not represent the full potential of the convergence of bioorthogonal chemistry and cell therapy. Pan *et. al* have demonstrated the *in vivo* reaction of azide-modified CAR-T cells with cyclooctyne-modified xenograft tumors to increase the efficacy of blood cancer treatment.[80] While not directly therapeutically relevant because the tumor cells were also labeled *ex vivo*, this work demonstrates that bioorthogonal chemistry can be used as a targeting strategy for cell therapy if the appropriate chemical reporter could be introduced to the cancerous site potentially through the increased metabolism of cancerous cells or implantation of a chemical reporter-modified hydrogel at the tumor site. Additional future applications may involve *in vivo* controlled activation/deactivation of CAR-T cells via bioorthogonal reactions.

A challenge in the delivery of some therapeutics is the tradeoff between the size of the drug and its permeability or solubility. The ability to form covalent bonds *in situ* using bioorthogonal chemistry allows for the introduction of smaller components of a larger system that can form the active compound post-delivery (Figure 1.7B). Such an idea was tested with proteolysis-targeting chimeras (PROTACs). PROTACs are heterobifunctional molecules featuring a targeting ligand for a protein of interest linked to an E3 ubiquitin ligase recruiter molecule. In a cell, the PROTAC brings a protein of interest and a ubiquitin ligase into close proximity such that the target is ubiquitinated and designated for degradation. While PROTACs are a distinctly promising approach for controlling dysregulated proteins implicated in many diseases, they are large molecules with non-druglike properties, including low cell permeability and solubility. In a creative approach to solving this issue, Heightman and co-workers labeled the individual targeting ligand and recruiter with bioorthogonal handles (*trans*-cyclooctene and tetrazine, respectively) such that the whole PROTAC could be formed after the more soluble and permeable components were delivered separately to a cell.[81] This *in situ* drug formation is applicable currently toward therapeutics with flexibility in the linkage. Future *in situ* therapeutic synthesis would benefit from traceless bioorthogonal reactions or those that are designed to result in pharmacophores. Another aspect that would enhance this approach would be to develop bioorthogonal reactions that are catalyzed by the intracellular environment (*e.g.* high glutathione levels) such that only intracellular, not extracellular, drug synthesis would occur. The concept of local environment-promoted click reactions has been demonstrated by the Qu group, who exploited elevated levels of Cu(I) in an Alzheimer's disease model to catalyze a click reaction for in situ drug formation.[82] Overall, as chemical advances to bioorthogonal chemistries are made (*vida supra*) the scope of *in situ* therapeutic synthesis will increase.

1.5.3 First use in humans

Finally, as a remarkable sign of the field's explosion into relevancy on many scales, bioorthogonal chemistry is now being performed in humans (Figure 1.7C). The tetrazine-*trans*-cyclooctene reaction is the subject of an ongoing US clinical trial.[83] A two-component cancer treatment system features a tetrazine-displaying biopolymer that is injected once at the tumor site, followed by dosing of a *trans*-cyclooctene-caged prodrug form of doxorubicin, a potent chemotherapeutic.[84] Functional doxorubicin is freed from the fast click-and-release reaction, which will only occur where the biopolymer is injected, garnering a high degree of control over where the drug is released. This system demonstrates reduced off-target toxicity and is expected to be a generalized cancer treatment independent of differences between cancer types or individual patients. The general approach of targeting specific locales in a patient with one bioorthogonal reaction partner to bring drugs to the disease site has potential to be used for other disorders as well. One can also imagine using implanted functional biopolymers to target cell therapies to disease sites. Overall, this first instance of click chemistry performed in humans sets an important precedent for future clinical applications, which we will undoubtedly see soon.

1.6 Conclusion

There was a time where the thought of performing non-native organic reactions in living systems without disruption would have seemed outlandish and all but impossible. But chemists are no strangers to creativity, and it is fitting that the pursuit of nature's attributes of selectivity and elegance should lead to chemistries that work in increasingly complex environments. The future of bioorthogonal chemistry is bursting with opportunity, and no doubt the field of

chemical biology will continue to evolve and influence applications such as disease diagnosis and treatment.

1.7 References

(1) Morrison, K. L.; Weiss, G. A. The Origins of Chemical Biology. *Nat. Chem. Biol.* **2006**, *2*, 3–6.

(2) Brik, A.; Keinan, E. Chemical Biology: Powerful Synergy Between Two Cultures. *Isr. .J Chem*. **2019**, *59*, 3–6.

(3) Sletten, E. M.; Bertozzi, C. R. Bioorthogonal Chemistry: Fishing for Selectivity in a Sea of Functionality. *Angew. Chem. Int. Ed.* **2009**, *48*, 6974–6998.

(4) Kolb, H. C.; Finn, M. G.; Sharpless, K. B. Click Chemistry: Diverse Chemical Function from a Few Good Reactions. *Angew. Chem. Int. Ed.* **2001**, *40*, 2004–2021.

(5) Saxon, E.; Bertozzi, C. R. Cell Surface Engineering by a Modified Staudinger Reaction. *Science* **2000**, *287*, 2007–2010.

(6) Tornøe, C. W.; Christensen, C.; Meldal, M. Peptidotriazoles on Solid Phase: [1,2,3]-Triazoles by Regiospecific Copper(I)-Catalyzed 1,3-Dipolar Cycloadditions of Terminal Alkynes to Azides. *J. Org. Chem.* **2002**, *67*, 3057–3064.

(7) Rostovtsev, V. v.; Green, L. G.; Fokin, V. v.; Sharpless, K. B. A Stepwise Huisgen Cycloaddition Process: Copper(I)-Catalyzed Regioselective "Ligation" of Azides and Terminal Alkynes. *Angew. Chem. Int. Ed.* **2002**, *41*, 2596–2599.

(8) Rigolot, V.; Biot, C.; Lion, C. To View Your Biomolecule, Click inside the Cell. *Angew. Chem. Int. Ed.* **2021**, *60*, 23084–23105.

(9) Bertozzi, C. A Special Virtual Issue Celebrating the 2022 Nobel Prize in Chemistry for the Development of Click Chemistry and Bioorthogonal Chemistry. *ACS Cent. Sci.* **2022**, *9*, 2–3.

(10) Agard, N. J.; Prescher, J. A.; Bertozzi, C. R. A Strain-Promoted [3 + 2] Azide-Alkyne Cycloaddition for Covalent Modification of Biomolecules in Living Systems. *J. Am. Chem. Soc.* **2004**, *126*, 15046–15047.

(11) Blackman, M. L.; Royzen, M.; Fox, J. M. Tetrazine Ligation: Fast Bioconjugation Based on Inverse-Electron-Demand Diels-Alder Reactivity. *J. Am. Chem. Soc.* **2008**, *130*, 13518–13519.

(12) Devaraj, N. K.; Weissleder, R.; Hilderbrand, S. A. Tetrazine-Based Cycloadditions: Application to Pretargeted Live Cell Imaging. *Bioconjugate Chem.* **2008**, *19*, 2297–2299.

(13) Nilsson, B. L.; Kiessling, L. L.; Raines, R. T. Staudinger Ligation: A Peptide from a Thioester and Azide. *Org. Lett.* **2000**, *2*, 1939–1941.

(14) Saxon, E.; Armstrong, J. I.; Bertozzi, C. R. A "Traceless" Staudinger Ligation for the Chemoselective Synthesis of Amide Bonds. *Org. Lett.* **2000**, *2*, 2141–2143.

(15) Serwa, R.; Wakening, L.; Signore, G. Del; Mühlberg, M.; Claußnitzer, I.; Weise, C.; Gerrits, M.; Hackenberger, C. P. R. Chemoselective Staudinger-Phosphite Reaction of Azides for the Phosphorylation of Proteins. *Angew. Chem. Int. Ed.* **2009**, *48*, 8234–8239.

(16) Vallée, M. R. J.; Majkut, P.; Wilkening, I.; Weise, C.; Müller, G.; Hackenberger, C. P. R. Staudinger-Phosphonite Reactions for the Chemoselective Transformation of Azido-Containing Peptides and Proteins. *Org. Lett.* **2011**, *13*, 5440–5443.

(17) Sundhoro, M.; Jeon, S.; Park, J.; Ramström, O.; Yan, M. Perfluoroaryl Azide Staudinger Reaction: A Fast and Bioorthogonal Reaction. *Aingew. Chem. Int. Ed.* **2017**, *56*, 12117–12121.

(18) Shih, H.-W.; Prescher, J. A. A Bioorthogonal Ligation of Cyclopropenones Mediated by Triarylphosphines. *J. Am. Chem. Soc.* **2015**, *137*, 10036–10039.

(19) Heiss, T. K.; Dorn, R. S.; Ferreira, A. J.; Love, A. C.; Prescher, J. A. Fluorogenic Cyclopropenones for Multicomponent, Real-Time Imaging. *J. Am. Chem. Soc.* **2022**, *144*, 7871–7880.

(20) Deb, T.; Tu, J.; Franzini, R. M. Mechanisms and Substituent Effects of Metal-Free Bioorthogonal Reactions. *Chem. Rev.* **2021**, *121*, 6850–6914.

(21) Wallace, S.; Chin, J. W. Strain-Promoted Sydnone Bicyclo-[6.1.0]-Nonyne Cycloaddition. *Chem. Sci.* **2014**, *5*, 1742–1744.

(22) Bernard, S.; Audisio, D.; Riomet, M.; Bregant, S.; Sallustrau, A.; Plougastel, L.; Decuypere, E.; Gabillet, S.; Kumar, R. A.; Elyian, J.; Trinh, M. N.; Koniev, O.; Wagner, A.; Kolodych, S.; Taran, F. Bioorthogonal Click and Release Reaction of Iminosydnones with Cycloalkynes. *Angew. Chem. Int. Ed.* **2017**, *56*, 15612–15616.

(23) McKay, C. S.; Moran, J.; Pezacki, J. P. Nitrones as Dipoles for Rapid Strain-Promoted 1,3-Dipolar Cycloadditions with Cyclooctynes. *Chem. Commun.* **2010**, *46*, 931–933.

(24) Ning, X.; Temming, R. P.; Dommerholt, J.; Guo, J.; Ania, D. B.; Debets, M. F.; Wolfert, M. A.; Boons, G. J.; van Delft, F. L. Protein Modification by Strain-Promoted Alkyne-Nitrone Cycloaddition. *Angew. Chem. Int. Ed.* **2010**, *49*, 3065–3068.

(25) Singh, I.; Heaney, F. Solid Phase Strain Promoted "Click" Modification of DNA via [3+2]-Nitrile Oxide–Cyclooctyne Cycloadditions. *Chem. Commun.* **2011**, *47*, 2706–2708.

(26) Sanders, B. C.; Friscourt, F.; Ledin, P. A.; Mbua, N. E.; Arumugam, S.; Guo, J.; Boltje, T. J.; Popik, V. v.; Boons, G. J. Metal-Free Sequential [3 + 2]-Dipolar Cycloadditions Using Cyclooctynes and 1,3-Dipoles of Different Reactivity. *J. Am. Chem. Soc.* **2011**, *133*, 949–957.

(27) Kaya, E.; Vrabel, M.; Deiml, C.; Prill, S.; Fluxa, V. S.; Carell, T. A Genetically Encoded Norbornene Amino Acid for the Mild and Selective Modification of Proteins in a Copper-Free Click Reaction. *Angew. Chem. Int. Ed.* **2012**, *51*, 4466–4469.

(28) McGrath, N. A.; Raines, R. T. Diazo Compounds as Highly Tunable Reactants in 1,3-Dipolar Cycloaddition Reactions with Cycloalkynes. *Chem. Sci.* **2012**, *3*, 3237–3240.

(29) Kamber, D. N.; Liang, Y.; Blizzard, R. J.; Liu, F.; Mehl, R. A.; Houk, K. N.; Prescher, J. A. 1,2,4-Triazines Are Versatile Bioorthogonal Reagents. *J. Am. Chem. Soc.* **2015**, *137*, 8388–8391.

(30) Levandowski, B. J.; Gamache, R. F.; Murphy, J. M.; Houk, K. N. Readily Accessible Ambiphilic Cyclopentadienes for Bioorthogonal Labeling. *J. Am. Chem. Soc.* **2018**, *140*, 6426–6431.

(31) Stuyver, T.; Coley, C. Machine Learning-Guided Computational Screening of New Candidate Reactions with High Bioorthogonal Click Potential. *Chem. Eur. J.* **2023**, *29*, e202300387.

(32) Kumar, G. S.; Lin, Q. Seeking Citius: Photochemical Access of Reactive Intermediates for Faster Bioorthogonal Reactions. *ChemBioChem* **2022**, *23*, e202200175.

(33) Yu, Z.; Ho, L. Y.; Lin, Q. Rapid, Photoactivatable Turn-on Fluorescent Probes Based on an Intramolecular Photoclick Reaction. *J. Am. Chem. Soc.* **2011**, *133*, 11912–11915.

(34) Poloukhtine, A. A.; Mbua, N. E.; Wolfert, M. A.; Boons, G. J.; Popik, V. v. Selective Labeling of Living Cells by a Photo-Triggered Click Reaction. *J. Am. Chem. Soc.* **2009**, *131*, 15769–15776.

(35) Liu, L.; Zhang, D.; Johnson, M.; Devaraj, N. K. Light-Activated Tetrazines Enable Precision Live-Cell Bioorthogonal Chemistry. *Nat. Chem.* **2022**, *14*, 1078–1085.

(36) Wang, C.; Zhang, H.; Zhang, T.; Zou, X.; Wang, H.; Rosenberger, J. E.; Vannam, R.; Trout, W. S.; Grimm, J. B.; Lavis, L. D.; Thorpe, C.; Jia, X.; Li, Z.; Fox, J. M. Enabling *In Vivo* Photocatalytic Activation of Rapid Bioorthogonal Chemistry by Repurposing Silicon-Rhodamine Fluorophores as Cytocompatible Far-Red Photocatalysts. *J. Am. Chem. Soc.* **2021**, *143*, 10793–10803.

(37) Jemas, A.; Xie, Y.; Pigga, J. E.; Caplan, J. L.; Am Ende, C. W.; Fox, J. M. Catalytic Activation of Bioorthogonal Chemistry with Light (CABL) Enables Rapid, Spatiotemporally Controlled Labeling and No-Wash, Subcellular 3D-Patterning in Live Cells Using Long Wavelength Light. *J. Am. Chem. Soc.* **2022**, *144*, 1647–1662.

(38) Lemieux, G. A.; de Graffenried, C. L.; Bertozzi, C. R. A Fluorogenic Dye Activated by the Staudinger Ligation. *J. Am. Chem. Soc.* **2003**, *125*, 4708–4709.

(39) Jewett, J. C.; Bertozzi, C. R. Synthesis of a Fluorogenic Cyclooctyne Activated by Cu-Free Click Chemistry. *Org. Lett.* **2011**, *13*, 5937–5939.

(40) Shie, J. J.; Liu, Y. C.; Hsiao, J. C.; Fang, J. M.; Wong, C. H. A Cell-Permeable and Triazole-Forming Fluorescent Probe for Glycoconjugate Imaging in Live Cells. *Chem. Commun.* **2017**, *53*, 1490–1493.

(41) Favre, C.; Friscourt, F. Fluorogenic Sydnone-Modified Coumarins Switched-On by Copper-Free Click Chemistry. *Org. Lett.* **2018**, *20*, 4213–4217.

(42) Carlson, J. C. T.; Meimetis, L. G.; Hilderbrand, S. A.; Weissleder, R. BODIPY-Tetrazine Derivatives as Superbright Bioorthogonal Turn-on Probes. *Angew. Chem. Int. Ed.* **2013**, *52*, 6917–6920.

(43) Werther, P.; Yserentant, K.; Braun, F.; Grußmayer, K.; Navikas, V.; Yu, M.; Zhang, Z.; Ziegler, M. J.; Mayer, C.; Gralak, A. J.; Busch, M.; Chi, W.; Rominger, F.; Radenovic, A.; Liu, X.; Lemke, E. A.; Buckup, T.; Herten, D. P.; Wombacher, R. Bio-Orthogonal Red and Far-Red Fluorogenic Probes for Wash-Free Live-Cell and Super-Resolution Microscopy. *ACS Cent. Sci.* **2021**, *7*, 1561–1571.

(44) Mao, W.; Chi, W.; He, X.; Wang, C.; Wang, X.; Yang, H.; Liu, X.; Wu, H. Overcoming Spectral Dependence: A General Strategy for Developing Far-Red and Near-Infrared Ultra-Fluorogenic Tetrazine Bioorthogonal Probes. *Angew. Chem. Int. Ed.* **2022**, *61*, e202117386.

(45) Wang, J.; Wang, X.; Fan, X.; Chen, P. R. Unleashing the Power of Bond Cleavage Chemistry in Living Systems. *ACS Cent. Sci.* **2021**, *7*, 929–943.

(46) Versteegen, R. M.; Rossin, R.; ten Hoeve, W.; Janssen, H. M.; Robillard, M. S. Click to Release: Instantaneous Doxorubicin Elimination upon Tetrazine Ligation. *Angew. Chem. Int. Ed.* **2013**, *52*, 14112–14116.

(47) Riomet, M.; Porte, K.; Wijkhuisen, A.; Audisio, D.; Taran, F. Fluorogenic Iminosydnones: Bioorthogonal Tools for Double Turn-on Click-and-Release Reactions. *Chem. Commun.* **2020**, *56*, 7183–7186.

(48) Kang, D.; Lee, S.; Kim, J. Bioorthogonal Click and Release: A General, Rapid, Chemically Revertible Bioconjugation Strategy Employing Enamine N-Oxides. *Chem* **2022**, *8*, 2260–2277.

(49) Schreiber, C. L.; Smith, B. D. Molecular Conjugation Using Non-Covalent Click Chemistry. *Nat. Rev. Chem.* **2019**, *3*, 393–400

(50) Kataki-Anastasakou, A.; Hernandez, S.; Sletten, E. M. Cell-Surface Labeling via Bioorthogonal Host–Guest Chemistry. *ACS Chem. Biol.* **2021**, *16*, 2124–2129.

(51) Cao, L.; Šekutor, M.; Zavalij, P. Y.; Mlinarič-Majerski, K.; Glaser, R.; Isaacs, L. Cucurbit[7]Uril×guest Pair with an Attomolar Dissociation Constant. *Angew. Chem. Int. Ed.* **2014**, *53*, 988–993.

(52) Shetty, D.; Khedkar, J. K.; Park, K. M.; Kim, K. Can We Beat the Biotin-Avidin Pair?: Cucurbit[7]Uril-Based Ultrahigh Affinity Host-Guest Complexes and Their Applications. *Chem. Soc. Rev.* **2015**, *44*, 8747–8761.

(53) Plumet, C.; Mohamed, A. S.; Vendeuvre, T.; Renoux, B.; Clarhaut, J.; Papot, S. Cell–Cell Interactions via Non-Covalent Click Chemistry. *Chem. Sci.* **2021**, *12*, 9017–9021.

(54) Ma, Y.-L.; Sun, C.; Li, Z.; Wang, Z.; Wei, J.; Cheng, Q.; Zheng, L.-S.; Chang, X.-Y.; Li, K.; Wang, R.; Jiang, W. Biomimetic Recognition-Based Bioorthogonal Host–Guest Pairs for Cell Targeting and Tissue Imaging in Living Animals. *CCS Chem.* **2022**, *4*, 1977–1989.

(55) Sasmal, R.; Som, A.; Kumari, P.; Nair, R. V.; Show, S.; Barge, N. S.; Pahwa, M.; Das Saha, N.; Rao, S.; Vasu, S.; Agarwal, R.; Agasti, S. S. Supramolecular Guest Exchange in Cucurbit[7]Uril for Bioorthogonal Fluorogenic Imaging across the Visible Spectrum. *ACS Cent. Sci.* **2024**, *10*, 1945–1959.

(56) Meyer, C. F.; Seath, C. P.; Knutson, S. D.; Lu, W.; Rabinowitz, J. D.; Macmillan, D. W. C. Photoproximity Labeling of Sialylated Glycoproteins (GlycoMap) Reveals

Sialylation-Dependent Regulation of Ion Transport. *J. Am. Chem. Soc.* **2022**, *144*, 23633–23641.

(57) Flynn, R. A.; Pedram, K.; Malaker, S. A.; Batista, P. J.; Smith, B. A. H.; Johnson, A. G.; George, B. M.; Majzoub, K.; Villalta, P. W.; Carette, J. E.; Bertozzi, C. R. Small RNAs Are Modified with N-Glycans and Displayed on the Surface of Living Cells. *Cell* **2021**, *184*, 3109-3124.

(58) Neef, A. B.; Schultz, C. Selective Fluorescence Labeling of Lipids in Living Cells. *Angew. Chem. Int. Ed.* **2009**, *48*, 1498–1500.

(59) Jao, C. Y.; Roth, M.; Welti, R.; Salic, A. Metabolic Labeling and Direct Imaging of Choline Phospholipids in Vivo. *Proc. Natl. Acad. Sci. U. S. A.* **2009**, *106*, 15332–15337.

(60) Bumpus, T. W.; Baskin, J. M. A Chemoenzymatic Strategy for Imaging Cellular Phosphatidic Acid Synthesis. *Angew. Chem. Int. Ed.* **2016**, *55*, 13155–13158.

(61) Bumpus, T. W.; Baskin, J. M. Clickable Substrate Mimics Enable Imaging of Phospholipase D Activity. *ACS Cent. Sci.* **2017**, *3*, 1070–1077.

(62) Liang, D.; Wu, K.; Tei, R.; Bumpus, T. W.; Ye, J.; Baskin, J. M. A Real-Time Click Chemistry Imaging Approach Reveals Stimulus-Specific Subcellular Locations of Phospholipase D Activity. *Proc. Natl. Acad. Sci. U. S. A.* **2019**, *116*, 15453–15462.

(63) White, B. M.; Kumar, P.; Conwell, A. N.; Wu, K.; Baskin, J. M. Lipid Expansion Microscopy. *J. Am. Chem. Soc.* **2022**, *144*, 18212–18217.

(64) Dieterich, D. C.; Lee, J. J.; Link, A. J.; Graumann, J.; Tirrell, D. A.; Schuman, E. M. Labeling, Detection and Identification of Newly Synthesized Proteomes with Bioorthogonal Non-Canonical Amino-Acid Tagging. *Nat. Protoc.* **2007**, *2*, 532–540.

(65) Li, X.-M.; Huang, S.; Li, X. D. Photo-ANA Enables Profiling of Host–Bacteria Protein Interactions during Infection. *Nat. Chem. Biol.* **2023**, *19*, 614–623.

(66) Liu, Y.; Patricelli, M. P.; Cravatt, B. F. Activity-Based Protein Profiling: The Serine Hydrolases. *Proc. Natl. Acad. Sci. U. S. A*. **1999**, *96*, 14694–14699.

(67) Cravatt, B. F.; Wright, A. T.; Kozarich, J. W. Activity-Based Protein Profiling: From Enzyme Chemistry to Proteomic Chemistry. *Annu. Rev. Biochem.* **2008**, *77*, 383–414.

(68) Zhang, G.; Li, J.; Xie, R.; Fan, X.; Liu, Y.; Zheng, S.; Ge, Y.; Chen, P. R. Bioorthogonal Chemical Activation of Kinases in Living Systems. *ACS Cent. Sci.* **2016**, *2*, 325–331.

(69) Luo, J.; Liu, Q.; Morihiro, K.; Deiters, A. Small-Molecule Control of Protein Function through Staudinger Reduction. *Nat. Chem.* **2016**, *8*, 1027–1034.

(70) Qin, G.; Yang, J.; Zhao, C.; Ren, J.; Qu, X. Manipulating Complex Chromatin Folding via CRISPR-Guided Bioorthogonal Chemistry. *Proc. Natl. Acad. Sci. U. S. A*. **2022**, *119*, 1–7.

(71) Bumpus, T. W.; Huang, S.; Tei, R.; Baskin, J. M. Click Chemistry-Enabled CRISPR Screening Reveals GSK3 as a Regulator of PLD Signaling. *Proc. Natl. Acad. Sci. U. S. A*. **2021**, *118*, 1–7.

(72) Peplow, M. Click Chemistry Targets Antibody-Drug Conjugates for the Clinic. *Nat. Biotechnol.* **2019**, *37*, 835–837.

(73) Ko, J.; Wilkovitsch, M.; Oh, J.; Kohler, R. H.; Bolli, E.; Pittet, M. J.; Vinegoni, C.; Sykes, D. B.; Mikula, H.; Weissleder, R.; Carlson, J. C. T. Spatiotemporal Multiplexed Immunofluorescence Imaging of Living Cells and Tissues with Bioorthogonal Cycling of Fluorescent Probes. *Nat. Biotechnol.* **2022**, *40*, 1654–1662.

(74) Song, W. F.; Yao, W. Q.; Chen, Q. W.; Zheng, D.; Han, Z. Y.; Zhang, X. Z. In Situ Bioorthogonal Conjugation of Delivered Bacteria with Gut Inhabitants for Enhancing Probiotics Colonization. *ACS Cent. Sci.* **2022**, *8*, 1306–1317.

(75) Rossin, R.; Verkerk, P. R.; Van Den Bosch, S. M.; Vulders, R. C. M.; Verel, I.; Lub, J.; Robillard, M. S. *In Vivo* Chemistry for Pretargeted Tumor Imaging in Live Mice. *Angew. Chem. Int. Ed.* **2010**, *49*, 3375–3378.

(76) Sarrett, S. M.; Keinänen, O.; Dayts, E. J.; Dewaele-Le Roi, G.; Rodriguez, C.; Carnazza, K. E.; Zeglis, B. M. Inverse Electron Demand Diels–Alder Click Chemistry for Pretargeted PET Imaging and Radioimmunotherapy. *Nat. Protoc.* **2021**, *16*, 3348–3381.

(77) Rondon, A.; Degoul, F. Antibody Pretargeting Based on Bioorthogonal Click Chemistry for Cancer Imaging and Targeted Radionuclide Therapy. *Bioconjugate Chem.* **2020**, *31*, 159–173.

(78) Pan, H.; Li, P.; Li, G.; Li, W.; Hu, B.; He, H.; Chen, Z.; Wang, F.; Liu, L.; Gong, Y.; Han, Y.; Luo, Y.; Zheng, M.; Ma, Y.; Cai, L.; Jin, Y. Glycometabolic Bioorthogonal Chemistry-Guided Viral Transduction for Robust Human T Cell Engineering. *Adv. Funct. Mater.* **2019**, *29*, 1807528.

(79) Zhao, Y.; Dong, Y.; Yang, S.; Tu, Y.; Wang, C.; Li, J.; Yuan, Y.; Lian, Z. Bioorthogonal Equipping CAR-T Cells with Hyaluronidase and Checkpoint Blocking Antibody for Enhanced Solid Tumor Immunotherapy. *ACS Cent. Sci.* **2022**, *8*, 603–614.

(80) Pan, H.; Li, W.; Chen, Z.; Luo, Y.; He, W.; Wang, M.; Tang, X.; He, H.; Liu, L.; Zheng, M.; Jiang, X.; Yin, T.; Liang, R.; Ma, Y.; Cai, L. Click CAR-T Cell Engineering for Robustly Boosting Cell Immunotherapy in Blood and Subcutaneous Xenograft Tumor. *Bioact. Mater.* **2021**, *6*, 951–962.

(81) Lebraud, H.; Wright, D. J.; Johnson, C. N.; Heightman, T. D. Protein Degradation by In-Cell Self-Assembly of Proteolysis Targeting Chimeras. *ACS Cent. Sci.* **2016**, *2*, 927–934.

(82) Du, Z.; Yu, D.; Du, X.; Scott, P.; Ren, J.; Qu, X. Self-Triggered Click Reaction in an Alzheimer's Disease Model: In Situ Bifunctional Drug Synthesis Catalyzed by Neurotoxic Copper Accumulated in Amyloid-β Plaques. *Chem. Sci.* **2019**, *10*, 10343–10350.

(83) Phase 1/2a Study of SQ3370 in Patients With Advanced Solid Tumors. ClinicalTrials.gov. https://clinicaltrials.gov/study/NCT04106492?term=shasqi&rank=1#study-overview (accessed 2025-06-09).

(84) Wu, K.; Yee, N. A.; Srinivasan, S.; Mahmoodi, A.; Zakharian, M.; Mejia Oneto, J. M.; Royzen, M. Click Activated Protodrugs against Cancer Increase the Therapeutic Potential of Chemotherapy through Local Capture and Activation. *Chem. Sci.* **2021**, *12*, 1259–1271.

CHAPTER TWO

Perfluoroarenes in chemical biology: A perspective on biomolecule modification and host–guest chemistry

2.1 Abstract

Given its rarity in nature, fluorine substitution has been utilized as part of many chemical biology studies that take advantage of its biorthogonality (non-interfering with natural processes) as well as the sensitivity of detection measures such as ^{19}F NMR. The perfluoroarene moiety (an aromatic ring with C–H bonds replaced with C–F bonds) has been used in many studies of biological structure and function. The distinct electronic properties of perfluoroarenes have made them useful for probing folding dynamics of biomolecules like DNA and peptides or as reactive groups for chemical modifications. The non-covalent arene-perfluoroarene interaction has also been used to probe biomolecule stabilities and to induce protein-protein interactions. This perspective begins by highlighting the ways perfluoroaromatic motifs are incorporated into biological metabolites and some key applications, then dives into studies capitalizing on the nucleophilic substitution of perfluoroarene by biological nucleophiles. Finally, the arene-perfluoroarene interaction is discussed, beginning with chemical biology studies. The final piece explores this interaction within host–guest chemistry, which is proposed to be a new avenue for chemical biology tool development; proposed directions of future work are included throughout. The multifaceted abilities of the bioorthogonal perfluoroaromatic motif have earned it a place in the chemical biology toolbox.

2.2 Introduction

Within chemical biology, alteration of biomolecules with strategic chemical motifs is employed to study natural systems.[1–3] For instance, tagging of nucleic acids or proteins with

fluorescent probes allows for cellular tracking, introduction of chemical reporters to glycans allows for cell-surface labeling via bioorthogonal chemistry, and new biomolecule interactions are induced by host–guest interactions (Figure 2.1A; see details in Chapter 1). The addition of new selective probes or new types of non-covalent interactions, especially those orthogonal to, or compatible with, existing methods enhances the abilities of chemical biologists to study biological processes in new, more detailed ways.

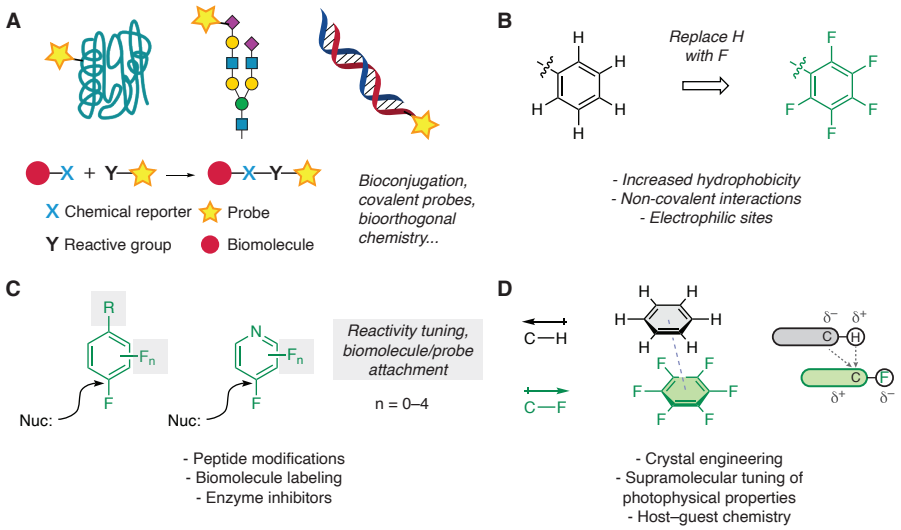

Figure 2.1 Overview of perfluoroaromatics in the context of chemical biology tools. (A) General motivations: labeling biomolecules through bioconjugation or bioorthogonal chemistry. (B) Fluorination and properties imparted by it. (C) Overview of reactivity of perfluoroaromatics and examples explored in this perspective. (D) Overview of arene-perfluoroarene interactions and examples of applications.

Increasingly, a single aromatic motif is employed in biological studies: perfluoroarenes (Figure 2.1B). These are aromatic compounds where C–H bonds are replaced with C–F bonds, and the unique properties of fluorine lead to specific reactivity and interactions of these structures. Fluorine's rarity in biology paired with its electronegativity and small size have proven useful in the development of bioorthogonal chemical tools.[4,5] For instance, perfluoroaromatic modifications to the building blocks of different biomolecules have been employed as ^{19}F NMR probes, which offers high sensitivity and benefits from the lack of natural

fluorine.[6,7] The hydrophobic pentafluoroaromatic motif has also been used to target fluorescent probes to the endoplasmic reticulum.[8–10] Many other applications using perfluoroaromatics take advantage of reactivity: fluorine's electronegativity leads to electrophilic spots on aromatic systems, good for reactions with strong nucleophiles like the sulfur atom of cysteine (Figure 2.1C).[11–14] Tuning the reactivity of perfluoroarenes further with different electron-withdrawing substituents and/or the number of fluorine atoms is employed to both modify natural metabolites for later incorporation in biomolecules, as well as to develop selective covalent probes.

In a different realm, the non-covalent interactions of perfluoroarenes offer another avenue for bioorthogonal modification. A strong non-covalent interaction occurs between electron-rich hydrocarbon aromatics and perfluoroaromatics, arising from electrostatic (opposite dipole moments of C–H versus C–F bonds) as well as dispersion forces. In the standard example of benzene and hexafluorobenzene, the overall quadrupole moments are similar in strength but opposite in sign, leading to a strong attraction (Figure 2.1D).[15–17] There have been many examples of solid-state crystal engineering applications of these interactions since their discovery in the 1960s and in recent years, more work has focused on using them in solution-phase studies.[18–20]

In this perspective, applications of covalent modifications to biologically relevant structures with perfluoroaromatics in biological studies will set the stage for current uses in chemical biology, including how they are incorporated into biomolecules. In the next portion, applications of the arene-perfluoroarene interaction will be explored, including some in biological systems, while proposing future applications for studying living systems via host–guest chemistry.

2.3 Biomolecule modifications with perfluoroaryl groups

2.3.1 Modified building blocks

The utility of fluorine in biological studies has led to the synthesis of numerous modified structures for different applications. Perfluoroaromatic-containing biological building blocks have been incorporated into biomolecules to probe macromolecular properties, as will be discussed in this section.

Analogs of natural nucleic acid bases with different degrees of aromatic fluorination have been made to probe hydrogen bonding in DNA base pairing (Figure 2.2A, **2.1**)[21] as well as base-stacking interactions (**2.2**).[22,23] In the latter case, incorporation of fluorinated bases helped show that dispersive interactions among aromatic bases contributed more to overall stability than electrostatic forces. Other fluorinated derivatives including **2.3**, **2.4**, and pentafluoro-substituted base, **2.5**, were made for a study probing RNA stacking with unnatural bases.[24] While nucleoside studies have largely focused on perturbing naturally occurring interactions, some of the chemistry described herein, including host–guest applications, may extend to nucleic acids in the future.

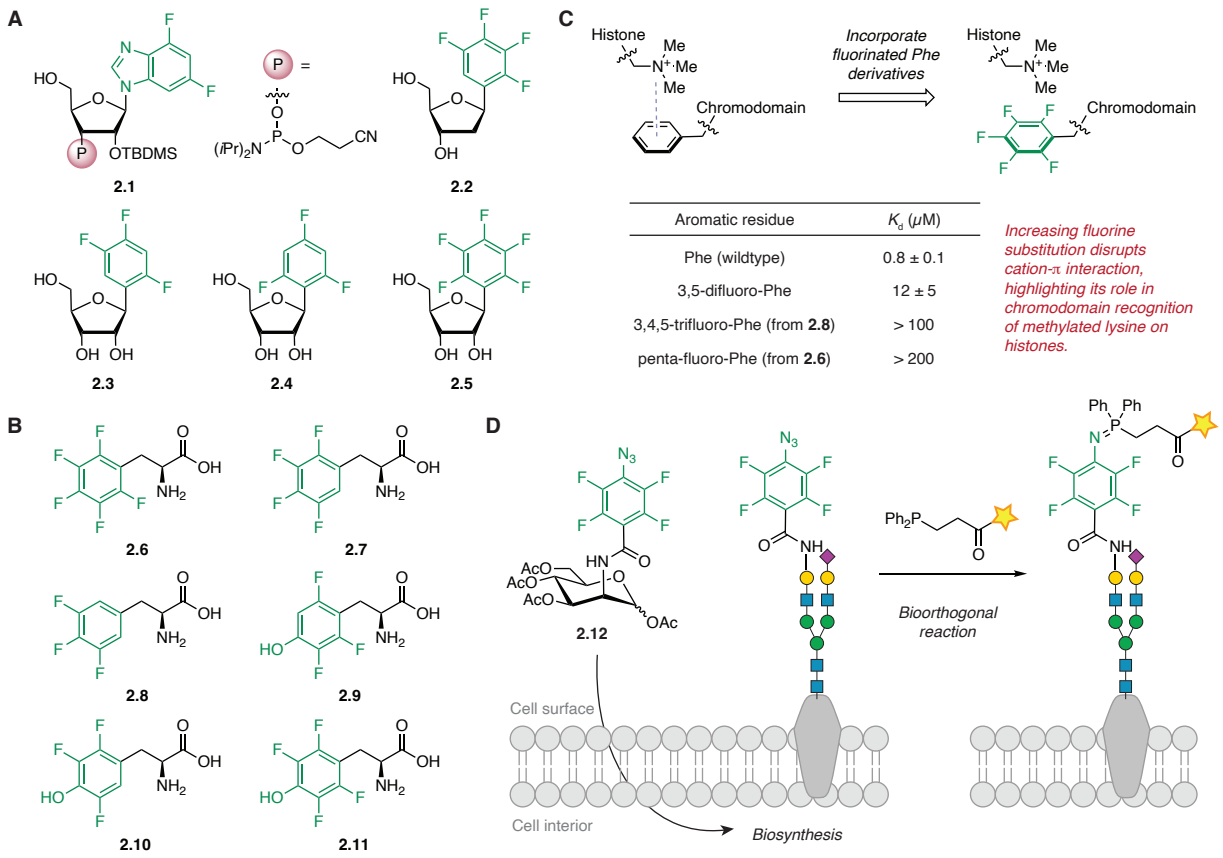

Figure 2.2 Perfluoroarene-containing synthetic metabolites. (A) Examples of modified nucleosides bearing aromatics of varying fluorination. (B) Examples of fluorinated phenylalaine and tyrosine derivatives. (C) Application of phenylalanine derivatives used to probe non-covalent cation-π interactions in protein recognition. (D) A modified mannosamine sugar is metabolically incorporated, displayed on cell surfaces, and labeled with bioorthogonal chemistry.

Many fluorinated derivatives of aromatic amino acids have been synthesized and incorporated into proteins to probe biological processes. Schultz and co-workers used pentafluoro derivative **2.6** as a tyrosine replacement to examine the impact of replacing a hydrogen-bond donor with repulsive interactions from a fluorine substituent.[25] The unnatural amino acid was loaded onto a synthesized aminoacyl tRNA and incorporated via amber stop codon recognition for *in vitro* Staphyloccal nuclease protein expression. The original hydrogen bond between tyrosine and glutamate was destabilized, as measured by overall mutant stability compared to wildtype. The same unnatural amino acid, along with **2.7** and **2.8** featuring different

degrees of fluorine substitution, was used to investigate another non-covalent interaction in proteins.[26] Histone proteins carry epigenetic information through covalent residue modifications such as methylation of lysine residues; recognition of these changes by chromodomain proteins is proposed to occur through cation-π interactions with phenylalanine residues.[27] Summerer, Liu, and co-workers site-specifically replaced a phenylalanine residue with **2.6**, **2.8**, and a disubstituted fluoroarene derivative using the amber stop codon and an evolved pyrrolysyl-tRNA synthetase, then measured the interaction strength (Figure 2.2C). As the fluorine substitution decreased the electron density over the aromatic residue, the interaction strength decreased, highlighting the role of cation-π interactions in this binding event.

Fluorophenol amino acid derivatives have also been used as unnatural versions of tyrosine. Schultz, Stubbe, and co-workers evolved an aminoacyl-tRNA synthetase to recognize unnatural derivative **2.9** over natural tyrosine, then tested incorporation of **2.9**, **2.10**, and **2.11** into green fluorescent protein (GFP) mutants.[28] The wide range of pK_a values and redox potentials represented by the fluorotyrosine derivatives allowed probing of biological tyrosyl radical pathways. Similarly, Wang and co-workers incorporated **2.10** and **2.11** as photoinduced electron-transfer (PET) probes on fluorogenic metalloenzyme mutants used to monitor manganese reduction.[29] These studies show that methods of unnatural amino acid incorporation are amenable to many perfluoroaromatic motifs, including those with a wide range of redox properties and pK_a values.

To date, perfluoroaromatics have not been widely added to glycan structures. Ramström and Yan generated modified mannosamine derivative **2.12** bearing a perfluoroaryl azide moiety (Figure 2.2D).[30] This unnatural sugar was taken up by cells in the sialic acid biosynthetic pathway and ultimately displayed on cell surfaces, where the azide motif was used as a substrate

for the bioorthogonal Staudinger ligation. This reaction, with an increased rate owing to the electron-withdrawing perfluoro group, was stabilized at the iminophosphorane reaction intermediate, allowing for probe attachment with just a simple phosphine. In addition to further the utility of the Staudinger ligation, this work highlights the potential of perfluoroaromatic structures to be metabolically incorporated via glycan biosynthetic pathways.

2.3.2 Biomolecules reacting with perfluoroaromatic probes

The selectivity of perfluoroarene reactivity with sulfur nucleophiles has led to precise modifications of biomolecular structures. Fluoroaromatic amino acids have been modified following synthetic incorporation, such as through S_NAr reactions with thiols to attach moieties that improve the antimicrobial activity of small peptides.[31] In contrast, the reaction of unmodified biological nucleophiles with perfluoroaromatics has been utilized more and will be discussed in this section.

Meldal, Diness, and co-workers found that simple substituent modifications on a single perfluoroaromatic structure could lead to impressively selective labeling of different cysteine residues.[32] In a selectivity experiment, the highly reactive perfluorinated aromatic sulfonamide **2.13** reacted with both surface and active-site cysteines on TEV protease, including denatured protein (Scheme 2.1). By decreasing the reactivity, either by removing electron-withdrawing fluorines (**2.14**) or reducing the electron-withdrawing power of the substituent *para* to the reactive site (**2.15**), reactivity was limited only to an active-site cysteine. These less-reactive probes did not label cysteine residues in denatured protein, and the authors posit the reason to be loss of a reaction-promoting hydrophobic local environment. Other examples of reaction-promoting local environments are discussed in this section.

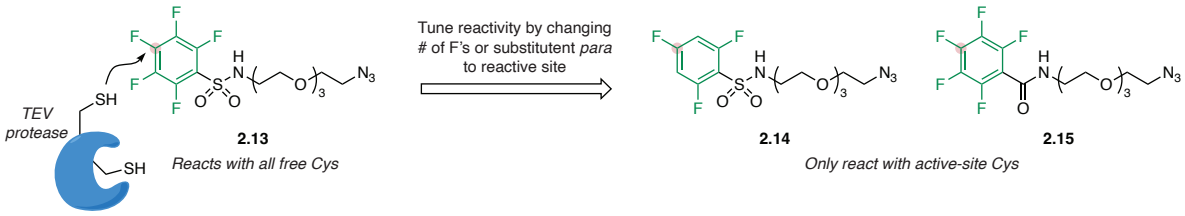

Scheme 2.1 Reactivity tuning of perfluoroaromatic probes. Azide handles were used for post-S_NAr attachment of fluorophores for visualization.

As peptides are utilized more in novel pharmaceuticals, improvements to their stability toward proteolysis or methods for increased cell penetration are required.[33] One strategy involves cyclizing peptides through side-chain coupling, or stapling. The Pentelute group took advantage of perfluoroaromatic S_NAr reactivity with cysteine nucleophiles to use both hexafluorobenzene **2.16** and decafluorobiphenyl **2.17** as peptide staples (Figure 2.3A).[34] The first nucleophilic addition activated the perfluoroaromatic for a second, regioselective addition. These staples increased the rigidity, lipophilicity, and stability of the modified peptides. Later, peptides stabled with biphenyl **2.17** showed increased penetration of the blood-brain barrier for improved pharmaceutical delivery[35,36] as well as enhanced activity in acute lung injury treatments.[37]

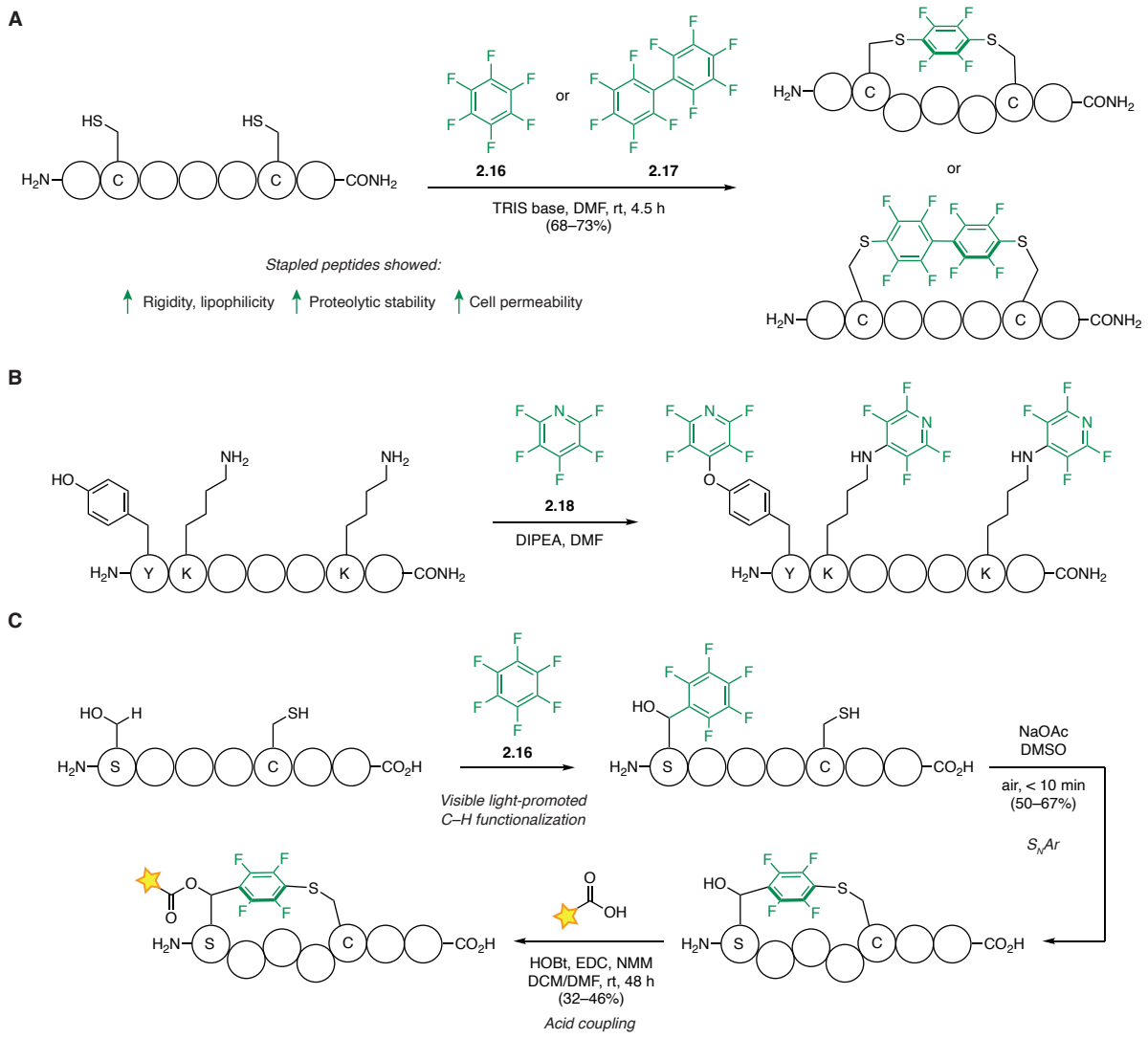

Figure 2.3 Peptide side-chain modifications using perfluoroaromatics. (A) Peptide stapling using hexafluorobenzene or decafluorobiphenyl. (B) Labeling beyond cysteine using pentafluoropyridine. (C) Unsymmetric peptide stapling with different examples of hexafluorobenzene reactivities.

The Cobb group reported in 2013 that pentafluoropyridine, **2.18**, reacts with nucleophilic amino acid side chains and can be used as protecting groups in peptide synthesis (Figure 2.3B).[38] Later, they showed that **2.18** reacts with multiple side chains on peptides: cysteine, tyrosine, serine, and lysine.[39] This contrasts with **2.16**, which reacted only with cysteine residues in the same conditions and suggests pentafluoropyridine may be useful for orthogonal modifications.

This work also showed that an attached tetrafluoropyridine group could prevent proteolysis by shielding certain protease cleavage motifs.

In 2024, Xu and co-workers designed a sequential, asymmetric peptide coupling sequence that was also compatible with late-stage peptide functionalization.[40] Through a visible light-promoted activation of a beta-hydrogenation on a serine side chain, hexafluorobenzene **2.16** was attached to a peptide, and subsequent S_NAr reaction with a nearby cysteine residue led to a stapled product (Figure 2.3C). The serine hydroxyl group was further modified through acid coupling conditions to give peptides tagged with groups such as azides for click chemistry or fluorescent probes. The stapled peptides showed increased stability and cellular uptake. This example highlights the orthogonality of perfluoroarene reactivity to other bioconjugation methods. It is possible radical defluorination to append the perfluoroarene moiety to a residue other than serine will be utilized further,[41] perhaps expanding to other biomolecules as well.

Researchers have engineered peptide sequences to promote the S_NAr reaction of perfluoroaromatic probes in aqueous environments. This expands labeling to biomolecules that are incompatible with organic solvents, the typical requirement for efficient S_NAr reactivity. The Pentelute group considered the enzyme glutathione S-transferase (GST), which catalyzes reactions between cysteine and different electrophiles (Figure 2.4A).[42] GST will catalyze reactions with many peptides so long as they feature the glutathione (GSH) sequence (N-terminal glutamate-cysteine-glycine). Site-selective coupling between perfluoroaromatic-modified peptides and GSH-sequence-containing peptides was successfully catalyzed by GST in aqueous conditions at physiological temperature. This work further showed that GST also successfully catalyzed intramolecular stapling, a complement to the work discussed above.

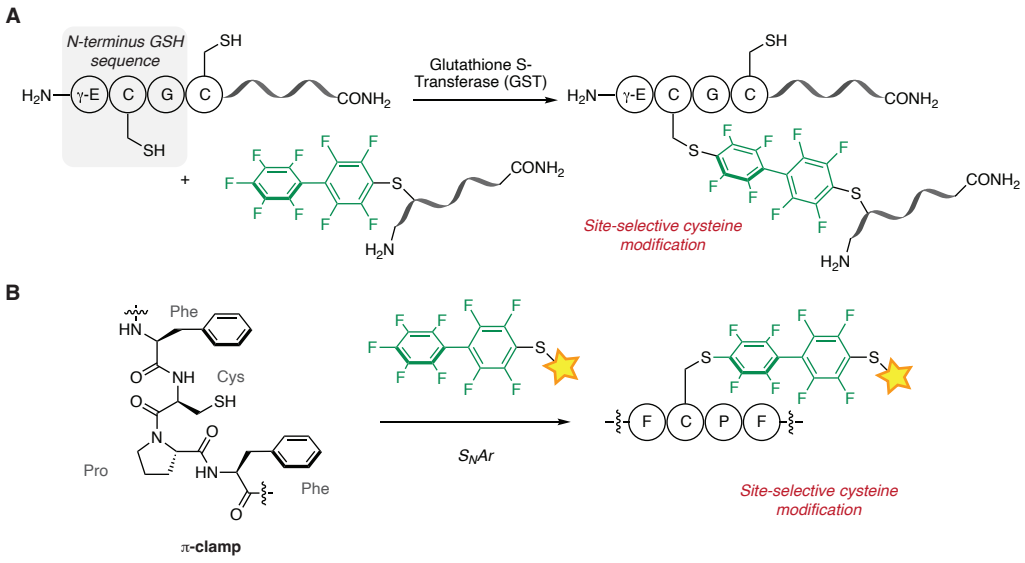

Figure 2.4 Engineering methods to promote S_NAr reactions in aqueous, biological settings. (A) GST-catalyzed coupling between a GSH sequence and a perfluoroaromatic-labeled peptide. (B) The π-clamp sequence sequesters perfluoroaromatics in a hydrophobic cavity for binding-promoted reactivity.

A few years later, the Pentelute group developed a second method for promoting the S_NAr reaction with perfluoroaromatic probes in aqueous settings (Figure 2.4B).[43,44] An engineered peptide sequence, phenylalanine-cysteine-proline-phenylalanine, formed a pocket that could bind a perfluoroaromatic probe and position it for attack by the present thiol. This hydrophobic cavity, termed a "π-clamp" in reference to the flanking phenylalanine residues, created a nonpolar local environment that promoted the reaction, in addition to the induced proximity between electrophile and nucleophile. This peptide sequence has been engineered into various proteins and used for site-selective attachment of various probes through reactivity with a perfluoroaromatic group.[45–47] The Pentelute group has since used high-throughput screening methods to identify other peptide sequences that can promote reactivity with perfluoroaromatic probes.[48,49]

Clearly, the reactivity of perfluoroaromatics is a useful tool for chemically modifying many biological structures site-selectively and has shown compatibility with many biological settings. We predict future work will focus on improving labeling in aqueous conditions, and these modifications may also enable labeling strategies involving non-covalent interactions of perfluoroarenes, like the π-clamp, and as discussed in the next section.

2.4 Arene-perfluoroarene interactions in chemical biology

2.4.1 Background

Since the first evidence of strong interactions between benzene and hexafluorobenzene (**2.16**) in the 1960s, the arene-perfluoroarene interaction has been studied and exploited for numerous applications (Figure 2.1D).[18,19,50,51] The slip-stack arrangement favored for this interaction is governed by a balance between favorable quadrupole-quadrupole and dispersion forces.[52] There is not an edge-to-face interaction, as the negatively charged face of benzene experiences repulsion with the negatively charged fluorine atoms of **2.16**. Computational work by Wheeler and Houk showed that perfluoroaromatics interact strongly with electron-rich aromatics; the same work showed that arene-(perfluoro)arene substituent effects arise from direct interactions rather than changes to the overall π system (Figure 2.5A).[53] Work from our lab explored the factors influencing arene-perfluoroarene interaction strength in solution and revealed that increasing aromatic surface areas and increasing the polarity of the solvent environment also increased binding (Figure 2.5B).[16] Such fundamental factors influencing arene-perfluoroarene interactions should be kept in mind when designing recognition tools.

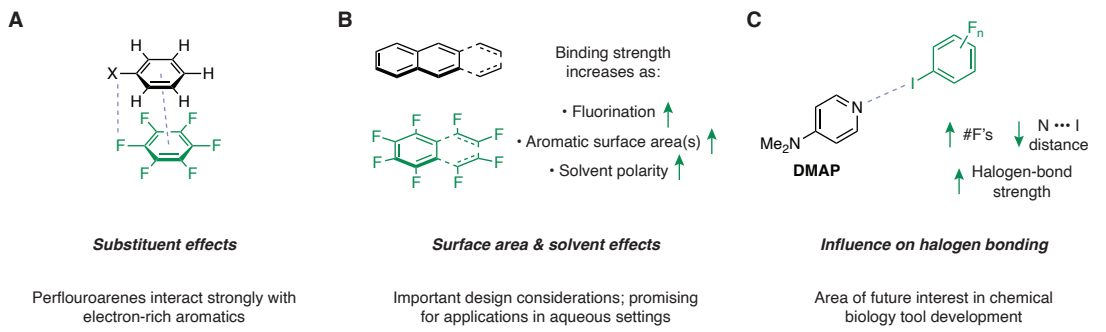

Figure 2.5 Non-covalent interactions and perfluoroaromatics. (A) Substituent effects and (B) solution-phase factors that influence the strength of arene-perfluoroarene interactions. (C) The influence of fluorination of aromatic halogen-bond donors.

The impact of perfluorinated rings on other non-covalent interactions has also been explored. Halogen bonding is a directional interaction analogous to hydrogen bonding, involving an electron-deficient region on a halogen atom (the donor) and a Lewis basic site (the acceptor) that, among many applications, has been studied in protein structures.[54,55] Perfluoroarenes are commonly used as halogen bond donors, as the electron-withdrawing nature of fluorine atoms increases the donating ability of other halogens like bromine and iodine (the larger, more polarizable halogens are better halogen bond donors overall) (Figure 2.5C).[56] Präsang et al. showed that for the simple case of DMAP as an acceptor and aryl iodides as halogen-bond donors, increasing the number of fluorine substituents linearly trended with a decrease in distance between donor and acceptor, corresponding to an increase in halogen bond strength.[57] The pentafluorinated aryl iodide was found to form the strongest halogen bond. While most work featuring this combination has focused on solid-state crystal engineering, it is likely future work will examine applications in the solution phase, as will be discussed in Chapter 5.

The solid-state applications of arene-perfluoroarene interactions have been recently comprehensively reviewed.[19] Here, the discussion will highlight biological studies that have utilized these interactions. It will end with host–guest chemistry applications that may lead to

future applications in chemical biology, bringing together proposed future directions from Chapter 1 and establishing motivations for the work described in Chapters 2–6.

2.4.2 Arene-perfluoroarene interactions in biological studies

As previously mentioned, perfluorinated versions of aromatic amino acids have been used to probe the contribution of different non-covalent interactions to overall protein stability. In addition to the cation- interaction discussed previously, perfluoroarenes have proven useful in determining arene-arene interaction contributions. Woll et al. showed that within a hydrophobic core containing three phenylalanine residues, replacing one with **2.6** increased overall folding stability.[58] Replacing others with **2.6** in different combinations did not provide stability, and the authors suggest the protein conformation must be able to fold to permit favorable arene-perfluoroarene interactions to experience stabilization.

Gao and co-workers showed that arene-perfluoroarene interactions could mediate protein-protein interactions in solution, remarking that even just a simple aromatic amino acid replacement led to enhanced protein complex stability (Figure 2.6).[59,60] In later work, the group systematically explored the role of different degrees of fluorination in the supramolecular assembly of designer polypeptides, highlighting the interplay of hydrophobic effect and dipole-dipole interactions. Interesting, they found that phenylalanine interactions with tetrafluorinated amino acid **2.7** provided increased stabilization over pentafluorinated **2.6**, suggesting modulation of overall quadrupole moments may provide another avenue of association strength tuning (Figure 2.6).[61] Other related examples and applications have been reviewed in detail.[50,62]

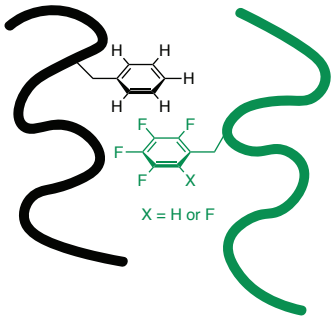

Amino acid pair	Relative stability ($\Delta\Delta G$, kcal/mol)
Phe, Phe	0.0
Phe, 4xF	6.7
Phe, 5xF	5.0

Influence of arene-perfluoroarene interaction strength on overall stabilities of protein dimers

Figure 2.6 Impact of arene-perfluoroarene interactions on overall peptide dimer stability when one phenylalanine peptide is fluorinated.

The π-clamp method of biomolecule modification described in the previous section is an example of arene-perfluoroarene interactions used in combination with the reactivity of perfluoroarenes to achieve site-selective labeling. Given the efficiency of the π-clamp and ensuing uses, it is reasonable to expect future examples pairing the two properties. Chapter 4 will summarize efforts toward one such development.

It is worth noting there are increasing uses of arene-perfluoroarene interactions in biomedical developments.[63] For instance, they have been used to drive the assembly of nanostructures that promote cell growth as a type of peptide-based therapeutic with increased stability.[64] Applications of the perfluoroaromatic motif in therapeutic and diagnostic settings have been recently reviewed and may yield even further avenues adept to chemical biology studies.[65]

2.4.3 Host–guest chemistry and arene-perfluoroarene interactions

Host–guest chemistry is an increasingly popular tool for modifying biomolecules.[66] To date, the use of simple perfluoroaromatics in 1:1 host–guest complexes is somewhat underexplored. Known hosts like cucurbiturils and calixarenes have moderate binding strengths with hexafluorobenzene, **2.16** (Figure 2.7A). In water, cucurbit[7]uril (CB[7]) binds **2.16** on the

order of 10^3 M^{-1}, which is about the same magnitude observed for small-molecule arene-perfluoroarene interactions in aqueous solution.[16,67] While CB[7] binds many guests with affinities over 10^{10} M^{-1}, it is not a remarkable host for perfluoroaromatics; binding is likely primarily driven by the hydrophobic effect, as there are no beneficial arene interactions. Calixarene host **2.19** also binds **2.16** on the order of 10^3 M^{-1} in an aqueous/organic mixture, though there was no discussion on how the host and guest interact.[68] Both examples show a hydrophobic core is beneficial for perfluoroaromatic binding in aqueous environments.

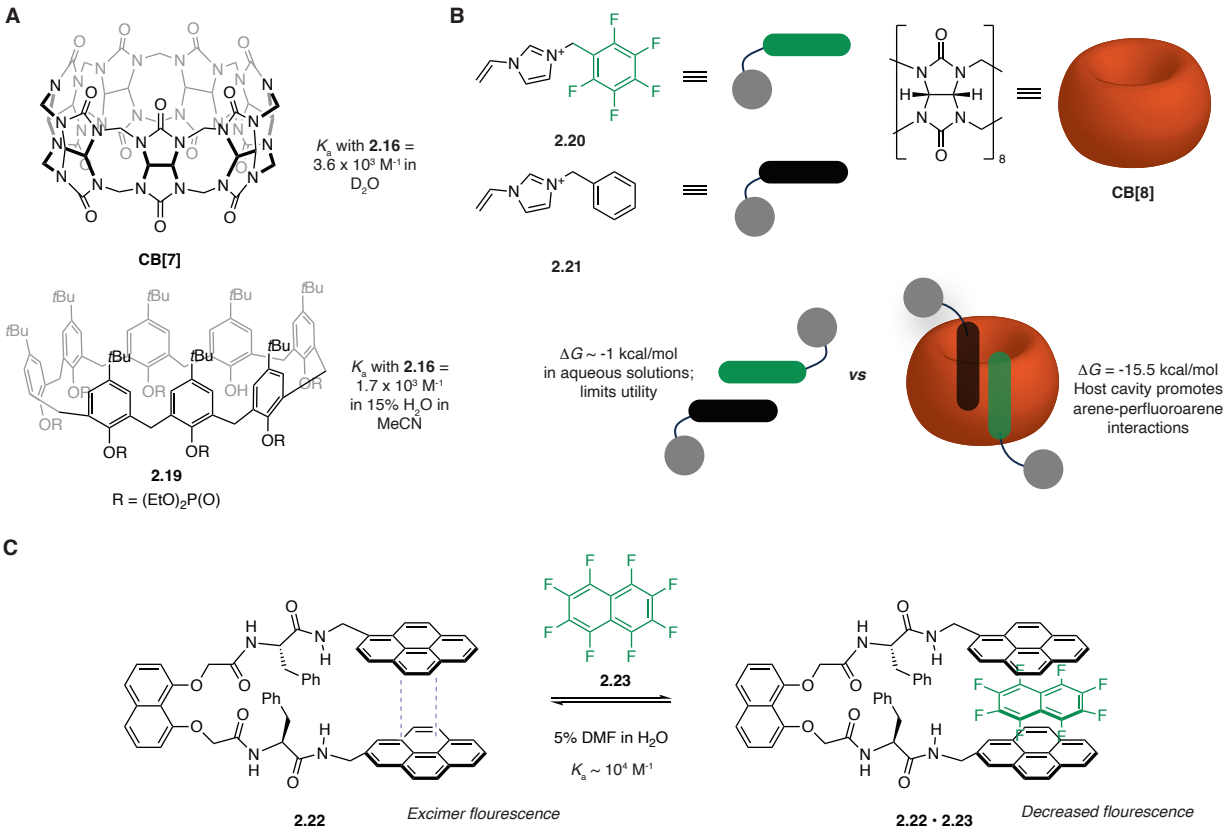

Figure 2.7 Examples of solution-phase host–guest chemistry with perfluoroaromatics. (A) Some common host types bind hexafluorobenzene **2.16**. (B) CB[8]-sequestration of (perfluoro)arenes increases arene-perfluoroarene interaction strength in water. (C) Perfluoroarene binding can be used to modulate photophysical properties in solution.

In 2020, Scherman and co-workers used host–guest sequestration to increase the strength of simple arene-perfluoroarene interactions.[69] In water, the association of solubilized **2.20** and

2.21 is relatively weak, with a free energy of ~ -1 kcal/mol (Figure 2.7B). Host CB[8] can accommodate both aromatic molecules simultaneously in its hydrophobic cavity. In doing so, the overall interaction increases significantly to just over -15 kcal/mol. The researchers found that the arene-perfluoroarene pair was sequestered preferentially over two equivalents of either **2.20** or **2.21**, highlighting the favorability of the mixed association in aqueous environments. Our lab's work on arene-perfluoroarene interactions in solution, while performed with small molecules rather than larger host–guest pairs, showed that both an increase in surface area and polarity of solvent environments enhance overall binding strengths.[16] Together, these examples demonstrate that host–guest assemblies that maximize arene-perfluoroarene interactions and benefit from the hydrophobic effect have the potential to strongly associate in biological settings.

Other host–guest systems that utilize arene-perfluoroarene interactions have not yet been employed in biology but may inspire such endeavors. In 2025, Xu et al. examined binding between pyrene-functionalized foldamer **2.22** and octafluoronaphthalene, **2.23** (Figure 2.7C).[70] Here, binding of **2.23** disrupted the arene-arene interactions of the pyrene clamp, causing a decrease in pyrene excimer fluorescence. The selective recognition of **2.23** over other perfluorinated aromatics and the measured responses from the foldamer gave researchers a tool for tuning foldamer photophysical properties. As pyrene excimers have been utilized to study protein-protein interactions,[71] it is possible introduction of arene-perfluoroarene interactions may facilitate studying the dynamics of such events. Other instances of using perfluoroaromatics to modulate emission in supramolecular assemblies may also inspire future biological applications.[72,73]

Other examples of the host–guest chemistry of perfluoroaromatics include large organometallic aromatic capsules that recognize perfluoroaromatics over perfluorocarbons of

similar size[74] and pyridine-based aromatic cages.[75] Association in the latter example was proposed to be driven by interactions between fluorine atoms and nitrogen-rich aromatic faces rather than arene-perfluoroarene interactions, which may be a useful design principle to incorporate in future hosts. Pentafluoropyridine **2.18**, discussed earlier as a useful peptide-modifying motif, may be an interesting guest to explore with future host types. Perfluoroaromatic hosts have also been synthesized and may be useful for recognizing electron-rich aromatic guests.[76]

To utilize host–guest chemistry in biological settings, relatively small complexes that capitalize on the hydrophobic effect to promote recognition are likely required. Our group seeks to synthesize electron-rich aromatic hosts that recognize simple perfluoroarenes. We plan to not only generate new, tunable synthetic chemical tools with which to study biology, but to fill a gap in the host–guest literature that pertains to simple systems based on arene-perfluoroarene interactions.

2.5 Conclusion

The perfluoroaromatic moiety is increasingly used in biological studies. Modifications to biomolecules have allowed for studying the perturbation of native non-covalent forces as well as improved properties of potential peptide therapeutics. The non-covalent arene-perfluoroarene interaction has already proved useful for modulating different supramolecular structures within and adjacent to biology, and new applications are likely on the horizon. With many methods to incorporate perfluoroaromatics into biological systems, there is still plenty of space to explore. The following chapters explore developments in the host–guest recognition of perfluoroarenes with an eye toward advancing non-covalent chemical biology tools.

2.6 Abbreviations and chemical formulas

Acetonitrile (MeCN); *tert*-Butyldimethylsilyl (TBDMS); Cysteine (Cys or C); Deoxyribonucleic acid (DNA); Deuterium oxide (D_2O); Dichloromethane (DCM); Diisopropylethylamine (DIPEA); 4-Dimethylaminopyridine (DMAP); Dimethylformamide (DMF); Dimethylsulfoxide (DMSO); Glutamate (Glu); Glutathione (GSH) 1-Hydroxybenzotriazole (HOBt); Lysine (Lys or K); *N*-Methylmorpholine (NMM); Nuclear magnetic resonance (NMR); Nucleophile (Nuc); Nucleophilic aromatic substitution (S_NAr); Phenylalanine (Phe); Proline (Pro); Ribonucleic acid (RNA); Serine (Ser or S); Sodium acetate (NaOAc); Tyrosine (Tyr or Y)

2.7 References

(1) Sletten, E. M.; Bertozzi, C. R. Bioorthogonal Chemistry: Fishing for Selectivity in a Sea of Functionality. *Angew. Chem. Int. Ed.* **2009**, *48*, 6974–6998.

(2) Rigolot, V.; Biot, C.; Lion, C. To View Your Biomolecule, Click inside the Cell. *Angew. Chem. Int. Ed.* **2021**, *60*, 23084–23105.

(3) Zielke, F. M.; Rutjes, F. P. J. T. Recent Advances in Bioorthogonal Ligation and Bioconjugation. *Top. Curr. Chem.* **2023**, *381*, 1–30.

(4) Harper, D. B.; O'Hagan, O. The Fluorinated Natural Products. *Nat. Prod. Rep.* **1994**, *11*, 123–133.

(5) Miller, M. A.; Sletten, E. M. Perfluorocarbons in Chemical Biology. *ChemBioChem* **2020**, *21*, 3451–3462.

(6) Qin, L.; Sheridan, C.; Gao, J. Synthesis of Tetrafluorinated Aromatic Amino Acids with Distinct Signatures in ^{19}F NMR. *Org. Lett.* **2012**, *14*, 528–531.

(7) Gimenez, D.; Phelan, A.; Murphy, C. D.; Cobb, S. L. ^{19}F NMR as a Tool in Chemical Biology. *Beilstein J. Org. Chem.* **2021**, *17*, 293–318.

(8) Wagner, N.; Stephan, M.; Höglinger, D.; Nadler, A. A Click Cage: Organelle-Specific Uncaging of Lipid Messengers. *Angew. Chem. Int. Ed*. **2018**, *57*, 13339–13343.

(9) Goujon, A.; Colom, A.; Straková, K.; Mercier, V.; Mahecic, D.; Manley, S.; Sakai, N.; Roux, A.; Matile, S. Mechanosensitive Fluorescent Probes to Image Membrane Tension in Mitochondria, Endoplasmic Reticulum, and Lysosomes. *J. Am. Chem. Soc.* **2019**, *141*, 3380–3384.

(10) Danylchuk, D. I.; Jouard, P. H.; Klymchenko, A. S. Targeted Solvatochromic Fluorescent Probes for Imaging Lipid Order in Organelles under Oxidative and Mechanical Stress. *J. Am. Chem. Soc.* **2021**, *143*, 912–924.

(11) Birchall, J. M.; Green, M.; Haszeldine, R. N.; Pitts, A. D. The Mechanism of the Nucleophilic Substitution Reactions of Polyfluoroarenes. *Chem. Commun. (London)* **1967**, *7*, 338–339.

(12) Amii, H.; Uneyama, K. C-F Bond Activation in Organic Synthesis. *Chem. Rev.* **2009**, *109*, 2119–2183.

(13) Zhang, C.; Vinogradova, E. V.; Spokoyny, A. M.; Buchwald, S. L.; Pentelute, B. L. Arylation Chemistry for Bioconjugation. *Angew. Chem. Int. Ed.* **2019**, *58*, 4810–4839.

(14) Brittain, W. D. G.; Coxon, C. R. Perfluoroaryl and Perfluoroheteroaryl Reagents as Emerging New Tools for Peptide Synthesis, Modification and Bioconjugation. *Chem. Eur. J.* **2022**, *28*, e202103305.

(15) Anslyn, E. V.; Dougherty, D. A. Modern Physical Organic Chemistry; University Science Books, 2006.

(16) Lee, G. Y.; Hu, E.; Rheingold, A. L.; Houk, K. N.; Sletten, E. M. Arene-Perfluoroarene Interactions in Solution. *J. Org. Chem.* **2021**, *86*, 8425–8436.

(17) Wang, W.; Wu, W. X.; Zhang, Y.; Jin, W. J. Perfluoroaryl⋯aryl Interaction: The Most Important Subset of π -Hole⋯ π Bonding. *Chem. Phys. Rev.* **2024**, *5*, 031303.

(18) Patrick, C. R.; Prosser, G. S. A Molecular Complex of Benzene and Hexafluorobenzene. *Nature* **1960**, *187*, 1021–1021.

(19) Zhang, S.; Chen, A.; An, Y.; Li, Q. Arene-Perfluoroarene Interaction: Properties, Constructions, and Applications in Materials Science. *Matter* **2024**, *7*, 3317–3350.

(20) Smith, C. E.; Smith, P. S.; Thomas, R. L.; Robins, E. G.; Collings, J. C.; Dai, C.; Scott, A. J.; Borwick, S.; Batsanov, A. S.; Watt, S. W.; Clark, S. J.; Viney, C.; Howard, J. A. K.; Clegg, W.; Marder, T. B. Arene-Perfluoroarene Interactions in Crystal Engineering: Structural Preferences in Polyfluorinated Tolans. *J. Mater. Chem.* **2004**, *14*, 413–420.

(21) Parsch, J.; Engels, J. W. C−F⋯H−C Hydrogen Bonds in Ribonucleic Acids. *J. Am. Chem. Soc.* **2002**, *124*, 5664–5672.

(22) Kool, E. T.; Morales, J. C.; Guckian, K. M. Mimicking the Structure and Function of DNA: Insights into DNA Stability and Replication. *Angew. Chem. Int. Ed.* **2000**, *39*, 990–1009

(23) Lai, J. S.; Qu, J.; Kool, E. T. Fluorinated DNA Bases as Probes of Electrostatic Effects in DNA Base Stacking. *Angew. Chem. Int. Ed.* **2003**, *42*, 5973–5977.

(24) Živković, A.; Engels, J. W. RNA Recognition by Fluor-Aromatic Substituted. *Nucleosides, Nucleotides Nucleic Acids* **2005**, *24*, 1023–1027.

(25) Thorson, J. S.; Chapman, E.; Schultz, P. G. Analysis of Hydrogen Bonding Strengths in Proteins Using Unnatural Amino Acids. *J. Am. Chem. Soc.* **1995**, *117*, 9361–9362.

(26) Lee, Y. J.; Schmidt, M. J.; Tharp, J. M.; Weber, A.; Koenig, A. L.; Zheng, H.; Gao, J.; Waters, M. L.; Summerer, D.; Liu, W. R. Genetically Encoded Fluorophenylalanines Enable Insights into the Recognition of Lysine Trimethylation by an Epigenetic Reader. *Chem. Commun.* **2016**, *52*, 12606–12609.

(27) Mellor, J. It Takes a PHD to Read the Histone Code. *Cell* **2006**, *126*, 22–24.

(28) Minnihan, E. C.; Young, D. D.; Schultz, P. G.; Stubbe, J. Incorporation of Fluorotyrosines into Ribonucleotide Reductase Using an Evolved, Polyspecific Aminoacyl-TRNA Synthetase. *J. Am. Chem. Soc.* **2011**, *133*, 15942–15945.

(29) Liu, X.; Jiang, L.; Li, J.; Wang, L.; Yu, Y.; Zhou, Q.; Lv, X.; Gong, W.; Lu, Y.; Wang, J. Significant Expansion of Fluorescent Protein Sensing Ability through the Genetic Incorporation of Superior Photo-Induced Electron-Transfer Quenchers. *J. Am. Chem. Soc.* **2014**, *136*, 13094–13097.

(30) Sundhoro, M.; Jeon, S.; Park, J.; Ramström, O.; Yan, M. Perfluoroaryl Azide Staudinger Reaction: A Fast and Bioorthogonal Reaction. *Angew. Chem. Int. Ed.* **2017**, *56*, 12117–12121.

(31) Glossop, H. D.; Sarojini, V. Accessing the Thiol Toolbox: Synthesis and Structure-Activity Studies on Fluoro-Thiol Conjugated Antimicrobial Peptides. *Bioconjugate Chem*. **2023**, *34*, 218–227.

(32) Embaby, A. M.; Schoffelen, S.; Kofoed, C.; Meldal, M.; Diness, F. Rational Tuning of Fluorobenzene Probes for Cysteine-Selective Protein Modification. *Angew. Chem. Int. Ed.* **2018**, *57*, 8022–8026.

(33) Vinogradov, A. A.; Yin, Y.; Suga, H. Macrocyclic Peptides as Drug Candidates: Recent Progress and Remaining Challenges. *J. Am. Chem. Soc.* **2019**, *141*, 4167–4181.

(34) Spokoyny, A. M.; Zou, Y.; Ling, J. J.; Yu, H.; Lin, Y.; Pentelute, B. L. A Perfluoroaryl-Cysteine S_NAr Chemistry Approach to Unprotected Peptide Stapling. *J. Am. Chem. Soc.* **2013**, *135*, 5946–5949.

(35) Fadzen, C. M.; Wolfe, J. M.; Cho, C. F.; Chiocca, E. A.; Lawler, S. E.; Pentelute, B. L. Perfluoroarene-Based Peptide Macrocycles to Enhance Penetration Across the Blood-Brain Barrier. *J. Am. Chem. Soc.* **2017**, *139*, 15628–15631.

(36) Fadzen, C. M.; Wolfe, J. M.; Zhou, W.; Cho, C. F.; Von Spreckelsen, N.; Hutchinson, K. T.; Lee, Y. C.; Chiocca, E. A.; Lawler, S. E.; Yilmaz, O. H.; Lippard, S. J.; Pentelute, B. L. A Platinum(IV) Prodrug - Perfluoroaryl Macrocyclic Peptide Conjugate Enhances Platinum Uptake in the Brain. *J. Med. Chem.* **2020**, *63*, 6741–6747.

(37) Li, S.; Song, S.; Liu, X.; Zhang, X.; Liang, X.; Chang, X.; Zhou, D.; Han, J.; Nie, Y.; Guo, C.; Yao, X.; Chang, M.; Peng, Y. Development of a Decafluorobiphenyl Cyclized Peptide Targeting the NEMO-IKKα/β Interaction That Enhances Cell Penetration and Attenuates Lipopolysaccharide-Induced Acute Lung Injury. *Bioconjugate Chem.* **2024**, *35*, 638–652.

(38) Hudson, A. S.; Hoose, A.; Coxon, C. R.; Sandford, G.; Cobb, S. L. Synthesis of a Novel Tetrafluoropyridine-Containing Amino Acid and Tripeptide. *Tetrahedron Lett.* **2013**, *54*, 4865–4867.

(39) Gimenez, D.; Mooney, C. A.; Dose, A.; Sandford, G.; Coxon, C. R.; Cobb, S. L. The Application of Perfluoroheteroaromatic Reagents in the Preparation of Modified Peptide Systems. *Org. Biomol. Chem.* **2017**, *15*, 4086–4095.

(40) Wang, M.; Pan, D.; Zhang, Q.; Lei, Y.; Wang, C.; Jia, H.; Mou, L.; Miao, X.; Ren, X.; Xu, Z. Site-Selective Polyfluoroaryl Modification and Unsymmetric Stapling of Unprotected Peptides. *J. Am. Chem. Soc.* **2024**, *146*, 6675–6685.

(41) Wang, J.; Gao, H.; Shi, C.; Chen, G.; Tan, X.; Chen, X.; Xu, L.; Cai, X.; Huang, B.; Li, H. Recent Advances in Radical-Based C-F Bond Activation of Polyfluoroarenes and: Gem -Difluoroalkenes. *Chem. Commun.* **2021**, *57*, 12203–12217.

(42) Zhang, C.; Spokoyny, A. M.; Zou, Y.; Simon, M. D.; Pentelute, B. L. Enzymatic "Click" Ligation: Selective Cysteine Modification in Polypeptides Enabled by Promiscuous Glutathione S-Transferase. *Angew. Chem. Int. Ed.* **2013**, *52*, 14001–14005.

(43) Zhang, C.; Welborn, M.; Zhu, T.; Yang, N. J.; Santos, M. S.; Van Voorhis, T.; Pentelute, B. L. π-Clamp-Mediated Cysteine Conjugation. *Nat. Chem.* **2016**, *8*, 120–128.

(44) Dai, P.; Williams, J. K.; Zhang, C.; Welborn, M.; Shepherd, J. J.; Zhu, T.; Van Voorhis, T.; Hong, M.; Pentelute, B. L. A Structural and Mechanistic Study of π-Clamp-Mediated Cysteine Perfluoroarylation. *Sci. Rep.* **2017**, *7*, 1–11.

(45) Dai, P.; Zhang, C.; Welborn, M.; Shepherd, J. J.; Zhu, T.; Van Voorhis, T.; Pentelute, B. L. Salt Effect Accelerates Site-Selective Cysteine Bioconjugation. *ACS Cent. Sci.* **2016**, *2*, 637–646.

(46) Baccile, J. A.; Voorhees, P. J.; Chillo, A. J.; Berry, M.; Morgenstern, R.; Schwertfeger, T. J.; Rossi, F. M.; Nelson, C. D. S. Site-Specific Small Molecule Labeling of an Internal Loop in JC Polyomavirus Pentamers Using the π-Clamp-Mediated Cysteine Conjugation. *ChemBioChem* **2021**, *22*, 3037–3041.

(47) Taylor, R. J.; Aguilar Rangel, M.; Geeson, M. B.; Sormanni, P.; Vendruscolo, M.; Bernardes, G. J. L. π-Clamp-Mediated Homo- and Heterodimerization of Single-Domain

Antibodies via Site-Specific Homobifunctional Conjugation. *J. Am. Chem. Soc.* **2022**, *144*, 13026–13031.

(48) Evans, E. D.; Pentelute, B. L. Discovery of a 29-Amino-Acid Reactive Abiotic Peptide for Selective Cysteine Arylation. *ACS Chem. Biol.* **2018**, *13*, 527–532.

(49) Evans, E. D.; Gates, Z. P.; Sun, Z. Y. J.; Mijalis, A. J.; Pentelute, B. L. Conformational Stabilization and Rapid Labeling of a 29-Residue Peptide by a Small Molecule Reaction Partner. *Biochemistry* **2019**, *58*, 1343–1353.

(50) Meyer, E. A.; Castellano, R. K.; Diederich, F. Interactions with Aromatic Rings in Chemical and Biological Recognition. *Angew. Chem. Int. Ed.* **2003**, *42*, 1210–1250.

(51) Cozzi, F.; Ponzini, F.; Annunziata, R.; Cinquini, M.; Siegel, J. S. Polar Interactions between Stacked π Systems in Fluorinated 1,8-Diarylnaphthalenes: Importance of Quadrupole Moments in Molecular Recognition. *Angew. Chem. Int. Ed.* **1995**, *34*, 1019–1020.

(52) Carter-Fenk, K.; Herbert, J. M. Electrostatics Does Not Dictate the Slip-Stacked Arrangement of Aromatic π-π Interactions. *Chem. Sci.* **2020**, *11*, 6758–6765.

(53) Wheeler, S. E.; Houk, K. N. Substituent Effects in the Benzene Dimer Are Due to Direct Interactions of the Substituents with the Unsubstituted Benzene. *J. Am. Chem. Soc.* **2008**, *130*, 10854–10855.

(54) Cavallo, G.; Metrangolo, P.; Milani, R.; Pilati, T.; Priimagi, A.; Resnati, G.; Terraneo, G. The Halogen Bond. *Chem. Rev.* **2016**, *116*, 2478–2601.

(55) Scholfield, M. R.; Vander Zanden, C. M.; Carter, M.; Ho, P. S. Halogen Bonding (X-Bonding): A Biological Perspective. *Protein Sci*. **2013**, *22*, pp 139–152.

(56) Sharber, S. A.; Mullin, W. J.; Thomas, S. W. Bridging the Void: Halogen Bonding and Aromatic Interactions to Program Luminescence and Electronic Properties of π-Conjugated Materials in the Solid State. *Chem. Mater.* **2021**, *33*, 6640–6661.

(57) Präsang, C.; Whitwood, A. C.; Bruce, D. W. Halogen-Bonded Cocrystals of 4-(N,N-Dimethylamino)Pyridine with Fluorinated Iodobenzenes. *Cryst. Growth Des.* **2009**, *9*, 5319–5326.

(58) Woll, M. G.; Hadley, E. B.; Mecozzi, S.; Gellman, S. H. Stabilizing and Destabilizing Effects of Phenylalanine → F 5-Phenylalanine Mutations on the Folding of a Small Protein. *J. Am. Chem. Soc.* **2006**, *128*, 15932–15933.

(59) Zheng, H.; Gao, J. Highly Specific Heterodimerization Mediated by Quadrupole Interactions. *Angew. Chem. Int. Ed.* **2010**, *49*, 8635–8639.

(60) Pace, C. J.; Gao, J. Exploring and Exploiting Polar-π Interactions with Fluorinated Aromatic Amino Acids. *Acc. Chem. Res.* **2013**, *46*, 907–915.

(61) Pace, C. J.; Zheng, H.; Mylvaganam, R.; Kim, D.; Gao, J. Stacked Fluoroaromatics as Supramolecular Synthons for Programming Protein Dimerization Specificity. *Angew. Chem. Int. Ed.* **2012**, *51*, 103–107.

(62) Salonen, L. M.; Ellermann, M.; Diederich, F. Aromatic Rings in Chemical and Biological Recognition: Energetics and Structures. *Angew. Chem. Int. Ed.* **2011**, *50*, 4808–4842.

(63) Veronese, E.; Metrangolo, P.; Dichiarante, V. Engineering Amino Acid and Peptide Supramolecular Architectures through Fluorination. *Chem. Eur. J.* **2024**, *30*, e202400617.

(64) Kim, T.; Hong, J.; Kim, J.; Cho, J.; Kim, Y. Two-Dimensional Peptide Assembly via Arene-Perfluoroarene Interactions for Proliferation and Differentiation of Myoblasts. *J. Am. Chem. Soc.* **2023**, *145*, 1793–1802.

(65) Nair, R. R.; Seo, E. W.; Hong, S.; Jung, K. O.; Kim, D. Pentafluorobenzene: Promising Applications in Diagnostics and Therapeutics. *ACS Appl. Bio Mater*. **2023**, *6*, 4081–4099.

(66) Wang, Y. C.; Bai, S. C.; Ye, W. L.; Jiang, J.; Li, G. Recent Progress in Site-Selective Modification of Peptides and Proteins Using Macrocycles. *Bioconjugate Chem.* **2024**, *35*, 277–285.

(67) Assaf, K. I.; Nau, W. M. Cucurbiturils as Fluorophilic Receptors. *Supramol. Chem.* **2014**, *26*, 657–669.

(68) Kalchenko, O. I.; Lipkowski, J.; Kalchenko, V. I.; Vysotsky, M. A.; Markovsky, L. N. Effect of Octakis(Diethoxyphosphoryloxy)-Tert-Butyl-Calix[8]Arene in Mobile Phase on the Reversed-Phase Retention Behavior of Aromatic Compounds: Host-Guest Complex Formation and Stability Constants Determination. *J Chromatogr. Sci.* **1998**, *36*, 269–273.

(69) Huang, Z.; Chen, X.; Wu, G.; Metrangolo, P.; Whitaker, D.; McCune, J. A.; Scherman, O. A. Host-Enhanced Phenyl-Perfluorophenyl Polar–π Interactions. *J. Am. Chem. Soc.* **2020**, *142*, 7356–7361.

(70) Xu, Y.; Hao, A.; Xing, P. Dynamic Chiral Folding for Arene-Perfluoroarene Force Driven Clamping. *Nano Lett.* **2025**, *25*, 7128–7136.

(71) Bains, G. K.; Kim, S. H.; Sorin, E. J.; Narayanaswami, V. The Extent of Pyrene Excimer Fluorescence Emission Is a Reflector of Distance and Flexibility: Analysis of the Segment Linking the LDL Receptor-Binding and Tetramerization Domains of Apolipoprotein E3. *Biochemistry* **2012**, *51*, 6207–6219.

(72) Wang, T.; Zhang, Z.; Hao, A.; Xing, P. Engineering Perfluoroarenes for Enhanced Molecular Barrier Effect and Chirality Transfer in Solutions. *Chem. Sci.* **2025**, *16*, 3498–3508.

(73) Yang, S.; Li, F.; Li, Q.; Han, J.; Cheng, Y. Chiral Coassembly-Activated CPL Amplification Promoted by Electrostatic and Arene-Perfluoroarene Interactions. *ACS Appl. Opt. Mater.* **2023**, *1*, 1492–1500.

(74) Kai, U.; Sumida, R.; Tanaka, Y.; Yoshizawa, M. Discrimination of Perfluorinated Arenes/Alkanes by Modulable Polyaromatic Capsules. *J. Am. Chem. Soc.* **2025**, *147*, 10640–10646.

(75) Takezawa, H.; Murase, T.; Resnati, G.; Metrangolo, P.; Fujita, M. Recognition of Polyfluorinated Compounds Through Self-Aggregation in a Cavity. *J. Am. Chem. Soc.* **2014**, *136*, 1786–1788.

(76) Sandford, G. Macrocycles from Perhalogenated Heterocycles. *Chem. Eur. J.* **2003**, *9*, 1464–1469.

CHAPTER THREE

The interplay between preorganization and hydrogen bonding in perfluoroaromatic-binding cyclophane hosts

3.1 Abstract

A significant goal within the field of host–guest chemistry is to achieve molecular recognition on par with the examples of strength and selectivity present in nature's binding partners. The principles of preorganization and complementarity, along with understanding the strength and tunability of individual non-covalent interactions, drive the design of complexes aiming to reach such recognition capabilities. To better design hosts for specific guests of interest, the role of different aspects of a binding complex must be well understood. Our group has successfully designed an organic host to bind perfluoroaromatic guests with reasonably high affinities in different solvent environments. Now, we have dissected the role of both host preorganization and hydrogen bonding through carefully crafted experiments to understand the individual components that drive binding in organic solvent. We find that while hydrogen bonding with guests is critical for strong binding in this system, the preorganized cavity plays an important role in not only what guests bind, but the overall strength of binding.

3.2 Introduction

The field of host–guest chemistry arose from chemists' desire to mimic the selective molecular recognition on display in nature, such as the non-covalent forces bringing together proteins and ligands or nucleic acid base pairs.[1] Nature's exquisite selectivity and high binding show the power of non-covalent forces when arranged properly. Chemists have spent decades trying to perfect such recognition in small-molecule systems, striving for high binding affinities (K_a) in various solvents by designing complexes with finely tuned shapes for maximum

interaction. The principles of preorganization and complementarity arose from this pursuit (Figure 3.1A).[2,3] When considering the binding of lithium ions, recognition increases as the binding cavity of hosts become more rigid, such as going from the linear, floppy triethylene glycol to the rigid, cyclized corresponding crown ether.[4,5] The entropic cost to binding, going from so many possible orientations to just one, becomes much lower when the unbound host's ground state is already preorganized for a guest.

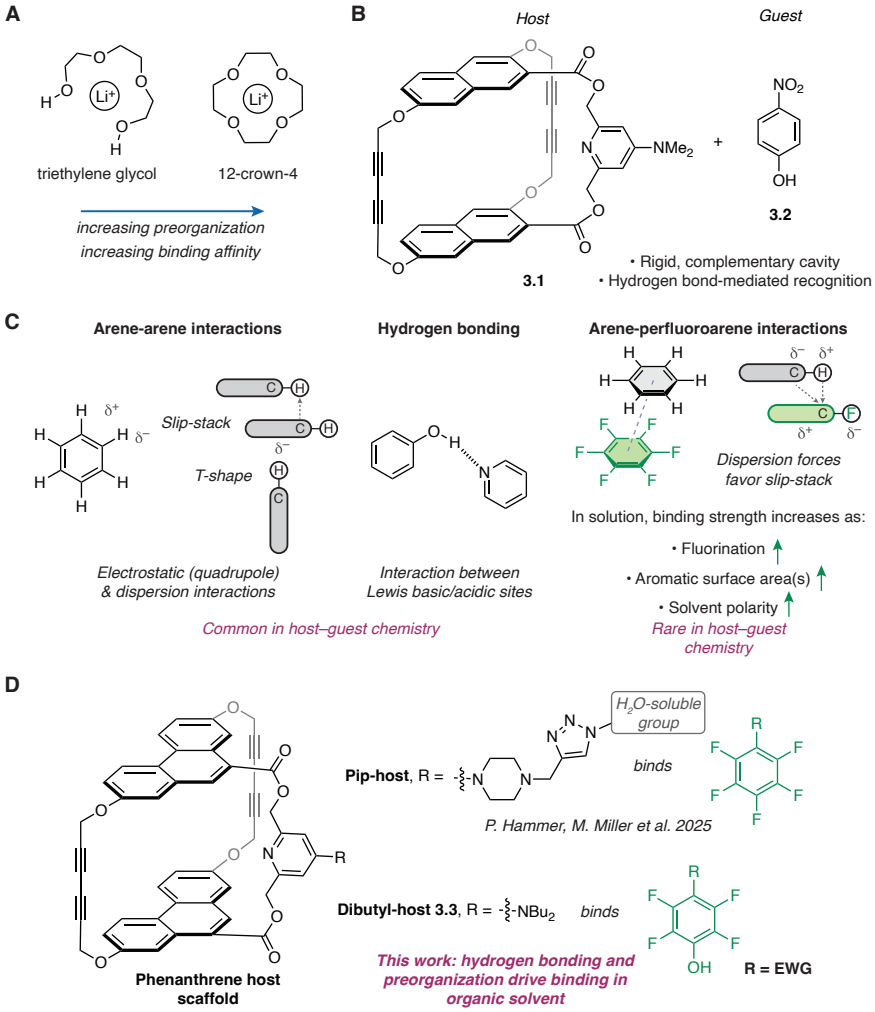

Figure 3.1 Design principles for host–guest complexes in organic solutions. (A) Principles of preorganization and complementarity with classic examples in lithium-ion binding. (B) Cyclophane host that binds electron-deficient guests strongly due to shape complementarity and hydrogen bonding (ref. 6). (C) Non-covalent interactions considered in this work. Depiction of arene interactions adapted (ref. 23). (D) Structure of cyclophane host (R = NBu_2, **3.3**) that is the

subject of this work (inspired by host **3.1**). Water-soluble piperazine-substituted host (**Pip-host**) is discussed in others' work. EWG = electron-withdrawing group.

The principles of complementarity and preorganization are on display throughout host–guest systems designed by chemists. The Whitlock group published a series of naphthalene-based hosts in the 1980s and 1990s such as **3.1** (Figure 3.1B).[6,7] These hosts were found to bind strongly to electron-deficient guests such as *p*-nitrophenol (**3.2**) in organic solvent (~10^4 M^{-1} in $CDCl_3$). Through a series of host iterations, they showed that increasing the hydrogen-bond interaction strength as well as modifying the cavity to optimally fit **3.2** increased the overall binding strength.[8–10]

The naphthalene hosts also highlight non-covalent interactions often employed for molecular recognition: arene-arene interactions and hydrogen bonding (Figure 3.1C). Through electrostatic and dispersion forces, aromatic groups experience attractive interactions in different geometries.[11–14] Hydrogen bonds are often incorporated into synthetic host–guest systems, with strengths that can be tuned through different substituents on host and/or guest.[15,16] In our own work, we aim to design hosts that recognize guests through a less-explored set of interactions: those between aromatic compounds and perfluoroaromatics (Figure 3.1C).

Perfluoroaromatics are aromatic rings where C–H bonds are replaced with C–F bonds (Figure 3.1C). A relatively strong non-covalent interaction can occur between electron-rich hydrocarbon aromatics and perfluoroaromatics, arising from electrostatics (opposite quadrupole moments arising from electronegativity changes going from C–H to C–F) and dispersion forces (induced dipoles).[12,17–19] The arene-perfluoroarene interaction is increasingly used in crystal engineering, materials science applications, and chemical biology (discussed in Chapter 2).[20–22] Our group's earlier work studying this force focused on the properties that influence interaction strength in solution.[23] It was found that arene-perfluoroarene interactions in solution increase as

fluorination, aromatic surface area, and/or solvent polarity increase. Despite increased interest in and use of arene-perfluoroarene interactions, there are still relatively few examples of them being enhanced through host–guest chemistry (Chapter 2).[20,24–26]

In previous work from our lab, Dr. Margeaux Miller synthesized a host, **3.3**, that accommodates perfluoroarenes (Figure 3.1D).[27] The host features electron-rich phenanthrene faces for arene recognition, rigid side linkers to increase host preorganization, and a bridging linker. The bridge serves to increase rigidity, preventing rotation of the aromatic rings, and provides a location for electron-accepting groups, such as pyridine, for interactions like hydrogen bonding. Dr. Miller's work showed that hydrogen bonding is necessary for strong interactions in organic solvents, while later work by Prairie Hammer showed that arene-perfluoroarene interactions drive binding in polar solvents like water (unpublished work). Both works used modified linkers to enhance solubility in different environments (Figure 3.1D). For the latter case, a piperazine linker (**Pip-host**) was used to append click chemistry-compatible groups. In this current work, we use organic-soluble dibutyl host **3.3** to investigate the roles of hydrogen bonding and preorganization in recognizing perfluoroaromatic guests in organic solvents.

3.3 Results and discussion

3.3.1 The complementarity of H-bonding and a preorganized host cavity

In the synthesis of phenanthrene-based host **3.3**, two isomers are isolated: a *twist* isomer, **3.3a**, and a *meso* isomer, **3.3b**, depending on the linker ester connections (Figure 3.2A). We used ^{1}H NMR titrations to determine the binding affinities of both hosts with fluorinated phenol **3.4** (Figure 3.2B; shown is a titration between **3.3a** and **3.4**). The calculated K_a's for each host were within error of each other, suggesting no major difference in guest binding between isomers (Figure 3.1A). This contrasts with the reported naphthalene host, **3.1**, whose corresponding

"twist" isomer binds its guest, **3.2**, an order of magnitude lower.[6] Considering the ^{1}H NMR titration of **3.3a** with **3.4**, we see that both the phenanthrene and pyridine proton signals shift as more guest is bound (Figure 3.2B). This supports binding in the cavity as well as interactions with the pyridine linker. Host **3.3a** also binds **3.2** with a binding affinity an order of magnitude higher than it binds **3.4**, nearly the same as naphthalene-based host **3.1** (Figure 3.2C). This may be the result of cavity size: **3.2** has a smaller width compared to fluorinated **3.4** and fits in both naphthalene- and phenanthrene-based hosts; **3.2** may have more space to adopt an optimized geometry for hydrogen bonding.

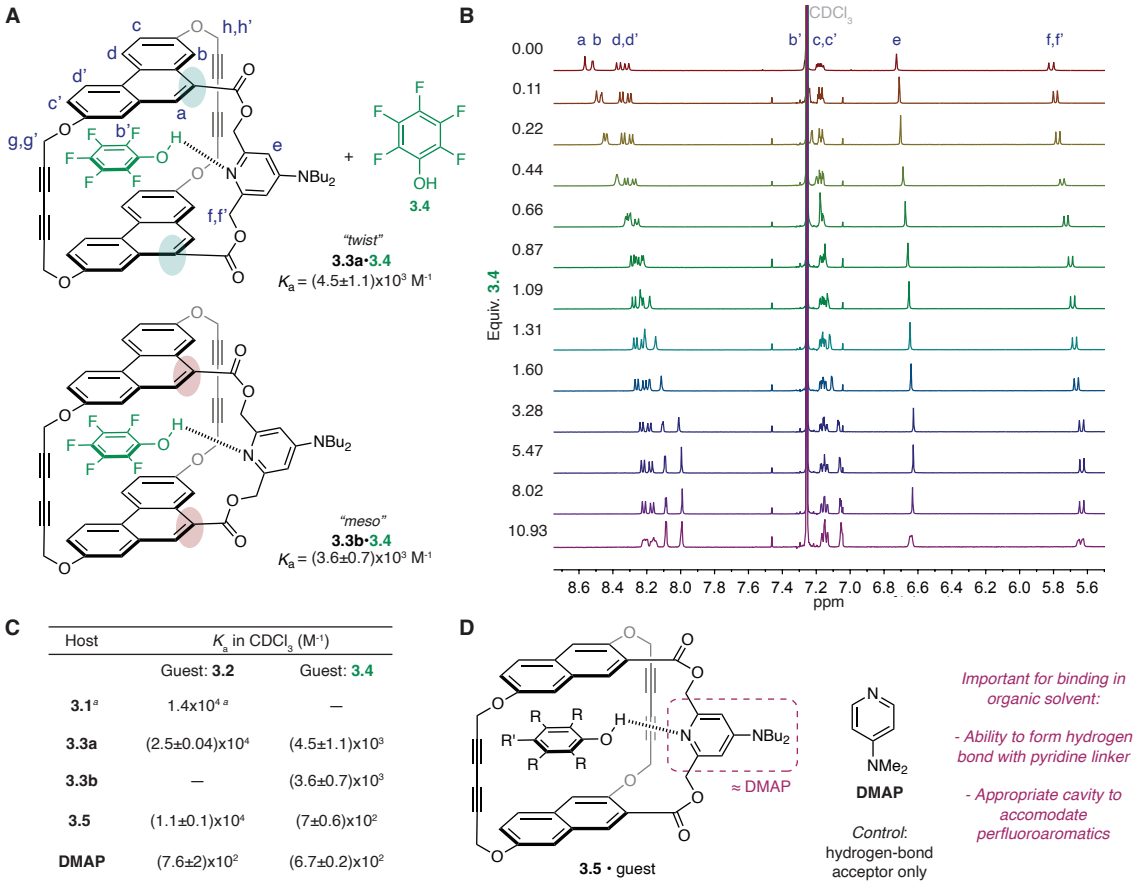

Host	K_a in $CDCl_3$ (M^{-1})	
	Guest: **3.2**	Guest: **3.4**
3.1[a]	1.4x10^4 [a]	—
3.3a	(2.5±0.04)x10^4	(4.5±1.1)x10^3
3.3b	—	(3.6±0.7)x10^3
3.5	(1.1±0.1)x10^4	(7±0.6)x10^2
DMAP	(7.6±2)x10^2	(6.7±0.2)x10^2

Figure 3.2 Comparison of different cavity sizes and binding to non-fluorinated versus fluorinated phenols. (A) Binding of pentafluorophenol, **3.4**, by two host isomers, with K_a's determined in $CDCl_3$. (B) Representative ^{1}H NMR titration: **3.3a** with **3.4**. (C) Table of binding affinities with *p*-nitrophenol, **3.2**, and pentafluorophenol, **3.4**. (D) Additional host structures. [a]Reported (ref. 6).

To begin probing the importance of hydrogen bonding and preorganization for binding perfluoroaromatics in organic solvent, we considered additional host structures. Dr. Margeaux Miller synthesized a version of naphthalene-based **3.1** with the dibutylamine linker used in the phenanthrene platform (**3.5**, Figure 3.2D). Butyl groups were chosen to enhance the solubility in organic solvent. To probe the binding contribution of hydrogen bonding alone, without any contribution from an appropriately shaped, rigid cavity, we considered DMAP, a truncated version of the pyridine linker.

We first checked the binding affinity of naphthalene dibutylamine host **3.5** with *p*-nitrophenol **3.2**, which was reported to bind with the dimethyl version on the order of 10^4 M^{-1} (Figure 3.2C). We found butyl-substituted **3.5** bound nitrophenol **3.2** with a similar affinity, which showed that swapping of the dimethylamino substituent for one with butyl groups was not detrimental to binding. We next tested binding with pentafluorophenol, **3.4**, as our model perfluorinated phenol guest. Here, we observed a nearly two-order-of-magnitude drop in binding affinity compared to **3.2**. This suggests the cavity of **3.5** is not ideal for perfluoroaromatic guests.

Curiously, the same experiments using DMAP as the host suggest that **3.2** and **3.4** should have similar hydrogen-bonding abilities (Figure 3.2C). We hypothesized the substantially higher binding with nitrophenol **3.2** must come from cavity contributions. Previous computational work by Dr. Gina Lee supported the idea that the naphthalene cavity is likely too small to favorably accommodate perfluoroaromatic guests.[28] Given that fluorophenol **3.4** binds with nearly the same affinity to naphthalene host **3.5** and DMAP, it may be hydrogen bonding with the linker of **3.5** but *outside* the cavity. We attempted to grow crystal structures of such a complex but were unsuccessful.

The results here suggest that while cavity size is important for accommodating guests of interest, the strength of the hydrogen bond interaction between host and guest in organic solvent is the main contributor to high binding affinities. We decided to further probe the role of the hydrogen bond with additional host controls.

3.3.2 Non-hydrogen bonding controls

We were curious how the presence or absence of hydrogen bonding would influence the binding equilibrium with pentafluorophenol **3.4** (Figure 3.3A). We proposed a "control" host, **3.6**, without a hydrogen-bond acceptor on the linker. The control host, synthesized by Erika Aguiluz Ramirez, was accessed by generating a modified linker, accessible in two steps. Starting with commercially available **3.7**, dialkylation proceeded to give **3.8** in great yield (Figure 3.3B). Reduction of both esters gave linker **3.9**. This was esterified with the activated ester **3.10** (prepared and used by Dr. Margeaux Miller in the synthesis of **3.3**)[27] to give prehost **3.11**, which was then cyclized in Eglinton coupling conditions to give control host **3.6**. Only the *twist* isomer was isolated and studied in this case, as the difference between isomers **3.3a** and **3.3b** was not significant. Control host **3.6** bound **3.4** with a K_a of about 10 M^{-1}, suggesting that while binding occurs with a complementary cavity, hydrogen bonding is critical for obtaining the high K_a's observed previously.

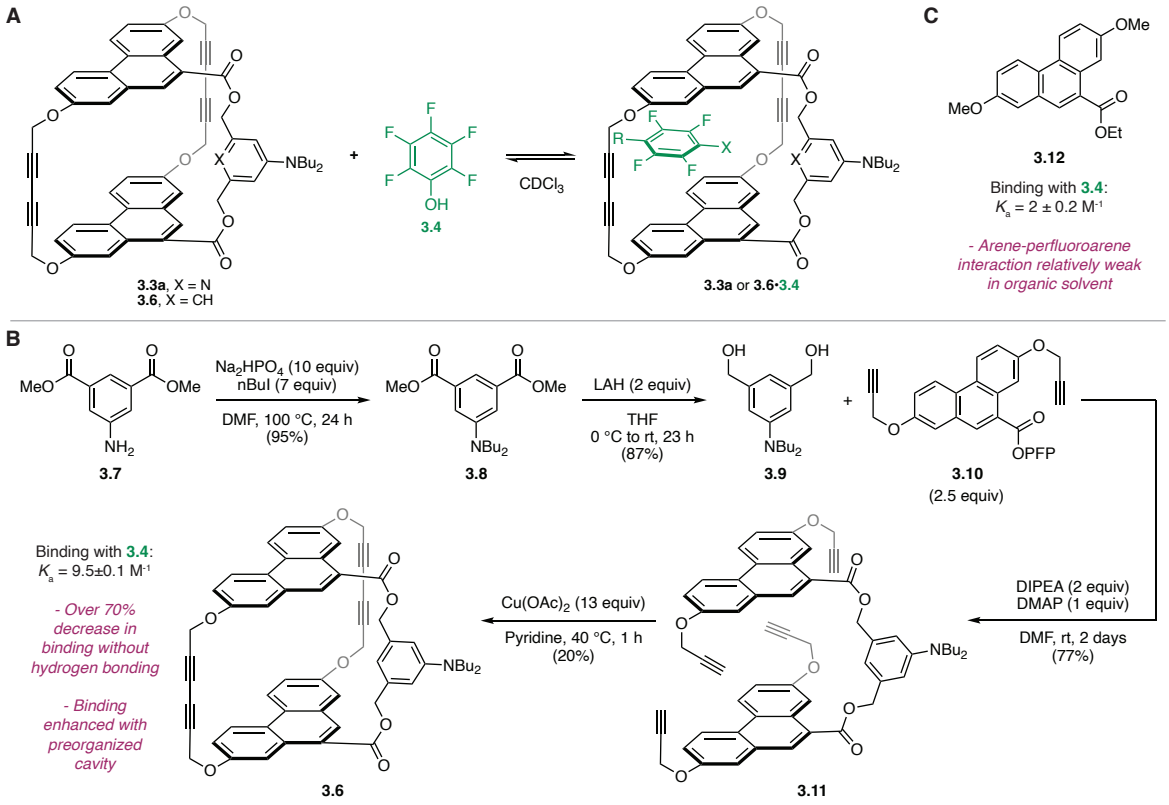

Figure 3.3 Non-hydrogen bonding control experiments. (A) Equilibrium being measured in experiments between **3.4** and phenanthrene hosts. (B) Synthesis of non-hydrogen bonding control host **3.6** by Erika Aguiluz Ramirez. Binding result with **3.4** given. (C) Phenanthrene-only "host" and binding results with **3.4** to probe contribution of both cavity complementarity and hydrogen bonding.

To test the arene-perfluoroarene interaction in $CDCl_3$ without either a rigid cavity or a hydrogen-bond interaction, Dr. Gina Lee measured the binding strength between a phenanthrene precursor, **3.12**, also synthesized by Dr. Margeaux Miller, and **3.4** (Figure 3.3C). Binding with **3.4** was only about 2 M^{-1}, barely above the detectable limit of K_a's in organic solvent.[23] The arene-perfluoroarene interaction is not strong in organic solvent, as further shown in this experiment, and the recognition of guests by host **3.3** in organic solvent is most dependent on hydrogen bonding, with a boost from an appropriately sized and shaped cavity.

3.3.3 Exploring an expanded scope of guests

Following control studies with respect to the host, we decided to expand our suite of guests to explore the influence of guest contributions on binding strength. In addition to guests nitrophenol **3.2** and pentafluorophenol **3.4**, we considered fluorinated phenols **3.13** and **3.14**, with electron-withdrawing groups expected to increase the hydrogen-bond donation ability of the guests (Figure 3.4A).[29] There was a marked increase in binding with **3.13** for both **3.3a** and **3.3b**, with K_a's ranging from 2.3–3.2x10^4 M^{-1} (Figure 3.4B). This suggests a stronger hydrogen bonding interaction, though there may also be favorable dispersion interactions between the amide substituent and the phenanthrene faces.[11] Given that both isomers of host **3.3** bound **3.4** or **3.13** with similar magnitude, we continued forward with **3.3a**, which gave slightly higher affinities for both guests. Fluorinated nitrophenol **3.14**, the perfluorinated analog of **3.2**, was expected to also show an increase in binding. Indeed, we observed binding over 10^5 M^{-1}, though with high error. This range is typically considered the upper limit for determining K_a values by NMR titrations, which likely contributes to the high error.[30–32] Together, these data show that modulating hydrogen bond strength through substitution *para* to the hydrogen-bond donating –OH is reflected in overall binding strength with host **3.3**.

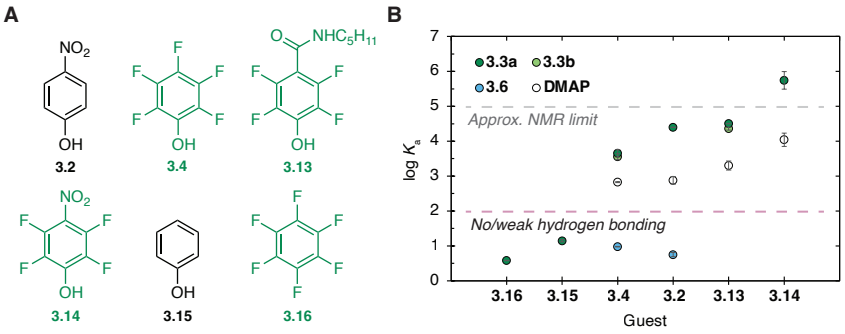

Figure 3.4 Summary of binding results. (A) Complete suite of guests, with non-fluorinated and non-hydrogen bonding representatives. (B) Log-scale plot of measured K_a values colored by host, with regions of interest noted. Error bars represent standard deviation of at least two replicates.

We also considered non-fluorinated phenol **3.15** and hexafluorobenzene **3.16**, a non-hydrogen-bond donating perfluorinated guest (Figure 3.4A). With phenol **3.15**, binding was just above 10 M^{-1}; this orders-of-magnitude decrease suggests the importance of substitution of phenolic guests for binding (Figure 3.4B). Similarly, binding with **3.16** was low, under 10 M^{-1}, though still above the NMR detection limit of 1, suggesting interactions in the cavity still occur. This was confirmed through crystals of host–guest complexes grown by Prairie Hammer, which were suitable for X-ray crystallography (Scheme 3.1).

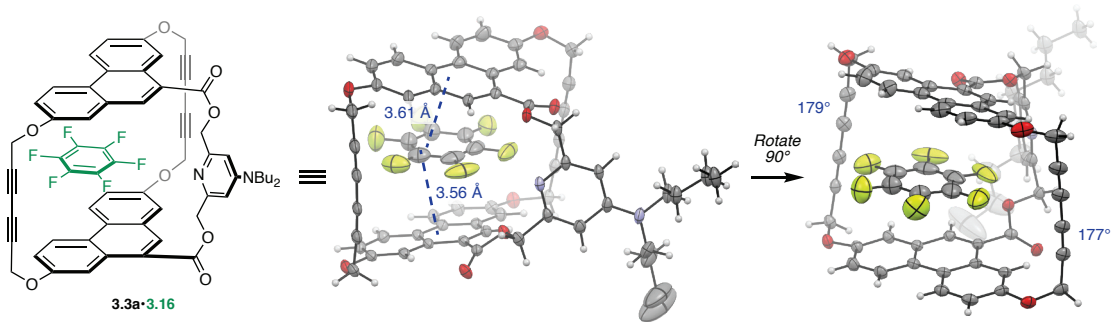

Scheme 3.1 Crystal structure of complex **3.3a•3.16**. Ellipsoids are set at 50% probability.

A summary of binding affinities and energies with various guests and hosts **3.3a**, **3.3b**, **3.6**, and DMAP is plotted in Figure 3.4B and listed in Table 3.1. We tested if control host **3.6** interacted with **3.2** without hydrogen bonding and found a K_a below 10 (Table 3.1, entry 11). This K_a was lower than **3.6** with pentafluorophenol **3.4** (entry 12), the opposite trend from what was observed with main host **3.3a** (entries 3–4). However, we caution against any conclusions regarding cavity interactions between guests with control host **3.6**, as due to guest solubility issues and the low K_a, saturation could not be reached in an experiment with nitrophenol **3.2**.

Entry	Host	Guest	K_a in $CDCl_3$ (M^{-1})	ΔG (kcal•mol^{-1})
1	**3.5**	**3.2**	$(1.1 \pm 0.1)x10^4$ [a]	-5.5 ± 0.06
2	**3.5**	**3.4**	$(7.0 \pm 0.6)x10^2$ [a]	-3.9 ± 0.05
3	**3.3a**	**3.2**	$(2.5 \pm 0.04)x10^4$	-6.0 ± 0.009

4	**3.3a**	**3.4**	$(4.5 \pm 1.1)\text{x}10^3$	-5.0 ± 0.1
5	**3.3b**	**3.4**	$(3.6 \pm 0.7)\text{x}10^3$	-4.8 ± 0.1
6	**3.3a**	**3.13**	$(3.2 \pm 0.07)\text{x}10^4$	-6.1 ± 0.01
7	**3.3b**	**3.13**	$(2.3 \pm 0.2)\text{x}10^4$	-5.9 ± 0.06
8	**3.3a**	**3.14**	$(5.5 \pm 3.2)\text{x}10^5$ [b]	-7.8 ± 0.3
9	**3.3a**	**3.15**	14 ± 1	-1.6 ± 0.04
10	**3.3a**	**3.16**	3.8 ± 0.05	-0.80 ± 0.008
11	**3.6**	**3.2**	5.6 ± 0.8	-1.0 ± 0.09
12	**3.6**	**3.4**	9.5 ± 0.1	-1.3 ± 0.006
13	**DMAP**	**3.2**	$(7.6 \pm 1.9)\text{x}10^2$	-3.9 ± 0.1
14	**DMAP**	**3.4**	$(7.2 \pm 0.8)\text{x}10^2$	-3.9 ± 0.07
15	**DMAP**	**3.13**	$(2.0 \pm 0.6)\text{x}10^3$	-4.5 ± 0.2
16	**DMAP**	**3.14**	$(1.1 \pm 0.5)\text{x}10^4$	-5.5 ± 0.3
17	**3.12**	**3.4**	2 ± 0.2	-0.5 ± 0.04
18	**3.12**	**3.16**	< 1 [c]	> 0

Table 3.1 Summary of K_a values in $CDCl_3$ and calculated binding energies. Values obtained in at least duplicate unless otherwise stated. [a]K_a determined from single experiment. [b]Guest displays 1:2 binding; $K_{a,1}$ given in table. [c]Below NMR detection limit.

With regards to hydrogen bonding interactions alone, guests **3.13** and **3.14** show similar trends in binding with DMAP as with **3.3a**, though about an order of magnitude lower in each case, which we attribute to the lack of a rigid cavity (Figure 3.4B; Table 3.1 entries 15–16). We also tested phenanthrene block **3.12** with hexafluorobenzene **3.16** but found the K_a to be below the NMR limit (Table 3.1, entry 18). The slight increase observed between pentafluorophenol **3.4** and **3.12** (Table 3.1, entry 17) suggests some benefit to arene-perfluoroarene interaction from aromatic substitution, which we have observed previously.[23]

3.3.4 Observations of 1:2 binding with fluorinated phenols

In some binding experiments with strong hydrogen-bond donating guests, we saw changes in ^{1}H NMR titrations at higher equivalents of guest that we considered indicative of 1:2 binding. This was particularly apparent in the spectra of host titrated with tetrafluoronitrophenol **3.14**, where the aromatic proton peak of the pyridine linker and the adjacent methylene proton peaks switch from shifting upfield to downfield beyond 1 equivalent of guest (Figure 3.5A,B). This is also clear when plotting proton shifts against amount of guest: the peaks on or adjacent to the pyridine linker give sigmoidal curves, while phenanthrene protons trend in a single direction, leveling out beyond 1 equivalent (Figure 3.5C). The broadening of host aromatic peaks when less than 1 equivalent of guest is present has been observed with other hosts with high K_a values.[33] The recorded shifts failed to fit a 1:1 binding model but gave more reasonable values in a 1:2 model, though with high error (Figure 3.5A). We again attribute the high error to reaching the upper NMR limit for accurate K_a detection (~10^5 M^{-1}). We also observed similar shifts in the spectra of titration experiments with amide guest **3.13** beyond 2 equivalents, and with pentafluorophenol **3.4** beyond 5 equivalents; we were able to fit those to 1:2 binding models as well (Figure 3.5D).

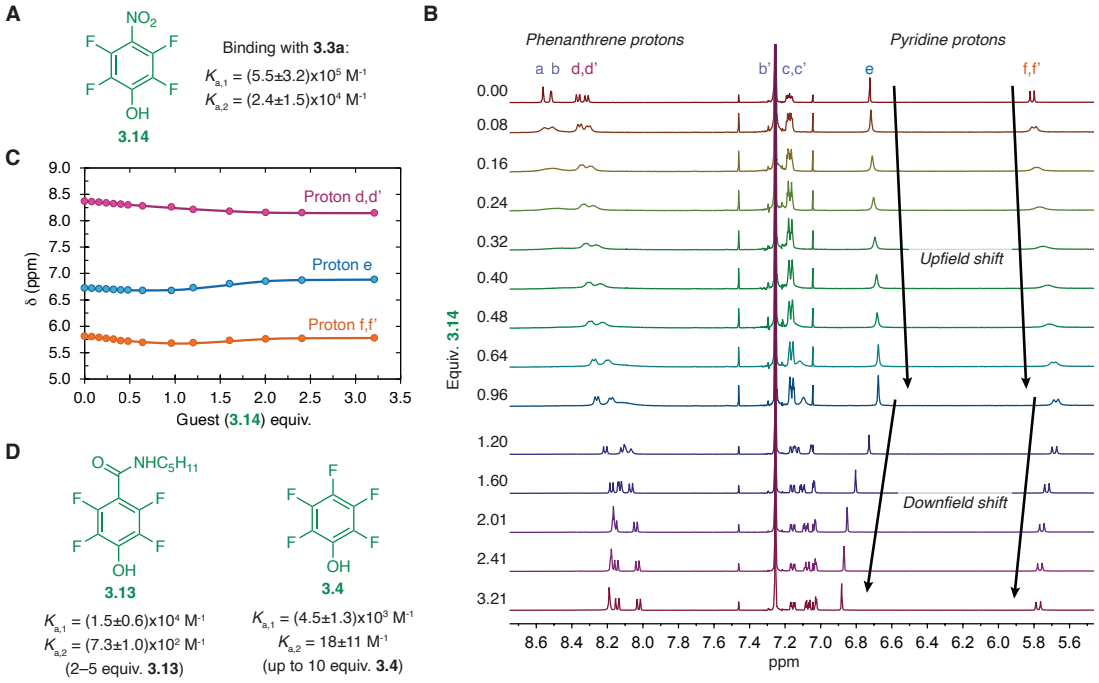

Figure 3.5 Evidence of 1:2 binding between **3.3a** and fluorinated phenols. (A) Structure of guest **3.14** and results of fitting ^{1}H NMR titration data to 1:2 model. (B) Stacked ^{1}H NMR spectra from a titration of **3.3a** with **3.14** with changes in shift direction highlighted. (C) Plot of chemical shifts (from spectra in [B]) for phenanthrene (d,d'), pyridine (e), and pyridyl methylene (f,f') protons as amount of guest increases; protons in/near pyridine display sigmoidal binding. (D) Results of 1:2 model fitting for other guests at higher equivalents that also displayed changes in ^{1}H NMR shift direction.

Fortunately, crystal structures of a complex between **3.3a** and **3.4**, again grown by Prairie Hammer, revealed the likely nature of the 1:2 binding event (Scheme 3.2). In the crystalline form, the cavity-bound guest appears to be hydrogen-bonded to another equivalent of guest that is located outside the cavity, with a distance of 2.59 Å. The exterior guest appears to form a second hydrogen bond, at a distance of 2.61 Å, with the pyridine nitrogen on the host linker. A similar binding phenomenon was observed in a 1:2 crystal published by the Whitlock group. There, a modified version of the original naphthalene host **3.1** interacts with two equivalents of a *p*-nitrophenol guest bearing a cyano substituent. One guest molecule is cavity-bound while another is outside, with an –OH directed toward the pyridine linker. The authors suggested the

second equivalent of guest was merely a crystallization artifact, but our NMR experiments suggest such 1:2 complexes can form in solution as well. Because phenanthrene proton signals stop shifting after one equivalent of guest is bound, we propose the first binding event occurs within the host cavity, while the second event is outside, as evidenced by the shift in direction by the pyridine linker protons.

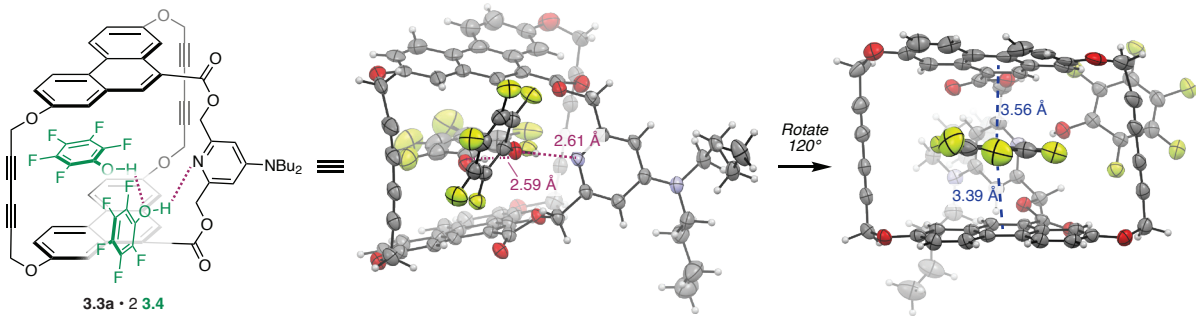

Scheme 3.2 Crystal structure of host **3.3a** showing interactions with 2 molecules of guest **3.4**. Ellipsoids set at 50% probability.

Curiously, we did not see evidence of 1:2 binding with higher equivalents of non-fluorinated nitrophenol **3.2**, despite it binding host **3.3a** with nearly the same affinity as **3.13**. It is possible that the smaller guest is able to form a more ideal hydrogen bond in the phenanthrene cavity, while the fluorinated guests cannot adopt the same, optimal geometry, so a second hydrogen bonding event occurs to maximize favorable interactions. Further investigation is needed to understand this distinction, and it is likely computation will be insightful.

We also observed possible trends with pK_a values (Figure 3.6A). In general, binding affinities increased as pK_a decreased (Figure 3.6B). However, there appeared to be separate trends emerging within guest groupings (fluorinated versus non-fluorinated phenols). This may be reflective of cavity differences as discussed earlier. Anslyn and co-workers have shown that basicity is not necessarily a key determinant of hydrogen-bond driven binding, but trends can arise among guests that are similar in shape and interaction with host.[34] Curiously, the

fluorinated phenols, all with lower pK_a values than that of *p*-nitrophenol **3.2**, are also the ones with observed 1:2 binding, though the role of acidity in this observation, if any, is unclear. Future work may involve expanding the scope of phenols to encompass a larger pK_a range and include more non-fluorinated phenols to detect any patterns.

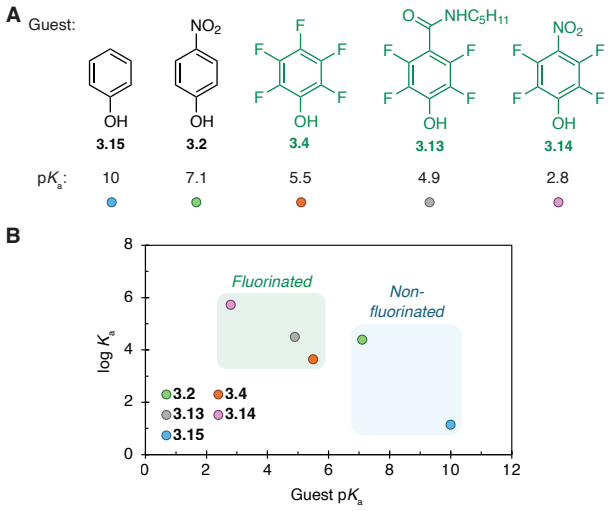

Figure 3.6 Exploring potential trends between guest pK_a and binding affinity, K_a. (A) Structures of phenolic guests and pK_a values. Value for **3.13** determined by Prairie Hammer. (B) Plot of logK_a versus pK_a.

3.4 Conclusion

This work analyzes the central interplay between host and guest shape complementarity and the strength of hydrogen bonding in organic solvent. Through comparisons with phenanthrene- and naphthalene-based hosts, in addition to DMAP as a small-molecule, hydrogen-bond only control, we show that despite hydrogen bonding being the main driver of strong recognition of electron-deficient guests (fluorinated and other), having a preorganized aromatic cavity can boost these affinities by an order of magnitude. We also showed that arene-perfluoroarene interactions are weak in organic solvent, and in contrast to our other work with host **3.3** in aqueous solutions, recognition of perfluoroaromatics is determined primarily by

cavity shape. We have also observed 1:2 binding in the case of fluorinated phenolic guests and future work could explore a potential relationship to guest acidity.

Future work will explore additional linker modifications that will allow for more fine-tuning of guest interactions, building on the systematic knowledge here. Other linker modifications may expand the utility of this host platform for future biological labeling studies; indeed, one such direction is explored in Chapter 4. In addition, further probing of the trends in binding affinity between fluorinated and non-fluorinated phenols, or even alternative aromatic hydrogen-bonding donating guests may be revealing. Finally, exploration of alternative aromatic scaffolds beyond naphthalene and phenanthrene will likely open doors to new guests and new types of interactions. A potential alternative scaffold, olympicene, will be explored in Chapters 5 and 6.

3.5 Experimental Procedures

Chemical reagents were purchased from Alfa Aesar, Sigma-Aldrich, Fisher Scientific, or Acros Organics and used without purification. Compounds were weighed on a Sartorius ENTRIS224-1S Analytical Balance (220 x 0.0001 g) or a Sartorius MSE6.6S-000-DM Cubis Micro Balance. NMR spectra were recorded on Bruker NEO-600 (^{1}H) or Bruker AV-500 (^{1}H) and processed with MestReNova software. Samples were taken in deuterated chloroform ($CDCl_3$) and NMR peaks were calibrated using residual non-deuterated solvent ($CHCl_3$ at 7.26 ppm ^{1}H NMR).

3.5.1 Synthetic abbreviations and chemical formulas

n-Butyliodide (*n*BuI); Chloroform ($CHCl_3$); Copper acetate ($Cu[OAc]_2$); Diisopropylethylamine (DIPEA); 4-Dimethylaminopyridine (DMAP); Dimethylformamide (DMF); Disodium

phosphate (Na_2HPO_4); Lithium aluminum hydride (LAH); Megahertz (MHz); Pentafluorophenyl (PFP); Tetrahydrofuran (THF); Trifluoroacetic acid (TFA).

3.5.2 General host–guest titration/K_a determination procedures

The host was measured on an analytical microbalance (when > 20 mg of guest were needed, an analytical balance was used instead). Host stock solutions were prepared with $CDCl_3$ neutralized by passing through aluminum oxide (alumina; basic, 50–200 μm, 60 Å pores [Acros Organics]) and dried over 4 Å molecular sieves.[35] Concentrations of host stock solutions were made below the solubility limit of the host. Guest stock solutions were prepared in basified $CDCl_3$. Stocks were added to NMR tubes using gas-tight Hamilton syringes. Preliminary titrations and the BindSim program (http://app.supramolecular.org/bindsim/) were used to determine the approximate equivalents of guest needed for saturation.[32] Ideally, > 70% saturation was achieved. Binding data were fit using BindFit (http://app.supramolecular.org/bindfit/).[31,32] Experiments were performed in duplicate unless otherwise noted.

3.5.3 Equations used

Average K_a:

$$K_{a,avg} = \frac{K_{a,1} + K_{a,2} + \ \ldots K_{a,n}}{n}$$

K_a standard deviation (error):

$$SD = \sqrt{\frac{(K_{a,1} - K_{a,avg})^2 + (K_{a,1} - K_{a,avg})^2 + \cdots (K_{a,n} - K_{a,avg})^2}{n}}$$

Binding energy:

$$\Delta G = -RTlnK_a$$

Binding energy error:

$$\text{Error} = \sqrt{\left(\frac{\Delta K_a / K_a}{\ln (K_a)}\right)^2} * \Delta G$$

3.5.4 ^{1}H NMR titrations

Complex of **3.3b** and **3.4** in $CDCl_3$ (KMH-V-014)

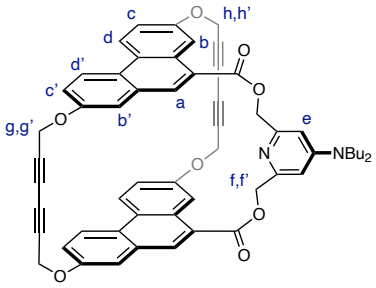

Host: **3.3b**

[H] = 0.84 mM

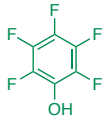

Guest: **3.4**

[G] = 0–7.3 mM

proton	K_a (bindfit)
a	4480 ± 8%
b	3655 ± 8%
d,d'	2971 ± 14%
e	6988 ± 17%
f,f'	3373 ± 7%
global fitting	4301 ± 4%

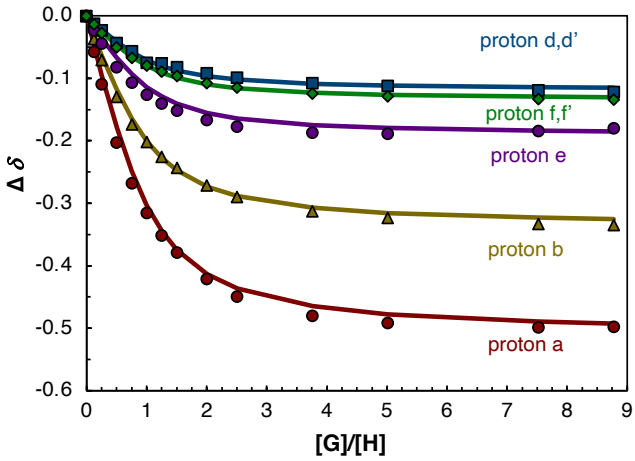

Trial 1 (MAM-IV-244) 0.10 to 7.4 equiv	Trial 2 (KMH-V-014) 0.13 to 8.8 equiv
2870 ± 5%	4301 ± 4%

$K_{a,avg}$ = 3590 ± 3%

$K_{a,avg}$ ± SD = 3590 ± 720

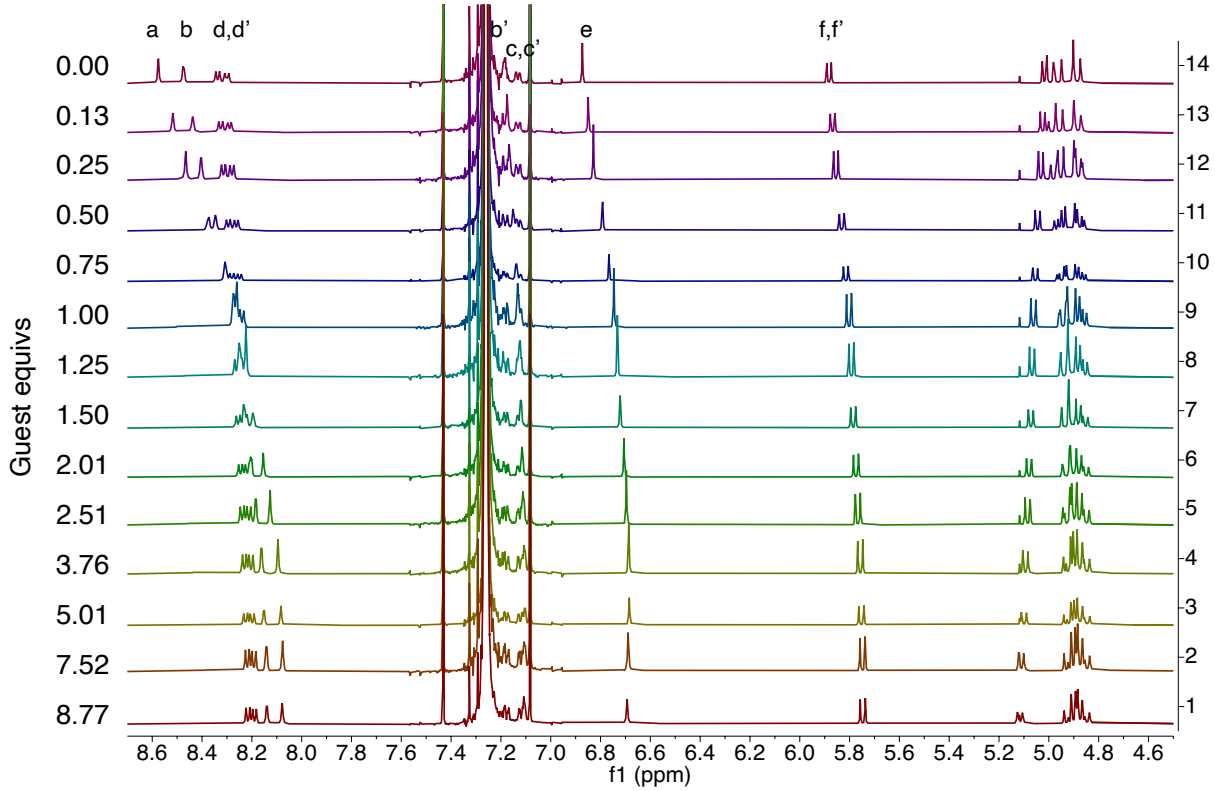

Complex of **DMAP** and **3.2** in $CDCl_3$ (KMH-II-005)

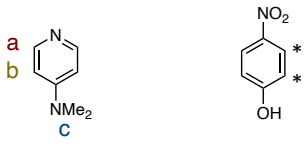

Host: **DMAP**

[H] = 2.1 mM

Guest: **3.2**

[G] = 0–4.9 mM

proton	K_a (bindfit)
b	862 ± 2%
c	732 ± 2%
global fitting	806 ± 1%

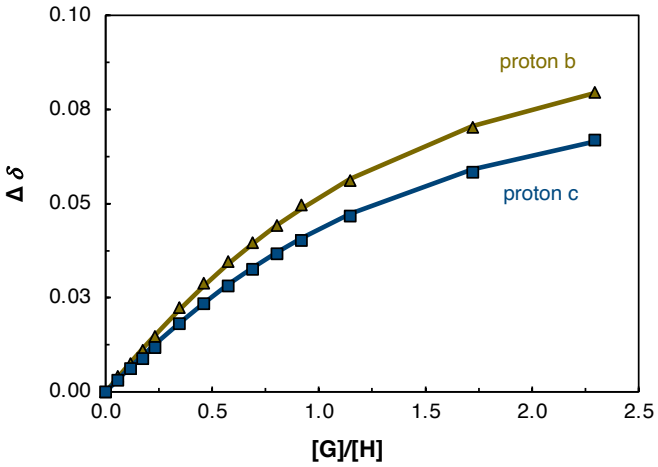

Trial 1	Trial 2	Trial 3	Trial 4	Trial 5	Trial 6
0.06–2.29	0.06–2.34	0.06–2.30	0.06–2.20	0.05–2.15	0.05—2.15
806 ± 1%	980 ± 6%	400 ± 2%	826 ± 2%	656 ± 1%	890 ± 3%

$K_{a,avg}$ = 760 ± 2%

$K_{a,avg}$ ± SD = 760 ± 190

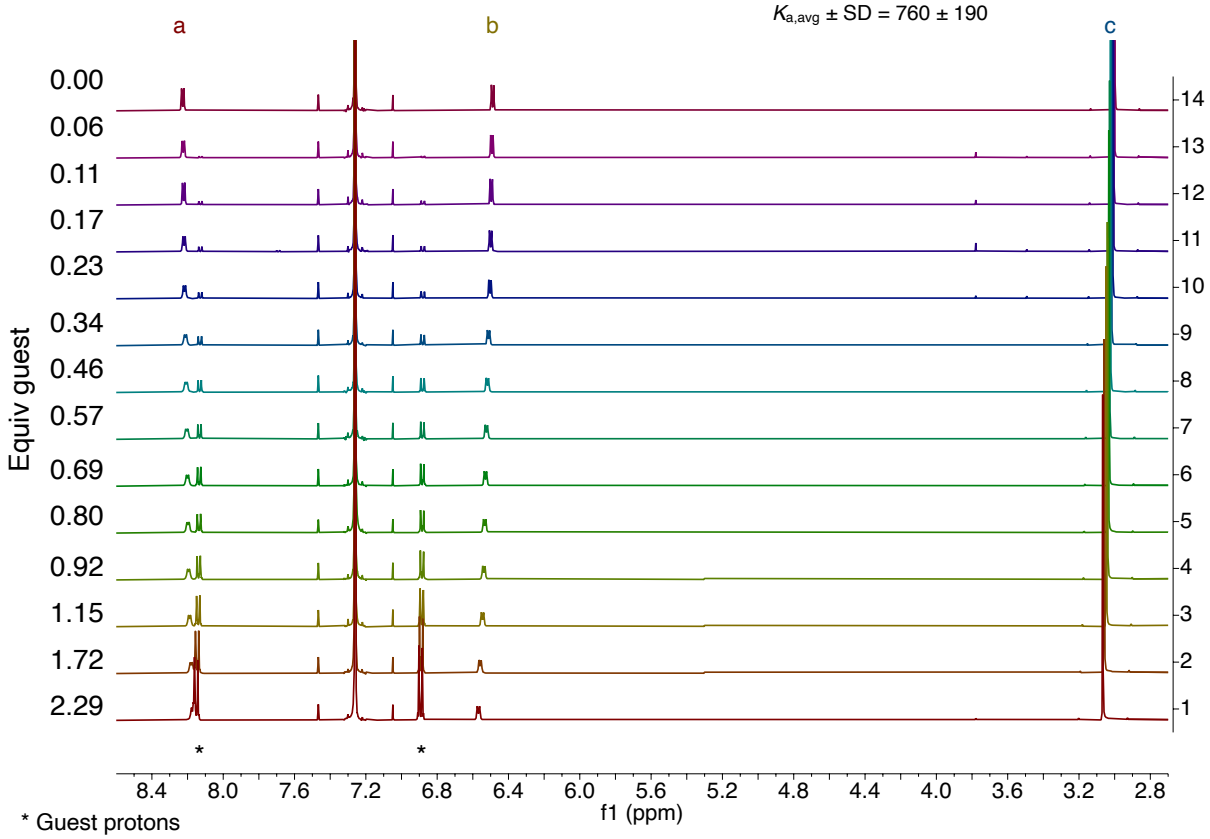

* Guest protons

Complex of **DMAP** and **3.4** in $CDCl_3$ (KMH-V-016)

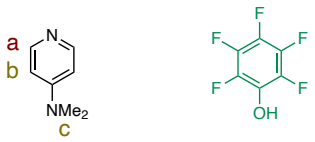

Host: **DMAP**

[H] = 2.1 mM

Guest: **3.4**

[G] = 0–23 mM

proton	K_a (bindfit)
b	627 ± 4%
c	742 ±5%
global fitting	684 ± 3%

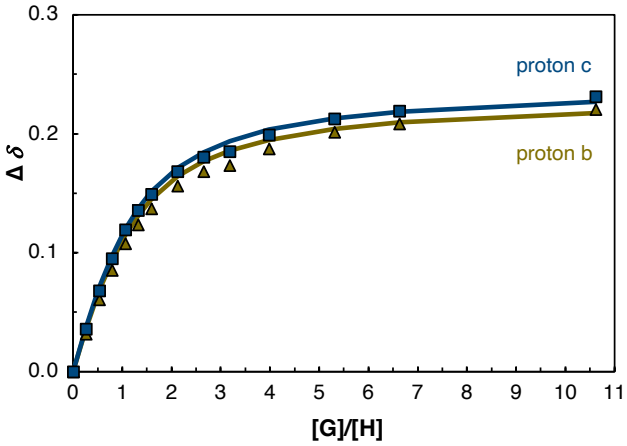

Trial 1	Trial 2	Trial 3
0.07–1.81	0.07–2.70	0.27–10.6
640 ± 7%	690 ± 6%	680 ± 3%

$K_{a,avg}$ = 670 ± 3%

$K_{a,avg}$ ± SD = 670 ± 22

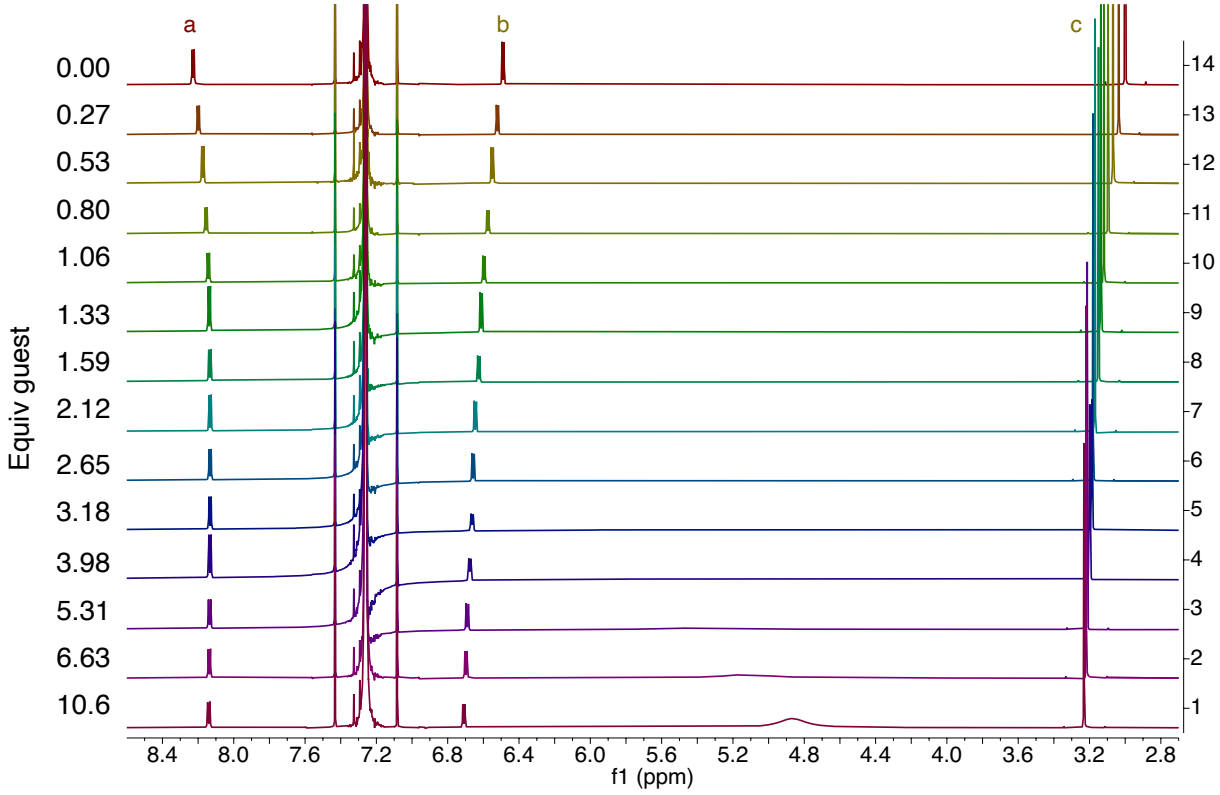

* Guest protons

Complex of **3.6** and **3.4** in $CDCl_3$ (KMH-II-057)

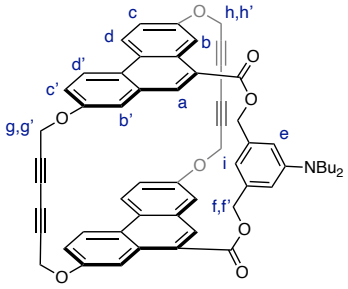

Host: **3.6**
[H] = 0.84 mM

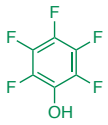

Guest: **3.4**
[G] = 0–252 mM

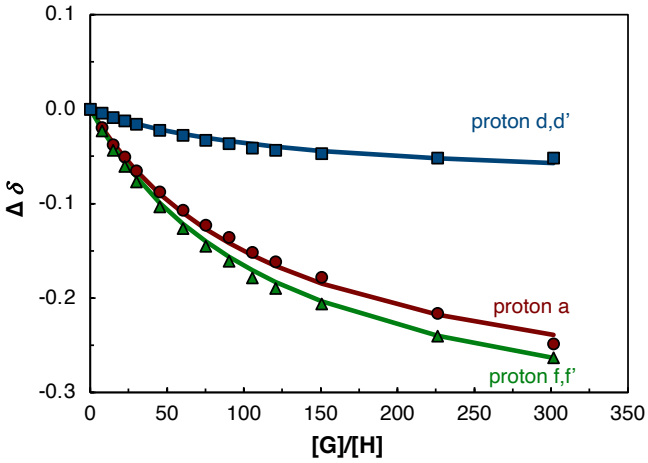

proton	K_a (bindfit)
a	7.8 ± 3%
d,d'	11.0 ± 1%
f,f'	14.4 ± 8%
global fitting	9.6 ± 2%

Trial 1 7.5 to 301 equiv	**Trial 2** 7.7 to 309 equiv
9.6 ± 2%	9.4 ± 2%

$K_{a,avg}$ = 9.5 ± 1%
$K_{a,avg}$ ± SD = 9.5 ± 0.1

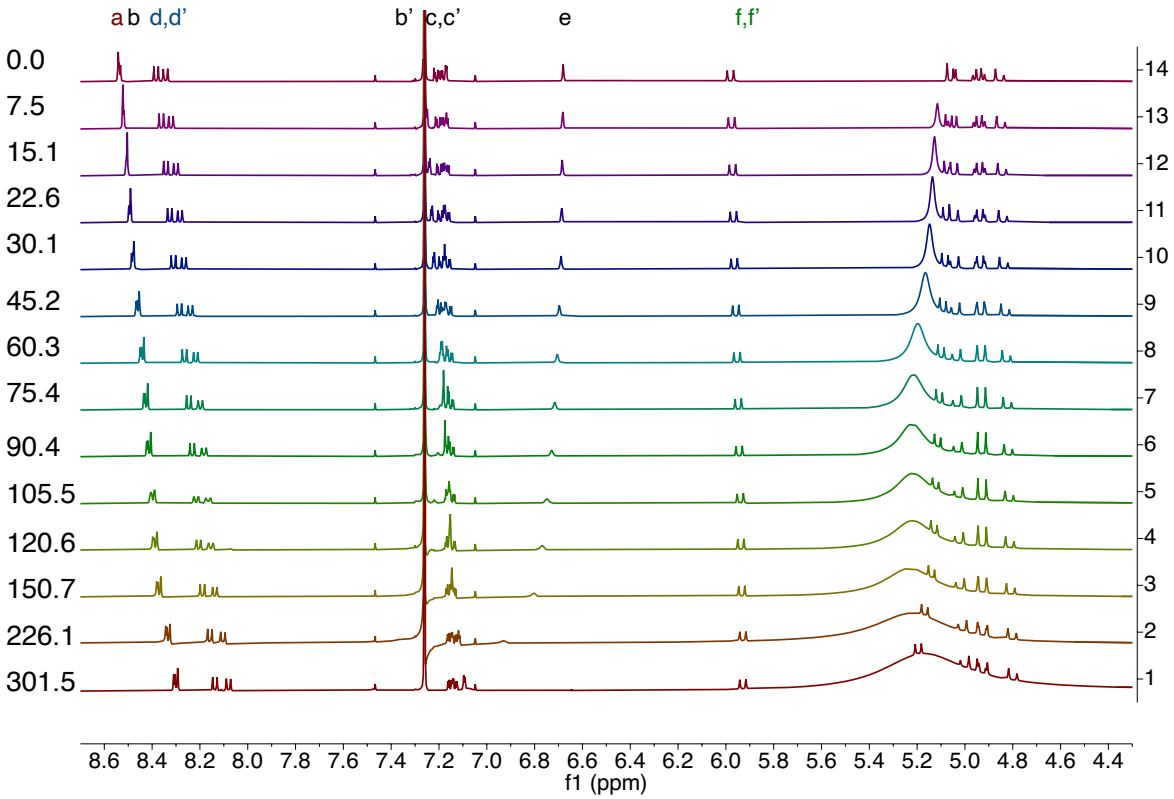

Complex of **3.6** and *p*-nitrophenol (**3.4**) in $CDCl_3$ (KMH-II-061)

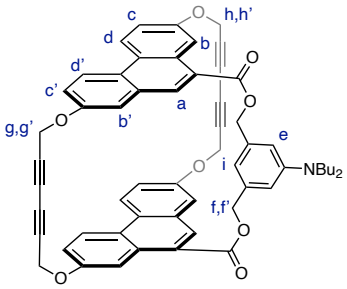

Host: **3.6**

[H] = 0.84 mM

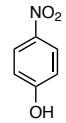

Guest: **3.2**

[G] = 0–46 mM

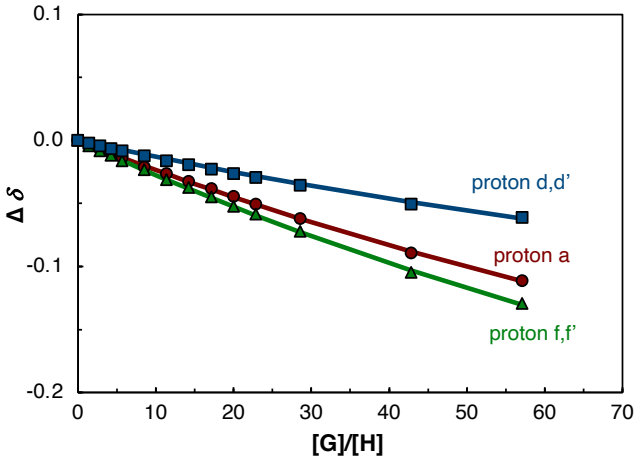

proton	K_a (bindfit)
a	5.1 ± 0.8%
d,d'	5.2 ± 1%
f,f'	8.0 ± 1%
global fitting	5.5 ± 0.5%

Trial 1 1.4 to 57 equiv	**Trial 2** 1.5 to 60 equiv	**Trial 3** 1.4 to 58 equiv
5.5 ± 0.5%	4.6 ± 2%	6.58 ± 1%

$K_{a,avg}$ = 5.6 ± 0.7%

$K_{a,avg}$ ± SD = 5.6 ± 0.8

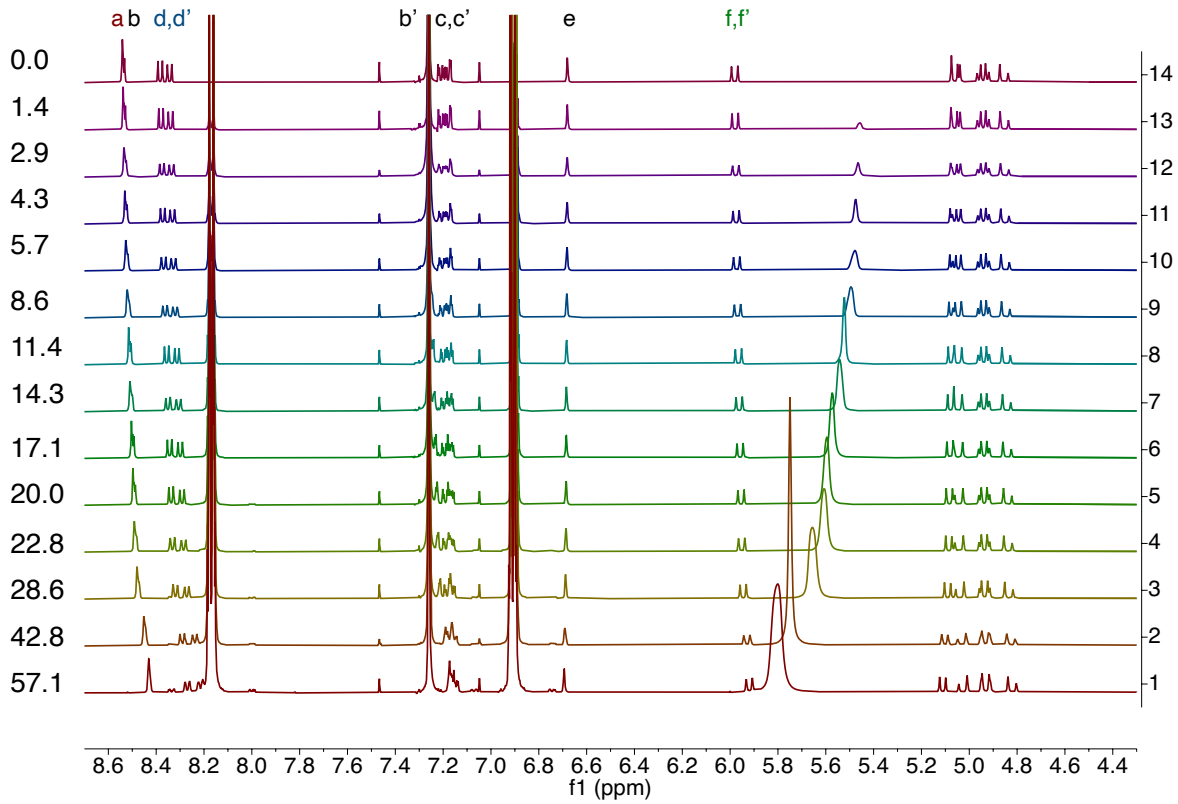

Complex of **DMAP** and **3.13** in $CDCl_3$ (KMH-II-020)

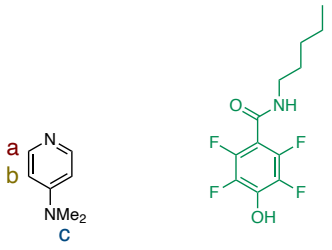

Host: **DMAP**

[H] = 2.1 mM

Guest: **3.13**

[G] = 0–5.1 mM

proton	K_a (bindfit)
a	1571 ± 7%
b	2018 ± 9 %
c	2406 ± 9%
global fitting	2111 ± 4%

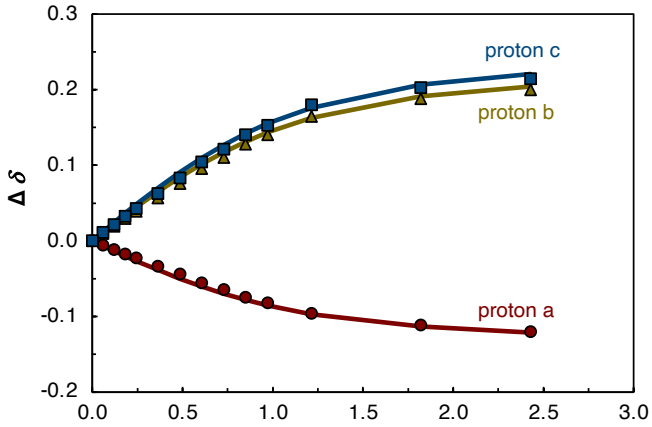

Trial 1	Trial 2	Trial 3	Trial 4	Trial 5	Trial 6
0.06–2.43	0.06—2.42	0.06—2.42	0.06–2.43	0.06–2.42	0.06—2.42
2111 ± 4%	1453 ± 5%	997 ± 6%	2398 ± 5%	2777 ± 6%	2285 ± 5%

$K_{a,avg}$ = 2004 ± 2%

$K_{a,avg}$ ± SD = 2000 ± 600

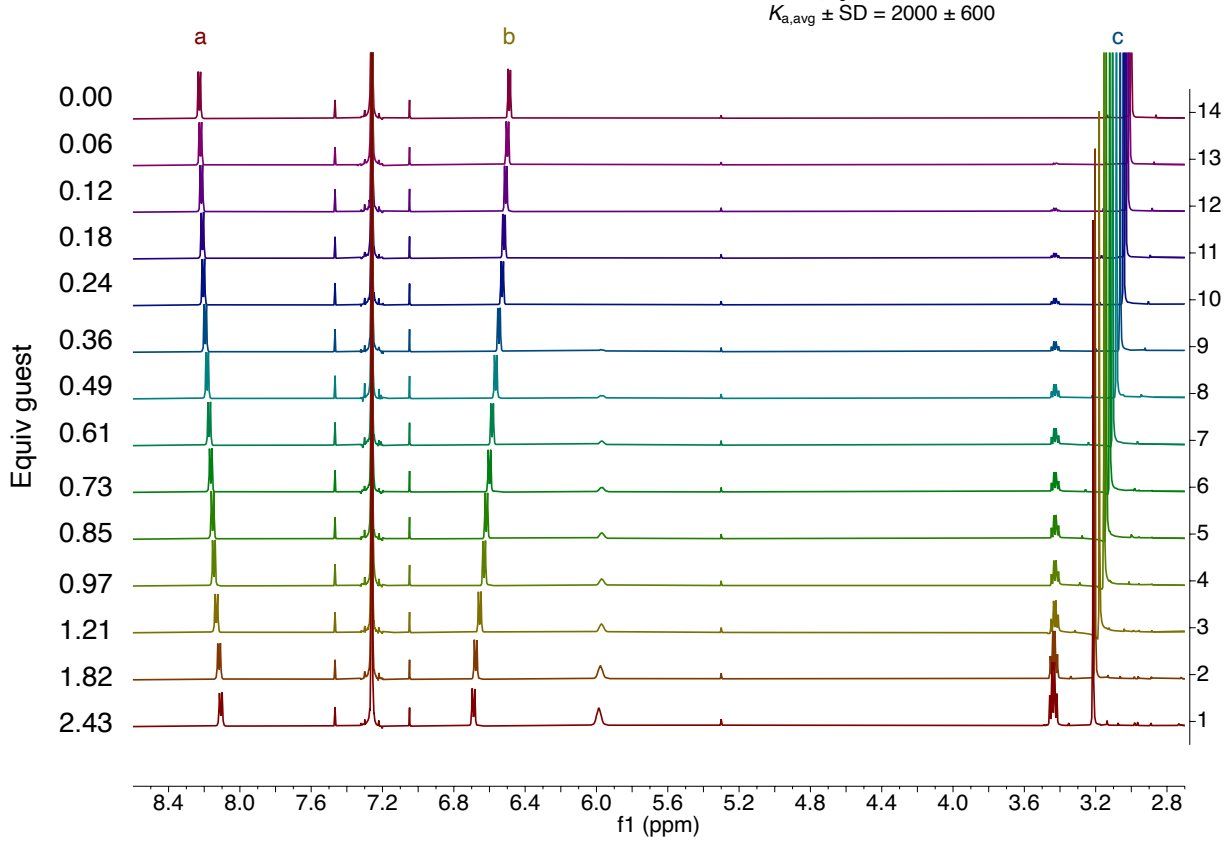

Complex of **DMAP** and **3.14** in $CDCl_3$ (KMH-II-027)

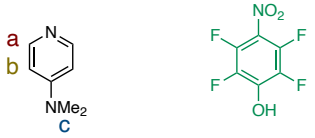

Host: **DMAP**

[H] = 2.1 mM

Guest: **3.14**

[G] = 0–4.7 mM

proton	K_a (bindfit)
a	8381 ± 35%
b	7452 ± 33%
c	11309 ± 41%
global fitting	9088 ± 19%

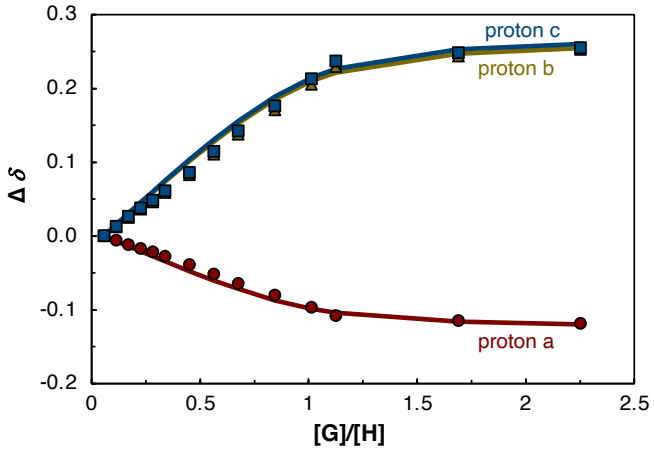

Trial 1 0.2–12.2 equiv	Trial 2 0.06—2.25 equiv	Trial 3 0.06—2.25 equiv	Trial 4 0.06–2.25 equiv	Trial 5 0.06–2.25 equiv
6400 ± 12%	7100 ± 19%	9100 ± 19%	14000 ± 25%	19000 ± 31%

$K_{a,avg}$ = 11000 ± 13%

$K_{a,avg}$ ± SD = 11000 ± 4800

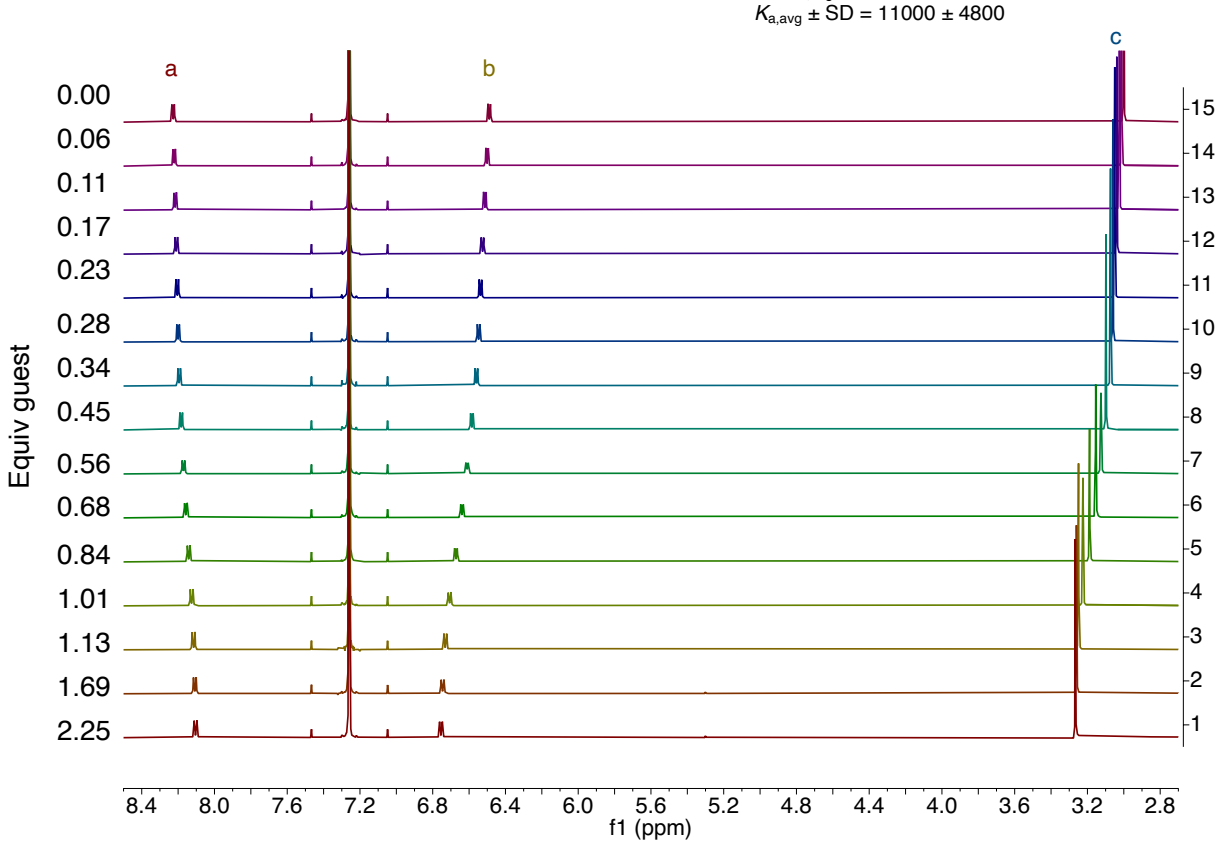

Complex of **3.3b** and **TFA** in $CDCl_3$ (KMH-V-020)

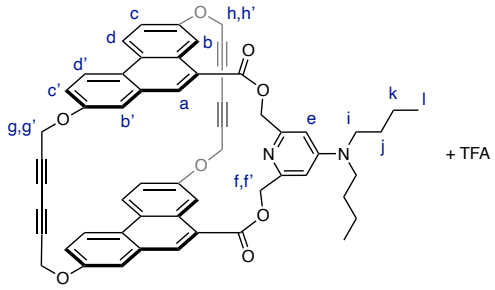

Host: **3.3b**

[H] = 0.88 mM

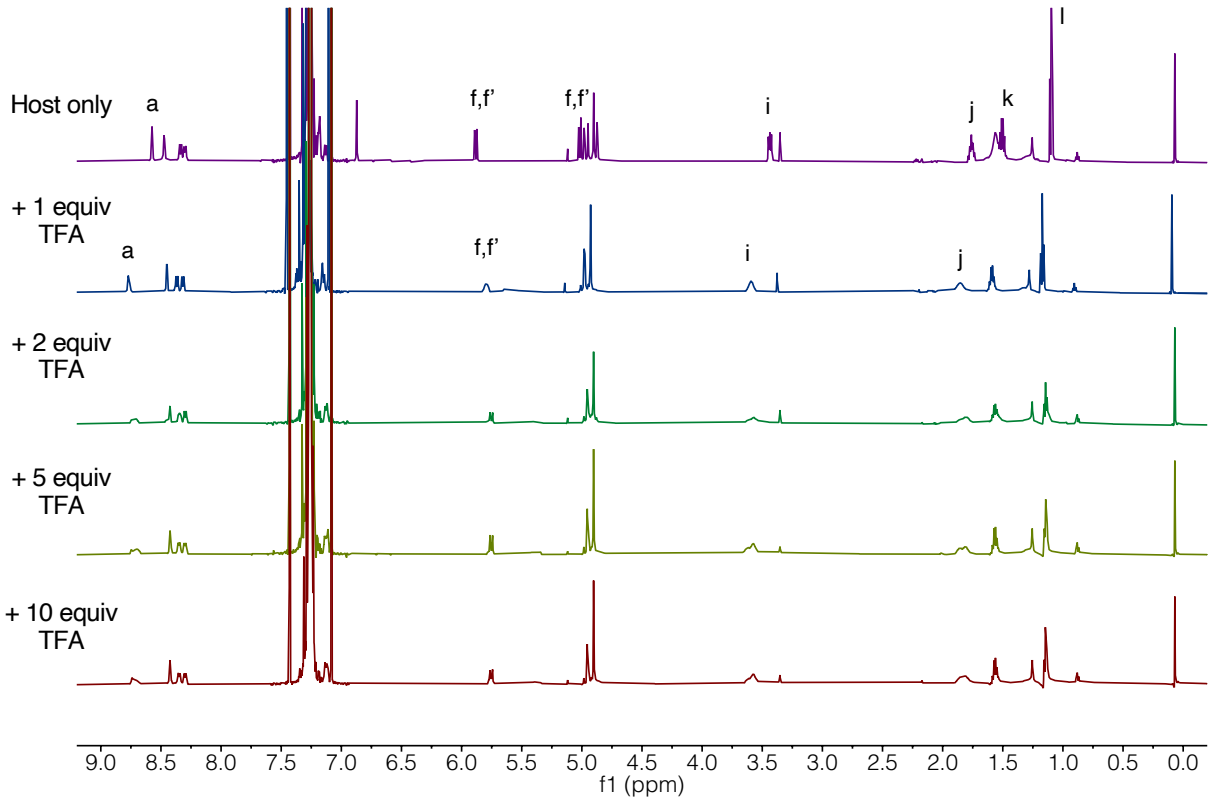

H_a, H_e, H_i, H_j, and H_k shift differently upon protonation compared to when bound to guest.

3.5.5 All NMR titration trials with BindFit links

Meso phenanthrene (**3.3b**) + pentafluorophenol (**3.4**)			
Trial	Notebook	K_a in $CDCl_3$ (M^{-1})	BindFit URL
1	MAM-IV-244	2870 ± 5%	http://app.supramolecular.org/bindfit/view/0d107f0c-daaf-493d-9bac-796bcdf758d9
2	KMH-V-014	4301 ± 4%	http://app.supramolecular.org/bindfit/view/ee7b7222-17a7-42b6-98a9-515a13e55b9e
DMAP + *p*-nitrophenol (**3.2**)			
Trial	Notebook	K_a in $CDCl_3$ (M^{-1})	BindFit URL
1	KMH-II-005	806 ± 1%	http://app.supramolecular.org/bindfit/view/195443a7-3aab-4fb3-8fa6-a8bc597313aa
2	GL_04_228	980 ± 6%	http://app.supramolecular.org/bindfit/view/17d5d395-edf4-4cb5-b160-1648bdba23b6
3	GL_04_241	400 ± 2%	http://app.supramolecular.org/bindfit/view/312acbaf-517b-4389-b4bc-7325ae06c301
4	KMH-II-007	826 ± 2%	http://app.supramolecular.org/bindfit/view/dcdd682c-a074-43dc-8441-0ba584cc06d1
5	KMH-II-011	656 ± 1%	http://app.supramolecular.org/bindfit/view/feacb3f6-0d3d-4457-b4c8-ec34d1f25168
6	KMH-II-012	890 ± 3%	http://app.supramolecular.org/bindfit/view/7c1a88ea-4d94-49ca-9573-bfebc3e8fac7
DMAP + pentafluorophenol (**3.4**)			
Trial	Notebook	K_a in $CDCl_3$ (M^{-1})	BindFit URL
1	GL_04_228	640 ± 7%	http://app.supramolecular.org/bindfit/view/87b04c56-b1d9-43de-b88a-1fd777c005a1
2	GL_04_244	690 ± 6%	http://app.supramolecular.org/bindfit/view/cc37fa5e-0939-4462-b229-a009554b9db5
3	KMH-V-016	680 ± 3%	http://app.supramolecular.org/bindfit/view/2b50dcd6-be8e-41ec-85cf-a75bc39909b5
Control host (**3.6**) + pentafluorophenol (**3.4**)			
Trial	Notebook	K_a in $CDCl_3$ (M^{-1})	BindFit URL
1	KMH-II-057	9.6 ± 2%	http://app.supramolecular.org/bindfit/view/071966b37-1b6b-4c34-9a6d-d909f7e9ab28
2	KMH-II-060	9.4 ± 2%	http://app.supramolecular.org/bindfit/view/c5f506ed-cab2-4df9-96d8-7ffc19b61efd
Control host (**3.6**) + *p*-nitrophenol (**3.2**)			
Trial	Notebook	K_a in $CDCl_3$ (M^{-1})	BindFit URL
1	KMH-II-061	5.5 ± 0.5%	http://app.supramolecular.org/bindfit/view/88c05c9b-4248-4549-b59c-57660c9a13a0
2	KMH-II-062	4.6 ± 2%	http://app.supramolecular.org/bindfit/view/8b15b640-00bd-4521-ae5b-2f3daa9ae53b
3	KMH-II-063	6.6 ± 1%	http://app.supramolecular.org/bindfit/view/9386be0a-96c0-405b-903b-827a14927a4e
DMAP + tetrafluorohydroxyamide (**3.13**)			
Trial	Notebook	K_a in $CDCl_3$ (M^{-1})	BindFit URL

1	KMH-II-020	2111 ± 4%	http://app.supramolecular.org/bindfit/view/1a7e5132-7f54-4535-bc0a-5560ed59b43c
2	GL_04_245	1453 ± 5%	http://app.supramolecular.org/bindfit/view/473df4c5-a86d-4d22-a11e-3d46201efece
3	GL_04_256	997 ± 6%	http://app.supramolecular.org/bindfit/view/0bac30a2-c666-43bc-be98-fc58aed5556b
4	KMH-II-021	2398 ± 5%	http://app.supramolecular.org/bindfit/view/fb7bfc00-6633-48b8-942d-680314e5951e
5	KMH-II-022	2777 ± 6%	http://app.supramolecular.org/bindfit/view/1a71c6b6-158f-4fbc-8d2f-02714f94fce3
6	KMH-II-023	2285 ± 5%	http://app.supramolecular.org/bindfit/view/643e55a3-273e-4aec-959e-b01c3aa2611f
DMAP + tetrafluoronitrophenol (**3.14**)			
Trial	Notebook	K_a in $CDCl_3$ (M^{-1})	BindFit URL
1	GL_04_208	6400 ± 12%	http://app.supramolecular.org/bindfit/view/17f292c8-2195-4a68-aaa9-e72818708859
2	KMH-II-026	7100 ± 19%	http://app.supramolecular.org/bindfit/view/f5ae6745-695a-4315-b013-e975028b49a9
3	KMH-II-027	9100 ± 19%	http://app.supramolecular.org/bindfit/view/69cbb53a-0c66-4224-b861-6efa72489cdc
4	KMH-II-030	14000 ± 25%	http://app.supramolecular.org/bindfit/view/b01c8b57-a487-4760-b402-c6d7f9ead151
5	KMH-II-031	19000 ± 31%	http://app.supramolecular.org/bindfit/view/5fa0ba07-93df-4385-96cc-2489038e3896

*3.5.6 Selection of 1:2 binding model for tetrafluoronitrophenol and host (**3.3a•3.14**)*

Online fitting program BindFit has four options for 1:2 binding models; we fit titration data to each and then compared the covariances of fit of the more complex models to the least complex (statistical) following the procedure of Hibbert and Thordarson.[32] As the "full" binding model gave the best (lowest) fit, those binding constants are reported. A representative example comparing the different models is shown below for one replicate experiment of **3.3a** titrated with guest **3.14**.

Binding model	Relationship between K_1 and K_2	K_1 (M^{-1})	K_2 (M^{-1})	cov_{fit}	cov_{fit} ratio
Full 1:2	$\boldsymbol{K_1 \neq 4K_2}$	**798385**	**46548**	**6.6997e-3**	**14.7**
Non-cooperative 1:2	$K_1 = 4K_2$	285024	71,256	8.0078e-3	12.3
Additive 1:2	$K_1 \neq 4K_2$	165	47	0.0983	1
Statistical 1:2	$K_1 = 4K_2$	175	44	0.0983	1

BindFit URLs:

Full: http://app.supramolecular.org/bindfit/view/80c477a5-d839-4f46-ac16-dcf4ab63d6f9

Non-cooperative: http://app.supramolecular.org/bindfit/view/da0c19f5-ef21-475f-9d72-1fb8ee3714e9

Additive: http://app.supramolecular.org/bindfit/view/39d014ac-16e5-4e5c-b369-bacd33b582d4

Statistical: http://app.supramolecular.org/bindfit/view/da0c19f5-ef21-475f-9d72-1fb8ee3714e9

3.6 References

(1) Cram, D. J.; Cram, J. M. Host-Guest Chemistry. *Science* **1974**, *183*, 803–809.

(2) Cram, D. J. Preorganization – From Solvents to Spherands. *Angew. Chem. Int. Ed.* **1986**, *25*, 1039–1057.

(3) Wittenberg, J. B.; Isaacs, L. Complementarity and Preorganization. In Supramolecular Chemistry; John Wiley & Sons, Ltd: Chichester, UK, 2012.

(4) Anslyn, E. V.; Dougherty, D. A. Modern Physical Organic Chemistry; University Science Books, 2006.

(5) Cobranchi, D. P.; Garland, B. A.; Masiker, M. C.; Eyring, E. M.; Firman, P.; Petrucci, S. Relaxation Kinetics and Infrared Spectra of the Complexation of Lithium Ion by Triethylene Glycol and by Tetraethylene Glycol in Acetonitrile. *J. Phys. Chem.* **1992**, *96*, 5856–5865.

(6) Sheridan, R. E.; Whitlock, H. W. Concave Functionality: Some Exceptionally Large Binding Constants of Phenol Sticky Hosts. *J. Am. Chem. Soc.* **1988**, *110*, 4071–4073.

(7) Sheridan, R. E.; Whitlock, H. W. Concave Functionality: Design of a Phenol Sticky Host. *J. Am. Chem. Soc.* **1986**, *108*, 7120–7121.

(8) Whitlock, B. J.; Whitlock, H. W. Concave Functionality: Design Criteria for Nonaqueous Binding Sites. *J. Am. Chem. Soc.* **1990**, *112*, 3910–3915.

(9) Neder, K. M.; Whitlock, H. W. Importance of Hydrogen Bond Acceptor Ability in Design of Host Molecules Capable of Molecular Recognition. *J. Am. Chem. Soc.* **1990**, *112*, 9412–9414.

(10) Whitlock, B. J.; Whitlock, H. W. Effect of Cavity Size on Supramolecular Stability. *J. Am. Chem. Soc.* **1994**, *116*, 2301–2311.

(11) Wheeler, S. E.; Houk, K. N. Substituent Effects in the Benzene Dimer Are Due to Direct Interactions of the Substituents with the Unsubstituted Benzene. *J. Am. Chem. Soc.* **2008**, *130*, 10854–10855.

(12) Hunter, C. A.; Lawson, K. R.; Perkins, J.; Urch, C. J. Aromatic Interactions. *J. Chem. Soc., Perkin Trans. 2* **2001**, *5*, 651–669.

(13) Riwar, L.-J.; Trapp, N.; Kuhn, B.; Diederich, F. Substituent Effects in Parallel-Displaced π-π Stacking Interactions: Distance Matters. *Angew. Chem. Int. Ed.* **2017**, *56*, 11252–11257.

(14) Martinez, C. R.; Iverson, B. L. Rethinking the Term "Pi-Stacking." *Chem. Sci.* **2012**, *3*, 2191–2201.

(15) Cooke, G.; Rotello, V. M. Methods of Modulating Hydrogen Bonded Interactions in Synthetic Host-Guest Systems. *Chem. Soc. Rev.* **2002**, *31*, 275–286.

(16) Wilson, A. J. Hydrogen-Bonding Receptors for Molecular Guests. In Supramolecular Chemistry; Wiley, 2012.

(17) Hernández-Trujillo, J.; Costas, M.; Vela, A. Quadrupole Interactions in Pure Non-Dipolar Fluorinated or Methylated Benzenes and Their Binary Mixtures. *J. Chem. Soc., Faraday Trans.* **1993**, *89*, 2441–2443.

(18) Tsuzuki, S.; Uchimaru, T.; Mikami, M. Intermolecular Interaction between Hexafluorobenzene and Benzene: Ab Initio Calculations Including CCSD(T) Level Electron Correlation Correction. *J. Phys. Chem. A* **2006**, *110*, 2027–2033.

(19) Carter-Fenk, K.; Herbert, J. M. Electrostatics Does Not Dictate the Slip-Stacked Arrangement of Aromatic π-π Interactions. *Chem. Sci.* **2020**, *11*, 6758–6765.

(20) Zhang, S.; Chen, A.; An, Y.; Li, Q. Arene-Perfluoroarene Interaction: Properties, Constructions, and Applications in Materials Science. *Matter* **2024**, *7*, 3317–3350.

(21) Smith, C. E.; Smith, P. S.; Thomas, R. L.; Robins, E. G.; Collings, J. C.; Dai, C.; Scott, A. J.; Borwick, S.; Batsanov, A. S.; Watt, S. W.; Clark, S. J.; Viney, C.; Howard, J. A. K.; Clegg, W.; Marder, T. B. Arene-Perfluoroarene Interactions in Crystal Engineering: Structural Preferences in Polyfluorinated Tolans. *J. Mater. Chem.* **2004**, *14*, 413–420.

(22) Brittain, W. D. G.; Coxon, C. R. Perfluoroaryl and Perfluoroheteroaryl Reagents as Emerging New Tools for Peptide Synthesis, Modification and Bioconjugation. *Chem. Eur. J.* **2022**, *28*, e202103305.

(23) Lee, G. Y.; Hu, E.; Rheingold, A. L.; Houk, K. N.; Sletten, E. M. Arene-Perfluoroarene Interactions in Solution. *J. Org. Chem.* **2021**, *86*, 8425–8436.

(24) Huang, Z.; Chen, X.; Wu, G.; Metrangolo, P.; Whitaker, D.; McCune, J. A.; Scherman, O. A. Host-Enhanced Phenyl-Perfluorophenyl Polar– π Interactions. *J. Am. Chem. Soc.* **2020**, *142*, 7356–7361.

(25) Kai, U.; Sumida, R.; Tanaka, Y.; Yoshizawa, M. Discrimination of Perfluorinated Arenes/Alkanes by Modulable Polyaromatic Capsules. *J. Am. Chem. Soc.* **2025**, *147*, 10640–10646.

(26) Xu, Y.; Hao, A.; Xing, P. Dynamic Chiral Folding for Arene-Perfluoroarene Force Driven Clamping. *Nano Lett.* **2025**, *25*, 7128–7136.

(27) Miller, M. A. Methods for the Synthesis and Detection of Perfluorinated Small Molecules as Tools for Chemical Biology, University of California, Los Angeles, 2022.

(28) Lee, G. Y. The Study of Non-Covalent Interactions Using the Synergistic Combination of Experiment and Computation, UCLA, 2021.

(29) Gilli, P.; Pretto, L.; Bertolasi, V.; Gilli, G. Predicting Hydrogen-Bond Strengths from Acid-Base Molecular Properties. the PKa Slide Rule: Toward the Solution of a Long-Lasting Problem. *Acc. Chem. Res.* **2009**, *42*, 33–44.

(30) Thordarson, P. Binding Constants and Their Measurement. In Supramolecular Chemistry; Wiley, 2012.

(31) Thordarson, P. Determining Association Constants from Titration Experiments in Supramolecular Chemistry. *Chem. Soc. Rev.* **2011**, *40*, 1305–1323.

(32) Brynn Hibbert, D.; Thordarson, P. The Death of the Job Plot, Transparency, Open Science and Online Tools, Uncertainty Estimation Methods and Other Developments in Supramolecular Chemistry Data Analysis. *Chem. Commun.* **2016**, *52*, 12792–12805.

(33) Cloninger, M. J.; Whitlock, H. W. A Synthetic Receptor Which Uses Multiple Edge−Face Interactions To Bind Aromatic Guests. *J. Org. Chem.* **1998**, *63*, 6153–6159.

(34) Kelly-Rowley, A. M.; Lynch, V. M.; Anslyn, E. V. Molecular Recognition of Enolates of Active Methylene Compounds in Acetonitrile. The Interplay between Complementarity and Basicity, and the Use of Hydrogen Bonding to Lower Guest pK_as. *J. Am. Chem. Soc.* **1995**, *117*, 3438–3447.

(35) Armarego, W. L. F. .; Chai, C. L. Lin. Purification of Laboratory Chemicals (6th Ed.); Butterworth-Heinemann, 2009.

CHAPTER FOUR

Progress toward complexation-driven labeling of perfluoroaromatic-modified biomolecules via a modified phenanthrene-based host

4.1 Abstract

Perfluoroaromatics are increasingly used in chemical biology applications, including as covalent modifications to biomolecules. Their electrophilic nature makes them candidates for facile nucleophilic aromatic substitution (S_NAr) reactions, but the rates of such reactions are drastically decreased going from organic to aqueous reaction conditions. The work started here aims to take advantage of a phenanthrene-based host platform that binds perfluoroaromatic guests through arene-perfluoroarene interactions, which are enhanced in polar environments such as water, to create a nonpolar reaction microenvironment in which S_NAr can occur more readily. This requires installation of a nucleophile on the phenanthrene host, which would transform it into an affinity-guided covalent probe. Here, two strategies are explored for installing a nucleophilic thiol on final host structures. Additionally, an alternative strategy for bringing together the phenanthrene and linker components of the host is developed.

4.2 Introduction

As discussed in Chapter 2, aromatic substitution reactions of perfluoroarenes in aqueous biological settings have been accomplished by changing the immediate surroundings of the substrate, such as in the hydrophobic cavity formed by Pentelute's π-clamp that binds perfluoroarenes.[1] This also brings reaction partners into proximity to promote reactivity. The idea of proximity-induced or affinity-guided reactivity is to take an otherwise slow, intermolecular reaction, dependent on some second-order rate constant, k_2, and effectively turn it into an intramolecular reaction to enhance the overall rate (Figure 4.1).[2,3] This strategy is

employed by natural biomolecules and in chemical biology tools alike.[2–7] The relationship between an effective first-order, intramolecular reaction and the corresponding second-order one is termed the effective molarity.

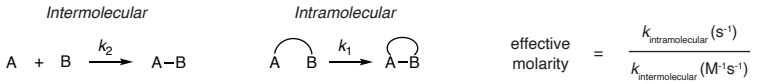

Figure 4.1 A general bimolecular reaction compared to a similar reaction with non-covalent or covalent bonds bringing reactants together to increase reactivity. Schematic adapted.[2,3]

The Whitlock group's naphthalene host **3.1**, discussed in Chapter 3, was adapted to serve as an "artificial enzyme," positioning an electron-deficient guest in its aromatic cavity to be deprotonated by the pyridine linker, which promoted a structural rearrangement of the guest.[8] After successfully expanding the Whitlock host platform into our own, phenanthrene-based system to bind perfluoroaromatic guests, we wondered if we could turn it into a probe capable of covalent guest modification. A thiol functionality near the host's cavity could react with electrophilic perfluoroaromatic guests, analogously to the π-clamp (Figure 4.2A). In a biological context, we imagine a binding event between thiol-functionalized host **4.1** with a perfluoroaromatic guest appended to some biomolecule of interest. This binding would position nucleophile and electrophile near each other in a host•guest complex, increasing the effective reaction molarity and reducing the polarity of the reaction medium. The subsequent reaction to form adduct **4.2** would result in a modified perfluoroaromatic guest, delivering whatever probe or payload was attached to the host structure.

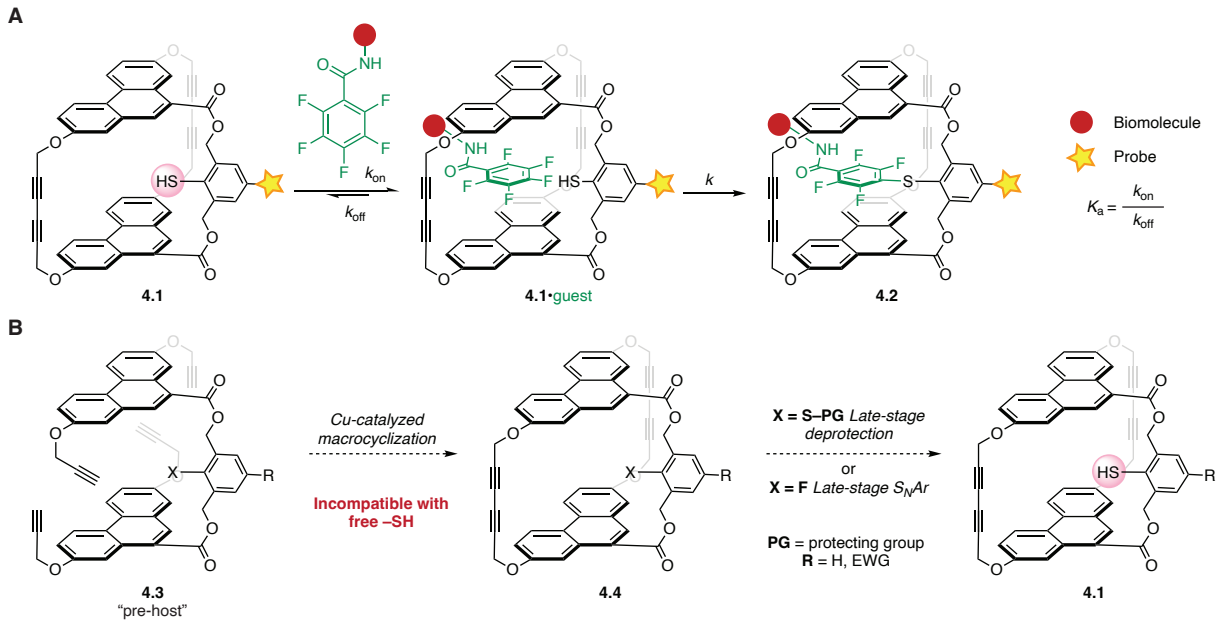

Figure 4.2 Overview of thiol-functionalized host project. (A) Proposed binding-promoted labeling reaction between host and perfluoroaromatic guest. (B) General proposed synthesis of thiol-functionalized host via different methods.

The goal of the present work was to design and synthesize a proof-of-concept system that would determine the feasibility of a host bearing a free thiol and of guest binding promoting nucleophilic substitution. We propose following the same synthetic strategy used in Chapter 3, with pre-host **4.3** bearing a masked group on the single-ring linker, as a free thiol would be incompatible with copper-catalyzed alkyne couplings (Figure 4.2B). Host **4.4** would feature either a protected thiol that could be subjected to mild deprotection conditions to reveal final host **4.1**, or an electrophilic substituent such as fluorine that could be transformed to a free thiol through a substitution reaction. In either case, the presence and choice of a substituent para to the ultimate thiol are chosen depending on the synthetic requirements of the linker. Here, both routes are explored, with the latter resulting in pre-host synthesis using new conditions, followed by successful formation of host **4.4**; however, installation of the free thiol is still a work in progress.

4.3 Results and discussion

4.3.1 Attempted late-stage deprotection route to thiol host

The first strategy toward a functionalized host was to reveal a free thiol through a final deprotection reaction. This would occur after the copper-catalyzed macrocyclization, the step necessitating masked or absent thiols. Final host **4.1a**, initially proposed without any additional linker substitution to streamline the synthesis, would come from deprotection of *para*-methoxybenzyl (PMB)-masked thiol following macrocyclization of prehost **4.3a** (Scheme 4.1). The PMB thiol protecting group has been successfully removed in the presence of esters, which we assume to be the most labile connections in the final host.[9] Pre-host **4.3a** could be made in the same fashion as phenanthrene host **3.3** — via esterification between two equivalents of phenanthrene face **4.5** and a new diol linker, **4.6**.

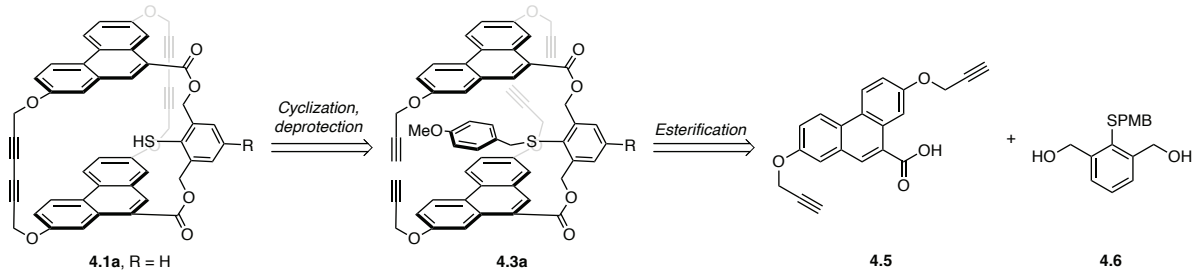

Scheme 4.1 Retrosynthesis of thiol-functionalized host with late-stage deprotection step.

Toward linker **4.6**, xylene **4.7** was treated with NBS to give di-brominated **4.8** (Scheme 4.2). Double displacement of the benzylic bromines by benzoic acid proceeded quickly, resulting in good yield of aryl bromide **4.9**. We planned to deprotect the benzoyl groups in a later step to reveal the benzylic hydroxy groups of **4.5**.

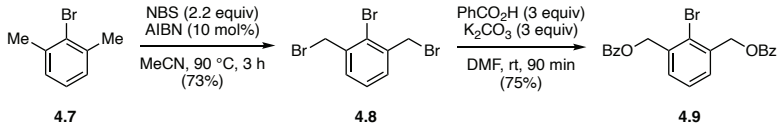

4.7 **4.8** **4.9**

Scheme 4.2 Synthesis of protected diol **4.9**.

We next attempted to install the PMB-protected thiol on **4.9** using C–S cross coupling methods (Scheme 4.3). Initially, following literature conditions utilizing thioacetate **4.10**, doubly protected linker **4.12** was successfully made, albeit in low yield (Table 4.1, entry 1).[10] By increasing the amounts of both thiol and base, both conversion and yield were improved, though only modestly, and still too low for an efficient early-stage reaction (Table 4.1, entry 2). An alternate ligand also resulted in a decrease in conversion (Table 4.1, entry 3).

We next tried reported conditions that utilized free thiol **4.11**, amine base instead of inorganic base, XantPhos as the ligand, and dioxane as solvent; this resulted in a similarly low conversion (Table 4.1, entry 4).[11] Including NaI as a co-catalyst further decreased conversion (Table 4.1, entry 5). Changing catalysts resulted in some recovery of conversion (Table 4.1, entry 6), though still lower than our best hit, and employment of a pre-catalyst system with a different base decreased conversion dramatically (entry 7). Finally, repeating some conditions in deoxygenated mixtures with or without inclusion of water did not improve conversion (Table 4.1, entries 8–9). It is possible that the benzoate ester groups result in too much steric congestion around the halide center of reactivity, slowing down formation of catalytic intermediates and lowering conversion; we did not however see improvements upon prolonged reaction time or higher temperatures. Should this route be revisited, alternative benzylic –OH protecting groups or substituents may need to be considered.

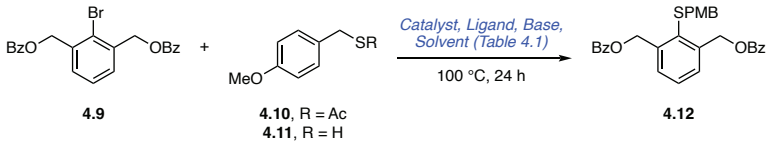

Scheme 4.3 General C–S cross-coupling scheme for installing protected thiol.

Entry	PMB reagent (equiv)	Catalyst	Ligand	Base (equiv)	Solvent	Conversion to **4.12** [a]
1	**4.10** (1.4 equiv)	$Pd(dba)_2$ (8 mol%)	XPhos (10 mol%)	K_2CO_3 (1.0 equiv)	THF:H_2O (4:1)	9% (5%[b])
2	**4.10** (1.6 equiv)	$Pd(dba)_2$ (9 mol%)	XPhos (11 mol%)	K_2CO_3 (1.6 equiv)	THF:H_2O (4:1)	38% (20%[b])
3	**4.10** (1.8 equiv)	$Pd(dba)_2$ (11 mol%)	XantPhos (10 mol%)	K_2CO_3 (1.8 equiv)	THF:H_2O (4:1)	13%
4	**4.11** (1.4 equiv)	$Pd(dba)_2$ (7 mol%)	XantPhos (9 mol%)	DIPEA (1.7 equiv)	1,4-dioxane	12%
5	**4.11** (1.4 equiv)	$Pd(dba)_2$ (10 mol%) *and* NaI (1.2 equiv)	XantPhos (11 mol%)	DIPEA (1.7 equiv)	1,4-dioxane	4%
6	**4.11** (1.6 equiv)	Pd_2dba_3 (10 mol%)	XPhos (15 mol%)	DIPEA (2.5 equiv)	1,4-dioxane	19%
7 [c]	**4.11** (1.2 equiv)	XPhos Pd G4 Pre-catalyst (11 mol%)		Et_3N (2.0 equiv)	1,4-dioxane	7%
8 [c]	**4.11** (1.2 equiv)	Pd_2dba_3 (10 mol%)	XPhos (21 mol%)	DIPEA (2.0 equiv)	1,4-dioxane	13%
9 [c]	**4.11** (1.2 equiv)	Pd_2dba_3 (10 mol%)	XPhos (21 mol%)	DIPEA (2.0 equiv)	1,4-dioxane:H_2O (50:1)	8%

Table 4.1 Conditions for improving yield of **4.12**. [a]Determined by ^{1}H NMR. [b]Isolated yield. [c]Deoxygenated reaction mixture before heating.

Alternative versions of the initial targeted linker, **4.6**, may be accessible through different reactions, including exploring alternative thiol protecting groups such as acetate or disulfides — groups that can be removed in mild conditions but are compatible with the preceding reactions.

At this point, however, given the challenges in improving the yield of aryl bromide **4.12**, we decided to focus on an alternative route that could lead to higher yields of a linker and its precursors.

4.3.2 Late-stage nucleophilic substitution route to thiol host

Instead of revealing a protected thiol on the final host structure, we also considered installing the thiol as the final step of the synthesis. Here, final host **4.1** would be made by S_NAr reaction at an electrophilic site on the linker of host **4.4** (Scheme 4.4). The linker could be additionally functionalized with a protected alkyne (**4.1b**) or ester (**4.1c**) for future modifications, such as the attachment of solubilizing groups. The electron-withdrawing nature of the substituents on **4.4b** or **4.4c** would promote the S_NAr reaction to install the thiol, though they would also likely reduce the nucleophilicity of the thiol, potentially slowing down the guest labeling step. If proximity effects prove insufficient for labeling, alternative substitution patterns could be explored; here, though, we decided to focus first on accessing **4.1b** or **4.1c**.

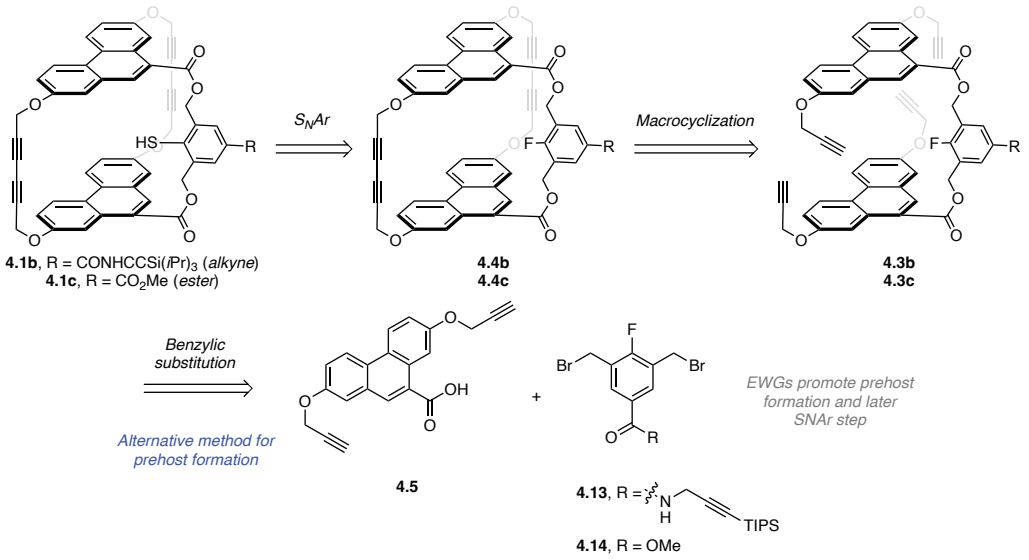

Scheme 4.4 Retrosynthesis of thiol-functionalized host featuring late-stage S_NAr. EWG = electron-withdrawing group.

Host **4.4b** or **4.4c** could come from macrocyclization of pre-host **4.3b** or **4.3c** (Scheme 4.4). Instead of the esterification step used to synthesize pre-host **3.11** in Chapter 3, we proposed benzylic substitution by phenanthrene acid **4.5** on dibromo linker **4.13** or **4.14**, with the electron-deficient nature of this linker promoting the benzylic S_N2 reaction. This method was used in some naphthalene-based host syntheses by the Whitlock group.[12] We decided to pursue alkyne-functionalized **4.13** first, as other work in our lab has successfully modified phenanthrene-platform hosts via copper-catalyzed alkyne-azide cycloaddition (CuAAC) click chemistry with an alkyne-functionalized linker.

Our first attempt toward **4.13** started with carboxylation of fluorinated xylene **4.15** to give acid precursor **4.16** in good yield (Scheme 4.5). Amide coupling with propargylamine under standard conditions over only a couple hours gave terminal alkyne **4.17**, which was easily cleaned with only a silica plug post workup. Protection of the terminal alkyne with a triisopropylsilyl (TIPS) group to give **4.18** also proceeded readily in approximately the same yield. Synthesizing TIPS propargyl amine **4.19** and then coupling it with acid **4.16** also gave rise to **4.18**. Though a lower coupling yield, it is approximately the same as the overall in the two-step sequence. Unfortunately, attempts to brominate the benzylic positions of **4.18** to access **4.13** failed, possibly due to reactivity between NBS and the alkyne, though the complex mess of products suggested additional undesired reactions. This logically invited exploring bromination first, then coupling second.

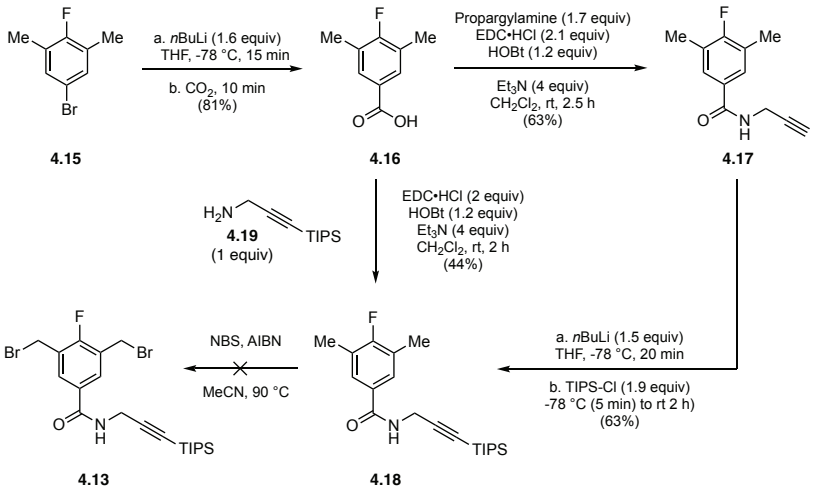

Scheme 4.5 Amide coupling, then bromination attempts toward **4.13**.

Bromination of acid **4.16** to give **4.20** was far less challenging (Scheme 4.6). Unfortunately, we were again unsuccessful in accessing **4.13**. Despite attempts with multiple conditions (via amide coupling reagents or acid chloride formation), each case resulted in a complex mixture of products without signs of success. We hypothesize some of this side reactivity may be from nucleophilic attack by amine **4.19** on the benzylic positions; this would again point to an incompatibility between an alkyne and electrophilic bromine handles.

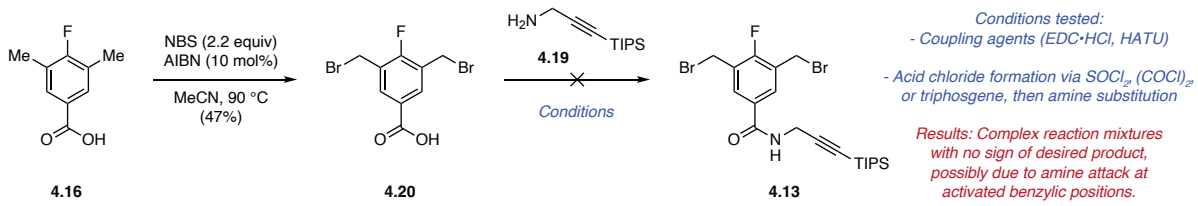

Scheme 4.6 Bromination first, then amide coupling attempts toward **4.13**.

Due to the synthetic compatibility challenges with amide and bromine functionalization, we decided to switch to a different electron-withdrawing substituent para to the fluorine that could be transformed later. Esterfication of **4.16** via acid chloride formation in methanol gave ester **4.21** in decent yield (Scheme 4.7). As an aside, acid **4.16** proved to be an excellent

precursor for both amide and ester formation, with relatively quick reaction times and facile product purifications with moderate to good yields, highlighting its general utility as a synthetic intermediate. Bromination proceeded to give **4.14**, though with lots of product stuck at mono-bromination (**4.22**), contributing to a decreased yield. Optimization of this step would be needed if this linker is utilized further.

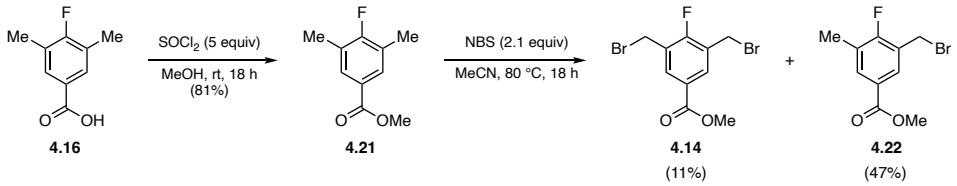

Scheme 4.7 Synthesis of ester linker **4.14**.

Having successfully formed linker **4.14** via a short synthesis, we attempted benzylic substitution with two equivalents of phenanthrene acid **4.5** (Figure 4.3A). Excitingly, clean pre-host **4.3c** was accessed in high yield (approximately the same as the esterified linkers in Chapter 3) after only a wash step post-workup. This simple purification contrasts with the recrystallization/column chromatography sequence required for previous pre-host iterations. Next, subjection to copper conditions for Eglinton coupling gave rise to two host isomers, *twist* **4.4c** and *meso* **4.23**, clearly observed by LC–MS (Figure 4.3B). Interestingly, past phenanthrene host isomer mixes, such as those in Chapter 3, were observed as a single broad peak in the same LC–MS conditions. Similarly, the fluorine atom of the linker allows for observation of isomers by ^{19}F NMR (Figure 4.3C). Unfortunately, attempts to characterize individual isomers were challenged by an inability to separate them by standard silica gel and alumina chromatography, despite success with previous host iterations. Purification by high-performance liquid chromatography (HPLC) may be possible, or modifications to the ester linker may help with the separation in other chromatography methods.

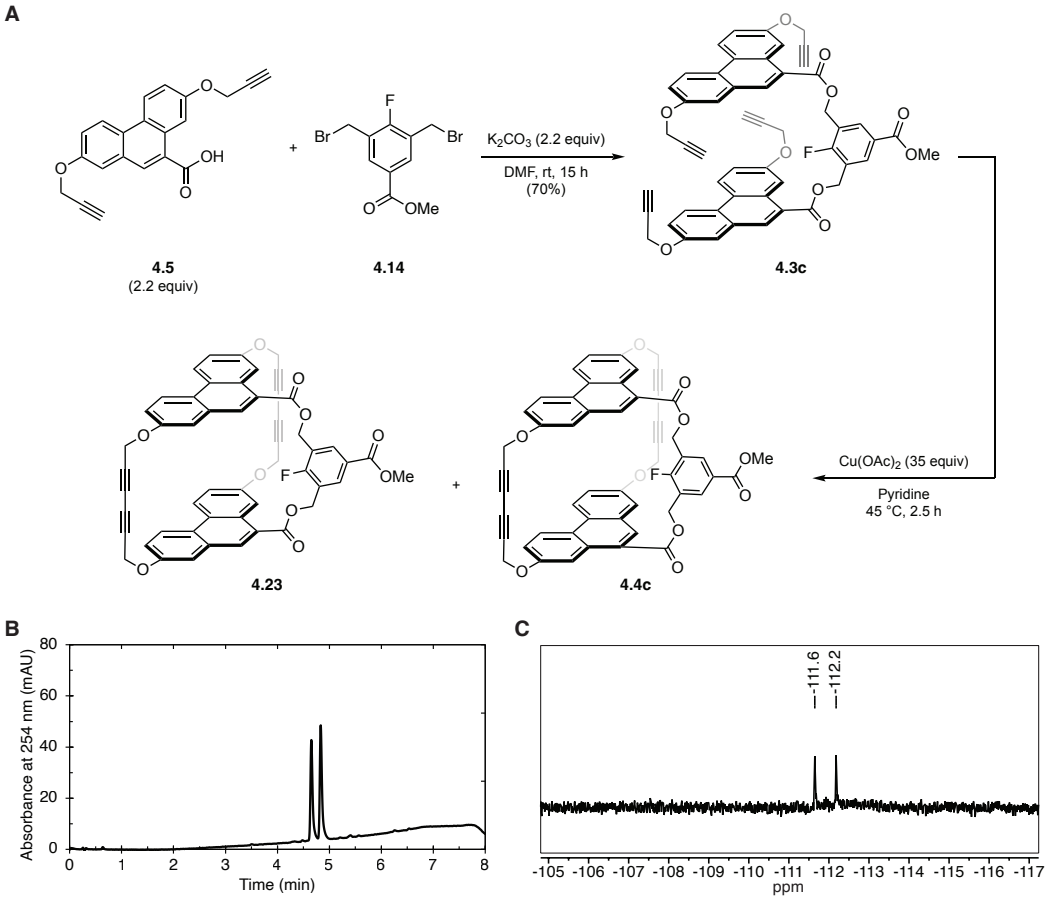

Figure 4.3 Formation of host with electrophilic site for late-stage thiol installation. (A) Reaction scheme featuring new method for pre-host (**4.3c**) synthesis, followed by successful macrocyclization to give a mixture of host isomers. (B) LC–MS trace of isomer mixture showing two distinct peaks. (C) ^{19}F NMR spectrum of isomer mixture showing two peaks.

We decided to test S_NAr conditions on the host isomer mix and check for successful fluorine displacement on the linker (Scheme 4.8). While complete structural analyses were limited due to small reaction scales, LC–MS data suggested both salt Na_2S and organic thiol **4.11** failed to substitute at the desired position. Mass data support thiol addition at the alkyne linkers in the former case, with proposed structures **4.A** and **4.B**, suggesting inorganic thiol sources are poor choices for on-host modifications. The basic conditions used with **4.11** appeared to hydrolyze the host methyl ester to give proposed acid **4.C**; while the acid itself is still useful, there was no evidence of thiol substitution by mass. An organic base may yield better results.

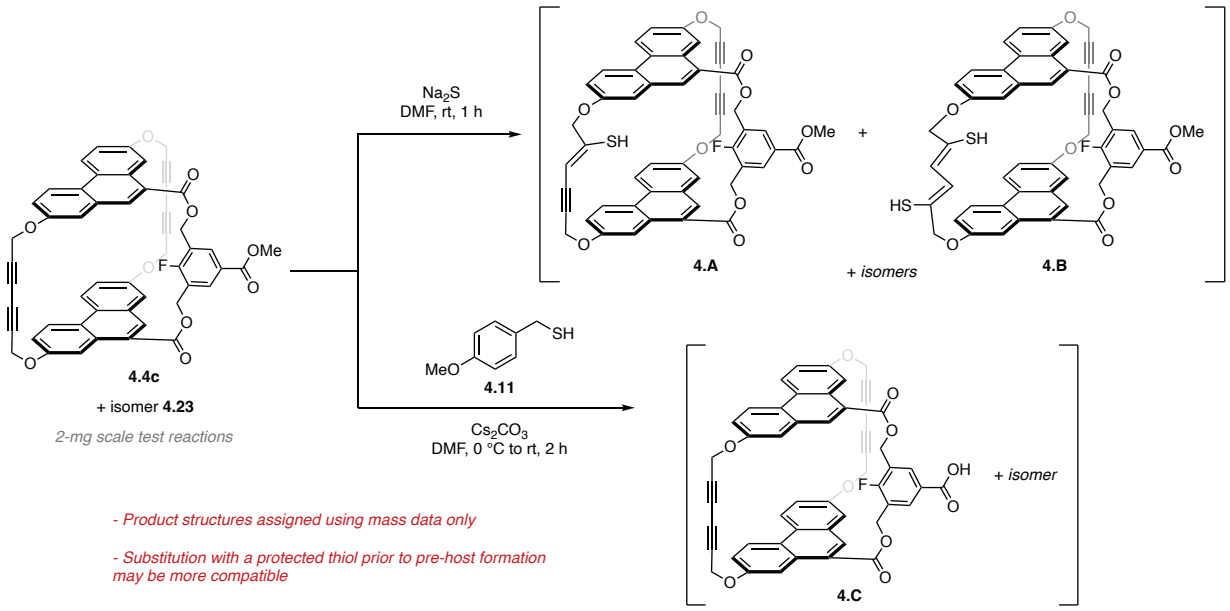

Scheme 4.8 Attempts at late-stage thiol installation on mix of host isomers.

The next most useful step would be to screen conditions to install a thiol on the linker alone before forming host. Different electron-withdrawing substituents, temperatures, bases, and solvents could be examining without compromising a final host structure.[13] More forceful conditions could be required as the present linker may not be sufficiently activated for substitution.[14] If a method to install a free thiol on the final host structure cannot be found, installing a protected thiol on linker **4.16** or **4.21** via S_NAr chemistry prior to bromination and pre-host formation may be amenable. A final mild deprotection step would reveal functionalized host. This would avoid any incompatibilities between the alkyne linkers and thiol reagents observed in Scheme 4.8. There are still many possible directions to the final covalent host probe target, and a combination of the chemistries shown here may be the key.

4.4 Conclusion

Two different strategies for late-stage installation of a free thiol on a host for perfluoroarenes were explored. The first route, based on the idea of late-stage deprotection of a masked thiol incorporated via the host linker, hit a snag in functionalizing said linker. The second route featured a linker with an electrophilic site for late-stage thiol substitution. Here, an ester-substituted linker was successfully synthesized and used to make the penultimate host structure, but a method for thiol substitution remains unknown.

There are many possible future directions for this work, beyond any attempts to access a thiol-bearing version of the phenanthrene host. First, hosts **4.4c** and **4.23** may be useful in guest binding scenarios where arene-perfluoroarene interactions are the primary non-covalent force driving recognition, such as in aqueous solutions, in contrast to the hydrogen-bonding pyridine linker featured in Chapter 3. Additionally, the ester handle may facilitate smooth installation of solubilizing groups through hydrolysis and ester- or amide-bond formation. Finally, the chemistry used to install linker **4.14** and non-chromatographic purification of the pre-host should make any future swapping of linkers relatively straightforward, so long as benzylic leaving groups are installed. This strategy will likely work best for linkers with electron-withdrawing substituents. The linker chemistry developed here contributes to one of our goals of designing a perfluoroaromatic recognition platform with a high degree of synthetic modularity.

4.5 Experimental Procedures

4.5.1 Synthetic abbreviations and chemical formulas

Acetic acid (AcOH); Acetonitrile (MeCN); Aluminum chloride ($AlCl_3$); Ammonium chloride (NH_4Cl); Azobisisobutyronitrile (AIBN); *n*-Butyllithium (*n*BuLi); Carbon dioxide (CO_2);

Cesium carbonate (Cs_2CO_3); Chloroform ($CHCl_3$); Copper acetate ($Cu[OAc]_2$); Dibenzylideneacetone (dba); 4-Dimethylaminopyridine (DMAP); Dichloromethane (CH_2Cl_2); Diethyl ether (Et_2O); Dimethylformamide (DMF); Electrospray ionization (ESI); Ethyl acetate (EtOAc); 1-Ethyl-3-(3-dimethylaminopropyl)carbodiimide (EDC); Hexafluorophosphate azabenzotriazole tetramethyl uronium (HATU); High-resolution mass spectrometry (HRMS); Hydrochloric acid (HCl); 1-Hydroxybenzotriazole (HOBt); Liquid chromatography–mass spectrometry (LC–MS); Low-resolution mass spectrometry (LRMS); Magnesium sulfate ($MgSO_4$); Megahertz (MHz); Methanol (MeOH); *N*-Bromosuccinimide (NBS); Nitrogen gas (N_2); Oxalyl chloride ($[COCl]_2$); Potassium carbonate (K_2CO_3); Sodium bicarbonate ($NaHCO_3$); Sodium hydroxide (NaOH); Sodium iodide (NaI); Sodium sulfate (Na_2SO_4); Sodium sulfide (Na_2S); Sodium sulfite (Na_2SO_3); Tetrahydrofuran (THF); Thionyl chloride ($SOCl_2$); Toluene (PhMe); Triethylamine (Et_3N); Triisopropylsilyl (TIPS); Trimethylsilyl (TMS)

4.5.2 Materials and instrumentation

Chemical reagents were purchased from Alfa Aesar, Sigma-Aldrich, Fisher Scientific, Acros Organics, TCI, Oakwood Chemicals, or Combi-Blocks and used without purification, unless otherwise noted. Reagents and products were weighed on a Sartorius ENTRIS224-1S Analytical Balance (220 x 0.0001 g). Anhydrous, deoxygenated solvents CH_2Cl_2, DMF, MeCN, MeOH, PhMe, and THF were dispensed from a Grubb's-type Phoenix Solvent Drying System. Thin-layer chromatography (TLC) was performed using silica gel 60 F_{254} (EMD Millipore) plates (0.5 mm thickness for preparatory TLC) and visualized under short- and/or long-wave UV light (UVGL-25, 254/365 nm). Flash column chromatography was performed using technical grade silica gel with 60 Å pores and 40–63 μm mesh particle size (Sorbtech Technologies) or

aluminum oxide (alumina; basic, 50–200 μm, 60 Å pores [Acros Organics]). Solvent was removed under reduced pressure with a Büchi or Ika Rotovapor with a Welch self-cleaning dry vacuum pump and further dried with a Welch DuoSeal pump attached to a Schlenk manifold. NMR spectra were recorded on Bruker NEO-600 (^{1}H, ^{13}C, and ^{19}F), Bruker AV-500 (^{1}H and ^{13}C), Bruker DRX-500 (^{1}H), and Bruker AV-400 (^{1}H, ^{13}C, and ^{19}F) instruments and processed with MestReNova software. Samples were taken in deuterated chloroform ($CDCl_3$ or deuterated DMSO (DMSO-d_6), and NMR peaks were calibrated using residual non-deuterated solvent ($CHCl_3$ at 7.26 ppm ^{1}H NMR, 77.16 ppm ^{13}C NMR; DMSO at 2.50 ppm ^{1}H NMR, 39.52 ppm ^{13}C NMR). Multiplicities are as indicated: s (singlet), bs (broad singlet), d (doublet), dd (doublet of doublets), ddt (doublet of doublet of triplets), t (triplet), td (triplet of doublets), q (quartet), and m (multiplet). Coupling constants, *J*, are reported in Hz and integrations are provided. LRMS (electrospray ionization [ESI]) were collected on an Agilent 1260 Infinity II HPLC-tandem MS system with InfinityLab Poroshell 120 EC-C8 column (3.0 x 50 mm, 2.7 μm). LC method: gradient of 40% MeCN in water to 95% over 5.5 min, 95% MeCN over 2 min, then back to 40% MeCN over 0.5 min, after first equilibrating with 40% MeCN/water. HRMS (ESI-MS) were collected on an Agilent 6545 Q-TOF LC/MS with 1260 Infinity LC.

4.5.3 Synthetic experimental procedures

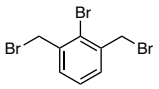

4.8

2-bromo-1,3-bis(bromomethyl)benzene (4.8). To an oven-dried, 20-mL scintillation vial was added anhydrous MeCN (5.8 mL, 0.40 M) and 2-bromo-1,3-dimethylbenzene **4.7** (0.30 mL, 420 mg, 2.3 mmol, 1.0 equiv). NBS (900.1 mg, 5.057 mmol, 2.2 equiv) and AIBN (37.8 mg, 0.230

mmol, 10 mol%) were added sequentially and the mixture stirred at 90 °C in an aluminum reaction block. After 2.5 h, the reaction was cooled to room temperature and quenched with saturated aqueous Na_2SO_3 (5 mL). The aqueous layer was extracted with $CHCl_3$ (3 x 10 mL). The combined organic layers were dried (Na_2SO_4), filtered, and concentrated. The off-white crude solid was loaded onto silica gel and purified by column chromatography (silica gel, 1% EtOAc/hexanes). Product **4.8** was isolated as a white solid (578 mg, 1.69 mmol, 73%). R_f = 0.5 in 10% EtOAc/hexanes. ^{1}H NMR (500 MHz, $CDCl_3$): δ 7.42 (d, *J* = 7.5 Hz, 2H), 7.29 (t, *J* = 7.5 Hz, 1H), 4.65 (s, 4H) ppm. The spectral data are consistent with a literature report.[15]

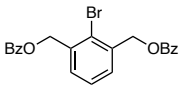

4.9

(2-bromo-1,3-phenylene)bis(methylene) dibenzoate (4.9). To an oven-dried, 20-mL scintillation vial was added: **4.8** (73.4 mg, 0.214 mmol, 1.00 equiv), benzoic acid (79.9 mg, 0.654 mmol, 3.06 equiv), and flame-dried K_2CO_3 (88.9 mg, 0.643 mmol, 3.00 equiv). Anhydrous DMF (2.1 mL, 0.10 M) was added and the mixture stirred at room temperature for 4.5 h. DMF was blown off with a stream of air, then the crude product was re-dissolved in CH_2Cl_2 and H_2O (2 mL each). The aqueous layer was extracted with CH_2Cl_2 (3 x 2 mL), and the combined organic layers were washed with H_2O (1 x 2 mL), then dried (Na_2SO_4), filtered, and concentrated. The crude white solid was evaporated onto silica gel and purified by column chromatography (silica gel, 100% hexanes → 5% EtOAc/hexanes). Aryl bromide product **4.9** was isolated as a white solid (68 mg, 0.16 mmol, 75%). R_f = 0.3 in 10% EtOAc/hexanes. ^{1}H NMR (500 MHz, $CDCl_3$): δ 8.11 (dd, *J* = 8.4, 1.4 Hz, 4H), 7.59 (ddt, *J* = 8.7, 7.2, 1.3 Hz, 2H), 7.51–7.45 (m, 6H), 7.41 – 7.35 (m, 1H), 5.51 (s, 4H) ppm. ^{13}C NMR (126 MHz, $CDCl_3$): δ

166.3, 136.5, 133.4, 130.0, 129.9, 129.6, 128.6, 127.7, 124.5, 66.5 ppm. LRMS (ESI) m/z: $[M+NH_4]^+$ calcd for $C_{22}H_{21}BrNO_4^+$ 442.1; found 442.0.

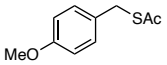

4.10

***S*-(4-methoxybenzyl) ethanethioate (4.10)**. Made following a literature procedure.[10] To an oven-dried reaction vial was added DMAP (3.4 mg, 0.028 mmol, 2 mol%). The vial was purged and backfilled with N_2, then anhydrous CH_2Cl_2 (0.90 mL, 1.6 M), pyridine (0.09 mL, 90 mg, 1 mmol, 0.7 equiv), Ac_2O (0.16 mL, 170 mg, 1.7 mmol, 1.2 equiv), and 4-methoxybenzyl mercaptan **4.11** (0.20 mL, 220 mg, 1.4 mmol, 1.0 equiv) were added sequentially. The mixture was stirred at room temperature for 20 h, then quenched with 1 M HCl (2 mL). The aqueous layer was extracted with CH_2Cl_2 (3 x 1 mL), then the combined organic layers were washed with H_2O (3 x 1 mL) and brine (3 x 1 mL) then dried (Na_2SO_4), filtered, and concentrated. The crude product was purified by column chromatography (silica gel, 5% EtOAc/hexanes). Thioacetate **4.10** was isolated as a clear oil (232 mg, 1.18 mmol, 84%). R_f = 0.3 in 5% EtOAc/hexanes. ^{1}H NMR (500 MHz, $CDCl_3$): δ 7.23 – 7.19 (m, 2H), 6.85 – 6.80 (m, 2H), 4.08 (s, 2H), 3.78 (s, 3H), 2.34 (s, 3H) ppm. The spectral data were consistent with the literature report.

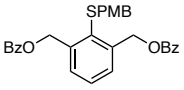

4.12

(2-((4-methoxybenzyl)thio)-1,3-phenylene)bis(methylene) dibenzoate (4.12). Aryl bromide **4.9** (20.5 mg, 0.0482 mmol, 1.00 equiv), flame-dried K_2CO_3 (10.5 mg, 0.0760 mmol, 1.58 equiv), XPhos ligand (2.5 mg, 0.0052 mmol, 11 mol%), and $Pd(dba)_2$ (2.4 mg, 0.0042 mmol, 8.7 mol%) were added to an oven-dried dram vial. The mixture was purged and backfilled with N_2,

then thioacetate **4.10** (14.7 mg, 0.0749 mmol, 1.55 equiv) in anhydrous THF (0.18 mL, 0.27 M) was added followed by H_2O (40 µL, 1.2 M). The solution was stirred at 100 °C in an aluminum reaction block for 24 h, then cooled to room temperature. The solution was diluted in CH_2Cl_2 (5 mL), filtered through celite, and concentrated. The crude mixture was evaporated onto silica gel and purified by column chromatography (100% hexanes → 5% EtOAc/hexanes). Product **4.12** was isolated as an off-white solid (7.5 mg, 0.015 mmol, 20%). R_f = 0.5 in 25% EtOAc/hexanes. ^{1}H NMR (500 MHz, $CDCl_3$): δ 8.12 – 8.04 (m, 4H), 7.57 (td, *J* = 7.3, 1.4 Hz, 2H), 7.52 (d, *J* = 7.7 Hz, 2H), 7.48 – 7.39 (m, 6H), 6.98 (d, *J* = 8.7 Hz, 2H), 6.73 (d, *J* = 8.7 Hz, 2H), 5.53 (s, 4H), 3.93 (s, 2H), 3.71 (s, 3H) ppm. ^{13}C NMR (126 MHz, $CDCl_3$): δ 166.4, 159.0, 141.8, 133.2, 132.6, 130.2, 130.2, 129.8, 129.6, 129.5, 129.1, 128.6, 114.0, 65.5, 55.3, 41.2 ppm. LRMS (ESI) m/z: $[M+NH_4]^+$ calcd for $C_{30}H_{30}NO_5S^+$ 516.2; found 516.2.

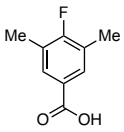

4.16

4-fluoro-3,5-dimethylbenzoic acid (4.16) To a flame-dried, 25-mL flask was added 5-bromo-2-fluoro-*m*-xylene **4.15** (1.08 g, 5.30 mmol, 1.00 equiv). The flask was briefly purged and backfilled with N_2 before adding anhydrous THF (23 mL, 0.23 M). The solution was cooled to -78 °C in a dry ice/acetone bath, then *n*-BuLi (1.6 M in hexanes, 3.8 mL, 6.1 mmol, 1.2 equiv) was added dropwise and the solution stirred at -78 °C for 10 min. To a separate, 500-mL single-neck flask, equipped with a rubber septum fitted with a cannula needle, was added anhydrous $MgSO_4$ (enough to fill ~1/4 of the flask) and enough dry ice to maintain a flow of CO_2 out the needle. Taking care to avoid excess pressure buildup, the cannula needle was added to the main

reaction mixture and CO_2 was bubbled in over 5 min. After 5 min, the cannula was removed, and the reaction mixture was warmed to room temperature. The reaction was diluted with Et_2O (50 mL), and the organic layer was extracted with 1 M NaOH (2 x 10 mL). The combined aqueous layers were then acidified to pH 3–4 (checked with pH paper and appearance of an insoluble white solid) using 1 M HCl, then extracted with EtOAc (3 x 20 mL). The organic layers were dried (Na_2SO_4), filtered, and concentrated under reduced pressure to give **4.16** as a white-brown solid (721 mg, 4.29 mmol, 81%). R_f = 0.5 in 50% EtOAc/hexanes. ^{1}H NMR (500 MHz, $CDCl_3$): δ 7.80 (d, *J* = 6.9 Hz, 2H), 2.31 (d, *J* = 2.2 Hz, 6H) ppm. ^{13}C NMR (126 MHz, $CDCl_3$): δ 172.1, 163.7 (d, *J* = 252.3 Hz), 131.5 (d, *J* = 6.5 Hz), 125.1 (d, *J* = 19.0 Hz), 124.6 (d, *J* = 3.7 Hz), 14.7 (d, *J* = 4.0 Hz) ppm. ^{19}F NMR (376 MHz, $CDCl_3$) δ -112.4 ppm. LRMS (ESI) m/z: $[M–H]^-$ calcd for $C_9H_8FO_2^-$ 167.1; found 167.2.

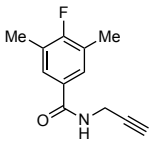

4.17

4-fluoro-3,5-dimethyl-N-(prop-2-yn-1-yl)benzamide (4.17). To an oven-dried, 2-mL dram vial was added EDC•HCl (47 mg, 0.25 mmol, 2.1 equiv; weighed separately into a capped, tared, oven-dried scintillation vial) in CH_2Cl_2 (0.8 mL). Propargylamine (13 µL, 11 mg, 0.20 mmol, 1.7 equiv), acid **4.16** (19.9 mg, 0.118 mmol, 1.00 equiv), and HOBt (19 mg, 0.14 mmol, 1.2 equiv) were added to the solution. Triethylamine (66 µL, 48 mg 0.47 mmol, 4.0 equiv) was added and the solution stirred at room temperature for 2.5 h. The reaction mixture was concentrated under reduced pressure, dissolved in minimal CH_2Cl_2 and passed through a silica plug in a Monster pipette, eluted with 50% EtOAc/hexanes. The product **4.17** was isolated as a white, flaky solid

(15 mg, 0.073 mmol, 63%). R_f = 0.3 in 25% EtOAc/hexanes. ^{1}H NMR (500 MHz, $CDCl_3$): δ 7.45 (d, *J* = 6.7 Hz, 2H), 6.14 (s, 1H), 4.24 (m, 2H), 2.30 (s, 7H [methyl and alkyne peaks overlapping]) ppm. ^{13}C NMR (126 MHz, $CDCl_3$): δ 166.7, 162.2 (d, *J* = 250.4 Hz), 129.1 (d, *J* = 3.5 Hz) , 128.1 (d, *J* = 6.4 Hz), 125.1 (d, *J* = 19.6 Hz), 79.6, 72.1, 29.9, 14.8 (d, *J* = 4.0 Hz) ppm. ^{19}F NMR (376 MHz, $CDCl_3$): δ -115.9 ppm. LRMS (ESI) m/z: $[M+H]^+$ calcd for $C_{12}H_{13}FNO^+$ 206.1; found 206.2.

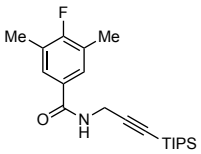

4.18

4-fluoro-3,5-dimethyl-N-(3-(triisopropylsilyl)prop-2-yn-1-yl)benzamide (4.18) from 4.17. To a flame-dried, 15-mL flask was added **4.17** (10.7 mg, 0.0521 mmol, 1.00 equiv), which was then purged and backfilled with N_2. Anhydrous THF (0.5 mL, 0.1 M) was added and the solution cooled to -78 °C using a dry ice/acetone bath. At -78 °C, *n*-BuLi (1.6 M, 0.05 mL, 0.08 mmol, 2 equiv) was added dropwise; the resulting dark orange solution was stirred at -78 °C for 20 min before adding TIPS-Cl (21 µL, 19 mg, 0.099 mmol, 1.9 equiv). The dark reddish pink solution was stirred for 5 min before removing dry ice/acetone bath, then stirred at room temperature for 2 h. The reaction was quenched with saturated aqueous NH_4Cl (1 mL). The aqueous layer was extracted with CH_2Cl_2 (3 x 2 mL) and the combined organic layers dried (Na_2SO_4), filtered, and concentrated. The crude orange oil was passed through a silica plug (25% EtOAc/hexanes) to give **4.18** as a clear oil (12 mg, 0.033 mmol, 63%). R_f = 0.6 in 25% EtOAc/hexanes. ^{1}H NMR (500 MHz, $CDCl_3$): δ 7.43 (d, *J* = 6.7 Hz, 2H), 6.11 (s, 1H), 4.29 (d, *J* = 5.0 Hz, 2H), 2.29 (d, *J* = 2.1 Hz, 6H), 1.07 (d, *J* = 2.4 Hz, 21H) ppm. ^{13}C NMR (126 MHz, $CDCl_3$): δ 166.5, 162.1 (d, *J* =

250.5 Hz), 129.4 (d, J = 3.6 Hz), 128.1 (d, J = 6.1 Hz), 125.1 (d, J = 18.8 Hz), 103.0, 85.2, 31.1, 18.7, 14.8, 11.3 ppm. ^{19}F NMR (376 MHz, $CDCl_3$): δ -116.1 ppm. HRMS (ESI/Q-TOF) m/z: $[M+H]^+$ calcd for $C_{21}H_{33}FNOSi^+$ 362.2315; found 362.2303.

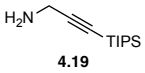

4.19

3-(triisopropylsilyl)prop-2-yn-1-amine (4.19). Following a modified literature procedure,[16] propargylamine (0.20 mL, 170 mg, 3.1 mmol, 1.0 equiv) and anhydrous THF (10 mL, 0.31 M) were added to a flame-dried, 50-mL flask under N_2. The solution was cooled to -78 °C using a dry ice/acetone bath. At -78 °C, *n*-BuLi (1.6 M, 2.2 mL, 3.5 mmol, 1.1 equiv) was added dropwise and stirred at -78 °C. After 15 min, the solution was warmed to 0 °C; TIPS-Cl (0.79 mL, 710 mg, 3.7 mmol, 1.2 equiv) was added and the resulting mixture stirred at 0 °C for 1 h, then warmed to room temperature. The reaction was quenched with saturated aqueous $NaHCO_3$ (5 mL) and stirred for 5 min. The mixture was diluted with H_2O (5 mL) and the aqueous layer was extracted with Et_2O (3 x 10 mL). The combined organic layers were washed with brine (1 x 5 mL), then dried (Na_2SO_4), filtered, and concentrated. The crude product was purified by column chromatography (silica gel, 50% → 75% EtOAc/hexanes + 0.1% triethylamine) to give **4.19** as a yellow oil (380 mg, 1.8 mmol, 58%). R_f = 0.2 in 50% EtOAc/hexanes (visualized with ninhydrin stain). ^{1}H NMR (500 MHz, $CDCl_3$): δ 3.47 (s, 2H), 2.01 (bs, 2H), 1.07 (m, 21H) ppm. The spectral data are consistent with the literature report.

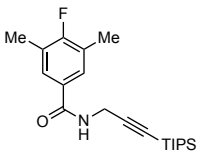

4.18

4-fluoro-3,5-dimethyl-N-(3-(triisopropylsilyl)prop-2-yn-1-yl)benzamide (4.18) from 4.16. To an oven-dried, 2-mL dram vial was added EDC•HCl (23.5 mg, 0.123 mmol, 1.9 equiv), followed by **4.16** (11.0 mg, 0.0654 mmol, 1.00 equiv). Anhydrous CH_2Cl_2 (0.4 mL, 0.2 M) was added, followed by HOBt (10.7 mg, 0.079 mmol, 1.2 equiv), then amine **4.19** (20 mg, 0.1 mmol, 1 equiv) and finally triethylamine (36 µL, 26 mg, 0.26 mmol, 4.0 equiv). The mixture was stirred at room temperature for 2 h, then diluted with H_2O (2 mL). The aqueous layer was extracted with CH_2Cl_2 (2 x 2 mL) and the combined organic layers washed with brine (1 x 2 mL). The organic layers were dried (Na_2SO_4), filtered, and concentrated, then passed through a silica gel plug (25% EtOAc/hexanes) to give **4.18** as a yellow oil (10.3 mg, 0.0285 mmol, 44%). R_f = 0.6 in 25% EtOAc/hexanes. The spectral data were consistent with those listed above.

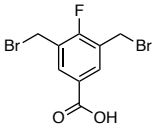

4.20

3,5-bis(bromomethyl)-4-fluorobenzoic acid (4.20). To an oven-dried, 20-mL scintillation vial was added acid **4.16** (105.8 mg, 0.6291 mmol, 1.000 equiv). Anhydrous MeCN was added (1.7 mL, 0.37 M), followed by AIBN (10.6 mg, 0.0646 mmol, 10.3 mol%), then NBS (247.5 mg, 1.391 mmol, 2.211 equiv). The mixture was stirred in an aluminum heat block at 80 °C for 3.5 h. The solution was cooled, quenched with saturated aq. Na_2SO_3 (5 mL). The aqueous layer was extracted with $CHCl_3$ (3 x 5 mL). The organic layers were combined, dried (Na_2SO_4), filtered, and concentrated to give a crude yellow solid, which was evaporated onto silica and purified by

column chromatography (silica gel, 1% → 5% → 10% EtOAc/hexanes + 1% AcOH). Product **4.20** was isolated as a white solid (97 mg, 0.30 mmol, 47%). R_f = 0.2 in 25% EtOAc/hexanes. ^{1}H NMR (500 MHz, $CDCl_3$): δ 8.14 (d, *J* = 6.8 Hz, 2H), 4.54 (s, 4H) ppm. ^{13}C NMR (126 MHz, $CDCl_3$): δ 168.4, 162.0 (d, *J* = 264.7 Hz), 134.0 (d, *J* = 4.7 Hz), 126.7 (d, *J* = 16.0 Hz), 126.1 (d, *J* = 4.2 Hz), 24.4 (d, *J* = 4.6 Hz) ppm. ^{19}F NMR (376 MHz, $CDCl_3$): δ -112.4. HRMS (ESI/Q-TOF) m/z: $[M+H]^+$ calcd for $C_9H_8Br_2FO_2$ 326.8855 (100% relative intensity Br isotope peak); found 326.8969.

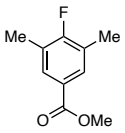

4.21

methyl 4-fluoro-3,5-dimethylbenzoate (4.21). To a flame-dried 25-mL flask was added 4-fluoro-3,5-dimethylbenzoic acid **4.16** (308 mg, 1.83 mmol, 1.00 equiv). The flask was purged and backfilled with N_2. Anhydrous MeOH was added (3.8 mL, 0.48 M), followed by dropwise addition of $SOCl_2$ (0.66 mL, 9.1 mmol, 5.0 equiv). The mixture was stirred at room temperature for 16 h. Volatiles were removed via rotatory evaporation to give a dark brown, oily solid, which was then dissolved in CH_2Cl_2/EtOAc (20 mL). The organic layer was washed with saturated aq. $NaHCO_3$ (10 mL). The organic layer was dried (Na_2SO_4), filtered, and concentrated to yield **4.21** as a light brown solid (271 mg, 1.49 mmol, 81%). R_f = 0.6 in 25% EtOAc/hexanes. ^{1}H NMR (400 MHz, $CDCl_3$): δ 7.72 (d, *J* = 7.1 Hz, 2H), 3.89 (s, 3H), 2.29 (d, *J* = 2.1 Hz, 6H) ppm. ^{13}C NMR (126 MHz, $CDCl_3$): δ 166.8, 163.7 (d *J* = 251.8 Hz), 130.8 (d, *J* = 6.3 Hz), 125.4 (d, *J* = 3.9 Hz), 124.8 (d, *J* = 18.7 Hz), 52.2, 14.7 (d, *J* = 4.2 Hz) ppm. ^{19}F NMR (376 MHz, $CDCl_3$): δ -

114.1 ppm. HRMS (ESI/Q-TOF) m/z: $[M]^+$ calcd for $C_{10}H_{11}FO_2$ 182.0743; found 182.0792. LRMS (ESI) m/z: $[M+H]^+$ calcd for $C_{10}H_{12}FO_2^+$ 183.1; found 183.0.

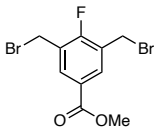

4.14

methyl 3,5-bis(bromomethyl)-4-fluorobenzoate (4.14). To an oven-dried, 20-mL scintillation vial was added methyl 4-fluoro-3,5-dimethylbenzoate **4.21** (100.4 mg, 0.5511 mmol, 1.000 equiv). Anhydrous MeCN was added (1.8 mL, 0.31 M), followed by AIBN (9.0 mg, 0.055 mmol, 10 mol%), then NBS (203.7 mg, 1.144 mmol, 2.076 equiv). The mixture was stirred in an aluminum heat block at 80 °C. After 6 h, more NBS was added (11.6 mg, 0.0652 mmol, 0.118 equiv) and the mixture was stirred at 80 °C. After a total of 26 h at 80 °C, the solution was cooled, quenched with saturated aq. Na_2SO_3 (5 mL). The aqueous layer was extracted with $CHCl_3$ (3 x 5 mL). The organic layers were combined, dried (Na_2SO_4), filtered, and concentrated to give a crude yellow solid, which was evaporated onto silica and purified by column chromatography (silica gel, 5% EtOAc/hexanes). The final compound **4.14** was isolated as an off-white solid (20 mg, 0.059 mmol, 11%). R_f = 0.3 in 10% EtOAc/hexanes. ^{1}H NMR (400 MHz, $CDCl_3$): δ 8.07 (d, J = 6.9 Hz, 2H), 4.52 (s, 4H), 3.93 (s, 3H) ppm. ^{13}C NMR (126 MHz, $CDCl_3$): δ 165.3, 161.5 (d, J = 258.3 Hz), 133.3 (d, J = 5.6 Hz), 127.1 (d, J = 4.0 Hz), 126.4 (d, J = 16.1 Hz), 52.6, 24.5 (d, J = 4.1 Hz) ppm. ^{19}F NMR (376 MHz, $CDCl_3$) δ -113.9 ppm. HRMS (ESI/Q-TOF) m/z: $[M+H]^+$ calcd for $C_{10}H_{10}Br_2FO_2^+$ 338.9032; found 338.8999. The mono-brominated product **4.22** was also isolated (68 mg, 0.26 mmol, 47%).^{1}H NMR (400 MHz,

$CDCl_3$) δ 7.93 (dd, *J* = 6.8, 2.3 Hz, 1H), 7.87 (d, *J* = 7.2 Hz, 1H), 4.51 (d, *J* = 1.2 Hz, 2H), 3.91 (s, 3H), 2.33 (d, *J* = 2.2 Hz, 3H).

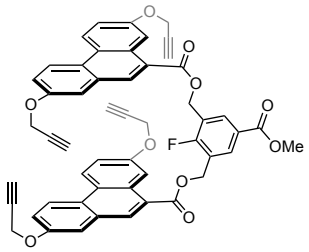

4.3c

(2-fluoro-5-(methoxycarbonyl)-1,3-phenylene)bis(methylene) bis(2,7-bis(prop-2-yn-1-yloxy)phenanthrene-9-carboxylate) (4.3c) (pre-host). To an oven-dried, 2-mL dram vial was added **4.14** (5.0 mg, 0.015 mmol, 1.0 equiv), **4.5** (10.8 mg, 0.033 mmol, 2.2 equiv), and flame-dried K_2CO_3 (4.5 mg, 0.033 mmol, 2.2 equiv). The solid mixture was purged and backfilled with N_2, then anhydrous DMF was added (0.1 mL, 0.2 M). The solution was stirred at room temperature for 15 h. DMF was blown off with a stream of air, and the resulting yellow solid was washed with EtOAc to give **4.3c** as a pale yellow solid (9 mg, 0.01 mmol, 70%). R_f = 0.1 in 25% EtOAc/hexanes. ^{1}H NMR (500 MHz, DMSO-d_6): δ 8.78 (d, *J* = 9.4 Hz, 2H), 8.73 (d, *J* = 9.2 Hz, 2H), 8.49 (s, 2H), 8.35 – 8.30 (m, 4H), 7.64 (d, *J* = 2.7 Hz, 2H), 7.45 (dd, *J* = 9.1, 2.7 Hz, 2H), 7.41 (dd, *J* = 9.2, 2.7 Hz, 2H), 5.66 (s, 4H), 4.92 (d, *J* = 2.4 Hz, 4H), 4.88 (d, *J* = 2.4 Hz, 4H), 3.87 (s, 3H), 3.59 (t, *J* = 2.4 Hz, 2H), 3.56 (t, *J* = 2.3 Hz, 2H) ppm. ^{13}C NMR (126 MHz, DMSO-d_6): δ 166.5, 165.0, 155.8, 155.6, 132.8, 132.5, 129.7, 128.5, 126.5, 125.2, 125.1, 124.8, 124.4, 124.3, 124.2, 120.4, 117.5, 111.4, 108.6, 79.0, 78.9, 78.5, 78.4, 60.4, 55.7, 55.5, 54.9, 52.5 ppm. ^{19}F NMR (565 MHz, DMSO-d_6): δ -114.8 ppm. HRMS (ESI/Q-TOF) m/z: $[M+Na]^+$ calcd for $C_{52}H_{35}FNaO_{10}^+$ 861.2112; found 861.2051.

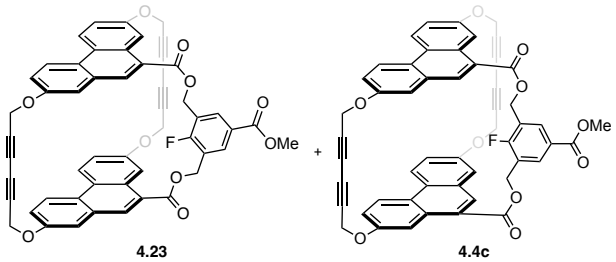

Host (4.3c+4.23). To an oven-dried, 20-mL scintillation vial was added $Cu(OAc)_2$ (15.7 mg, 0.0864 mmol, 14 equiv). The vial was purged and backfilled with N_2 and pyridine was added (1.0 mL), then the solution warmed to 45 °C in an oil bath. Pre-host **4.3c** (5.0 mg, 0.0060 mmol, 1.0 equiv) was dissolved in DMF (0.7 mL) and pyridine (0.3 mL, 0.006 M final [**4.3c**]). The prehost solution was added dropwise to the $Cu(OAc)_2$ solution at 45 °C over about 4 min, then stirred at 45 °C for 2 h. The solution was cooled to room temperature and solvents evaporated. The crude mixture was re-dissolved in $CHCl_3$ (5 mL) and the organic layer washed with 1 M HCl (1 x 2 mL). The aqueous layer was extracted with $CHCl_3$ (3 x 5 mL). The combined organic layers were dried (Na_2SO_4), filtered, and concentrated, then passed through a silica gel plug (100% EtOAc) to give a mixture of host isomers, **4.4c** and **4.23** (4 mg, 0.005 mmol, 80%). R_f = 0.8 in 75% EtOAc/hexanes. LRMS (ESI) m/z: $[M+NH_4]^+$ calcd for $C_{52}H_{35}FNO_{10}^+$ 852.2; found 852.2 (isomer 1), 852.4 (isomer 2); $[M+Na]^+$ calcd for $C_{52}H_{31}FO_{10}Na^+$ 857.2; found 857.4 (isomer 1), 857.4 (isomer 2). HRMS (ESI/Q-TOF) m/z: $[M+NH_4]^+$ calcd for $C_{52}H_{35}FNO_{10}^+$ 852.2240; found 852.2244. The host isomers proved inseparable by standard silica gel chromatography methods, but a comparison to known host isomers allowed for approximating peak assignments in 1H NMR (see next section). Using three methods, it was found the isomers were present in a roughly 1:1 mixture: LC–MS (1:1.14), ^{1}H NMR (1.04:1 **4.23**:**4.4c**), and ^{19}F NMR (1:1.1, unknown assignments).

4.5.4 ^{1}H NMR spectra

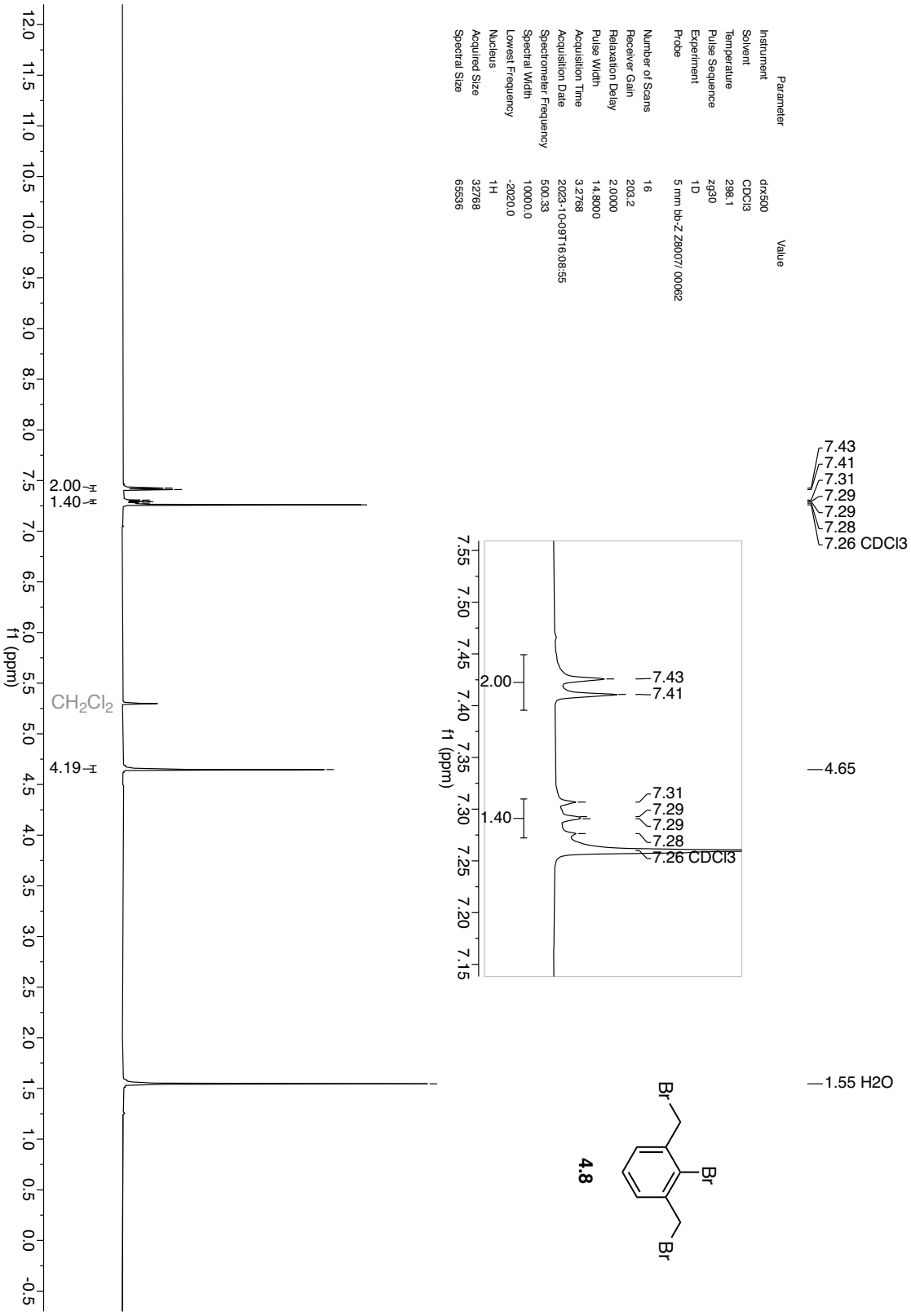

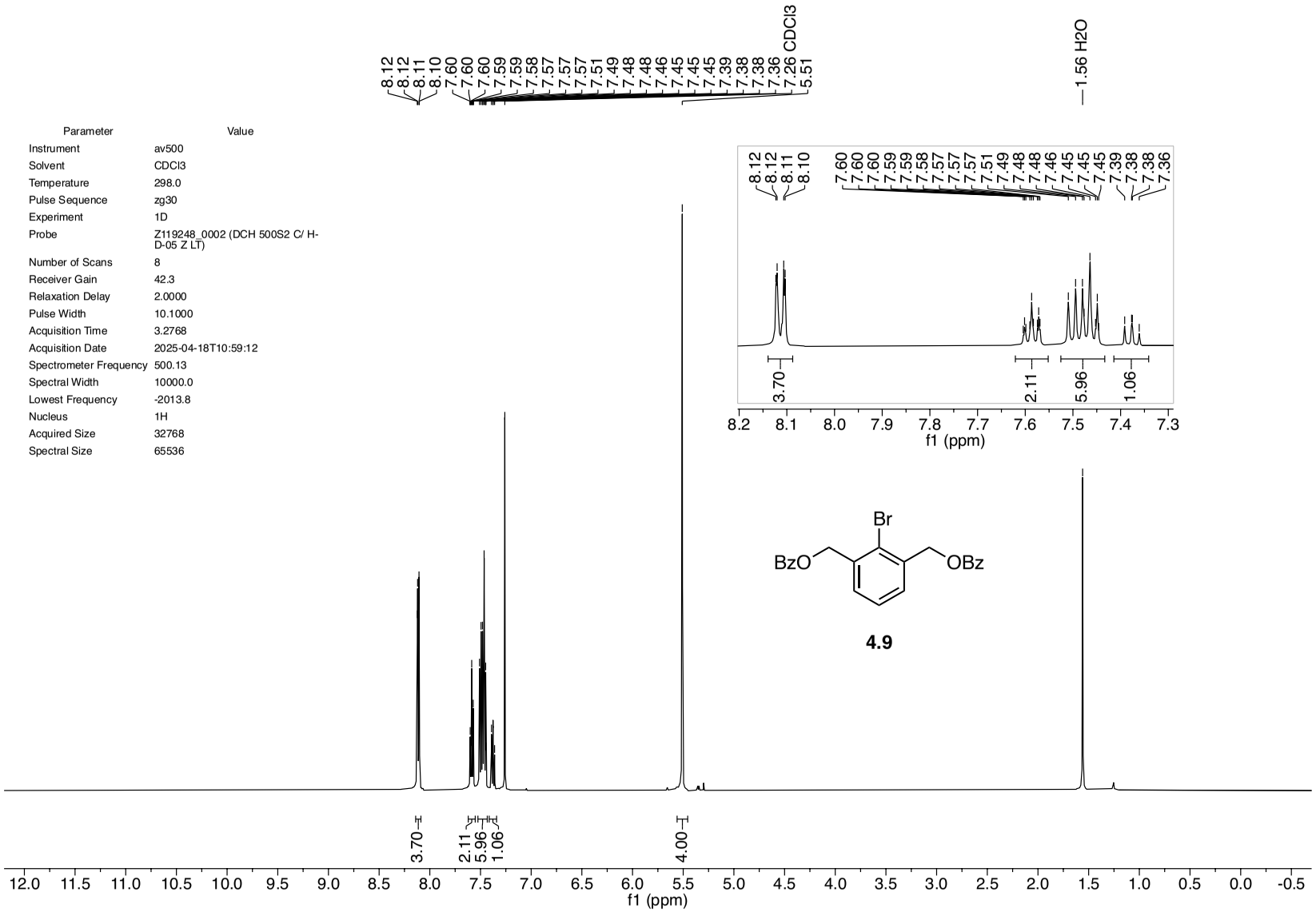
8.12 8.12 8.11 8.10 7.60 7.60 7.60 7.59 7.59 7.58 7.57 7.57 7.57 7.51 7.49 7.48 7.48 7.46 7.45 7.45 7.45 7.39 7.38 7.36 CDCl3 5.51
1.56 H2O
Parameter Value
Instrument av500
Solvent CDCl3
Temperature 298.0
Pulse Sequence zg30
Experiment 1D
Probe Z119248_0002 (DCH 500S2 C/ H-D-05 Z LT)
Number of Scans 8
Receiver Gain 42.3
Relaxation Delay 2.0000
Pulse Width 10.1000
Acquisition Time 3.2768
Acquisition Date 2025-04-18T10:59:12
Spectrometer Frequency 500.13
Spectral Width 10000.0
Lowest Frequency -2013.8
Nucleus 1H
Acquired Size 32768
Spectral Size 65536
3.70 2.11 5.96 1.06
f1 (ppm)
Br
BzO
OBz
4.9
3.70 2.11 5.96 1.06 4.00
f1 (ppm)

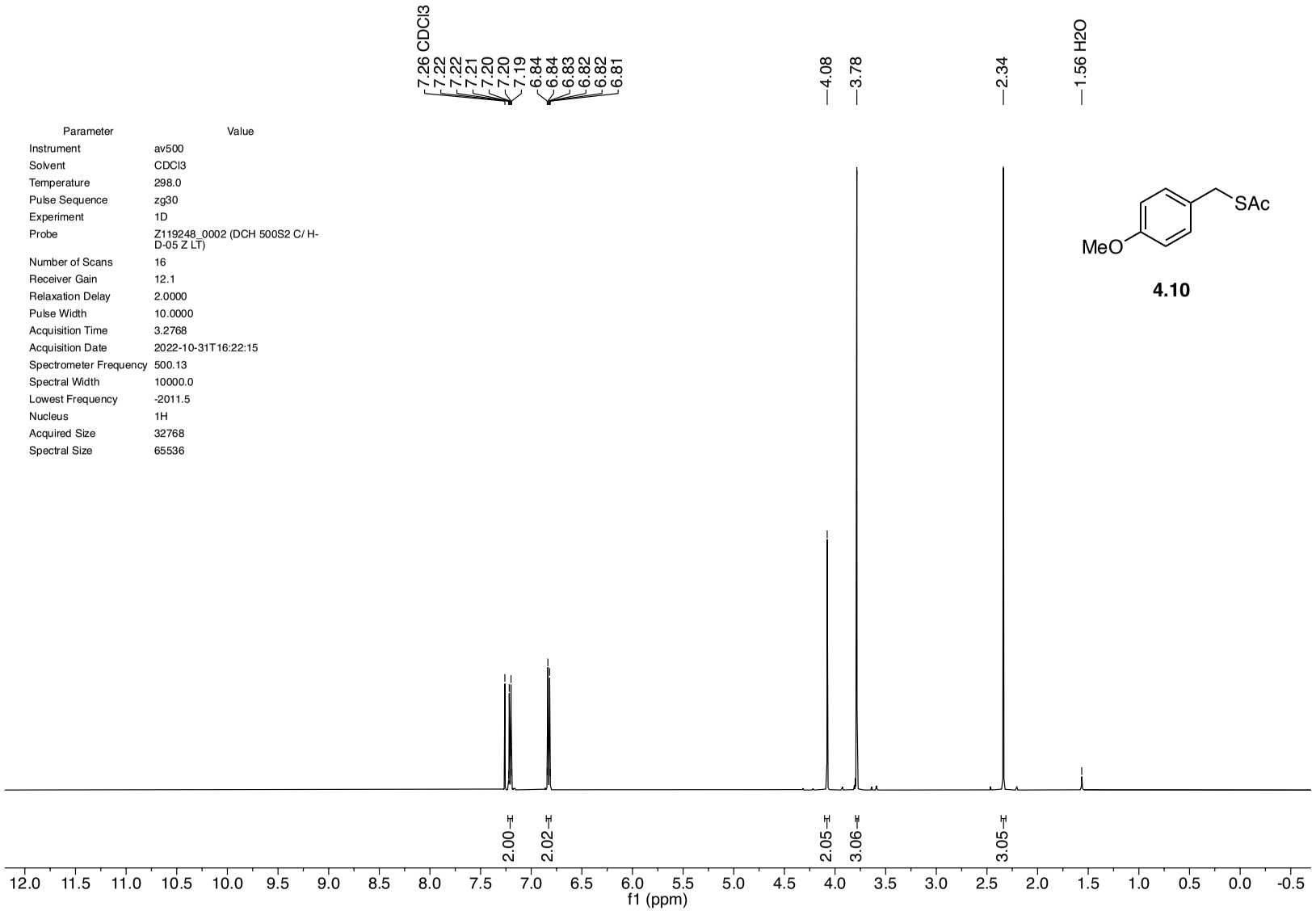
7.26 CDCl3
7.22
7.22
7.21
7.20
7.20
7.19
6.84
6.84
6.83
6.82
6.82
6.81
4.08
3.78
2.34
1.56 H2O
Parameter Value
Instrument av500
Solvent CDCl3
Temperature 298.0
Pulse Sequence zg30
Experiment 1D
Probe Z119248_0002 (DCH 500S2 C/ H-D-05 Z LT)
Number of Scans 16
Receiver Gain 12.1
Relaxation Delay 2.0000
Pulse Width 10.0000
Acquisition Time 3.2768
Acquisition Date 2022-10-31T16:22:15
Spectrometer Frequency 500.13
Spectral Width 10000.0
Lowest Frequency -2011.5
Nucleus 1H
Acquired Size 32768
Spectral Size 65536
SAc
MeO
4.10
2.00
2.02
2.05
3.06
3.05
12.0 11.5 11.0 10.5 10.0 9.5 9.0 8.5 8.0 7.5 7.0 6.5 6.0 5.5 5.0 4.5 4.0 3.5 3.0 2.5 2.0 1.5 1.0 0.5 0.0 -0.5
f1 (ppm)

Parameter	Value
Instrument	av500
Solvent	CDCl3
Temperature	298.0
Pulse Sequence	zg30
Experiment	1D
Probe	Z119248_0002 (DCH 500S2 C/ H-D-05 Z LT)
Number of Scans	16
Receiver Gain	42.3
Relaxation Delay	2.0000
Pulse Width	10.1000
Acquisition Time	3.2768
Acquisition Date	2025-04-18T09:43:40
Spectrometer Frequency	500.13
Spectral Width	10000.0
Lowest Frequency	-2013.8
Nucleus	1H
Acquired Size	32768
Spectral Size	65536

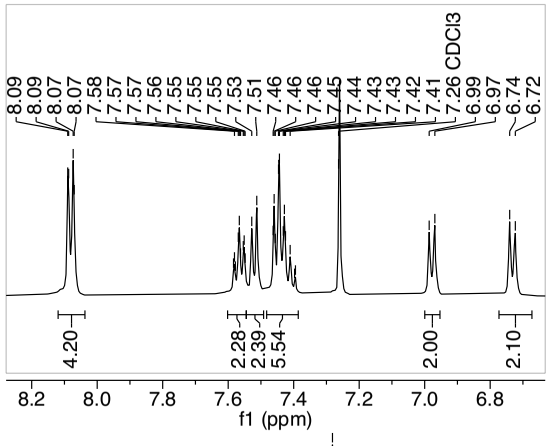

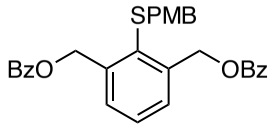

4.12

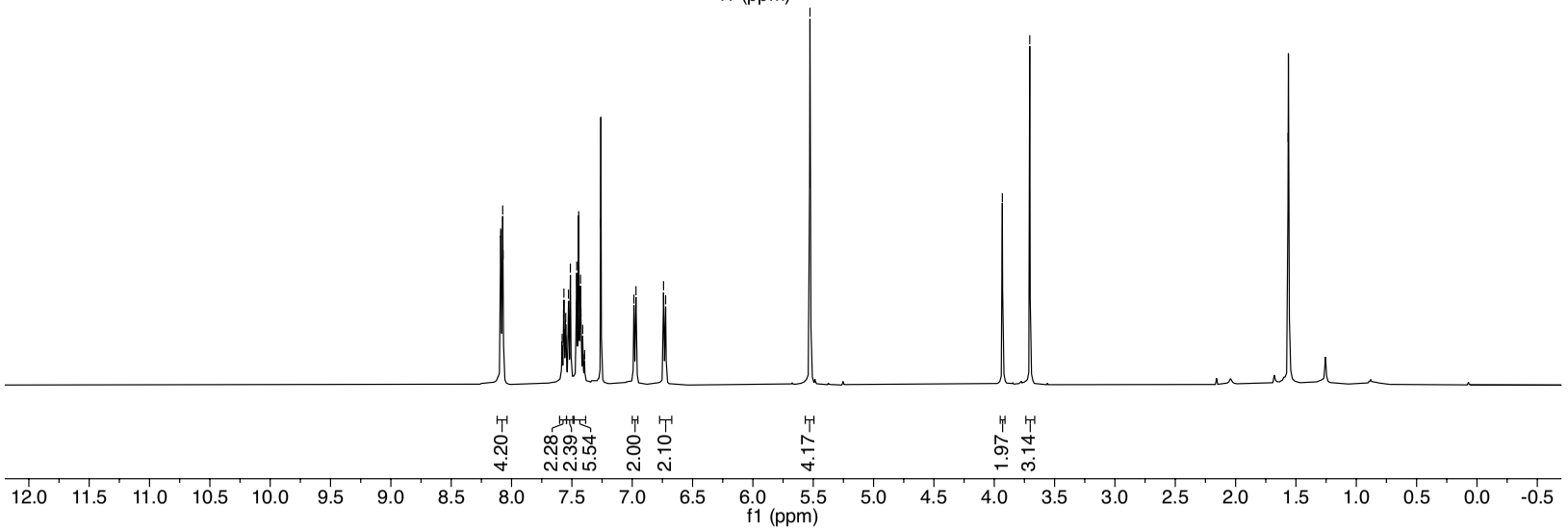

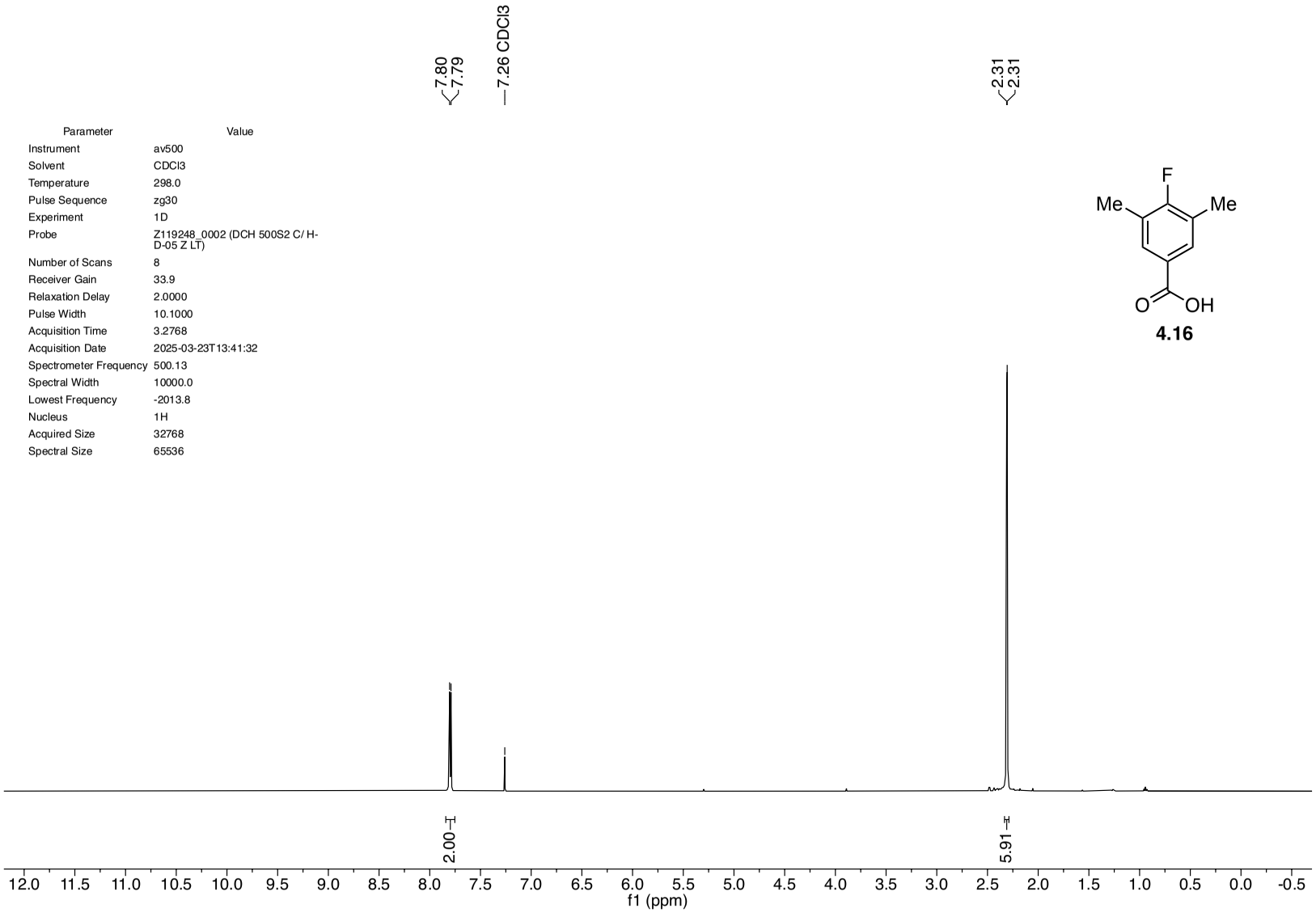
7.80
7.79
7.26 CDCl3
2.31
2.31
Parameter Value
Instrument av500
Solvent CDCl3
Temperature 298.0
Pulse Sequence zg30
Experiment 1D
Probe Z119248_0002 (DCH 500S2 C/ H-D-05 Z LT)
Number of Scans 8
Receiver Gain 33.9
Relaxation Delay 2.0000
Pulse Width 10.1000
Acquisition Time 3.2768
Acquisition Date 2025-03-23T13:41:32
Spectrometer Frequency 500.13
Spectral Width 10000.0
Lowest Frequency -2013.8
Nucleus 1H
Acquired Size 32768
Spectral Size 65536
F
Me
Me
O
OH
4.16
2.00
5.91
12.0 11.5 11.0 10.5 10.0 9.5 9.0 8.5 8.0 7.5 7.0 6.5 6.0 5.5 5.0 4.5 4.0 3.5 3.0 2.5 2.0 1.5 1.0 0.5 0.0 -0.5
f1 (ppm)

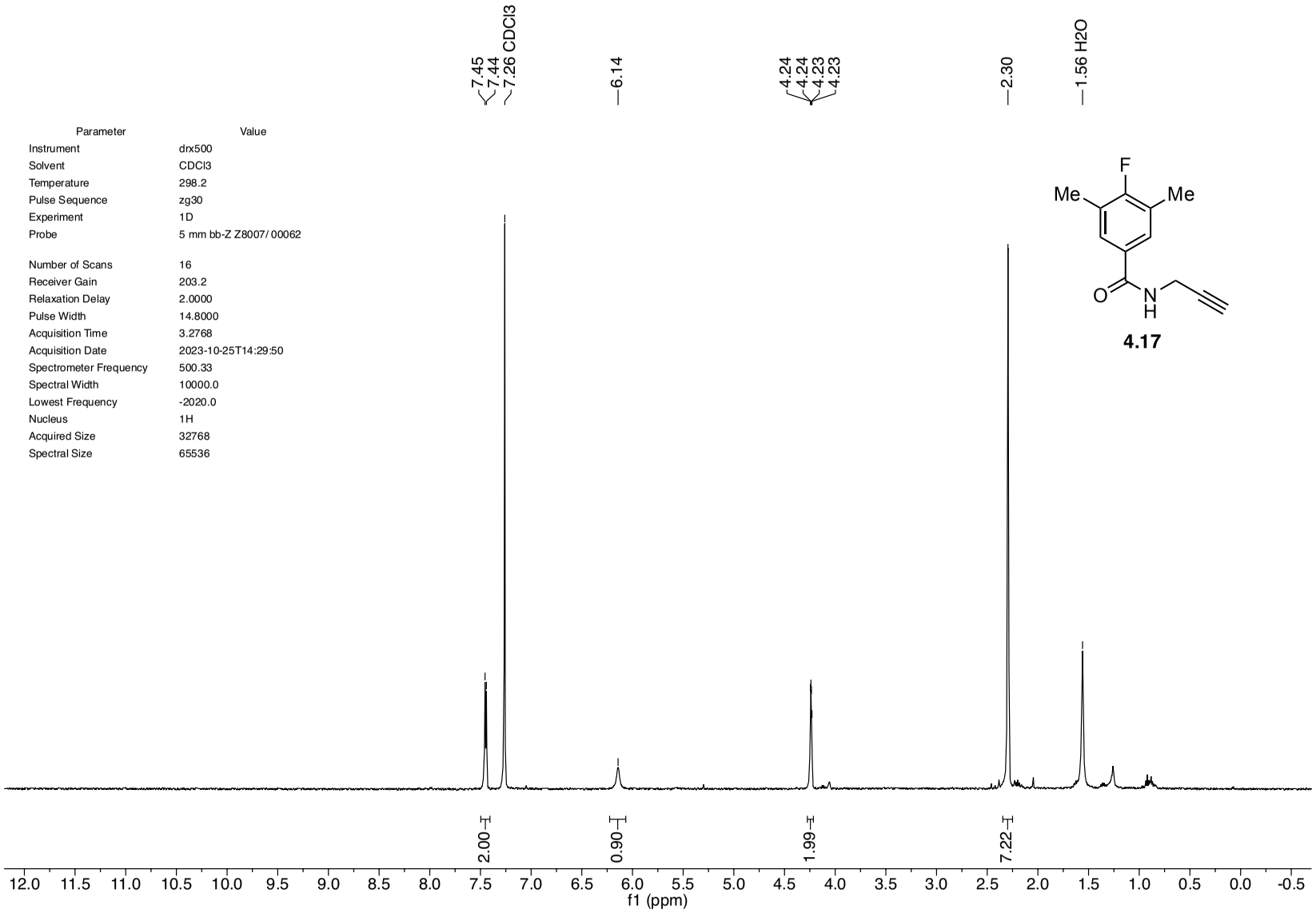
7.45
7.44
7.26 CDCl3
6.14
4.24
4.24
4.23
4.23
2.30
1.56 H2O
Parameter Value
Instrument dnx500
Solvent CDCl3
Temperature 298.2
Pulse Sequence zg30
Experiment 1D
Probe 5 mm bb-Z Z8007/ 00062
Number of Scans 16
Receiver Gain 203.2
Relaxation Delay 2.0000
Pulse Width 14.8000
Acquisition Time 3.2768
Acquisition Date 2023-10-25T14:29:50
Spectrometer Frequency 500.33
Spectral Width 10000.0
Lowest Frequency -2020.0
Nucleus 1H
Acquired Size 32768
Spectral Size 65536
F
Me
Me
O
N
H
4.17
2.00
0.90
1.99
7.22
12.0 11.5 11.0 10.5 10.0 9.5 9.0 8.5 8.0 7.5 7.0 6.5 6.0 5.5 5.0 4.5 4.0 3.5 3.0 2.5 2.0 1.5 1.0 0.5 0.0 -0.5
f1 (ppm)

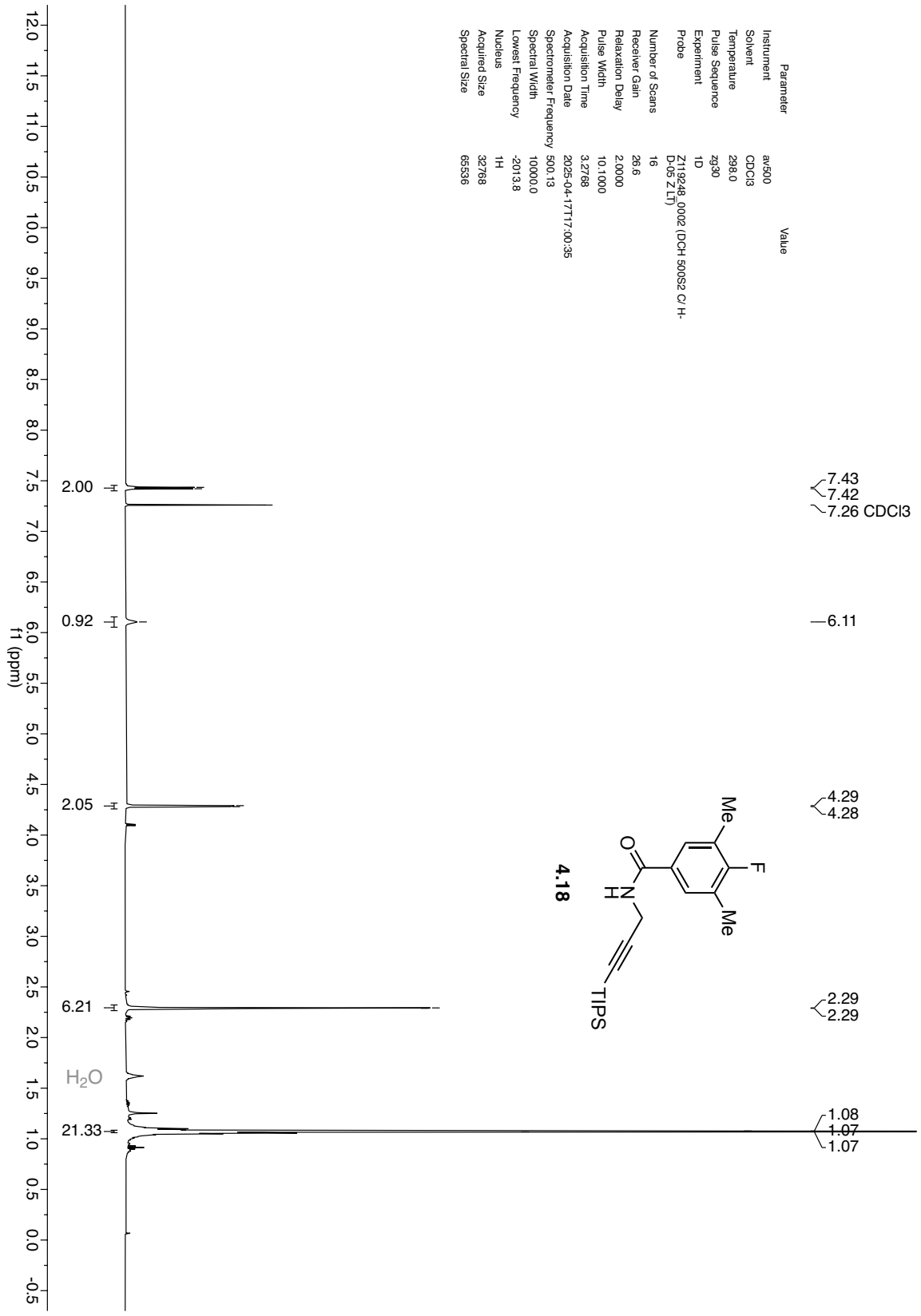
Parameter Value
Instrument av500
Solvent CDCl3
Temperature 298.0
Pulse Sequence zg30
Experiment 1D
Probe Z119248_0002 (DCH 500S2 C/ H-D-05 Z LT)
Number of Scans 16
Receiver Gain 26.6
Relaxation Delay 2.0000
Pulse Width 10.1000
Acquisition Time 3.2768
Acquisition Date 2025-04-17T17:00:35
Spectrometer Frequency 500.13
Spectral Width 10000.0
Lowest Frequency -2013.8
Nucleus 1H
Acquired Size 32768
Spectral Size 65536
4.18
Me
F
Me
O
N
H
TIPS
2.00
0.92
2.05
6.21
21.33
H2O
7.43
7.42
7.26 CDCl3
6.11
4.29
4.28
2.29
2.29
1.08
1.07
1.07
f1 (ppm)

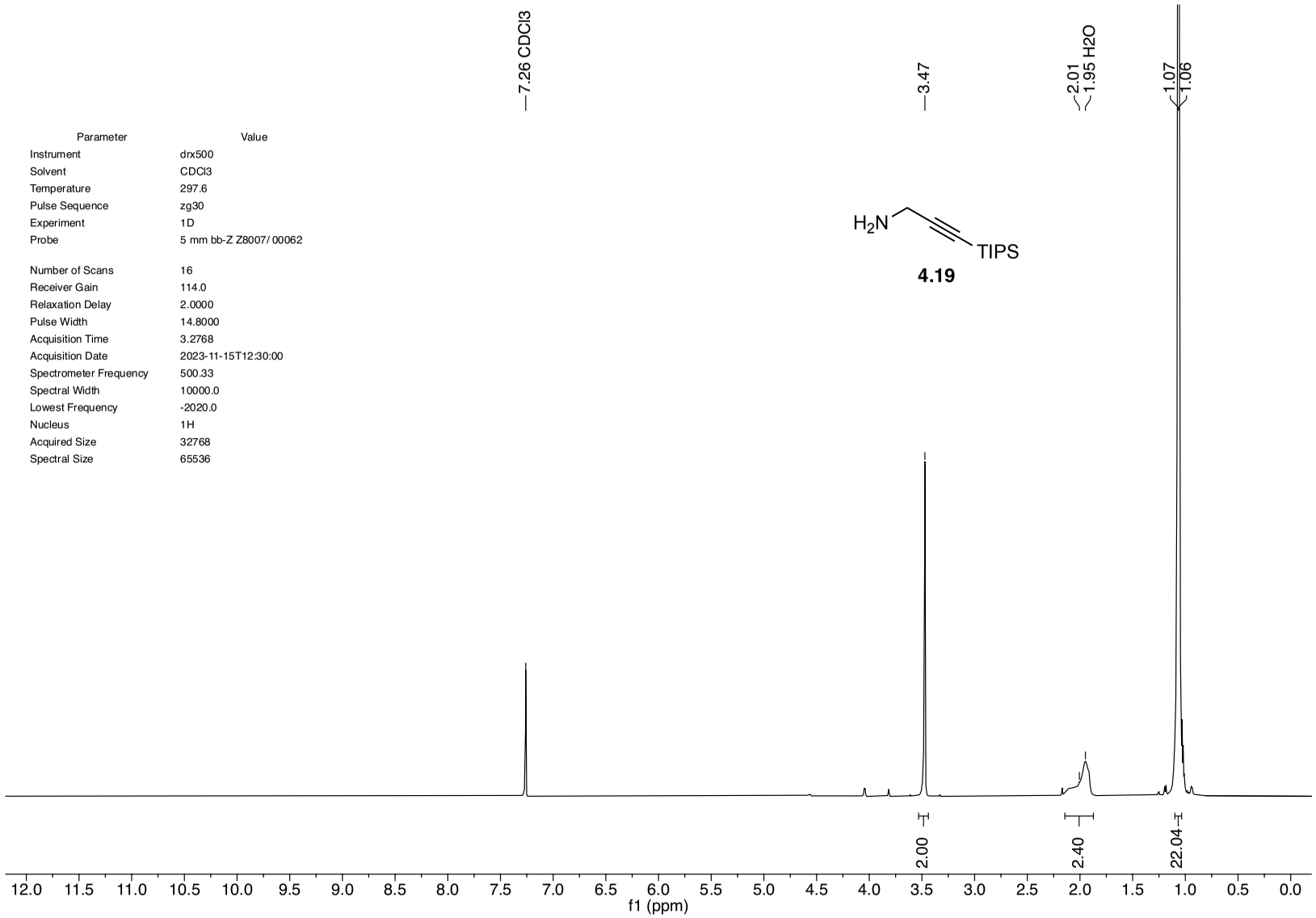
7.26 CDCl3
3.47
2.01
1.95 H2O
1.07
1.06
H2N
TIPS
4.19
Parameter Value
Instrument drx500
Solvent CDCl3
Temperature 297.6
Pulse Sequence zg30
Experiment 1D
Probe 5 mm bb-Z Z8007/ 00062
Number of Scans 16
Receiver Gain 114.0
Relaxation Delay 2.0000
Pulse Width 14.8000
Acquisition Time 3.2768
Acquisition Date 2023-11-15T12:30:00
Spectrometer Frequency 500.33
Spectral Width 10000.0
Lowest Frequency -2020.0
Nucleus 1H
Acquired Size 32768
Spectral Size 65536
2.00
2.40
22.04
12.0 11.5 11.0 10.5 10.0 9.5 9.0 8.5 8.0 7.5 7.0 6.5 6.0 5.5 5.0 4.5 4.0 3.5 3.0 2.5 2.0 1.5 1.0 0.5 0.0
f1 (ppm)

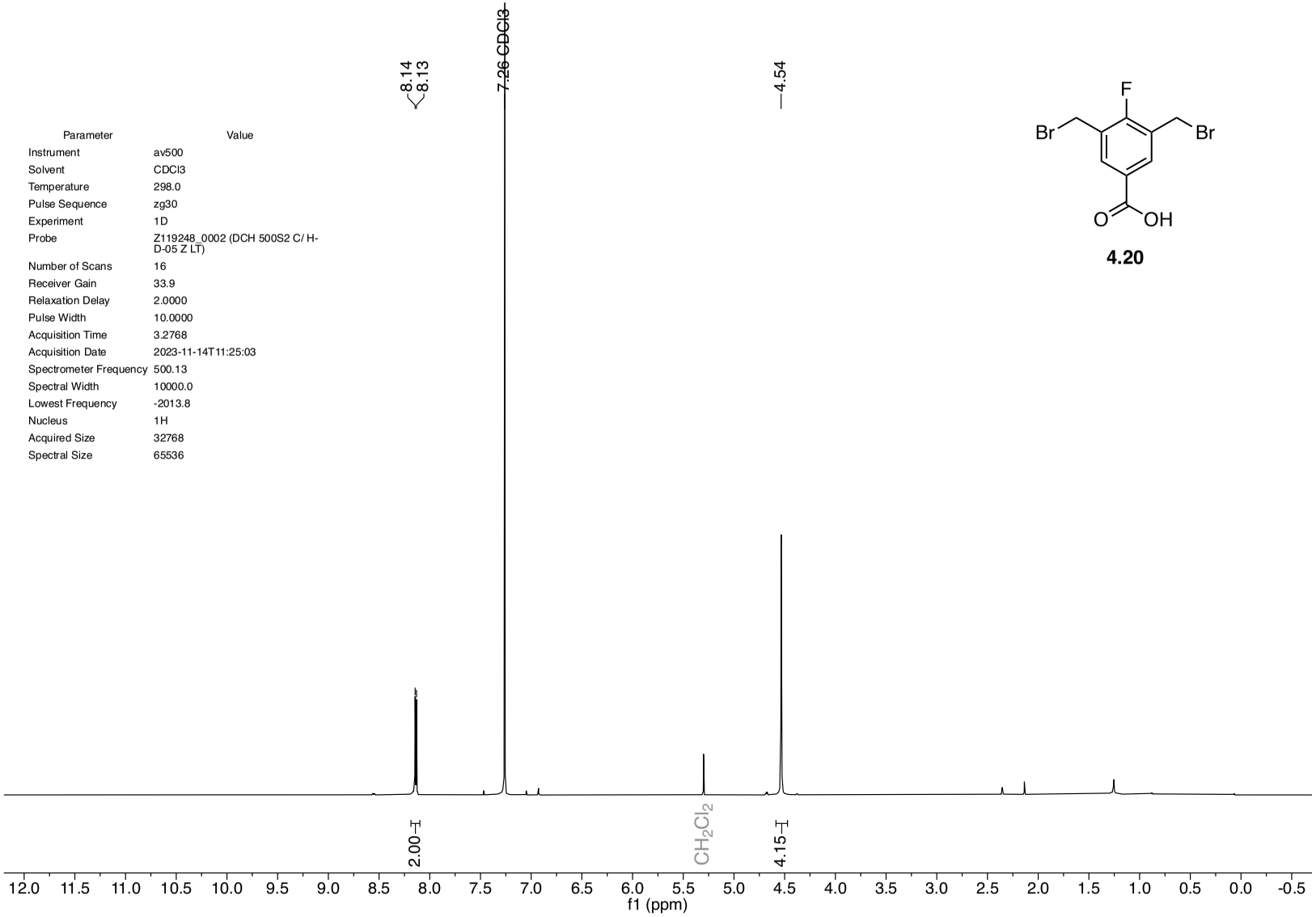
8.14
8.13
7.26 CDCl3
4.54
F
Br
Br
O
OH
4.20
Parameter Value
Instrument av500
Solvent CDCl3
Temperature 298.0
Pulse Sequence zg30
Experiment 1D
Probe Z119248_0002 (DCH 500S2 C/ H-D-05 Z LT)
Number of Scans 16
Receiver Gain 33.9
Relaxation Delay 2.0000
Pulse Width 10.0000
Acquisition Time 3.2768
Acquisition Date 2023-11-14T11:25:03
Spectrometer Frequency 500.13
Spectral Width 10000.0
Lowest Frequency -2013.8
Nucleus 1H
Acquired Size 32768
Spectral Size 65536
2.00
CH2Cl2
4.15
12.0 11.5 11.0 10.5 10.0 9.5 9.0 8.5 8.0 7.5 7.0 6.5 6.0 5.5 5.0 4.5 4.0 3.5 3.0 2.5 2.0 1.5 1.0 0.5 0.0 -0.5
f1 (ppm)

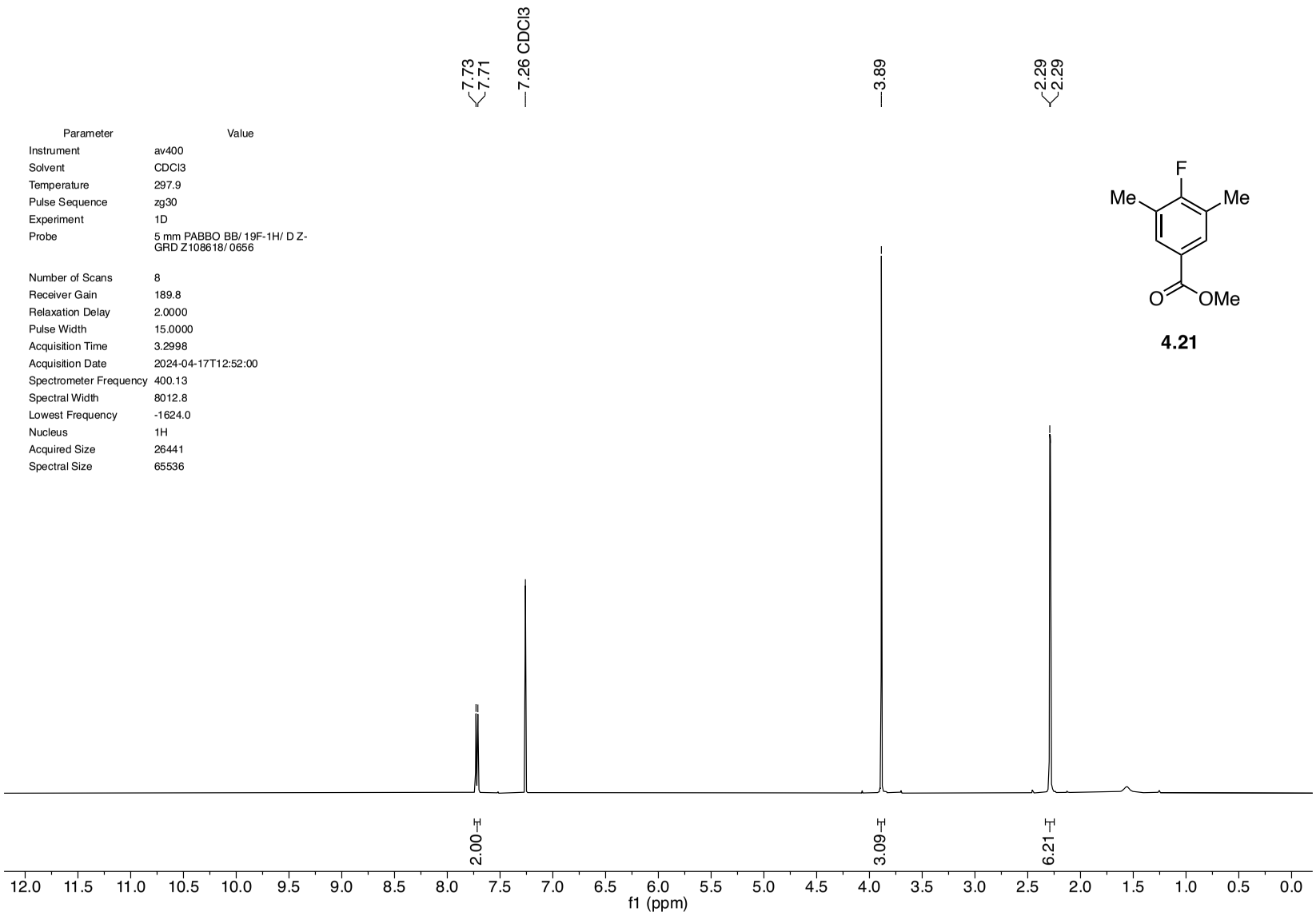
7.73
7.71
7.26 CDCl3
3.89
2.29
2.29
Parameter Value
Instrument av400
Solvent CDCl3
Temperature 297.9
Pulse Sequence zg30
Experiment 1D
Probe 5 mm PABBO BB/ 19F-1H/ D Z-GRD Z108618/ 0656
Number of Scans 8
Receiver Gain 189.8
Relaxation Delay 2.0000
Pulse Width 15.0000
Acquisition Time 3.2998
Acquisition Date 2024-04-17T12:52:00
Spectrometer Frequency 400.13
Spectral Width 8012.8
Lowest Frequency -1624.0
Nucleus 1H
Acquired Size 26441
Spectral Size 65536
F
Me
Me
O
OMe
4.21
2.00
3.09
6.21
12.0 11.5 11.0 10.5 10.0 9.5 9.0 8.5 8.0 7.5 7.0 6.5 6.0 5.5 5.0 4.5 4.0 3.5 3.0 2.5 2.0 1.5 1.0 0.5 0.0
f1 (ppm)

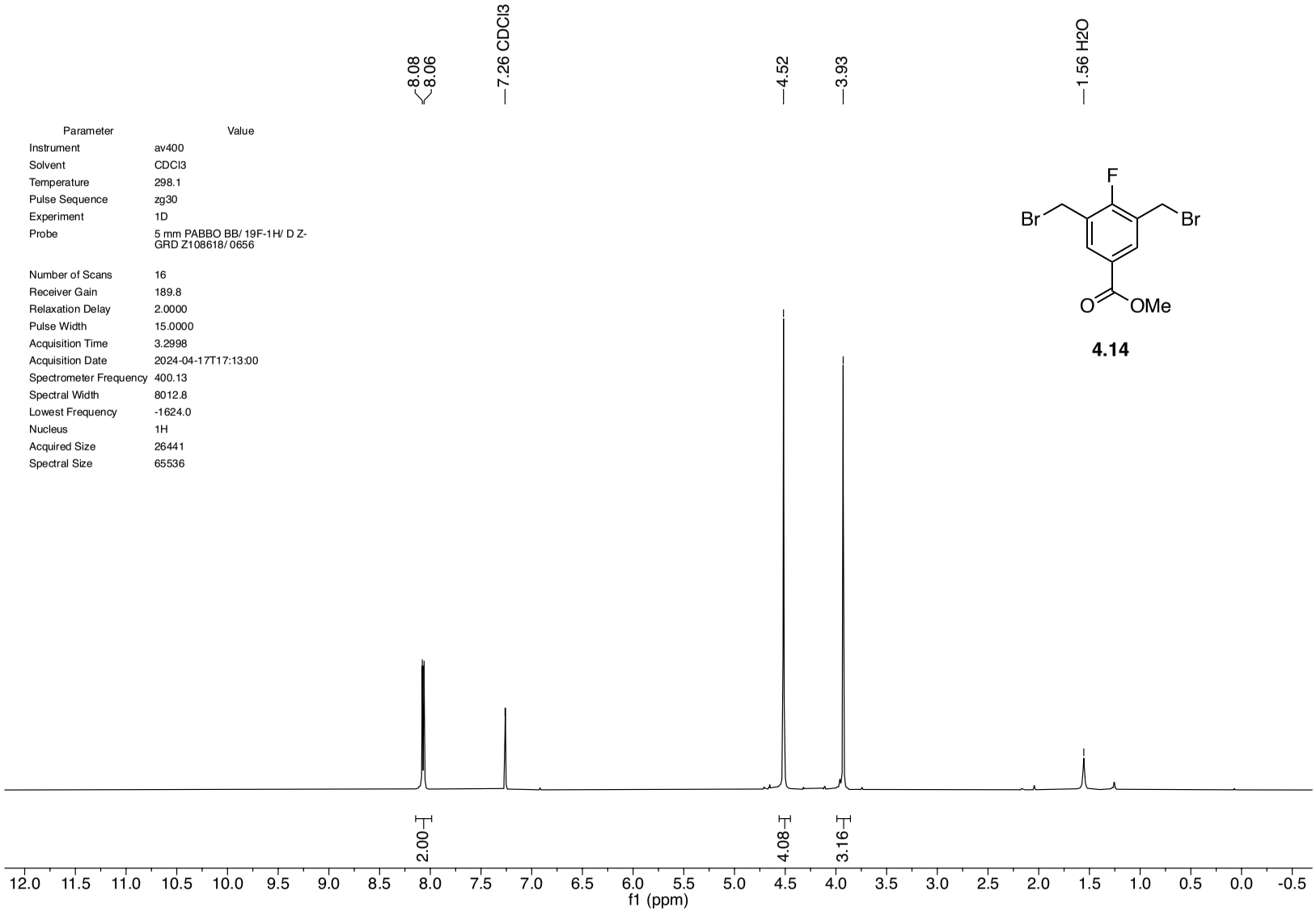
8.08
8.06
7.26 CDCl3
4.52
3.93
1.56 H2O
Parameter Value
Instrument av400
Solvent CDCl3
Temperature 298.1
Pulse Sequence zg30
Experiment 1D
Probe 5 mm PABBO BB/ 19F-1H/ D Z-GRD Z108618/ 0656
Number of Scans 16
Receiver Gain 189.8
Relaxation Delay 2.0000
Pulse Width 15.0000
Acquisition Time 3.2998
Acquisition Date 2024-04-17T17:13:00
Spectrometer Frequency 400.13
Spectral Width 8012.8
Lowest Frequency -1624.0
Nucleus 1H
Acquired Size 26441
Spectral Size 65536
F
Br
Br
O
OMe
2.00
4.08
3.16
12.0 11.5 11.0 10.5 10.0 9.5 9.0 8.5 8.0 7.5 7.0 6.5 6.0 5.5 5.0 4.5 4.0 3.5 3.0 2.5 2.0 1.5 1.0 0.5 0.0 -0.5
f1 (ppm)

4.14

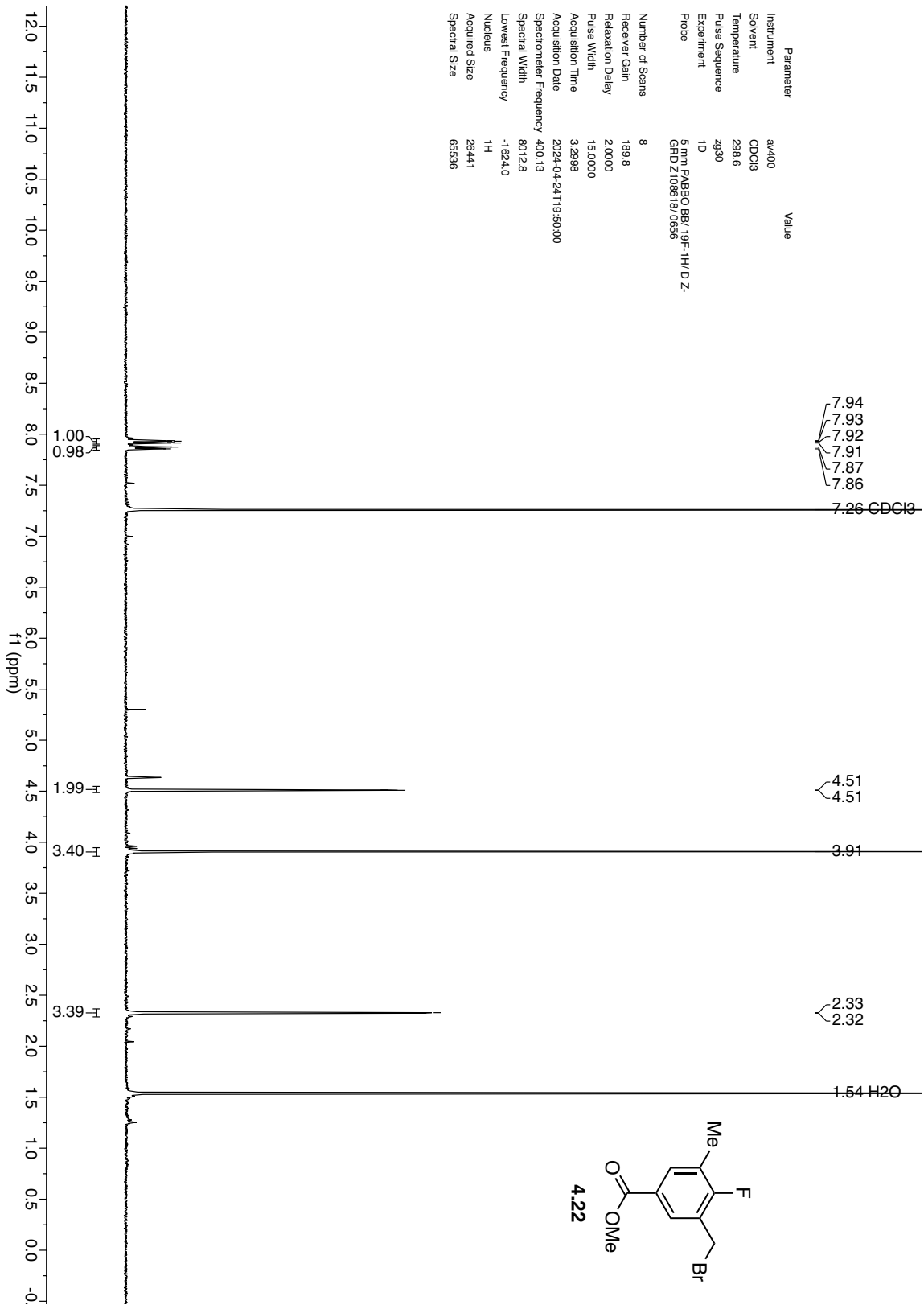
Parameter Value
Instrument av400
Solvent CDCl3
Temperature 298.6
Pulse Sequence zg30
Experiment 1D
Probe 5 mm PABBO BB/ 19F-1H/ D Z-GRD Z108618/ 0656
Number of Scans 8
Receiver Gain 189.8
Relaxation Delay 2.0000
Pulse Width 15.0000
Acquisition Time 3.2998
Acquisition Date 2024-04-24T19:50:00
Spectrometer Frequency 400.13
Spectral Width 8012.8
Lowest Frequency -1624.0
Nucleus 1H
Acquired Size 26441
Spectral Size 65536
7.94
7.93
7.92
7.91
7.87
7.86
7.26 CDCl3
4.51
4.51
3.91
2.33
2.32
1.54 H2O
1.00
0.98
1.99
3.40
3.39
Me
F
Br
OMe
O
4.22
f1 (ppm)

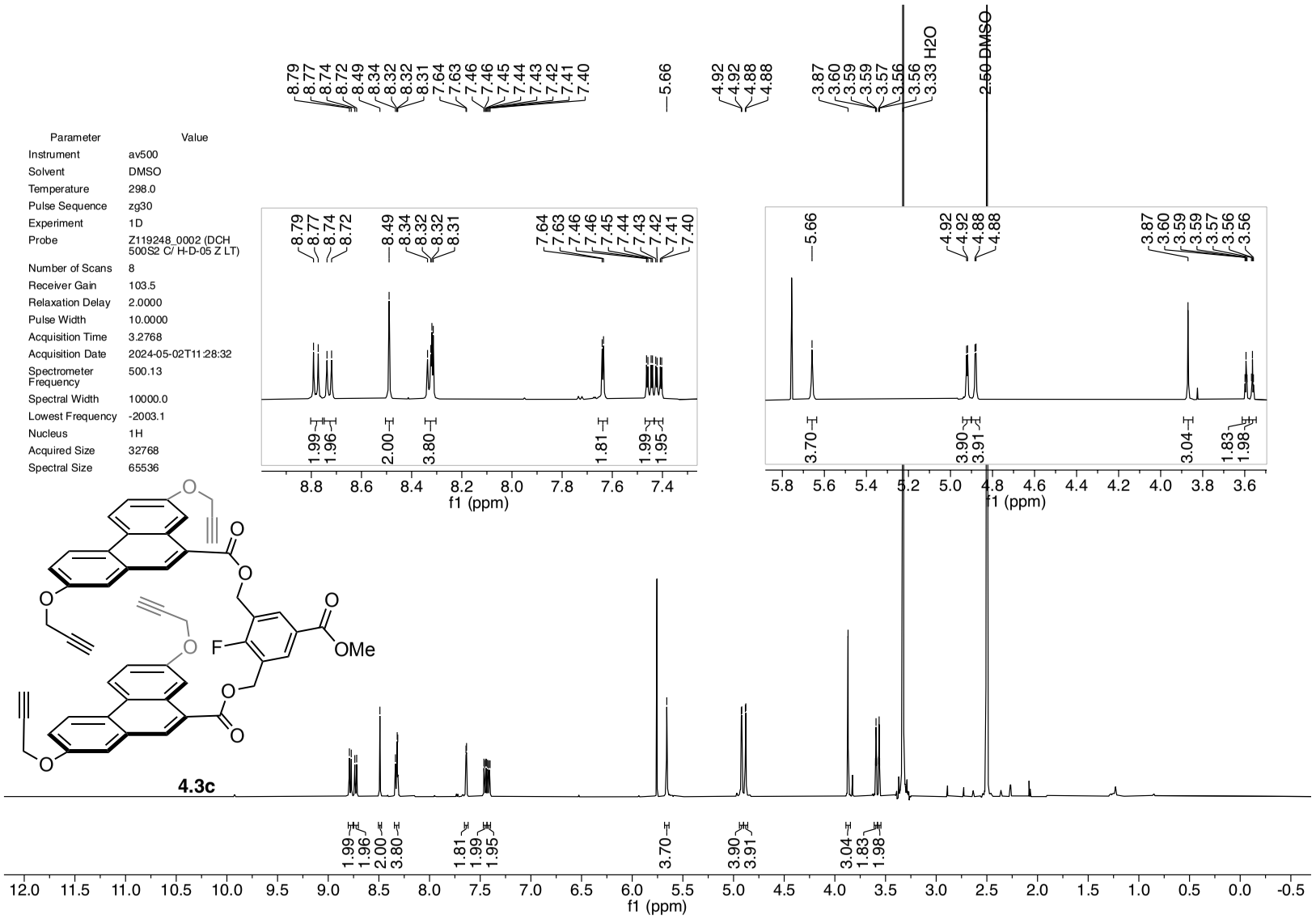
8.79
8.77
8.74
8.72
8.49
8.34
8.32
8.32
8.31
7.64
7.63
7.46
7.46
7.45
7.44
7.43
7.42
7.41
7.40
5.66
4.92
4.92
4.88
4.88
3.87
3.60
3.59
3.59
3.57
3.56
3.56
3.33 H2O
2.50 DMSO
Parameter Value
Instrument av500
Solvent DMSO
Temperature 298.0
Pulse Sequence zg30
Experiment 1D
Probe Z119248_0002 (DCH 500S2 C/ H-D-05 Z LT)
Number of Scans 8
Receiver Gain 103.5
Relaxation Delay 2.0000
Pulse Width 10.0000
Acquisition Time 3.2768
Acquisition Date 2024-05-02T11:28:32
Spectrometer Frequency 500.13
Spectral Width 10000.0
Lowest Frequency -2003.1
Nucleus 1H
Acquired Size 32768
Spectral Size 65536
1.99
1.96
2.00
3.80
1.81
1.99
1.95
3.70
3.90
3.91
3.04
1.83
1.98
f1 (ppm)
F
OMe
4.3c

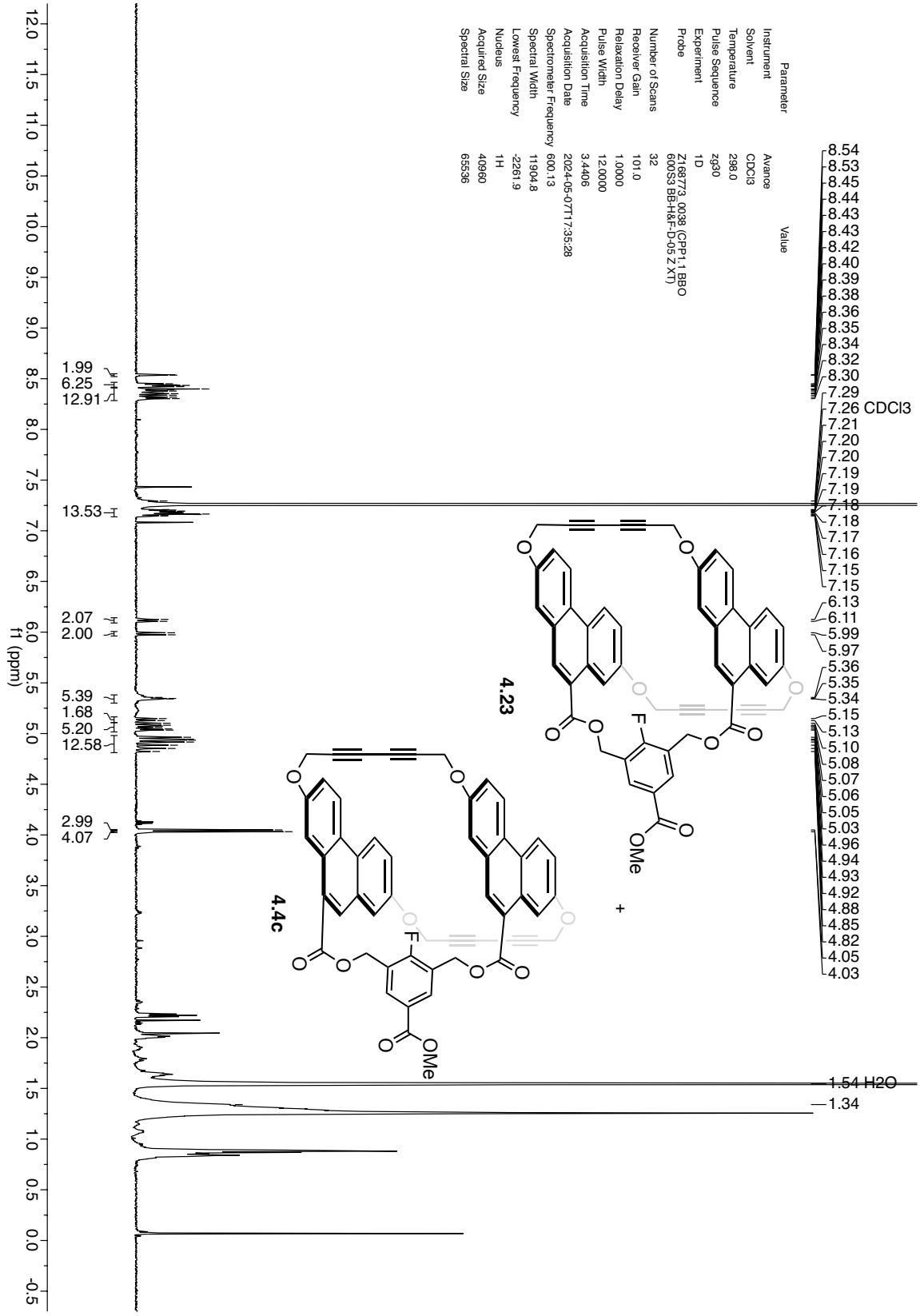
Parameter Value
Instrument Avance
Solvent CDCl3
Temperature 298.0
Pulse Sequence zg30
Experiment 1D
Probe Z168773_0038 (CPP1;1 BBO 600S3 BB-H&F-D-05 Z XT)
Number of Scans 32
Receiver Gain 101.0
Relaxation Delay 1.0000
Pulse Width 12.0000
Acquisition Time 3.4406
Acquisition Date 2024-05-07T17:35:28
Spectrometer Frequency 600.13
Spectral Width 11904.8
Lowest Frequency -2261.9
Nucleus 1H
Acquired Size 4096
Spectral Size 65536
8.54
8.53
8.45
8.44
8.43
8.43
8.42
8.40
8.39
8.38
8.36
8.35
8.34
8.32
8.30
7.29
7.26 CDCl3
7.21
7.20
7.20
7.19
7.19
7.18
7.18
7.17
7.16
7.15
7.15
6.13
6.11
5.99
5.97
5.36
5.35
5.34
5.15
5.13
5.10
5.08
5.07
5.06
5.05
5.03
4.96
4.94
4.93
4.92
4.88
4.85
4.82
4.05
4.03
1.54 H2O
1.34
1.99
6.25
12.91
13.53
2.07
2.00
5.39
1.68
5.20
12.58
2.99
4.07
4.23
4.4c
OMe
OMe
F
F
+
f1 (ppm)

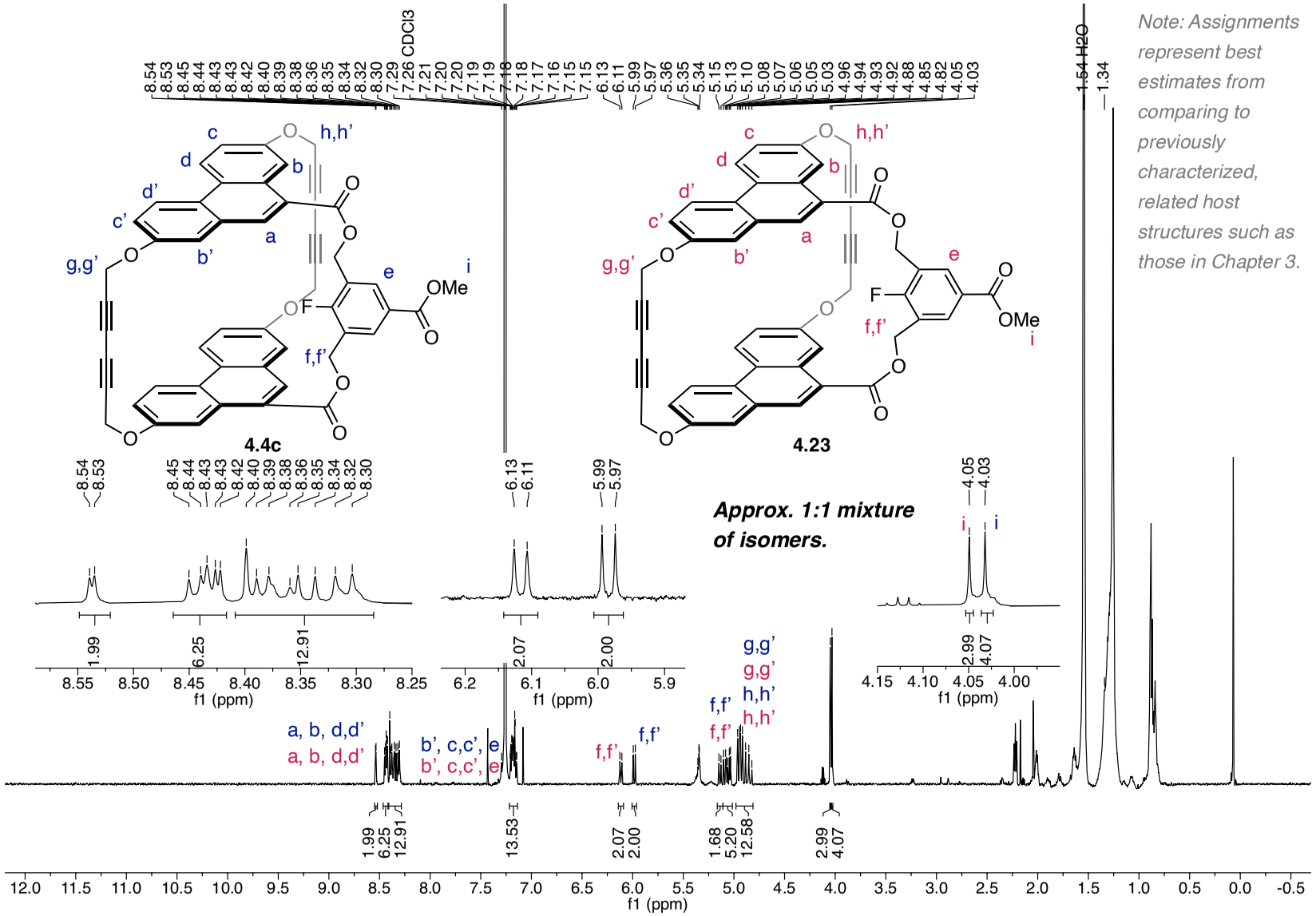

Note: Assignments represent best estimates from comparing to previously characterized, related host structures such as those in Chapter 3.

4.5.5 ^{13}C NMR spectra

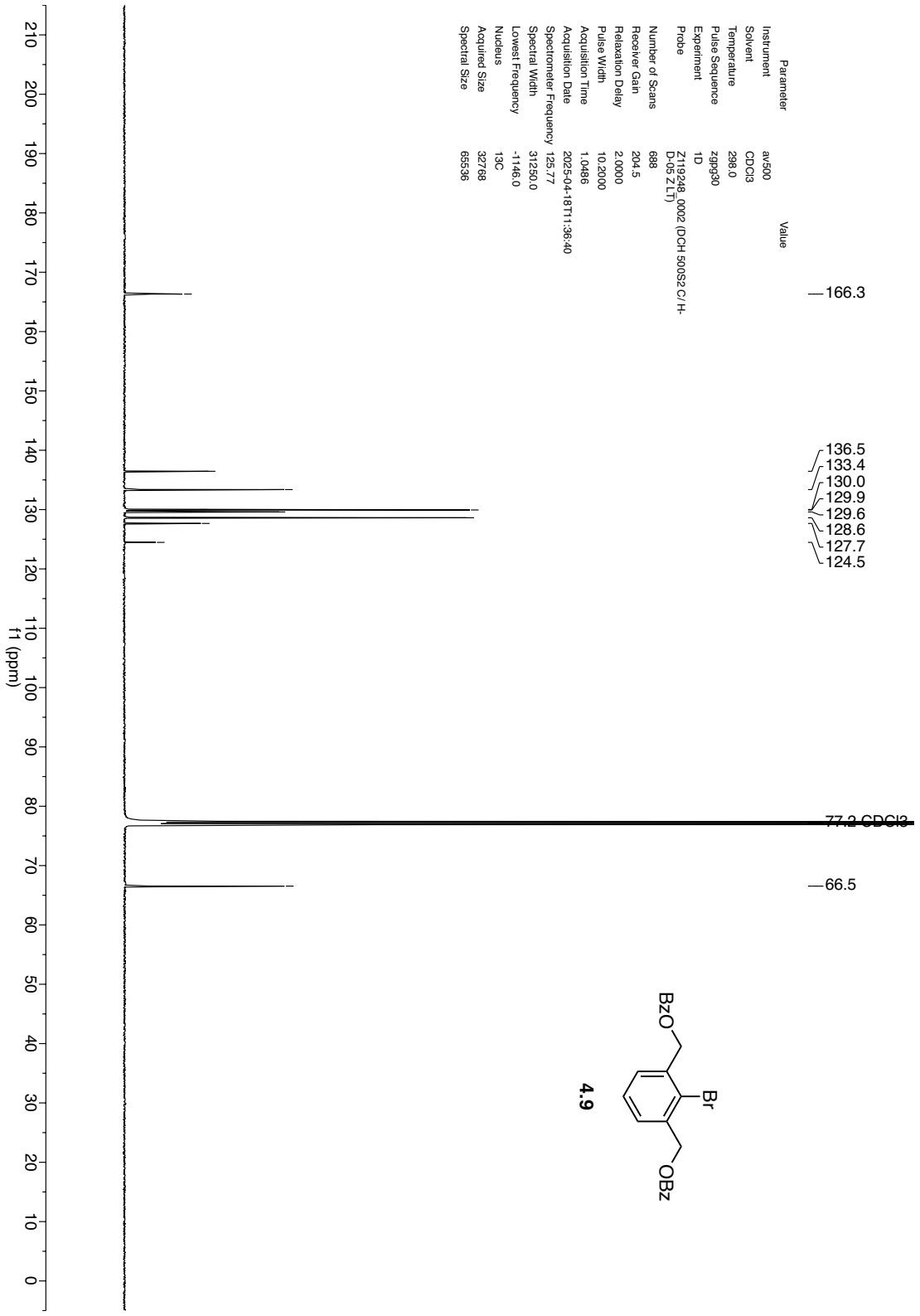

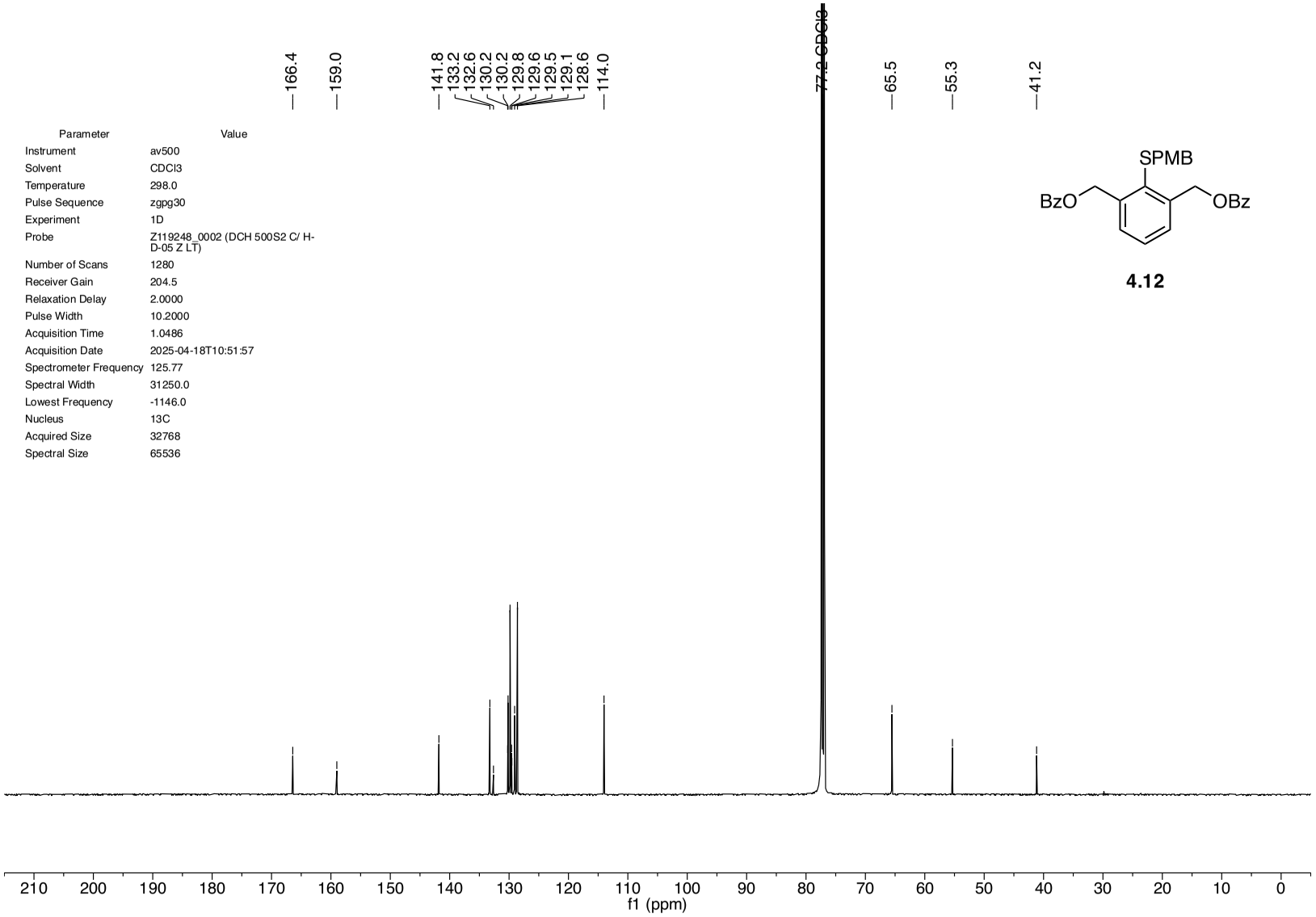
166.4
159.0
141.8
133.2
132.6
130.2
130.2
129.8
129.6
129.5
129.1
128.6
114.0
77.2 CDCl3
65.5
55.3
41.2
Parameter Value
Instrument av500
Solvent CDCl3
Temperature 298.0
Pulse Sequence zgpg30
Experiment 1D
Probe Z119248_0002 (DCH 500S2 C/ H-D-05 Z LT)
Number of Scans 1280
Receiver Gain 204.5
Relaxation Delay 2.0000
Pulse Width 10.2000
Acquisition Time 1.0486
Acquisition Date 2025-04-18T10:51:57
Spectrometer Frequency 125.77
Spectral Width 31250.0
Lowest Frequency -1146.0
Nucleus 13C
Acquired Size 32768
Spectral Size 65536
SPMB
BzO
OBz
4.12
210 200 190 180 170 160 150 140 130 120 110 100 90 80 70 60 50 40 30 20 10 0
f1 (ppm)

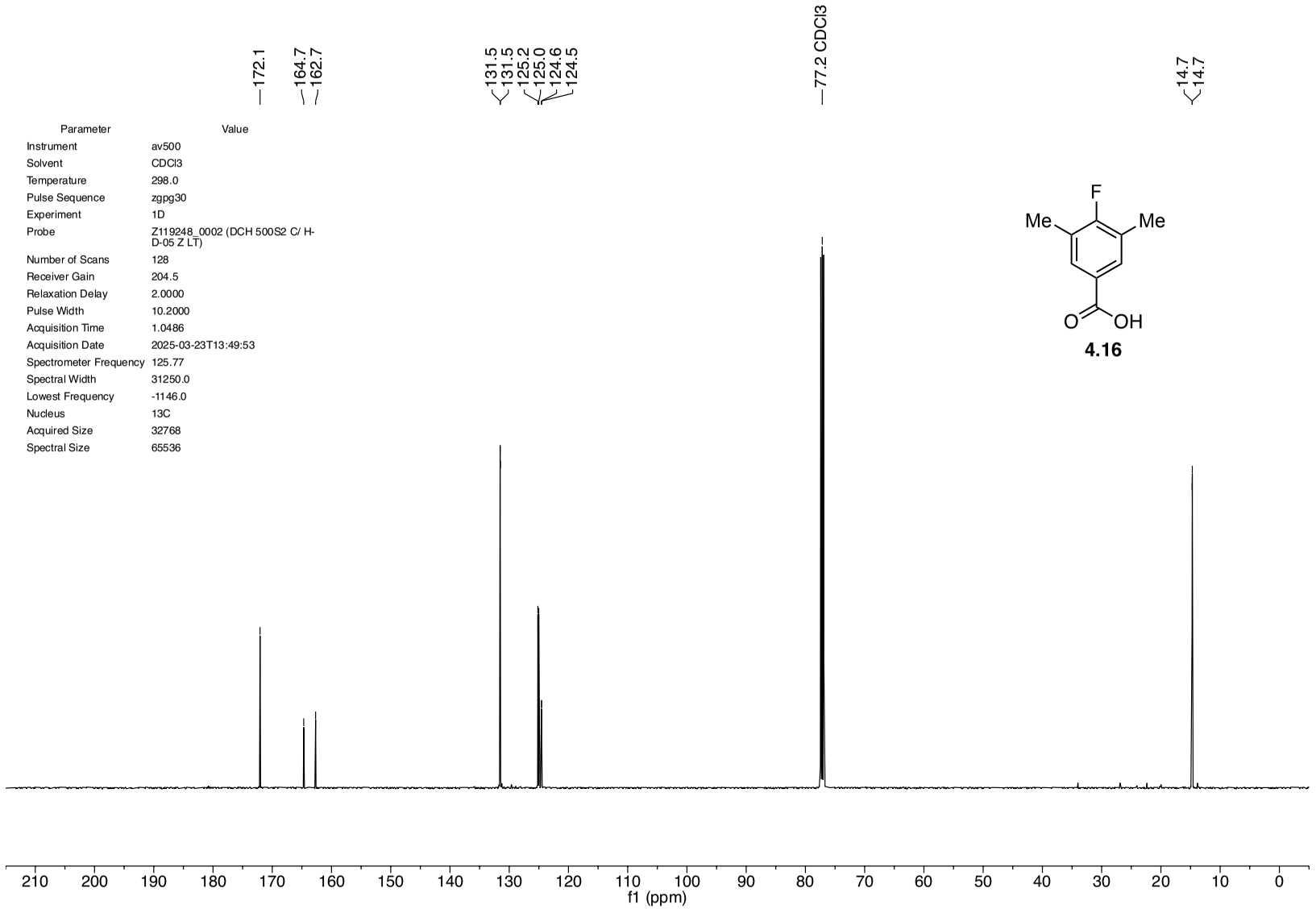
172.1
164.7
162.7
131.5
131.5
125.2
125.0
124.6
124.5
77.2 CDCl3
14.7
14.7
Parameter Value
Instrument av500
Solvent CDCl3
Temperature 298.0
Pulse Sequence zgpg30
Experiment 1D
Probe Z119248_0002 (DCH 500S2 C/ H-D-05 Z LT)
Number of Scans 128
Receiver Gain 204.5
Relaxation Delay 2.0000
Pulse Width 10.2000
Acquisition Time 1.0486
Acquisition Date 2025-03-23T13:49:53
Spectrometer Frequency 125.77
Spectral Width 31250.0
Lowest Frequency -1146.0
Nucleus 13C
Acquired Size 32768
Spectral Size 65536
F
Me
Me
O
OH
4.16
210 200 190 180 170 160 150 140 130 120 110 100 90 80 70 60 50 40 30 20 10 0
f1 (ppm)

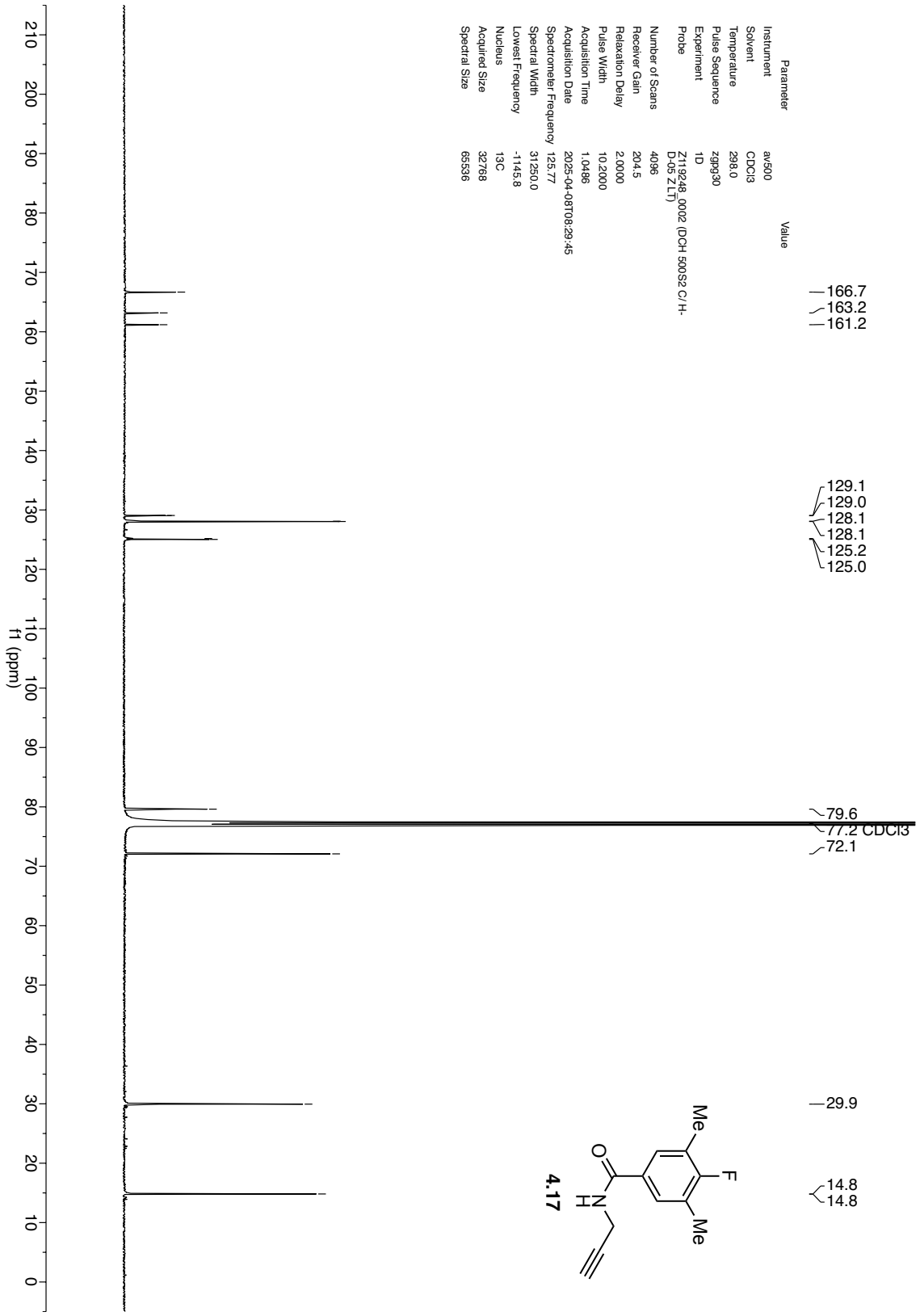
Parameter Value
Instrument av500
Solvent CDCl3
Temperature 298.0
Pulse Sequence zgpg30
Experiment 1D
Probe Z119248_0002 (DCH 500S2 C/ H-D-05 Z LT)
Number of Scans 4096
Receiver Gain 204.5
Relaxation Delay 2.0000
Pulse Width 10.2000
Acquisition Time 1.0486
Acquisition Date 2025-04-08T08:29:45
Spectrometer Frequency 125.77
Spectral Width 31250.0
Lowest Frequency -1145.8
Nucleus 13C
Acquired Size 32768
Spectral Size 65536
166.7
163.2
161.2
129.1
129.0
128.1
128.1
125.2
125.0
79.6
77.2 CDCl3
72.1
29.9
14.8
14.8
f1 (ppm)
Me
F
Me
O
N
H
4.17

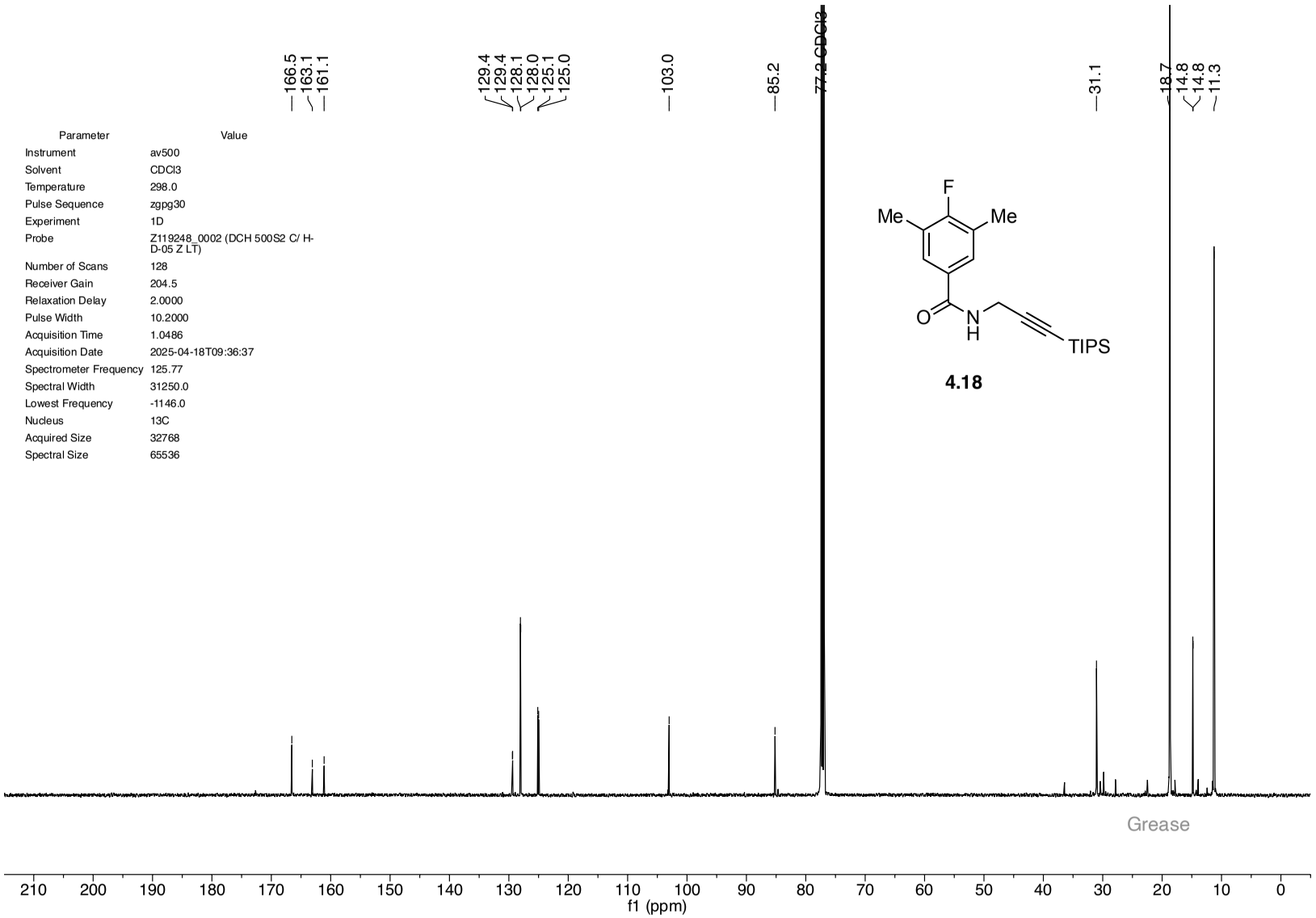
166.5
163.1
161.1
129.4
129.4
128.1
128.0
125.1
125.0
103.0
85.2
77.2 CDCl3
31.1
18.7
14.8
14.8
11.3
Parameter Value
Instrument av500
Solvent CDCl3
Temperature 298.0
Pulse Sequence zgpg30
Experiment 1D
Probe Z119248_0002 (DCH 500S2 C/ H-D-05 Z LT)
Number of Scans 128
Receiver Gain 204.5
Relaxation Delay 2.0000
Pulse Width 10.2000
Acquisition Time 1.0486
Acquisition Date 2025-04-18T09:36:37
Spectrometer Frequency 125.77
Spectral Width 31250.0
Lowest Frequency -1146.0
Nucleus 13C
Acquired Size 32768
Spectral Size 65536
F
Me
Me
O
N
H
TIPS
4.18
Grease
210 200 190 180 170 160 150 140 130 120 110 100 90 80 70 60 50 40 30 20 10 0
f1 (ppm)

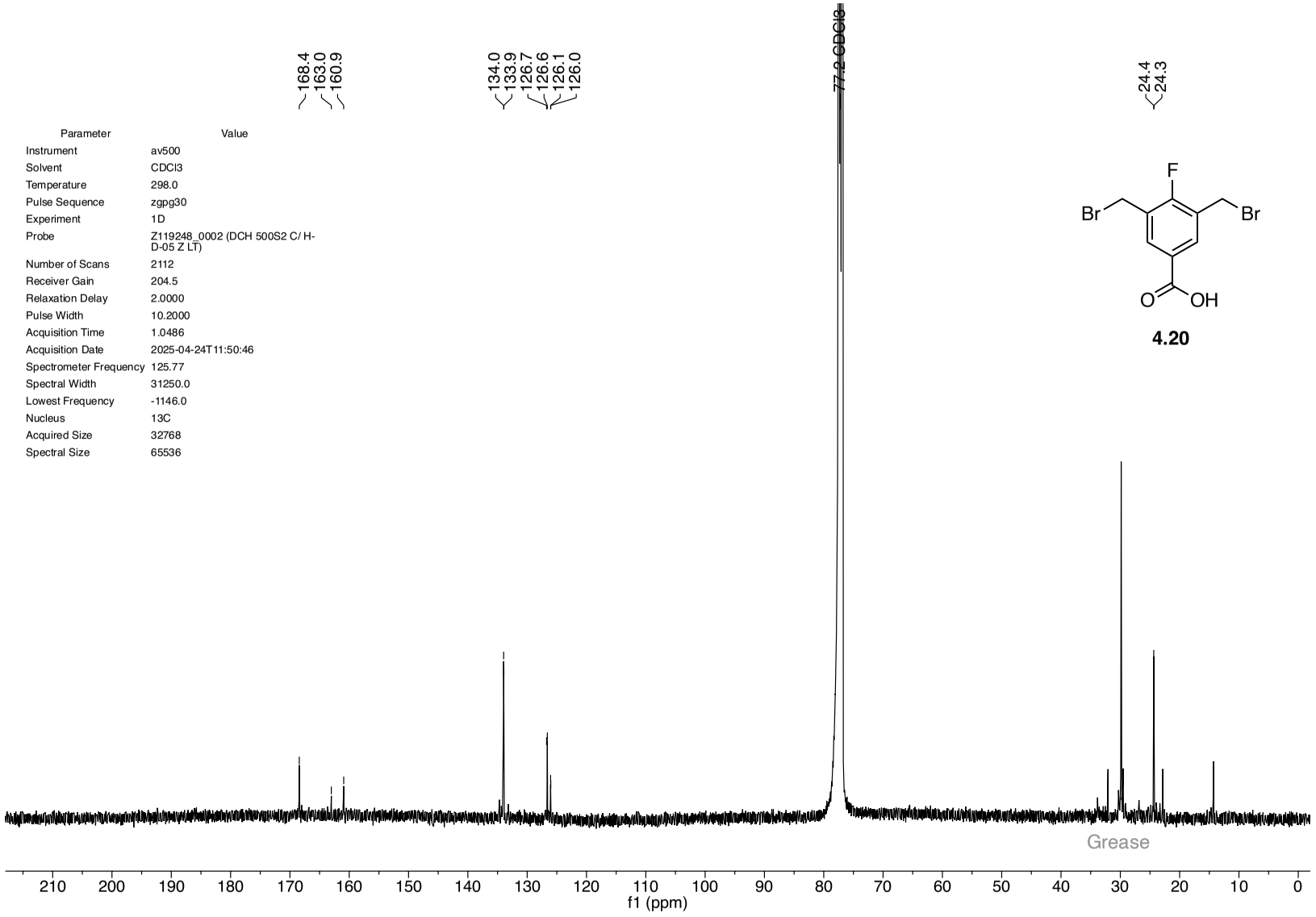
168.4
163.0
160.9
134.0
133.9
126.7
126.6
126.1
126.0
77.2 CDCl3
24.4
24.3
Parameter Value
Instrument av500
Solvent CDCl3
Temperature 298.0
Pulse Sequence zgpg30
Experiment 1D
Probe Z119248_0002 (DCH 500S2 C/ H-D-05 Z LT)
Number of Scans 2112
Receiver Gain 204.5
Relaxation Delay 2.0000
Pulse Width 10.2000
Acquisition Time 1.0486
Acquisition Date 2025-04-24T11:50:46
Spectrometer Frequency 125.77
Spectral Width 31250.0
Lowest Frequency -1146.0
Nucleus 13C
Acquired Size 32768
Spectral Size 65536
F
Br
Br
O
OH
4.20
Grease
210 200 190 180 170 160 150 140 130 120 110 100 90 80 70 60 50 40 30 20 10 0
f1 (ppm)

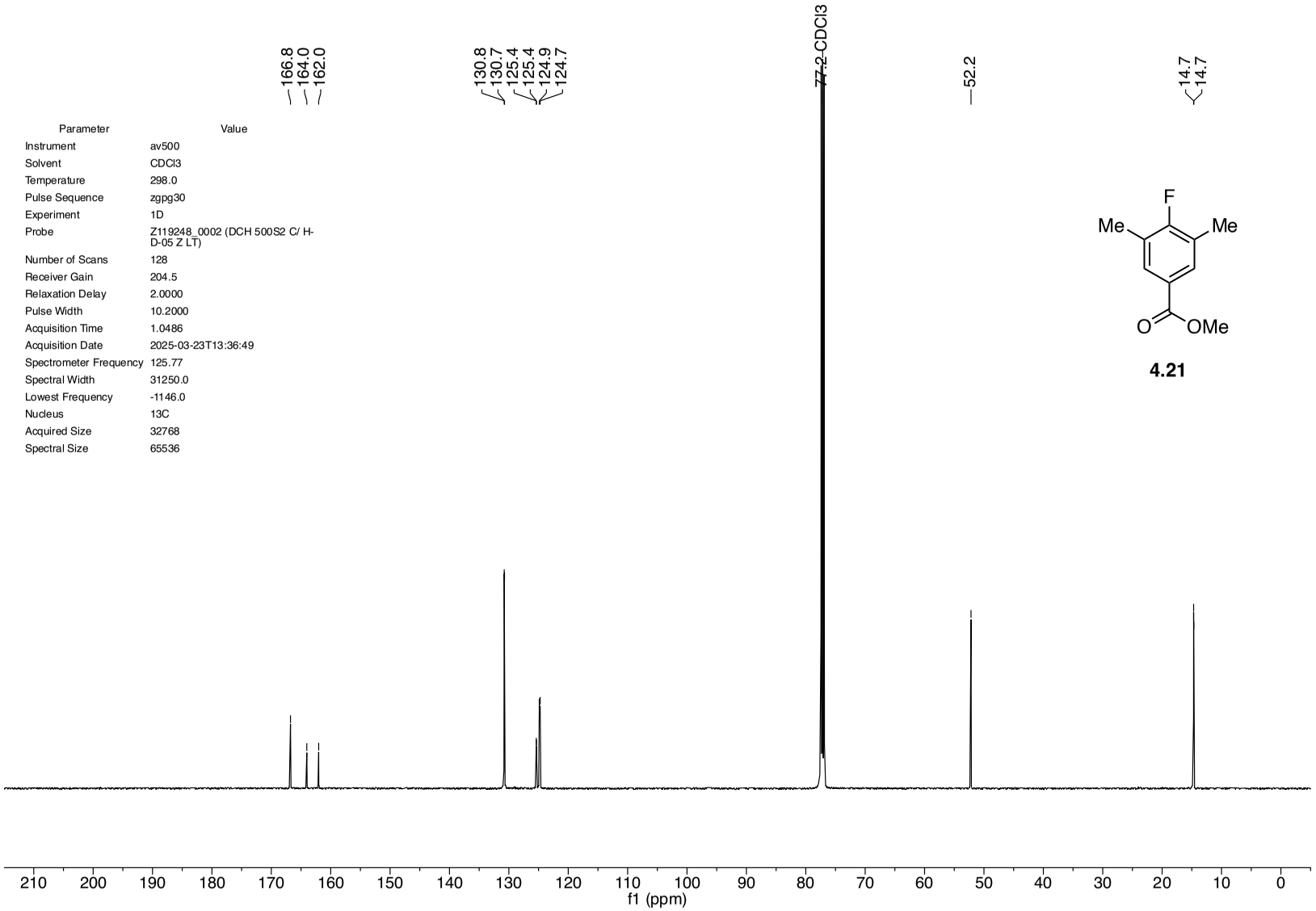
166.8
164.0
162.0
130.8
130.7
125.4
125.4
124.9
124.7
77.2-CDCl3
52.2
14.7
14.7
Parameter Value
Instrument av500
Solvent CDCl3
Temperature 298.0
Pulse Sequence zgpg30
Experiment 1D
Probe Z119248_0002 (DCH 500S2 C/ H-D-05 Z LT)
Number of Scans 128
Receiver Gain 204.5
Relaxation Delay 2.0000
Pulse Width 10.2000
Acquisition Time 1.0486
Acquisition Date 2025-03-23T13:36:49
Spectrometer Frequency 125.77
Spectral Width 31250.0
Lowest Frequency -1146.0
Nucleus 13C
Acquired Size 32768
Spectral Size 65536
F
Me
Me
O
OMe
4.21
210 200 190 180 170 160 150 140 130 120 110 100 90 80 70 60 50 40 30 20 10 0
f1 (ppm)

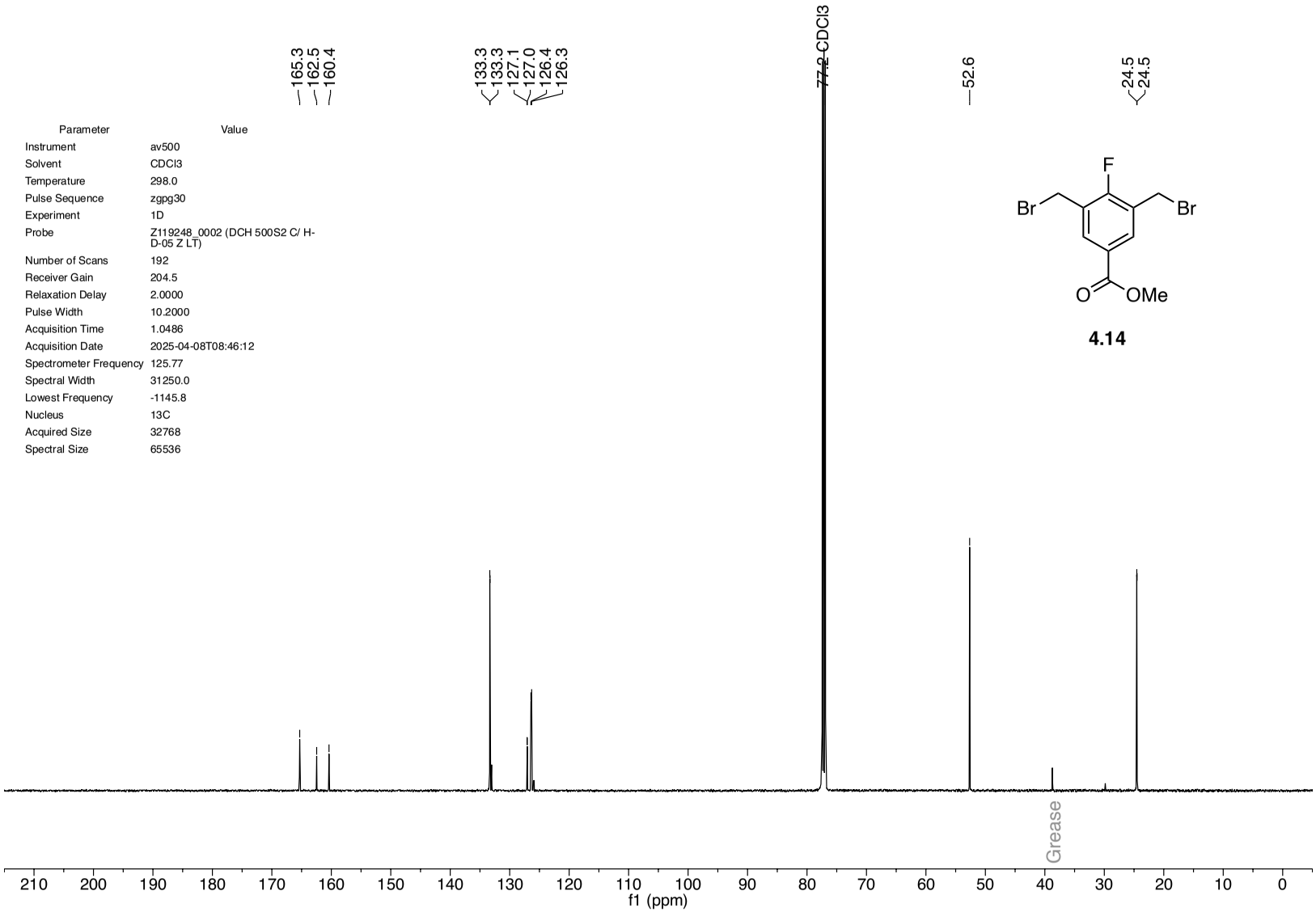
165.3
162.5
160.4
133.3
133.3
127.1
127.0
126.4
126.3
77.2 CDCl3
52.6
24.5
24.5
Parameter Value
Instrument av500
Solvent CDCl3
Temperature 298.0
Pulse Sequence zgpg30
Experiment 1D
Probe Z119248_0002 (DCH 500S2 C/ H-D-05 Z LT)
Number of Scans 192
Receiver Gain 204.5
Relaxation Delay 2.0000
Pulse Width 10.2000
Acquisition Time 1.0486
Acquisition Date 2025-04-08T08:46:12
Spectrometer Frequency 125.77
Spectral Width 31250.0
Lowest Frequency -1145.8
Nucleus 13C
Acquired Size 32768
Spectral Size 65536
F
Br
Br
O
OMe
4.14
Grease
210 200 190 180 170 160 150 140 130 120 110 100 90 80 70 60 50 40 30 20 10 0
f1 (ppm)

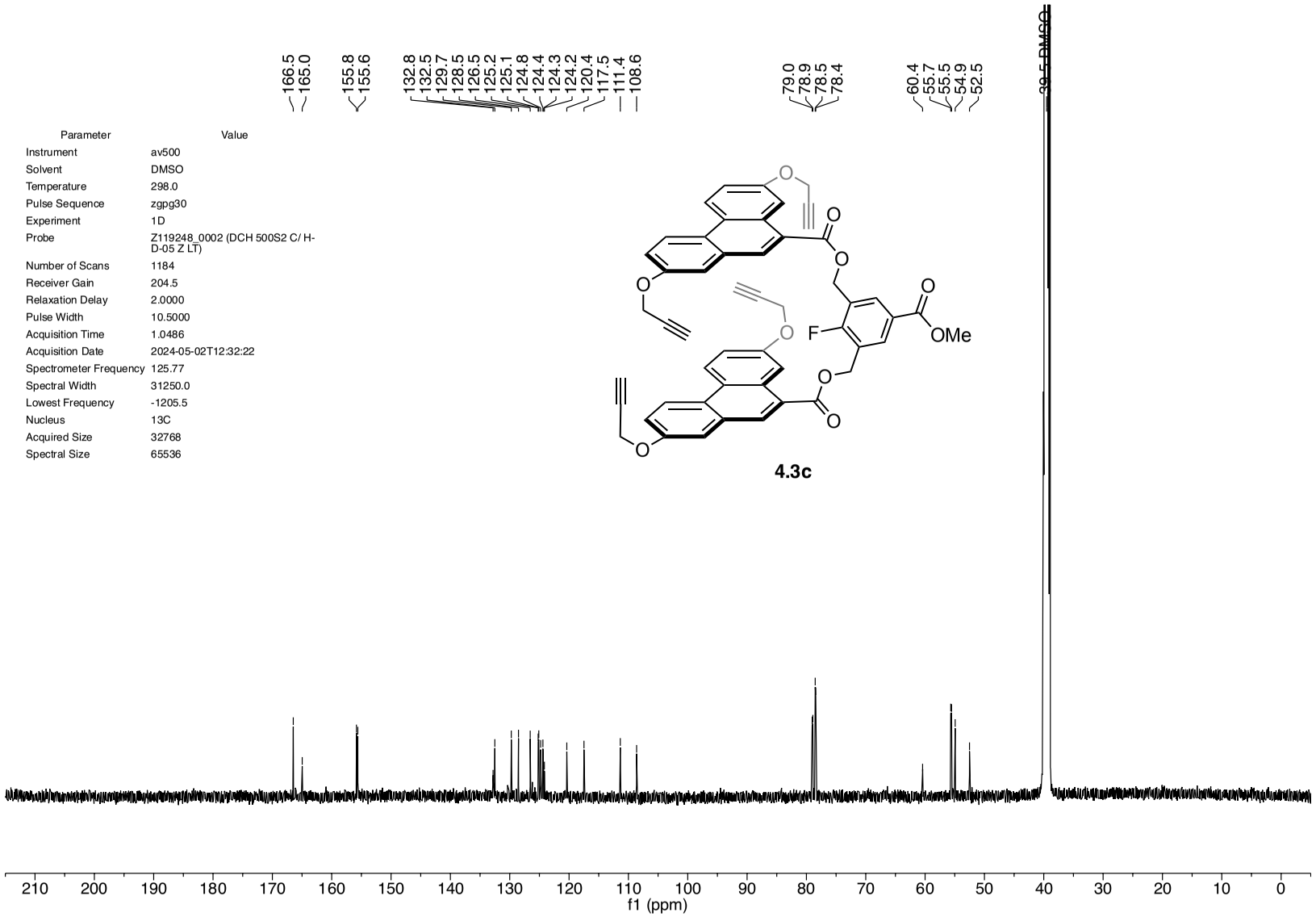
166.5
165.0
155.8
155.6
132.8
132.5
129.7
128.5
126.5
125.2
125.1
124.8
124.4
124.3
124.2
120.4
117.5
111.4
108.6
79.0
78.9
78.5
78.4
60.4
55.7
55.5
54.9
52.5
39.5 DMSO
Parameter Value
Instrument av500
Solvent DMSO
Temperature 298.0
Pulse Sequence zgpg30
Experiment 1D
Probe Z119248_0002 (DCH 500S2 C/ H-D-05 Z LT)
Number of Scans 1184
Receiver Gain 204.5
Relaxation Delay 2.0000
Pulse Width 10.5000
Acquisition Time 1.0486
Acquisition Date 2024-05-02T12:32:22
Spectrometer Frequency 125.77
Spectral Width 31250.0
Lowest Frequency -1205.5
Nucleus 13C
Acquired Size 32768
Spectral Size 65536
O
O
O
O
O
F
OMe
O
O
O
O
4.3c
210 200 190 180 170 160 150 140 130 120 110 100 90 80 70 60 50 40 30 20 10 0
f1 (ppm)

4.5.6 ^{19}F NMR spectra

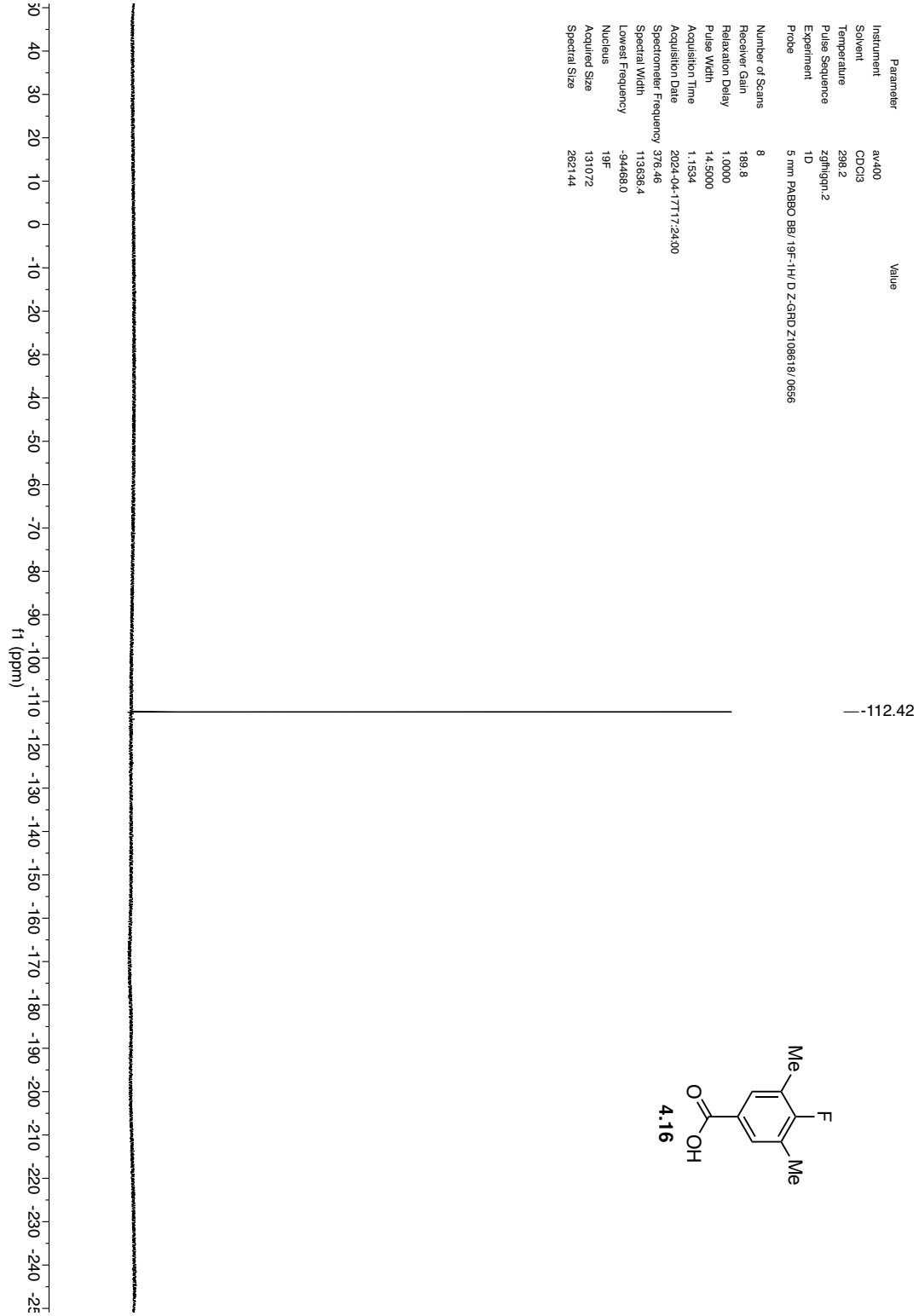

Parameter	Value
Instrument	av400
Solvent	CDCl3
Temperature	296.0
Pulse Sequence	zgfhigqn.2
Experiment	1D
Probe	5 mm PABBO BB/ 19F-1H/ D Z-GRD Z108618/ 0656
Number of Scans	16
Receiver Gain	189.8
Relaxation Delay	1.0000
Pulse Width	15.3000
Acquisition Time	1.3981
Acquisition Date	2025-04-24T09:49:00
Spectrometer Frequency	376.46
Spectral Width	93750.0
Lowest Frequency	-84524.8
Nucleus	19F
Acquired Size	131072
Spectral Size	262144

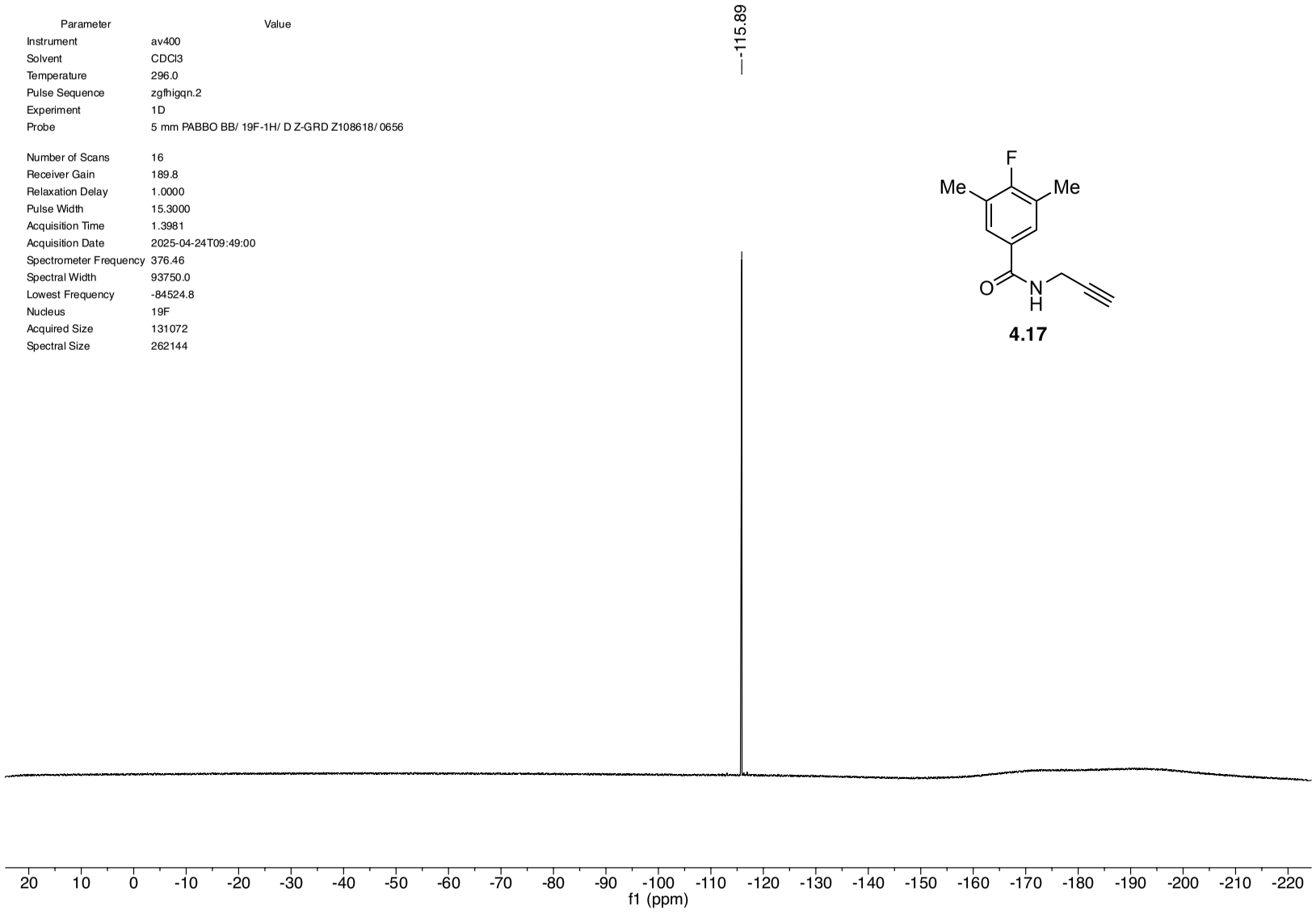

4.17

Parameter	Value
Instrument	av400
Solvent	CDCl3
Temperature	296.0
Pulse Sequence	zgfhigqn.2
Experiment	1D
Probe	5 mm PABBO BB/ 19F-1H/ D Z-GRD Z108618/ 0656
Number of Scans	8
Receiver Gain	189.8
Relaxation Delay	1.0000
Pulse Width	15.3000
Acquisition Time	1.3981
Acquisition Date	2025-04-18T10:02:00
Spectrometer Frequency	376.46
Spectral Width	93750.0
Lowest Frequency	-84524.8
Nucleus	19F
Acquired Size	131072
Spectral Size	262144

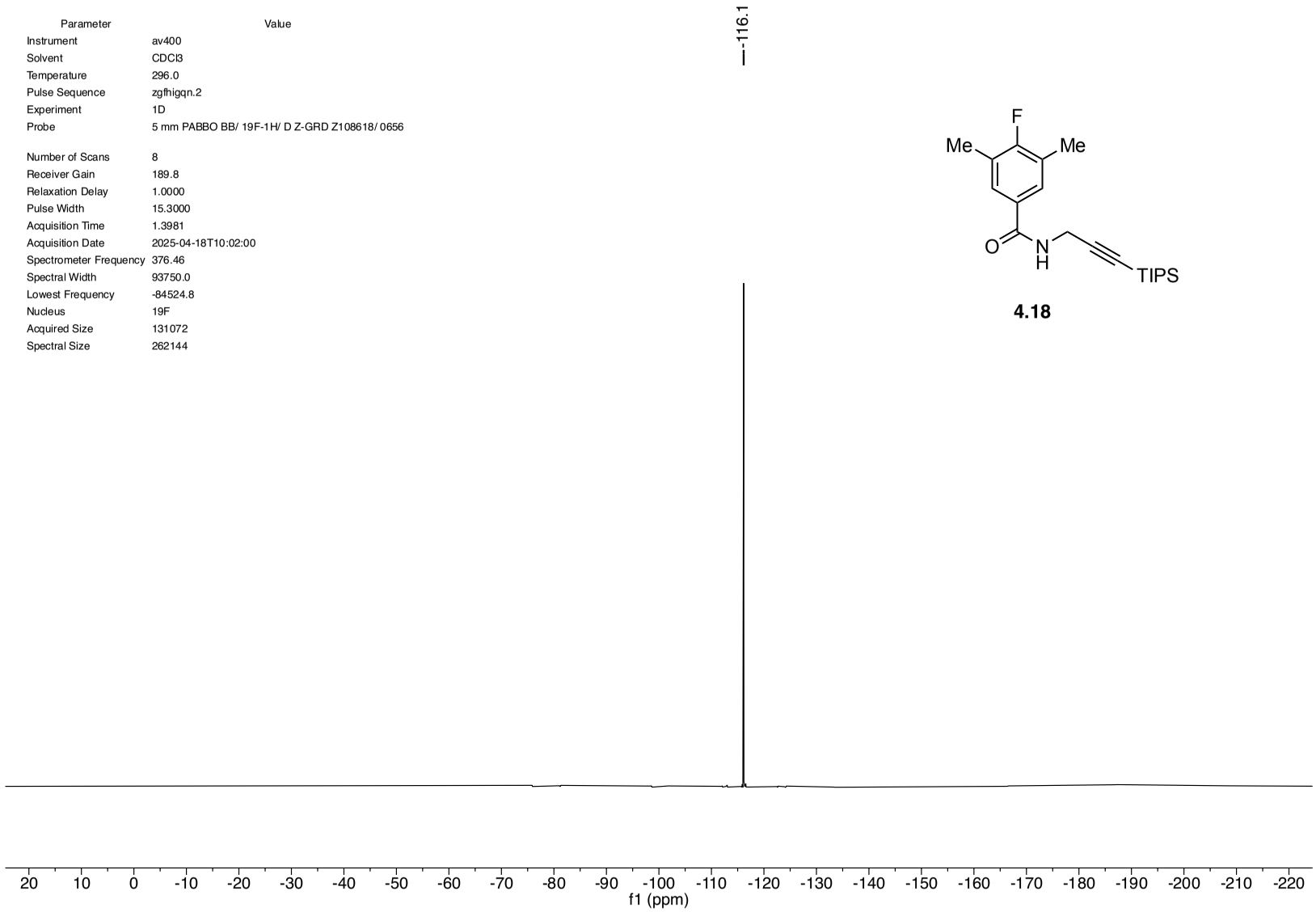

4.18

Parameter	Value
Instrument	av400
Solvent	CDCl3
Temperature	296.4
Pulse Sequence	zgfhigqn.2
Experiment	1D
Probe	5 mm PABBO BB/ 19F-1H/ D Z-GRD Z108618/ 0656
Number of Scans	16
Receiver Gain	189.8
Relaxation Delay	1.0000
Pulse Width	15.3000
Acquisition Time	1.3981
Acquisition Date	2025-04-24T12:49:00
Spectrometer Frequency	376.46
Spectral Width	93750.0
Lowest Frequency	-84524.8
Nucleus	19F
Acquired Size	131072
Spectral Size	262144

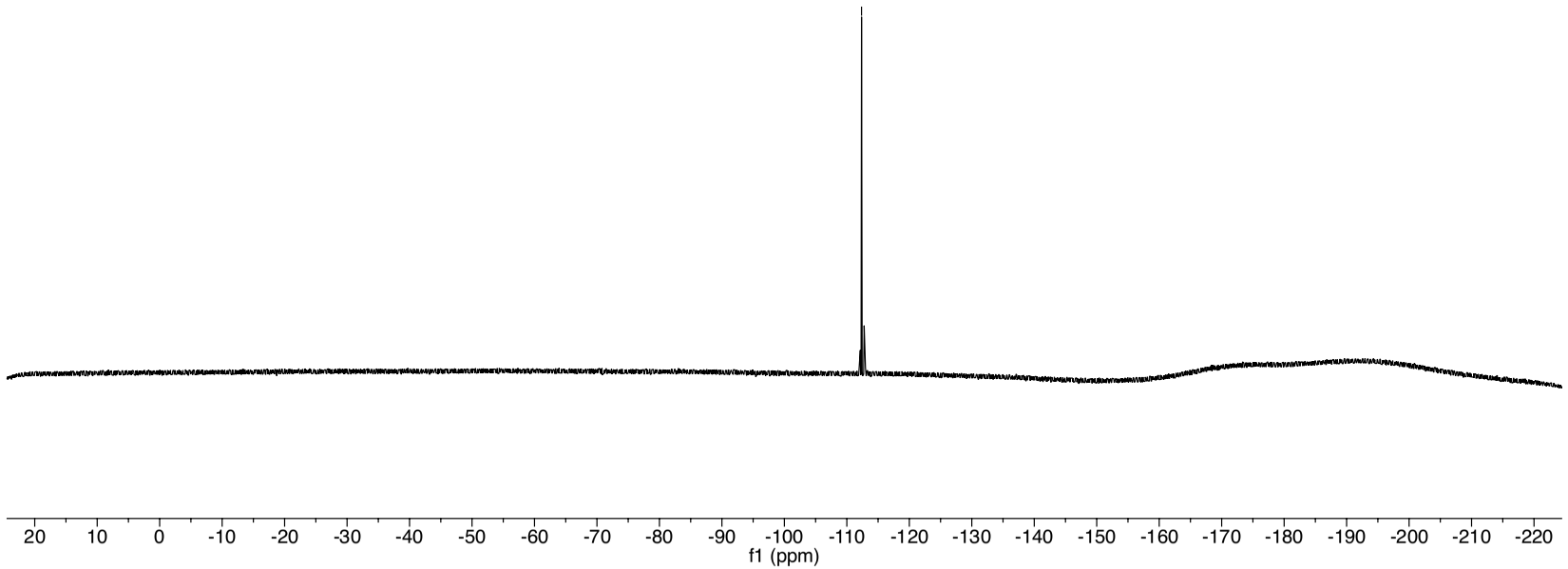

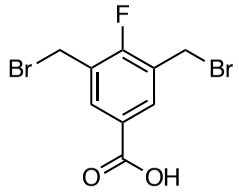

4.20

Parameter	Value
Instrument	av400
Solvent	CDCl3
Temperature	298.0
Pulse Sequence	zgfhigqn.2
Experiment	1D
Probe	5 mm PABBO BB/ 19F-1H/ D Z-GRD Z108618/ 0656
Number of Scans	8
Receiver Gain	189.8
Relaxation Delay	1.0000
Pulse Width	14.5000
Acquisition Time	1.1534
Acquisition Date	2024-04-17T12:57:00
Spectrometer Frequency	376.48
Spectral Width	113636.4
Lowest Frequency	-75643.1
Nucleus	19F
Acquired Size	131072
Spectral Size	262144

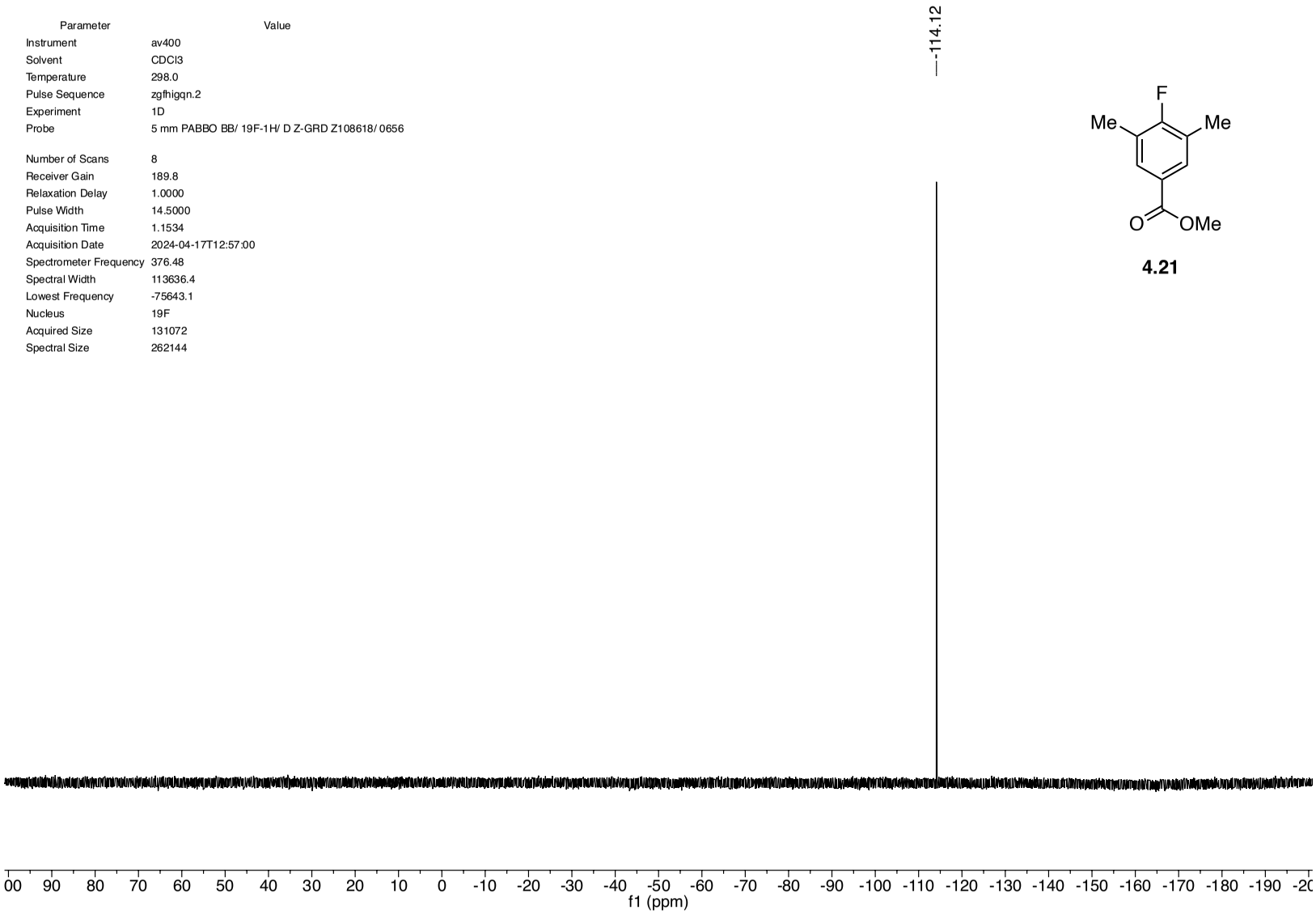

Parameter	Value
Instrument	av400
Solvent	CDCl3
Temperature	298.2
Pulse Sequence	zgfhigqn.2
Experiment	1D
Probe	5 mm PABBO BB/ 19F-1H/ D Z-GRD Z108618/ 0656
Number of Scans	8
Receiver Gain	189.8
Relaxation Delay	1.0000
Pulse Width	14.5000
Acquisition Time	1.1534
Acquisition Date	2024-04-17T17:16:00
Spectrometer Frequency	376.46
Spectral Width	113636.4
Lowest Frequency	-94468.0
Nucleus	19F
Acquired Size	131072
Spectral Size	262144

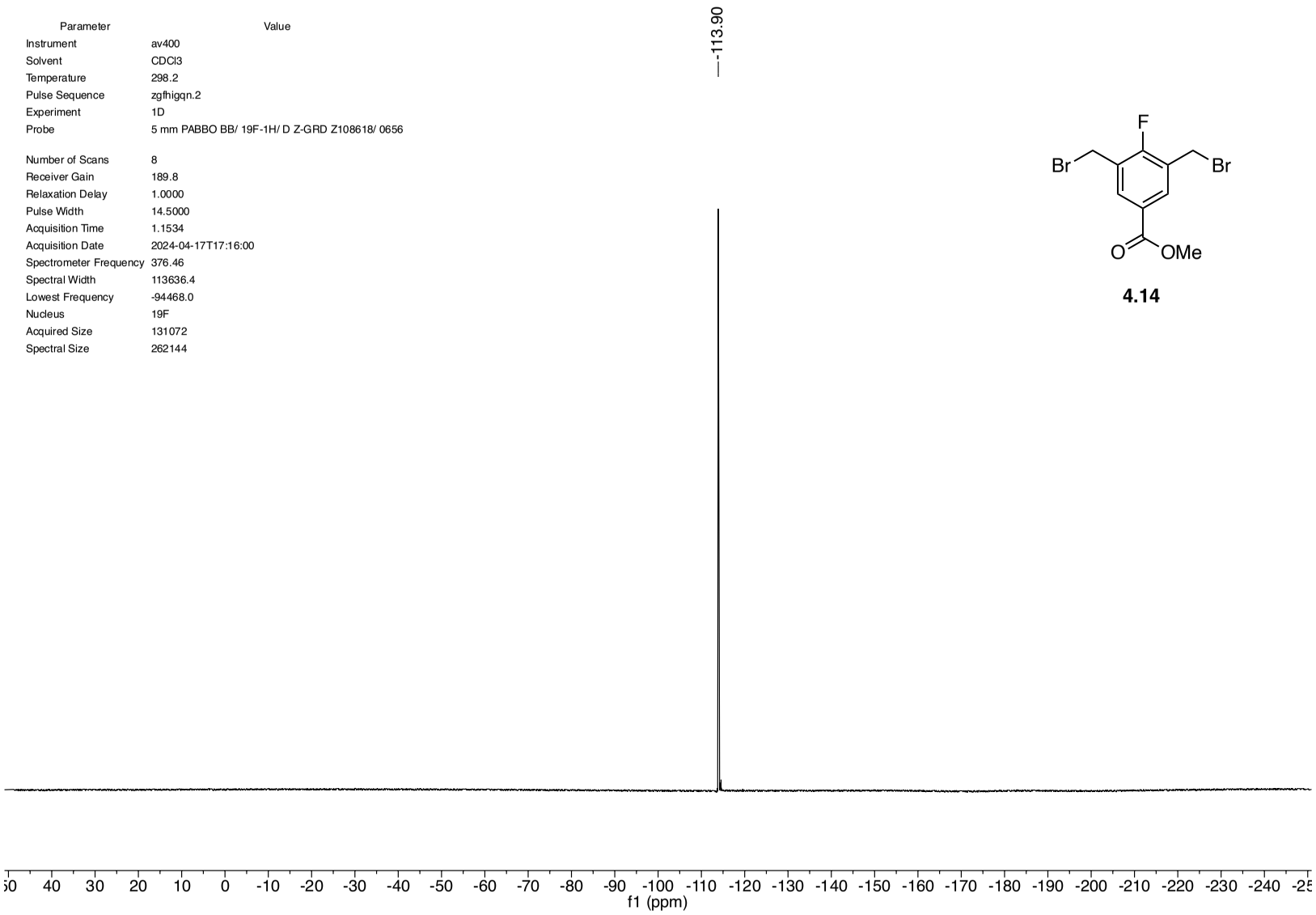

4.14

Parameter	Value
Instrument	Avance
Solvent	DMSO
Temperature	298.0
Pulse Sequence	zg30
Experiment	1D
Probe	Z168773_0038 (CPP1.1 BBO 600S3 BB-H&F-D-05 Z XT)
Number of Scans	16
Receiver Gain	16.0
Relaxation Delay	1.0000
Pulse Width	15.0000
Acquisition Time	0.4981
Acquisition Date	2024-04-26T17:03:46
Spectrometer Frequency	564.63
Spectral Width	131578.9
Lowest Frequency	-122258.1
Nucleus	19F
Acquired Size	65536
Spectral Size	131072

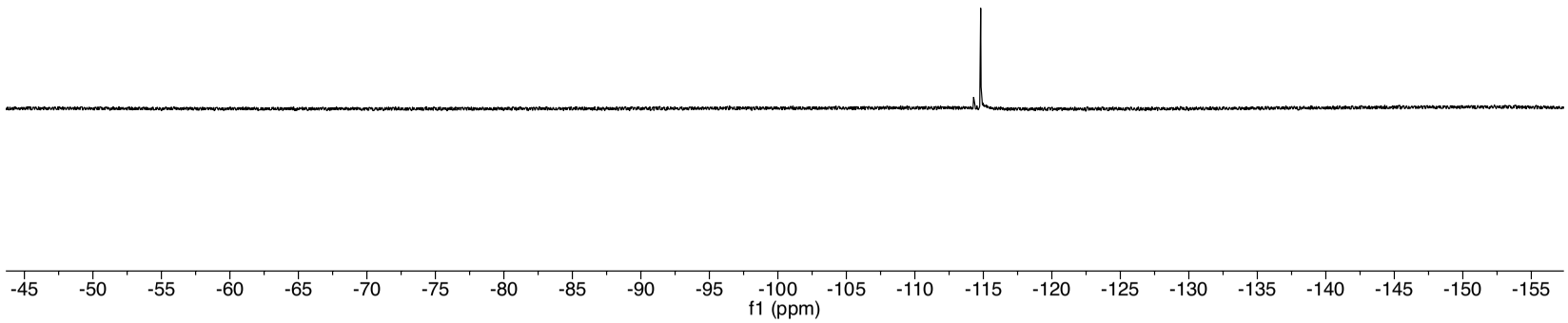

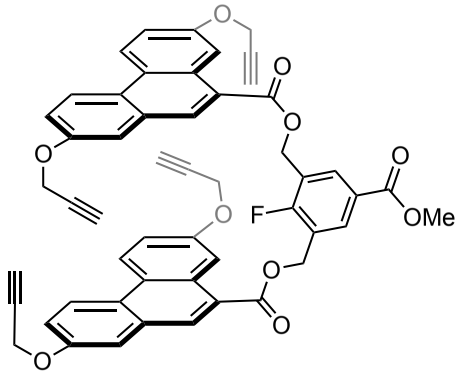

4.3c

Parameter	Value
Instrument	Avance
Solvent	CDCl3
Temperature	298.0
Pulse Sequence	zg30
Experiment	1D
Probe	Z168773_0038 (CPP1.1 BBO 600S3 BB-H&F-D-05 Z XT)
Number of Scans	32
Receiver Gain	16.0
Relaxation Delay	1.0000
Pulse Width	15.0000
Acquisition Time	0.7602
Acquisition Date	2024-05-07T17:38:35
Spectrometer Frequency	564.63
Spectral Width	86206.9
Lowest Frequency	-99572.1
Nucleus	19F
Acquired Size	65536
Spectral Size	131072

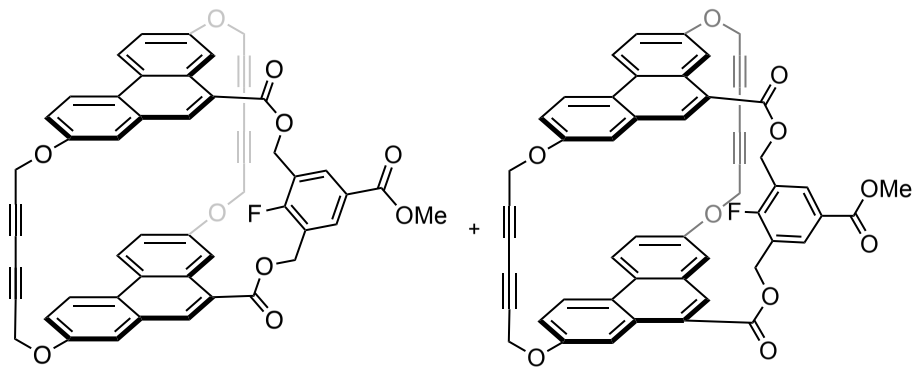

4.23 **4.4c**

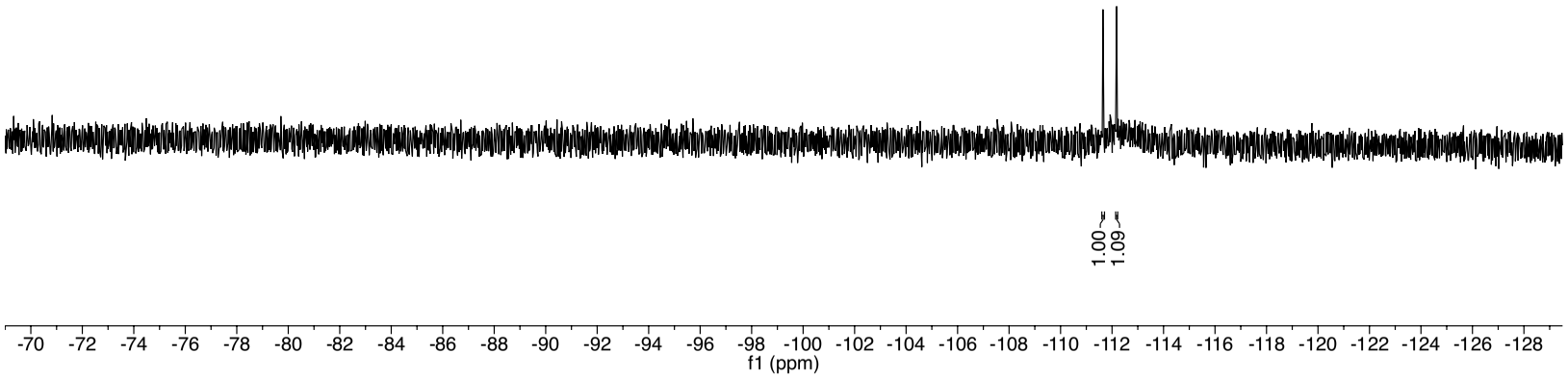

4.6 References

(1) Zhang, C.; Welborn, M.; Zhu, T.; Yang, N. J.; Santos, M. S.; Van Voorhis, T.; Pentelute, B. L. π-Clamp-Mediated Cysteine Conjugation. *Nat. Chem*. **2016**, *8*, 120–128.

(2) Hobert, E. M.; Doerner, A. E.; Walker, A. S.; Schepartz, A. Effective Molarity Redux: Proximity as a Guiding Force in Chemistry and Biology. *Isr. J. Chem.* **2013**, *53*, 567–576.

(3) Chmura, A. J.; Orton, M. S.; Meares, C. F.; Hawthorne, M. F. Antibodies with Infinite Affinity. *Proc. Natl. Acad. Sci*. **2001**, *98*, 8480–8484.

(4) Gartner, Z. J.; Liu, D. R. The Generality of DNA-Templated Synthesis as a Basis for Evolving Non-Natural Small Molecules. *J. Am. Chem. Soc*. **2001**, *123*, 6961–6963.

(5) Kim, S.; Kim, S.; Kim, S.; Kim, N.; Lee, S. W.; Yi, H.; Lee, S.; Sim, T.; Kwon, Y.; Lee, H. S. Affinity-Directed Site-Specific Protein Labeling and Its Application to Antibody-Drug Conjugates. *Adv. Sci.* **2024**, *11*, 1–10

(6) Lake, B. P. M.; Rullo, A. F. Offsetting Low-Affinity Carbohydrate Binding with Covalency to Engage Sugar-Specific Proteins for Tumor-Immune Proximity Induction. *ACS Cent. Sci.* **2023**, *9*, 2064–2075.

(7) Dong, R.; Yang, X.; Wang, B.; Ji, X. Mutual Leveraging of Proximity Effects and Click Chemistry in Chemical Biology. *Med. Res. Rev.* **2023**, *43*, 319–342

(8) Kennan, A. J.; Whitlock, H. W. Host-Catalyzed Isoxazole Ring Opening: A Rationally Designed Artificial Enzyme. *J. Am. Chem. Soc.* **1996**, *118*, 3027–3028.

(9) Turner, W. W.; Arnold, L. D.; Maag, H.; Zlotnick, A. Hepatitis b Core Protein Allosteric Modulators. WO2015138895A1, 2015.

(10) Wager, K. M.; Daniels, M. H. Palladium-Catalyzed Cross-Coupling of Benzyl Thioacetates and Aryl Halides. *Org. Lett.* **2011**, *13*, 4052–4055.

(11) Itoh, T.; Mase, T. A General Palladium-Catalyzed Coupling of Aryl Bromides/Triflates and Thiols. *Org. Lett.* **2004**, *6*, 4587–4590.

(12) Whitlock, B. J.; Whitlock, H. W. Effect of Cavity Size on Supramolecular Stability. *J. Am. Chem. Soc.* **1994**, *116*, 2301–2311.

(13) Gimenez, D.; Mooney, C. A.; Dose, A.; Sandford, G.; Coxon, C. R.; Cobb, S. L. The Application of Perfluoroheteroaromatic Reagents in the Preparation of Modified Peptide Systems. *Org. Biomol. Chem.* **2017**, *15*, 4086–4095.

(14) Embaby, A. M.; Schoffelen, S.; Kofoed, C.; Meldal, M.; Diness, F. Rational Tuning of Fluorobenzene Probes for Cysteine-Selective Protein Modification. *Angew. Chem. Int. Ed.* **2018**, *57*, 8022–8026.

(15) Ariff, P. N. A. M.; Sedgwick, D. M.; Iwasawa, K.; Kiyono, T.; Sumii, Y.; Ikuta, R.; Uranagase, M.; Kawahara, H.; Fustero, S.; Ogata, S.; Shibata, N. Design and Mechanistic Insights into α-Helical p-Terphenyl Guanidines as Potent Small-Molecule Antifreeze Agents. *J. Am. Chem. Soc.* **2024**, *146*, 26435–26441.

(16) Núñez-Villanueva, D.; Ciaccia, M.; Hunter, C. A. Cap Control: Cyclic: Versus Linear Oligomerisation in Covalent Template-Directed Synthesis. *RSC Adv.* **2019**, *9*, 29566–29569.

CHAPTER FIVE

Toward an olympicene-based host for perfluoroaromatics

5.1 Abstract

The syntheses of molecular recognition units based on olympicene, a five-ring polycyclic aromatic hydrocarbon (PAH) that is not fully conjugated, are explored. The ability to reliably and robustly synthesize olympicene derivatives with specific substitution at desired sites would enable broad development of olympicene-based materials, including receptors for applications in host–guest chemistry. To expand our synthetic host platform based on recognition of perfluoroaromatic compounds, we sought to establish synthetic methods for accessing desired olympicene building blocks, as well as demonstrate incorporation in a proof-of-concept host platform. We explored different routes based on building up from other PAH scaffolds (anthraquinone, pyrene, and benzanthrone) to access new 3-,8-disubstituted olympicene ketone building blocks. Though these efforts ultimately did not result in the final desired product, they highlight directions that are promising for future endeavors. Our pursuit of a simplified olympicene host revealed patterns of instability that, while preventing our desired application, highlight an important knowledge gap regarding olympicene derivatives that sets the stage for our later investigations.

5.2 Introduction

Following success in designing a host for perfluoroaromatic guests as discussed in Chapter 3, we next sought methods to improve arene-perfluoroarene interactions within a synthetic host–guest system. Based on previous work, it is known that expanding the aromatic surface area of either, or both, aromatic compounds will lead to an increase in interaction

strength.[1] Computational work by Dr. Gina Lee suggested that a host based on olympicene, a five-ring aromatic scaffold, would bind strongly to a perfluoroaromatic guest (Figure 5.1A). The computed host structure features large aromatic faces for maximizing arene interactions (spaced ~7 Å apart, ideal for interacting with perfluoroarenes). The computed complex also featured a halogen-bonding interaction, which is analogous to hydrogen bonding in strength and acceptor types but has a strict geometry requirement of 180° between donor and acceptor atoms.[2] The halogen bond is intriguing as it is relatively rare in biological systems,[3] compared to hydrogen bonding, which is present in our other host platform. This may lend more bioorthogonality for a system that we hope will function as a biological labeling tool.

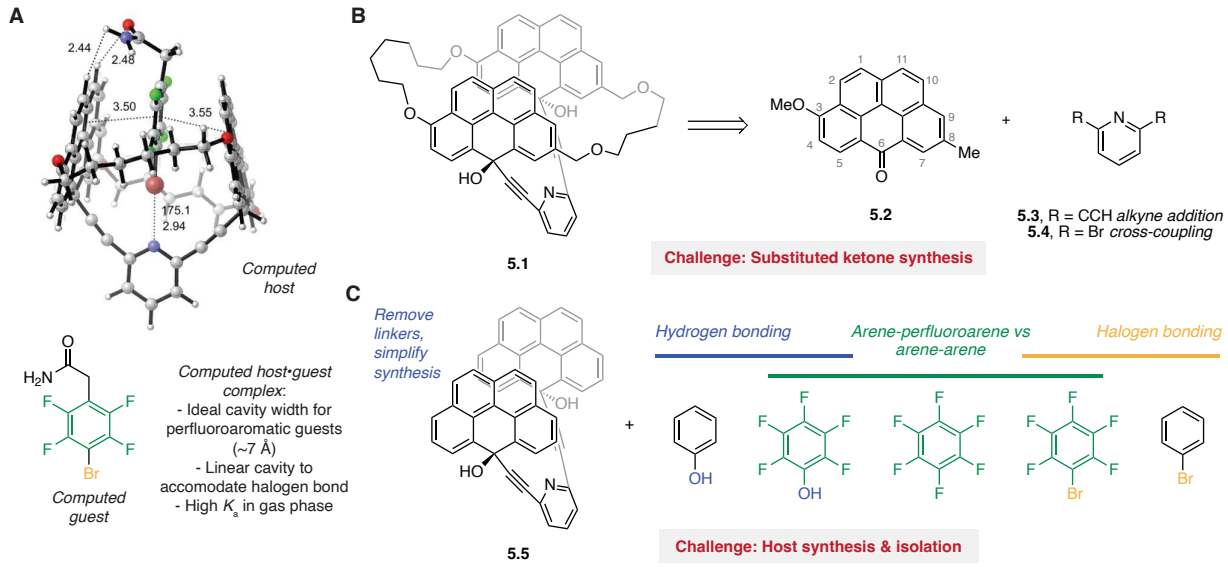

Figure 5.1 Target host structures: motivation and challenges. (A) Computationally derived host–guest complex designed by Dr. Gina Lee (geometry optimization: B97D/6-31G[d]; single-point calculations: B3LYP-D3/6-311+G[d,p]). (B) Retrosynthesis of host **5.1**; requires synthesis of substituted ketone **5.2**, a pattern not found in the literature for the olympicene scaffold. (C) Flexible "tweezer" host target **5.5** based on known olympicene starting materials, with proposed suite of guests to measure non-covalent interactions of interest.

The structure we decided to target synthetically is that of **5.1** (Figure 5.1B). We envisioned bringing two olympicene faces and a pyridine acceptor bridge together stepwise via three linkages with different connections, requiring an olympicene building block with different

functional handles. By connecting each host linker in a different manner and step, we expected more control over the regiochemistry of the final assembled host. Importantly, the sp^3 geometry allowed by the non-conjugated carbon at the 6-position of olympicene allows for formation of a linear cavity with alkyne linkers to the pyridine acceptor, which is key for accommodating a halogen bond interaction. Retrosynthetically, the host would come from a substituted olympicene ketone **5.2** and a di-substituted pyridine, with either alkyne groups for addition into the ketone (**5.3**) or bromine atoms as cross-coupling handles (**5.4**) to react with alkyne-containing derivatives of **5.2**. The challenge here, before ever approaching the synthesis of **5.1**, was that no methods existed for accessing an olympicene ketone like **5.2**, with variable substituents at the 3- and 8-positions, thus requiring development of new olympicene chemistry. To further the challenge, the route would also need to be robust, scalable, and high-yielding, as was learned in the synthesis of our phenanthrene-based host for binding experiments (Chapter 3).

Given the challenges faced in accessing ketone **5.2**, we also pursued the synthesis of flexible host **5.5**, without side linkers connecting the aromatic faces, which could come from known starting materials and potentially remove many challenging synthetic steps. This host fits the model of molecular tweezers (Figure 5.2A).[4] The flexibility of such hosts can limit binding strengths due to entropically costly reorganization upon binding a guest, but that can be improved if multiple non-covalent interactions are present. The first tweezer published by Chen and Whitlock, based on caffeine, recognized aromatic guests and bears similar design principles to our host platform (Figure 5.2B; Chapter 3).[5] With host **5.5**, we could measure the binding affinities of different perfluoroaromatic guests with or without hydrogen or halogen bonding present; these results would inform our designs going forward, even if the actual strengths are diminished by having a less preorganized host.

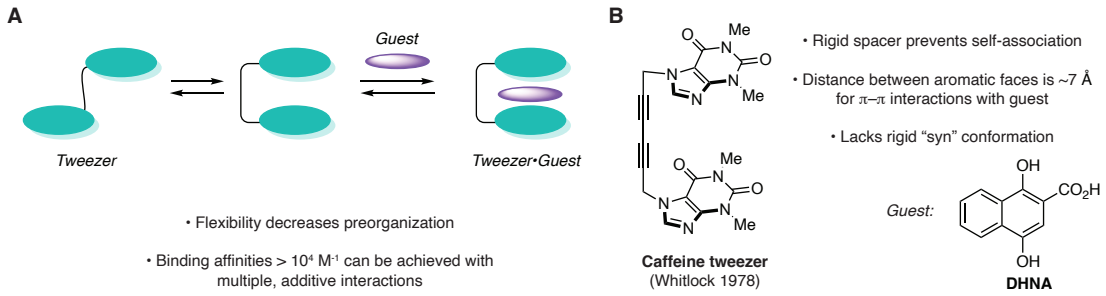

Figure 5.2 Molecular tweezers, an overview. (A) Binding equation highlighting the flexibility of tweezer-type hosts. (B) The first tweezer and design elements important for binding guests like 1,3-dihydroxy-2-naphthoic acid (**DNHA**).

Here, efforts toward synthesizing a substituted olympicene ketone via multiple routes, based on different polycyclic aromatic hydrocarbon (PAH) starting materials, are summarized, including issues encountered and potential future directions. Second, the synthesis of host **5.5** via two methods is presented along with challenges that precluded its final isolation, characterization, and application.

5.3 Results and discussion

5.3.1 Attempts to synthesize a 3,8-substituted olympicene ketone

Anthraquinone route. Our first substituted olympicene ketone target was **5.6**, with identical –OMe substituents at the 3- and 8-positions, which allowed us to use substituted anthraquinone as a starting material (Figure 5.3A). We envisioned the cyclization of an ene-diyne motif on di-methoxy ketone **5.7** would afford the final substituted product. Such a cyclization was precedented on unsubstituted, non-ketone-containing anthraquinone derivatives to access large aromatics like coronene.[6] The required alkynes could come from Sonogashira coupling of dibromoolefin **5.8**, which could come from di-methoxy substituted anthraquinone **5.9**. Selective olefination of only one ketone had been shown on unsubstituted anthraquinone.[7]

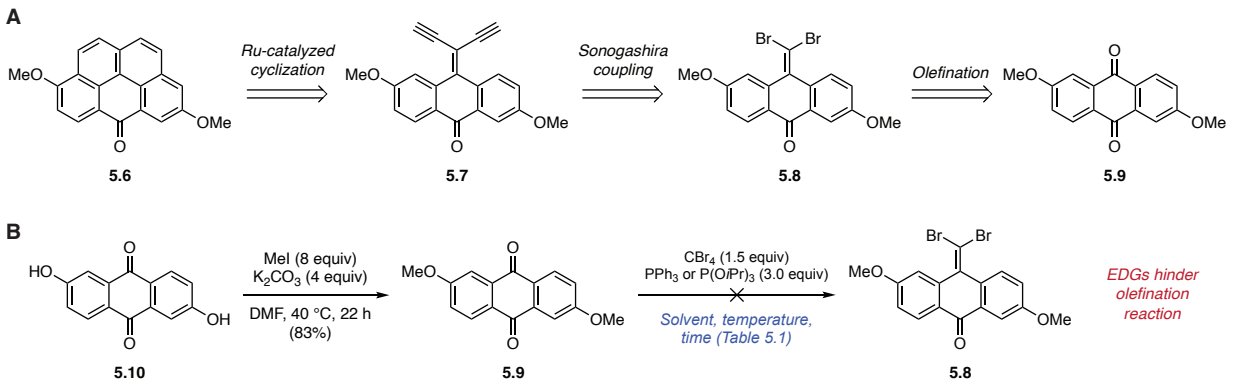

Figure 5.3 Anthraquinone-based route to substituted olympicene ketone. (A) Retrosynthesis of ketone **5.6**. (B) Progress in forward synthesis. (EDG = electron-donating group)

Methylated **5.9** was accessed readily through simple alkylation of anthraflavic acid **5.10** in yields acceptable for a first step (Figure 5.3B). However, the following olefination did not prove successful; various attempts are summarized in Table 5.1. Despite changing solvent to allow increased reaction temperatures (entries 1–3), using alternative phosphorus reagents (entry 4),[7] or using microwave conditions with precedent for unsubstituted anthraquinone olefination,[8] no conversion to **5.8** was observed. Starting material **5.9** could be recovered but the presence of by-products often complicated purification. The observation of triphenylphosphine oxide suggests ylide formation may have been successful, with **5.8** being too inactivated for subsequent addition. A mass corresponding to the expected ylide was observed by mass spectrometry in conditions with CH_2Cl_2 as the solvent (entries 1, 5). It is likely the two electron-donating methoxy groups reduce the electrophilicity of the carbonyl carbon sufficiently to prevent addition by the ylide intermediate.[9] Future attempts at this route would likely benefit from employing electron-withdrawing groups on the anthraquinone core that could be transformed later in the synthesis, though additional steps may be detrimental to final ketone yields.

Entry	Solvent	P reagent	Temperature	Time	Result
1	CH_2Cl_2	PPh_3	rt	21 h	No reaction; ylide formation[a]
2	DCE	PPh_3	84 °C	24 h	No reaction
3	PhMe	PPh_3	111 °C	65 h	No reaction
4	CH_2Cl_2	$P(OiPr)_3$	rt	24 h	No reaction
5	CH_2Cl_2	PPh_3	80 °C (μwave)	20 min	No reaction; ylide formation[a]

Table 5.1 Summary of olefination attempts on **5.9** to synthesize **5.8**. [a]Ylide formation observed by liquid chromatography–mass spectrometry.

Pyrene route. A second route based on a pyrene scaffold was inspired by existing methods to access an unsubstituted olympicene ketone.[10] Mirroring the unsubstituted route, an acid-catalyzed cyclization of tethered carboxylic acid **5.11** would result in the desired ketone **5.2** (Scheme 5.1). The required non-pyrene carbons would come via an olefination-reduction sequence on pyrene aldehyde **5.12**, which could come from formylation of bromine-functionalized **5.13** via lithium-halogen exchange and DMF-quenching, which is precedented on 1-bromopyrene.[11]

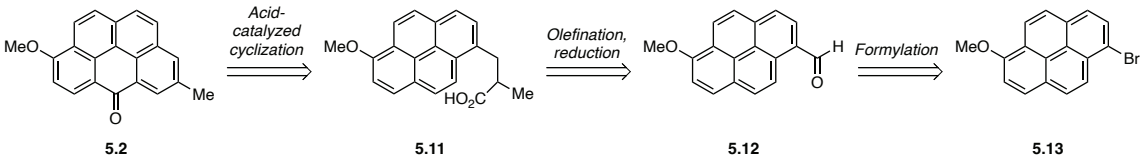

5.2 **5.11** **5.12** **5.13**

Scheme 5.1 Retrosynthesis of ketone **5.2** via pyrene-based route.

Asymmetrically substituted pyrene **5.13** was accessed after a series of optimization trials (Scheme 5.1, Table 5.2). Sodium methoxide (NaOMe) was made fresh from methanol (MeOH) and sodium metal, but no reaction occurred with starting material 1,6-dibromopyrene, **5.14** (Table 5.2, entry 1). As still no appreciable product was made after including CuI as a catalyst (often employed for methoxide additions to aryl halides[12]), the poor solubility of **5.14** in MeOH

was considered a factor (Table 5.2, entry 2). Instead, **5.14** was dissolved in DMAc, and fresh NaOMe solution was added to this solution and heated. The reaction proceeded readily, though with over-substitution to give **5.15** when greater than 2 equivalents of NaOMe were added (Table 5.2, entries 3–4). The doubly substituted product was identified using published NMR data,[13] but separation of **5.13** and **5.15** proved difficult, and absolute yields were not found. Overlapping peaks in crude ^{1}H NMR also complicated percent composition calculations. However, using fewer than 2 equivalents of NaOMe, DMAc, and catalytic CuI, and heating to 80 °C for 20 h resulted in an acceptable yield of product **5.13** without over-substitution (Table 5.2, entry 5). Cooling to 50 °C resulted in poor conversion (Table 5.1, entry 6), and the use of premade NaOMe salt also resulted in a lower yield of **5.13** (Table 5.1, entry 7).

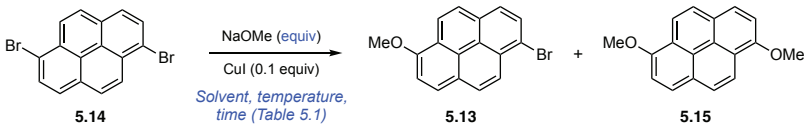

5.14 **5.13** **5.15**

Scheme 5.2 Synthesis of methoxy- and bromine-substituted pyrene **5.13**.

Entry	Solvent	Catalyst	Equiv NaOMe	Temperature	Time	Result
1	MeOH	None	4.9 [a]	65 °C	24 h	Only recovered **5.14**
2	MeOH	CuI	5.3 [a]	65 °C	21 h	Only recovered **5.14**
3	DMAc	CuI	4.6 [a]	80 °C	20 h	Mix of **5.13**, **5.15** [b]
4	DMAc	CuI	9.0 [a]	80 °C	20 h	Mix of **5.13**, **5.15** [b]
5	**DMAc**	**CuI**	**1.7** [a]	**80 °C**	**20 h**	**57% yield of 5.13**
6	DMAc	CuI	1.6 [a]	50 °C	25 h	<1% conversion to **5.13**
7	DMAc	CuI	1.5 [c]	80 °C	25 h	20% yield of **5.13**

Table 5.2 Optimization of substitution conditions to access pyrene **5.13**. [a]NaOMe was prepared from sodium metal and MeOH. [b]Inseparable mix of products. [c]Commercially available, solid NaOMe was used.

Formylation of **5.13** led to aldehyde product **5.12**, but with low yield, as many insoluble by-products were also made, complicating purification (Figure 5.4A,B). The overall yield may be improved if formation of side products could be reduced, potentially through lower temperature and shorter reaction time, either during the lithiation and/or quenching steps. It may also be worth attempting alternative formylation reactions and starting materials, such as a Vilsmeier-Haack reaction with 1-methoxypyrene.[14] Overall though, the low yields of both the substitution and formylation steps of this pyrene-based route to **5.2** were considered too limiting to warrant further investigation at the time, as from the aldehyde there were still many steps required to access **5.2**.

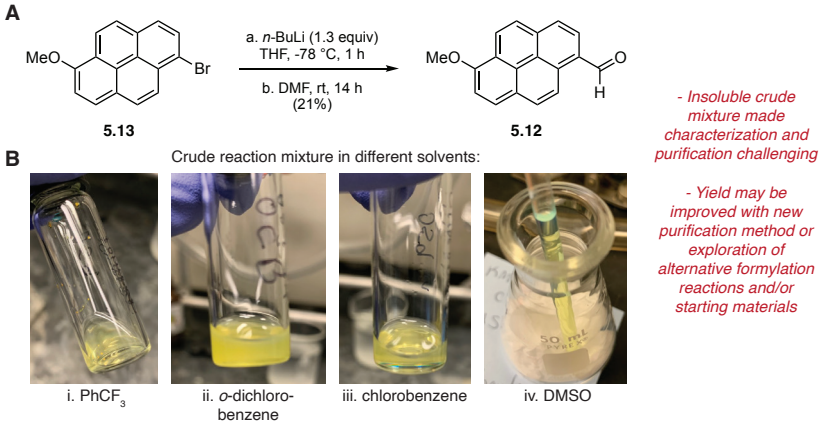

Figure 5.4 Synthesis of aldehyde **5.12** and purification challenges. (A) Synthesis of aldehyde. (B) Pictures of crude mixture in various solvents, with cloudiness indicative of insolubility; only DMSO fully dissolved the crude solid. Challenges and future directions are given.

Benzanthrone route. The final PAH scaffold employed toward a substituted olympicene ketone was benzanthrone, an aromatic ketone with four out of five final fused rings in place (Figure 5.5A). We envisioned final ketone **5.2** or the alternative **5.6** could arise from a platinum-catalyzed cyclization of terminal alkyne on benzanthrone compound **5.16** or **5.17**. Such cyclization procedures are often used to form phenanthrene (the three-membered PAH featured in Chapters 3 and 4).[15] Use of differently substituted alkynes could also allow for substitution at

the 11-position of olympicene if desired. The required alkyne could be installed on halogen-functionalized benzanthrone **5.18a**–**b** or **5.19a**–**b**. We decided to pursue both Cl and Br handles as it was unclear which halogen, if either, would be tolerated in the preceding cyclization step to form the benzanthrone scaffold. This transformation proceeds first via acid-directed arylation of naphthalene **5.20** by a diaryliodonium triflate salt, **5.21**–**22**, to form intermediate **5.A**, followed by acid-mediated intramolecular acylation to yield a benzanthrone product (Figure 5.5B).[16] While the initial report of this methodology had a reasonable substrate scope, there were no examples with *ortho* halogen substituents on the diaryliodonium triflate component.

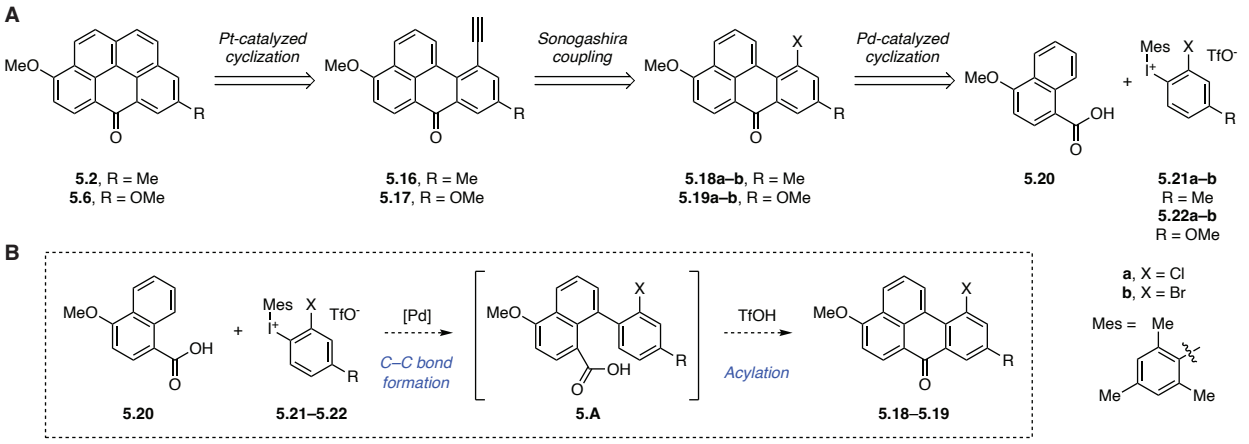

Figure 5.5 Approach to substituted ketone based on benzanthrone. (A) Retrosynthetic scheme for accessing either of two options for final substituted ketone. (B) Proposed mechanism of benzanthrone formation.[16]

Known naphthoic acid **5.20** was readily made in two high-yielding steps: bromination of **5.23** followed by carboxylation of **5.24** (Figure 5.6A). Four different diaryliodonium triflate salts (**5.21a,b**–**5.22a,b**) were synthesized with a combination of substituents (Figure 5.6B). Following a procedure for forming asymmetric iodonium triflates with electron-rich aryl components, the iodonium tosylate was made first from mesitylene, **5.25**, and the appropriate aryl iodide (**5.26a,b**–**5.27a,b**), followed by facile anion exchange with triflic acid (TfOH) to access the more reactive diaryliodonium triflates **5.21a,b**–**5.22a,b**.[17,18] The use of mesitylene removes the need

for a matching non-iodo arene to form a symmetric salt, and mesitylene with its two ortho substituents is not a productive arylating group for the benzanthrone cyclization reaction. The aryl iodides were commercially available except for **5.27a**, which was synthesized from 3-chloroanisole **5.28** according to literature procedure (Figure 5.6C).[19] Minor isomer **5.29** was also isolated.

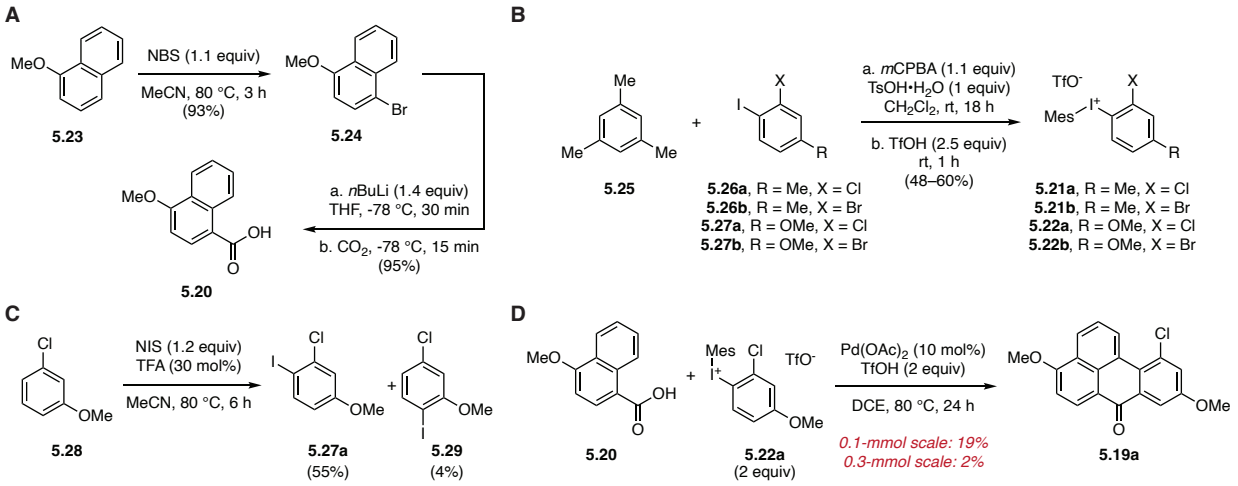

Figure 5.6 Starting material syntheses and benzanthrone cyclization reaction. (A) Two-step synthesis of naphthoic acid **5.20**. (B) Synthesis of diaryliodonium triflates with *in situ* anion exchange. (C) Synthesis of aryl iodide **5.27a**. (D) Benzanthrone synthesis.

Unfortunately, it was quickly apparent that halogen substituents at the desired position were not well-tolerated in the Pd-catalyzed benzanthrone cyclization conditions; only methoxy/chloro product **5.19a** was made successfully (Figure 5.6D). Upon scaling up, the relatively poor yield of 19% decreased significantly, accompanied by an increase in the amount of side products observed by NMR and TLC. The additional products may have resulted from competing reactions facilitated by Pd catalysis at the halogen site. It is also possible **5.20** was arylated by mesitylene, which would prevent acylation, though no such products were detected.

We briefly explored alternative methods for benzanthrone synthesis to improve the yield of **5.19a**. A related method employed iodoarenes alone, instead of diaryliodonium salts, in Pd-

catalyzed arylation of naphthoic acids using Ag_2O as an oxidative additive.[20] In acidic conditions (TfOH with hexafluoroisopropanol [HFIP] as solvent), cyclization occurred to access many benzanthrone derivatives, including those with halogens at the desired position. Again, however, these conditions failed to give the desired product, with the now known **5.19a** not detected from attempted cyclization of **5.20** and **5.27a** (Scheme 5.3). In comparing these results to the successful report products, the combination of halogen and electron-donating group appears to hinder this particular palladium-catalyzed transformation, less so than steric factors.

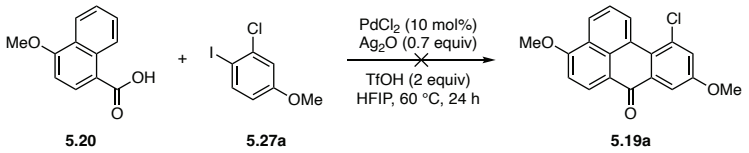

Scheme 5.3 Alternative conditions attempted for accessing benzanthrone **5.19a**.

As a final attempt to increase the yield of **5.19a**, a reported two-step benzanthrone synthesis was attempted.[21] It was thought that separating the arylation and acylation steps might lead to an overall increase in yield, or at least pinpoint where the problem step was occurring. Acid **5.20** was subjected to coupling conditions with pyrrolidine to give known amide **5.30**; pyrrolidine amides were used in the original report. Amide **5.30** was arylated with **5.22a** to give **5.31** in acceptable yield (Scheme 5.4). Unfortunately, despite an improved arylation step, cyclization attempts by many, varied methods still failed to result in the desired benzanthrone scaffold (Table 5.3, entries 1–7). Interestingly, **5.31** was returned mostly clean (except in the case of excess TfOH, entry 7), and neither this nor the preceding step resulted in the mess of side products as seen in the attempts above. A wider screen of more forceful acylation conditions may prove fruitful. Since these trials, a similar two-step approach was used to access extended aromatic ketones via ester intermediates, instead of amides;[22] this modified methodology may be amendable to accessing olympicene ketones.

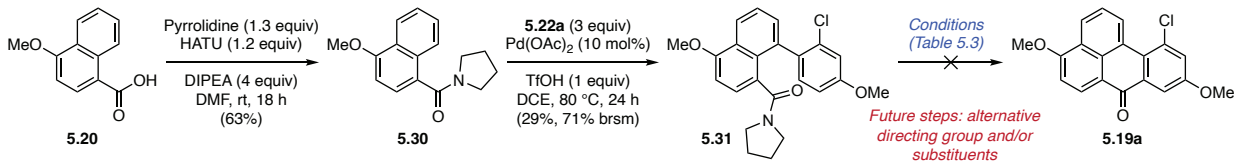

Scheme 5.4 Attempted two-step, amide cyclization to access benzanthrone **5.19a**.

Entry	Reagent(s)	Solvent	Temperature	Time	Result
1	$POCl_3$	—	100 °C	14 h	Recovered **5.31**
2	$POCl_3$	—	100 °C	4 days	Recovered **5.31**
3	$POCl_3$, Et_3N	CH_2Cl_2	rt	4 days	Recovered **5.31**
4	LDA	THF	-46 °C to rt	3.5 h	Recovered **5.31**
5	TfOH (2.5 equiv)	DCE	80 °C	27 h	Recovered **5.31**
6	TfOH (4 equiv)	CH_2Cl_2	rt	27 h	Recovered **5.31**
7	TfOH (12 equiv)	DCE	80 °C	24 h	Decomposition of **5.31**

Table 5.3 Attempts to access **5.19a** via cyclization of amide **5.31**. Recovered **5.31** was re-subjected to subsequent trials.

Ultimately, accessing substituted ketone **5.2** or **5.6** proved challenging, and it was likely worth taking a step back to verify that pursuit of olympicene as a host aromatic scaffold was worthwhile. To do so, we needed to access some version of a receptor that would bind with measurable affinity to our perfluoroaromatic guests of interest. Switching focus from substituted olympicene to the unsubstituted version allowed us to use more established chemistry to push toward a host target.

5.3.2 Synthesis of a flexible olympicene molecular tweezer

Given the struggles in obtaining a substituted olympicene ketone, we considered pursuing a flexible version of host **5.1**, tweezer host **5.5**, that could potentially be synthesized more quickly from known starting materials and allow us to probe the relative contributions of non-

covalent interactions of interest (Scheme 5.5). We envisioned two routes to **5.5**: one via alkyne addition by **5.3** into two equivalents of ketone **5.32**, or via cross-coupling between dibromopyridine **5.4** and two equivalents of propargyl alcohol **5.33**. In contrast to the above efforts, all four potential building blocks were already known in the literature.

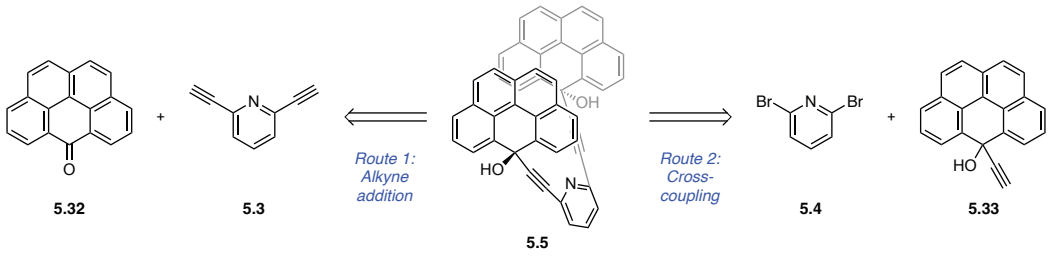

Scheme 5.5 Retrosynthetic analysis of tweezer host **5.5** via two routes.

Toward the first route, Sonogashira coupling between **5.4** and trimethylsilyl (TMS) acetylene gave TMS-protected **5.34**, which was readily deprotected in basic conditions to give diyne **5.3** in decent yield (Figure 5.7A). While the intermediates used to access ketone **5.32** were all known, here, new procedures in a new sequence were developed that could be performed on multigram scales (1–2 g) and in high yields (> 80% for each step) (Figure 5.7B). First, commercially available pyrene aldehyde **5.35** was transformed to conjugated ester **5.36** via Horner-Wadsworth-Emmons olefination conditions. The ester was reduced to **5.37** by hydrogenation and easily hydrolyzed to acid **5.38**. These three steps were performed in excellent yields, requiring only precipitations and filtrations for purification, which was a marked change from the substituted ketone route attempts.

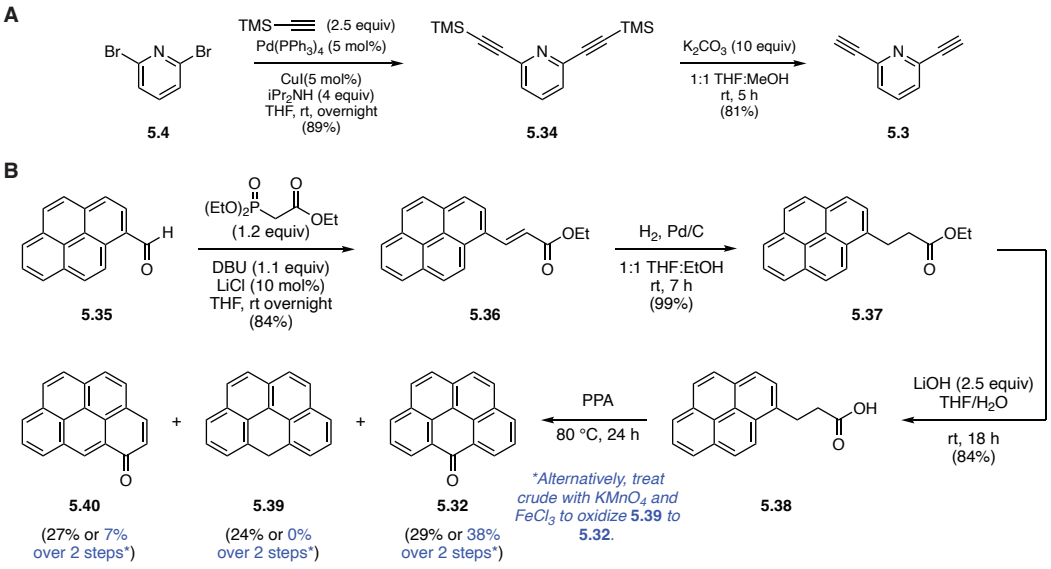

Figure 5.7 Synthesis of starting materials for tweezer host **5.5**. (A) Synthesis of diyne **5.3**. (B) New route to acid **5.38** for subsequent PPA cyclization to access ketone **5.32** and related olympicene compounds.

Following literature procedure, acid **5.38** was treated with polyphosphoric acid (PPA) for 24 h to give a mixture of many aromatic products, though with 3 major ones: desired symmetric ketone **5.32**, reduced olympicene **5.39**, and ketone isomer **5.40** (Figure 5.7B). While the individual yields are not particularly impressive on their own, in the context of such a messy reaction, it is remarkable these yields are both reproducible in our hands and in line with the reported values. We found this reaction to be reliable only up to a 300-mg reaction scale but deemed this only a mild limitation. Pleasingly, we also found that subjecting the crude mixture to oxidizing conditions as a second step improved the yield of **5.32** to 38%, as any **5.39** was fully oxidized to the symmetric ketone. Though here only ketone **5.32** is utilized, **5.39** and **5.40** and their synthetic applications will be examined in Chapter 6.

Synthesis of **5.5** via alkyne additions was attempted first. Diyne **5.3** was lithiated and added to two equivalents of **5.32** to access the desired host (Figure 5.8A). Crude analysis by liquid chromatography–mass spectrometry (LC–MS) was initially promising: while dwarfed by a

large **5.32** peak, a small preceding peak had a mass corresponding to **5.41**, the result of a single alkyne addition (Figure 5.8B). The mass presented as loss of the hydroxyl group, which has been observed in other similar compounds during electrospray ionization (ESI) like LC–MS.[23] Much smaller peaks with later retention times were promising signs of product formation: a peak at 2.7 minutes matched the parent ion expected for **5.5**, while at 3.1 minutes, the [M–OH] mass for **5.5** appeared (Figure 5.8C). Despite this initial hit, efforts to pursue this route further faltered. Re-subjection of crude **5.41** to similar conditions did not result in greater formation of presumed product and, even more discouragingly, attempts to purify any products were met with decomposition. The consistent observation of a loss-of-water mass from the propargyl alcohol products led us to propose carbocation **5.B** as a possible intermediate that could form, react, and degrade during purification (e.g. acidic or basic silica gel) or transformation attempts (Figure 5.8D). This intermediate and other explanations for olympicene propargyl alcohol instability will be explored in Chapter 6.

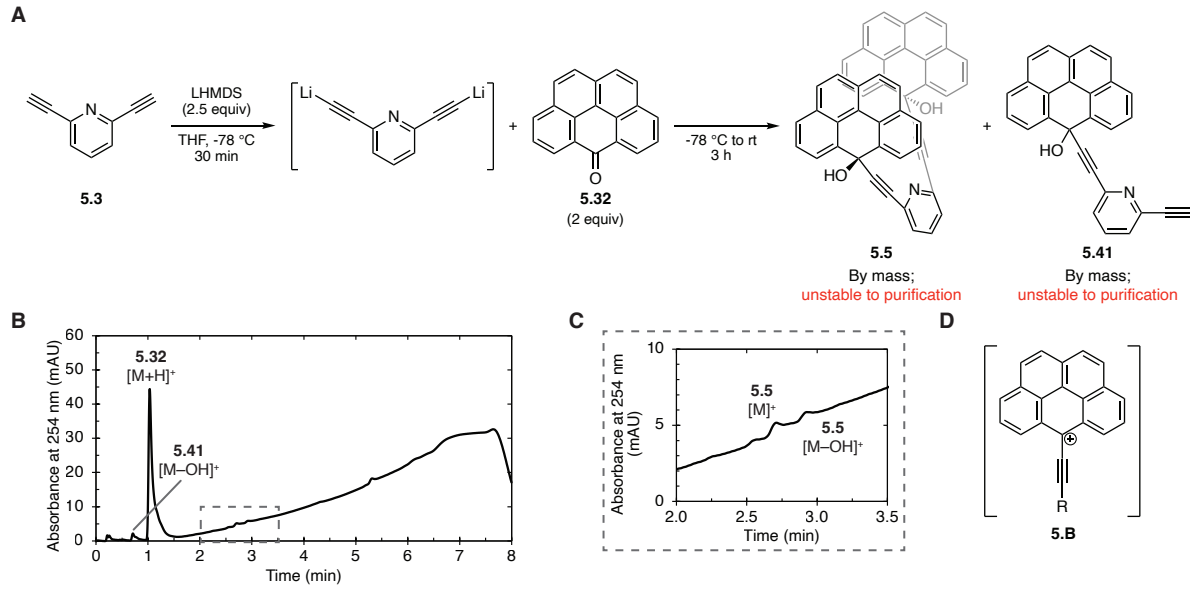

Figure 5.8 Attempted synthesis of tweezer **5.5** via alkyne addition. (A) Reaction scheme. (B) Crude LC–MS trace of reaction in part A. (C) View of small peaks from chromatogram (2–3.5

min) in part B. (D) Proposed general structure of loss-of-water intermediate observed in mass spectrometry experiments.

Despite signs of propargyl alcohol instabilities, we still attempted to synthesize tweezer **5.5** via cross-coupling reactions. First, following a reported procedure, ketone **5.32** was subjected to addition by lithiated TMS acetylene to give **5.42**, which was then deprotected in basic conditions to give **5.33** (Figure 5.9A).[24] If **5.32** was completely consumed, the reaction to form **5.42** was remarkably clean by ^{1}H NMR, and LC–MS only showed product and loss-of-water peak, and the deprotection was similarly very clean. This was fortunate, as just like previous propargyl alcohols, **5.42** and **5.33** did not withstand chromatographic purification attempts and were unstable in solution for prolonged periods of time.

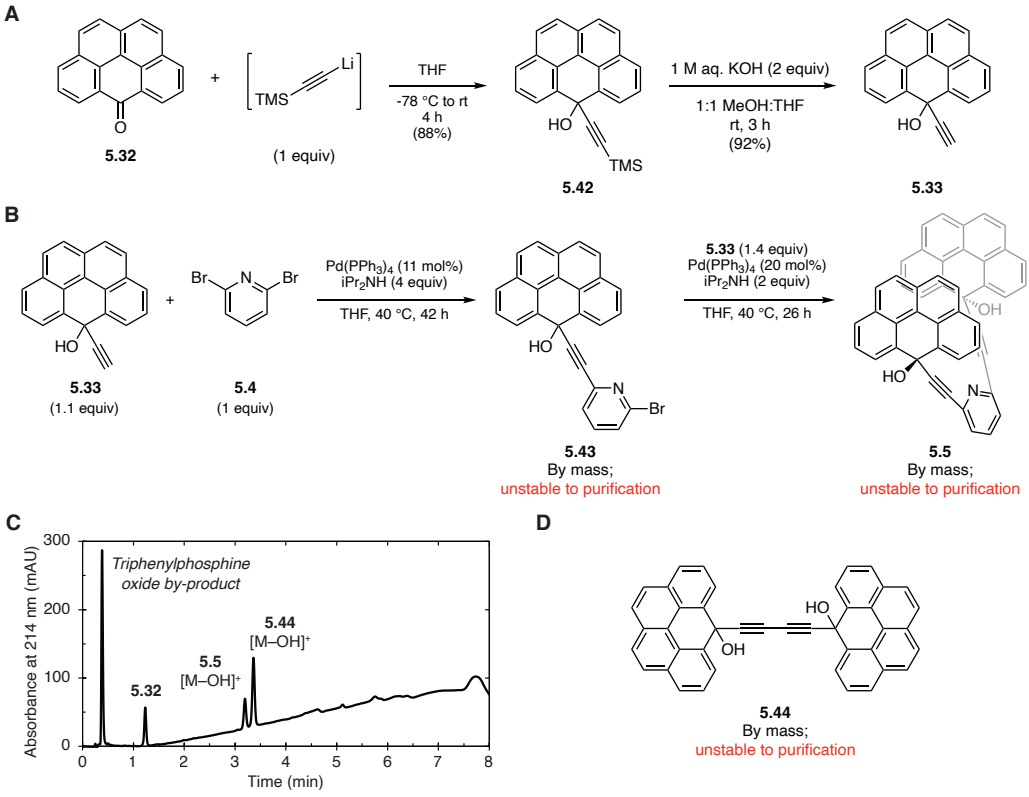

Figure 5.9 Attempt to access tweezer **5.5** via cross-coupling. (A) Synthesis of propargyl alcohol **5.33**. (B) Route to presumed product via single addition intermediate **5.43**. (C) Crude LC–MS analysis of reaction in Part B with peaks of interest and corresponding mass patterns noted. (D) Proposed structure of alkyne product **5.44** based on mass results in Part C.

Initial attempts at traditional Pd-catalyzed Sonogashira coupling between **5.4** and two molecules of **5.33** with a copper co-catalyst did not provide evidence of product formation. Mass spectrometry suggested alkyne-alkyne coupling products from two equivalents of **5.33** was a favored reaction pathway. By removing copper and heating the reaction to 40 °C, evidence of a new, useful product arose: single coupling between **5.33** and **5.4** to give **5.43** (Figure 5.9B). As with previous propargyl alcohols, mass spectrometry revealed an [M–OH] peak; in the case of **5.43**, the isotope pattern associated with the presence of a single bromine atom was also observed, lending stronger evidence to its formation despite the inability to isolate it for full characterization. Even when excess **5.33** was employed, **5.43** was the only product, so a second, re-subjection step was carried out with additional **5.33** (Figure 5.9B). Here, evidence of tweezer formation matched that of Figure 5.8B; at a retention time of 3.1 minutes in the LC–MS chromatogram, the loss-of-water peak for **5.5** is observed, in greater abundance via the cross-coupling route (Figure 5.9C). The other major peaks corresponded to: triphenylphosphine oxide, an expected side product of the coupling conditions; ketone **5.32**, presumably unreacted in the formation of **5.42**/**5.33** (a consequence of the purification challenges with propargyl alcohols); and a mass that again suggested coupling between two equivalents of **5.33**, with a proposed structure of **5.44** (Figure 5.9D). It is curious that this alkyne coupling still occurred without added copper but such olympicene dimers may be of interest for other applications, if the issue of stability is addressed.

Ultimately, while there was some evidence for the formation of **5.5**, particularly via the cross-coupling route, the inability to purify and characterize it and the other propargyl alcohol products not only prevents full characterization, but any likelihood that the final host would be stable enough for binding experiments. It was clear that the stability of olympicene derivatives

with sp^3-hybridzed 6-positions was understudied and would need addressing before achieving useful final products. This need led to an exploration of alternative olympicene starting materials chronicled in Chapter 6.

5.4 Conclusion

An olympicene-based macrocyclic host for perfluoroaromatic guests would feature a large aromatic surface area and a linear cavity made possible by the presence of a tetrahedral center on olympicene scaffolds. In this work, progress toward and challenges in synthesizing a 3,8-disubstituted olympicene ketone, unknown in literature, are summarized. Three different PAH starting frameworks — anthraquinone, pyrene, and benzanthrone — were utilized, with pyrene and benzanthrone being the most promising. Despite not being able to access final ketones **5.2** or **5.6**, there are potential avenues to explore and push these syntheses forward in the future, particularly those based on pyrene or benzanthrone.

Two synthetic routes toward flexible host **5.5** showed signs of success by mass spectrometry, but intermediates and final products were unable to be purified and fully characterized. The instabilities of the propargyl alcohols observed here highlight a weakness in the olympicene scaffold: the presence of a labile group at the reaction 6-position limits the stability and applicability of certain olympicene derivatives. The chemistry of these alcohols is explored in depth in Chapter 6, along with an examination of alternative olympicene starting materials for potentially accessing more stable architectures, including modified host designs.

5.5 Experimental Procedures

5.5.1 Synthetic abbreviations and chemical formulas

Acetonitrile (MeCN); Ammonium chloride (NH_4Cl); *n*-Butyllithium (*n*BuLi); Carbon dioxide (CO_2); Chloroform ($CHCl_3$); Copper iodide (CuI); Direct analysis in real time (DART); 1,8-Diazabicyclo[5.4.0]undec-7-ene (DBU); 1,2-Dichloroethane (DCE); Dichloromethane (CH_2Cl_2); Diethyl ether (Et_2O); Diisopropylethylamine (DIPEA); Diisopropyamine (*i*Pr_2NH); Dimethylacetamide (DMAc); Dimethylformamide (DMF); Dimethylsulfoxide (DMSO); Electrospray ionization (ESI); Ethanol (EtOH); Ethyl acetate (EtOAc); Hexafluoroisopropanol (HFIP); Hexafluorophosphate azabenzotriazole tetramethyl uranium (HATU); High-resolution mass spectrometry (HRMS); Hydrochloric acid (HCl); Iron(III) chloride ($FeCl_3$); isopropanol (*i*PrOH); Liquid chromatography–mass spectrometry (LC–MS); Lithium bis(trimethylsilyl)amide (LHMDS); Lithium chloride (LiCl); Lithium hydroxide (LiOH); Low-resolution mass spectrometry (LRMS); Magnesium sulfate ($MgSO_4$); Megahertz (MHz); *meta*-Chloroperoxybenzoic acid (*m*CPBA); Methanol (MeOH); Methyl iodide (MeI); Mesitylene (Mes); *N*-Bromosuccinimide (NBS); *N*-iodosuccinimide (NIS); Nitrogen gas (N_2); Nuclear magnetic resonance (NMR); Polyphosphoric acid (PPA); Potassium carbonate (K_2CO_3); Potassium hydroxide (KOH); Potassium permanganate ($KMnO_4$); Silver oxide (Ag_2O). Sodium bicarbonate ($NaHCO_3$); Sodium hydroxide (NaOH); Sodium methoxide (NaOMe); Sodium sulfate (Na_2SO_4); Sodium thiosulfate ($Na_2S_2O_3$); Tetrahydrofuran (THF); Thin-layer chromatography (TLC); Toluene (PhMe); Tosic acid (TsOH); Triethylamine (TEA); Triflic acid (TfOH); Trifluoroacetic acid (TFA); Trimethylsilyl (TMS); Ultraviolet-visible (UV-vis).

5.5.2 Materials and instrumentation

Chemical reagents were purchased from Alfa Aesar, Sigma-Aldrich, Fisher Scientific, Acros Organics, TCI, Oakwood Chemicals, or Combi-Blocks and used without purification, unless otherwise noted. Reagents and products were weighed on a Sartorius ENTRIS224-1S Analytical Balance (220 x 0.0001 g). Anhydrous, deoxygenated solvents CH_2Cl_2, DMF, MeCN, MeOH, PhMe, and THF were dispensed from a Grubb's-type Phoenix Solvent Drying System. Thin-layer chromatography (TLC) was performed using silica gel 60 F_{254} (EMD Millipore) plates (0.5 mm thickness for preparative TLC) and visualized under short- and/or long-wave UV light (UVGL-25, 254/365 nm). Flash column chromatography was performed using technical grade silica gel with 60 Å pores and 40–63 μm mesh particle size (Sorbtech Technologies) or aluminum oxide (alumina; basic, 50–200 μm, 60 Å pores [Acros Organics]). Solvent was removed under reduced pressure with a Büchi or Ika Rotovapor with a Welch self-cleaning dry vacuum pump and further dried with a Welch DuoSeal pump attached to a Schlenk manifold. NMR spectra were recorded on Bruker AV-500 (^{1}H and ^{13}C), Bruker DRX-500 (^{1}H), and Bruker AV-400 (^{1}H, ^{13}C, and ^{19}F) instruments and processed with MestReNova software. Samples were taken in deuterated chloroform ($CDCl_3$) or deuterated DMSO (DMSO-d_6), and NMR peaks were calibrated using residual non-deuterated solvent ($CHCl_3$ at 7.26 ppm ^{1}H NMR, 77.16 ppm ^{13}C NMR; DMSO at 2.50 ppm ^{1}H NMR, 39.52 ppm ^{13}C NMR). Multiplicities are as indicated: s (singlet), d (doublet), dd (doublet of doublets), ddd (doublet of doublets of doublets), ddt (doublet of doublet of triplets), dq (doublet of quartets), dt (doublet of triplets), tt (triplet of triplets), t (triplet), q (quartet), and m (multiplet). Coupling constants, *J*, are reported in Hz and integrations are provided. LRMS (electrospray ionization [ESI]) were collected on an Agilent 1260 Infinity II HPLC-tandem MS system with InfinityLab Poroshell 120 EC-C8 column (3.0 x

50 mm, 2.7 μm). LC method: gradient of 65% MeCN in water to 100% over 5.5 min, 100% MeCN over 2 min, then back to 65% MeCN over 0.5 min, after first equilibrating with 65% MeCN/water. HRMS (ESI-MS) were collected on an Agilent 6545 Q-TOF LC/MS with 1260 Infinity LC. HRMS (DART-MS) were collected on a Thermo Exactive Plus Orbitrap with IonSense ID-CUBE DART source and a Vapur Interface (IonSense Inc.), with samples in CH_2Cl_2 spotted onto OpenSpot sample cards (IonSense Inc.) and ionization performed using UHP He plasma.

5.5.3 Note on observed masses

Many compounds (**5.5**, **5.33**, **5.41**, **5.42**, **5.43**, and **5.44**) were observed with oxidized masses by LRMS and HRMS (both ESI). This has been reported for other related compounds observed via electrospray ionization.[25–28]

5.5.4 Synthetic experimental procedures

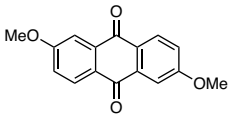

5.9

2,6-dimethoxyanthracene-9,10-dione (5.9). Following a modified literature procedure,[29] anthraflavic acid **5.10** (96.8 mg, 0.403 mmol, 1.00 equiv) and flame-dried K_2CO_3 (234 mg, 1.69 mmol, 4.19 equiv) were added to a flame-dried, 15-mL flask, followed by anhydrous DMF (1.0 mL, 0.40 M). Methyl iodide (0.20 mL, 450 mg, 3.2 mmol, 7.9 equiv) was added dropwise and the solution stirred at 40 °C in an oil bath, under N_2, for 22 h. After cooling to room temperature, the mixture was poured into a beaker containing H_2O (20 mL). The aqueous layer was extracted with $CHCl_3$ (3 x 25 mL) and the combined organic layers dried ($MgSO_4$), filtered, and

concentrated. The crude was evaporated onto silica and purified by column chromatography (silica gel, 50% → 100% EtOAc/hexanes; flush with 2% MeOH/EtOAc; product sticks to column) to yield **5.9** as a yellow-orange solid (90 mg, 0.34 mmol, 83%). R_f = 0.7 in 50% EtOAc/hexanes. ^{1}H NMR (400 MHz, $CDCl_3$) δ 8.25 (d, *J* = 8.7 Hz, 2H), 7.73 (d, *J* = 2.7 Hz, 2H), 7.26 – 7.22 (m, 2H), 3.99 (s, 6H). The spectral data were consistent with the literature report.[30]

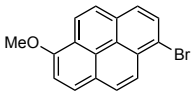

5.13

1-bromo-6-methoxypyrene (5.13). Based on a modified literature procedure.[31] A 2-neck, 25-mL flask equipped with stir bar and condenser was flame-dried under vacuum and backfilled with N_2 three times. With water flowing through condenser, anhydrous MeOH (2.0 mL) was added to flask, followed by sodium metal (Na^0, 123.5 mg, 5.372 mmol). The solution exothermed and was stirred, cooling to room temperature, for 50 minutes to make a fresh NaOMe solution (2.7 M in MeOH). To a separate, flame-dried 15-mL flask with a condenser was added 1,6-dibromopyrene **5.14** (101.6 mg, 0.2822 mmol, 1.000 equiv), DMAc (2.3 mL, 0.12 M), and CuI (5.6 mg, 0.029 mmol, 10 mol %). Freshly prepared NaOMe solution (2.7 M, 0.18 mL, 0.48 mmol, 1.7 equiv) was added via syringe, and the mixture lowered into 80 °C oil bath and stirred for 18 h. The mixture was cooled to room temperature, then quenched with cold H_2O (15 mL). The aqueous layer was acidified to ~pH 3–4 using 2 M HCl (check using pH paper). The acidified aqueous layer was extracted with CH_2Cl_2 (3 x 20 mL, until yellow color disappeared from aqueous layer). The combined organic layers were washed with brine (1 x 20 mL), then dried ($MgSO_4$), filtered, and concentrated. The crude product was evaporated onto

silica and purified by column chromatography (silica gel, 10% PhMe in hexanes) to give **5.13** as a yellow solid (48 mg, 0.15 mmol, 55%). R_f = 0.2 in 10% PhMe/hexanes. ^{1}H NMR (400 MHz, $CDCl_3$): δ 8.47 (d, *J* = 9.2 Hz, 1H), 8.24 (d, *J* = 9.2 Hz, 1H), 8.18 (d, *J* = 8.2 Hz, 1H), 8.16 (d, *J* = 8.4 Hz, 1H), 8.05 (d, *J* = 9.2 Hz, 1H), 7.99 (d, *J* = 9.2 Hz, 1H), 7.94 (d, *J* = 8.2 Hz, 1H), 7.58 (d, *J* = 8.4 Hz, 1H), 4.18 (s, 3H) ppm. ^{13}C NMR (126 MHz, $CDCl_3$): δ 154.3, 131.3, 130.43, 130.36, 129.0, 126.3, 126.3, 126.2, 125.3, 125.2, 124.9, 123.6, 121.6, 120.4, 119.1, 108.8, 56.3 ppm. HRMS (ESI/Q-TOF) m/z: [M]+ calcd for $C_{17}H_{11}BrO$ 309.9993; found 309.9970. *Safety note*: NaOMe solution was quenched via slow addition of *i*PrOH, then MeOH, then H_2O while immersed in ice bath.

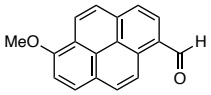

5.12

6-methoxypyrene-1-carbaldehyde (5.12). Based on a modified literature procedure.[11] To a flame-dried, 10-mL flask was added **5.13** (39.0 mg, 0.125 mmol, 1.00 equiv); the flask was then purged and backfilled with N_2. Anhydrous THF (0.8 mL, 0.2 M) was added and the flask cooled to -78 °C in a dry ice/acetone bath. At -78 °C, *n*-BuLi (1.6 M, 0.10 mL, 0.16 mmol, 1.3 equiv) was added dropwise; the mixture was stirred at -78 °C for 1 h. After 1 h, still at -78 °C, anhydrous DMF (15 µL, 14 mg, 0.19 mmol, 1.5 equiv) was added, then the dry ice/acetone bath removed. The reaction was stirred at room temperature for 14 h. The flask was lowered into an ice bath and quenched with aqueous HCl (6 M, 10 mL). The quenched solution was stirred for 10 minutes, warming to room temperature, then transferred to a beaker. The aqueous layer was extracted with Et_2O (30 mL) and concentrated. The crude yellow solid was insoluble in many

solvents (Et_2O, CH_2Cl_2, EtOAc, PhMe, $CHCl_3$). The crude was dissolved in DMF and purified via preparative TLC (50% EtOAc/hexanes). Aldehyde **5.12** was isolated as a bright yellow, sticky powder (7.1 mg, 0.027 mmol, 21%). R_f = 0.5 in 25% EtOAc/hexanes. ^{1}H NMR (400 MHz, DMSO-d_6): δ 10.77 (s, 1H), 9.24 (d, J = 9.3 Hz, 1H), 8.60 (d, J = 9.1 Hz, 1H), 8.54 (d, J = 8.0 Hz, 1H), 8.48 (d, J = 8.5 Hz, 1H), 8.38 (m, 2H), 8.24 (d, J = 9.2 Hz, 1H), 7.90 (d, J = 8.6 Hz, 1H), 4.20 (s, 3H) ppm. ^{13}C NMR (126 MHz, $CDCl_3$): δ 193.1, 155.5, 136.3, 132.4, 131.8, 131.0, 128.1, 126.9, 126.3, 125.4, 125.1, 124.8, 124.7, 123.8, 120.6, 120.3, 109.0, 56.4 ppm. LRMS (ESI) m/z: $[M]^+$ calcd for $C_{18}H_{12}O_2$ 260.1; found 260.8; $[M+2\ Na–H]^+$ calcd for $C_{18}H_{11}O_2Na_2$ 305.1; found 305.0.

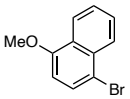

5.24

1-bromo-4-methoxynaphthalene (5.24). Based on a modified literature procedure,[32] recrystallized NBS (1.35 g, 7.58 mmol, 1.1 equiv), anhydrous MeCN (32 mL, 0.24 M), and 1-methoxynaphthalene **5.23** (1.0 mL, 6.9 mmol, 1.0 equiv) were added sequentially to a flame-dried, 250-mL, 3-neck flask under N_2. The reaction was stirred at 80 °C for 3 h, then cooled to room temperature. The reaction was then quenched with saturated aq. $Na_2S_2O_3$ (15 mL) and the aqueous layer extracted with CH_2Cl_2 (3 x 10 mL). The combined organic layers were washed once with brine (10 mL) then dried ($MgSO_4$), filtered, and concentrated to give the crude product as a yellow oil. The crude product was purified by column chromatography (silica gel, 5% EtOAc/hexanes → 25% EtOAc/hexanes). Product **5.24** was obtained as a pale yellow oil (1.53 g, 6.45 mmol, 93%). R_f = 0.4 in 10% EtOAc/hexanes. ^{1}H NMR (400 MHz, $CDCl_3$): δ 8.28 (d, J =

8.1 Hz, 1H), 8.17 (d, J = 8.2 Hz, 1H), 7.66 (d, J = 8.2 Hz, 1H), 7.61 (m, 1H), 7.53 (m. 1H), 6.69 (d, J = 8.3 Hz, 1H), 4.00 (s, 3H) ppm. The spectral data were consistent with a literature report.[33]

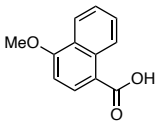

5.20

4-methoxy-1-naphthoic acid (5.20). Based on a modified literature procedure,[32] 1-bromo-4-methoxynaphthalene (**5.24**) (657 mg, 2.77 mmol, 1.00 equiv) was added to a flame-dried, 100-mL, 3-neck flask, which was then purged and backfilled with N_2 three times. Anhydrous THF (28 mL, 0.10 M) was added, and the mixture cooled to -78 °C. At -78 °C, *n*-BuLi (1.4 M, 2.8 mL, 3.9 mmol, 1.4 equiv) was added dropwise, and the reaction was stirred at -78 °C for 30 minutes. To a separate, 500-mL single-neck flask, equipped with a rubber septum fitted with a cannula needle, was added anhydrous $MgSO_4$ (enough to fill ~1/4 of the flask) and enough dry ice to maintain a flow of CO_2 out the needle. Taking care to avoid excess pressure buildup, the cannula needle was added to the main reaction mixture (still at -78 °C) and CO_2 was bubbled in over 15 minutes, accompanied by the formation of a white precipitate. After 15 minutes, CO_2 flow was removed, and the reaction mixture was warmed to room temperature. The crude mixture was diluted with Et_2O (50 mL), and the organic layer extracted with 1 M NaOH (3 x 10 mL). The combined aqueous layers were then acidified to pH 3–4 using 2 M HCl (checked with pH paper), then extracted with EtOAc (3 x 20 mL). The organic layers were dried ($MgSO_4$), filtered, and concentrated under reduced pressure to give **5.20** as a white solid (534 mg, 2.64 mmol, 95%). R_f = 0.41 in 50% EtOAc/hexanes. ^{1}H NMR (400 MHz, DMSO-d_6): δ 12.79 (s, 1H), 9.04 (d, J = 8.8 Hz, 1H), 8.24 (dd, J = 8.4, 0.8 Hz), 8.23 (d, J = 8.3 Hz, 1H), 7.65 (m, 1H), 7.55 (m, 1H), 7.03 (d, J = 8.3 Hz, 1H), 4.03 (s, 3H) ppm. ^{13}C NMR (101 MHz, DMSO-d_6) δ 168.3,

158.5, 132.4, 132.3, 128.0, 125.6, 125.5, 124.9, 121.9, 118.9, 103.4, 56.0 ppm. The spectral data were consistent with the literature report.[34]

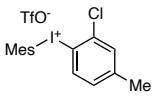

5.21a

(2-chloro-4-methylphenyl)(mesityl)iodonium triflate (5.21a). Based on modified literature procedures,[17,18] to a 20-mL scintillation vial with a stir bar were added, in order: 70–75% *m*CPBA (dried under vacuum) (240 mg, 1.0–1.1 equiv), CH_2Cl_2 (4.5 mL, 0.21 M), mesitylene (0.14 mL, 1.0 mmol, 1.1 equiv), 2-chloro-1-iodo-4-methylbenzene **5.26a** (0.13 mL, 0.93 mmol, 1.0 equiv), and TsOH•H_2O (193 mg, 1.09 mmol, 1.2 equiv). The reaction was stirred at room temperature overnight. The mixture was cooled to 0 °C and TfOH (80 μL, 0.91 mmol, 0.98 equiv) was added dropwise. The reaction was warmed to room temperature and stirred for an additional 2 h. The mixture was concentrated under reduced pressure, then Et_2O (4 mL) was added. This mixture was stirred for 30 minutes, then cooled to 0 °C for about 1 h. The product was then collected by vacuum filtration, rinsing with cold Et_2O. Product **5.21a** was obtained as a pink solid (248 mg, 0.476 mmol, 51%). R_f = 0.2 in 4% MeOH in CH_2Cl_2. ^{1}H NMR (400 MHz, DMSO-d_6): δ 8.13 (d, J = 8.2 Hz, 1H), 7.66 (d, J = 1.1 Hz, 1H), 7.26 (dd, J = 8.2, 1.2 Hz, 1H), 7.20 (s, 2H), 2.60 (s, 6H), 2.35 (s, 3H), 2.28 (s, 3H) ppm. ^{13}C NMR (101 MHz, DMSO-d_6): δ 145.4, 143.1, 141.8, 138.6, 135.6, 131.1, 130.8, 129.9, 122.7, 122.3, 119.1, 112.7, 26.2, 20.5, 20.4 ppm. ^{19}F NMR (376 MHz, DMSO-d_6): δ -77.73 ppm. LRMS (ESI) m/z: $[M\text{-}OTf]^+$ calcd for $C_{16}H_{17}ClI$ 371.0; found 371.0.

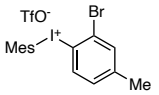

5.21b

(2-bromo-4-methylphenyl)(mesityl)iodonium triflate (5.21b). Based on modified literature procedures, [17,18] to a 20-mL scintillation vial with a stir bar were added, in order: 70–75% *m*CPBA (dried under vacuum) (465 mg, 1.1–1.2 equiv), CH_2Cl_2 (7.5 mL, 0.2 M), mesitylene (0.26 mL, 1.9 mmol, 1.1 equiv), 2-bromo-1-iodo-4-methylbenzene **5.26b** (0.24 mL, 1.7 mmol, 1.0 equiv), and TsOH•H_2O (357 mg, 1.88 mmol, 1.1 equiv). The reaction was stirred at room temperature overnight. The mixture was cooled to 0 °C and TfOH (150 µL, 1.7 mmol, 1.0 equiv) was added dropwise. The reaction was warmed to room temperature and stirred for an additional 2 h. The mixture was concentrated under reduced pressure, then Et_2O (~4 mL) was added. This mixture was stirred for 30 minutes, then cooled to 0 °C for about 1 h. The product was then collected by vacuum filtration, rinsing with cold Et_2O. Product **5.21b** was obtained as a pink solid (507 mg, 0.897 mmol, 53%). R_f = 0.2 in 4% MeOH in CH_2Cl_2. ^{1}H NMR (400 MHz, DMSO-d_6): δ 8.02 (d, J = 8.2 Hz, 1H), 7.75 (d, J = 1.2 Hz, 1H), 7.24 (dd, J = 8.2, 1.2 Hz, 1H), 7.17 (s, 2H), 2.58 (s, 6H), 2.30 (s, 3H), 2.25 (s, 3H) ppm. ^{13}C NMR (101 MHz, DMSO-d_6): δ 145.2, 143.1, 141.8, 138.8, 134.4, 131.2, 130.0, 126.4, 123.0, 122.3, 119.1, 115.7, 26.3, 20.4, 20.4 ppm. ^{19}F NMR (376 MHz, DMSO-d_6): δ -77.72 ppm. LRMS (ESI) m/z: $[M\text{-}OTf]^+$ calcd for $C_{16}H_{17}BrI$ $(M\text{-}OTf)^+$: 415.0; found 415.0.

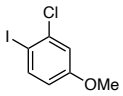

5.27a

2-chloro-1-iodo-4-methoxybenzene (5.27a). Based on a modified literature procedure,[19] anhydrous MeCN (16 mL, 0.25 M), 3-chloroanisole **5.28** (0.50 mL, 4.1 mmol, 1.0 equiv), and

TFA (0.10 mL, 1.3 mmol, 0.3 equiv) were added to a flame-dried, 50 mL, 2-neck flask, equipped with a reflux condenser, under N_2. *N*-iodosuccinimide (1.01 g, 4.80 mmol, 1.2 equiv) was added, and the flask immediately lowered into an 80 °C oil bath. The reaction was stirred at 80 °C for 6 h, then cooled to room temperature. The crude product was concentrated under reduced pressure, then purified by column chromatography (silica gel, 1%→2%→3%→4%→5%→6%→7% EtOAc/heptane). Product **5.27a** was obtained as a clear oil (596 mg, 2.22 mmol, 55% yield). R_f = 0.69 in 15% EtOAc/heptane. ^{1}H NMR (400 MHz, $CDCl_3$): δ 7.69 (d, J = 8.8 Hz, 1H), 7.03 (d, J = 2.8 Hz, 1H), 6.57 (dd, J = 8.8, 2.8 Hz, 1H), 3.78 (s, 3H) ppm. Minor isomer 4-chloro-1-iodo-2-methoxybenzene **5.29** was obtained as a clear oil (41 mg, 4% yield). The column also yielded 310 mg of a 1.4:1 mixture of both isomers that could be further purified if needed. The spectral data for both isomers were consistent with a literature report.[35]

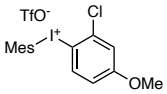

5.22a

(2-chloro-4-methoxyphenyl)(mesityl)iodonium triflate (5.22a). Based on modified literature procedures, [17,18] to a 20-mL scintillation vial with a stir bar were added, in order: 70–75% *m*CPBA (dried under vacuum) (240 mg, 1.1–1.2 equiv), CH_2Cl_2 (4.5 mL, 0.21 M), mesitylene (0.14 mL, 1.0 mmol, 1.1 equiv), 2-chloro-1-iodo-4-methoxybenzene **5.27a** (252 mg, 0.940 mmol, 1.00 equiv), and TsOH•H_2O (195 mg, 1.03 mmol, 1.10 equiv). The reaction was stirred at room temperature overnight. The mixture was cooled to 0 °C and TfOH (85 µL, 0.97 mmol, 1.0 equiv) was added dropwise. The reaction was warmed to room temperature and stirred for an additional 2 h. The mixture was concentrated under reduced pressure, then Et_2O (4 mL) was added. This mixture was stirred for 30 minutes, then cooled to 0 °C for about 1 h. The product

was then collected by vacuum filtration, rinsing with cold Et_2O. Product **5.22a** was obtained as a pale brown solid (244 mg, 0.456 mmol, 48% yield). R_f = 0.2 in 4% MeOH in CH_2Cl_2. ^1H NMR (400 MHz, $CDCl_3$): δ 7.33 (d, J = 9.1 Hz, 1H), 7.12 (d, J = 2.8 Hz, 1H), 7.11 (s, 2H), 6.83 (dd, J = 9.1, 2.8 Hz, 1H), 3.85 (s, 3H), 2.63 (s, 6H), 2.35 (s, 3H) ppm. ^{13}C NMR (101 MHz, $CDCl_3$): δ 163.6, 144.7, 142.6, 137.2, 135.7, 130.7, 121.9, 121.4, 118.7, 117.0, 116.6, 101.1, 56.2, 27.0, 21.1 ppm. ^{19}F NMR (376 MHz, $CDCl_3$): δ -78.30 ppm. LRMS (ESI) m/z: $[M\text{-}OTf]^+$ calcd for $C_{16}H_{17}ClIO$ 387.0; found 387.0.

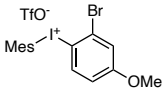

5.22b

(2-bromo-4-methoxyphenyl)(mesityl)iodonium triflate (5.22b). Based on modified literature procedures, [17,18] to a 20 mL scintillation vial with a stir bar were added, in order: 70–75% *m*CPBA (dried under vacuum) (250 mg, 1.1–1.2 equiv), CH_2Cl_2 (4.5 mL, 0.21 M), mesitylene (0.14 mL, 1.0 mmol, 1.1 equiv), 2-bromo-1-iodo-4-methoxybenzene **5.27b** (0.14 mL, 0.94 mmol, 1.0 equiv), and TsOH•H_2O (197 mg, 1.04 mmol, 1.1 equiv). The reaction was stirred at room temperature overnight. The mixture was cooled to 0 °C and TfOH (83 µL, 0.93 mmol, 1.0 equiv) was added dropwise. The reaction was warmed to room temperature and stirred for an additional 2 h. The mixture was concentrated under reduced pressure, then Et_2O (4 mL) was added. This mixture was stirred for 30 minutes, then cooled to 0 °C for about 1 h. The product was then collected by vacuum filtration, rinsing with cold Et_2O. Product **5.22b** was obtained as a white solid (285 mg, 0.490 mmol, 52%). R_f = 0.2 in 4% MeOH in CH_2Cl_2. ^1H NMR (500 MHz, $CDCl_3$): δ 7.27 (d, J = 2.7 Hz, 1H), 7.16 (s, 2H), 6.96 (d, J = 9.1 Hz, 1H), 6.84 (dd, J = 9.1, 2.8 Hz, 1H), 3.83 (s, 3H), 2.63 (s, 6H), 2.39 (s, 3H) ppm. ^{13}C NMR (101 MHz, $CDCl_3$): δ 163.2,

145.1, 142.6, 134.3, 130.8, 125.9, 121.9, 121.9, 120.3, 118.7, 117.3, 103.7, 56.2, 27.0, 21.2 ppm. ^{19}F NMR (376 MHz, $CDCl_3$): δ -78.28 ppm. LRMS (ESI) m/z: $[M\text{-}OTf]^+$ calcd for $C_{16}H_{17}ClIO$ 431.0; found 431.0.

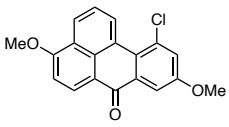

5.19a

11-chloro-4,9-dimethoxy-7*H*-benzo[*de*]anthracen-7-one (5.19a). Based on a literature procedure,[16] naphthoic acid **5.20** (61 mg, 0.30 mmol, 1.0 equiv), iodonium triflate **5.22a** (320 mg, 0.60 mmol, 2.0 equiv), and $Pd(OAc)_2$ (6.9 mg, 0.031 mmol, 10 mol%) were added to a flame-dried, 15-mL two-neck flask equipped with a stir bar and reflux condenser. The flask was then purged and backfilled with N_2 three times. Anhydrous DCE (3.0 mL, 0.10 M) was added. TfOH (53 μL, 0.60 mmol, 2.0 equiv) was added dropwise, and the mixture was stirred at 80 °C for 24 h. The crude mixture was filtered through celite, rinsing with CH_2Cl_2. The filtrate was concentrated under reduced pressure, then purified by column chromatography (silica gel, 25% EtOAc/hexanes→50% EtOAc/hexanes). Product **5.19a** was further purified by preparative thin-layer chromatography (30% EtOAc/hexanes) to yield a dark orange solid (2.1 mg, 0.0065 mmol, 2%). R_f = 0.30 in 25% EtOAc/hexanes. ^{1}H NMR (500 MHz, $CDCl_3$): δ 9.58 (dd, J = 7.8, 1.1 Hz, 1H), 8.77 (d, J = 8.4 Hz, 1H), 8.43 (dd, J = 8.4, 1.1 Hz, 1H), 8.08 (d, J = 3.0 Hz, 1H), 7.66 (t, J = 8.1 Hz, 1H), 7.40 (d, J = 3.0 Hz, 1H), 7.14 (d, J = 8.4 Hz, 1H), 4.15 (s, 3H), 3.98 (s, 3H) ppm. ^{13}C NMR (126 MHz, $CDCl_3$): δ 181.7, 162.2, 158.4, 135.5, 132.6, 132.6, 129.2, 129.2, 127.1, 125.4, 125.3, 124.7, 124.2, 123.9, 120.9, 110.1, 105.6, 56.2, 55.9 ppm. HRMS (ESI/Q-TOF) m/z: [M+H]+ calcd for $C_{19}H_{14}ClO_3^+$ 325.0631; found 325.0612.

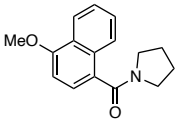

5.30

(4-methoxynaphthalen-1-yl)(pyrrolidin-1-yl)methanone (5.30). Naphthoic acid **5.20** (76.0 mg, 0.376 mmol, 1.00 equiv) was added to a flame-dried 20-mL scintillation vial and purged and backfilled with N_2. HATU (172.2 mg, 0.4529 mmol, 1.20 equiv; weighed separately in a tared vial with cap) was added with anhydrous DMF (1.3 mL, 0.29 M). DIPEA (0.26 mL, 190 mg, 1.5 mmol, 4.0 equiv), then pyrrolidine (0.040 mL, 34 mg, 0.5 mmol, 1.3 equiv) were added and the bright yellow mixture was stirred at room temperature for 16 h. The crude was diluted in EtOAc (10 mL) and added to saturated aqueous $NaHCO_3$ (10 mL). The aqueous layer was extracted with EtOAc (5 x 5 mL). The combined organic layers were washed with H_2O (10 x 5 mL) to remove the HATU urea by-product. The combined organic layers were dried (Na_2SO_4), filtered, and concentrated, then evaporated onto silica and purified by column chromatography (silica gel, hexanes flush, then 70% EtOAc/hexanes). Amide **5.30** was isolated as an off-white solid (60.1 mg, 0.235 mmol, 63%). R_f = 0.2 in 70% EtOAc/hexanes. ^{1}H NMR (500 MHz, DMSO-d_6): δ 8.22–8.20 (m, 1H), 7.81 – 7.75 (m, 1H), 7.56 (m, 2H), 7.43 (d, J = 7.9 Hz, 1H), 6.99 (d, J = 7.9 Hz, 1H), 4.00 (s, 3H), 3.58 (t, J = 7.0 Hz, 2H), 3.07 (t, J = 6.7 Hz, 2H), 1.90 (p, J = 6.8 Hz, 2H), 1.76 (p, J = 6.8 Hz, 2H) ppm. The spectral data were consistent with a literature report.[21]

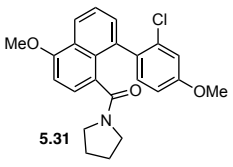

5.31

(8-(2-chloro-4-methoxyphenyl)-4-methoxynaphthalen-1-yl)(pyrrolidin-1-yl)methanone (5.31). Based on a literature procedure.[21] To a flame-dried, 20-mL scintillation vial under N_2

were added iodonium triflate **5.22a** (160.9 mg, 0.2998 mmol, 3.0 equiv) and $Pd(OAc)_2$ (2.4 mg, 0.011 mmol, 11 mol %). The vial was purged and backfilled with N_2 three times. Amide **5.30** (26 mg, 0.10 mmol, 1.0 equiv) in anhydrous DCE (2.0 mL, 0.050 M) was added, followed by TfOH (9.0 µL, 15 mg, 0.10 mmol, 1.0 equiv), added dropwise. The vial was stirred at 80 °C in an aluminum reaction block for 24 h, then allowed to cool to room temperature. The mixture was diluted with CH_2Cl_2 (2 mL) and filtered through celite, rinsing with additional CH_2Cl_2. The organic layer was washed with saturated aqueous $NaHCO_3$ (1 x 5 mL) and brine (1 x 5 mL), then dried ($MgSO_4$), filtered, and concentrated to give a crude, dark orange oil. The crude was evaporated onto silica and purified by column chromatography (silica gel, 90% EtOAc/hexanes) to give **5.31** as a pale orange solid (11.7 mg, 0.0296 mmol, 29%). R_f = 0.1 in 90% EtOAc/hexanes. ^{1}H NMR (500 MHz, $CDCl_3$): δ 8.41 (dd, *J* = 8.6, 4.2 Hz, 1H), 7.53 (dd, *J* = 8.6, 7.0 Hz, 1H), 7.42 – 7.37 (m, 1H), 7.35 – 7.30 (m, 1H), 7.11 – 7.03 (m, 1H), 6.98 – 6.95 (m, 1H), 6.89 (dd, *J* = 8.6, 2.6 Hz, 1H), 6.82 (dd, *J* = 7.9, 2.8 Hz, 1H), 4.04 (s, 3H), 3.85 (d, *J* = 1.5 Hz, 3H), 3.33 – 3.26 (m, 2H), 3.04–3.00 (m 1H), 2.91 – 2.80 (m, 1H), 2.67 – 2.54 (m, 1H), 1.79–1.71 (m, 4H) ppm. ^{13}C NMR (126 MHz, $CDCl_3$) δ 156.4, 135.3, 133.4, 132.9, 132.0, 131.9, 131.4, 130.7, 128.4, 127.0, 126.9, 124.9, 122.6, 114.6, 112.3, 111.6, 103.0, 55.8, 48.6, 45.4, 29.9, 25.9, 24.6 ppm. (Peaks in NMR split due to a mixture of rotamers.) LRMS (ESI) m/z: $[M+H]^+$ calcd for $C_{23}H_{23}ClNO_3^+$ 396.1; found 396.2; $[2M+Na]^+$ calcd for $C_{46}H_{46}Cl_2N_2O_6Na^+$ 815.3; found 815.2. Starting material **5.30** was also recovered (15 mg, 0.038 mmol, 38% recovery).

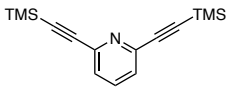

5.34

2,6-bis((trimethylsilyl)ethynyl)pyridine (5.34). Based on modified literature procedures,[36,37] 2,6-dibromopyridine **5.4** (450 mg, 1.9 mmol, 1.0 equiv), CuI (20 mg, 0.1 mmol, 5 mol%), and $Pd(PPh_3)_4$ (111 mg, 0.0957 mmol, 5.0 mol%) were added to a 15 mL two-neck flask. Anhydrous THF (6.0 mL, 0.32 M) was added, followed by *i*Pr_2NH (1.0 mL, 7.1 mmol, 3.7 equiv). Then TMS-acetylene (0.64 mL, 4.6 mmol, 2.4 equiv) was added dropwise. The mixture was stirred at room temperature overnight, then filtered through celite, rinsing with CH_2Cl_2. Aqueous, saturated NH_4Cl (2 mL) was added to the filtrate. The aqueous layer was extracted with CH_2Cl_2 (3 x 5 mL). The combined organic layers were washed once with brine (5 mL) then dried ($MgSO_4$), filtered, and concentrated under reduced pressure. The crude product was purified by column chromatography (silica gel, 25% EtOAc/hexanes) to yield **5.34** as a fluffy, white solid (461 mg, 1.70 mmol, 89%). R_f = 0.75 in 25% EtOAc/hexanes. ^{1}H NMR (400 Hz, $CDCl_3$): δ 7.59 (t, J = 7.8 Hz, 1H), 7.38 (d, J = 7.8 Hz, 2H), 0.25 (s, 18H) ppm. The spectral data were consistent with the literature report.[38]

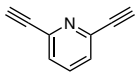

5.3

2,6-diethynylpyridine (5.3). Based on modified literature procedures,[36,37] **5.34** (230 mg, 0.85 mmol, 1.0 equiv) and dried K_2CO_3 (1.1 g, 8.0 mmol, 9.5 equiv) were added to a flame-dried, 15-mL, 2-neck flask, which was then purged and backfilled with N_2. Anhydrous THF (1.5 mL, 0.57 M) and anhydrous MeOH (1.5 mL, 0.57 M) were added and the reaction stirred at room temperature for 5 h. H_2O (5 mL) was added and the aqueous layer extracted with EtOAc (3 x 5

mL). The combined organic layers were washed once with brine (5 mL), then dried ($MgSO_4$), filtered, and concentrated under reduced pressure. The crude product was purified by column chromatography (silica gel, 25% EtOAc/hexanes) to give **5.3** as a fluffy off-white solid (88 mg, 0.69 mmol, 81%). R_f = 0.38 in 25% EtOAc/hexanes. ^{1}H NMR (400 Hz, $CDCl_3$): δ 7.65 (t, J = 7.8 Hz, 1H), 7.45 (d, J = 7.8 Hz, 2H), 3.16 (s, 2H) ppm. The spectral data were consistent with the literature report.[38]

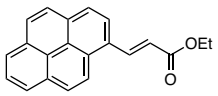

5.36

ethyl (*E*)-3-(pyren-1-yl)acrylate (5.36). The synthesis of this compound was based on a literature procedure.[39] Commercial 1-pyrenecarboxaldehyde (**5.35**) (1.40 g, 6.08 mmol, 1.00 equiv) and LiCl (29 mg, 0.68 mmol, 11 mol %) were added to a flame-dried 100-mL, 3-neck flask, which was then purged and backfilled with N_2 three times. Anhydrous THF (28 mL, 0.22 M) was added, followed by triethyl phosphonoacetate (1.4 mL, 7.1 mmol, 1.2 equiv) and then DBU (1.1 mL, 7.3 mmol, 1.2 equiv). The reaction was stirred at room temperature for 18 h, then neutralized with 1 M HCl (check with pH paper). The neutralized mixture was poured into a beaker of ice (approx. 20 g). The aqueous layer was extracted with PhMe (3 x 30 mL) after the ice melted. The combined organic layers were dried (Na_2SO_4), filtered, and concentrated under reduced pressure. To the resulting oil/solid mixture was added cold MeOH (10 mL), and the precipitate was collected by vacuum filtration, rinsing with cold MeOH, then dried to give **5.36** as a bright yellow solid (1.53 g, 5.09 mmol, 84%). R_f = 0.6 in 25% EtOAc/hexanes. ^{1}H NMR (500 MHz, $CDCl_3$): δ 8.84 (d, J = 15.7 Hz, 1H), 8.50 (d, J = 9.3 Hz, 1H), 8.29 (d, J = 7.9 Hz,

1H), 8.25–8.02 (m, 7H), 6.72 (d, J = 15.7 Hz, 1H), 4.37 (q, J = 7.2 Hz, 2H), 1.42 (t, J = 7.1 Hz, 3H) ppm. The spectral data were consistent with the literature report.[39]

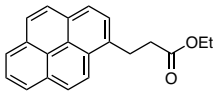

5.37

ethyl 3-(pyren-1-yl)propanoate (5.37). A 100-mL, 3-neck flask was equipped with a stir bar, septum, and two stopcock-controlled N_2 adapters; one attached to N_2/vacuum Schlenk line and the other to control H_2 release from a balloon. The flask was evacuated and backfilled with N_2, and **5.36** (503 mg, 1.68 mmol, 1.00 equiv) was added, followed by anhydrous THF (8 mL, 0.2 M) and EtOH (8 mL, 0.2 M), then Pd (10 wt% on carbon, 81 mg, 4.5 mol%). With stirring, the flask was evacuated briefly (until solvent began bubbling) and backfilled with N_2; this was repeated five times. A balloon attached to a 4-inch needle via tubing was purged then filled with hydrogen gas (H_2) and added to the second adapter on the flask. Controlling H_2 flow into the flask with the stopcock, the flask was evacuated and backfilled with H_2 three times, leaving the flask open to H_2 after. The reaction was stirred at room temperature for 7 h. The H_2 stopcock was closed and the flask was briefly evacuated, then purged with N_2 for 20 minutes to fully remove H_2. The reaction was filtered through a pad of celite, washing with THF. The filtrate was concentrated under reduced pressure to yield **5.37** as an off-white solid (503 mg, 1.66 mmol, quant.). R_f = 0.3 in 5% EtOAc in hexanes. ^{1}H NMR (500 MHz, $CDCl_3$): δ 8.29 (d, J = 9.2 Hz, 1H), 8.21 – 8.16 (m, 2H), 8.15 – 8.10 (m, 2H), 8.04 (s, 2H), 8.00 (t, J = 7.6 Hz, 1H), 7.91 (d, J = 7.8 Hz, 1H), 4.17 (q, J = 7.1 Hz, 2H), 3.70 (t, J = 8.0 Hz, 2H), 2.86 (t, J = 8.0 Hz, 2H), 1.25 (t, J = 7.2 Hz, 3H) ppm. This compound has been made previously by a different method, and the spectral data were consistent with the literature report.[39]

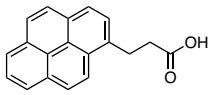

5.38

3-(pyren-1-yl)propanoic acid (5.38). Ester **5.37** (210 mg, 0.69 mmol, 1.0 equiv) was added to a 20-mL scintillation vial with a stir bar. THF (5 mL, 0.3 M) was added, followed by 1 M LiOH (aq) (1.6 mL, 1.6 mmol, 2.3 equiv). The reaction was stirred overnight for 18 h, with progress checked via TLC. The solvent was evaporated under reduced pressure, then 1 M HCl was added until the mixture acidified to pH 3–4 (checked via pH paper) and a yellow solid formed, which was collected by vacuum filtration, rinsing with cold water. The collected solid was dissolved in a THF/CH_2Cl_2 mixture (~3:1, ~50 mL total), dried (Na_2SO_4), filtered, and concentrated under reduced pressure to give **5.38** as an off-white flaky solid (158 mg, 0.576 mmol, 84%). R_f = 0.1 in 25% EtOAc/hexanes. ^{1}H NMR (500 MHz, $CDCl_3$): δ 8.28 (d, *J* = 9.2 Hz, 1H), 8.21 – 8.17 (m, 2H), 8.17 – 8.11 (m, 2H), 8.04 (s, 2H), 8.01 (t, *J* = 7.6 Hz, 1H), 7.92 (d, *J* = 7.7 Hz, 1H), 3.72 (t, *J* = 8.0 Hz, 2H), 2.94 (t, *J* = 8.0 Hz, 2H) ppm. This compound has been made previously by a different method, and the spectral data were consistent with the literature report.[39]

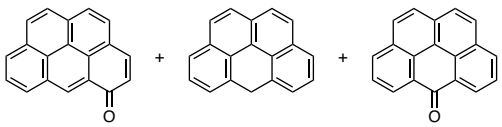

5.40 5.39 5.32

Mixture of 5.32, 5.39, and 5.40. Following the literature procedure,[10] **5.38** (55 mg, 0.20 mmol, 1.0 equiv) was added to a flame-dried 20-mL scintillation vial. Warm (60 °C) polyphosphoric acid (PPA) (0.5 mL, 0.4 M) was added. The mixture was stirred for 24 h at 80 °C in an aluminum reaction block. After cooling to room temperature, the reaction was further cooled in an ice bath before quenching with H_2O (1 mL) and transferring to a separatory funnel with more H_2O (20 mL). The aqueous layer was extracted with CH_2Cl_2 (5 x 25 mL). The combined organic layers

were dried (Na_2SO_4), filtered, and concentrated under reduced pressure to give a dark red crude mixture of **5.32**, **5.39**, and **5.40**. The three major products were isolated by column chromatography (crude material was evaporated onto silica; silica gel column, 0% → 5% → 10% → 15% → 20% → 25% → 50% EtOAc/hexanes). *We note that this reaction became more challenging (both workup and purification) upon scaling up, with 300 mg of **5.38** the largest scale performed, finding a 200-mg scale to be the most optimal for balancing consumption of workup materials, safety of PPA volumes, and overall yields.*

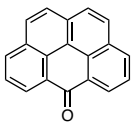

5.32

6*H*-benzo[*cd*]pyren-6-one (5.32). Compound **5.32** was isolated as a dark yellow solid (15 mg, 0.060 mmol, 29%). R_f = 0.7 in 25% EtOAc/hexanes. ^{1}H NMR (500 MHz, $CDCl_3$): δ 8.89 (dd, J = 7.4, 1.2 Hz, 2H), 8.35 (dd, J = 8.0, 1.3 Hz, 2H), 8.13 (d, J = 8.7 Hz, 2H), 8.03 (d, J = 8.7, 2H), 7.90 (dd, J = 8.0, 7.4 Hz, 2H) ppm. The spectral data were consistent with the literature report.[10]

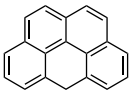

5.39

6*H*-benzo[*cd*]pyrene (5.39). Compound **5.39** was isolated as an off-white solid (12 mg, 0.050 mmol, 24%). R_f = 0.8 in 25% EtOAc/hexanes. ^{1}H NMR (500 MHz, $CDCl_3$): δ 7.82 (d, J = 8.7 Hz, 2H), 7.78 (d, J = 8.7 Hz, 2H), 7.74 (d, J = 7.8 Hz, 2H), 7.56–7.45 (m, 4H), 5.00 (s, 2H) ppm. The spectral data were consistent with the literature report.[10]

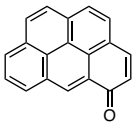

5.40

5*H*-benzo[*cd*]pyren-5-one (5.40). Compound **5.40** was isolated as a dark red solid (14 mg, 0.055 mmol, 27%). R_f= 0.3 in 25% EtOAc/hexanes. ^{1}H NMR (400 MHz, $CDCl_3$): δ 9.43 (s, 1H), 8.60 (d, J = 7.6 Hz, 1H), 8.46 (d, J = 7.7 Hz, 1 H), 8.26 (d, J = 7.9 Hz, 1H), 8.22–8.13 (m, 4H), 8.05 (d, J = 9.7 Hz, 1H), 6.88 (d, J = 9.7 Hz, 1H) ppm. The spectral data were consistent with the literature report.[10]

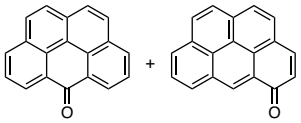

5.32 5.40

Mixture of 5.32 and 5.40 *via* PPA-oxidation sequence (*new procedure to access* 5.32 *in greater yields*). According to the literature procedure,[10] **5.38** (209 mg, 0.762 mmol, 1.00 equiv) was added to a flame-dried 20-mL scintillation vial. Warm (60 °C) PPA (2 mL, 0.4 M) was added. The mixture was stirred for 24 h at 80 °C in an aluminum reaction block. After cooling to room temperature, the reaction was further cooled in an ice bath before quenching with H_2O (~30 mL). The aqueous layer was extracted with CH_2Cl_2 (5 x 50 mL), and the combined organic layers were washed with brine (1 x 20 mL). The combined organic layers were dried (Na_2SO_4), filtered, and concentrated under reduced pressure to give a dark red crude mixture of **5.32**, **5.39**, and **5.40** (165 mg). Based on another literature procedure,[40] acetone (5 mL) was added to the crude mixture and cooled to -78 °C in a dry ice/acetone bath. $KMnO_4$ (122 mg, 0.772 mmol, 1.01 equiv) and $FeCl_3 \cdot 6\ H_2O$ (111 mg, 0.411 mmol, 0.539 equiv) were added and the reaction was stirred at -78 °C for 1 hour, then warmed to room temperature and stirred another 1 h. The crude mixture was filtered through filter paper, rinsing with CH_2Cl_2. The dark green organic filtrate was washed with

saturated aqueous $Na_2S_2O_3$ (1 x 10 mL) (this was repeated if the resulting orange solution turned green again), then H_2O (1 x 20 mL). The orange-colored organic layer was dried ($MgSO_4$), filtered, and concentrated to give a dark red solid. The two major products were isolated by column chromatography (crude material was evaporated onto silica gel; silica gel column, 0%→7%, then 25%→50% EtOAc/heptane). *Note: using heptane as the nonpolar component of chromatography solvent system led to better separation than hexanes, a mixture of isomers.*

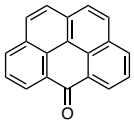

5.32

6*H*-benzo[*cd*]pyren-6-one (5.32). Compound **5.32** was isolated as lightweight, bright yellow crystals (73 mg, 0.29 mmol, 38% over two steps). The spectral data were consistent with those reported above.

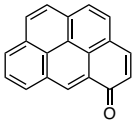

5.40

5*H*-benzo[*cd*]pyren-5-one (5.40). Compound **5.40** was isolated as a dark red solid (13 mg, 0.050 mmol, 7% over two steps). The spectral data were consistent with those reported above.

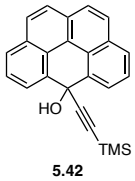

5.42

6-((trimethylsilyl)ethynyl)-6*H*-benzo[*cd*]pyren-6-ol (5.42). This procedure was based on a literature report.[24] To prepare TMS-acetylide solution: anhydrous THF (0.3 mL) and TMS

acetylene (0.06 mL, 0.4 mmol, 1 equiv) were added sequentially to a flame-dried 15-mL two-neck flask and the solution was cooled to -78 °C in a dry ice/acetone bath. *n*-BuLi (1.2 M in hexanes, 0.30 mL, 0.36 mmol, 1.0 equiv) was then added dropwise. The solution was warmed to room temperature and stirred for 45 minutes to give lithium TMS-acetylide solution.

6*H*-Benzo[*cd*]pyren-6-one **5.32** (18.0 mg, 0.0708 mmol, 1.00 equiv) was added to a separate flame-dried, 15-mL two-neck flask, followed by anhydrous THF (1.3 mL, 0.055 M). The solution was cooled to -78 °C in a dry ice/acetone bath before adding TMS acetylide (0.6 M, 0.20 mL, 0.12 mmol, 1.7 equiv) dropwise. The mixture was warmed to room temperature and stirred for 5 h. The reaction was then quenched with H_2O (2 mL) and extracted with CH_2Cl_2 (4 x 2 mL). The combined organic layers were dried (Na_2SO_4), filtered, and concentrated to give **5.42** as a dark green-brown solid (22 mg, 0.062 mmol, 88%). R_f = 0.6 in 25% EtOAc/hexanes. ^{1}H NMR (500 MHz, $CDCl_3$): δ 8.49 (dd, *J* = 7.4, 1.1 Hz, 2H), 8.06 (dd, *J* = 8.0, 1.2 Hz, 2H), 8.02 (d, *J* = 8.6 Hz, 2H), 7.95 (d, *J* = 8.8 Hz, 2H), 7.81 (dd, *J* = 8.0, 7.4 Hz, 2H), 2.71 (–OH, s, 1H), 0.25 (s, 9H) ppm. The spectral data were consistent with the literature report.[24]

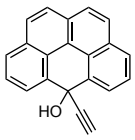

5.33

6-ethynyl-6*H*-benzo[*cd*]pyren-6-ol (5.33). Based on a modified literature procedure.[24] To a dram vial was added **5.42** (18 mg, 0.051 mmol, 1.0 equiv), followed by THF (0.5 mL, 0.1 M) and MeOH (0.5 mL, 0.1 M). Aqueous KOH (1 M, 0.1 mL, 0.1 mmol, 2 equiv) was added and the mixture stirred at room temperature for 3 hours. H_2O (1 mL) was added and the aqueous layer

extracted with CH_2Cl_2 (4 x 2 mL). The combined organic layers were dried (Na_2SO_4), filtered, and concentrated to give **5.31** as a dark brown solid (13 mg, 0.046 mmol, 97%). ^{1}H NMR (500 MHz, $CDCl_3$): δ 8.48 (dd, *J* = 7.4, 1.2 Hz, 2H), 8.07 (dd, *J* = 7.9, 1.3 Hz, 2H), 8.02 (d, *J* = 8.6 Hz, 2H), 7.95 (d, *J* = 8.7 Hz, 2H), 7.84 – 7.77 (m, 2H), 3.04 (s, 1H), 2.78 (s, 1H) ppm. The spectral data were consistent with the literature report.[24]

Attempted synthesis of 5.5 via Route 1: Alkyne addition

To a flame-dried, 15-mL two-neck flask was added **5.3** (12.9 mg, 0.101 mmol, 1.00 equiv), followed by anhydrous THF (0.35 mL). The solution was cooled to -78 °C in a dry ice/acetone bath, then LHMDS (1.0 M, 0.25 mL, 0.25 mmol, 2.5 equiv) was added and the mixture was stirred at -78 °C for 30 minutes to give a 0.17 M solution of lithiate.

Ketone **5.32** (20.3 mg, 0.0798 mmol, 1.00 equiv) was added to a separate flame-dried 10-mL flask, followed by anhydrous THF (0.8 mL, 0.1 M). The solution was cooled to -78 °C in a dry ice/acetone bath. Lithiated **5.3** solution (0.17 M, 0.23 mL, 0.039 mmol, 0.49 equiv) was then added dropwise. The reaction was allowed to warm to room temperature and then stirred for 3 h. The reaction was quenched with saturated aqueous NH_4Cl (2 mL), then extracted with CH_2Cl_2 (3 x 2 mL). The combined organic layers were washed once with saturated aqueous $NaHCO_3$ (1 mL), then dried (Na_2SO_4), filtered, and concentrated to give a dark yellow crude mixture containing single addition product **5.41** according to LCMS (LRMS) and HRMS. HRMS (APCI/DART) m/z: $[M–OH]^+$ calcd for $C_{28}H_{14}N^+$ 364.1121; found 364.1120.

Crude **5.41** (20 mg, contains unreacted **5.32**) was added to a flame-dried 15-mL flask, followed by anhydrous THF (0.8 mL, 0.06 M). The solution was cooled to -78 °C in a dry ice/acetone bath, then LHMDS (1.0 M, 0.18 mL, 0.18 mmol, 4 equiv) was added dropwise. The

mixture was stirred at -78 °C for 30 min before additional ketone **5.32** (4.3 mg, 0.017 mmol) was added in anhdryous THF (0.2 mL). The mixture was allowed to warm to room temperature and stirred an additional 2.5 h. The reaction was quenched with saturated aqueous NH_4Cl (2 mL), then extracted with CH_2Cl_2 (3 x 2 mL). The combined organic layers were washed once with saturated aqueous $NaHCO_3$ (1 mL), then dried (Na_2SO_4), filtered, and concentrated to give a dark brown crude mixture. LCMS analysis showed peaks with masses corresponding to **5.32** (LRMS [ESI] m/z: $[M+H]^+$ calcd for $C_{19}H_{11}O^+$ 255.3; found 255.1), **5.41** (LRMS [ESI] m/z: $[M–OH]^+$ calcd for $C_{28}H_{14}N^+$ 364.1; found 364.0), and **5.5** (LRMS [ESI] m/z: $[M]^+$ calcd for $C_{47}H_{25}NO_2^+$ 635.2; found 635.2; $[M–OH]^+$ calcd for $C_{47}H_{24}NO^+$ 618.2; found 618.2). Purification attempts (silica gel, neutralized silica gel with TEA, basic or neutralized alumina) caused decomposition of presumed products **5.41** and **5.5**, preventing confirmation of proposed structures.

Attempted synthesis of 5.5 via Route 2: Cross-coupling

To an oven-dried, 8-mL reaction vial was added 2,6-dibromopyridine **5.4** (3.8 mg, 0.016 mmol, 1.0 equiv), followed by propargyl alcohol **5.33** (10 mg, 0.04 mmol, 2 equiv), then $Pd(PPh_3)_4$ (2.6 mg, 0.002 mmol, 13 mol%). The vial was purged and backfilled with N_2, then anhydrous THF (0.2 mL, 0.08 M) was added, followed by *i*Pr_2NH (10 µL, 7 mg, 0.07 mmol, 4 equiv). The vial was lowered into a 40 °C aluminum reaction block and stirred for 3 days, monitored by TLC for appearance of new and disappearance of starting material **5.4**. After cooling to room temperature, the crude mixture was diluted with CH_2Cl_2 (2 mL) and filtered through Celite. The organic layer was washed with saturated aqueous $NaHCO_3$ (1 mL), then dried (Na_2SO_4), filtered, and concentrated to give a dark brown crude mixture, containing **5.43**

according to LCMS (LRMS) and HRMS. HRMS (APCI/DART) m/z: $[M–OH]^+$ calcd for $C_{26}H_{13}BrN^+$ 418.0226; found 418.0230.

To an oven-dried, 8-mL reaction vial was added **5.33** (6 mg, 0.02 mmol, 1 equiv*) and $Pd(PPh_3)_4$ (1.7 mg, 0.0015 mmol, 10 mol %*); the vial was purged and backfilled with N_2. Crude **5.43** (0.02 mmol, 1 equiv*) was added along with anhydrous THF (0.2 mL, 0.1 M*) and *i*Pr_2NH (8 μL, 7 mg, 0.06 mmol, 4 equiv*). The reaction was stirred in a 40 °C aluminum reaction block for 34 h, again monitoring by TLC, then cooled to room temperature. The mixture was diluted with CH_2Cl_2 (2 mL) and filtered through celite. The organic layer was washed with saturated aqueous $NaHCO_3$ (1 x 2 mL) and the resulting aqueous layer extracted more with CH_2Cl_2 (3 x 2 mL). The combined organic layers were dried (Na_2SO_4), filtered, and concentrated to give a dark brown crude solid. LCMS analysis showed peaks with masses corresponding to triphenylphosphine oxide (LRMS [ESI] m/z: $[M+H]^+$ calcd for $C_{18}H_{16}OP^+$ 279.1; found 279.0), **5.32** (LRMS [ESI] m/z: $[M+H]^+$ calcd for $C_{19}H_{11}O^+$ 255.3; found 255.1), and **5.5** (LRMS [ESI] m/z: $[M–OH]^+$ calcd for $C_{47}H_{24}NO^+$ 618.2; found 618.2), and **5.44** (LRMS [ESI] m/z: $[M–OH]^+$ calcd for $C_{42}H_{21}O^+$ 541.2; found 541.2). Purification attempts (silica gel, neutralized silica gel with TEA, basic or neutralized alumina) caused decomposition of presumed products **5.43**, **5.44**, and **5.5**, preventing confirmation of proposed structures. (*Assuming full conversion from step 1.)

5.5.5 ^{1}H NMR spectra

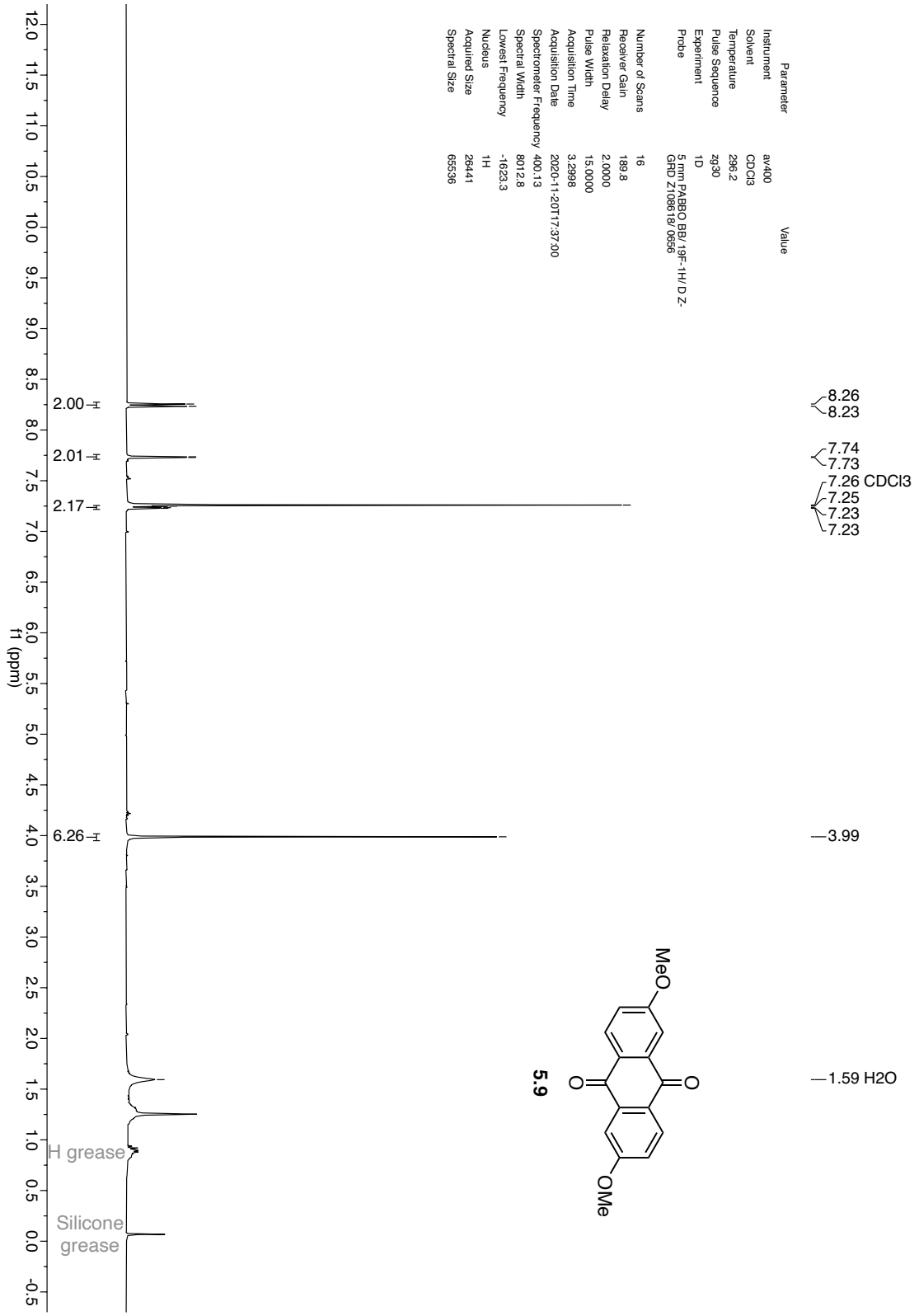

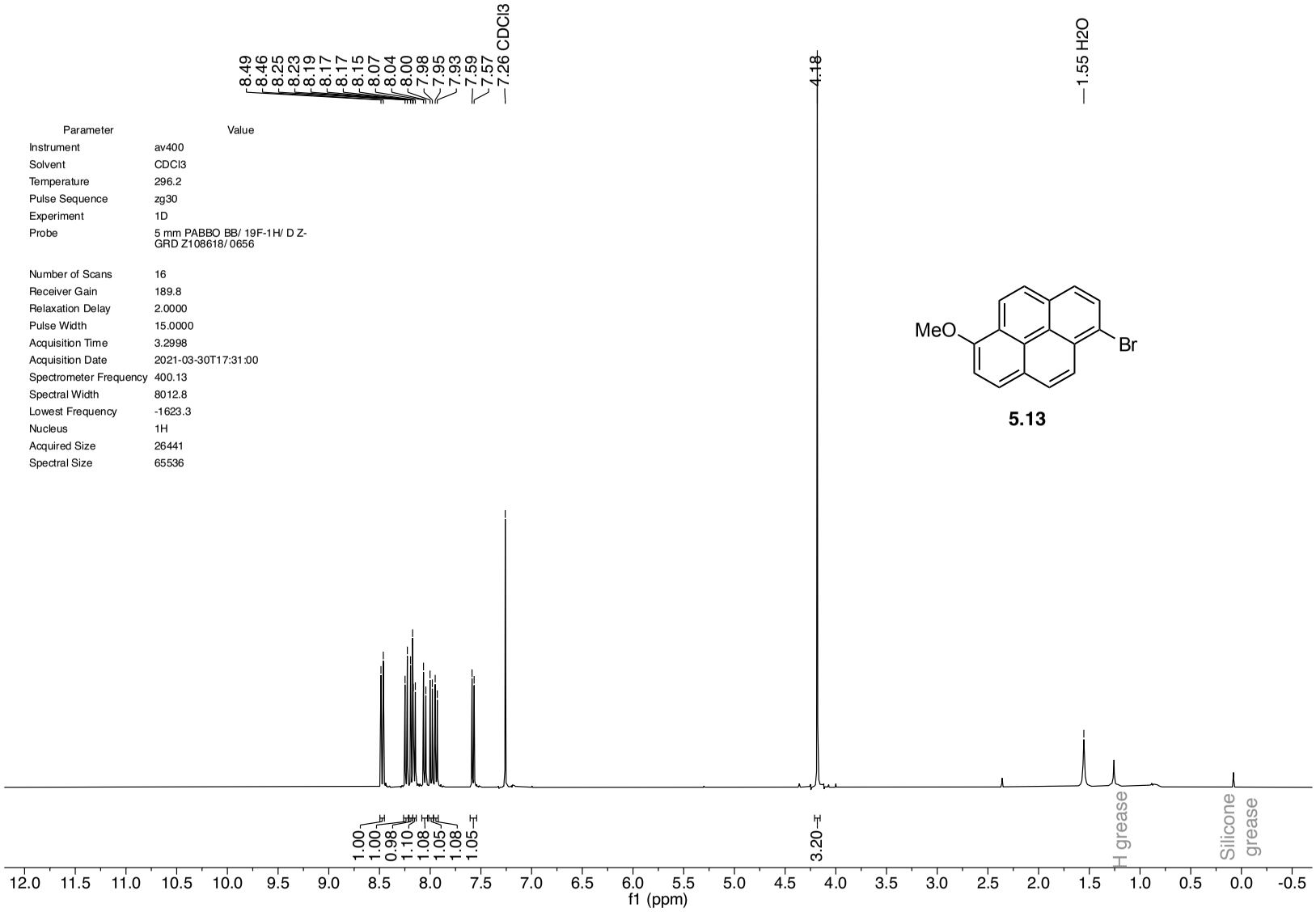
8.49
8.46
8.25
8.23
8.19
8.17
8.17
8.15
8.07
8.04
8.00
7.98
7.95
7.93
7.59
7.57
7.26 CDCl3
4.18
1.55 H2O
Parameter Value
Instrument av400
Solvent CDCl3
Temperature 296.2
Pulse Sequence zg30
Experiment 1D
Probe 5 mm PABBO BB/ 19F-1H/ D Z-GRD Z108618/ 0656
Number of Scans 16
Receiver Gain 189.8
Relaxation Delay 2.0000
Pulse Width 15.0000
Acquisition Time 3.2998
Acquisition Date 2021-03-30T17:31:00
Spectrometer Frequency 400.13
Spectral Width 8012.8
Lowest Frequency -1623.3
Nucleus 1H
Acquired Size 26441
Spectral Size 65536
MeO
Br
5.13
1.00
1.00
0.98
1.10
1.08
1.05
1.08
1.05
3.20
H grease
Silicone grease
12.0 11.5 11.0 10.5 10.0 9.5 9.0 8.5 8.0 7.5 7.0 6.5 6.0 5.5 5.0 4.5 4.0 3.5 3.0 2.5 2.0 1.5 1.0 0.5 0.0 -0.5
f1 (ppm)

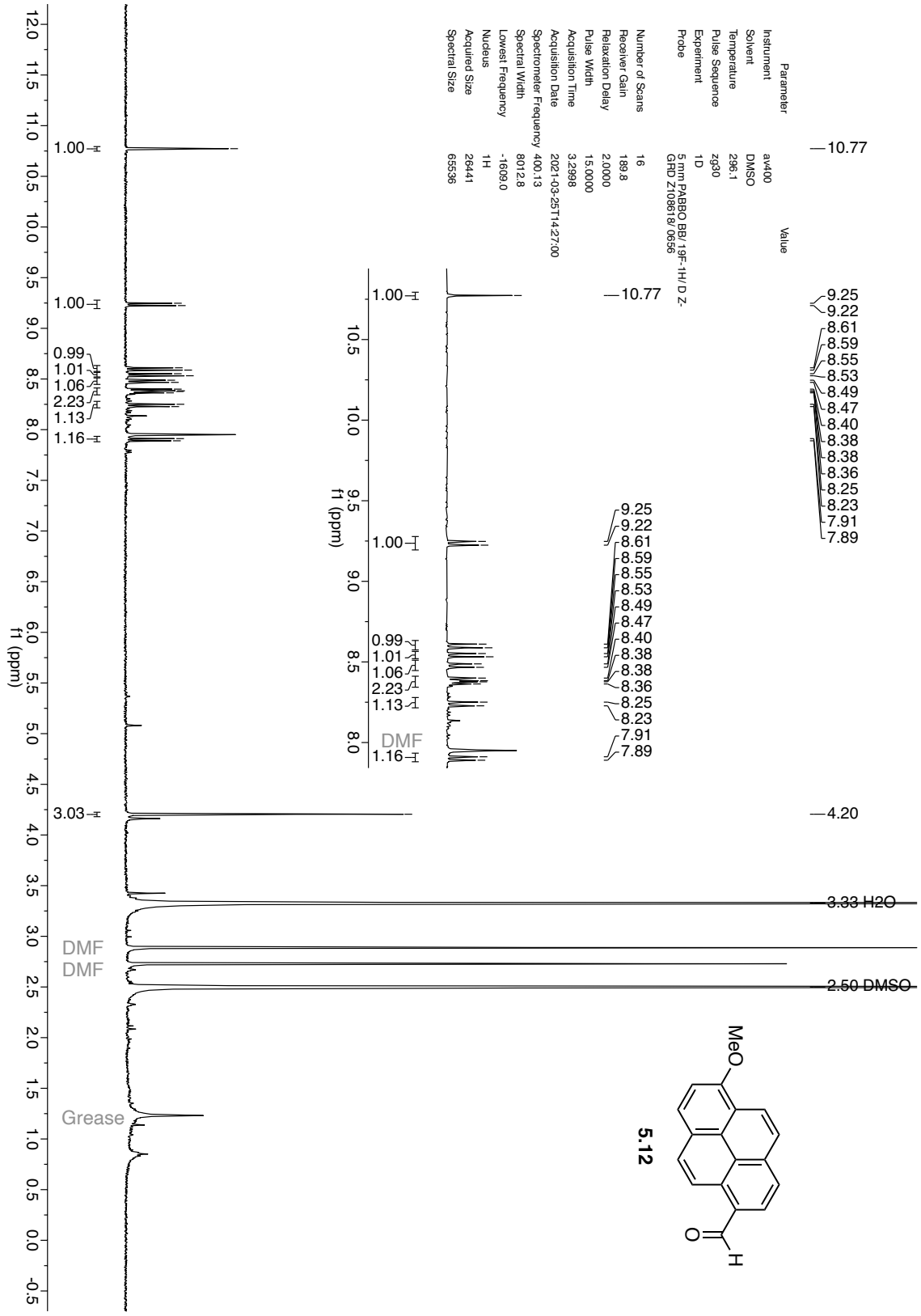
Parameter
Value
Instrument
av400
Solvent
DMSO
Temperature
296.1
Pulse Sequence
zg30
Experiment
1D
Probe
5 mm PABBO BB/ 19F-1H/ D Z-GRD Z108618/ 0656
Number of Scans
16
Receiver Gain
189.8
Relaxation Delay
2.0000
Pulse Width
15.0000
Acquisition Time
3.2998
Acquisition Date
2021-03-25T14:27:00
Spectrometer Frequency
400.13
Spectral Width
8012.8
Lowest Frequency
-1609.0
Nucleus
1H
Acquired Size
26441
Spectral Size
65536
10.77
9.25
9.22
8.61
8.59
8.55
8.53
8.49
8.47
8.40
8.38
8.38
8.36
8.25
8.23
7.91
7.89
4.20
3.33 H2O
2.50 DMSO
1.00
0.99
1.01
1.06
2.23
1.13
1.16
3.03
DMF
DMF
Grease
f1 (ppm)
MeO
O
H
5.12

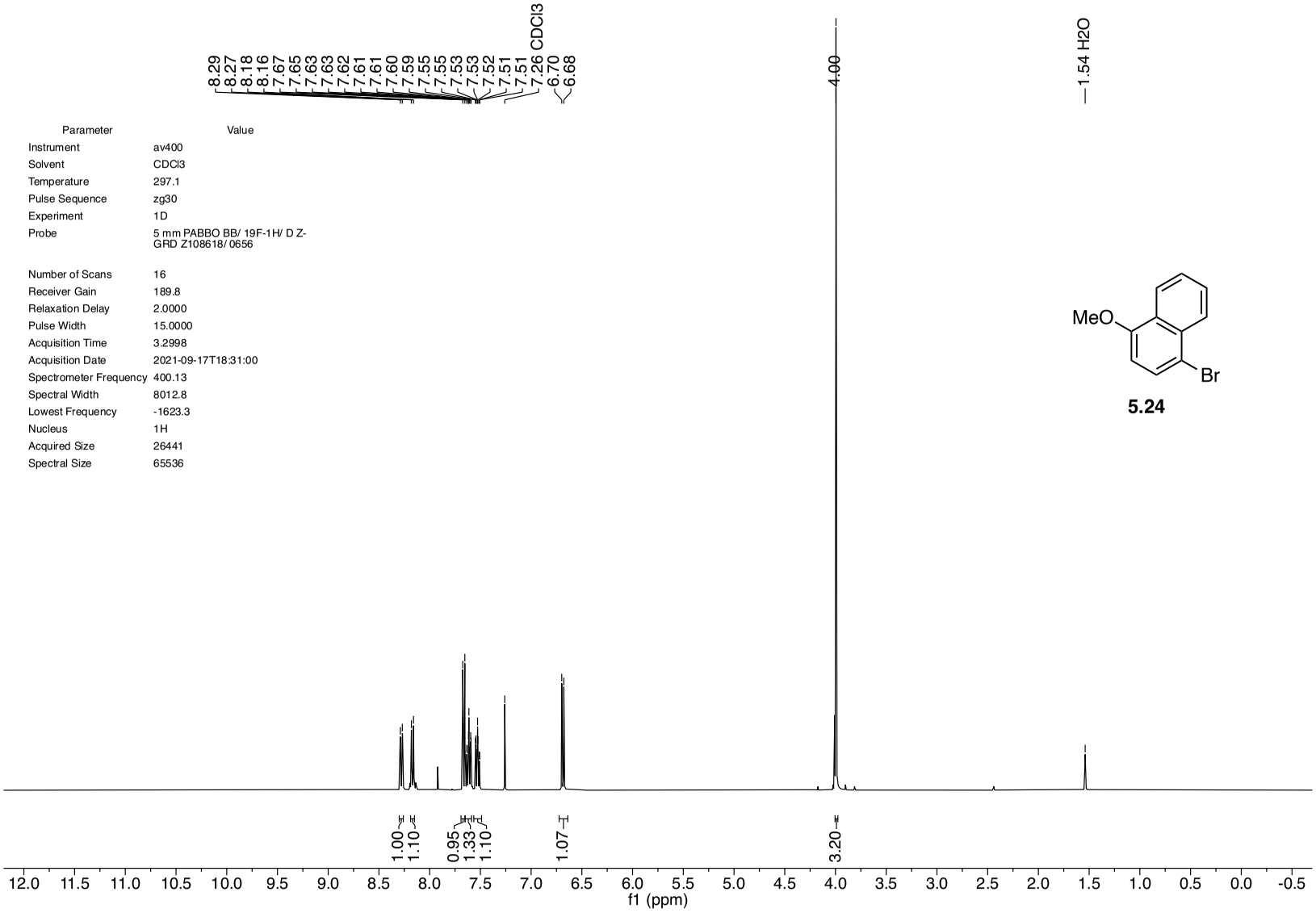
8.29
8.27
8.18
8.16
7.67
7.65
7.63
7.63
7.62
7.61
7.61
7.60
7.59
7.55
7.55
7.53
7.53
7.52
7.51
7.51
7.26 CDCl3
6.70
6.68
4.00
1.54 H2O
Parameter Value
Instrument av400
Solvent CDCl3
Temperature 297.1
Pulse Sequence zg30
Experiment 1D
Probe 5 mm PABBO BB/ 19F-1H/ D Z-GRD Z108618/ 0656
Number of Scans 16
Receiver Gain 189.8
Relaxation Delay 2.0000
Pulse Width 15.0000
Acquisition Time 3.2998
Acquisition Date 2021-09-17T18:31:00
Spectrometer Frequency 400.13
Spectral Width 8012.8
Lowest Frequency -1623.3
Nucleus 1H
Acquired Size 26441
Spectral Size 65536
MeO
Br
5.24
1.00
1.10
0.95
1.33
1.10
1.07
3.20
12.0 11.5 11.0 10.5 10.0 9.5 9.0 8.5 8.0 7.5 7.0 6.5 6.0 5.5 5.0 4.5 4.0 3.5 3.0 2.5 2.0 1.5 1.0 0.5 0.0 -0.5
f1 (ppm)

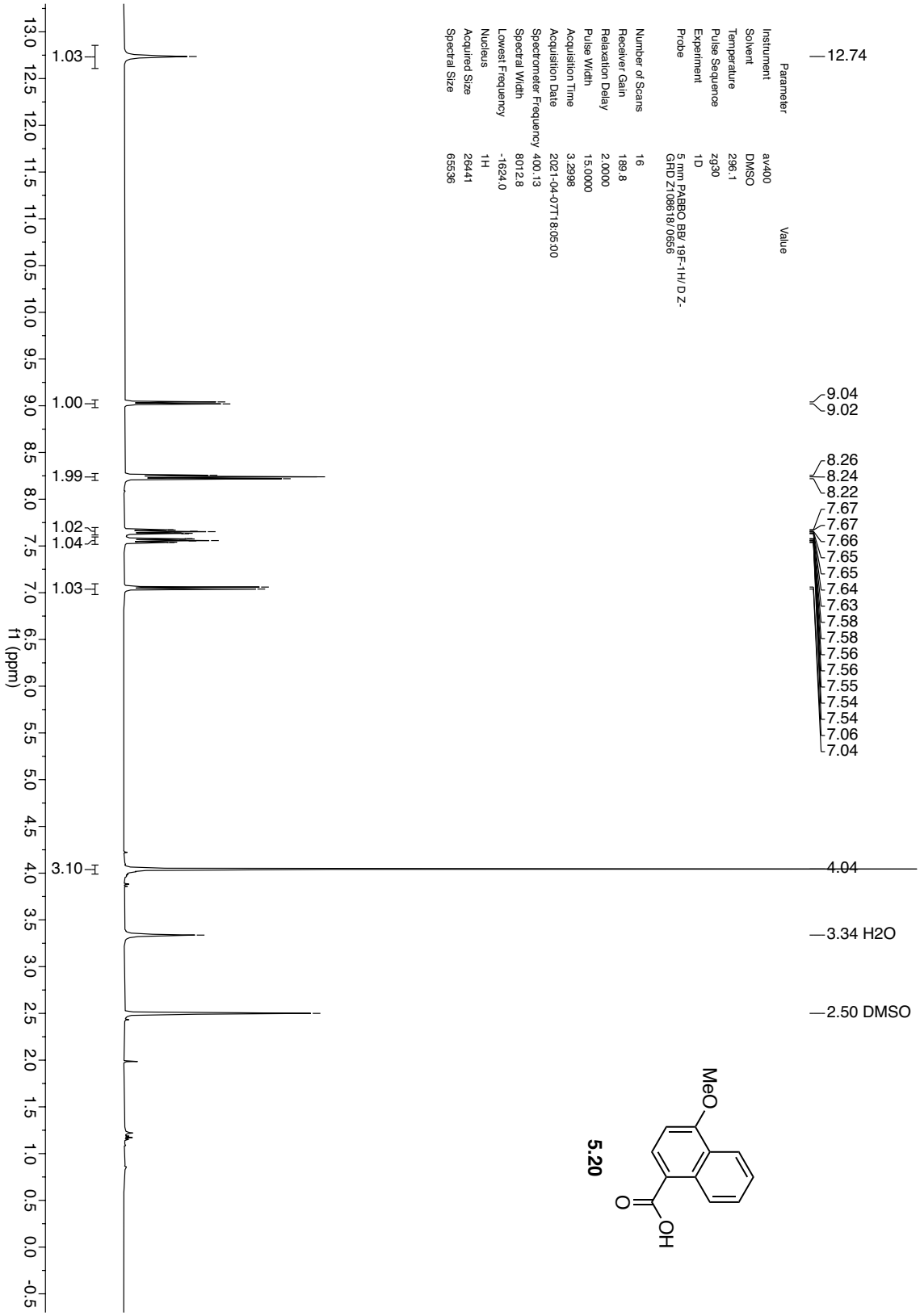
Parameter Value
Instrument av400
Solvent DMSO
Temperature 296.1
Pulse Sequence zg30
Experiment 1D
Probe 5 mm PABBO BB/ 19F-1H/ D Z-GRD Z108618/ 0656
Number of Scans 16
Receiver Gain 189.8
Relaxation Delay 2.0000
Pulse Width 15.0000
Acquisition Time 3.2998
Acquisition Date 2021-04-07T18:05:00
Spectrometer Frequency 400.13
Spectral Width 8012.8
Lowest Frequency -1624.0
Nucleus 1H
Acquired Size 26441
Spectral Size 65536
12.74
9.04
9.02
8.26
8.24
8.22
7.67
7.67
7.66
7.65
7.65
7.64
7.63
7.58
7.58
7.56
7.56
7.55
7.54
7.54
7.06
7.04
4.04
3.34 H2O
2.50 DMSO
1.03
1.00
1.99
1.02
1.04
1.03
3.10
f1 (ppm)
MeO
O
OH
5.20

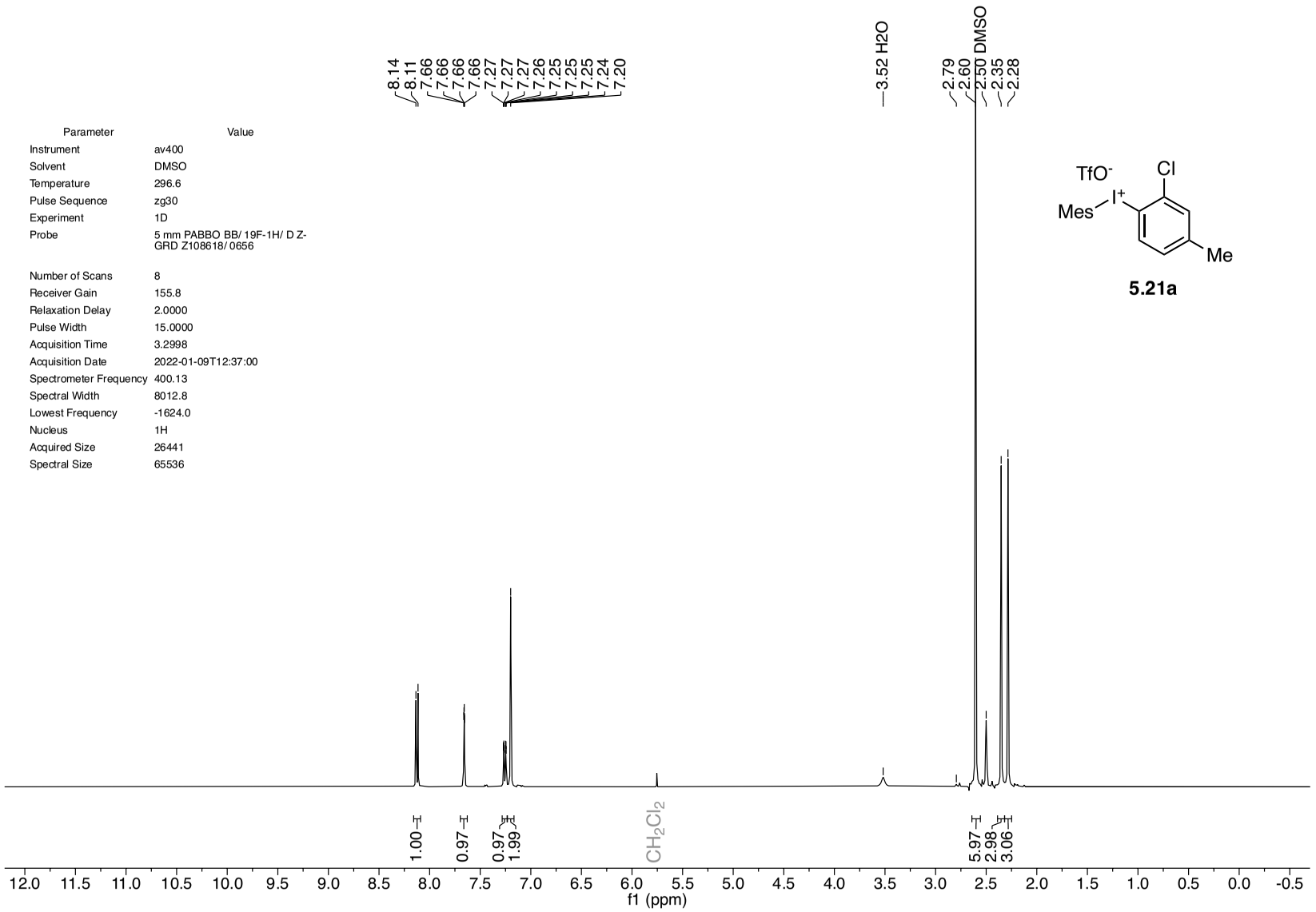
8.14
8.11
7.66
7.66
7.66
7.66
7.27
7.27
7.27
7.26
7.25
7.25
7.25
7.24
7.20
3.52 H2O
2.79
2.60
2.50 DMSO
2.35
2.28
Parameter Value
Instrument av400
Solvent DMSO
Temperature 296.6
Pulse Sequence zg30
Experiment 1D
Probe 5 mm PABBO BB/ 19F-1H/ D Z-GRD Z108618/ 0656
Number of Scans 8
Receiver Gain 155.8
Relaxation Delay 2.0000
Pulse Width 15.0000
Acquisition Time 3.2998
Acquisition Date 2022-01-09T12:37:00
Spectrometer Frequency 400.13
Spectral Width 8012.8
Lowest Frequency -1624.0
Nucleus 1H
Acquired Size 26441
Spectral Size 65536
TfO-
Cl
I+
Mes
Me
5.21a
1.00
0.97
0.97
1.99
CH2Cl2
5.97
2.98
3.06
f1 (ppm)

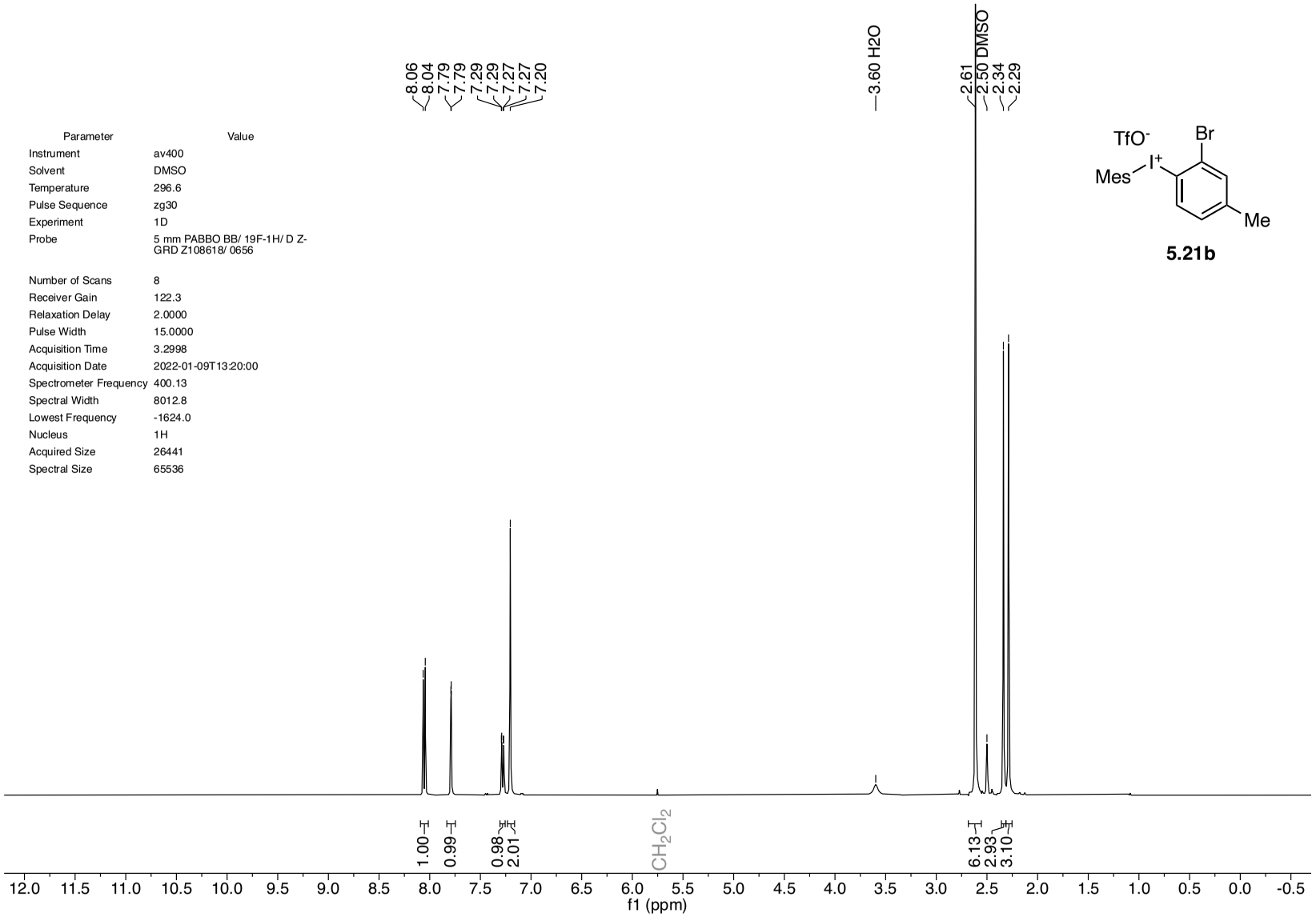
8.06
8.04
7.79
7.79
7.29
7.29
7.27
7.27
7.20
3.60 H2O
2.61
2.50 DMSO
2.34
2.29
Parameter Value
Instrument av400
Solvent DMSO
Temperature 296.6
Pulse Sequence zg30
Experiment 1D
Probe 5 mm PABBO BB/ 19F-1H/ D Z-GRD Z108618/ 0656
Number of Scans 8
Receiver Gain 122.3
Relaxation Delay 2.0000
Pulse Width 15.0000
Acquisition Time 3.2998
Acquisition Date 2022-01-09T13:20:00
Spectrometer Frequency 400.13
Spectral Width 8012.8
Lowest Frequency -1624.0
Nucleus 1H
Acquired Size 26441
Spectral Size 65536
TfO-
Br
Mes
I+
Me
5.21b
1.00
0.99
0.98
2.01
CH2Cl2
6.13
2.93
3.10
f1 (ppm)

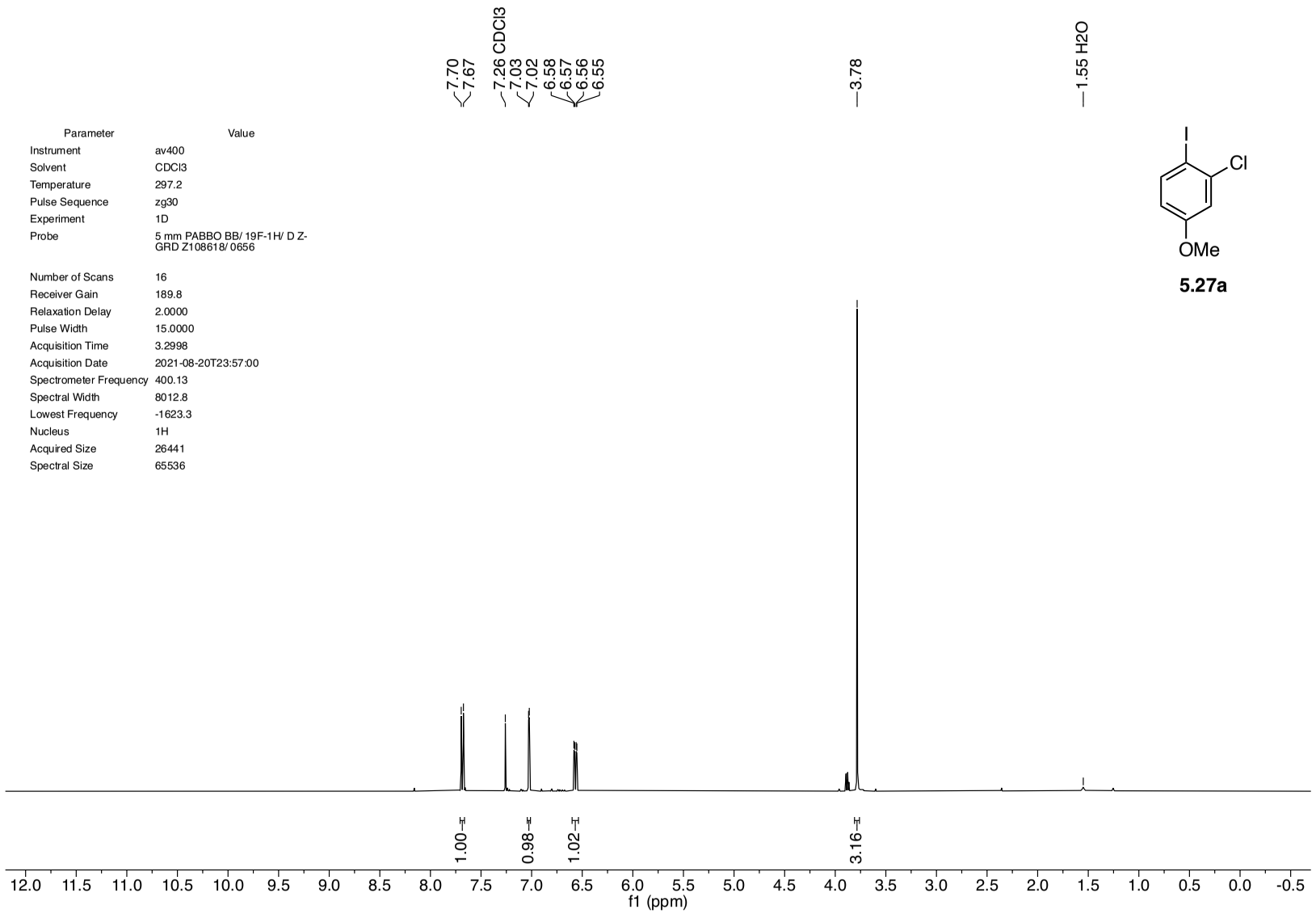
7.70
7.67
7.26 CDCl3
7.03
7.02
6.58
6.57
6.56
6.55
3.78
1.55 H2O
Parameter Value
Instrument av400
Solvent CDCl3
Temperature 297.2
Pulse Sequence zg30
Experiment 1D
Probe 5 mm PABBO BB/ 19F-1H/ D Z-GRD Z108618/ 0656
Number of Scans 16
Receiver Gain 189.8
Relaxation Delay 2.0000
Pulse Width 15.0000
Acquisition Time 3.2998
Acquisition Date 2021-08-20T23:57:00
Spectrometer Frequency 400.13
Spectral Width 8012.8
Lowest Frequency -1623.3
Nucleus 1H
Acquired Size 26441
Spectral Size 65536
Cl
OMe
5.27a
1.00
0.98
1.02
3.16
12.0 11.5 11.0 10.5 10.0 9.5 9.0 8.5 8.0 7.5 7.0 6.5 6.0 5.5 5.0 4.5 4.0 3.5 3.0 2.5 2.0 1.5 1.0 0.5 0.0 -0.5
f1 (ppm)

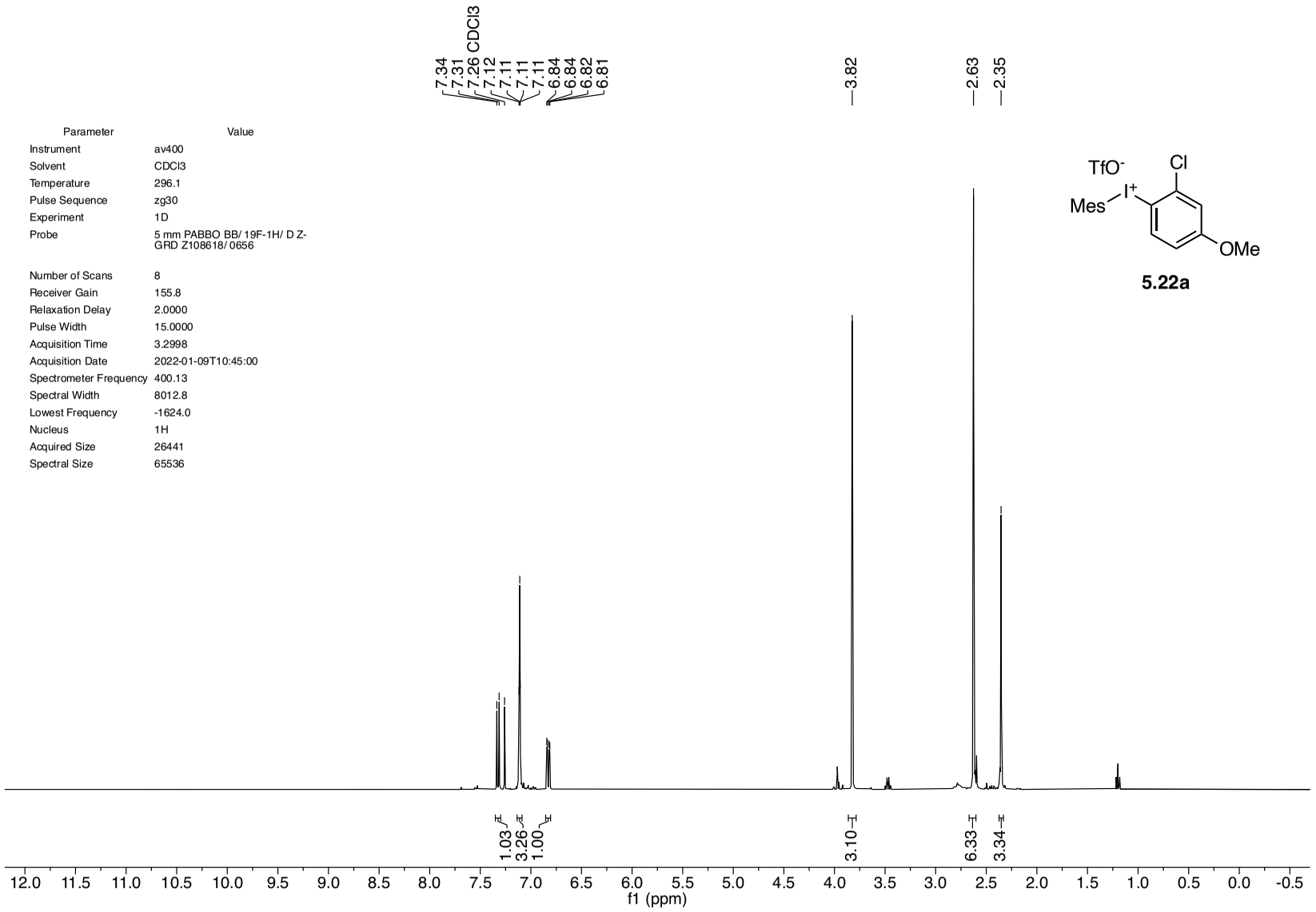
7.34
7.31
7.26 CDCl3
7.12
7.11
7.11
7.11
6.84
6.84
6.82
6.81
3.82
2.63
2.35
Parameter Value
Instrument av400
Solvent CDCl3
Temperature 296.1
Pulse Sequence zg30
Experiment 1D
Probe 5 mm PABBO BB/ 19F-1H/ D Z-GRD Z108618/ 0656
Number of Scans 8
Receiver Gain 155.8
Relaxation Delay 2.0000
Pulse Width 15.0000
Acquisition Time 3.2998
Acquisition Date 2022-01-09T10:45:00
Spectrometer Frequency 400.13
Spectral Width 8012.8
Lowest Frequency -1624.0
Nucleus 1H
Acquired Size 26441
Spectral Size 65536
TfO-
Cl
Mes
I+
OMe
5.22a
1.03
3.26
1.00
3.10
6.33
3.34
12.0 11.5 11.0 10.5 10.0 9.5 9.0 8.5 8.0 7.5 7.0 6.5 6.0 5.5 5.0 4.5 4.0 3.5 3.0 2.5 2.0 1.5 1.0 0.5 0.0 -0.5
f1 (ppm)

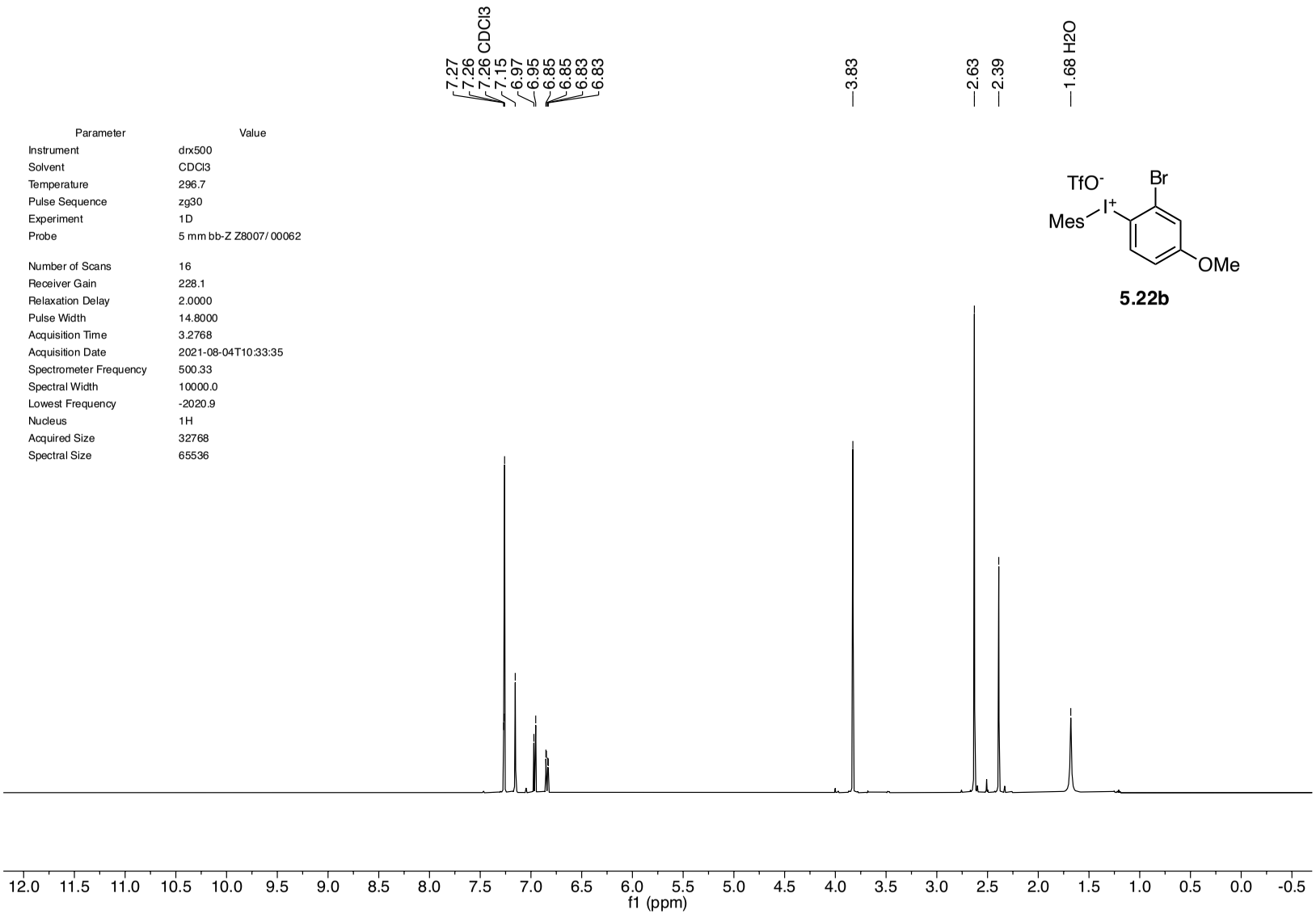
7.27
7.26
7.26 CDCl3
7.15
6.97
6.95
6.85
6.85
6.83
6.83
3.83
2.63
2.39
1.68 H2O
Parameter Value
Instrument drx500
Solvent CDCl3
Temperature 296.7
Pulse Sequence zg30
Experiment 1D
Probe 5 mm bb-Z Z8007/ 00062
Number of Scans 16
Receiver Gain 228.1
Relaxation Delay 2.0000
Pulse Width 14.8000
Acquisition Time 3.2768
Acquisition Date 2021-08-04T10:33:35
Spectrometer Frequency 500.33
Spectral Width 10000.0
Lowest Frequency -2020.9
Nucleus 1H
Acquired Size 32768
Spectral Size 65536
TfO-
Br
I+
Mes
OMe
5.22b
12.0 11.5 11.0 10.5 10.0 9.5 9.0 8.5 8.0 7.5 7.0 6.5 6.0 5.5 5.0 4.5 4.0 3.5 3.0 2.5 2.0 1.5 1.0 0.5 0.0 -0.5
f1 (ppm)

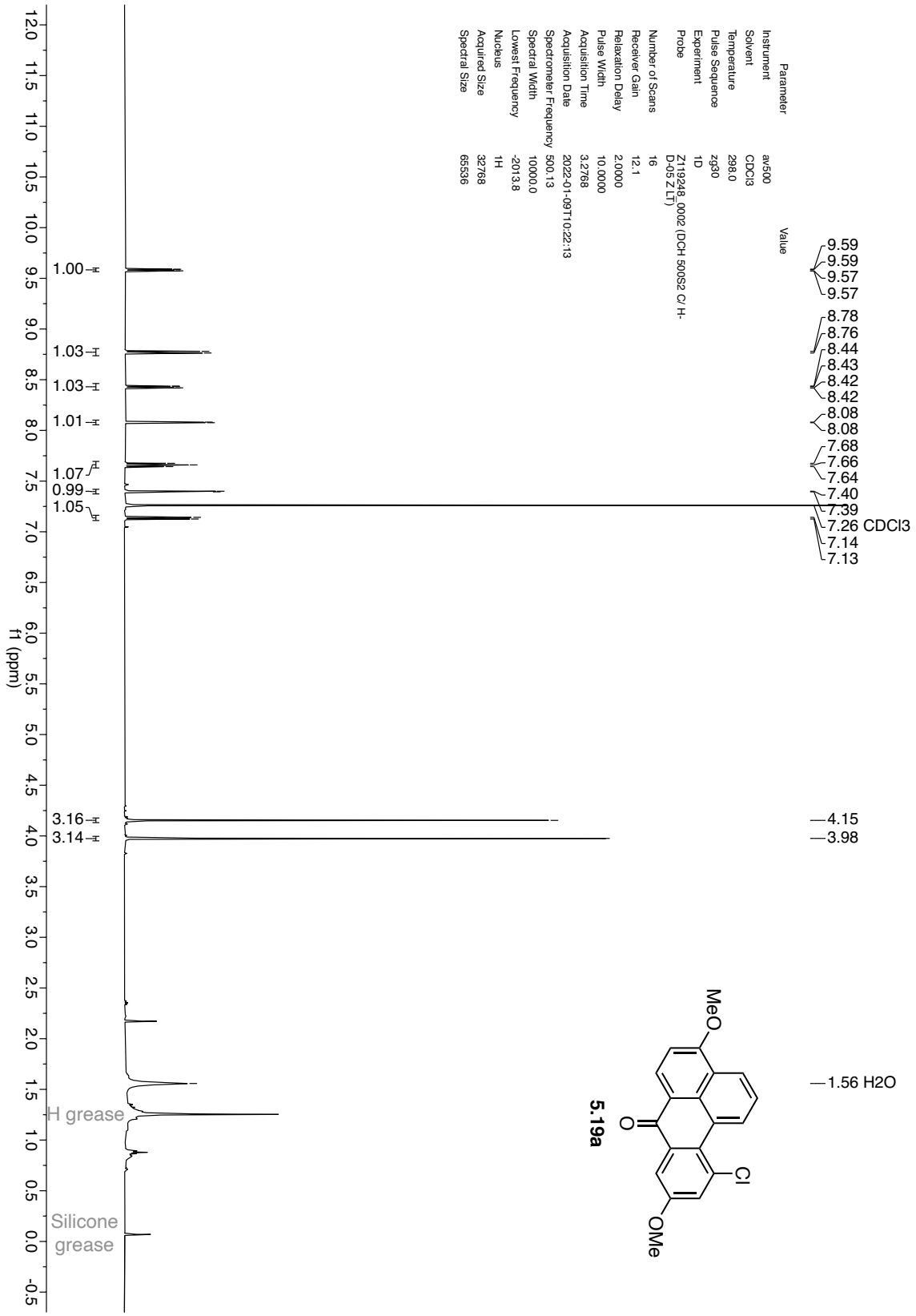
Parameter Value
Instrument av500
Solvent CDCl3
Temperature 298.0
Pulse Sequence zg30
Experiment 1D
Probe Z119248_0002 (DCH 500S2 C/ H-D-05 Z LT)
Number of Scans 16
Receiver Gain 12.1
Relaxation Delay 2.0000
Pulse Width 10.0000
Acquisition Time 3.2768
Acquisition Date 2022-01-09T10:22:13
Spectrometer Frequency 500.13
Spectral Width 10000.0
Lowest Frequency -2013.8
Nucleus 1H
Acquired Size 32768
Spectral Size 65536
9.59
9.59
9.57
9.57
8.78
8.76
8.44
8.43
8.42
8.42
8.08
8.08
7.68
7.66
7.64
7.40
7.39
7.26 CDCl3
7.14
7.13
4.15
3.98
1.56 H2O
1.00
1.03
1.03
1.01
1.07
0.99
1.05
3.16
3.14
H grease
Silicone grease
f1 (ppm)
MeO
O
Cl
OMe
5.19a

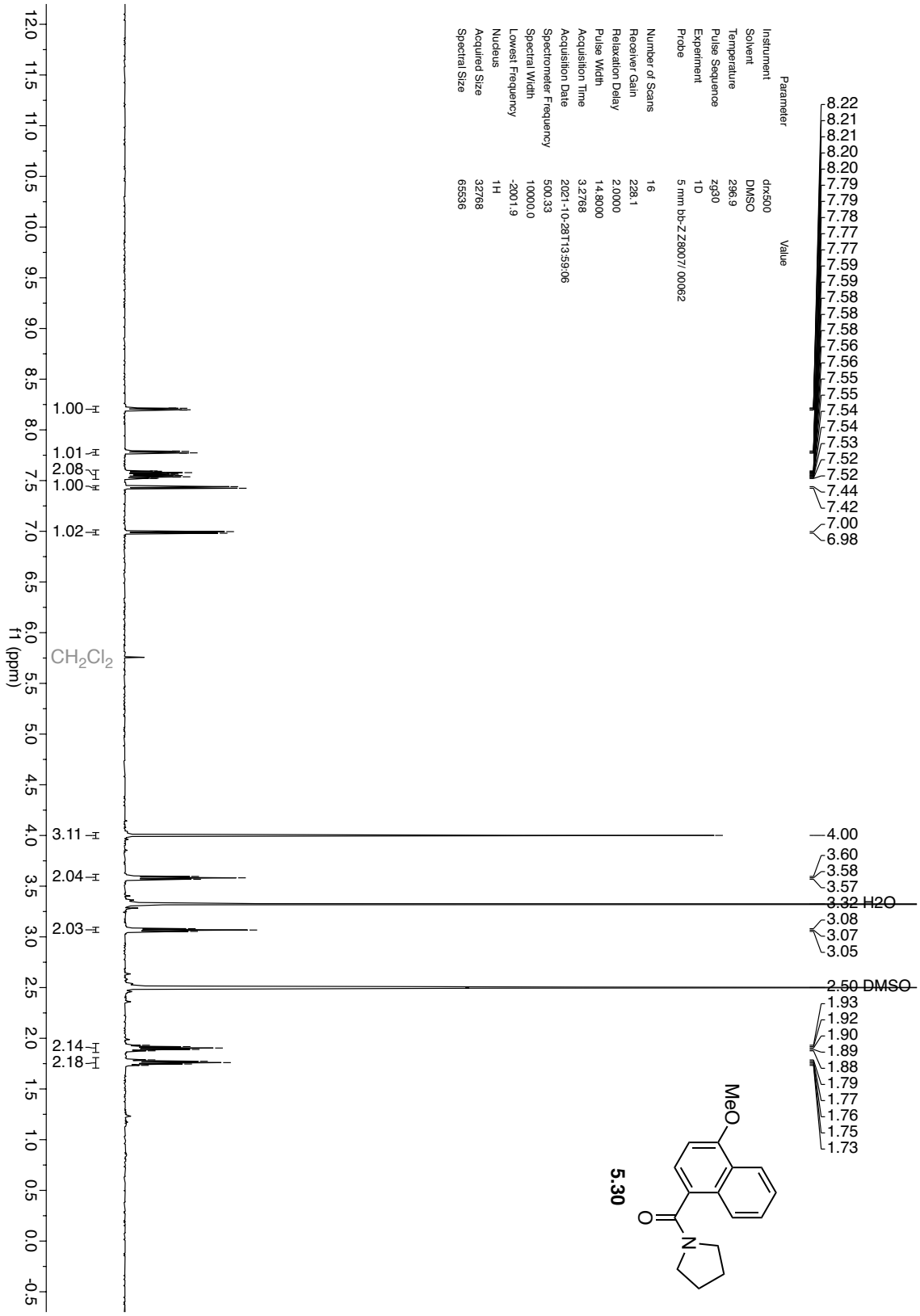
Parameter Value
Instrument drx500
Solvent DMSO
Temperature 296.9
Pulse Sequence zg30
Experiment 1D
Probe 5 mm bb-Z Z8007/ 00062
Number of Scans 16
Receiver Gain 228.1
Relaxation Delay 2.0000
Pulse Width 14.8000
Acquisition Time 3.2768
Acquisition Date 2021-10-28T13:59:06
Spectrometer Frequency 500.33
Spectral Width 10000.0
Lowest Frequency -2001.9
Nucleus 1H
Acquired Size 32768
Spectral Size 65536
8.22
8.21
8.21
8.20
8.20
7.79
7.79
7.78
7.77
7.77
7.59
7.59
7.58
7.58
7.58
7.56
7.56
7.55
7.55
7.54
7.54
7.53
7.52
7.52
7.44
7.42
7.00
6.98
4.00
3.60
3.58
3.57
3.32 H2O
3.08
3.07
3.05
2.50 DMSO
1.93
1.92
1.90
1.89
1.88
1.79
1.77
1.76
1.75
1.73
1.00
1.01
2.08
1.00
1.02
3.11
2.04
2.03
2.14
2.18
CH2Cl2
f1 (ppm)
MeO
O
N
5.30

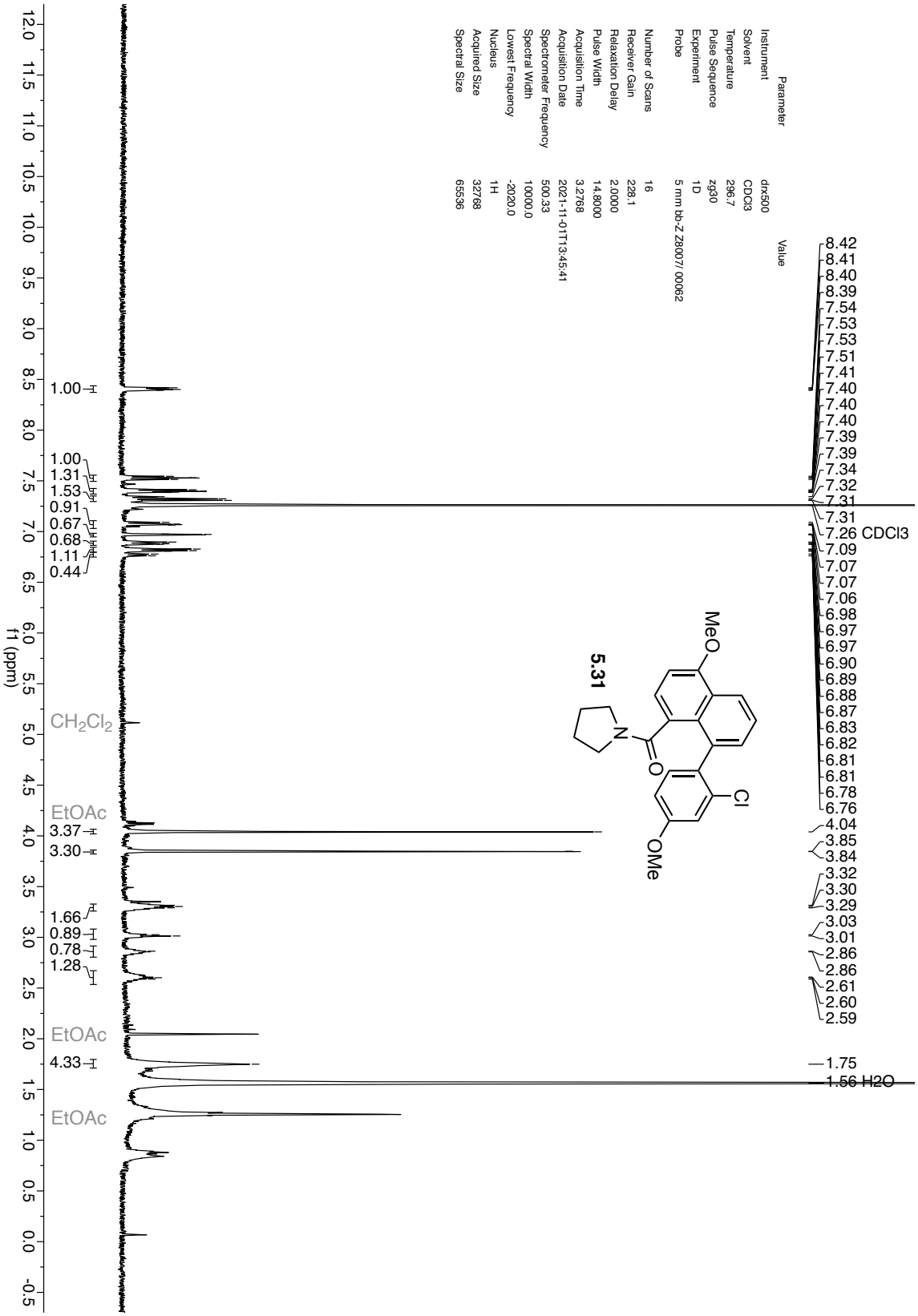
Parameter Value
Instrument drx500
Solvent CDCl3
Temperature 296.7
Pulse Sequence zg30
Experiment 1D
Probe 5 mm bb-Z Z8007/ 00062
Number of Scans 16
Receiver Gain 228.1
Relaxation Delay 2.0000
Pulse Width 14.8000
Acquisition Time 3.2768
Acquisition Date 2021-11-01T13:45:41
Spectrometer Frequency 500.33
Spectral Width 10000.0
Lowest Frequency -2020.0
Nucleus 1H
Acquired Size 32768
Spectral Size 65536
8.42
8.41
8.40
8.39
7.54
7.53
7.53
7.51
7.41
7.40
7.40
7.40
7.39
7.39
7.34
7.32
7.31
7.31
7.26 CDCl3
7.09
7.07
7.07
7.06
6.98
6.97
6.97
6.90
6.89
6.88
6.87
6.83
6.82
6.81
6.81
6.78
6.76
4.04
3.85
3.84
3.32
3.30
3.29
3.03
3.01
2.86
2.86
2.61
2.60
2.59
1.75
1.56 H2O
5.31
MeO
Cl
OMe
N
O
1.00
1.00
1.31
1.53
0.91
0.67
0.68
1.11
0.44
CH2Cl2
EtOAc
3.37
3.30
1.66
0.89
0.78
1.28
EtOAc
4.33
EtOAc
f1 (ppm)

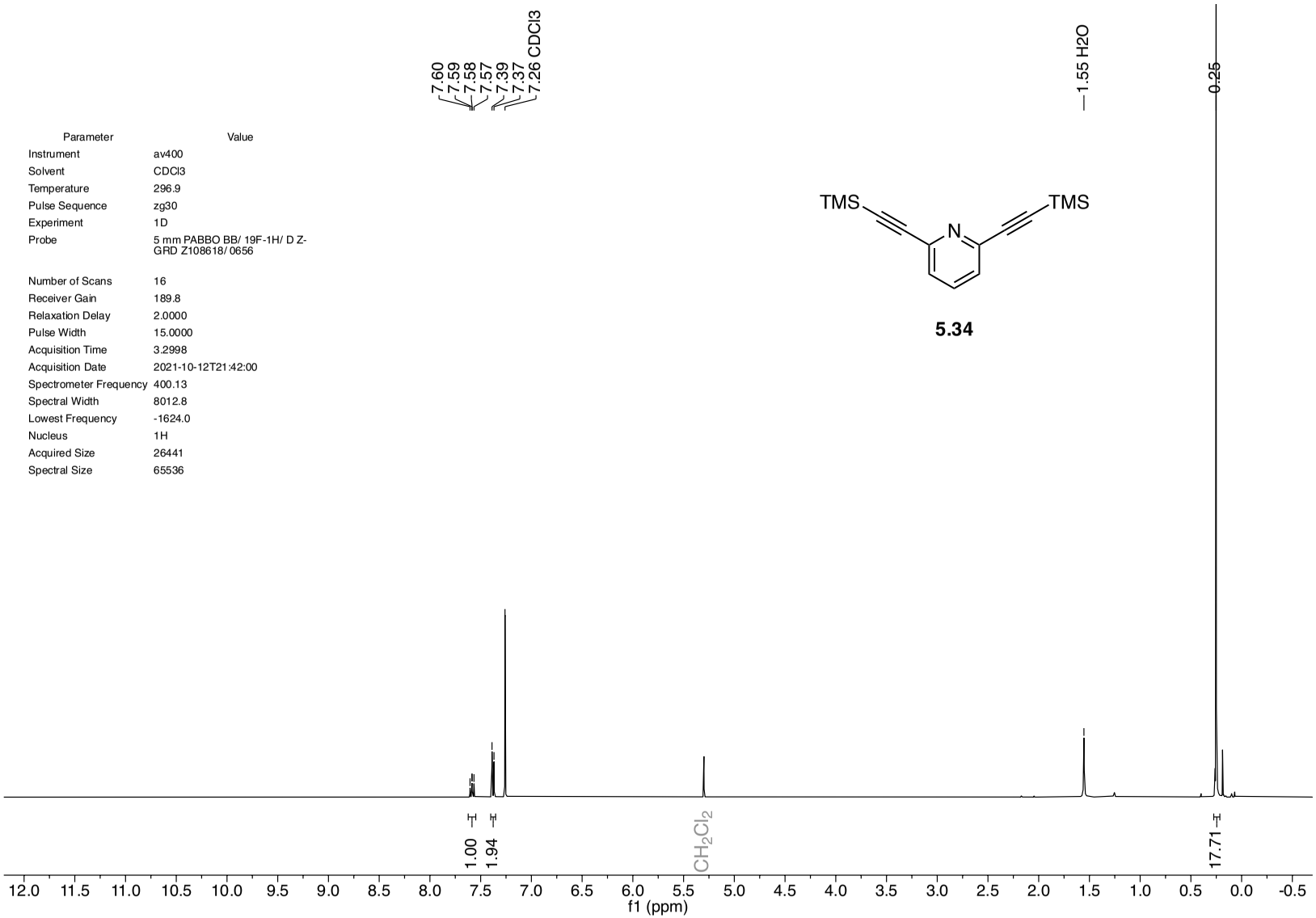
7.60
7.59
7.58
7.57
7.39
7.37
7.26 CDCl3
1.55 H2O
0.25
TMS
TMS
N
5.34
Parameter Value
Instrument av400
Solvent CDCl3
Temperature 296.9
Pulse Sequence zg30
Experiment 1D
Probe 5 mm PABBO BB/ 19F-1H/ D Z-GRD Z108618/ 0656
Number of Scans 16
Receiver Gain 189.8
Relaxation Delay 2.0000
Pulse Width 15.0000
Acquisition Time 3.2998
Acquisition Date 2021-10-12T21:42:00
Spectrometer Frequency 400.13
Spectral Width 8012.8
Lowest Frequency -1624.0
Nucleus 1H
Acquired Size 26441
Spectral Size 65536
1.00
1.94
CH2Cl2
17.71
12.0 11.5 11.0 10.5 10.0 9.5 9.0 8.5 8.0 7.5 7.0 6.5 6.0 5.5 5.0 4.5 4.0 3.5 3.0 2.5 2.0 1.5 1.0 0.5 0.0 -0.5
f1 (ppm)

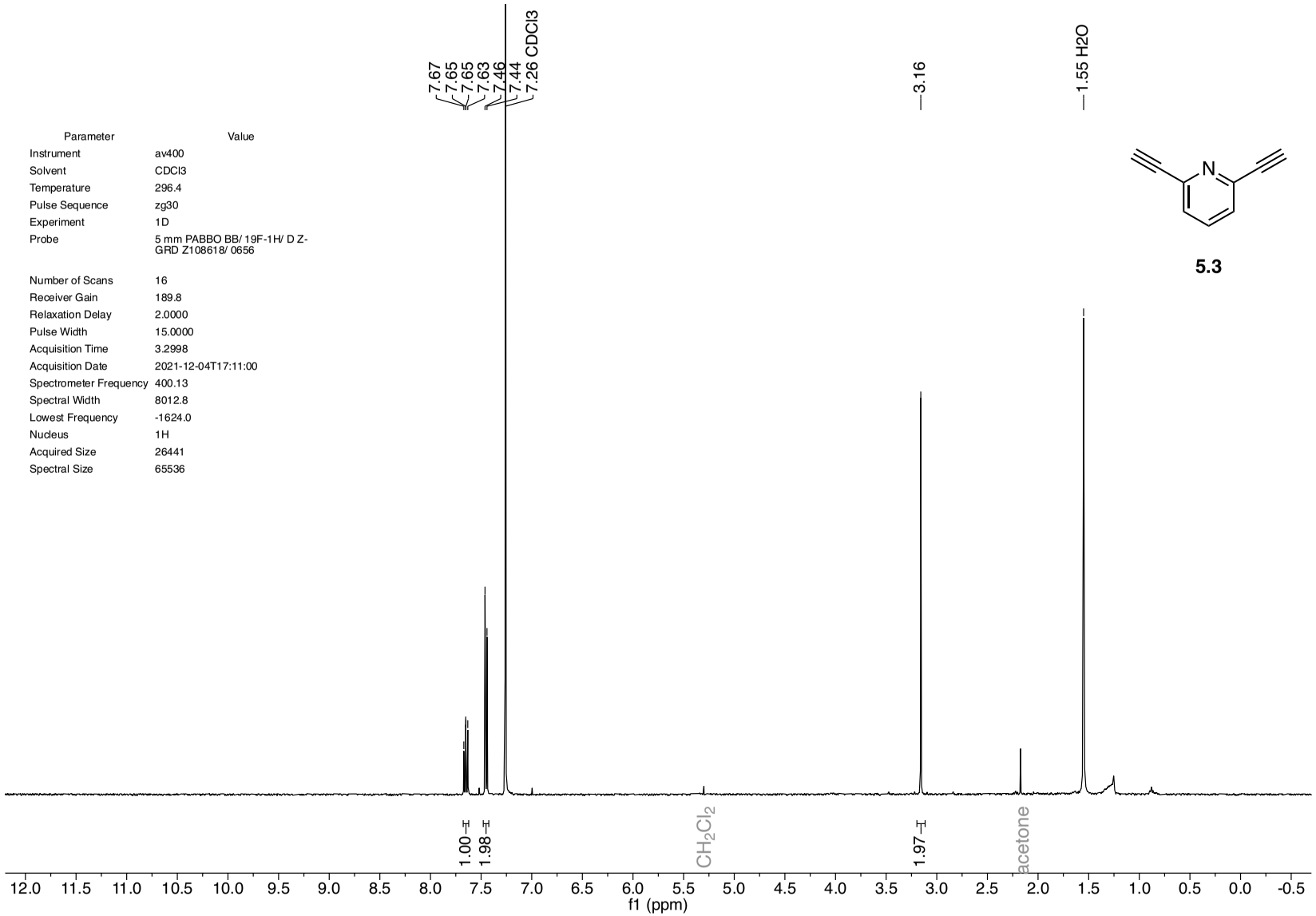
7.67
7.65
7.65
7.63
7.46
7.44
7.26 CDCl3
3.16
1.55 H2O
N
5.3
Parameter Value
Instrument av400
Solvent CDCl3
Temperature 296.4
Pulse Sequence zg30
Experiment 1D
Probe 5 mm PABBO BB/ 19F-1H/ D Z-GRD Z108618/ 0656
Number of Scans 16
Receiver Gain 189.8
Relaxation Delay 2.0000
Pulse Width 15.0000
Acquisition Time 3.2998
Acquisition Date 2021-12-04T17:11:00
Spectrometer Frequency 400.13
Spectral Width 8012.8
Lowest Frequency -1624.0
Nucleus 1H
Acquired Size 26441
Spectral Size 65536
1.00
1.98
CH2Cl2
1.97
acetone
12.0 11.5 11.0 10.5 10.0 9.5 9.0 8.5 8.0 7.5 7.0 6.5 6.0 5.5 5.0 4.5 4.0 3.5 3.0 2.5 2.0 1.5 1.0 0.5 0.0 -0.5
f1 (ppm)

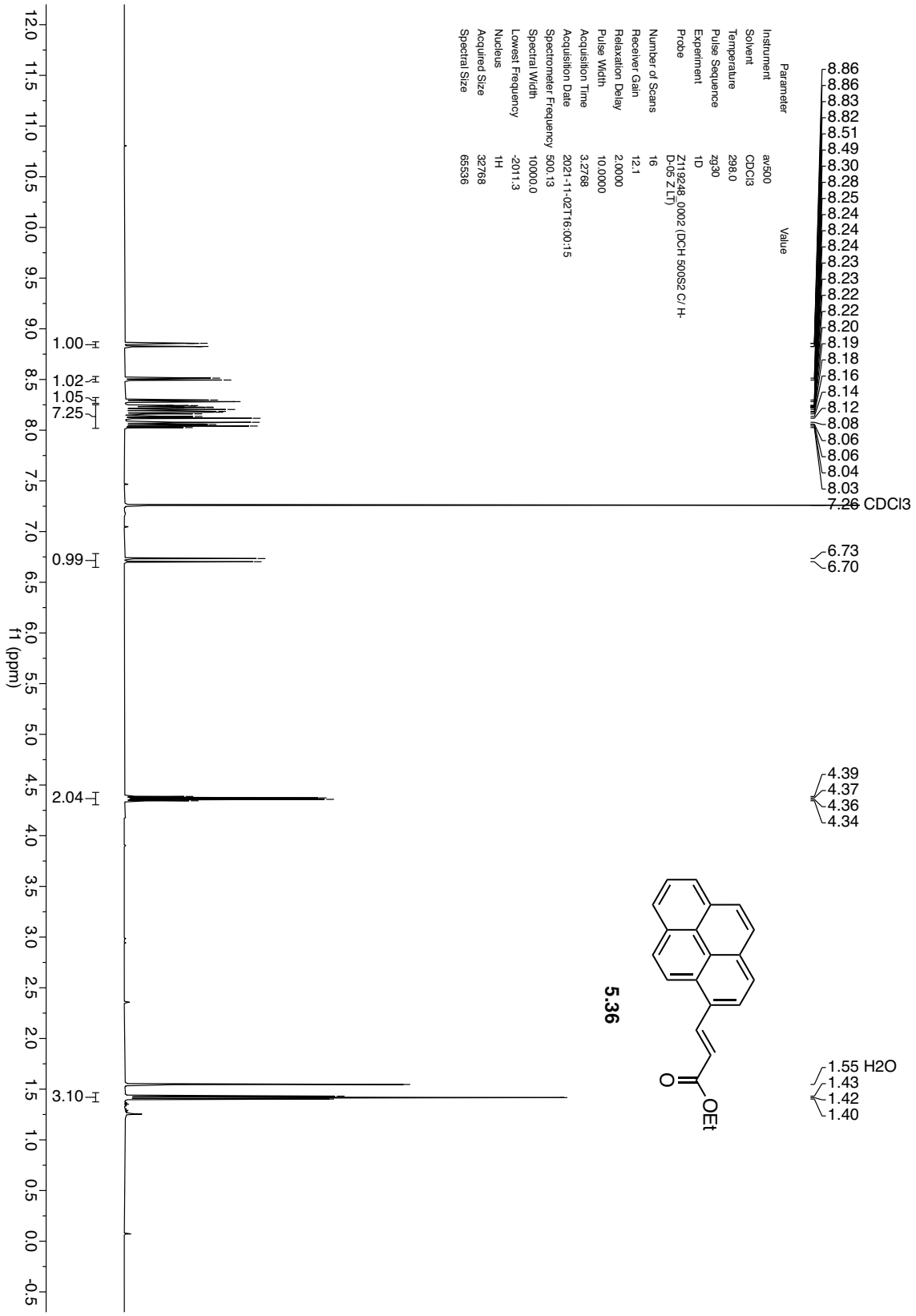
Parameter Value
Instrument av500
Solvent CDCl3
Temperature 298.0
Pulse Sequence zg30
Experiment 1D
Probe Z119248_0002 (DCH 500S2 C/ H-D-05 Z LT)
Number of Scans 16
Receiver Gain 12.1
Relaxation Delay 2.0000
Pulse Width 10.0000
Acquisition Time 3.2768
Acquisition Date 2021-11-02T16:00:15
Spectrometer Frequency 500.13
Spectral Width 10000.0
Lowest Frequency -2011.3
Nucleus 1H
Acquired Size 32768
Spectral Size 65536
8.86
8.86
8.83
8.82
8.51
8.49
8.30
8.28
8.25
8.24
8.24
8.24
8.23
8.23
8.22
8.22
8.20
8.19
8.18
8.16
8.14
8.12
8.08
8.06
8.06
8.04
8.03
7.26 CDCl3
6.73
6.70
4.39
4.37
4.36
4.34
1.55 H2O
1.43
1.42
1.40
1.00
1.02
1.05
7.25
0.99
2.04
3.10
5.36
OEt
O
f1 (ppm)

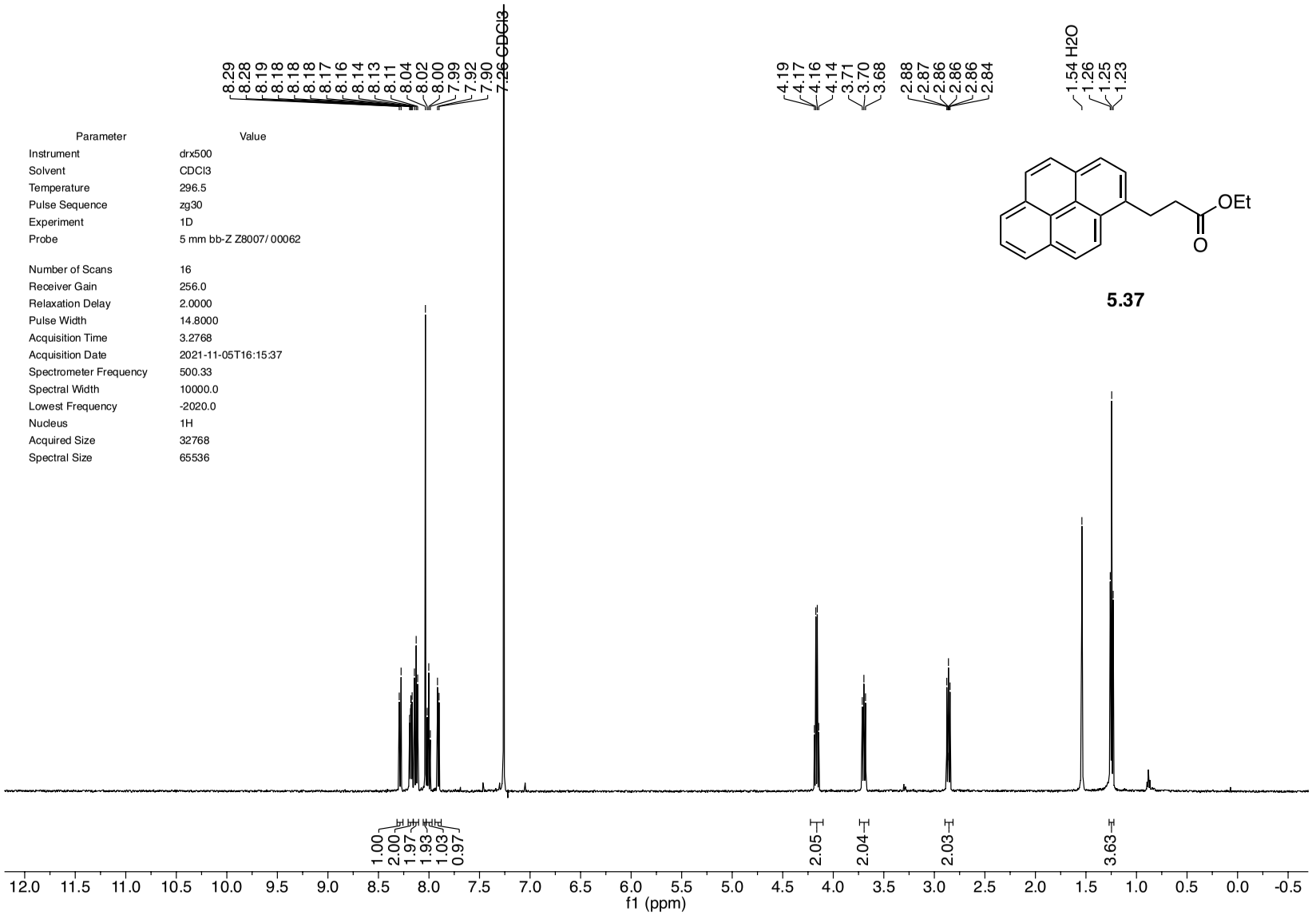
8.29
8.28
8.19
8.18
8.18
8.18
8.17
8.16
8.14
8.13
8.11
8.04
8.02
8.00
7.99
7.92
7.90
7.26 CDCl3
4.19
4.17
4.16
4.14
3.71
3.70
3.68
2.88
2.87
2.86
2.86
2.86
2.84
1.54 H2O
1.26
1.25
1.23
Parameter Value
Instrument drx500
Solvent CDCl3
Temperature 296.5
Pulse Sequence zg30
Experiment 1D
Probe 5 mm bb-Z Z8007/ 00062
Number of Scans 16
Receiver Gain 256.0
Relaxation Delay 2.0000
Pulse Width 14.8000
Acquisition Time 3.2768
Acquisition Date 2021-11-05T16:15:37
Spectrometer Frequency 500.33
Spectral Width 10000.0
Lowest Frequency -2020.0
Nucleus 1H
Acquired Size 32768
Spectral Size 65536
OEt
O
5.37
1.00
2.00
1.97
1.93
1.03
0.97
2.05
2.04
2.03
3.63
12.0 11.5 11.0 10.5 10.0 9.5 9.0 8.5 8.0 7.5 7.0 6.5 6.0 5.5 5.0 4.5 4.0 3.5 3.0 2.5 2.0 1.5 1.0 0.5 0.0 -0.5
f1 (ppm)

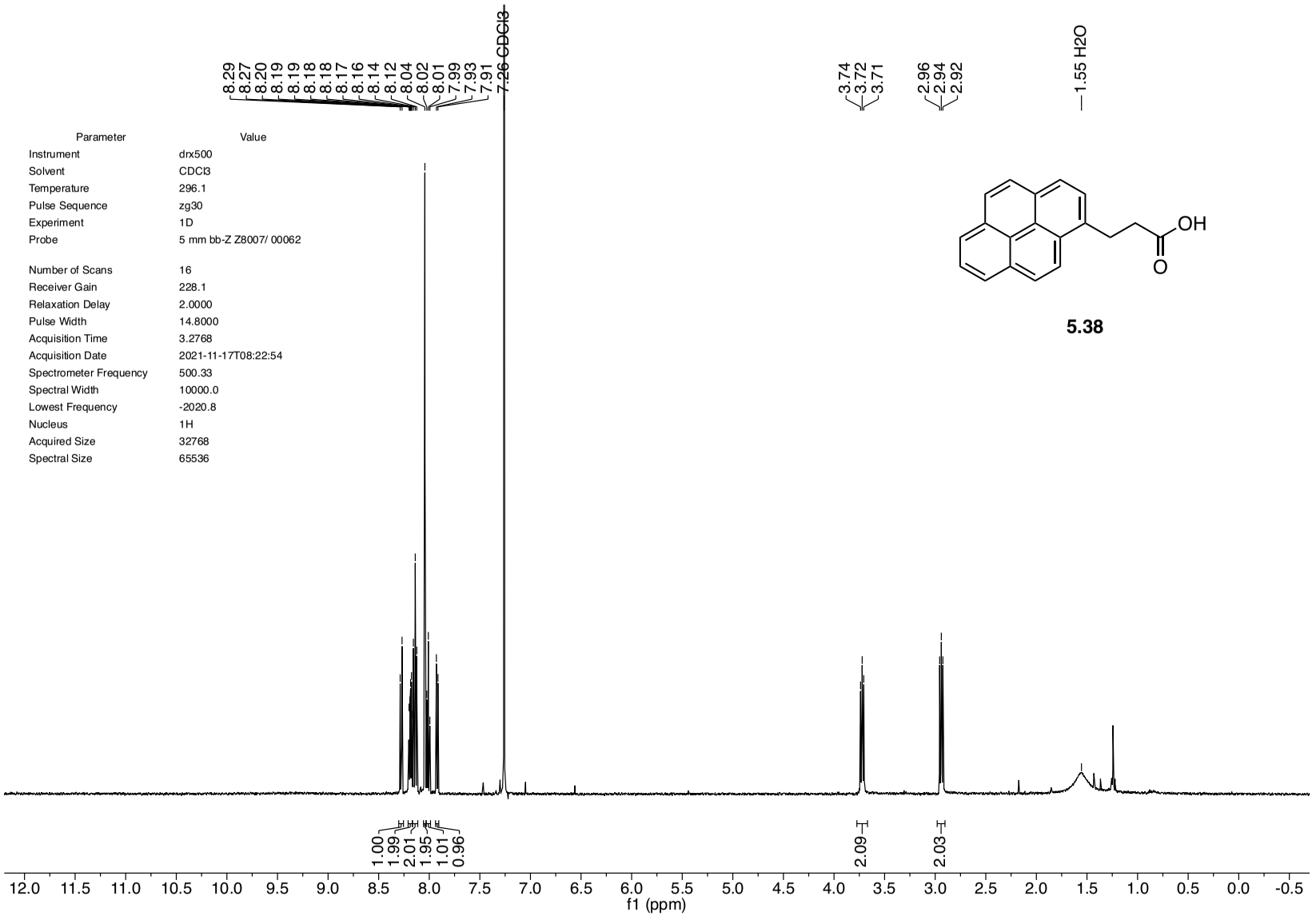
8.29
8.27
8.20
8.19
8.19
8.18
8.18
8.17
8.16
8.14
8.12
8.04
8.02
8.01
7.99
7.93
7.91
7.26 CDCl3
3.74
3.72
3.71
2.96
2.94
2.92
1.55 H2O
OH
O
5.38
Parameter Value
Instrument drx500
Solvent CDCl3
Temperature 296.1
Pulse Sequence zg30
Experiment 1D
Probe 5 mm bb-Z Z8007/ 00062
Number of Scans 16
Receiver Gain 228.1
Relaxation Delay 2.0000
Pulse Width 14.8000
Acquisition Time 3.2768
Acquisition Date 2021-11-17T08:22:54
Spectrometer Frequency 500.33
Spectral Width 10000.0
Lowest Frequency -2020.8
Nucleus 1H
Acquired Size 32768
Spectral Size 65536
1.00
1.99
2.01
1.95
1.01
0.96
2.09
2.03
12.0 11.5 11.0 10.5 10.0 9.5 9.0 8.5 8.0 7.5 7.0 6.5 6.0 5.5 5.0 4.5 4.0 3.5 3.0 2.5 2.0 1.5 1.0 0.5 0.0 -0.5
f1 (ppm)

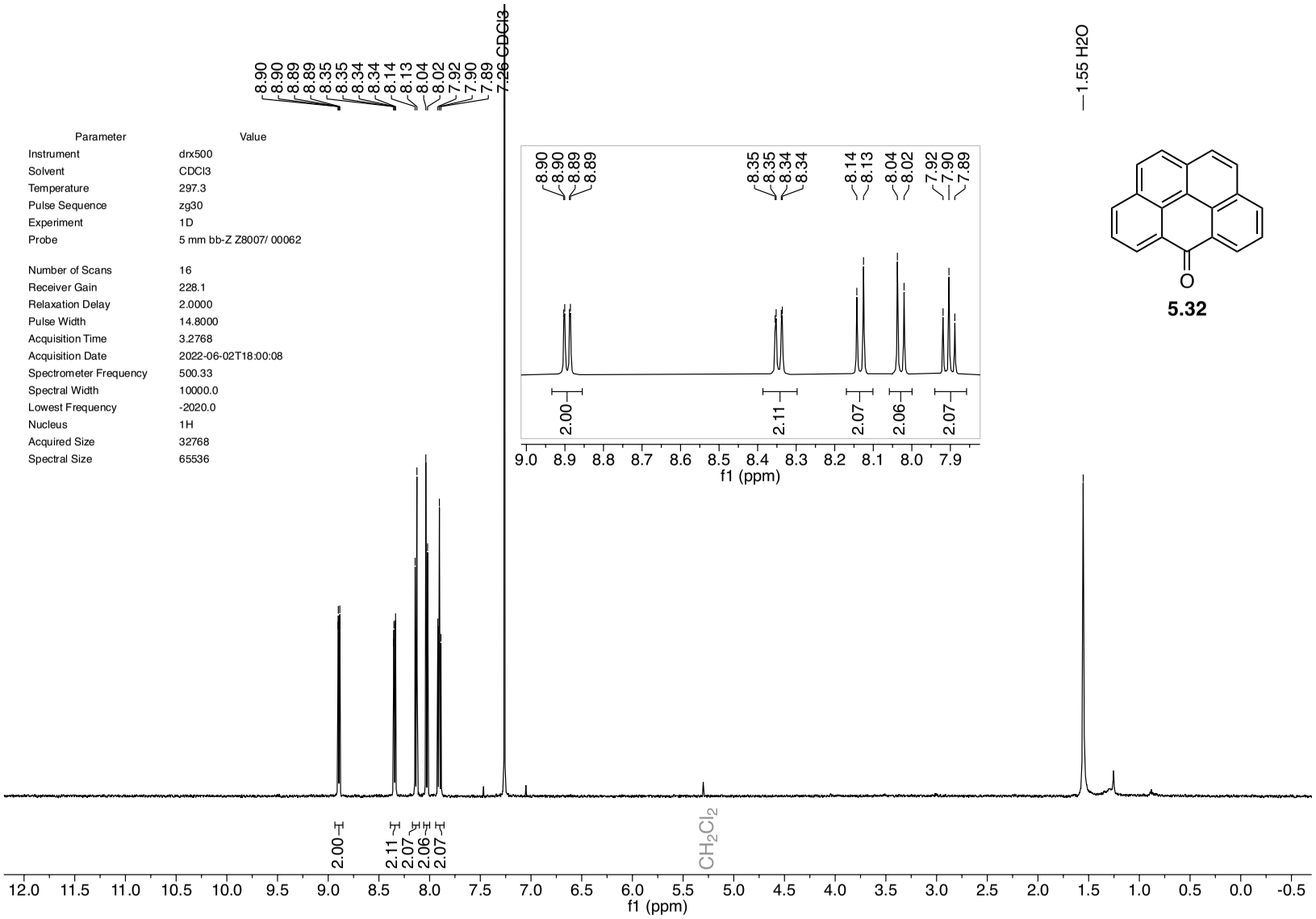
8.90
8.90
8.89
8.89
8.35
8.35
8.34
8.34
8.14
8.13
8.04
8.02
7.92
7.90
7.89
7.26 CDCl3
1.55 H2O
Parameter Value
Instrument drx500
Solvent CDCl3
Temperature 297.3
Pulse Sequence zg30
Experiment 1D
Probe 5 mm bb-Z Z8007/ 00062
Number of Scans 16
Receiver Gain 228.1
Relaxation Delay 2.0000
Pulse Width 14.8000
Acquisition Time 3.2768
Acquisition Date 2022-06-02T18:00:08
Spectrometer Frequency 500.33
Spectral Width 10000.0
Lowest Frequency -2020.0
Nucleus 1H
Acquired Size 32768
Spectral Size 65536
2.00
2.11
2.07
2.06
2.07
f1 (ppm)
CH2Cl2
O
5.32

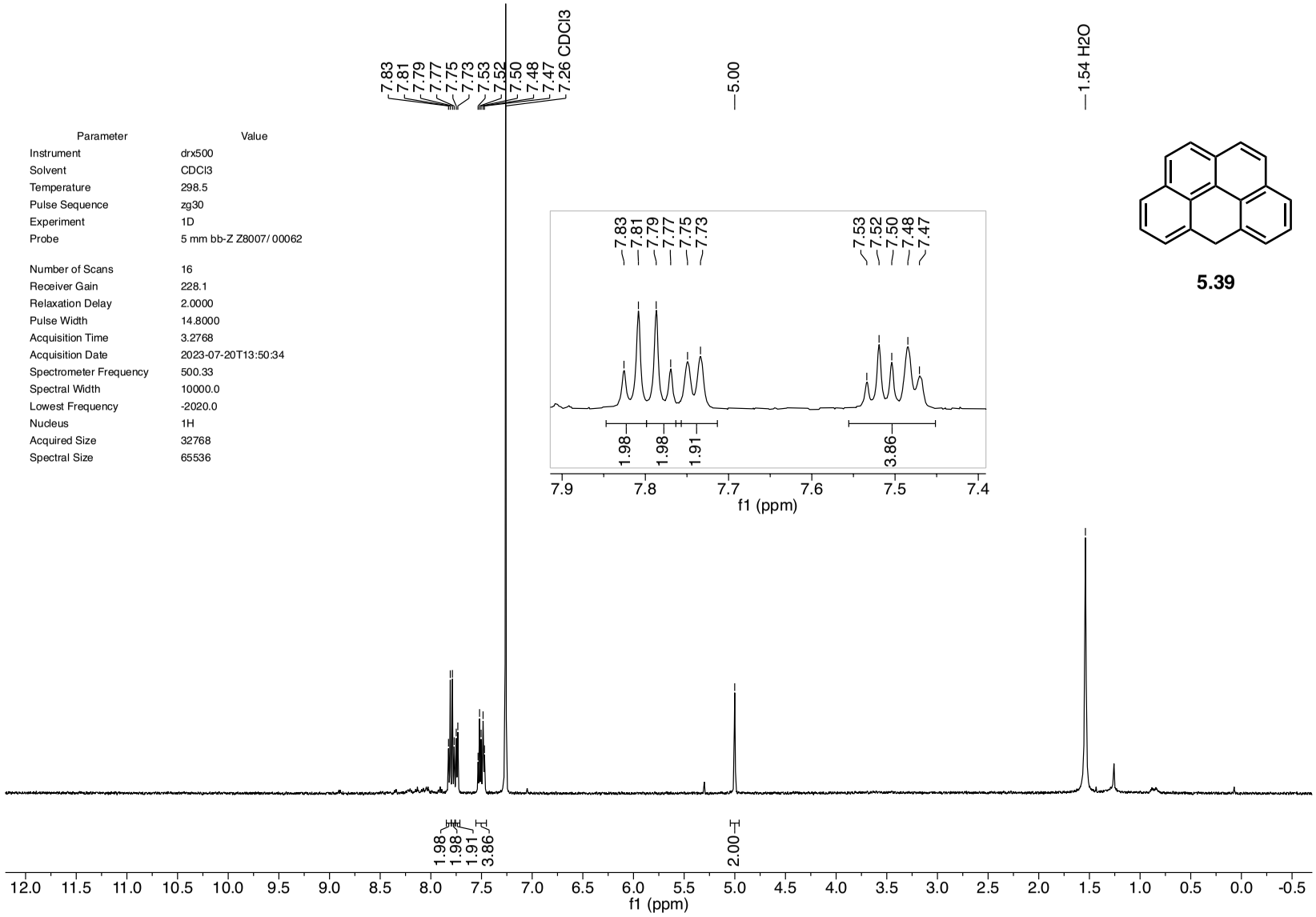
7.83
7.81
7.79
7.77
7.75
7.73
7.53
7.52
7.50
7.48
7.47
7.26 CDCl3
5.00
1.54 H2O
Parameter Value
Instrument drx500
Solvent CDCl3
Temperature 298.5
Pulse Sequence zg30
Experiment 1D
Probe 5 mm bb-Z Z8007/ 00062
Number of Scans 16
Receiver Gain 228.1
Relaxation Delay 2.0000
Pulse Width 14.8000
Acquisition Time 3.2768
Acquisition Date 2023-07-20T13:50:34
Spectrometer Frequency 500.33
Spectral Width 10000.0
Lowest Frequency -2020.0
Nucleus 1H
Acquired Size 32768
Spectral Size 65536
1.98
1.98
1.91
3.86
2.00
f1 (ppm)
5.39

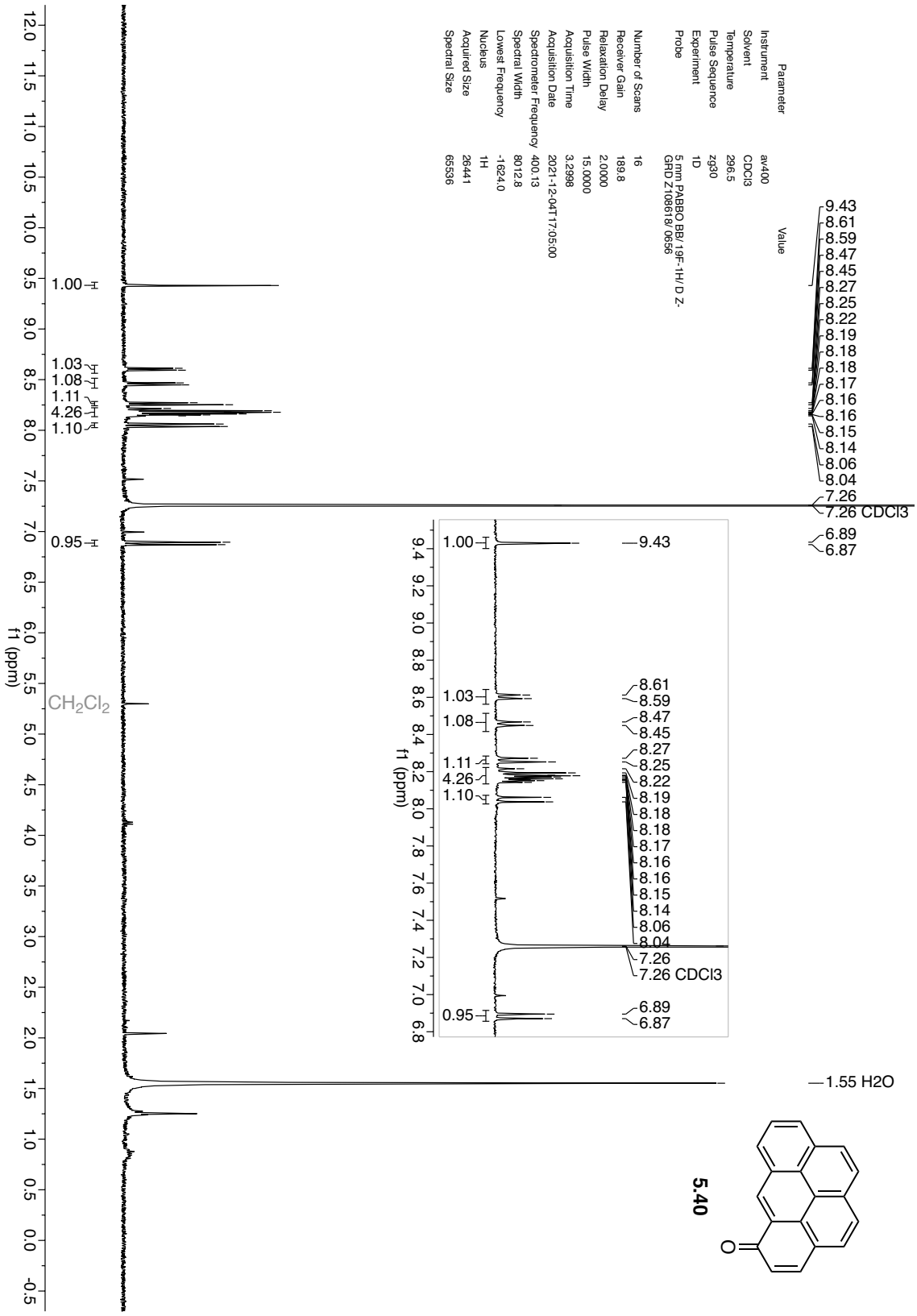
Parameter
Value
Instrument
av400
Solvent
CDCl3
Temperature
296.5
Pulse Sequence
zg30
Experiment
1D
Probe
5 mm PABBO BB/ 19F-1H/ D Z-GRD Z108618/ 0656
Number of Scans
16
Receiver Gain
189.8
Relaxation Delay
2.0000
Pulse Width
15.0000
Acquisition Time
3.2998
Acquisition Date
2021-12-04T17:05:00
Spectrometer Frequency
400.13
Spectral Width
8012.8
Lowest Frequency
-1624.0
Nucleus
1H
Acquired Size
26441
Spectral Size
65536
9.43
8.61
8.59
8.47
8.45
8.27
8.25
8.22
8.19
8.18
8.18
8.17
8.16
8.16
8.15
8.14
8.06
8.04
7.26
7.26 CDCl3
6.89
6.87
1.00
1.03
1.08
1.11
4.26
1.10
0.95
CH2Cl2
1.55 H2O
f1 (ppm)
5.40
O

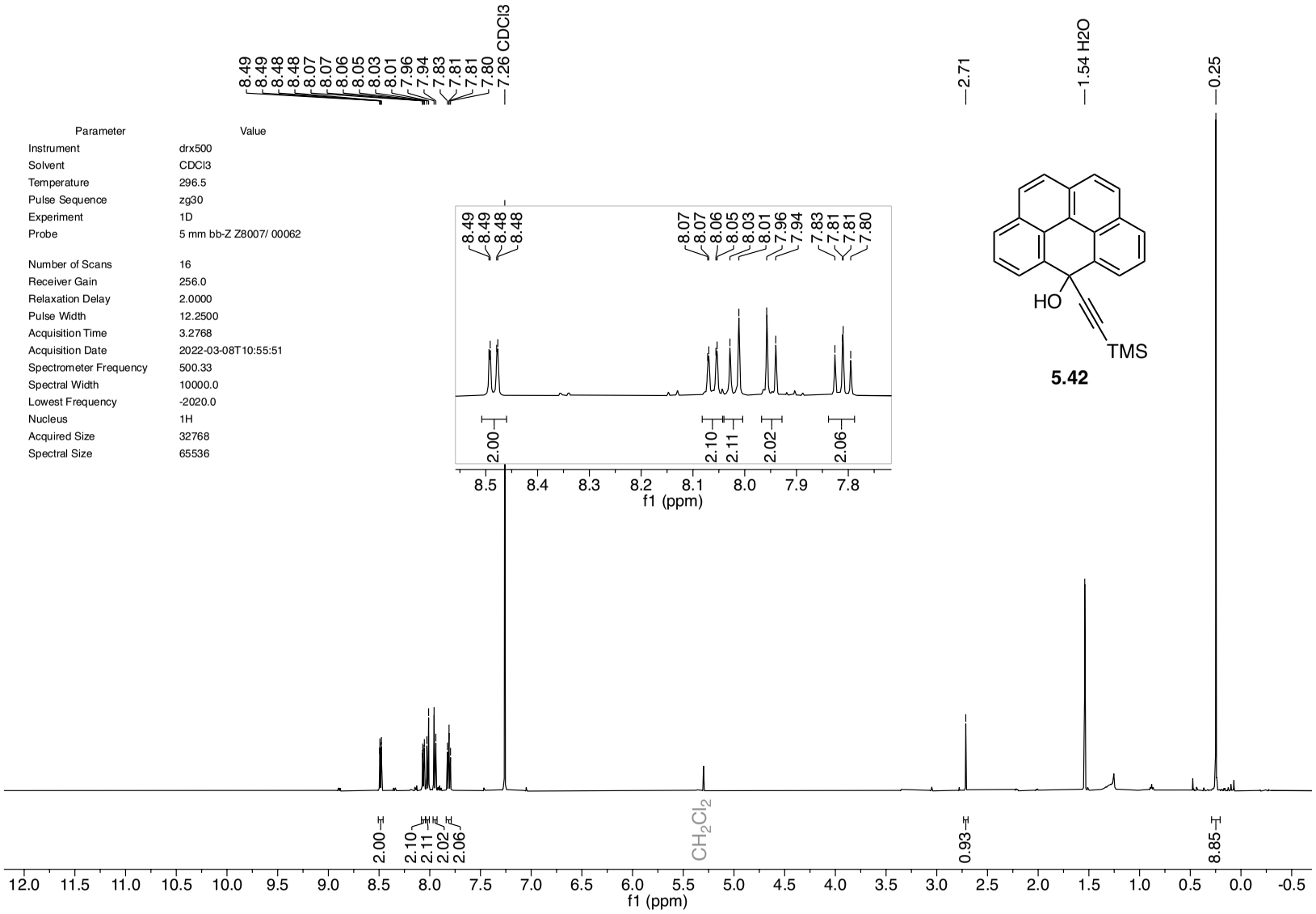
8.49
8.49
8.48
8.48
8.07
8.07
8.06
8.05
8.03
8.01
7.96
7.94
7.83
7.81
7.81
7.80
7.26 CDCl3
2.71
1.54 H2O
0.25
Parameter Value
Instrument drx500
Solvent CDCl3
Temperature 296.5
Pulse Sequence zg30
Experiment 1D
Probe 5 mm bb-Z Z8007/ 00062
Number of Scans 16
Receiver Gain 256.0
Relaxation Delay 2.0000
Pulse Width 12.2500
Acquisition Time 3.2768
Acquisition Date 2022-03-08T10:55:51
Spectrometer Frequency 500.33
Spectral Width 10000.0
Lowest Frequency -2020.0
Nucleus 1H
Acquired Size 32768
Spectral Size 65536
2.00
2.10
2.11
2.02
2.06
f1 (ppm)
HO
TMS
5.42
CH2Cl2
0.93
8.85
f1 (ppm)

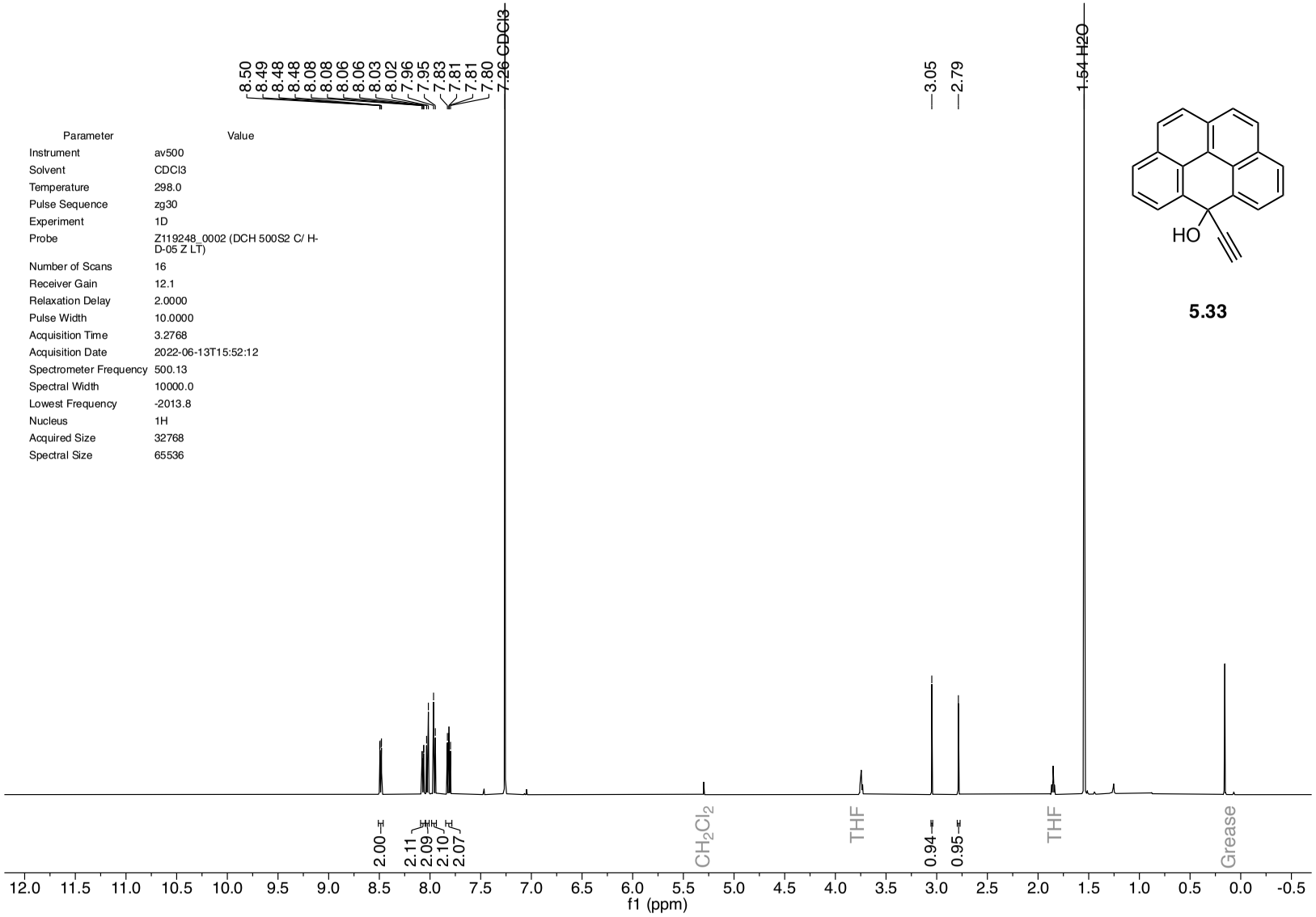
8.50
8.49
8.48
8.48
8.08
8.08
8.06
8.06
8.03
8.02
7.96
7.95
7.83
7.81
7.81
7.80
7.26 CDCl3
3.05
2.79
1.54 H2O
HO
Parameter Value
Instrument av500
Solvent CDCl3
Temperature 298.0
Pulse Sequence zg30
Experiment 1D
Probe Z119248_0002 (DCH 500S2 C/ H-D-05 Z LT)
Number of Scans 16
Receiver Gain 12.1
Relaxation Delay 2.0000
Pulse Width 10.0000
Acquisition Time 3.2768
Acquisition Date 2022-06-13T15:52:12
Spectrometer Frequency 500.13
Spectral Width 10000.0
Lowest Frequency -2013.8
Nucleus 1H
Acquired Size 32768
Spectral Size 65536
2.00
2.11
2.09
2.10
2.07
CH2Cl2
THF
0.94
0.95
THF
Grease
12.0 11.5 11.0 10.5 10.0 9.5 9.0 8.5 8.0 7.5 7.0 6.5 6.0 5.5 5.0 4.5 4.0 3.5 3.0 2.5 2.0 1.5 1.0 0.5 0.0 -0.5
f1 (ppm)

5.33

5.5.6 ^{13}C NMR spectra

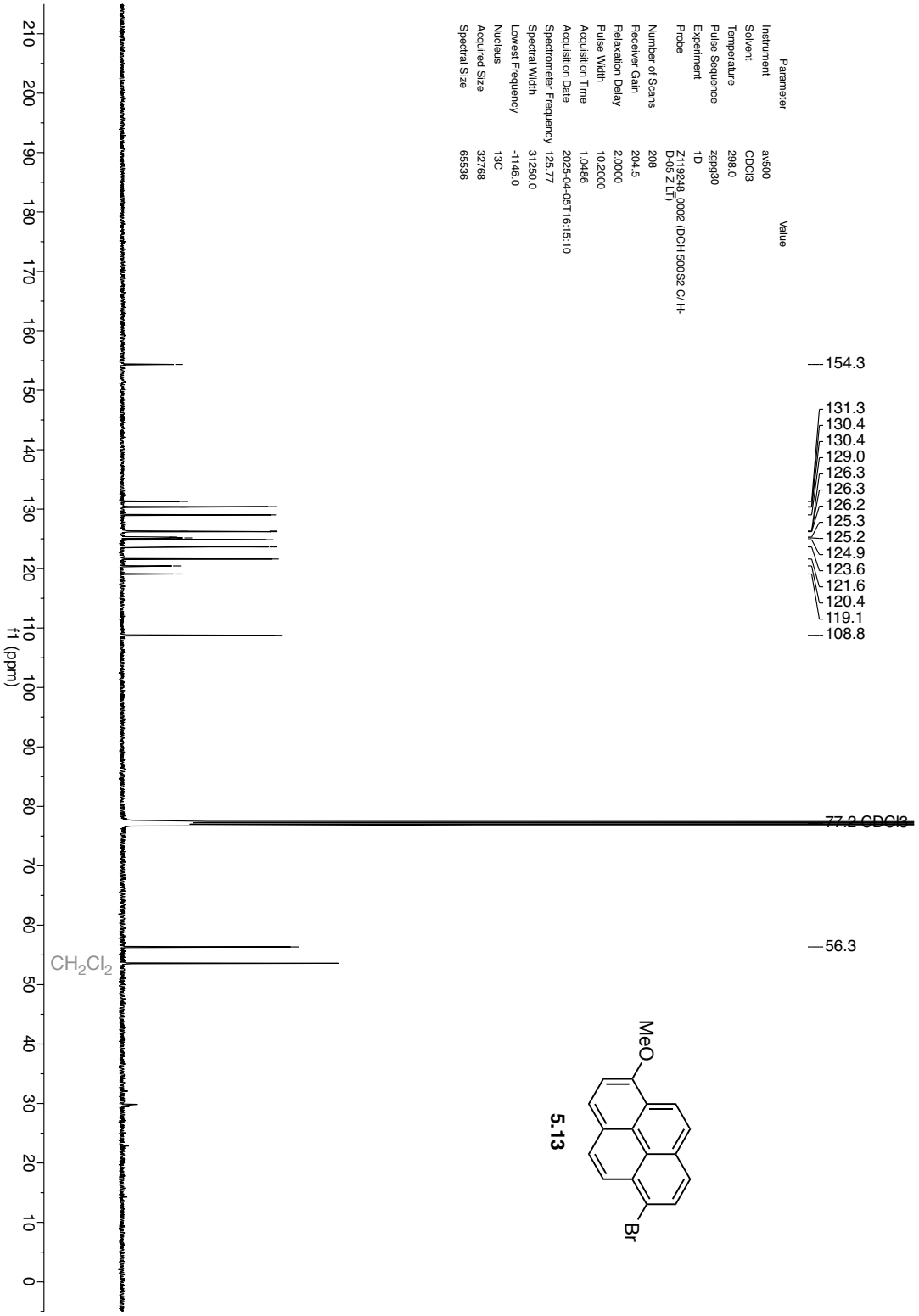

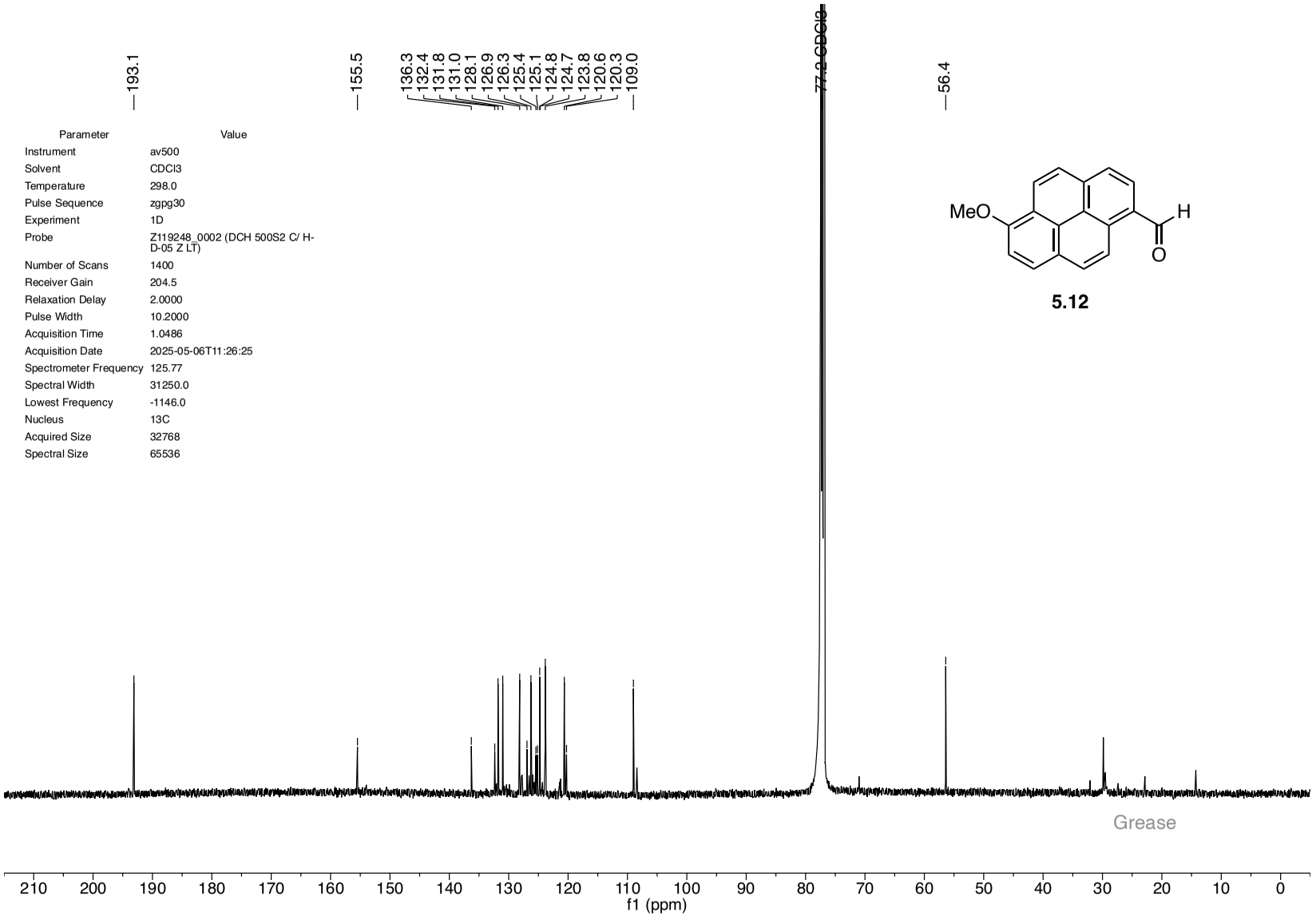

Parameter	Value
Instrument	av500
Solvent	CDCl3
Temperature	298.0
Pulse Sequence	zgpg30
Experiment	1D
Probe	Z119248_0002 (DCH 500S2 C/ H-D-05 Z LT)
Number of Scans	1400
Receiver Gain	204.5
Relaxation Delay	2.0000
Pulse Width	10.2000
Acquisition Time	1.0486
Acquisition Date	2025-05-06T11:26:25
Spectrometer Frequency	125.77
Spectral Width	31250.0
Lowest Frequency	-1146.0
Nucleus	13C
Acquired Size	32768
Spectral Size	65536

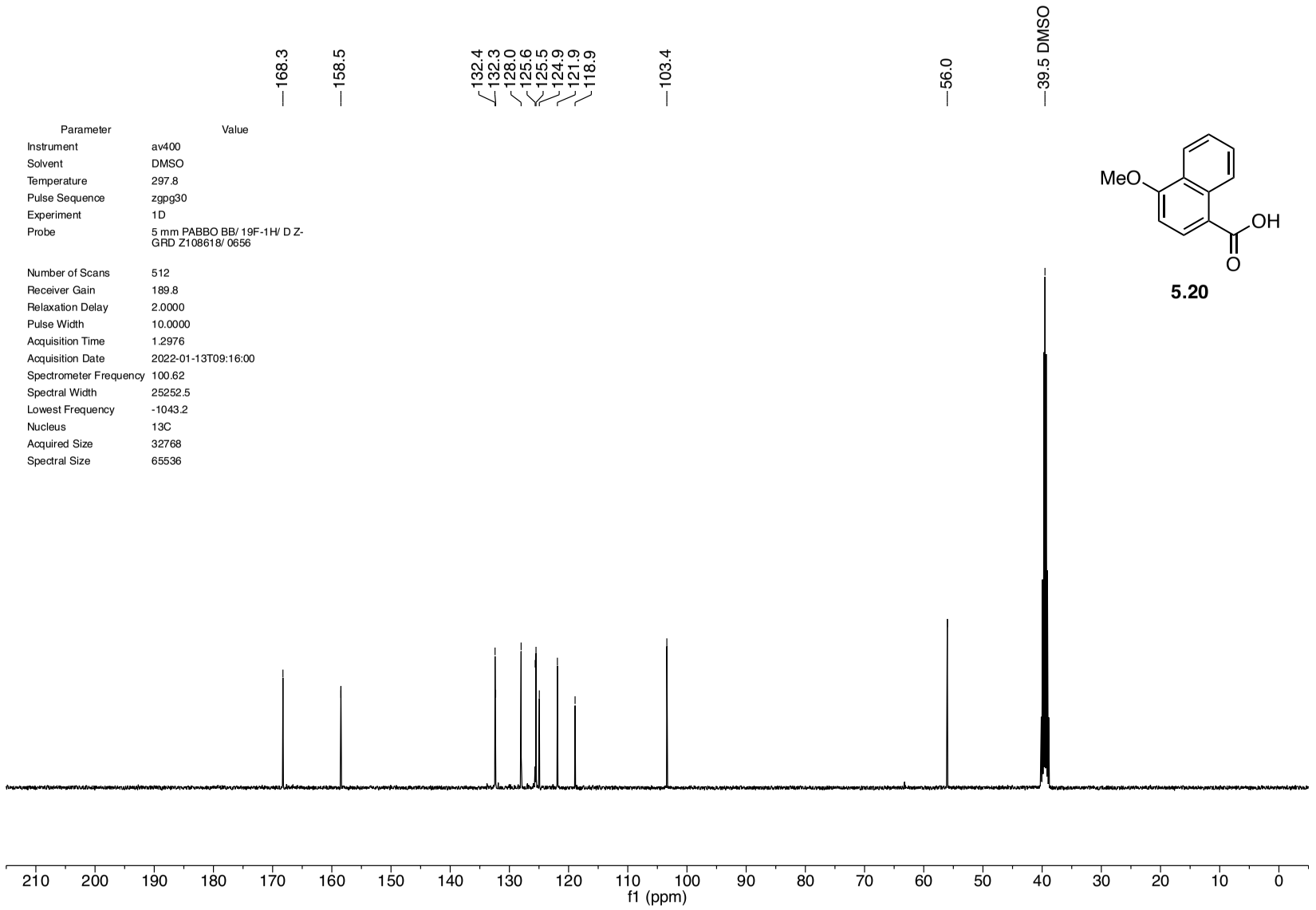
168.3
158.5
132.4
132.3
128.0
125.6
125.5
124.9
121.9
118.9
103.4
56.0
39.5 DMSO
Parameter Value
Instrument av400
Solvent DMSO
Temperature 297.8
Pulse Sequence zgpg30
Experiment 1D
Probe 5 mm PABBO BB/ 19F-1H/ D Z-GRD Z108618/ 0656
Number of Scans 512
Receiver Gain 189.8
Relaxation Delay 2.0000
Pulse Width 10.0000
Acquisition Time 1.2976
Acquisition Date 2022-01-13T09:16:00
Spectrometer Frequency 100.62
Spectral Width 25252.5
Lowest Frequency -1043.2
Nucleus 13C
Acquired Size 32768
Spectral Size 65536
MeO
OH
O
5.20
210 200 190 180 170 160 150 140 130 120 110 100 90 80 70 60 50 40 30 20 10 0
f1 (ppm)

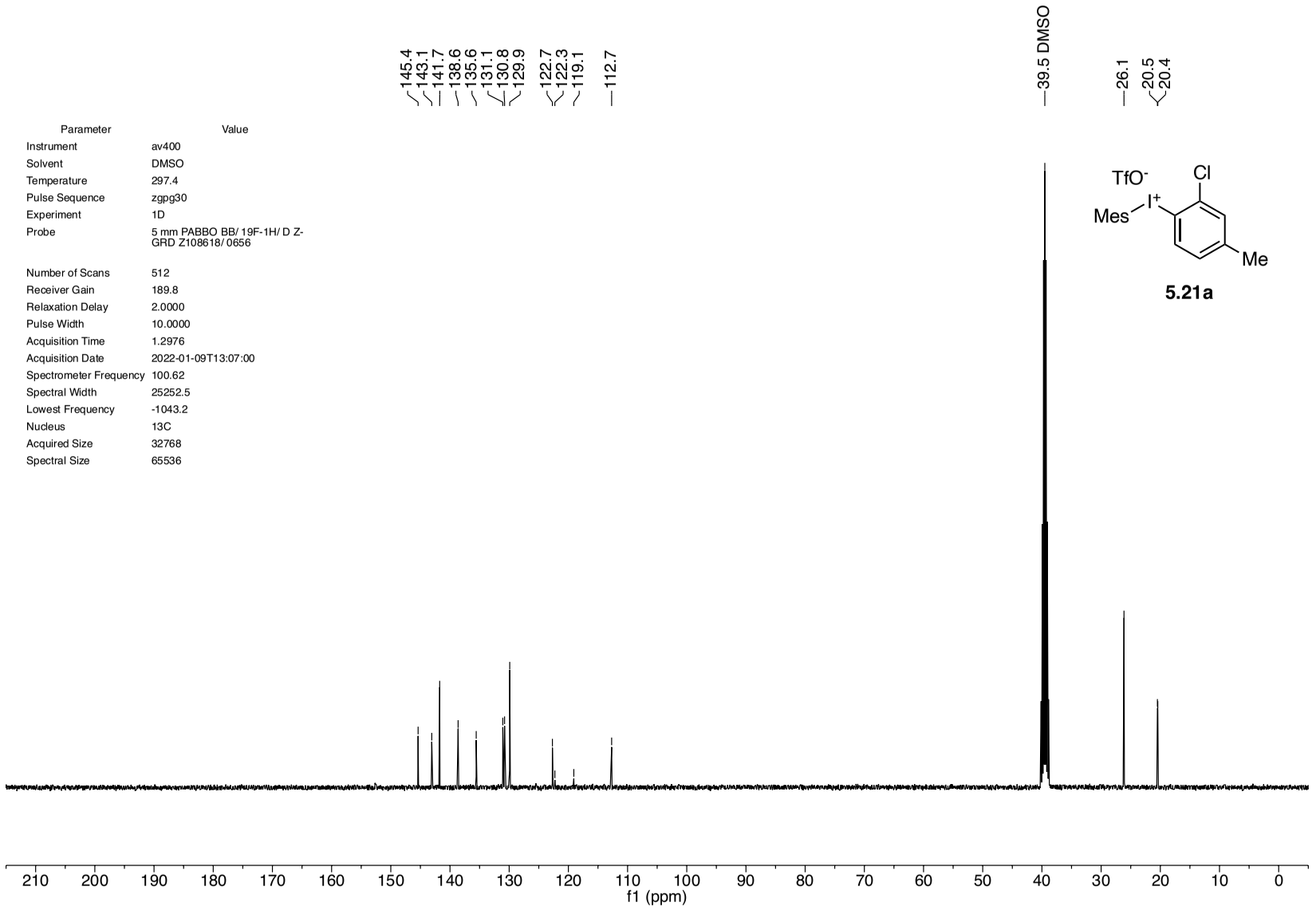

Parameter	Value
Instrument	av400
Solvent	DMSO
Temperature	297.4
Pulse Sequence	zgpg30
Experiment	1D
Probe	5 mm PABBO BB/ 19F-1H/ D Z-GRD Z108618/ 0656
Number of Scans	512
Receiver Gain	189.8
Relaxation Delay	2.0000
Pulse Width	10.0000
Acquisition Time	1.2976
Acquisition Date	2022-01-09T13:07:00
Spectrometer Frequency	100.62
Spectral Width	25252.5
Lowest Frequency	-1043.2
Nucleus	13C
Acquired Size	32768
Spectral Size	65536

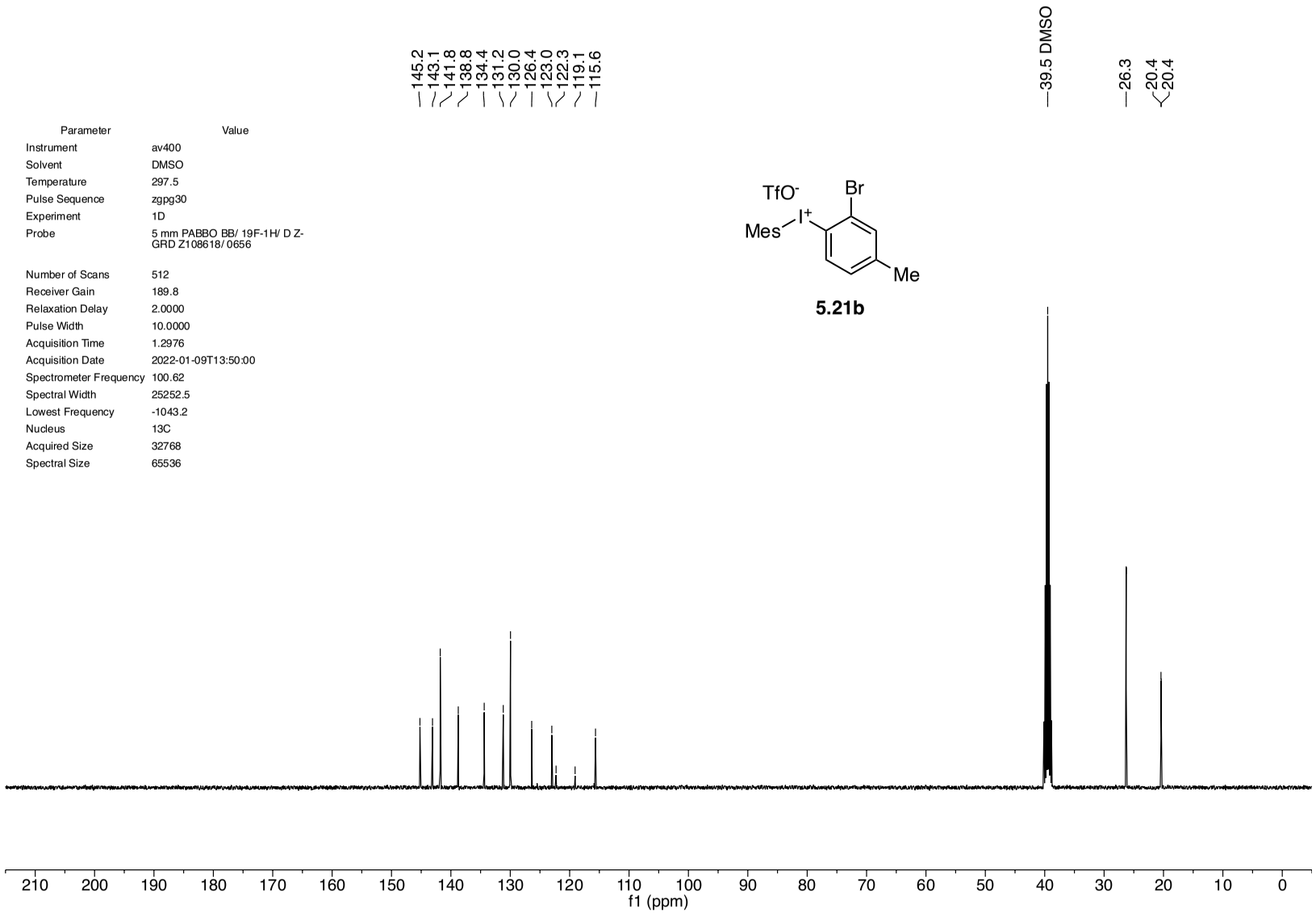
145.2
143.1
141.8
138.8
134.4
131.2
130.0
126.4
123.0
122.3
119.1
115.6
39.5 DMSO
26.3
20.4
20.4
TfO-
Br
Mes
I+
Me
5.21b
Parameter
Value
Instrument
av400
Solvent
DMSO
Temperature
297.5
Pulse Sequence
zgpg30
Experiment
1D
Probe
5 mm PABBO BB/ 19F-1H/ D Z-GRD Z108618/ 0656
Number of Scans
512
Receiver Gain
189.8
Relaxation Delay
2.0000
Pulse Width
10.0000
Acquisition Time
1.2976
Acquisition Date
2022-01-09T13:50:00
Spectrometer Frequency
100.62
Spectral Width
25252.5
Lowest Frequency
-1043.2
Nucleus
13C
Acquired Size
32768
Spectral Size
65536
210 200 190 180 170 160 150 140 130 120 110 100 90 80 70 60 50 40 30 20 10 0
f1 (ppm)

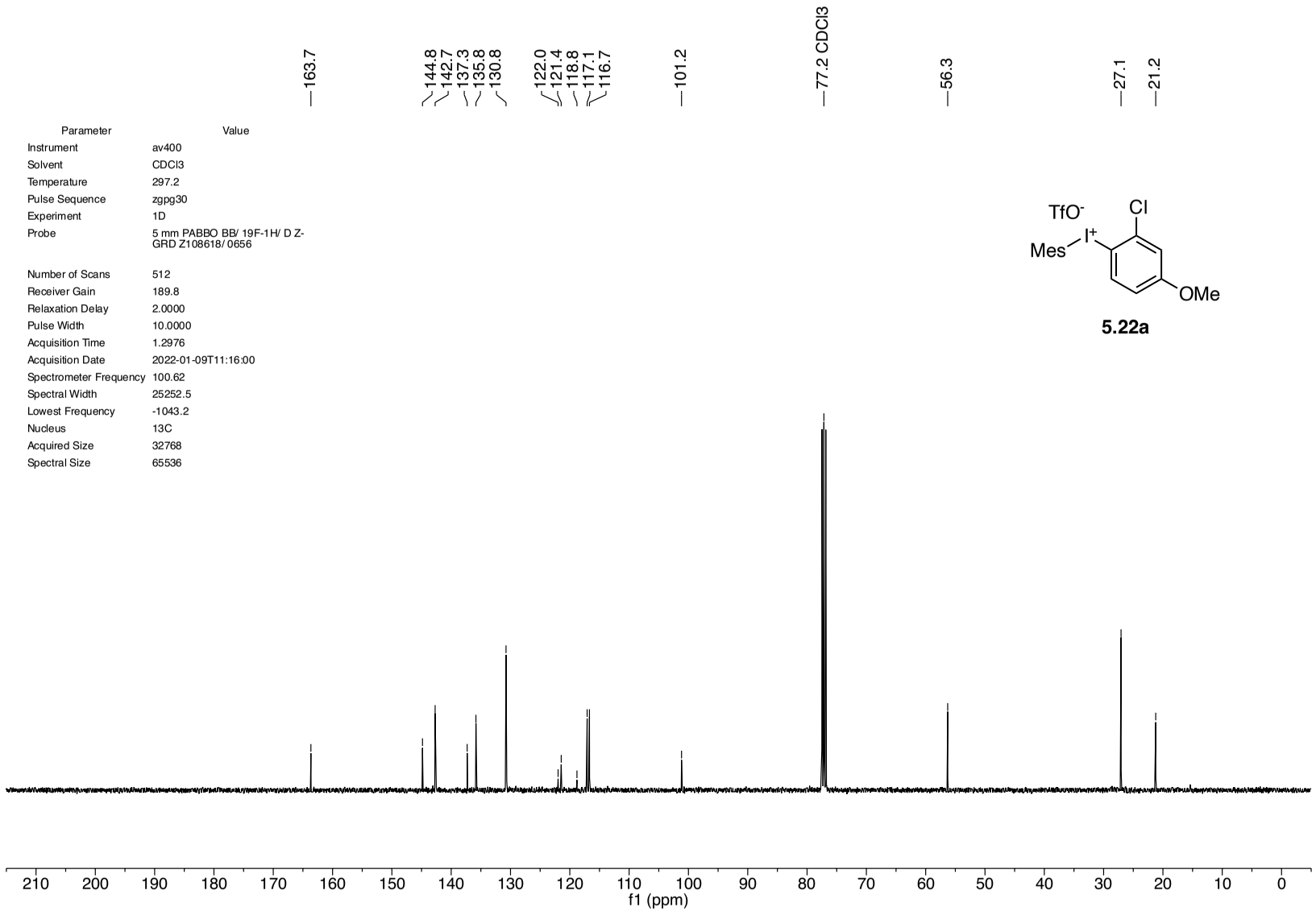
163.7
144.8
142.7
137.3
135.8
130.8
122.0
121.4
118.8
117.1
116.7
101.2
77.2 CDCl3
56.3
27.1
21.2
Parameter Value
Instrument av400
Solvent CDCl3
Temperature 297.2
Pulse Sequence zgpg30
Experiment 1D
Probe 5 mm PABBO BB/ 19F-1H/ D Z-GRD Z108618/ 0656
Number of Scans 512
Receiver Gain 189.8
Relaxation Delay 2.0000
Pulse Width 10.0000
Acquisition Time 1.2976
Acquisition Date 2022-01-09T11:16:00
Spectrometer Frequency 100.62
Spectral Width 25252.5
Lowest Frequency -1043.2
Nucleus 13C
Acquired Size 32768
Spectral Size 65536
TfO-
I+
Mes
Cl
OMe
5.22a
210 200 190 180 170 160 150 140 130 120 110 100 90 80 70 60 50 40 30 20 10 0
f1 (ppm)

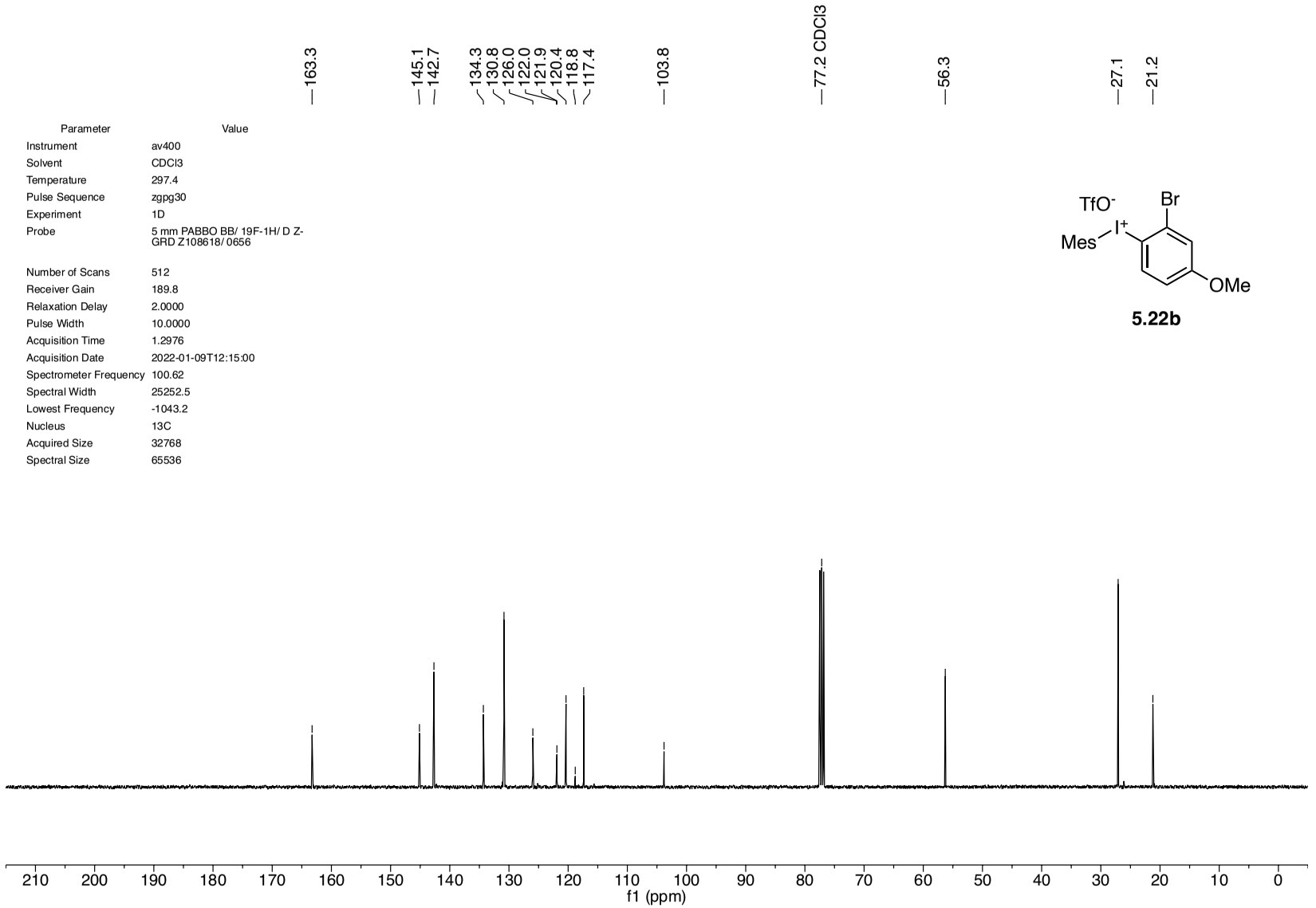
163.3
145.1
142.7
134.3
130.8
126.0
122.0
121.9
120.4
118.8
117.4
103.8
77.2 CDCl3
56.3
27.1
21.2
Parameter Value
Instrument av400
Solvent CDCl3
Temperature 297.4
Pulse Sequence zgpg30
Experiment 1D
Probe 5 mm PABBO BB/ 19F-1H/ D Z-GRD Z108618/ 0656
Number of Scans 512
Receiver Gain 189.8
Relaxation Delay 2.0000
Pulse Width 10.0000
Acquisition Time 1.2976
Acquisition Date 2022-01-09T12:15:00
Spectrometer Frequency 100.62
Spectral Width 25252.5
Lowest Frequency -1043.2
Nucleus 13C
Acquired Size 32768
Spectral Size 65536
TfO-
Br
I+
Mes
OMe
5.22b
210 200 190 180 170 160 150 140 130 120 110 100 90 80 70 60 50 40 30 20 10 0
f1 (ppm)

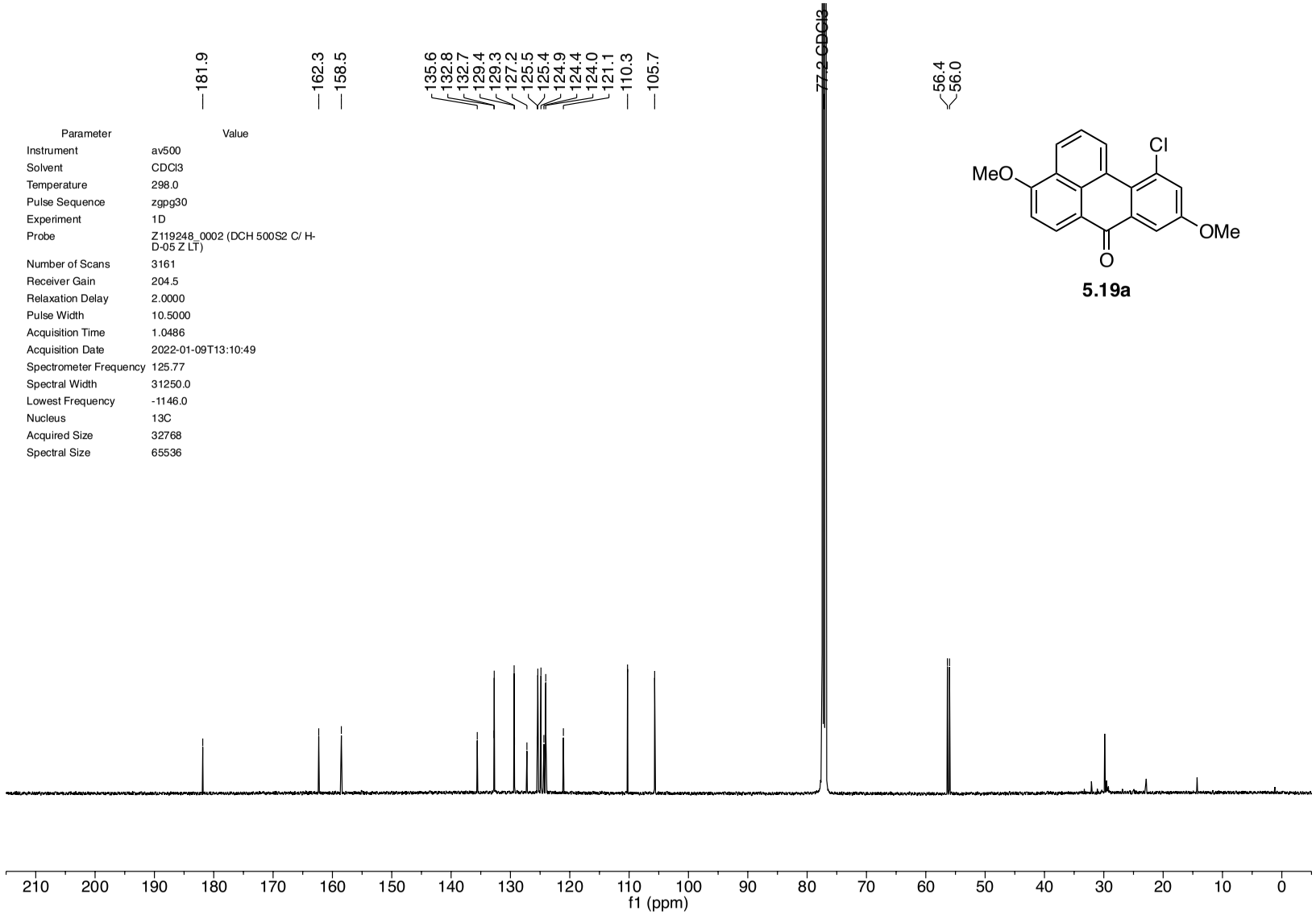
181.9
162.3
158.5
135.6
132.8
132.7
129.4
129.3
127.2
125.5
125.4
124.9
124.4
124.0
121.1
110.3
105.7
77.2 CDCl3
56.4
56.0
Parameter Value
Instrument av500
Solvent CDCl3
Temperature 298.0
Pulse Sequence zgpg30
Experiment 1D
Probe Z119248_0002 (DCH 500S2 C/ H-D-05 Z LT)
Number of Scans 3161
Receiver Gain 204.5
Relaxation Delay 2.0000
Pulse Width 10.5000
Acquisition Time 1.0486
Acquisition Date 2022-01-09T13:10:49
Spectrometer Frequency 125.77
Spectral Width 31250.0
Lowest Frequency -1146.0
Nucleus 13C
Acquired Size 32768
Spectral Size 65536
MeO
Cl
OMe
O
5.19a
210 200 190 180 170 160 150 140 130 120 110 100 90 80 70 60 50 40 30 20 10 0
f1 (ppm)

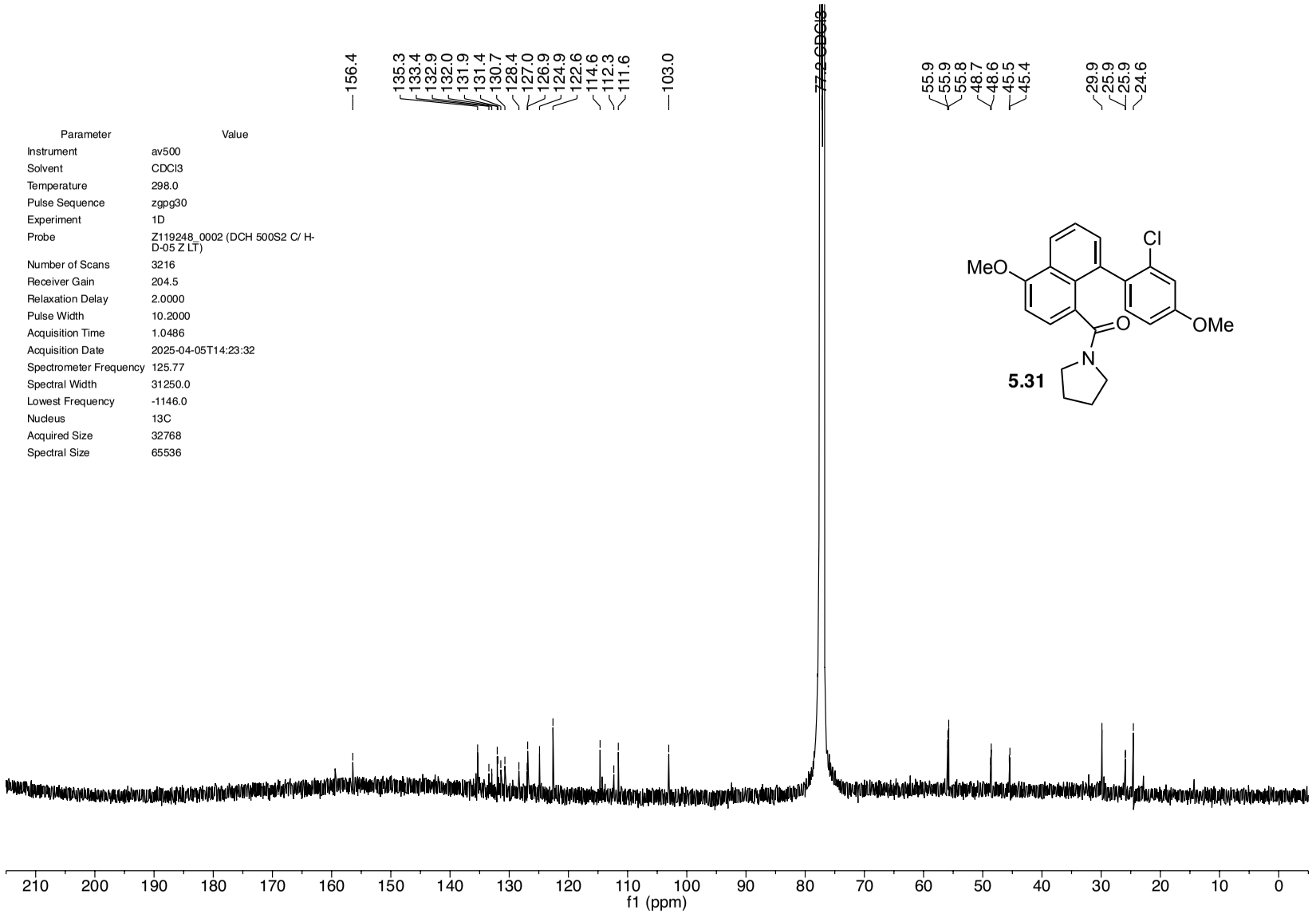
156.4
135.3
133.4
132.9
132.0
131.9
131.4
130.7
128.4
127.0
126.9
124.9
122.6
114.6
112.3
111.6
103.0
77.2 CDCl3
55.9
55.9
55.8
48.7
48.6
45.5
45.4
29.9
25.9
25.9
24.6
Parameter Value
Instrument av500
Solvent CDCl3
Temperature 298.0
Pulse Sequence zgpg30
Experiment 1D
Probe Z119248_0002 (DCH 500S2 C/ H-D-05 Z LT)
Number of Scans 3216
Receiver Gain 204.5
Relaxation Delay 2.0000
Pulse Width 10.2000
Acquisition Time 1.0486
Acquisition Date 2025-04-05T14:23:32
Spectrometer Frequency 125.77
Spectral Width 31250.0
Lowest Frequency -1146.0
Nucleus 13C
Acquired Size 32768
Spectral Size 65536
MeO
Cl
OMe
O
N
5.31
210 200 190 180 170 160 150 140 130 120 110 100 90 80 70 60 50 40 30 20 10 0
f1 (ppm)

5.5.7 ^{19}F NMR spectra

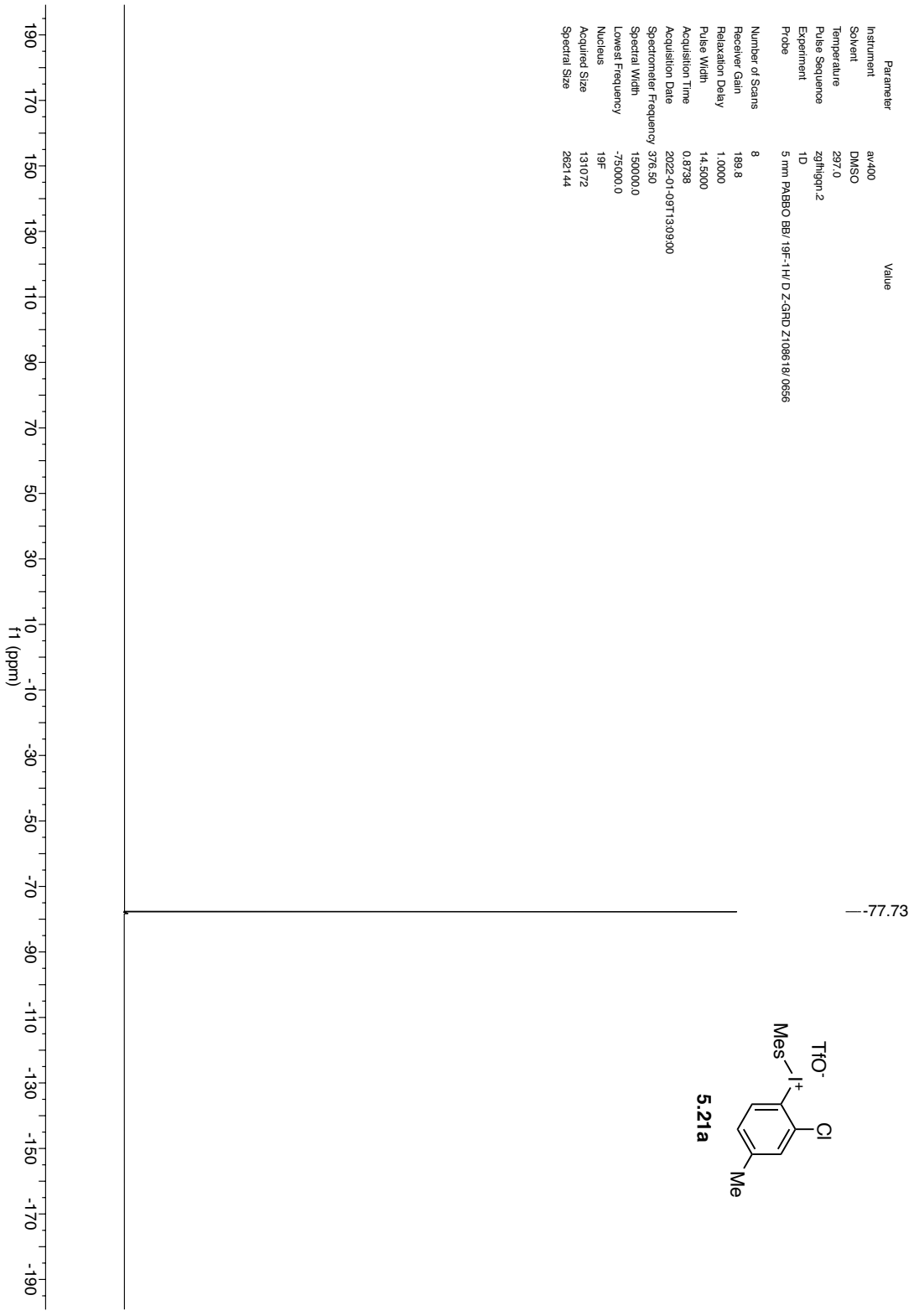

Parameter	Value
Instrument	av400
Solvent	DMSO
Temperature	297.1
Pulse Sequence	zgfhigqn.2
Experiment	1D
Probe	5 mm PABBO BB/ 19F-1H/ D Z-GRD Z108618/ 0656
Number of Scans	8
Receiver Gain	189.8
Relaxation Delay	1.0000
Pulse Width	14.5000
Acquisition Time	0.8738
Acquisition Date	2022-01-09T13:52:00
Spectrometer Frequency	376.50
Spectral Width	150000.0
Lowest Frequency	-75000.0
Nucleus	19F
Acquired Size	131072
Spectral Size	262144

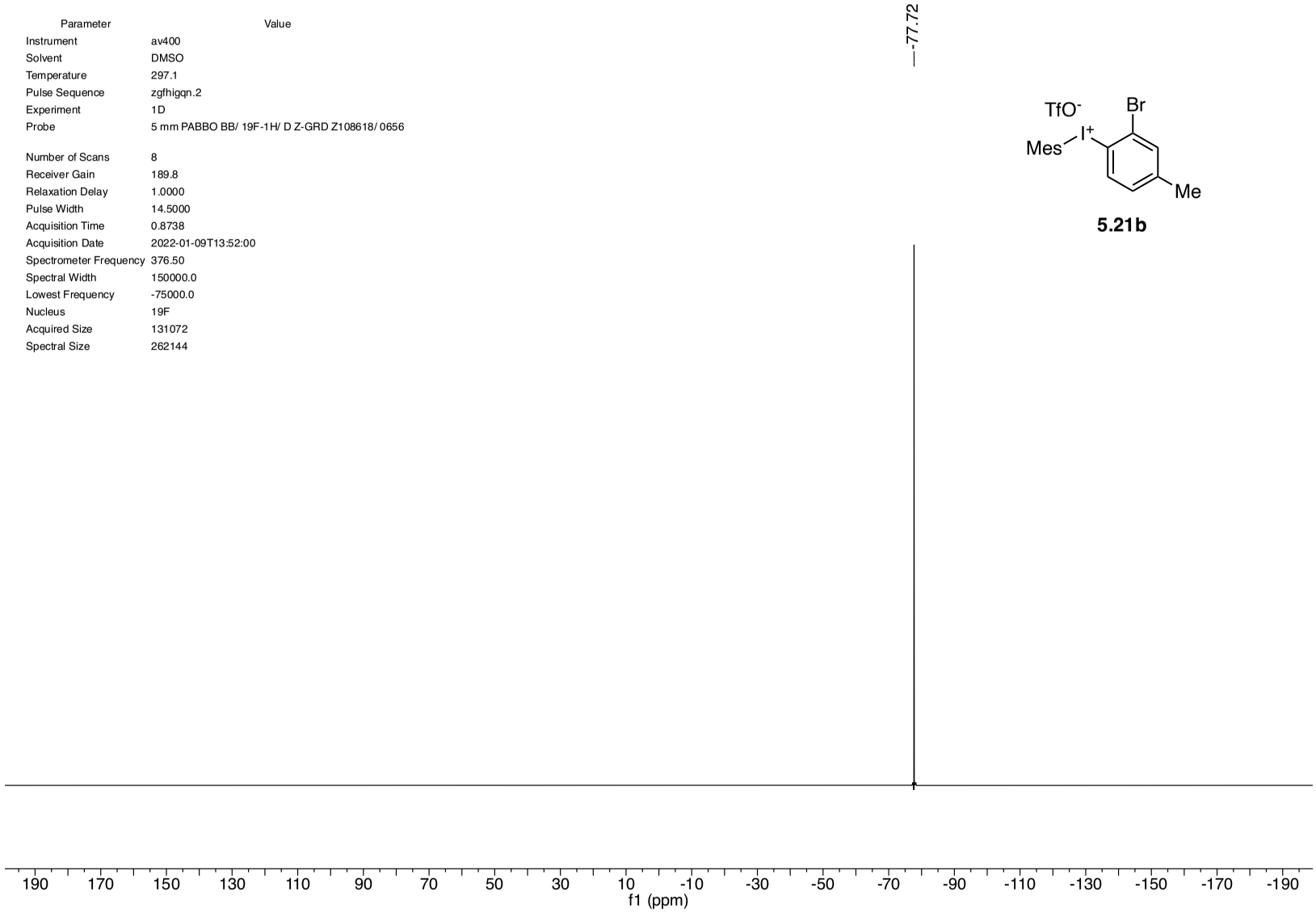

Parameter	Value
Instrument	av400
Solvent	CDCl3
Temperature	297.2
Pulse Sequence	zgflqn30
Experiment	1D
Probe	5 mm PABBO BB/ 19F-1H/ D Z-GRD Z108618/ 0656
Number of Scans	8
Receiver Gain	189.8
Relaxation Delay	2.0000
Pulse Width	14.5000
Acquisition Time	0.8738
Acquisition Date	2021-09-24T17:28:00
Spectrometer Frequency	376.50
Spectral Width	150000.0
Lowest Frequency	-75000.0
Nucleus	19F
Acquired Size	131072
Spectral Size	262144

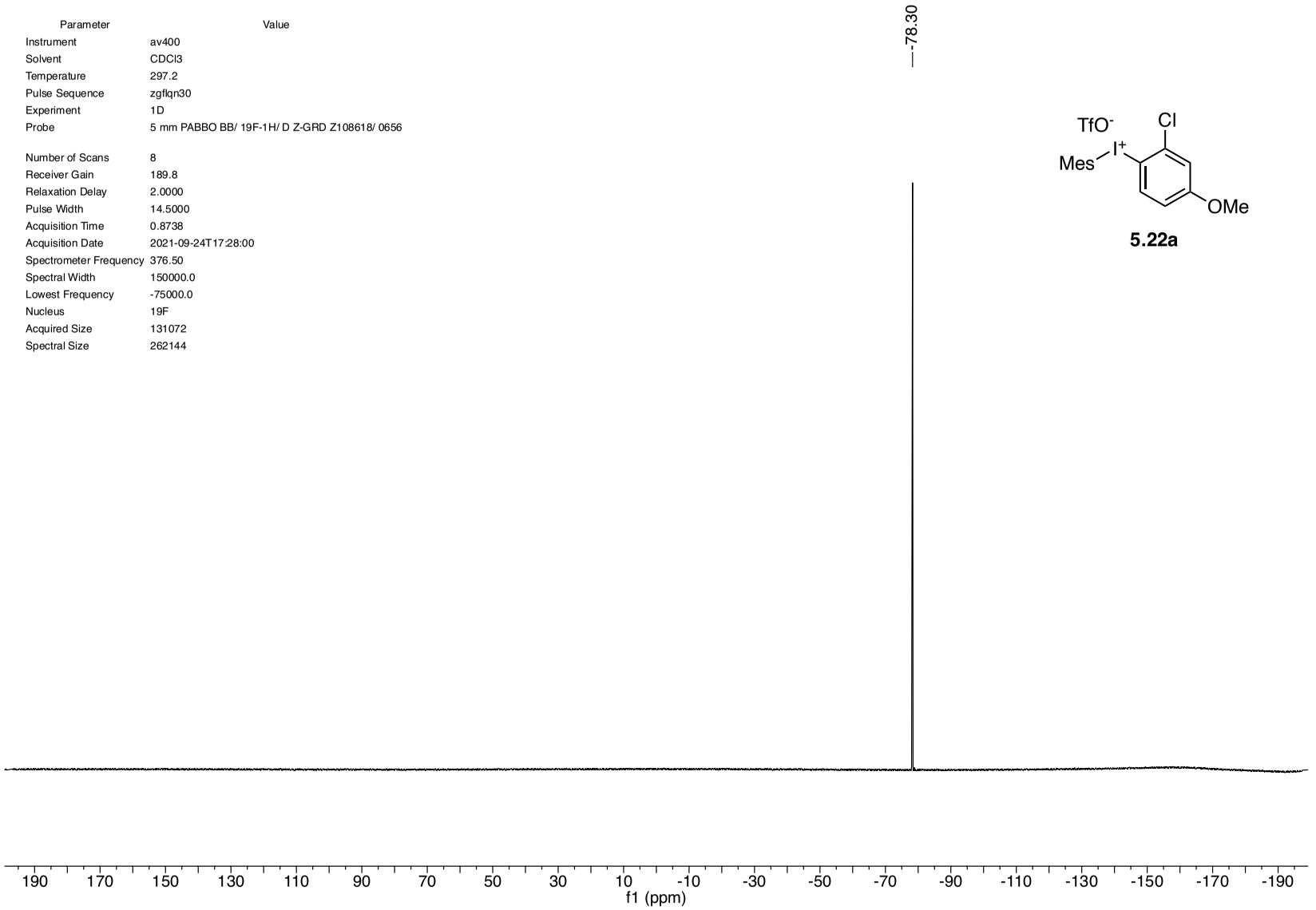

Parameter	Value
Instrument	av400
Solvent	CDCl3
Temperature	296.9
Pulse Sequence	zgfhigqn.2
Experiment	1D
Probe	5 mm PABBO BB/ 19F-1H/ D Z-GRD Z108618/ 0656
Number of Scans	8
Receiver Gain	189.8
Relaxation Delay	1.0000
Pulse Width	14.5000
Acquisition Time	0.8738
Acquisition Date	2022-01-09T12:17:00
Spectrometer Frequency	376.50
Spectral Width	150000.0
Lowest Frequency	-75000.0
Nucleus	19F
Acquired Size	131072
Spectral Size	262144

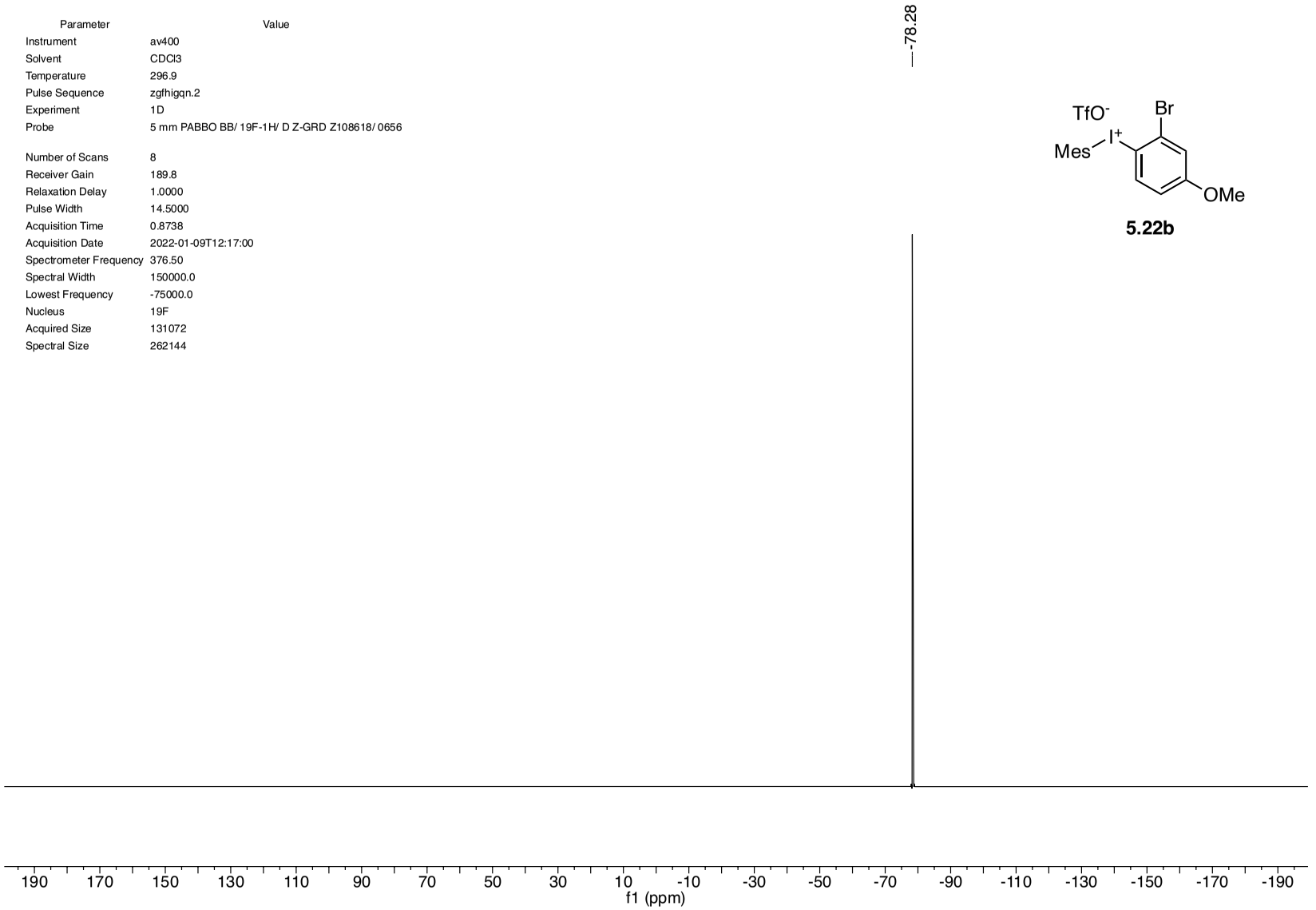

5.22b

5.6 References

(1) Lee, G. Y.; Hu, E.; Rheingold, A. L.; Houk, K. N.; Sletten, E. M. Arene-Perfluoroarene Interactions in Solution. *J. Org. Chem.* **2021**, *86*, 8425–8436.

(2) Cavallo, G.; Metrangolo, P.; Milani, R.; Pilati, T.; Priimagi, A.; Resnati, G.; Terraneo, G. The Halogen Bond. *Chem. Rev.* **2016**, *116*, 2478–2601.

(3) Scholfield, M. R.; Vander Zanden, C. M.; Carter, M.; Ho, P. S. Halogen Bonding (X-Bonding): A Biological Perspective. *Protein Sci*. **2013**, 139–152.

(4) Kahl, G. Molecular Tweezers. In Molecular Devices; Wiley: Hoboken, NJ, USA, 2018; 213–309.

(5) Chen, C. W.; Whitlock, H. W. Molecular Tweezers: A Simple Model of Bifunctional Intercalation. *J. Am. Chem. Soc.* **1978**, *100*, 4921–4922.

(6) Donovan, P. M.; Scott, L. T. Elaboration of Diaryl Ketones into Naphthalenes Fused on Two or Four Sides: A Naphthoannulation Procedure. *J. Am. Chem. Soc.* **2004**, *126*, 3108–3112.

(7) Nishiuchi, T.; Aibara, S.; Kubo, T. Synthesis and Properties of a Highly Congested Tri(9-anthryl)Methyl Radical. *Angew. Chem. Int. Ed.* **2018**, *57*, 16516–16519.

(8) Nauroozi, D.; Bruhn, C.; Fürmeier, S.; Holzhauer, J.; Faust, R. Microwave-Assisted Dibromoolefination of Aromatic and Heteroaromatic Aldehydes and Ketones. *J. Heterocycl. Chem.* **2016**, *53*, 615–619.

(9) Desai, N. B.; McKelvie, N.; Ramirez, F. A New Synthesis of 1,1-Dibromoölefins via Phosphine-Dibromomethylenes. the Reaction of Triphenylphosphine with Carbon Tetrabromide. *J. Am. Chem. Soc.* **1962**, *84*, 1745–1747.

(10) Mistry, A.; Moreton, B.; Schuler, B.; Mohn, F.; Meyer, G.; Gross, L.; Williams, A.; Scott, P.; Costantini, G.; Fox, D. J. The Synthesis and STM/AFM Imaging of "Olympicene" Benzo[Cd]Pyrenes. *Chem. Eur. J.* **2015**, *21*, 2011–2018.

(11) Schulze, M. Synthesis of 1-Bromopyrene and 1-Pyrenecarbaldehyde. *Org. Synth.* **2016**, *93*, 100–114.

(12) Aalten, H. L.; van Koten, G.; Grove, D. M.; Kuilman, T.; Piekstra, O. G.; Hulshof, L. A.; Sheldon, R. A. The Copper Catalysed Reaction of Sodium Methoxide with Aryl Bromides. A Mechanistic Study Leading to a Facile Synthesis of Anisole Derivatives. *Tetrahedron* **1989**, *45*, 5565–5578.

(13) Hasegawa, E.; Hirose, H.; Sasaki, K.; Takizawa, S.; Seida, T.; Chiba, N. Benzimidazoline-Dimethoxypyrene. An Effective Promoter System for Photoinduced Electron Transfer Promoted Reductive Transformations of Organic Compounds. *Heterocycles* **2009**, *77*, 1147–1161.

(14) Profft, E.; Biela, R. Zur Chemie Des Pyrens, I. 3-Alkoxy-pyrene Und 3-Alkoxy-pyrenaldehyde. *Chem. Ber.* **1961**, *94*, 2374–2382.

(15) Fürstner, A.; Mamane, V. Flexible Synthesis of Phenanthrenes by a PtCl2-Catalyzed Cycloisomerization Reaction. *J. Org. Chem.* **2002**, *67*, 6264–6267.

(16) Xue, C.; Wang, L.; Han, J. Palladium-Catalyzed Site-Selective Benzocyclization of Naphthoic Acids with Diaryliodonium Salts: Efficient Access to Benzanthrones. *J. Org. Chem.* **2020**, *85*, 15406–15414.

(17) Lindstedt, E.; Reitti, M.; Olofsson, B. One-Pot Synthesis of Unsymmetric Diaryliodonium Salts from Iodine and Arenes. *J. Org. Chem.* **2017**, *82*, 11909–11914.

(18) Zhu, M.; Jalalian, N.; Olofsson, B. One-Pot Synthesis of Diaryliodonium Salts Using Toluenesulfonic Acid: A Fast Entry to Electron-Rich Diaryliodonium Tosylates and Triflates. *Synlett* **2008**, *4*, 592–596.

(19) Castanet, A.-S.; Colobert, F.; Broutin, P.-E. Mild and Regioselective Iodination of Electron-Rich Aromatics with N -Iodosuccinimide and Catalytic Trifluoroacetic Acid. *Tetrahedron Lett.* **2002**, *43*, 5047–5048.

(20) Zhang, M.; Fu, Z.; Luo, A.; Pu, X.; Wang, M.; Huang, Y.; Yang, Y.; You, J. Palladium-Catalyzed C8–H Arylation and Annulation of 1-Naphthalene Carboxylic Acid Derivatives with Aryl Iodides. *Org. Chem. Front.* **2021**, *8*, 3274–3279.

(21) Garrec, J.; Cordier, M.; Frison, G.; Prévost, S. Palladium-Catalyzed C8-Arylation of Naphthalenes through C−H Activation: A Combined Experimental and Computational Study. *Chem. Eur. J.* **2019**, *25*, 14441–14446.

(22) Guo, Y.; Ding, S.; Zhang, N.; Xu, Z.; Wu, S.; Hu, J.; Xiang, Q.; Li, Z. Y.; Chen, X.; Sato, S.; Wu, J.; Sun, Z. π-Extended Doublet Open-Shell Graphene Fragments Exhibiting One-Dimensional Chain Stacking. *J. Am. Chem. Soc.* **2022**, *144*, 2095–2100.

(23) Strinitz, F.; Tucher, J.; Januszewski, J. A.; Waterloo, A. R.; Stegner, P.; Förtsch, S.; Hübner, E.; Tykwinski, R. R.; Burzlaff, N. Carbon-Rich Ruthenium Allenylidene Complexes Bearing Heteroscorpionate Ligands. *Organometallics* **2014**, *33*, 5129–5144.

(24) Spörler, S.; Strinitz, F.; Rodehutskors, P.; Müller, L.; Waterloo, A. R.; Dürr, M.; Hübner, E.; Ivanović-Burmazović, I.; Tykwinski, R. R.; Burzlaff, N. Carbon-Rich Cyclopentadienyl Ruthenium Allenylidene Complexes. *New. J. Chem.* **2016**, *40*, 6127–6134.

(25) Fernandez De La Mora, J.; Van Berkel, G. J.; Enke, C. G.; Cole, R. B.; Martinez-Sanchez, M.; Fenn, J. B. Electrochemical Processes in Electrospray Ionization Mass Spectrometry. *J. Mass Spectrom.* **2000**, *35*, 939–952.

(26) Chai, Y.; Sun, H.; Wan, J.; Pan, Y.; Sun, C. Hydride Abstraction in Positive-Ion Electrospray Interface: Oxidation of 1,4-Dihydropyridines in Electrospray Ionization Mass Spectrometry. *Analyst* **2011**, *136*, 4667–4669.

(27) Xu, X.; He, G.; Xu, X.; Wu, Z.; Cai, T. Investigation of the Electrochemical Oxidation of 2,3′-Bisindolylmethanes in Positive-Ion Electrospray Ionization Mass Spectrometry. *RSC Adv.* **2019**, *9*, 10727–10732.

(28) Okoročenkova, J.; Filgas, J.; Khan, N. M.; Slavíček, P.; Klán, P. Thermal Truncation of Heptamethine Cyanine Dyes. *J. Am. Chem. Soc.* **2024**, *146*, 19768–19781.

(29) Newson, H. L.; Wild, D. A.; Yeung, S. Y.; Skelton, B. W.; Flematti, G. R.; Allan, J. E.; Piggott, M. J. Access to 1,2,3,4-Tetraoxygenated Benzenes via a Double Baeyer-Villiger Reaction of Quinizarin Dimethyl Ether: Application to the Synthesis of Bioactive Natural Products from Antrodia Camphorata. *J. Org. Chem.* **2016**, *81*, 3127–3135.

(30) Kim, K.; Min, M.; Hong, S. Efficient Synthesis of Anthraquinones from Diaryl Carboxylic Acids via Palladium(II)-Catalyzed and Visible Light-Mediated Transformations. *Ad.v Synth. Catal.* **2017**, *359*, 848–852.

(31) Zhou, Y.; Wang, F.; Kim, Y.; Kim, S. J.; Yoon, J. Cu^{2+}-Selective Ratiometric and "off-on" Sensor Based on the Rhodamine Derivative Bearing Pyrene Group. *Org. Lett.* **2009**, *11*, 4442–4445.

(32) O'Meara, J. A.; Yoakim, C.; Bonneau, P. R.; Bös, M.; Cordingley, M. G.; Déziel, R.; Doyon, L.; Duan, J.; Garneau, M.; Guse, I.; Landry, S.; Malenfant, E.; Naud, J.; Ogilvie,

W. W.; Thavonekham, B.; Simoneau, B. Novel 8-Substituted Dipyridodiazepinone Inhibitors with a Broad-Spectrum of Activity against HIV-1 Strains Resistant to Non-Nucleoside Reverse Transcriptase Inhibitors. *J. Med. Chem.* **2005**, *48*, 5580–5588.

(33) Hirose, Y.; Yamazaki, M.; Nogata, M.; Nakamura, A.; Maegawa, T. Aromatic Halogenation Using N-Halosuccinimide and $PhSSiMe_3$ or PhSSPh. *J. Org. Chem.* **2019**, *84*, 7405–7410.

(34) Tang, S.; Zhao, X.; Yang, L.; Li, B.; Wang, B. Copper-Catalyzed Carboxylation of Aryl Thianthrenium Salts with CO_2. *Angew. Chem. Int. Ed.* **2022**, *61*, e202212975.

(35) Jakab, G.; Hosseini, A.; Hausmann, H.; Schreiner, P. Mild and Selective Organocatalytic Iodination of Activated Aromatic Compounds. *Synthesis* **2013**, *45*, 1635–1640.

(36) Orita, A.; Nakano, T.; An, D. L.; Tanikawa, K.; Wakamatsu, K.; Otera, J. Metal-Assisted Assembly of Pyridine-Containing Arylene Ethynylene Strands to Enantiopure Double Helicates. *J. Am. Chem. Soc.* **2004**, *126*, 10389–10396.

(37) Li, Q.; Huang, F.; Fan, Y.; Wang, Y.; Li, J.; He, Y.; Jiang, H. AgI-Directed Triple-Stranded Helicates with Meta -Ethynylpyridine Ligands. *Eur. J. Inorg. Chem.* **2014**, 3235–3244.

(38) Yuan, J.; Fang, X.; Zhang, L.; Hong, G.; Lin, Y.; Zheng, Q.; Xu, Y.; Ruan, Y.; Weng, W.; Xia, H.; Chen, G. Multi-Responsive Self-Healing Metallo-Supramolecular Gels Based on “Click” Ligand. *J. Mater. Chem.* **2012**, *22*, 11515.

(39) Fujii, A.; Sekiguchi, Y.; Matsumura, H.; Inoue, T.; Chung, W.-S.; Hirota, S.; Matsuo, T. Excimer Emission Properties on Pyrene-Labeled Protein Surface: Correlation between Emission Spectra, Ring Stacking Modes, and Flexibilities of Pyrene Probes. *Bioconjugate Chem.* **2015**, *26*, 537–548.

(40) Lai, S.; Lee, D. G. Lewis Acid Assisted Permanganate Oxidations. *Tetrahedron* **2002**, *58*, 9879–9887.

CHAPTER SIX

Characterization of the chemistry of olympicene derivatives

Adapted with permission from: Kaitlin M. Hartung, Ellen M. Sletten. Achieving Olympicene Functionalization Three Ways. *J. Org. Chem.* **2025**, *90*, 889–893. (DOI: 10.1021/acs.joc.4c02471) Copyright 2025 American Chemical Society. Includes unpublished work.

6.1 Abstract

Polycyclic aromatic hydrocarbons (PAHs) and their derivatives are of interest in many fields, from materials science to supramolecular chemistry. 6*H*-Benzo[*cd*]pyrene, or olympicene, is a PAH bearing a central sp^3-carbon bridge. We sought methods to modify this center position while maintaining stable tetrahedral geometry. Here, we characterize reactivity patterns of three olympicene core starting materials, with two of the three leading to center functionalization of the olympicene core, including the first use of 5*H*-benzo[*cd*]pyren-5-one as an olympicene synthon.

6.2 Introduction

Polycyclic aromatic hydrocarbons (PAHs) are utilized in multiple fields, including materials science as organic electronics or sensitizers for semiconductors,[1–4] and supramolecular chemistry as noncovalent molecular recognition units.[5–7] Synthetic modifications of the shape, substitution, and/or functionalities of fused aromatic cores are essential for tailoring properties to different applications. One PAH, 6*H*-benzo[*cd*]pyrene, or olympicene, has been considered for new materials (**5.39**, Figure 6.1A). The center, or 6-position, of **5.39** bears a methylene bridge that forces the otherwise helical four-ring benzo[*c*]phenanthrene scaffold into a planar conformation.[8] This sp^3-hybridized position can react to form stabilized cationic,[9,10] anionic,[11,12] or radical[13–15] intermediates.

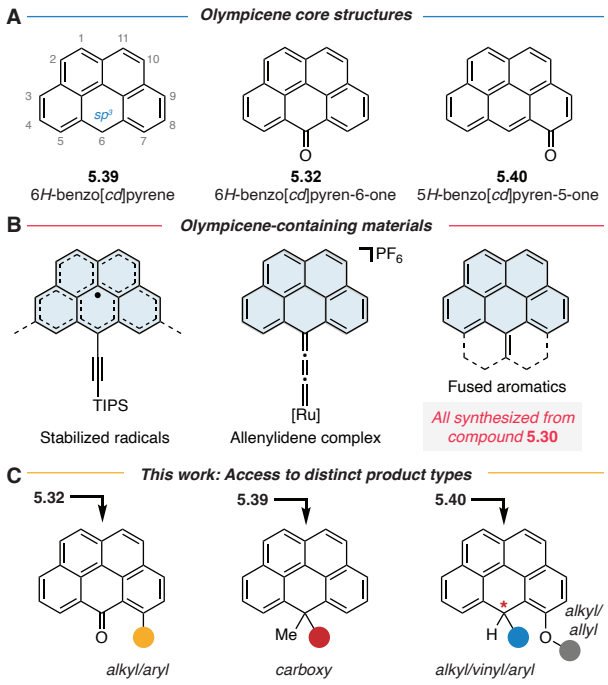

Figure 6.1 Olympicene and its derivatives. (A) Olympicene synthons, with all three accessed in a single reaction. (B) Structures previously accessed from **5.32**. (C) Present work on core substitution.

As introduced in Chapter 5, three building blocks can be accessed through a single cyclization reaction of pyrene derivative **5.38** (Figure 5.6B). Olympicene **5.39**, symmetric ketone **5.32**, and asymmetric ketone **5.40** are made in similar yields (Table 6.1, entry 1).[16] The yield of **5.32** can be increased by employing a second step to oxidize **5.39** (Table 6.1, entry 2), and the yield of **5.40** is maximized by treating **5.38** with Eaton's reagent (Table 6.1, entry 3). Finally, **5.32** can be readily reduced to **5.39** in high yield (Table 6.1, entry 4). Curiously, only ketone **5.32** has been used to synthesize new materials — including stabilized radicals,[17,18] ruthenium complexes,[19] and extended aromatic systems (Figure 6.1B)[20] — while the synthetic capabilities of **5.39** and **5.40** remain unexplored.

Entry	Reactant	Conditions	Yield of **5.39**	Yield of **5.32**	Yield of **5.40**
1	**5.38**	*a*	24%	29%	27%
2	**5.38**	*b*	0%	38%	7%
3	**5.38**	*c*	0%	<5%	40%
4	**5.32**	*d*	86%	—	—

Table 6.1 Methods to synthesize olympicene synthons. Conditions: (a) PPA, 80°C, 24 h; (b) i. PPA, 80 °C, 24 h, ii. $KMnO_4$, $FeCl_3$•6 H_2O, acetone, -78 °C, 1 h then rt, 1 h; (c) P_2O_5 in $MeSO_3H$ (Eaton's reagent), 80 °C, 24 h; (d) LAH, $AlCl_3$, THF, 0 °C to rt, 90 min.

We aimed to functionalize the center position of olympicene for molecular recognition applications (Chapter 5), where fine-tuning of structure and conformation are required. Notably, there are no syntheses where tetrahedral geometry is maintained in final products, even though strategic functionalization of this position could offer control over material properties like crystal packing or supramolecular behavior, while retaining the planarity of the benzo[*c*]phenanthrene moiety. In this work, we establish an olympicene reactivity roadmap using three different starting materials. We find that **5.32**, the widely used olympicene precursor, is a poor option for center substitution due to product instabilities, and we instead demonstrate substitution at the 5-position (Figure 6.1C). Conversely, we characterize olympicene **5.39** as a reasonable alternative for 6-position modification. Finally, we are the first to document reactivity of asymmetric ketone **5.40**, revealing simple installation of a new 6-position stereocenter and subsequent oxygen substitution. Our findings establish new synthetic procedures for functional olympicenes starting from **5.39**, **5.32**, or **5.40**.

6.3 Results and discussion

6.3.1 Chemistry of symmetric ketone

We began pursuing center functionalization with symmetric ketone **5.32**, synthesizing known propargyl alcohol **5.42** via 1,2-addition of (trimethylsilyl[TMS])acetylide (Figure 5.8A,

6.2A).[19] While this reaction went to conversion, we encountered stability issues during purification, as mentioned briefly in Chapter 5 (*vide infra*). To aid our stability investigation, we made phenylacetylene product **6.1**, removing the variable of TMS group lability. Neither **5.42** nor **6.1** was stable to purification conditions (e.g., variations of silica gel) or transformations (e.g., reduction), so we analyzed the crude products. The ^{1}H NMR spectra of both alcohols showed single, symmetric species (Figures 6.2B). However, the same samples consistently showed two peaks by liquid chromatography–mass spectrometry (LC–MS; Figure 6.2C). The mass of the first peak corresponded to oxidized product **6.2** or **6.3**[21,22] (Figures 6.2D, 6.3).[18] The second LC–MS peak's mass corresponded to a loss of water, previously reported for a similar alcohol.[23] This led us to consider formation of cationic intermediate **6.A** as a potential pathway for degradation, though other intermediates such as radicals are also possible (Figure 6.2D). Collectively, these observations led us to conclude that acetylide addition to **5.32** is unsuitable for center substitution.

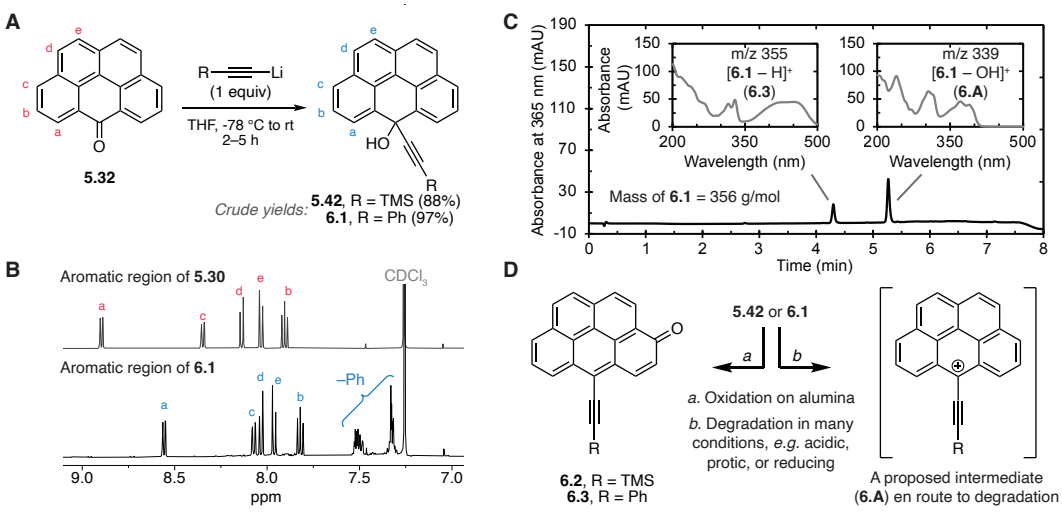

Figure 6.2 Olympicene propargyl alcohol instability. (A) Reactions of **5.32** with acetylides. (B) ^{1}H NMR spectra of **5.32** and **6.1**. (C) LC–MS analysis of **6.1**: chromatogram with insets of peak UV-vis spectra and masses. (D) Pathways to either oxidation (*a*) or degradation (*b*), with a proposed cationic intermediate.

We briefly considered further transformations of propargyl alcohols **5.42** and **6.1**. As mentioned, the oxidized products of both alcohols were characterized after attempted purification on alumina. In the case of **6.1**, brief treatment with alumina led to product **6.3**, confirmed by NMR studies and comparison to known decomposition products of related radicals (Figure 6.3A).[18] By LC–MS, the peak at 4.3 minutes for **6.3** (Figure 6.3B) matches that of **6.1** (Figure 6.2C) but without a later loss-of-water peak. This suggests **6.1** oxidizes to **6.3** (or an isomer) during electrospray ionization, a known phenomenon.[21,22] Independent UV-vis spectra of **6.1** and **6.3** show that **6.3** matches the species observed by LC–MS, while **6.1** has a trace not observed by LC–MS (Figure 6.3C).

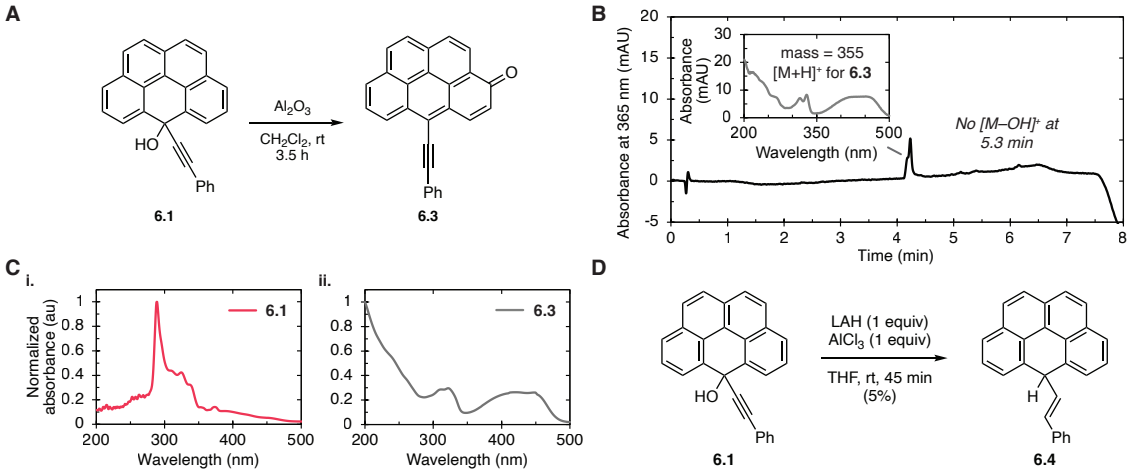

Figure 6.3 Further analysis of alcohol **6.1**. (A) Transformation of **6.1** on basic alumina to ketone **6.3**. (B) LC–MS analysis of **6.3**. (C) Normalized absorption spectra of **6.1** (i) and **6.3** (ii) in acetonitrile. Measurements were taken at concentrations with non-normalized absorbance values < 1 au in a 1-cm cuvette. (D) Reduction of **6.1**.

Given that the olympicene propargyl alcohols were unable to be purified, we briefly explored reduction of the 6-position hydroxy to a hydride to see if such a product type would be more stable. Treatment of **6.1** with lithium aluminum hydride (LAH) led to overreduction, forming alkene **6.4** (Figure 6.3D). This product did seem slightly more stable than its precursor,

as it could be isolated chromatographically on silica gel, but it still showed evidence of decomposition in a 2-D TLC experiment and decomposed when left in solution for more than a few hours.

Another attempt at reduction using $SnCl_2$, this time with alcohol **5.42**, led to a new product type entirely. While this reagent is successfully used to reduce propargyl alcohols in other aromatic systems,[24,25] it is also known to facilitate allene formation.[26,27] With **5.42**, the latter appeared to occur. By mass spectrometry, the product of this reaction appeared the same as **5.42**, suggesting a rearrangement, possibly to allene **6.5**, though with unexpected hydroxy/TMS substitution (Figure 6.4A). Of note, all **5.42** reacted, and the following analyses were done on just the isolated reaction mixture, with no further purification. A peak was identified in FTIR in the range typical for allenes and lower in frequency than expected for alkynes (Figure 6.4B).[28] The ^{1}H NMR spectrum displayed an aromatic shift pattern resembling that of **5.39**, reduced olympicene, though without a 6-position proton peak around 5 ppm (Figure 6.4C). Finally, ^{13}C NMR gives strong evidence of allene presence, with a carbon shift at 211 ppm (Figure 6.4D). This peak is much further downfield than would be expected for a carbonyl, and other similar allenes had shifts at 210 ppm or greater. Allene chemistry off aromatic scaffolds related to olympicene have been explored,[26,27] and it may be worthwhile in the materials community to pursue this avenue on olympicene scaffolds.

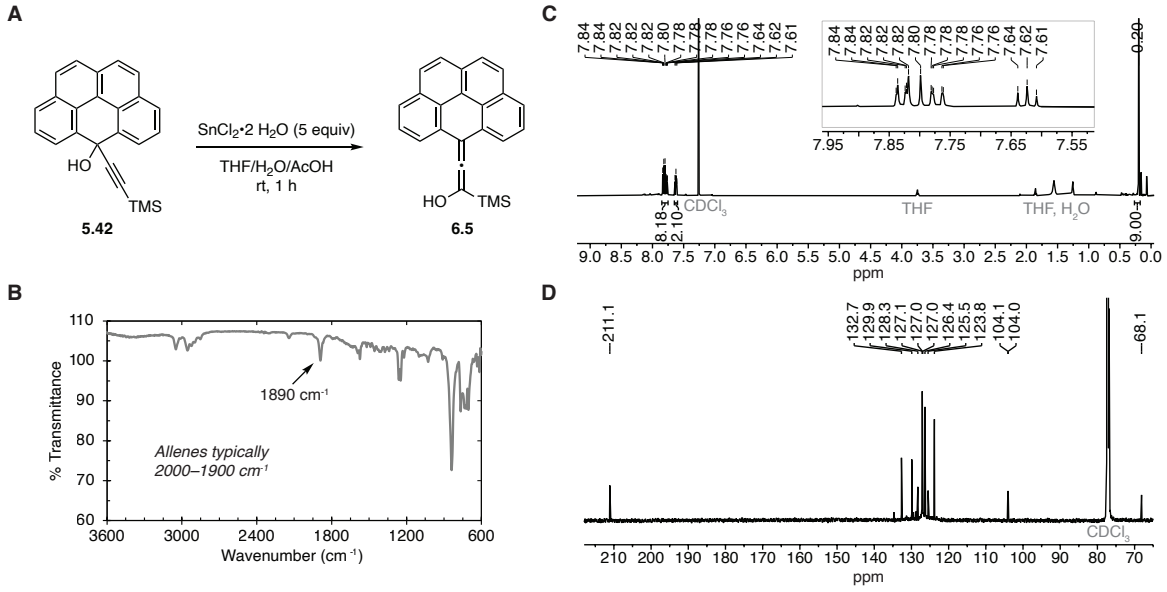

Figure 6.4 Evidence for formation of allene **6.5**. (A) Reaction scheme with proposed product. (B) FTIR spectrum of **6.5**. (C) ^{1}H NMR spectrum of **6.5**. (D) ^{13}C NMR spectrum of **6.5**.

Next, we tested if removing alkyne conjugation would make expulsion of water less likely, thus leading to less degradation, by examining alkyl additions to **5.32**. Instead of clean alcohol products from 1,2-addition, a complex mixture was obtained. Here, the only stable product isolated chromatographically was methyl-substituted **6.6** (Figure 6.5A), while a slew of other products in trace quantities was challenging to identify. Attempts to limit side reactions by keeping the reaction temperatures low were unfruitful. Formation of **6.6** presumably proceeds through an enol intermediate (**6.B**),[29–31] which is then oxidized. We tested both Grignard (MeMgBr) and organolithiate (MeLi) nucleophiles, as the former are more likely to undergo 1,4-additions than the more reactive lithiates.[32] However, the yields did not differ between reagents (Figure 6.5B).

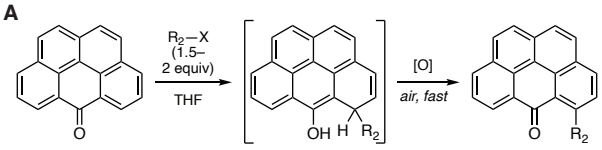

B

Product	Nucleophile	Temperature, time	Yield
6.6	MeMgBr	0 °C to rt, 3.5 h	11%
6.6	MeLi	-78 °C, 2 h to rt, 1 h	14%
6.7	PhMgBr	0 °C, 1.5 to rt, 1 h	23%
6.7	PhLi	-78 °C, 1 h to rt, 1 h	42%
–	 MgBr	0 °C, 2 h	–

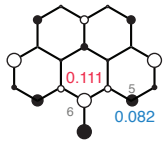

Figure 6.5 Exploring chemistry of **5.32** beyond alkyne additions. (A) Reactions of **5.32** with alkyl or aryl nucleophiles. (B) Summary of reactions. (C) LUMO densities on **5.32** with 1,2- (red) and 1,4 (blue) addition sites.

With *sp*- and sp^3-hybridized carbon nucleophiles yielding distinct results, we next looked to sp^2-hybridzed phenyl nucleophiles; these also gave the 1,4-addition/oxidation product, **6.7** (Figure 6.5A). Previously 1,4-addition had been reported with a bulkier aryl Grignard, though no hypothesis was suggested for the absence of 1,2-addition.[17] Ketone **6.7** was obtained in slightly higher yields than **6.6**, although overall yields remained low (Figure 6.5B). Finally, we attempted vinyl Grignard as a less sterically encumbered sp^2 nucleophile; however, complex reaction mixtures were observed upon $BrMgCHCH_2$ addition, with no isolable products. Overall, these results are consistent with lithiate and Grignard additions into other related aromatic ketones.[29–31,33,34]

Computation provided some insight into the observed reactivities. Considering the LUMO of **5.32**, we would expect a preference for 1,2- over 1,4-addition as the highest localization percentage is at the 1,2-addition site (6-position, Figure 6.5C). Electronic preference may be overridden by the steric effects of larger π-systems such as observed in the phenyl nucleophiles clashing with olympicene while approaching the carbonyl carbon, which could explain the increased yield of **6.7** compared to that of **6.6**. We believe that competing 1,2-

addition may still occur and contribute to the low yields of **6.6** and **6.7**, but the instability of these products precludes their identification. For acetylides, harder nucleophiles paired with slimmer steric profiles likely make 1,2-addition the most favorable. Overall, despite the precedence for **5.32** as an olympicene precursor, we deem it unideal for achieving center-functionalized products.

6.3.2 Chemistry of reduced olympicene

The most successful products from ketone **5.32** were acetylide-addition products **5.42** and **6.1**, despite stability issues. We attributed the instabilities of **5.42** and **6.1** to the labile 6-position hydroxyl and thus hypothesized that alkylation of the center position would stabilize functional olympicene derivatives. For this approach, we investigated olympicene **5.39** as a synthon. Following a single report of alkylation of **5.39**, we were able to access methyl olympicene **6.8** in 95% yield (Scheme 6.1).[35] The storage of **5.39** is limited by ready oxidation to **5.32** in air, but methylation prevents this, providing an alternative, stabilized starting material. In all conditions, **6.8** appeared stable.

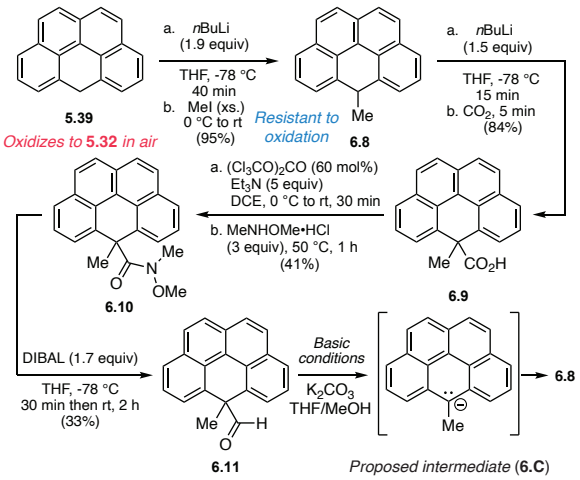

Scheme 6.1 Transformations of **5.39** and derivatives.

The further synthetic capability of **6.8** was highlighted with a second deprotonation, followed by a quench with CO_2. We were pleased to access carboxylic acid **6.9** in good yield employing a basic extraction/acidic workup sequence. Acid **6.9** was transformed to versatile Weinreb amide **6.10**, which was then readily reduced to aldehyde **6.11**. We tried to make **6.11** in a single step from **6.8** by first deprotonating with *n*BuLi, quenching with DMF, and performing an acidic workup, but saw no conversion and only returned starting material. The yields of **6.10** and **6.11** were lessened due to purification inefficiencies, but neither demonstrated significant decomposition on silica gel, in stark contrast to the 1,2-addition products from **5.32**. We further attempted to convert aldehyde **6.11** to a terminal alkyne but were unsuccessful. We we attempted to use the Bestmann−Ohira reagent, but under mildly basic conditions with K_2CO_3 we obtained **6.11** and in more basic conditions (with NaOMe) observed decomposition of starting material. We also attempted the two-step Corey−Fuchs method, but the first olefination step was unsuccessful with **6.11**. During these trials, we found that aldehyde **6.11** did not withstand basic conditions, instead returning **6.8**. We posit that a base-mediated decarbonylation occurs, proceeding through an olympicenyl anion intermediate (**6**.**C**), which is stabilized by conjugation with the benzo[*c*]phenanthrene system (Scheme 6.2).[11,36]

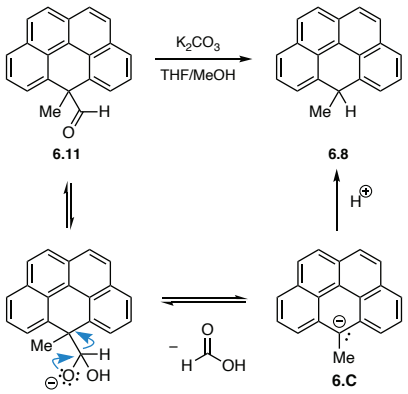

Scheme 6.2 Proposed mechanism of decarbonylation to yield **6.8** from **6.11**.

Ultimately, derivatives from **5.39** demonstrate greater stability than propargyl alcohols from **5.32**, suggesting that **5.39** is a superior choice for center substitution. Additionally, we highlight the ability to append acid, amide, and aldehyde handles to olympicene. However, we also caution that olympicene functionalization chemistry approaches should consider the potential to form highly stabilized intermediates, as evidenced by the proposed cationic (**6.A**) and anionic (**6.C**) structures.

6.3.3 Chemistry of asymmetric ketone

Finally, we examined the reactivity of asymmetric ketone **5.40**, which had remained undocumented until now. We predicted that, as with **5.32**, 1,4-addition could occur with carbon nucleophiles, and a potential 1,4-addition site on **5.40** would give center substitution. This reactivity was indeed observed with sp^3- and sp^2-hybridized nucleophiles (Figure 6.6A). Phenols **6.12**–**6.14**, resulting directly from 1,4-addition, are stable and isolable, unlike the presumed enol intermediate in previous additions (**6.B**, Figure 6.5A). Also contrasting with additions to **5.32**, we did not isolate further oxidized products. We attempted to oxidize product **6.12** by stirring in $CHCl_3$ in air and sitting in $CDCl_3$ in an NMR tube, both over multiple weeks, but did not see conversion of the phenol. We also subjected **6.12** and **6.14** to oxidizing conditions with I_2, which led to decomposition.

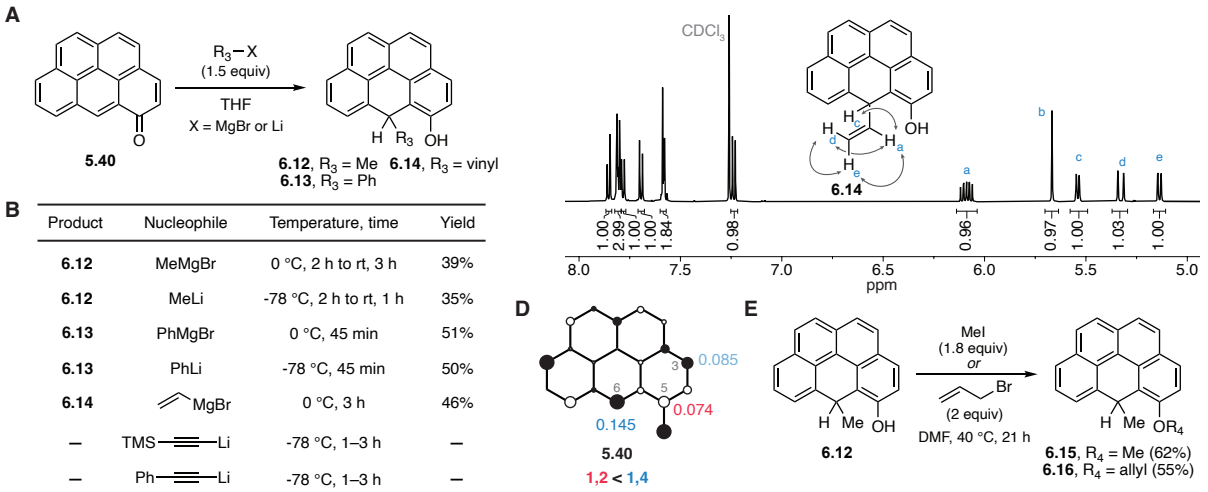

Figure 6.6 Chemistry of asymmetric ketone **5.40**. (A) Reactions of **5.40** with carbon nucleophiles. (B) Summary of reactions. (C) ^{1}H NMR spectrum of **6.14** highlighting coupling of protons in the vinyl region. (D) LUMO densities on **5.40** with 1,4-addition (blue), alternative 1,4-addition (light blue), and 1,2-addition (red) sites. (E) Reactions of **6.12**.

Employing a Grignard or organolithiate did not alter the resulting products, with methyl-substituted **6.12** and phenyl-substituted **6.13** accessed in similar yields with either organometallic reagent (Figure 6.6B). Curiously, vinyl Grignard reacted to give **6.14**, in contrast to the poor results with **5.32**. The ^{1}H NMR spectrum of **6.14** clearly showed the expected vinyl coupling pattern in addition to a new allylic proton, H_c, while a former singlet in the aromatic region had disappeared (Figure 6.6C). To complete the comparison between **5.32** and **5.40**, we attempted acetylide additions (Figure 6.6B). In stark contrast to **5.32**, acetylides reacted messily with **5.40**, producing complex mixtures even at reduced temperatures. For all addition reactions into **5.40**, the temperature was kept low to minimize side products, which at times prevented complete conversion. While these reactions were overall cleaner than additions to **5.32** and the products could be purified on silica gel, the isolated yields were still moderate. We cannot completely rule out instability on silica gel or reaction pathways other than 1,4-addition.

The computed LUMO densities of **5.40** show a sizable localization at the center position (Figure 6.6D). The large difference in LUMO between the center 1,4-addition site (6-position),

alternative 1,4-addition site (3-position), and 1,2-addition site (5-position) suggests reactivity at the latter two are unlikely competing pathways, as reflected by the overall higher yields for **5.40** compared to **5.32**. The low orbital character at the 1,2-site may also explain why acetylides, which show a greater tendency toward 1,2-additions, do not react cleanly with **5.40**. We did not observe loss-of-water masses on LC–MS for additions to **5.40,** further suggesting 1,2-addition and subsequent carbocation formation are unlikely. The relative differences between 1,2- and 1,4-positions are much closer in the symmetric (**5.32**) case, with the 1,2-position slightly higher, providing support to the competing 1,2-/1,4-additions hypothesis above (Figure 6.5C). Competing or unexpected 1,2-/1,4-additions have been investigated in similar systems.[30,31,37,38] Overall, the stabilities of **6.12**‑**6.14** were satisfactory, with **5.40** excitingly establishing a new olympicene stereocenter at the center position in one step.

The 1,4-addition into ketone **5.40** not only provides functionalization at the bridge position but also introduces an oxygen substituent at the 5-position. To probe the usefulness of this new functional handle, we further transformed phenol **6.12** (Figure 6.6E). Alkylation and allylation proceeded readily under standard conditions to give **6.15** and **6.16**, respectively. The crystal structure of **6.15** also shows the newly installed chiral center at the 6-position (Scheme 6.3). This brief foray into phenol functionalization suggests there are ample opportunities for elaborating from olympicene **5.40**.

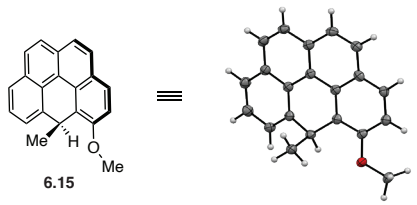

Scheme 6.3 Crystal structure of **6.15**. Ellipsoids are set at 50% probability.

We briefly considered other types of reactions with ketones **5.32** and **5.40**. Interestingly, bromination of **5.40** proceeded readily to give alpha-substituted **6.17**, while no reactivity was observed between NBS and symmetric ketone **5.32** (Scheme 6.4). The newly installed bromine atom proved useful in Suzuki-Miyaura cross-coupling, with product **6.18** accessed readily from **6.17** and phenylboronic acid. The limited work on cross-coupling off olympicene scaffolds, and the near-complete lack of chemistry known starting from **5.40**, make this type of chemistry an exciting future avenue for olympicene derivatization.

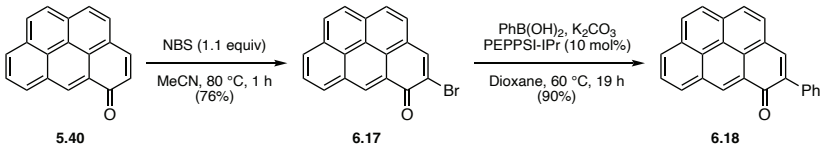

Scheme 6.4 Bromination of **5.40** and subsequent cross-coupling. PEPPSI-IPr = [1,3-Bis(2,6-Diisopropylphenyl)imidazol-2-ylidene](3-chloropyridyl)palladium(II) dichloride.

Finally, we considered the photophysical properties of **6.17** after observing fluorescence in different solvents (Figure 6.7A). There are a few examples of asymmetric ketone **5.40** being used as a photosensitizer,[39,40] including in cells,[41] which suggests there may be interest in exploring its derivatives. Additionally, derivatives of related aromatic ketones phenalenone and benzanthrone have been employed as fluorescent probes and for solvatochromism studies.[42–45]

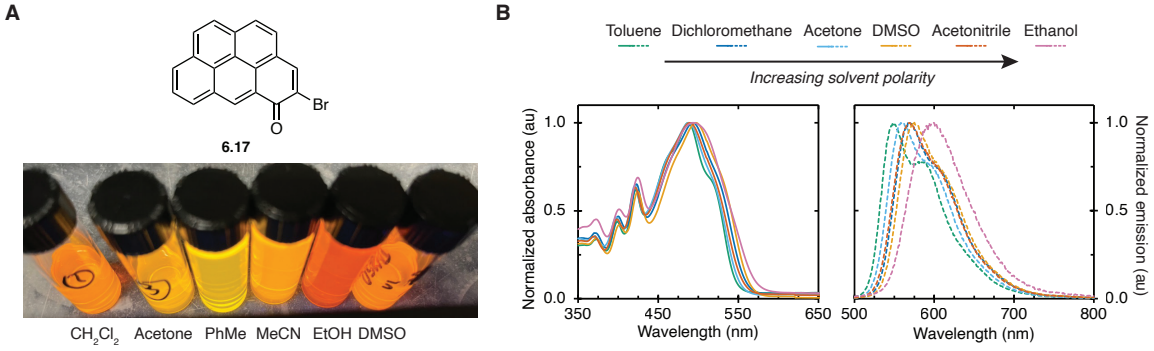

Figure 6.7 Preliminary photophysical investigation of **6.17**. (A) Solutions of **6.17** visualized under long-wave UV light. (B) Absorption (left) and emission (right, λ_{ex} 480 nm) spectra of **6.17** in

solvents of varying polarities. Absorbance-matched measurements were taken at concentrations with non-normalized absorbance intensities < 1 au in a 1-cm cuvette.

For **6.17**, the λ_{max} of absorption doesn't shift much with changing solvent polarity while the λ_{max} of emission does (Figure 6.7B). The largest switch, from nonpolar PhMe to polar EtOH, results in a 51-nm redshift in emission wavelength. Based on work with benzanthrone derivatives, substituting the bromine handle with sulfur- or nitrogen-containing substituents may increase this difference and lead to useful polarity-responsive probes. Ultimately, the chemistry of asymmetric ketone **5.40** and the properties of its derivatives is a vastly underexplored space ready for discovery.

6.4 Conclusion

In conclusion, the olympicene scaffold has potential for new applications in fields ranging from supramolecular chemistry to organic electronics, but to be fully realized, methods to achieve new substitution patterns and access stabilized structures are needed. We have expanded the reactivity knowledge of three olympicene compounds for functionalizing directly off the olympicene core, demonstrating distinct product types accessible from starting compounds **5.39**, **5.32**, and **5.40**. In particular, compounds **5.39** and **5.40** displayed the most successful functionalization at the advantageous sp^3 center of olympicene. Additionally, our first exploration of the synthetic utility of **5.40** and properties of its synthetic derivatives should ignite further pursuit of this synthon. The results presented here, from new products to limitations, will guide others utilizing these core scaffolds for the development of olympicene-containing materials.

6.5 Experimental Procedures

6.5.1 Synthetic abbreviations and chemical formulas

Acetonitrile (MeCN); Aluminum chloride ($AlCl_3$); Ammonium chloride (NH_4Cl); *n*-Butyllithium (*n*BuLi); Carbon dioxide (CO_2); Chloroform ($CHCl_3$); Direct analysis in real time (DART); Diisobutylaluminum hydride (DIBAL); 1,2-Dichloroethane (DCE); Dichloromethane (CH_2Cl_2); Diethyl ether (Et_2O); Dimethylformamide (DMF), Electrospray ionization (ESI); Ethanol (EtOH); Ethyl acetate (EtOAc); High-resolution mass spectrometry (HRMS); Hydrochloric acid (HCl); Iron(III) chloride ($FeCl_3$); Liquid chromatography–mass spectrometry (LC–MS); Lithium aluminum hydride (LAH); Lithium bis(trimethylsilyl)amide (LHMDS); Low-resolution mass spectrometry (LRMS); Magnesium sulfate ($MgSO_4$); Megahertz (MHz); Methanol (MeOH); Methyllithium (MeLi); Methylmagnesium bromide or methyl Grignard (MeMgBr); *N*-Bromosuccinimide (NBS); Nitrogen gas (N_2); Phenyllithium (PhLi); Phenylmagnesium bromide or phenyl Grignard (PhMgBr); Polyphosphoric acid (PPA); Potassium carbonate (K_2CO_3); Potassium permanganate ($KMnO_4$); Sodium bicarbonate ($NaHCO_3$); Sodium hydroxide (NaOH); Sodium sulfite (Na_2SO_3); Sodium sulfate (Na_2SO_4); Sodium thiosulfate ($Na_2S_2O_3$); Tetrahydrofuran (THF); Tin(II) chloride ($SnCl_2$); Toluene (PhMe); Trimethylsilyl (TMS); Ultraviolet-visible (UV-vis).

6.5.2 Materials and instrumentation

Chemical reagents were purchased from Alfa Aesar, Sigma-Aldrich, Fisher Scientific, Acros Organics, TCI, Oakwood Chemicals, or Combi-Blocks and used without purification, unless otherwise noted. Reagents and products were weighed on a Sartorius ENTRIS224-1S Analytical Balance (220 x 0.0001 g). Anhydrous, deoxygenated solvents CH_2Cl_2, DMF, MeCN, MeOH,

PhMe, and THF were dispensed from a Grubb's-type Phoenix Solvent Drying System. Thin-layer chromatography (TLC) was performed using silica gel 60 F_{254} (EMD Millipore) plates (0.5 mm thickness for preparative TLC) and visualized under short- and/or long-wave UV light (UVGL-25, 254/365 nm). Flash column chromatography was performed using technical grade silica gel with 60 Å pores and 40–63 μm mesh particle size (Sorbtech Technologies) or aluminum oxide (alumina; basic, 50–200 μm, 60 Å pores [Acros Organics]). Solvent was removed under reduced pressure with a Büchi or Ika Rotovapor with a Welch self-cleaning dry vacuum pump and further dried with a Welch DuoSeal pump attached to a Schlenk manifold. NMR spectra were recorded on Bruker NEO-600 (^{1}H and ^{13}C), Bruker AV-500 (^{1}H and ^{13}C), Bruker DRX-500 (^{1}H), and Bruker AV-400 (^{1}H and ^{13}C) instruments and processed with MestReNova software. Samples were taken in deuterated chloroform ($CDCl_3$), and NMR peaks were calibrated using residual non-deuterated solvent ($CHCl_3$ at 7.26 ppm ^{1}H NMR, 77.16 ppm ^{13}C NMR). Multiplicities are as indicated: s (singlet), d (doublet), dd (doublet of doublets), ddd (doublet of doublets of doublets), ddt (doublet of doublet of triplets), dq (doublet of quartets), dt (doublet of triplets), tt (triplet of triplets), t (triplet), q (quartet), and m (multiplet). Coupling constants, *J*, are reported in Hz and integrations are provided. LRMS (electrospray ionization [ESI]) were collected on an Agilent 1260 Infinity II HPLC-tandem MS system with InfinityLab Poroshell 120 EC-C8 column (3.0 x 50 mm, 2.7 μm). LC method: gradient of 40% MeCN in water to 95% over 5.5 min, 95% MeCN over 2 min, then back to 40% MeCN over 0.5 min, after first equilibrating with 40% MeCN/water. HRMS (ESI-MS) were collected on an Agilent 6545 Q-TOF LC/MS with 1260 Infinity LC. HRMS (DART-MS) were collected on a Thermo Exactive Plus Orbitrap with IonSense ID-CUBE DART source and a Vapur Interface (IonSense Inc.), with samples in CH_2Cl_2 spotted onto OpenSpot sample cards (IonSense Inc.) and

ionization performed using UHP He plasma. Absorbance spectra were collected on a JASCO V-770 UVVis/NIR spectrophotometer with a 4000 nm/min scan rate, 2-nm step size, and 800–200 nm spectral range in a 1-cm fused quartz cuvette (ThorLabs) after blanking with the appropriate solvent. Fluorescence was measured on a Horiba Instruments PTI QuantaMaster Series fluorometer with the following settings: 480-nm excitation, collection window 500–800 nm, 25-mm neutral density filter, slit width 5 nm, step size 1 sec, integration time 0.1 sec.

6.5.3 Note on observed masses

Many compounds (**6.1**, **6.8**, **6.12**, **6.13**, **6.14**, and **6.15**) were observed with oxidized masses by LRMS and HRMS (both ESI). This has been reported for other related compounds observed via electrospray ionization.[21,22,46,47]

6.5.4 Synthetic experimental procedures

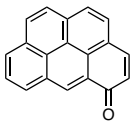

5.40

5*H*-benzo[*cd*]pyren-5-one (5.40) *via* Eaton's reagent (*new procedure to access* 5.40 *in greater yields*). To an oven-dried, 20-mL scintillation vial was added 3-(pyren-1-yl)propanoic acid **5.38** (104 mg, 0.379 mmol, 1.00 equiv), followed by Eaton's reagent (7.5% w/w P_2O_5 in methanesulfonic acid) (1.5 mL, 0.25 M). The mixture was stirred at 80 °C in an aluminum reaction block for 24 h. The solution was cooled to room temperature, then poured into a beaker with ice (mixture was diluted and rinsed with H_2O [10 mL] and CH_2Cl_2 [5 ml] for transfer). The solution was neutralized with saturated aqueous $NaHCO_3$ (checked via pH paper) and extracted with CH_2Cl_2 (5 x 20 mL). The combined organic layers were washed with brine (1 x 10 mL),

dried ($MgSO_4$), filtered, and concentrated under reduced pressure. The crude product was purified by column chromatography (the crude material was evaporated onto silica gel; silica gel column, 5% EtOAc/heptane) to give **5.40** as a red solid (38 mg, 0.15 mmol, 40%). The spectral data were consistent with those reported in Chapter 5.

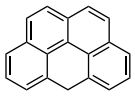

5.39

6*H*-benzo[*cd*]pyrene (5.39) via reduction of 5.32. Following the literature procedure,[48] $AlCl_3$ (266 mg, 1.99 mmol, 4.05 equiv) and anhydrous THF (3.0 mL, 0.66 M with respect to $AlCl_3$) were added to a flame-dried, 50-mL round-bottom flask. The solution was cooled to 0 °C, then LAH (1 M in THF, 2.0 mL, 2.0 mmol, 4.1 equiv) was added dropwise. The cloudy solution was stirred at 0 °C for five minutes before the addition of 6*H*-benzo[*cd*]pyren-6-one (**5.32**) (125 mg, 0.492 mmol, 1.00 equiv) dissolved in anhydrous THF (5 mL, 0.1 M) via syringe. The ice bath was removed, and the reaction was stirred at room temperature for 90 minutes (consumption of starting material was monitored by TLC, 25% EtOAc in hexanes). In contrast to the literature procedure, the Fieser workup[49] was employed to quench the reaction and isolate clean product: Et_2O was added (7 mL) and the solution was cooled to 0 °C. The following were added, in order, to the cooled solution: water (75 µL), 15% aqueous NaOH (75 µL), and then water (225 µL). The ice bath was removed, and the solution stirred at room temperature for 15 minutes. A spatula-tip amount of $MgSO_4$ was added and the solution was stirred for 5 minutes before filtering through celite and concentrating to give **5.39** as an off-white solid (102 mg, 0.424 mmol, 86%). Full conversion was indicated by TLC and ^1H NMR, and the product was stored

under N_2 and used quickly in next steps to avoid background oxidation to **5.32**. The spectral data were consistent with those reported in Chapter 5.

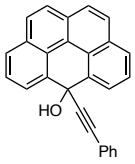

6.1

6-(phenylethynyl)-6*H*-benzo[*cd*]pyren-6-ol (6.1). To make 0.2 M phenylacetylide solution: to a flame-dried, 15-mL two-neck flask was added anhydrous THF (0.35 mL), followed by phenylacetylene (11 µL, 0.10 mmol, 1.0 equiv). The solution was cooled to -78 °C in a dry ice/acetone bath, then LHMDS (1.0 M, 0.15 mL, 0.15 mmol, 1.5 equiv) was added and the mixture was stirred at -78 °C for 30 minutes to give lithium phenylacetylide solution. *Note: this acetylide was also made using* n-*BuLi instead of LHMDS.*

6*H*-Benzo[*cd*]pyren-6-one **5.32** (10.2 mg, 0.0401 mmol, 1.00 equiv) was added to a separate flame-dried 10-mL flask, followed by anhydrous THF (0.4 mL, 0.1 M). The solution was cooled to -78 °C in a dry ice/acetone bath. Phenylacetylide (0.2 M, 0.2 mL, 0.04 mmol, 1 equiv) was then added dropwise. The reaction was allowed to warm to room temperature and then stirred for 2 h. The reaction was quenched with saturated aqueous NH_4Cl (2 mL), then extracted with CH_2Cl_2 (3 x 2 mL). The combined organic layers were dried (Na_2SO_4), filtered, and concentrated to give **6.1** as a dark brown solid (14 mg, 0.039 mmol, 97%). R_f = 0.2 in 10% EtOAc/hexanes. ^{1}H NMR (500 MHz, $CDCl_3$) δ 8.56 (dd, *J* = 7.5, 1.2 Hz, 2H), 8.06 (dd, *J* = 8.0, 1.2 Hz, 2H), 8.02 (d, *J* = 8.7 Hz, 2H), 7.95 (d, *J* = 8.7 Hz, 2H), 7.82 (dd, *J* = 8.0, 7.4 Hz, 2H), 7.55 – 7.49 (m, 2H), 7.33 (dd, *J* = 5.1, 1.9 Hz, 3H), 2.87 (–OH, s, 1H) ppm. ^{13}C NMR (126 MHz, $CDCl_3$) δ 136.8, 131.8, 131.4, 129.6, 129.0, 128.7, 128.4, 127.8, 127.1, 126.9, 124.3, 122.7, 122.2, 92.9, 88.6,

69.2 ppm. HRMS (APCI/DART) m/z: $[M–OH]^+$ calcd for $C_{27}H_{15}^+$ $[M–OH]^+$: 339.1168; found 339.1174. $\lambda_{max,abs}$ (CH_2Cl_2): 289 nm.

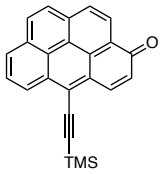

6.2

6-((trimethylsilyl)ethynyl)-3*H*-benzo[*cd*]pyren-3-one (6.2). 6-((Trimethylsilyl)ethynyl)-6*H*-benzo[*cd*]pyren-6-ol (**5.42**) (19 mg, 0.054 mmol) was evaporated onto basic alumina and loaded onto a column also packed with basic alumina. The column was eluted with 10% EtOAc/hexanes. Unreacted ketone **5.32** was obtained in fractions mixed with **6.2** (6.1 mg total). Oxidized product **6.2** was obtained as a dark green solid (4.4 mg, 0.013 mmol, 23%). R_f = 0.1 in 10% EtOAc/hexanes. ^{1}H NMR (500 MHz, $CDCl_3$) δ 8.95 (d, *J* = 8.1 Hz, 1H), 8.94 (dd, *J* = 7.7, 1.0 Hz, 1H), 8.62 (d, *J* = 9.9 Hz, 1H), 8.43 (dd, *J* = 7.6, 0.7 Hz, 1H), 8.38 (d, *J* = 8.1 Hz, 1H), 8.28 (d, *J* = 8.9 Hz, 1H), 8.21–8.16 (m, 2H), 7.01 (d, *J* = 9.9 Hz, 1H), 0.47 (s, 9H) ppm. ^{13}C NMR (126 MHz, $CDCl_3$) δ 185.7, 139.3, 135.1, 130.8, 130.5, 130.4, 130.1, 130.0, 129.8, 128.9, 127.6, 127.4, 126.9, 126.6, 126.5, 126.2, 126.1, 123.5, 122.7, 111.0, 100.0, 0.1 ppm. HRMS (ESI/Q-TOF) m/z: $[M+H]^+$ calcd for $C_{24}H_{19}OSi^+$ 351.1205; found 351.1216. $\lambda_{max,abs}$ (CH_2Cl_2): 232 nm.

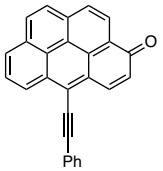

6.3

6-(phenylethynyl)-3*H*-benzo[*cd*]pyren-3-one (6.3). 6-(Phenylethynyl)-6*H*-benzo[*cd*]pyren-6-ol (**6.1**) (5.3 mg, 0.015 mmol) was evaporated onto basic alumina and loaded onto a column packed with basic alumina. The column was eluted with 25% EtOAc/hexanes. Clean oxidized product **6.3** was obtained as a yellow-brown solid (1.6 mg, 0.0045 mmol, 30%). R_f = 0.4 in 25% EtOAc/hexanes. ^{1}H NMR (600 MHz, $CDCl_3$) δ 9.01 (dd, *J* = 7.8, 1.1 Hz, 1H), 8.93 (d, *J* = 8.0 Hz, 1H), 8.69 (d, *J* = 9.9 Hz, 1H), 8.42 (dd, *J* = 7.6, 1.5 Hz, 1H), 8.35 (d, *J* = 8.2 Hz, 1H), 8.26 (d, *J* = 8.8 Hz, 1H), 8.18 (d, *J* = 8.8 Hz, 1H), 8.17 (dd, *J* = 7.9, 7.5 Hz, 1H), 7.85 – 7.81 (m, 2H), 7.53 – 7.50 (m, 3H), 7.01 (d, *J* = 9.8 Hz, 1H) ppm. ^{13}C NMR (126 MHz, $CDCl_3$) δ 185.7, 139.2, 135.1, 132.2, 130.8, 130.5, 130.3, 130.0, 129.83, 129.79, 129.5, 128.9, 128.8, 127.7, 127.4, 126.8, 126.7, 126.6, 126.5, 126.2, 123.6, 122.7, 122.5, 104.3, 85.2 ppm. HRMS (ESI/Q-TOF) m/z: $[M+H]^+$ calcd for $C_{27}H_{15}O^+$ 355.1123; found 355.1125. $\lambda_{max,abs}$ (CH_2Cl_2): 236 nm.

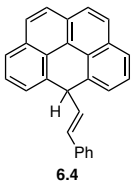

6.4

(*E*)-6-styryl-6*H*-benzo[*cd*]pyrene (6.4). To a flame-dried, 10-mL pear-shaped flask was added anhydrous THF (0.1 mL), followed by LAH (1 M in THF, 0.06 mL, 0.06 mmol, 1 equiv) and $AlCl_3$ (1 M in THF, 0.06 mL, 0.06 mmol, 1 equiv). The mixture was stirred for five minutes (bubbled for first minute), then **6.1** (20 mg, 0.06 mmol, 1 equiv) was added in anhydrous THF

(0.44 mL, 0.1 M). The mixture was stirred at room temperature for 45 minutes. The Fieser workup[49] was employed to quench the reaction: Et_2O was added (2 mL) and the solution cooled to 0 °C. The following were added, in order, to the cooled solution: water (3 μL), 15% aqueous NaOH (3 μL), and water (9 μL). The ice bath was removed and the solution stirred at room temperature for 15 minutes. A small amount of $MgSO_4$ was added; the solution was stirred for 5 minutes before filtering through celite and concentrating. The crude mixture was purified by preparative TLC (blank plate run first in 25% EtOAc/hexanes + 0.5% triethylamine, dried, loaded, run in 25% EtOAc/hexanes) to give **6.3** as a brown solid (0.9 mg, 0.003 mmol, 5% yield). R_f = 0.77 in 25% EtOAc/hexanes. ^{1}H NMR (500 MHz, $CDCl_3$): δ 7.90 – 7.83 (m, 4H), 7.81 (dt, *J* = 7.9, 1.2 Hz, 2H), 7.66 – 7.62 (m, 2H), 7.60 – 7.54 (m, 2H), 7.39 – 7.35 (m, 2H), 7.28 (d, *J* = 7.2 Hz, 2H), 7.23 – 7.17 (m, 1H), 6.63 (d, *J* = 15.6 Hz, 1H), 6.46 (dd, *J* = 15.6, 8.8 Hz, 1H), 5.63 (d, *J* = 8.9 Hz, 1H) ppm. ^{13}C NMR (126 MHz, $CDCl_3$): δ 137.2, 136.1, 134.8, 132.0, 129.0, 128.7, 127.5, 127.3, 127.3, 127.0, 126.9, 126.7, 126.6, 126.5, 125.0, 48.2 ppm. HRMS (APCI/DART) m/z: $[M - H]^+$ calcd for $C_{27}H_{17}^+$ 341.1330; found 341.1309.

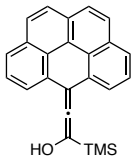

6.5

2-(6*H*-benzo[*cd*]pyren-6-ylidene)-1-(trimethylsilyl)ethen-1-ol (6.5). Alcohol **5.42** (10.8 mg, 0.0306 mmol, 1.00 equiv) was added to an oven-dried dram vial and dissolved in anhydrous THF (0.2 mL, 0.2 M). This solution was added to a new dram vial containing $SnCl_2 \bullet 2\ H_2O$ (32.0 mg, 0.142 mmol, 4.64 equiv), H_2O (0.05 mL) and AcOH (0.05 mL). The reaction was stirred at room

temperature for 1 hour. The mixture was added to H_2O (1 mL) and extracted with CH_2Cl_2 (4 x 2 mL). The combined organic layers were washed with aqueous NaOH (1 M, 1 x 1 mL), then dried (Na_2SO_4), filtered, and concentrated to give **6.5** as a dark green solid (5 mg, 45% yield). ^{1}H NMR (500 MHz, $CDCl_3$): δ 7.85 – 7.75 (m, 8H), 7.62 (t, *J* = 7.7 Hz, 2H), 0.20 (s, 8H) ppm. ^{13}C NMR (126 MHz, $CDCl_3$): δ 211.0, 132.6, 129.8, 128.1, 127.0, 126.9, 126.8, 126.2, 125.4, 123.7, 103.9, 103.8, 68.0, -0.6 ppm. IR 3048, 2953, 1890, 1247, 839 cm^{-1}. HRMS (APCI/DART) m/z: $[M - H]^+$ calcd for $C_{24}H_{19}OSi^+$ 351.1205; found 351.1195.

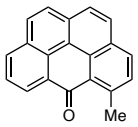

6.6

5-methyl-6*H*-benzo[*cd*]pyren-6-one (6.6) via Grignard reagent. 6*H*-Benzo[*cd*]pyren-6-one **5.32** (13.7 mg, 0.0539 mmol, 1.00 equiv) was added to a flame-dried, 15-mL two-neck flask, then was purged and backfilled with N_2 three times. Anhydrous THF (0.8 mL, 0.07 M) was added and the solution cooled to 0 °C once **5.32** had dissolved. MeMgBr (1.5 M in THF, 0.05 mL, 0.08 mmol, 2 equiv) was added dropwise at 0 °C. The ice bath was removed and the mixture was stirred at room temperature for 3.5 h. Saturated aqueous NH_4Cl (2 mL) was added and the aqueous layer extracted with CH_2Cl_2 (3 x 3 mL). The combined organic layers were then dried (Na_2SO_4), filtered, and concentrated. The crude mixture was purified by preparative TLC (25% EtOAc/hexanes) to give **6.6** as an orange solid (1.6 mg, 0.0060 mmol, 11%). R_f = 0.4 in 10% EtOAc/hexanes. ^{1}H NMR (500 MHz, $CDCl_3$): δ 8.86 (dd, *J* = 7.5, 1.3 Hz, 1H), 8.32 (dd, *J* = 7.9, 1.3 Hz, 1H), 8.20 (d, *J* = 8.1 Hz, 1H), 8.11 (d, *J* = 8.7 Hz, 1H), 8.10 (d, *J* = 8.6 Hz, 1H), 8.01 (d,

J = 8.7 Hz, 1H), 7.99 (d, *J* = 8.6 Hz, 1H), 7.90 (t, *J* = 7.7 Hz, 1H), 7.70 (d, *J* = 8.7 Hz, 1H), 3.18 (s, 3H) ppm. ^{13}C NMR (126 MHz, $CDCl_3$) δ 186.3, 145.9, 134.1, 133.7, 132.3, 132.2, 131.03, 131.02, 130.1, 129.4, 128.9, 128.9, 128.3, 127.9, 127.4, 127.2, 126.9, 126.3, 121.4, 25.3 ppm. HRMS (APCI/DART) m/z: $[M + H]^+$ calcd for $C_{20}H_{13}O^+$ 269.0966; found 269.0969. $\lambda_{max,abs}$ (CH_2Cl_2): 303 nm.

5-methyl-6*H*-benzo[*cd*]pyren-6-one (6.6) via organolithium reagent. 6*H*-Benzo[*cd*]pyren-6-one **5.32** (13.5 mg, 0.0531 mmol, 1.00 equiv) was added to a flame-dried 15-mL, two-neck flask, which was then purged and backfilled with N_2 three times. Anhydrous THF (0.5 mL, 0.1 M) was added and the solution was cooled to -78 °C in a dry ice/acetone bath. While at -78 °C, MeLi (1.6 M in Et_2O, 0.05 mL, 0.08 mmol, 2 equiv) was added dropwise; the solution went from a bright orange color to a dark yellow-brown. This was stirred at -78 °C for 2 h, then warmed to room temperature and stirred for an additional hour. The solution was then cooled to 0 °C and quenched by addition of saturated aqueous NH_4Cl (2 mL). After warming to room temperature, the aqueous layer was extracted with CH_2Cl_2 (3 x 3 mL), then the combined organic layers were dried (Na_2SO_4), filtered, and concentrated. The crude mixture was purified by preparative TLC (10% EtOAc in hexanes) to give **6.6** as an orange solid (2.0 mg, 0.0075 mmol, 14%). R_f = 0.4 in 10% EtOAc/hexanes. The spectral data were consistent with those listed above.

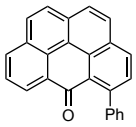

6.7

5-phenyl-6*H*-benzo[*cd*]pyren-6-one (6.7) via Grignard reagent. 6*H*-Benzo[*cd*]pyren-6-one **5.32** (9.9 mg, 0.039 mmol, 1.0 equiv) was added to a flame-dried, 15-mL two-neck flask, then purged and backfilled with N_2 three times. Anhydrous THF (0.56 mL, 0.070 M) was added, and the solution was cooled to 0 °C once **5.32** had dissolved. PhMgBr (0.5 M in THF, 0.12 mL, 0.060 mmol, 1.5 equiv) was added dropwise at 0 °C. The mixture was stirred at 0 °C for 1.5 h, then allowed to warm to room temperature. Saturated aqueous NH_4Cl (2 mL) was added and the aqueous layer extracted with CH_2Cl_2 (3 x 3 mL). The combined organic layers were then dried (Na_2SO_4), filtered, and concentrated. The crude mixture was purified by preparative TLC (10% EtOAc/hexanes) to give **6.7** as an orange solid (3.0 mg, 0.0091 mmol, 23%). R_f = 0.3 in 10% EtOAc/hexanes. ^{1}H NMR (500 MHz, $CDCl_3$) δ 8.70 (dd, *J* = 7.5, 1.2 Hz, 1H), 8.30 (d, *J* = 8.0 Hz), 8.29 (dd, *J* = 7.8, 1.3), 8.14 (d, *J* = 8.6 Hz, 1H), 8.12 (d, *J* = 8.7 Hz, 1H), 8.05 (d, *J* = 8.5 Hz), 8.03 (d, *J* = 8.5 Hz), 7.83 (dd, *J* = 8.0, 7.3 Hz, 1H), 7.69 (d, *J* = 8.1 Hz, 1H), 7.55 – 7.51 (m, 2H), 7.49 – 7.45 (m, 3H) ppm. ^{13}C NMR (126 MHz, $CDCl_3$) δ 184.7, 146.8, 144.1, 134.0, 133.5, 132.5, 131.4, 131.1, 130.98, 130.96, 129.4, 129.3, 128.8, 128.6, 128.3, 128.1, 128.0, 127.3, 127.3, 127.1, 127.1, 126.8, 121.9 ppm. HRMS (ESI/Q-TOF) m/z: $[M+H]^+$ calcd for $C_{25}H_{15}O^+$ 331.1123; found 331.1148. The ^{1}H NMR spectral data were consistent with a literature report (^{13}C NMR, HRMS data were not previously reported, and the product was made with different starting materials).[50]

5-phenyl-6*H*-benzo[*cd*]pyren-6-one (6.7) via organolithium reagent. 6*H*-Benzo[*cd*]pyren-6-one **5.32** (9.5 mg, 0.037 mmol, 1.0 equiv) was added to a flame-dried 15-mL, two-neck flask,

which was then purged and backfilled with N_2 three times. Anhydrous THF (0.5 mL, 0.07 M) was added, and the solution was cooled to -78 °C in a dry ice/acetone bath. While at -78 °C, PhLi (0.6 M in THF, 0.10 mL, 0.060 mmol, 1.6 equiv) was added dropwise; the solution went from a bright orange to a dark yellow-brown color. This was stirred at -78 °C for 1 h, then warmed to room temperature and stirred an additional 1 h. The solution was then quenched by addition of saturated aqueous NH_4Cl (2 mL). The aqueous layer was extracted with CH_2Cl_2 (3 x 2 mL), and the combined organic layers were then dried (Na_2SO_4), filtered, and concentrated. The crude product was purified by preparative TLC (10% EtOAc in hexanes) to give **6.7** as a yellow solid (5.0 mg, 0.015 mmol, 42%). R_f = 0.3 in 10% EtOAc/hexanes. The spectral data were consistent with those listed above.

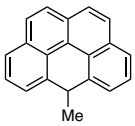

6.8

6-methyl-6*H*-benzo[*cd*]pyrene (6.8). 6*H*-Benzo[*cd*]pyrene **5.39** (95.4 mg, 0.397 mmol, 1.00 equiv) was added to a flame-dried, 25-mL, 2-neck round-bottom flask, which was then purged and backfilled with N_2 three times. Anhydrous THF (4.0 mL, 0.10 M) was added, and the solution was cooled to -78 °C in a dry ice/acetone bath. While at -78 °C, *n*-BuLi (1.5 M in hexanes, 0.50 mL, 0.75 mmol, 1.9 equiv) was added dropwise. The solution was stirred at -78 °C for 40 min, then MeI (0.25 mL, 4.0 mmol, 10 equiv) was added to quench the reaction. The quenched reaction was stirred at -78 °C for 20 min, then allowed to warm to room temperature and stirred an additional 20 min. Water (3 mL) and saturated aqueous NH_4Cl (1 mL) were added. The aqueous layer was extracted with CH_2Cl_2 (3 x 5 mL), and then the combined organic layers were dried (Na_2SO_4), filtered, and concentrated to give **6.8** as an orange solid (96 mg, 0.38

mmol, 95%). R_f = 0.8 in 25% EtOAc/hexanes. ^{1}H NMR (500 MHz, $CDCl_3$): δ 7.89 (d, *J* = 8.7 Hz, 2H), 7.85 (d, *J* = 8.7 Hz, 2H), 7.81 (dd, *J* = 7.4, 1.8 Hz, 2H), 7.63 – 7.56 (m, 4H), 4.85 (q, *J* = 7.4 Hz, 1H), 1.62 (d, *J* = 7.4 Hz, 3H) ppm. ^{13}C NMR (101 MHz, $CDCl_3$): δ 140.4, 131.9, 128.2, 127.1, 126.7, 126.64, 126.58, 125.76, 125.75, 125.0, 39.1, 32.5 ppm. HRMS (APCI/DART) m/z: $[M–H]^+$ calcd for $C_{20}H_{13}^+$ 253.1017; found 253.0995. HRMS (ESI/Q-TOF) m/z: $[M–H]^+$ calcd for $C_{20}H_{13}^+$ 253.1017, found 253.1012. $\lambda_{max,abs}$ (CH_2Cl_2): 289 nm. This compound has been previously reported but without complete characterization.[35]

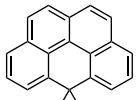

6.9

6-methyl-6*H*-benzo[*cd*]pyrene-6-carboxylic acid (6.9). To a flame-dried, 25-mL flask was added 6-methyl-6*H*-benzo[*cd*]pyrene **6.8** (90.6 mg, 0.356 mmol, 1.00 equiv). The flask was purged and backfilled with N_2 three times before adding anhydrous THF (3.6 mL, 0.10 M). The solution was cooled to -78 °C in a dry ice/acetone bath, then *n*-BuLi (1.5 M in hexanes, 0.40 mL, 0.60 mmol, 1.7 equiv) was added dropwise and the solution stirred at -78 °C for 15 min. To a separate, 500-mL single-neck flask, equipped with a rubber septum fitted with a cannula needle, was added anhydrous $MgSO_4$ (enough to fill ~1/4 of the flask) and enough dry ice to maintain a flow of CO_2 out the needle. Taking care to avoid excess pressure buildup, the cannula needle was added to the main reaction mixture and CO_2 was bubbled in over 5 min. After 5 min, the cannula was removed, and the reaction mixture was warmed to room temperature. The reaction was diluted with Et_2O (10 mL), and the organic layer was extracted with 1 M NaOH (3 x 1 mL). The combined aqueous layers were then acidified to pH 3–4 (checked with pH paper) using 1 M HCl,

then extracted with EtOAc (3 x 5 mL). The organic layers were dried (Na_2SO_4), filtered, and concentrated under reduced pressure to give **6.9** as a pale yellow solid (89 mg, 0.30 mmol, 84%). R_f = 0.05 in 25% EtOAc/hexanes. ^{1}H NMR (500 MHz, $CDCl_3$): δ 7.97 – 7.88 (m, 6H), 7.66 – 7.64 (m, 4H), 1.97 (s, 3H) ppm. ^{13}C NMR (126 MHz, $CDCl_3$): δ 179.7, 137.4, 132.0, 128.8, 127.6, 127.4, 127.0, 126.8, 125.7, 125.0, 123.6, 51.6, 34.6 ppm. HRMS (APCI/DART) m/z: [M – CO_2]$^-$ calcd for $C_{20}H_{13}^-$ 253.1023; found 253.1023.

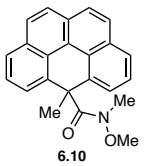

6.10

***N*-methoxy-*N*,6-dimethyl-6*H*-benzo[*cd*]pyrene-6-carboxamide (6.10).** To an oven-dried dram vial under a flow of N_2 was added 6-methyl-6*H*-benzo[*cd*]pyrene-6-carboxylic acid **6.9** (18 mg, 0.060 mmol, 1.0 equiv), followed by dry DCE (0.35 mL, 0.17 M). The solution was cooled to 0 °C. Triphosgene (11.3 mg, 0.0381 mmol, 0.64 equiv) was weighed in a separate, oven-dried, tared vial with cap, then dissolved in DCE (0.05 mL, 0.8 M with respect to triphosgene) and transferred via syringe to the 0 °C reaction mixture. Triethylamine was then added (41 μL, 0.30 mmol, 5.0 equiv). The ice bath removed and the reaction was stirred at room temperature for 30 min. After 30 min, *N*,*O*-dimethylhydroxylamine hydrochloride was added (18 mg, 0.18 mmol, 3.0 equiv) and the reaction stirred at 50 °C in an aluminum reaction block for 1 h. The mixture was cooled to room temperature, diluted with CH_2Cl_2 (5 mL), filtered through celite, and concentrated. The off-white, oily solid was resuspended in THF (2 mL) and filtered through celite to remove triethylammonium chloride. The final mixture was concentrated and purified by preparative TLC (25% EtOAc/hexanes) to give **6.10** as a brown solid (8.0 mg, 0.023 mmol,

41%). R_f = 0.3 in 25% EtOAc/hexanes. ^{1}H NMR (600 MHz, $CDCl_3$) δ 7.94 (d, *J* = 8.6 Hz, 2H), 7.89 (d, *J* = 8.7 Hz, 2H), 7.86 (dd, *J* = 7.8, 1.2 Hz, 2H), 7.61 (t, *J* = 7.6 Hz, 2H), 7.50 (dd, *J* = 7.4, 1.1 Hz, 2H), 3.06 (s [broad], 3H), 2.08 (s [broad], 3H), 1.86 (s, 3H) ppm. ^{13}C NMR (151 MHz, $CDCl_3$) δ 139.3, 131.9, 128.5, 127.4, 126.9, 126.7, 126.4, 125.8, 124.0, 123.8, 59.1, 51.4, 36.7, 29.9 ppm. HRMS (APCI/DART) m/z: $[M + H]^+$ calcd for $C_{23}H_{19}NO_2^+$ 342.1489; found 342.1515.

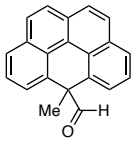

6.11

6-methyl-6*H*-benzo[*cd*]pyrene-6-carbaldehyde (6.11). To a flame-dried, 15-mL round-bottom flask was added *N*-methoxy-*N*,6-dimethyl-6*H*-benzo[*cd*]pyrene-6-carboxamide **6.10** (41 mg, 0.12 mmol, 1.0 equiv), which was then purged and backfilled with N_2. Anhydrous THF (1.2 mL, 0.10 M) was added and the solution was cooled to -78 °C in a dry ice/acetone bath. DIBAL (1.0 M in hexanes, 0.20 mL, 0.20 mmol, 1.7 equiv) was then added dropwise. The reaction was stirred at -78 °C for 30 min, then at room temperature for an additional 2 h. After 2 h, the solution was cooled to 0 °C. EtOAc (1 mL) was added, followed by a saturated aqueous mixture of Rochelle's salt (potassium sodium tartrate) (1.5 mL). This mixture was stirred at room temperature for 1 h (until two distinct layers had formed). The aqueous layer was extracted with EtOAc (2 x 2 mL), then the combined organic layers were dried (Na_2SO_4), filtered, and concentrated. The crude mixture was purified by column chromatography (the crude mixture was evaporated onto silica gel; 10% EtOAc/hexanes). Product **6.11** was obtained as a yellow solid (11 mg, 0.039 mmol, 33%). R_f = 0.9 in 25% EtOAc/hexanes. ^{1}H NMR (500 MHz, $CDCl_3$) δ 9.80 (s, 1H), 7.93 (d, *J* = 8.7 Hz, 2H), 7.91 – 7.88 (m, 4H), 7.63 (dd, *J* = 8.0, 7.3 Hz, 2H), 7.40 (dd, *J*

= 7.3, 1.2 Hz, 2H), 1.92 (s, 3H) ppm. ^{13}C NMR (126 MHz, $CDCl_3$) δ 194.2, 134.2, 132.4, 128.7, 127.8, 127.6, 127.2, 127.0, 126.9, 126.5, 124.0, 56.6, 30.8 ppm. HRMS (APCI/DART) m/z: [M + H]$^+$ calcd for $C_{21}H_{14}O^+$ 283.1117; found 283.1145.

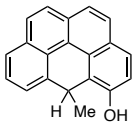

6.12

6-methyl-6*H*-benzo[*cd*]pyren-5-ol (6.12) via Grignard reagent. 5*H*-Benzo[*cd*]pyren-5-one **5.40** (6.1 mg, 0.024 mmol, 1.00 equiv) was added to a flame-dried, 15-mL two-neck flask, which was purged and backfilled with N_2. Anhydrous THF (0.25 mL, 0.08 M) was added and the solution was cooled to 0 °C. MeMgBr (0.7 M in THF, 0.06 mL, 0.04 mmol, 2 equiv) was then added dropwise and the solution stirred at 0 °C for 2 h, then warmed to room temperature and stirred for an additional 3 h. The reaction was quenched with saturated aqueous NH_4Cl (2 mL), and the aqueous layer extracted with CH_2Cl_2 (3 x 3 mL). The combined organic layers were dried (Na_2SO_4), filtered, and concentrated to give a red solid. The crude mixture was purified by preparative TLC (25% EtOAc/hexanes) to give **6.12** as a pale red solid (2.5 mg, 0.0092 mmol, 39%). R_f = 0.5 in 25% EtOAc/hexanes. ^{1}H NMR (500 MHz, $CDCl_3$): δ 7.89 (d, *J* = 8.7 Hz, 1H), 7.84 – 7.79 (m, 3H), 7.73 (d, *J* = 8.5 Hz, 1H), 7.71 (d, *J* = 8.6 Hz, 1H), 7.63 – 7.56 (m, 2H), 7.16 (d, *J* = 8.5 Hz, 1H), 5.10 (s, 1H), 5.01 (q, *J* = 7.1 Hz, 1H), 1.55 (d, *J* = 7.1 Hz, 3H) ppm. ^{13}C NMR (126 MHz, $CDCl_3$): δ 150.4, 139.8, 131.7, 128.7, 128.1, 127.3, 127.04, 127.02, 126.8, 126.7, 126.6, 125.84, 125.80, 124.6, 124.4, 123.0, 117.1, 34.1, 28.1 ppm. HRMS (ESI/Q-TOF) m/z: [M–H]$^+$ calcd for $C_{20}H_{13}O^+$: 269.0966; found 269.0972. $\lambda_{max,abs}$ (CH_2Cl_2): 291 nm.

6-methyl-6*H*-benzo[*cd*]pyren-5-ol (6.12) via organolithium reagent. 5*H*-Benzo[*cd*]pyren-5-one **5.40** (13.6 mg, 0.0535 mmol, 1.00 equiv) was added to a flame-dried, 15-mL two-neck flask, which was purged and backfilled with N_2. Anhydrous THF (0.55 mL, 0.10 M) was added, and the solution was cooled to -78 °C. MeLi (0.8 M in Et_2O, 0.13 mL, 0.10 mmol, 1.9 equiv) was added dropwise and the solution stirred at -78 °C for 2 h, then warmed to room temperature and stirred for an additional 1 h. The reaction was quenched with saturated aqueous NH_4Cl (2 mL), and the aqueous layer was then extracted with CH_2Cl_2 (3 x 3 mL). The combined organic layers were dried (Na_2SO_4), filtered, and concentrated to give a red solid. The crude mixture was purified by preparative TLC (25% EtOAc/hexanes) to give **6.12** as a pale red solid (5.0 mg, 0.018 mmol, 35%). R_f = 0.5 in 25% EtOAc/hexanes. The spectral data were consistent with those listed above.

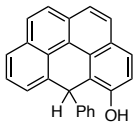

6.13

6-phenyl-6*H*-benzo[*cd*]pyren-5-ol (6.13) via Grignard reagent. 5*H*-Benzo[*cd*]pyren-5-one **5.40** (4.2 mg, 0.017 mmol, 1.0 equiv) was added to a flame-dried, 15-mL two-neck flask, which was purged and backfilled with N_2. Anhydrous THF (0.3 mL, 0.06 M) was added and the solution was cooled to 0 °C. Phenylmagnesium bromide (PhMgBr) (0.5 M in THF, 0.05 mL, 0.03 mmol, 2 equiv) was added dropwise and the solution stirred at 0 °C for 45 min. The reaction was quenched with saturated aqueous NH_4Cl (2 mL) and allowed to warm to room temperature. The aqueous layer was extracted with CH_2Cl_2 (3 x 2 mL), and then the combined organic layers were dried (Na_2SO_4), filtered, and concentrated to give a red solid. The crude mixture was purified by preparative TLC (25% EtOAc/hexanes) to give **6.13** as a pale orange solid (2.9 mg,

0.0087 mmol, 51%). R_f = 0.4 in 25% EtOAc/hexanes. ^{1}H NMR (600 MHz, $CDCl_3$) δ 7.88 (d, *J* = 8.7 Hz, 1H), 7.87 – 7.84 (m, 2H), 7.78 (d, *J* = 8.5 Hz, 1H), 7.75 (dd, *J* = 8.8, 2.0 Hz, 2H), 7.50 – 7.45 (m, 2H), 7.27 (m, 2H; overlaps with chloroform peak), 7.21 – 7.18 (m, 2H), 7.16 – 7.12 (m, 1H), 7.11 (d, *J* = 8.5 Hz, 1H), 6.09 (s, 1H), 5.00 (s, 1H) ppm. ^{13}C NMR (126 MHz, $CDCl_3$) δ 151.6, 147.1, 137.0, 131.8, 129.3, 129.0, 128.3, 128.1, 127.8, 127.5, 127.4, 127.3, 127.02, 126.97, 126.88, 126.7, 126.3, 126.2, 124.5, 124.3, 120.9, 118.1, 45.6 ppm. HRMS (ESI/Q-TOF) m/z: $[M–H]^+$ calcd for $C_{25}H_{15}O^+$ 331.1123; found 331.1138.

6-phenyl-6*H*-benzo[*cd*]pyren-5-ol (6.13) via organolithium reagent. 5*H*-Benzo[*cd*]pyren-5-one **5.40** (4.4 mg, 0.017 mmol, 1.0 equiv) was added to a flame-dried, 15-mL two-neck flask, which was then purged and backfilled with N_2. Anhydrous THF (0.3 mL, 0.06 M) was added, and the solution then cooled to -78 °C. Phenyllithium (PhLi) (0.4 M in THF, 0.07 mL, 0.03 mmol, 2 equiv) was added dropwise and the solution stirred at -78 °C for 45 min. The reaction was allowed to warm to room temperature, then quenched with saturated aqueous NH_4Cl (2 mL). The aqueous layer was extracted with CH_2Cl_2 (3 x 2 mL), and then the combined organic layers were dried (Na_2SO_4), filtered, and concentrated to give a red solid. The crude mixture was purified by preparative TLC (25% EtOAc/hexanes) to give **6.13** as a pale orange solid (2.9 mg, 0.0087 mmol, 50%). R_f = 0.4 in 25% EtOAc/hexanes. The spectral data were consistent with those listed above.

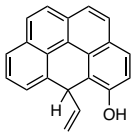

6.14

6-vinyl-6*H*-benzo[*cd*]pyren-5-ol (6.14). 5*H*-Benzo[*cd*]pyren-5-one **5.40** (5.0 mg, 0.020 mmol, 1.0 equiv) was added to a flame-dried, 15-mL two-neck flask, which was then purged and backfilled with N_2. Anhydrous THF (0.4 mL, 0.05 M) was added, then the solution cooled to 0 °C. At 0 °C, vinylmagnesium bromide (0.35 M in THF, 0.10 mL, 0.035 mmol, 1.8 equiv) was added dropwise. The solution was stirred at 0 °C for 3 h, then quenched with saturated aqueous NH_4Cl (2 mL) and allowed to warm to room temperature. The aqueous layer was extracted with CH_2Cl_2 (3 x 2 mL), and the combined organic layers were then dried (Na_2SO_4), filtered, and concentrated to give a crude red solid. The crude mixture was purified by preparative TLC (25% EtOAc/hexanes) to give **6.14** as a pale red solid (2.6 mg, 0.0092 mmol, 46%). R_f = 0.4 in 25% EtOAc/hexanes. ^{1}H NMR (600 MHz, $CDCl_3$): δ 7.85 (d, *J* = 8.7 Hz, 1H), 7.82 – 7.77 (m, 4H), 7.69 (d, *J* = 8.6 Hz, 1H), 7.60 – 7.56 (m, 2H), 7.24 (d, *J* = 8.6 Hz, 1H), 6.09 (ddd, *J* = 17.1, 9.8, 8.5 Hz, 1H), 5.67 (s, 1H), 5.54 (d, *J* = 8.5 Hz, 1H), 5.33 (dt, *J* = 16.9, 1.3 Hz, 1H), 5.14 (dt, *J* = 9.8, 1.5 Hz, 1H) ppm. ^{13}C NMR (126 MHz, $CDCl_3$): δ 152.3, 141.6, 134.4, 131.8, 128.8, 128.3, 128.0, 127.3, 127.2, 127.10, 127.08, 127.0, 126.8, 126.6, 126.5, 124.4, 124.2, 118.3, 117.6, 114.2, 44.4 ppm. HRMS (ESI/Q-TOF) m/z: $[M–H]^+$ calcd for $C_{21}H_{13}O^+$ 281.0966; found 281.0969.

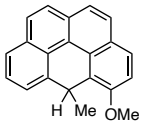

6.15

5-methoxy-6-methyl-6*H*-benzo[*cd*]pyrene (6.15). To an oven-dried, 2-mL dram vial was added flame-dried K_2CO_3 (10.7 mg, 0.0774 mmol, 1.85 equiv), followed by 6-methyl-6*H*-benzo[*cd*]pyren-5-ol **6.12** (11.3 mg, 0.0418 mmol, 1.00 equiv) dissolved in anhydrous DMF (0.40 mL, 0.10 M). Iodomethane (5.0 µL, 0.077 mmol, 1.8 equiv) was then added and the reaction stirred at 40 °C in an aluminum reaction block for 21 h. The reaction was allowed to cool to room temperature, then DMF was blown off with a stream of air. The resulting material was re-dissolved in H_2O (2 mL) and the aqueous layer was extracted with $CHCl_3$ (3 x 2 mL). The combined organic layers were washed with H_2O (1 x 3 mL), dried (Na_2SO_4), filtered, and concentrated to give an off-white solid. The crude mixture was purified by column chromatography (mixture was loaded dissolved in starting eluent; silica gel, 5% EtOAc in hexanes). Product **6.15** was obtained as an off-white solid (7.4 mg, 0.026 mmol, 62%). R_f = 0.5 in 25% EtOAc/hexanes. ^{1}H NMR (500 MHz, $CDCl_3$): δ 7.88 (d, *J* = 8.6 Hz, 1H), 7.84–7.81 (m, 3H), 7.79 (dd, *J* = 6.7, 2.5 Hz, 1H), 7.70 (d, *J* = 8.6 Hz, 1H), 7.61–7.56 (m, 2H), 7.36 (d, *J* = 8.7 Hz, 1H), 5.06 (q, *J* = 7.1 Hz, 1H), 4.07 (s, 3H), 1.49 (d, *J* = 7.1 Hz, 3H) ppm. ^{13}C NMR (151 MHz, $CDCl_3$): δ 154.3, 140.5, 131.7, 128.6, 127.8, 127.3, 127.0, 126.8, 126.7, 126.6, 125.8, 125.7, 125.6, 124.7, 124.4, 112.3, 56.2, 34.3, 28.7 ppm. HRMS (ESI/Q-TOF) m/z: $[M–H]^+$ calcd for $C_{21}H_{15}O^+$ 283.1123; found 283.1119.

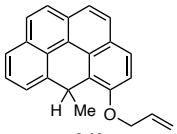

6.16

5-(allyloxy)-6-methyl-6*H*-benzo[*cd*]pyrene (6.16). To an oven-dried, 2-mL dram vial was added flame-dried K_2CO_3 (4.8 mg, 0.035 mmol, 2.1 equiv), followed by 6-methyl-6*H*-benzo[*cd*]pyren-5-ol **6.12** (4.7 mg, 0.017 mmol, 1.0 equiv) dissolved in anhydrous DMF (0.2 mL, 0.07 M). Allyl bromide (3 µL, 0.03 mmol, 2 equiv) was added and the reaction was stirred at 40 °C in an aluminum reaction block for 21 h. The reaction was allowed to cool to room temperature, then DMF was blown off with a stream of air. The resulting material was re-dissolved in H_2O (2 mL) and the aqueous layer was then extracted with $CHCl_3$ (3 x 2 mL). The combined organic layers were washed with H_2O (1 x 3 mL), dried (Na_2SO_4), filtered, and concentrated to give an off-white crude solid. The crude mixture was purified by preparative TLC (25% EtOAc in hexanes). Product **6.16** was obtained as an off-white solid (2.9 mg, 0.0093 mmol, 55%) along with unreacted starting material (2 mg, 40% recovery). R_f = 0.7 in 25% EtOAc/hexanes. ^{1}H NMR (600 MHz, $CDCl_3$): δ 7.88 (d, *J* = 8.6 Hz, 1H), 7.84–7.78 (m, 4H), 7.71 (d, *J* = 8.6 Hz, 1H), 7.59 (d, *J* = 5.6 Hz, 2H), 7.33 (d, *J* = 8.7 Hz, 1H), 6.21 (ddt, *J* = 17.2, 10.3, 5.0 Hz, 1H), 5.56 (dq, *J* = 17.3, 1.7 Hz, 1H), 5.37 (dq, *J* = 10.5, 1.5 Hz, 1H), 5.11 (q, *J* = 7.1 Hz, 1H), 4.81 (tt, *J* = 5.1, 1.7 Hz, 2H), 1.52 (d, *J* = 7.1 Hz, 3H) ppm. ^{13}C NMR (151 MHz, $CDCl_3$): δ 153.3, 140.5, 133.8, 131.7, 128.6, 127.9, 127.3, 126.9, 126.83, 126.77, 126.73, 126.66, 126.6, 126.1, 125.8, 125.6, 124.8, 124.5, 117.4, 113.5, 69.6, 34.3, 28.7 ppm. HRMS (ESI/Q-TOF) m/z: $[M+H]^+$ calcd for $C_{23}H_{19}O^+$ 311.1436; found 311.1427.

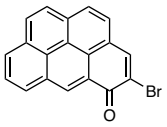

6.17

4-bromo-5*H*-benzo[*cd*]pyren-5-one (6.17). To an oven-dried dram vial was added 5*H*-benzo[*cd*]pyren-5-one (**5.40**) (13.1 mg, 0.0515 mmol, 1.00 equiv). The vial was purged under vacuum and backfilled with nitrogen, then dry MeCN (0.5 mL, 0.1 M) was added, followed by NBS (9.8 mg, 0.055 mmol, 1.1 equiv). The solution was stirred at 80 °C in an aluminum reaction block for 2 h, after which it was cooled to room temperature. The solution was diluted with CH_2Cl_2 (2 mL) and added to saturated aq. Na_2SO_3 (2 mL). The aqueous layer was extracted with CH_2Cl_2 (3 x 2 mL) and the organic layers dried (Na_2SO_4), filtered, and concentrated to give the crude as a dark red solid. The crude was purified by column chromatography (silica gel, 10% EtOAc in heptane). Product **6.17** was obtained as a red solid (143 mg, 0.429 mmol, 76% yield). R_f = 0.41 in 25% EtOAc/hexanes. ^{1}H NMR (500 MHz, $CDCl_3$): δ 9.41 (s, 1H), 8.56 (d, *J* = 7.8 Hz, 1H), 8.46 (d, *J* = 7.7 Hz, 1H), 8.45 (s, 1H), 8.20–8.18 (m, 2H), 8.16 (d, *J* = 7.6 Hz, 1H), 8.13 (t, *J* = 7.7, 7.7 Hz, 1H), 8.06 (d, *J* = 7.8 Hz, 1H) ppm. ^{13}C NMR (126 MHz, $CDCl_3$): δ 179.3, 144.5, 136.7, 135.1, 133.7, 131.7, 131.3, 130.8, 129.8, 129.0, 128.7, 128.3, 128.0, 127.65, 127.62, 127.5, 125.7, 124.95, 124.86, 124.8, 124.5, 123.7 ppm. HRMS (ESI/Q-TOF) m/z: $[M+H]^+$ calcd for $C_{19}H_{10}BrO^+$ 332.9915; found 332.9891. $\lambda_{max,abs}$ (CH_2Cl_2): 493 nm.

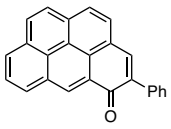

6.18

4-phenyl-5*H*-benzo[*cd*]pyren-5-one (6.18). To a flame-dried 8-mL reaction vial were added: **6.17** (1.00 mg, 0.00300 mmol, 1.00 equiv), phenylboronic acid (0.64 mg, 0.0052 mmol, 1.7 equiv), PEPPSI-IPr catalyst (0.22 mg, 0.00032 mmol, 11 mol%), and dried K_2CO_3 (1.64 mg,

0.0119 mmol, 3.97 equiv). The vial was purged and backfilled, then anhydrous dioxane was added (0.1 mL, 0.03 M). The reaction was stirred at 60 °C in an aluminum reaction block for 19 h, then allowed to cool to room temperature. The mixture was diluted with CH_2Cl_2 (2 mL) and the organic layer washed with H_2O (1 x 2 mL), then dried (Na_2SO_4), filtered, and concentrated. The crude product was purified via preparative TLC (25% EtOAc/hexanes) to give **6.18** as a pinkish red solid (0.90 mg, 0.0027 mmol, 90%). ^{1}H NMR (500 MHz, $CDCl_3$): δ 9.49 (s, 1H), 8.63 (d, *J* = 7.5 Hz, 1H), 8.46 (dd, *J* = 7.8, 1.0 Hz, 1H), 8.28 (d, *J* = 7.9 Hz, 1H), 8.22 – 8.15 (m, 5H), 7.80 (m, 2H), 7.51 (m, 2H), 7.46 – 7.41 (m, 1H) ppm. ^{13}C NMR (126 MHz, $CDCl_3$): δ 184.6, 141.2, 138.8, 137.0, 135.2, 133.2, 131.3, 131.0, 130.5, 130.2, 129.3, 129.1, 128.7, 128.6, 128.4, 128.2, 128.0, 127.3, 125.6, 125.3, 125.2, 125.1, 123.8 ppm. HRMS (ESI/Q-TOF) m/z: [M+H]+ calcd for $C_{25}H_{15}O^+$ 331.1123; found 331.1106.

6.5.5 ^{1}H NMR spectra

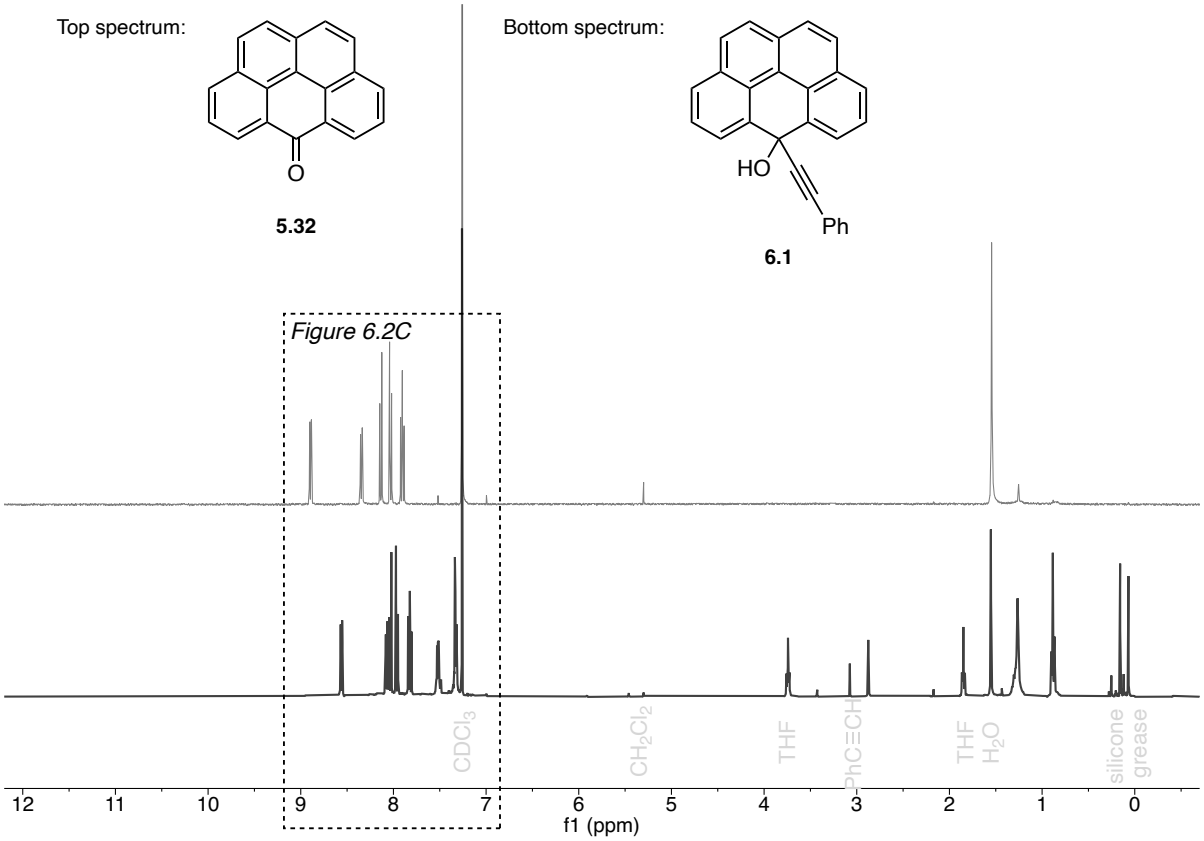

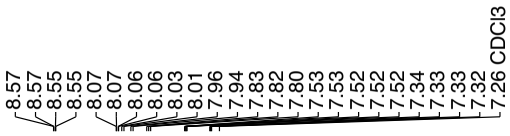

Parameter	Value
Instrument	av500
Solvent	CDCl3
Temperature	298.0
Pulse Sequence	zg30
Experiment	1D
Probe	Z119248_0002 (DCH 500S2 C/ H-D-05 Z LT)
Number of Scans	16
Receiver Gain	12.1
Relaxation Delay	2.0000
Pulse Width	10.0000
Acquisition Time	3.2768
Acquisition Date	2022-01-27T09:21:11
Spectrometer Frequency	500.13
Spectral Width	10000.0
Lowest Frequency	-2011.4
Nucleus	1H
Acquired Size	32768
Spectral Size	65536

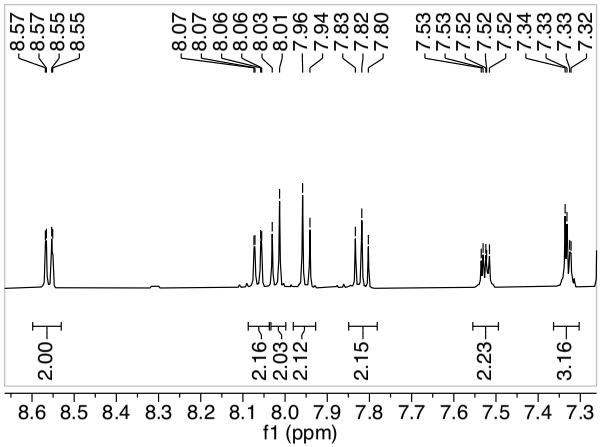

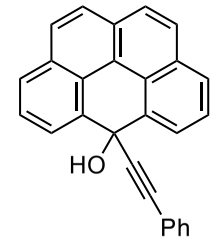

6.1

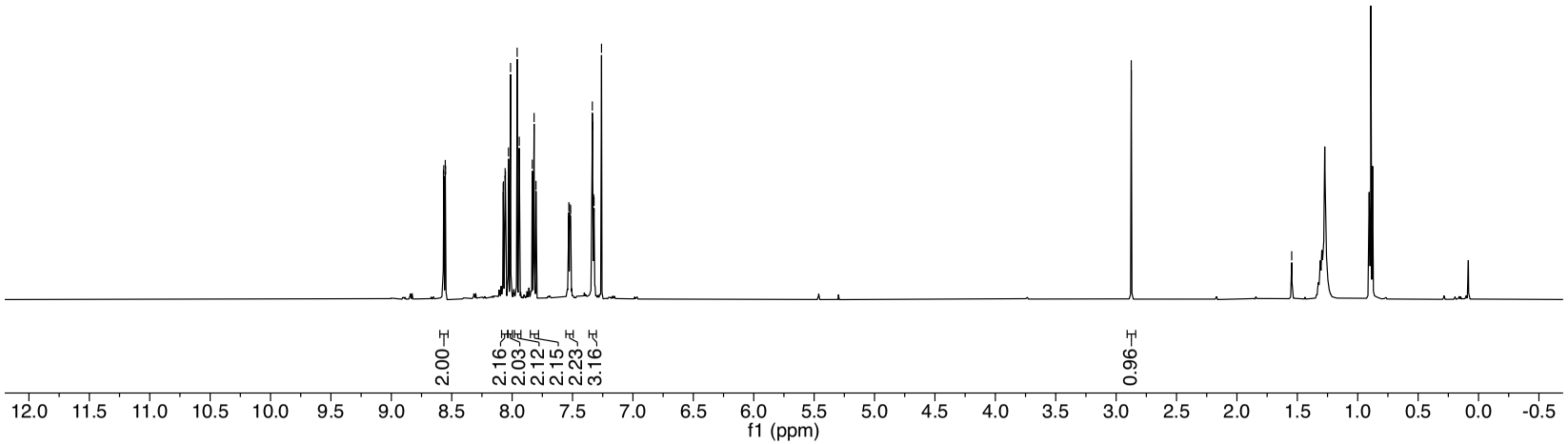

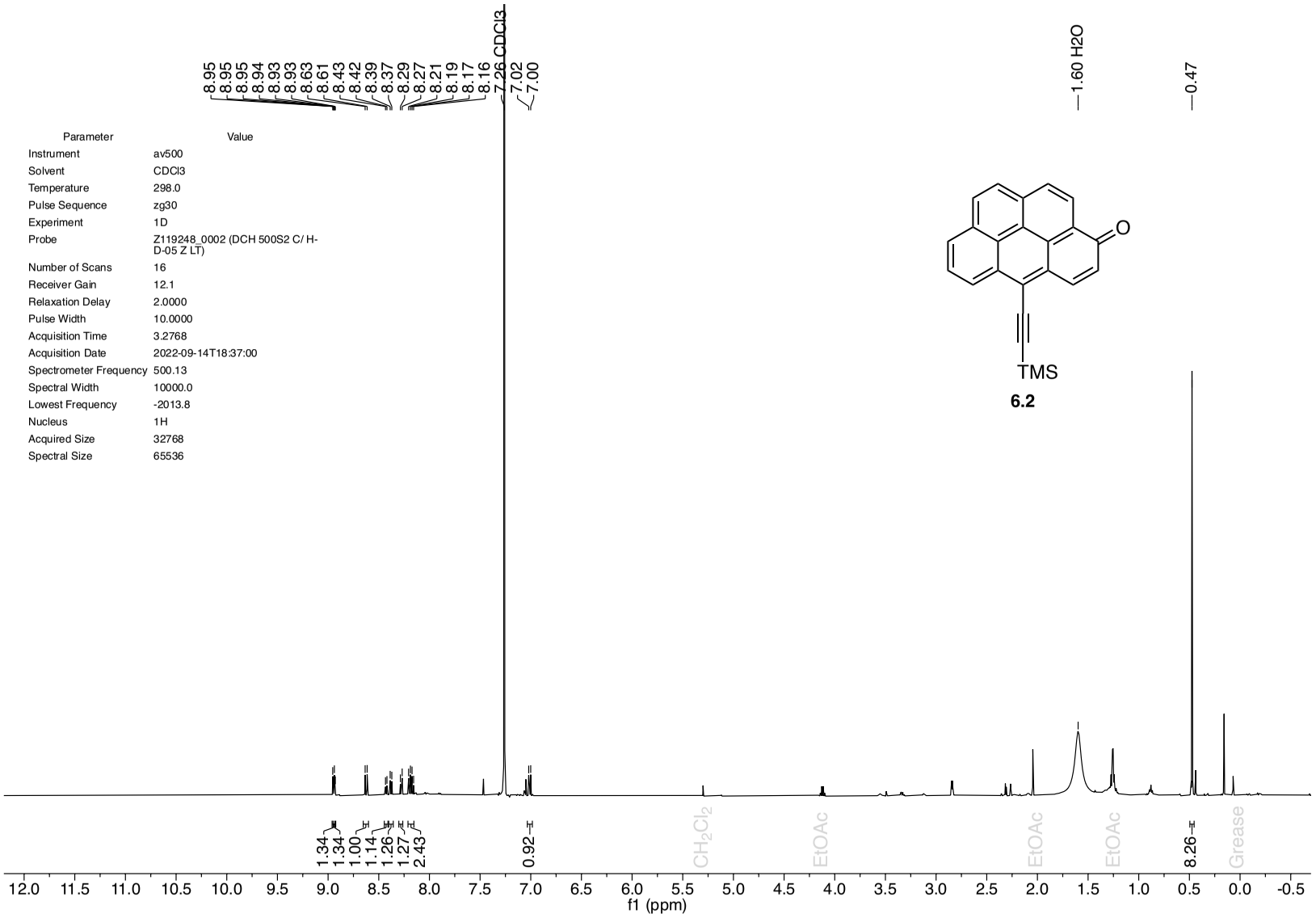
8.95
8.95
8.95
8.94
8.93
8.93
8.63
8.61
8.43
8.42
8.39
8.37
8.29
8.27
8.21
8.19
8.17
8.16
7.26 CDCl3
7.02
7.00
1.60 H2O
0.47
Parameter Value
Instrument av500
Solvent CDCl3
Temperature 298.0
Pulse Sequence zg30
Experiment 1D
Probe Z119248_0002 (DCH 500S2 C/ H-D-05 Z LT)
Number of Scans 16
Receiver Gain 12.1
Relaxation Delay 2.0000
Pulse Width 10.0000
Acquisition Time 3.2768
Acquisition Date 2022-09-14T18:37:00
Spectrometer Frequency 500.13
Spectral Width 10000.0
Lowest Frequency -2013.8
Nucleus 1H
Acquired Size 32768
Spectral Size 65536
O
TMS
6.2
1.34
1.34
1.00
1.14
1.26
1.27
2.43
0.92
CH2Cl2
EtOAc
EtOAc
EtOAc
8.26
Grease
12.0 11.5 11.0 10.5 10.0 9.5 9.0 8.5 8.0 7.5 7.0 6.5 6.0 5.5 5.0 4.5 4.0 3.5 3.0 2.5 2.0 1.5 1.0 0.5 0.0 -0.5
f1 (ppm)

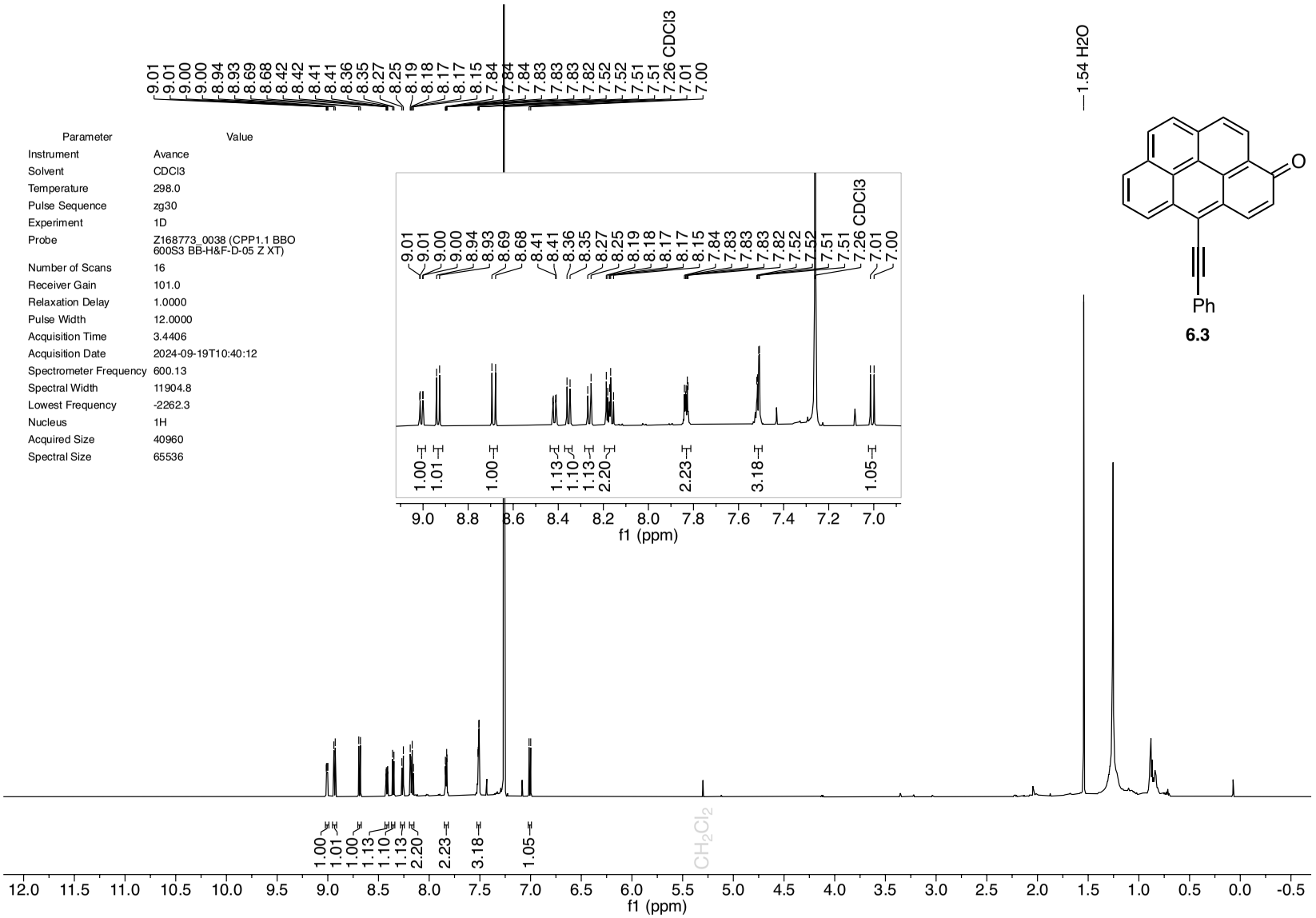
9.01 9.01 9.00 9.00 8.94 8.93 8.69 8.68 8.42 8.41 8.41 8.36 8.35 8.27 8.25 8.19 8.18 8.17 8.17 8.15 7.84 7.84 7.83 7.83 7.82 7.52 7.52 7.51 7.51 7.26 CDCl3 7.01 7.00
1.54 H2O
Parameter Value
Instrument Avance
Solvent CDCl3
Temperature 298.0
Pulse Sequence zg30
Experiment 1D
Probe Z168773_0038 (CPP1.1 BBO 600S3 BB-H&F-D-05 Z XT)
Number of Scans 16
Receiver Gain 101.0
Relaxation Delay 1.0000
Pulse Width 12.0000
Acquisition Time 3.4406
Acquisition Date 2024-09-19T10:40:12
Spectrometer Frequency 600.13
Spectral Width 11904.8
Lowest Frequency -2262.3
Nucleus 1H
Acquired Size 40960
Spectral Size 65536
1.00 1.01 1.00 1.13 1.10 1.13 2.20 2.23 3.18 1.05
f1 (ppm)
CH2Cl2
O
Ph
6.3

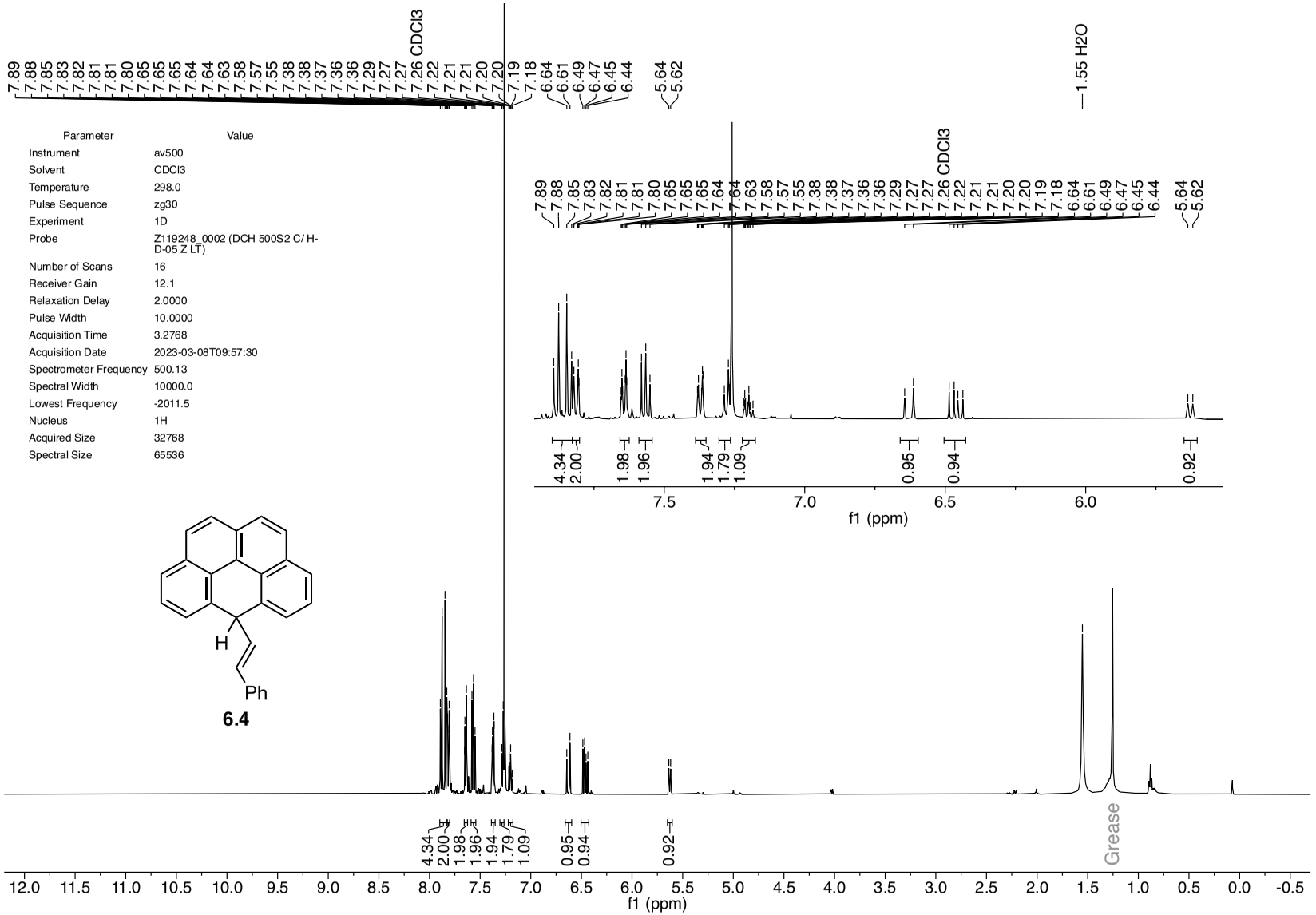
7.89 7.88 7.85 7.83 7.82 7.81 7.81 7.80 7.65 7.65 7.64 7.64 7.63 7.58 7.57 7.55 7.38 7.38 7.37 7.36 7.36 7.29 7.27 7.27 7.26 CDCl3 7.22 7.21 7.21 7.20 7.20 7.19 7.18 6.64 6.61 6.49 6.47 6.45 6.44 5.64 5.62 1.55 H2O
Parameter Value
Instrument av500
Solvent CDCl3
Temperature 298.0
Pulse Sequence zg30
Experiment 1D
Probe Z119248_0002 (DCH 500S2 C/ H-D-05 Z LT)
Number of Scans 16
Receiver Gain 12.1
Relaxation Delay 2.0000
Pulse Width 10.0000
Acquisition Time 3.2768
Acquisition Date 2023-03-08T09:57:30
Spectrometer Frequency 500.13
Spectral Width 10000.0
Lowest Frequency -2011.5
Nucleus 1H
Acquired Size 32768
Spectral Size 65536
4.34 2.00 1.98 1.96 1.94 1.79 1.09 0.95 0.94 0.92
Grease
f1 (ppm)
H
Ph
6.4

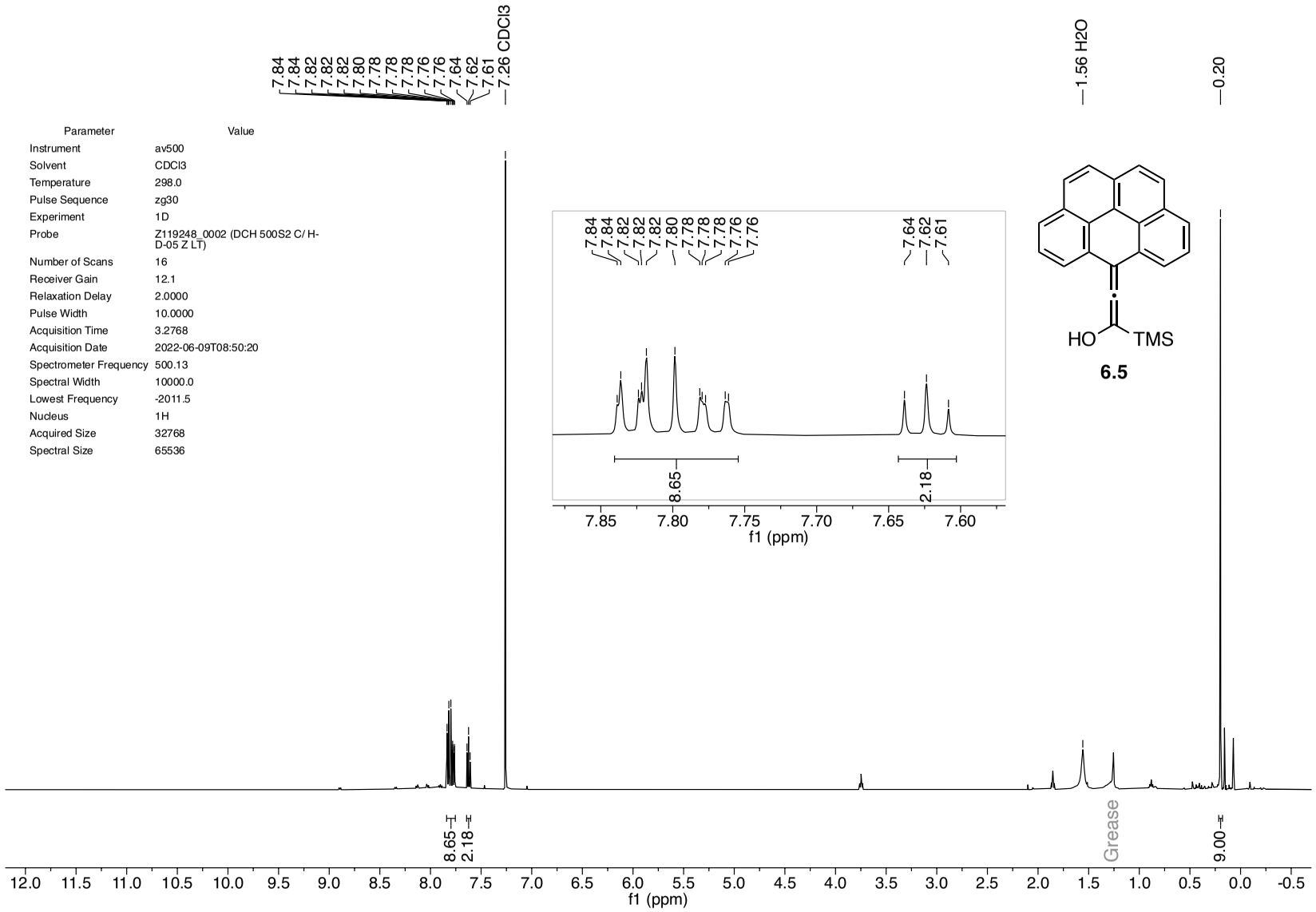
7.84
7.84
7.82
7.82
7.82
7.80
7.78
7.78
7.78
7.76
7.76
7.64
7.62
7.61
7.26 CDCl3
1.56 H2O
0.20
Parameter Value
Instrument av500
Solvent CDCl3
Temperature 298.0
Pulse Sequence zg30
Experiment 1D
Probe Z119248_0002 (DCH 500S2 C/ H-D-05 Z LT)
Number of Scans 16
Receiver Gain 12.1
Relaxation Delay 2.0000
Pulse Width 10.0000
Acquisition Time 3.2768
Acquisition Date 2022-06-09T08:50:20
Spectrometer Frequency 500.13
Spectral Width 10000.0
Lowest Frequency -2011.5
Nucleus 1H
Acquired Size 32768
Spectral Size 65536
8.65
2.18
f1 (ppm)
HO
TMS
6.5
Grease
9.00
f1 (ppm)

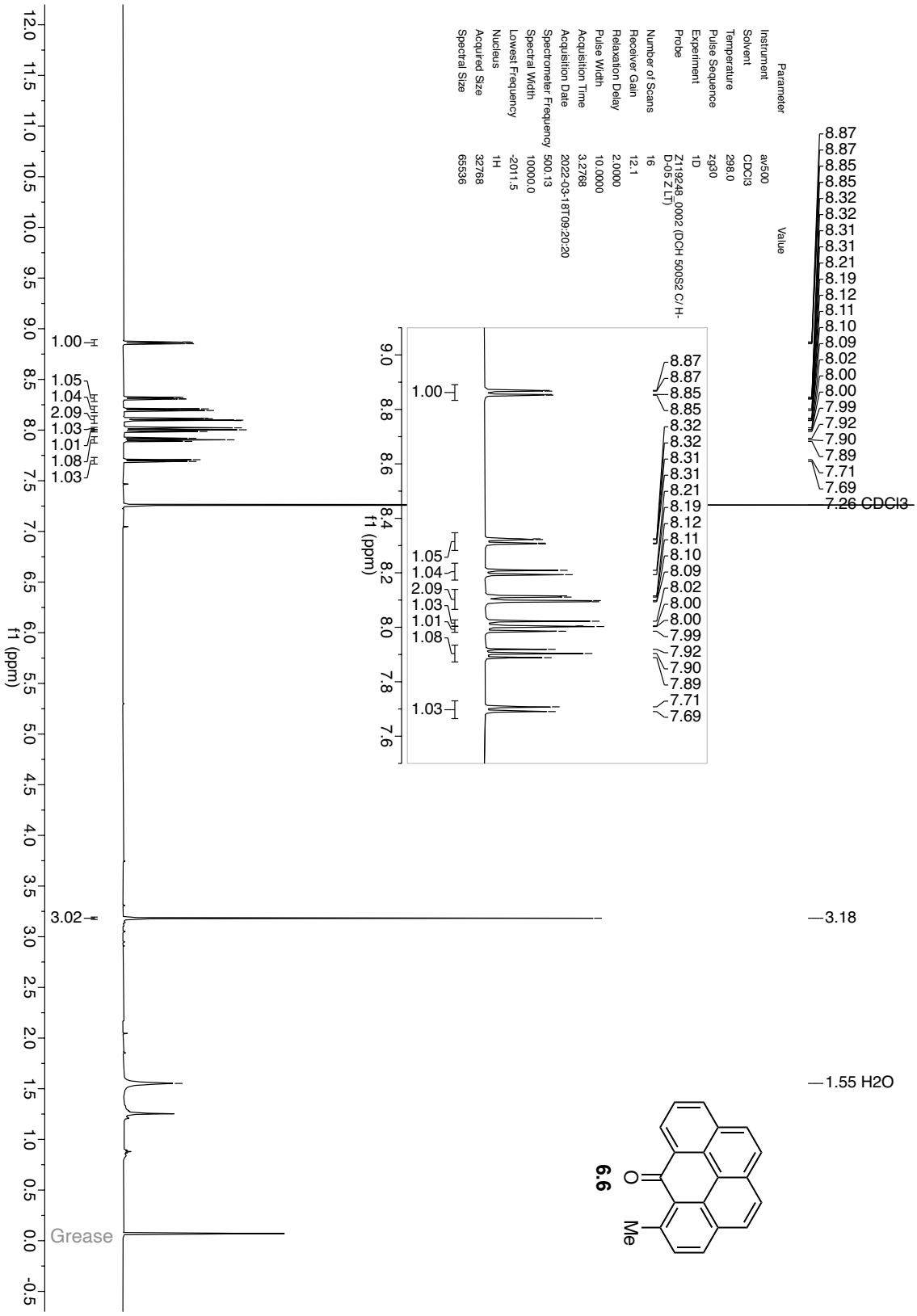
Parameter
Value
Instrument
av500
Solvent
CDCl3
Temperature
298.0
Pulse Sequence
zg30
Experiment
1D
Probe
Z119248_0002 (DCH 500S2 C/ H-D-05 Z LT)
Number of Scans
16
Receiver Gain
12.1
Relaxation Delay
2.0000
Pulse Width
10.0000
Acquisition Time
3.2768
Acquisition Date
2022-03-18T09:20:20
Spectrometer Frequency
500.13
Spectral Width
10000.0
Lowest Frequency
-2011.5
Nucleus
1H
Acquired Size
32768
Spectral Size
65536
8.87
8.87
8.85
8.85
8.32
8.32
8.31
8.31
8.21
8.19
8.12
8.11
8.10
8.09
8.02
8.00
8.00
7.99
7.92
7.90
7.89
7.71
7.69
7.26 CDCl3
1.00
1.05
1.04
2.09
1.03
1.01
1.08
1.03
3.02
3.18
1.55 H2O
Grease
f1 (ppm)
6.6
O
Me

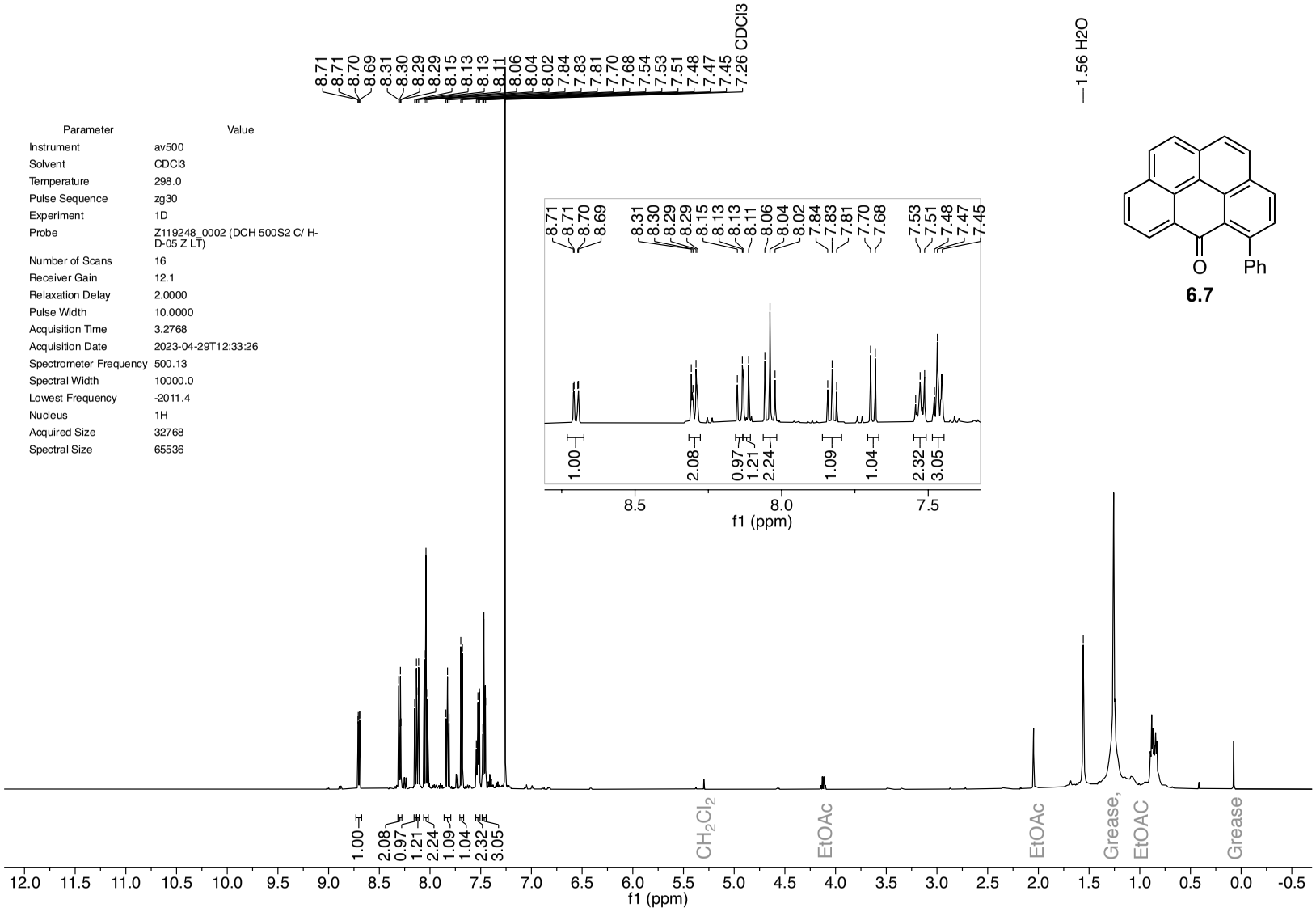
8.71
8.71
8.70
8.69
8.31
8.30
8.29
8.29
8.15
8.13
8.13
8.11
8.06
8.04
8.02
7.84
7.83
7.81
7.70
7.68
7.54
7.53
7.51
7.48
7.47
7.45
7.26 CDCl3
1.56 H2O
Parameter Value
Instrument av500
Solvent CDCl3
Temperature 298.0
Pulse Sequence zg30
Experiment 1D
Probe Z119248_0002 (DCH 500S2 C/ H-D-05 Z LT)
Number of Scans 16
Receiver Gain 12.1
Relaxation Delay 2.0000
Pulse Width 10.0000
Acquisition Time 3.2768
Acquisition Date 2023-04-29T12:33:26
Spectrometer Frequency 500.13
Spectral Width 10000.0
Lowest Frequency -2011.4
Nucleus 1H
Acquired Size 32768
Spectral Size 65536
1.00
2.08
0.97
1.21
2.24
1.09
1.04
2.32
3.05
CH2Cl2
EtOAc
EtOAc
Grease, EtOAC
Grease
f1 (ppm)
O
Ph
6.7

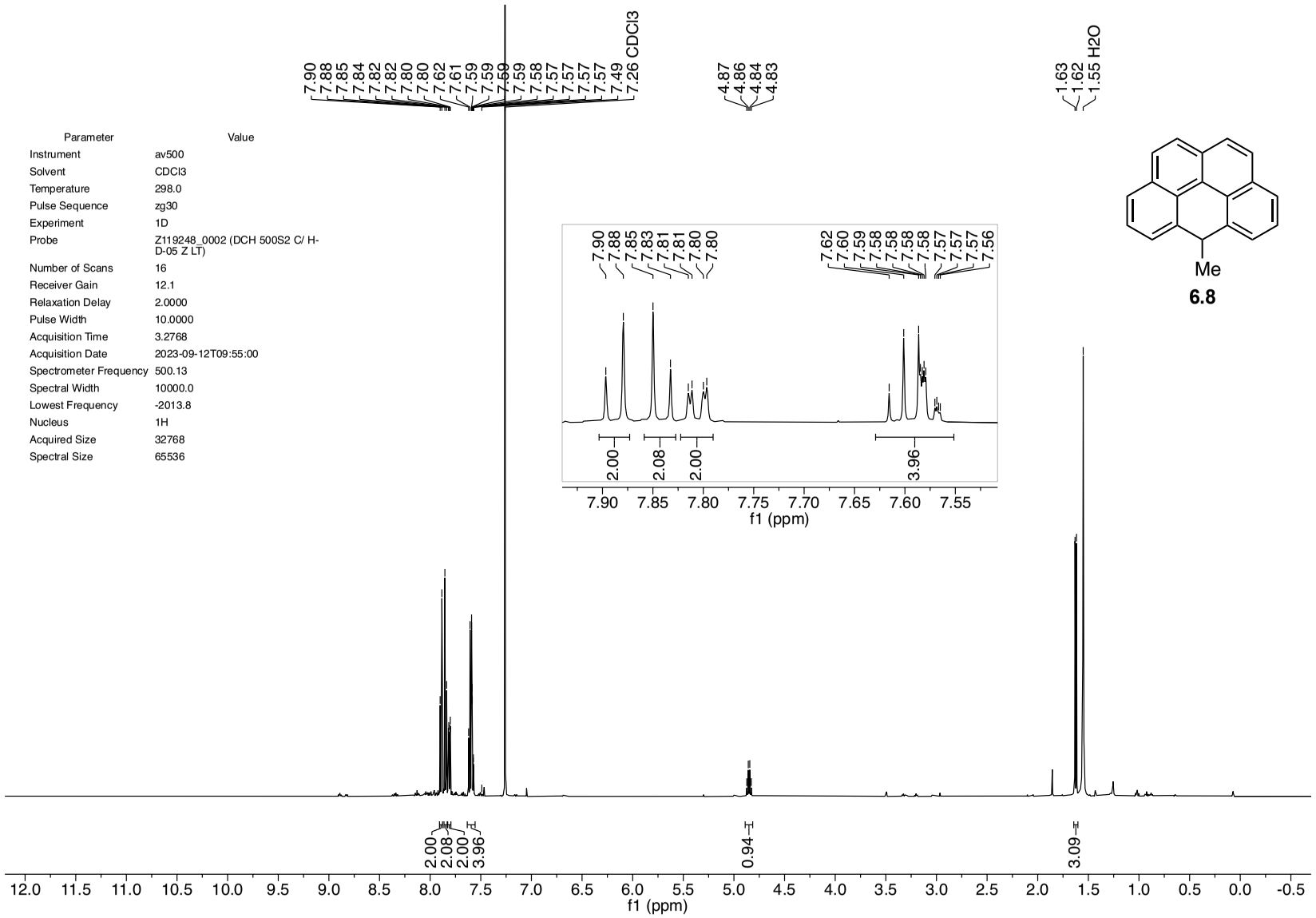
7.90
7.88
7.85
7.84
7.82
7.82
7.80
7.80
7.62
7.61
7.59
7.59
7.59
7.59
7.58
7.57
7.57
7.57
7.49
7.26 CDCl3
4.87
4.86
4.84
4.83
1.63
1.62
1.55 H2O
Parameter Value
Instrument av500
Solvent CDCl3
Temperature 298.0
Pulse Sequence zg30
Experiment 1D
Probe Z119248_0002 (DCH 500S2 C/ H-D-05 Z LT)
Number of Scans 16
Receiver Gain 12.1
Relaxation Delay 2.0000
Pulse Width 10.0000
Acquisition Time 3.2768
Acquisition Date 2023-09-12T09:55:00
Spectrometer Frequency 500.13
Spectral Width 10000.0
Lowest Frequency -2013.8
Nucleus 1H
Acquired Size 32768
Spectral Size 65536
7.90
7.88
7.85
7.83
7.81
7.80
7.80
7.62
7.60
7.59
7.58
7.58
7.58
7.57
7.57
7.57
7.56
2.00
2.08
2.00
3.96
7.90 7.85 7.80 7.75 7.70 7.65 7.60 7.55
f1 (ppm)
Me
6.8
2.00
2.08
2.00
3.96
0.94
3.09
12.0 11.5 11.0 10.5 10.0 9.5 9.0 8.5 8.0 7.5 7.0 6.5 6.0 5.5 5.0 4.5 4.0 3.5 3.0 2.5 2.0 1.5 1.0 0.5 0.0 -0.5
f1 (ppm)

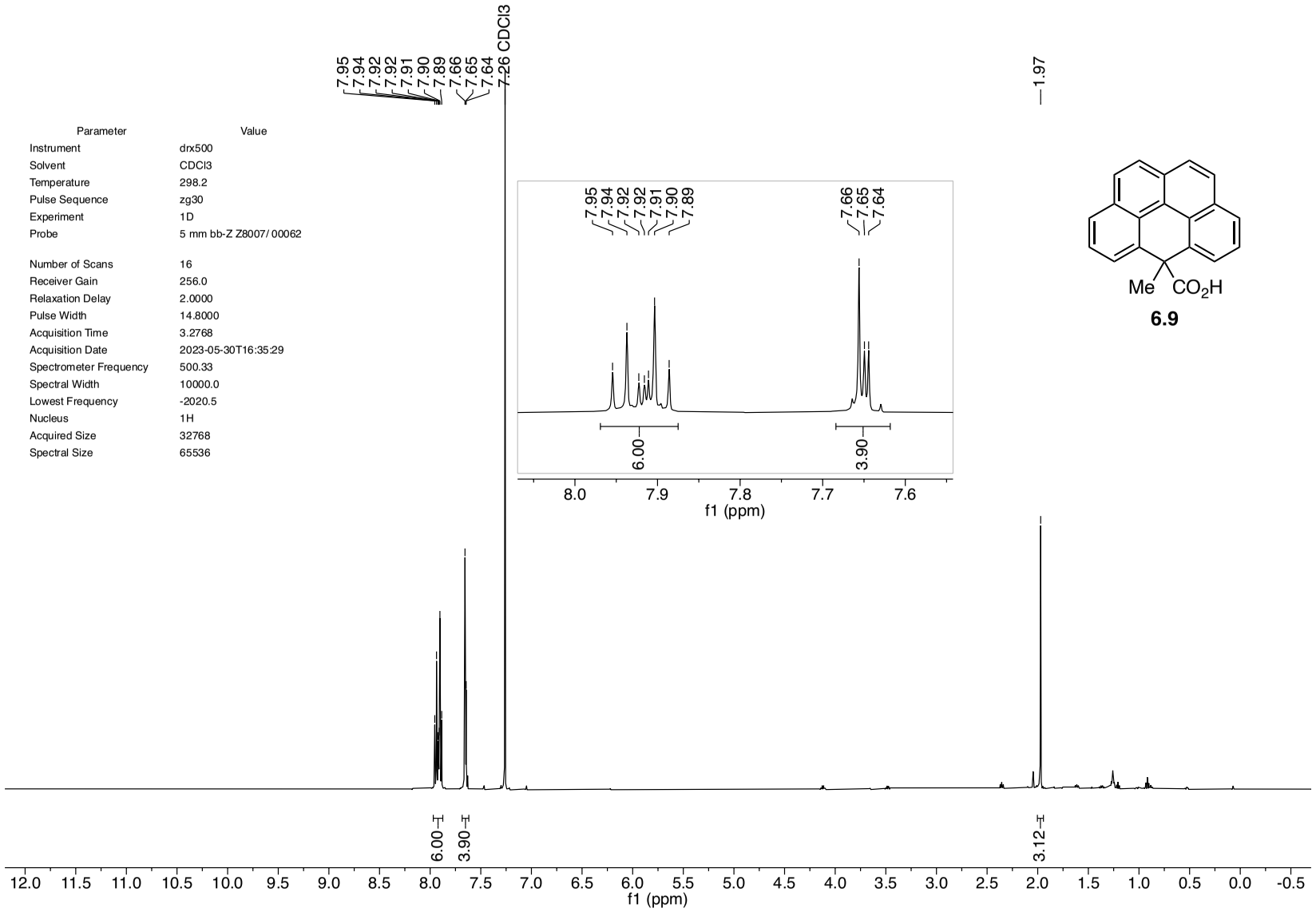

Parameter	Value
Instrument	drx500
Solvent	CDCl3
Temperature	298.2
Pulse Sequence	zg30
Experiment	1D
Probe	5 mm bb-Z Z8007/ 00062
Number of Scans	16
Receiver Gain	256.0
Relaxation Delay	2.0000
Pulse Width	14.8000
Acquisition Time	3.2768
Acquisition Date	2023-05-30T16:35:29
Spectrometer Frequency	500.33
Spectral Width	10000.0
Lowest Frequency	-2020.5
Nucleus	1H
Acquired Size	32768
Spectral Size	65536

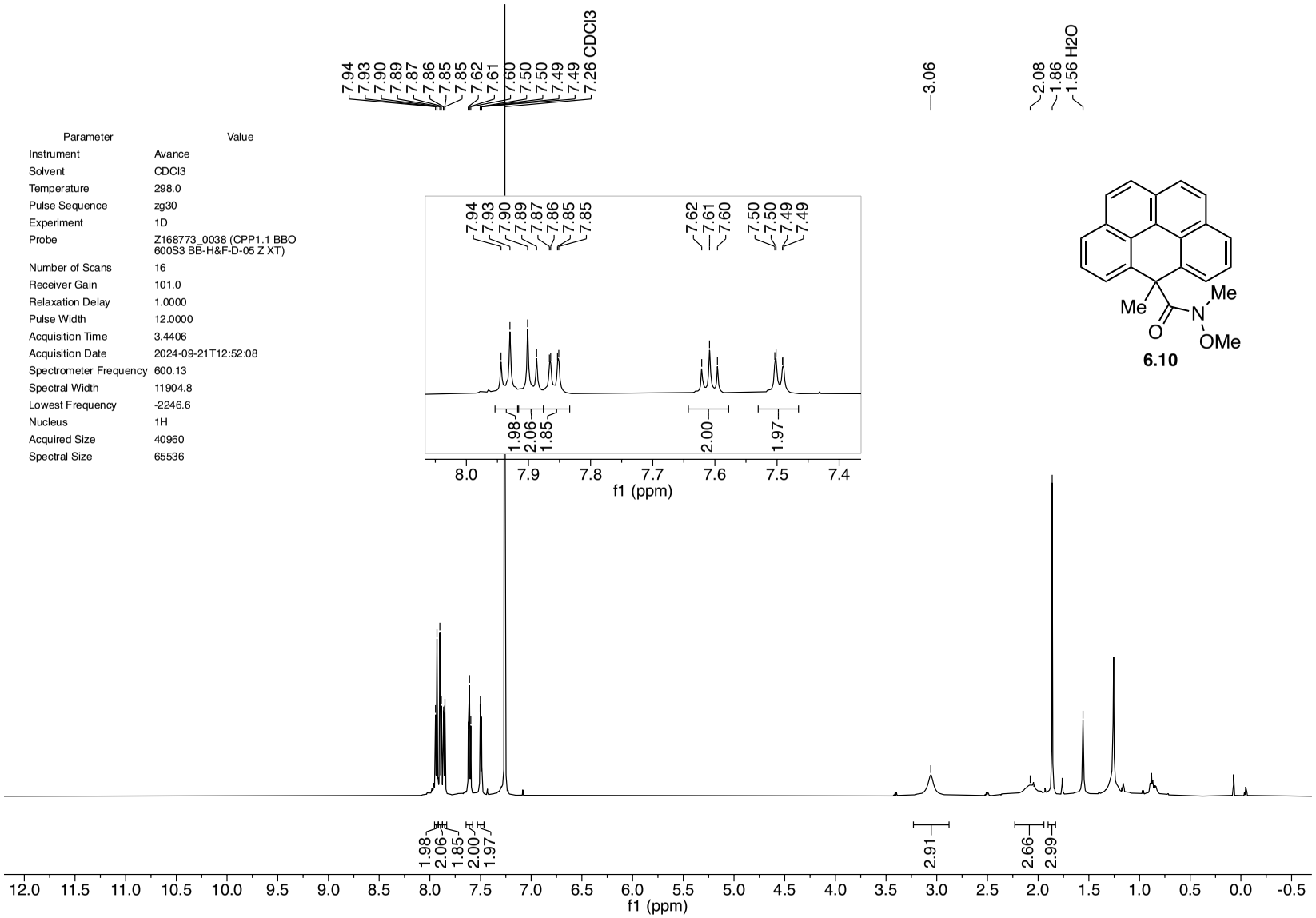
7.94
7.93
7.90
7.89
7.87
7.86
7.85
7.85
7.62
7.61
7.60
7.50
7.50
7.49
7.49
7.26 CDCl3
3.06
2.08
1.86
1.56 H2O
Parameter Value
Instrument Avance
Solvent CDCl3
Temperature 298.0
Pulse Sequence zg30
Experiment 1D
Probe Z168773_0038 (CPP1.1 BBO 600S3 BB-H&F-D-05 Z XT)
Number of Scans 16
Receiver Gain 101.0
Relaxation Delay 1.0000
Pulse Width 12.0000
Acquisition Time 3.4406
Acquisition Date 2024-09-21T12:52:08
Spectrometer Frequency 600.13
Spectral Width 11904.8
Lowest Frequency -2246.6
Nucleus 1H
Acquired Size 40960
Spectral Size 65536
1.98
2.06
1.85
2.00
1.97
8.0
7.9
7.8
7.7
7.6
7.5
7.4
f1 (ppm)
Me
Me
N
O
OMe
6.10
2.91
2.66
2.99
12.0
11.5
11.0
10.5
10.0
9.5
9.0
8.5
8.0
7.5
7.0
6.5
6.0
5.5
5.0
4.5
4.0
3.5
3.0
2.5
2.0
1.5
1.0
0.5
0.0
-0.5
f1 (ppm)

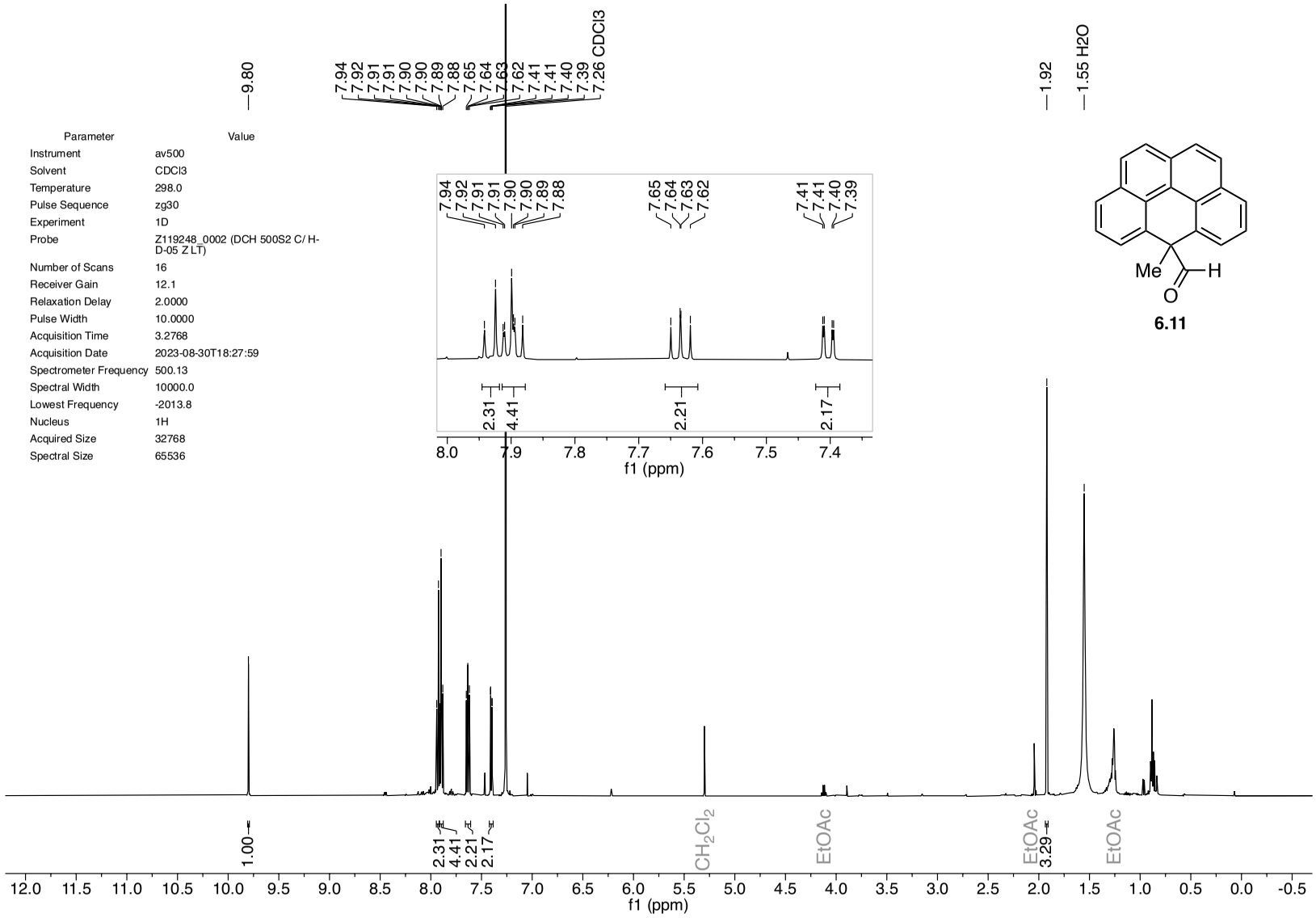
9.80
7.94
7.92
7.91
7.91
7.90
7.90
7.89
7.88
7.65
7.64
7.63
7.62
7.41
7.41
7.40
7.39
7.26 CDCl3
1.92
1.55 H2O
Parameter Value
Instrument av500
Solvent CDCl3
Temperature 298.0
Pulse Sequence zg30
Experiment 1D
Probe Z119248_0002 (DCH 500S2 C/ H-D-05 Z LT)
Number of Scans 16
Receiver Gain 12.1
Relaxation Delay 2.0000
Pulse Width 10.0000
Acquisition Time 3.2768
Acquisition Date 2023-08-30T18:27:59
Spectrometer Frequency 500.13
Spectral Width 10000.0
Lowest Frequency -2013.8
Nucleus 1H
Acquired Size 32768
Spectral Size 65536
2.31
4.41
2.21
2.17
f1 (ppm)
1.00
CH2Cl2
EtOAc
EtOAc
3.29
EtOAc
f1 (ppm)
Me
H
O
6.11

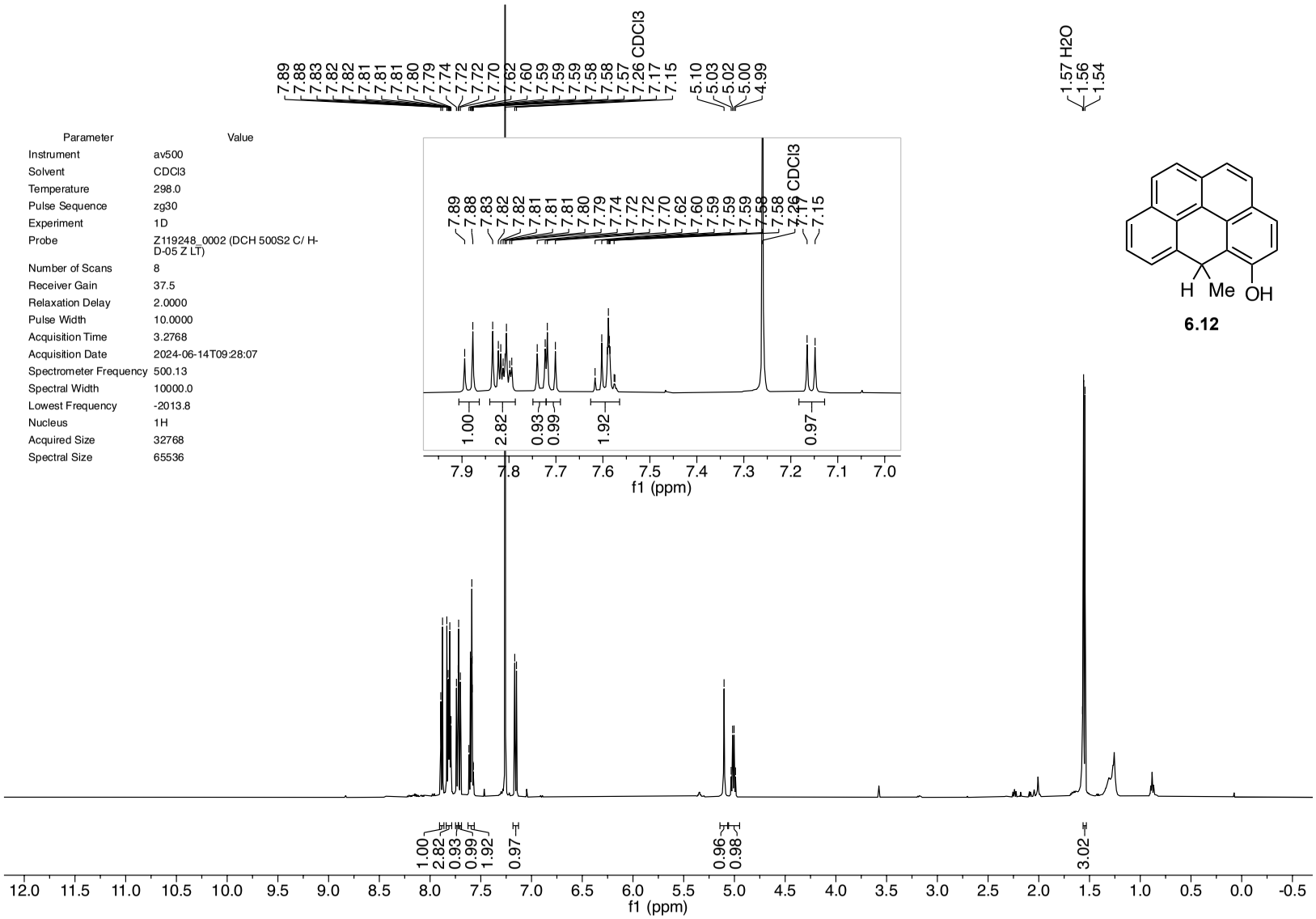
7.89 7.88 7.83 7.82 7.82 7.81 7.81 7.81 7.80 7.79 7.74 7.72 7.72 7.70 7.62 7.60 7.59 7.59 7.59 7.58 7.58 7.57 CDCl3 7.26 7.17 7.15 5.10 5.03 5.02 5.00 4.99
1.57 H2O 1.56 1.54
Parameter Value
Instrument av500
Solvent CDCl3
Temperature 298.0
Pulse Sequence zg30
Experiment 1D
Probe Z119248_0002 (DCH 500S2 C/ H-D-05 Z LT)
Number of Scans 8
Receiver Gain 37.5
Relaxation Delay 2.0000
Pulse Width 10.0000
Acquisition Time 3.2768
Acquisition Date 2024-06-14T09:28:07
Spectrometer Frequency 500.13
Spectral Width 10000.0
Lowest Frequency -2013.8
Nucleus 1H
Acquired Size 32768
Spectral Size 65536
1.00 2.82 0.93 0.99 1.92 0.97 0.96 0.98 3.02
f1 (ppm)
H Me OH
6.12

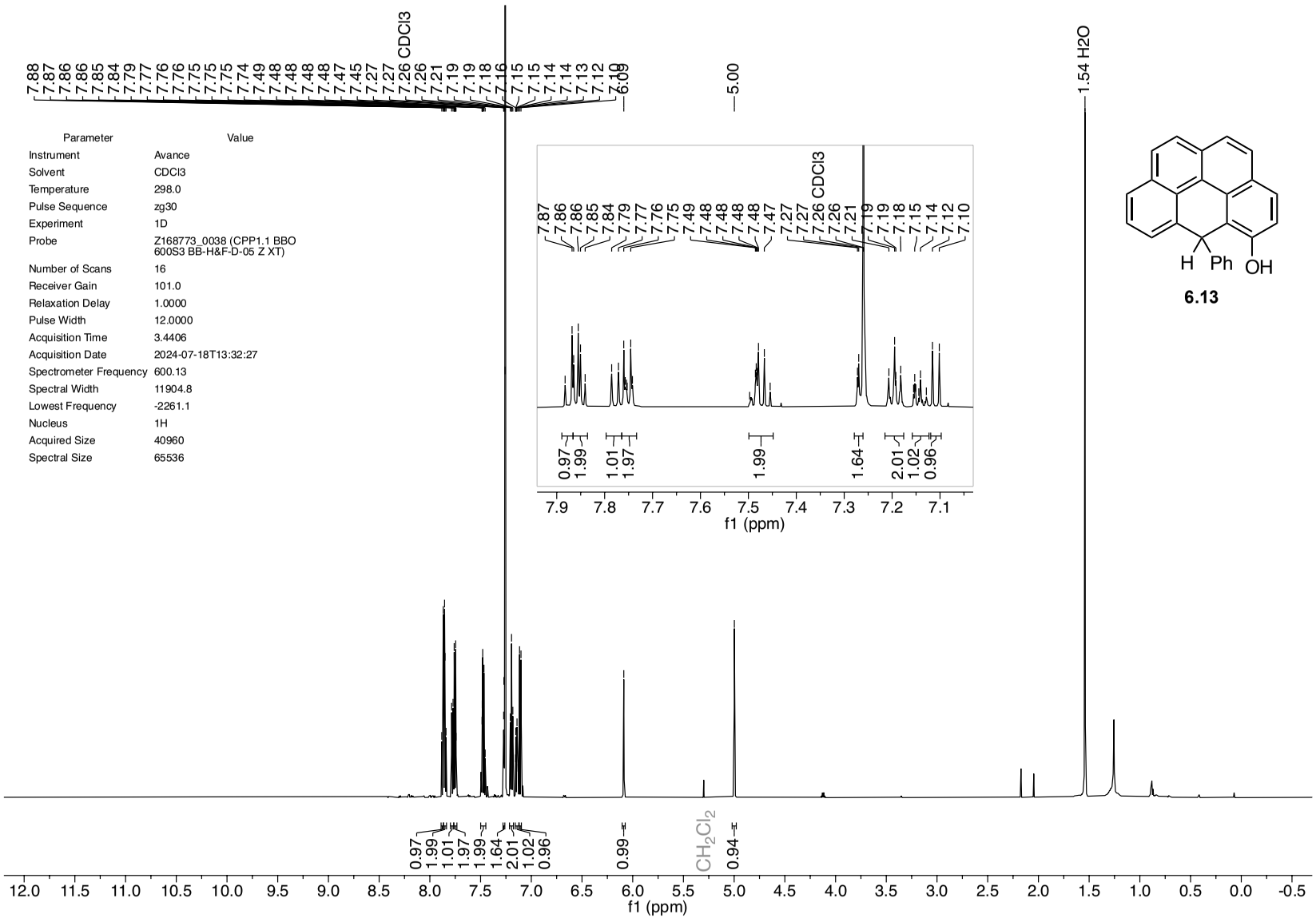
7.88 7.87 7.86 7.86 7.85 7.84 7.79 7.77 7.76 7.75 7.75 7.74 7.49 7.48 7.48 7.48 7.47 7.45 7.27 7.26 CDCl3 7.26 7.21 7.19 7.19 7.18 7.16 7.15 7.15 7.14 7.13 7.12 7.10 6.09
5.00
1.54 H2O
Parameter Value
Instrument Avance
Solvent CDCl3
Temperature 298.0
Pulse Sequence zg30
Experiment 1D
Probe Z168773_0038 (CPP1.1 BBO 600S3 BB-H&F-D-05 Z XT)
Number of Scans 16
Receiver Gain 101.0
Relaxation Delay 1.0000
Pulse Width 12.0000
Acquisition Time 3.4406
Acquisition Date 2024-07-18T13:32:27
Spectrometer Frequency 600.13
Spectral Width 11904.8
Lowest Frequency -2261.1
Nucleus 1H
Acquired Size 40960
Spectral Size 65536
7.87 7.86 7.86 7.85 7.84 7.79 7.77 7.76 7.75 7.49 7.48 7.48 7.48 7.47 7.27 7.27 7.26 CDCl3 7.26 7.21 7.19 7.19 7.18 7.15 7.14 7.12 7.10
0.97 1.99 1.01 1.97 1.99 1.64 2.01 1.02 0.96
7.9 7.8 7.7 7.6 7.5 7.4 7.3 7.2 7.1
f1 (ppm)
H Ph OH
6.13
0.97 1.99 1.01 1.97 1.99 1.64 2.01 1.02 0.96 0.99 CH2Cl2 0.94
12.0 11.5 11.0 10.5 10.0 9.5 9.0 8.5 8.0 7.5 7.0 6.5 6.0 5.5 5.0 4.5 4.0 3.5 3.0 2.5 2.0 1.5 1.0 0.5 0.0 -0.5
f1 (ppm)

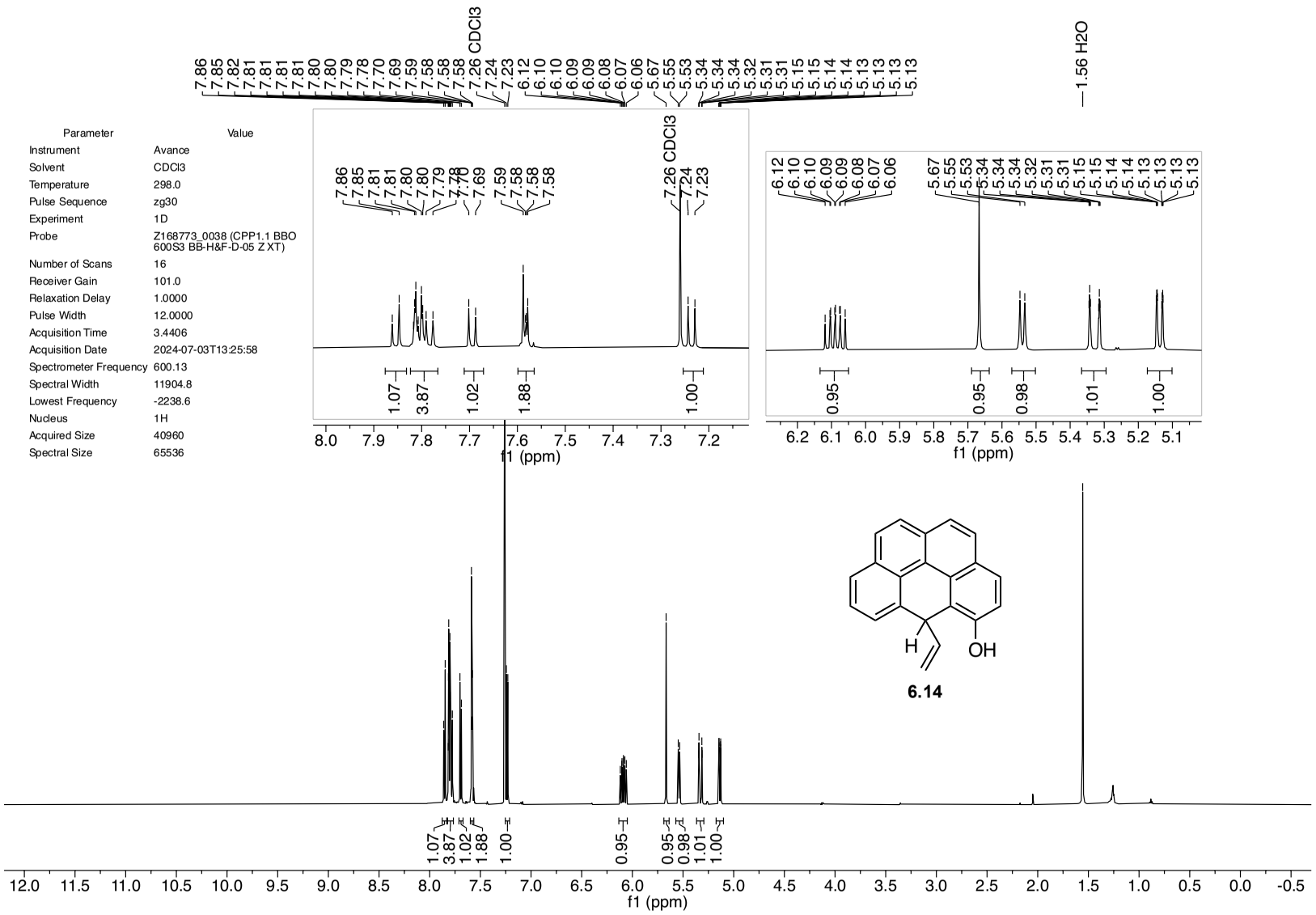
7.86 7.85 7.82 7.81 7.81 7.81 7.81 7.80 7.80 7.79 7.78 7.70 7.69 7.59 7.58 7.58 7.58 7.26 CDCl3 7.24 7.23 6.12 6.10 6.10 6.09 6.09 6.08 6.07 6.06 5.67 5.55 5.53 5.34 5.34 5.34 5.32 5.31 5.31 5.15 5.15 5.14 5.13 5.13 5.13 1.56 H2O
Parameter Value
Instrument Avance
Solvent CDCl3
Temperature 298.0
Pulse Sequence zg30
Experiment 1D
Probe Z168773_0038 (CPP1,1 BBO 600S3 BB-H&F-D-05 Z XT)
Number of Scans 16
Receiver Gain 101.0
Relaxation Delay 1.0000
Pulse Width 12.0000
Acquisition Time 3.4406
Acquisition Date 2024-07-03T13:25:58
Spectrometer Frequency 600.13
Spectral Width 11904.8
Lowest Frequency -2238.6
Nucleus 1H
Acquired Size 40960
Spectral Size 65536
1.07 3.87 1.02 1.88 1.00 0.95 0.95 0.98 1.01 1.00
f1 (ppm)
H
OH
6.14

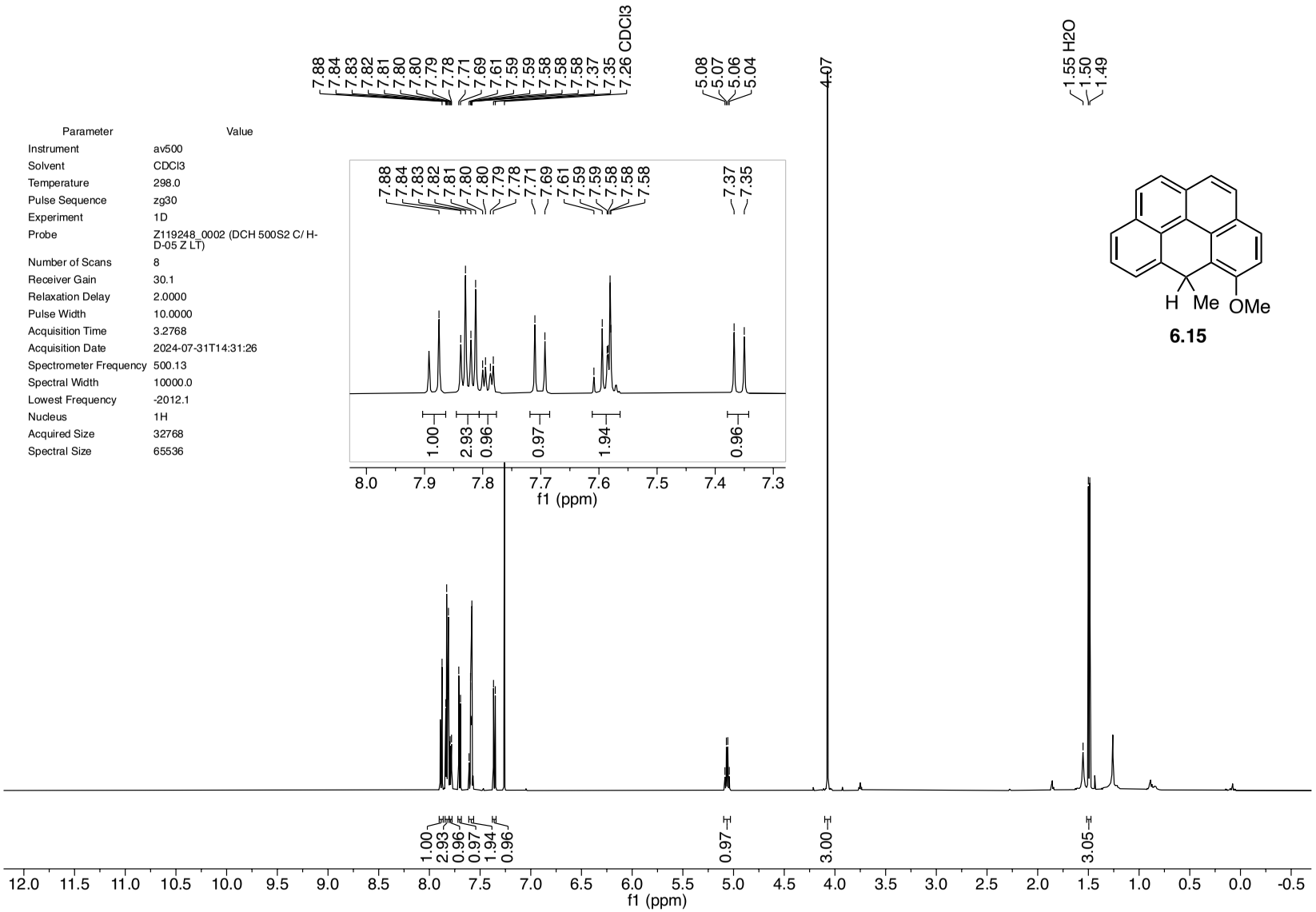
7.88
7.84
7.83
7.82
7.81
7.80
7.80
7.79
7.78
7.71
7.69
7.61
7.59
7.59
7.58
7.58
7.58
7.37
7.35
7.26 CDCl3
5.08
5.07
5.06
5.04
4.07
1.55 H2O
1.50
1.49
Parameter Value
Instrument av500
Solvent CDCl3
Temperature 298.0
Pulse Sequence zg30
Experiment 1D
Probe Z119248_0002 (DCH 500S2 C/ H-D-05 Z LT)
Number of Scans 8
Receiver Gain 30.1
Relaxation Delay 2.0000
Pulse Width 10.0000
Acquisition Time 3.2768
Acquisition Date 2024-07-31T14:31:26
Spectrometer Frequency 500.13
Spectral Width 10000.0
Lowest Frequency -2012.1
Nucleus 1H
Acquired Size 32768
Spectral Size 65536
1.00
2.93
0.96
0.97
1.94
0.96
0.97
3.00
3.05
f1 (ppm)
H Me OMe
6.15

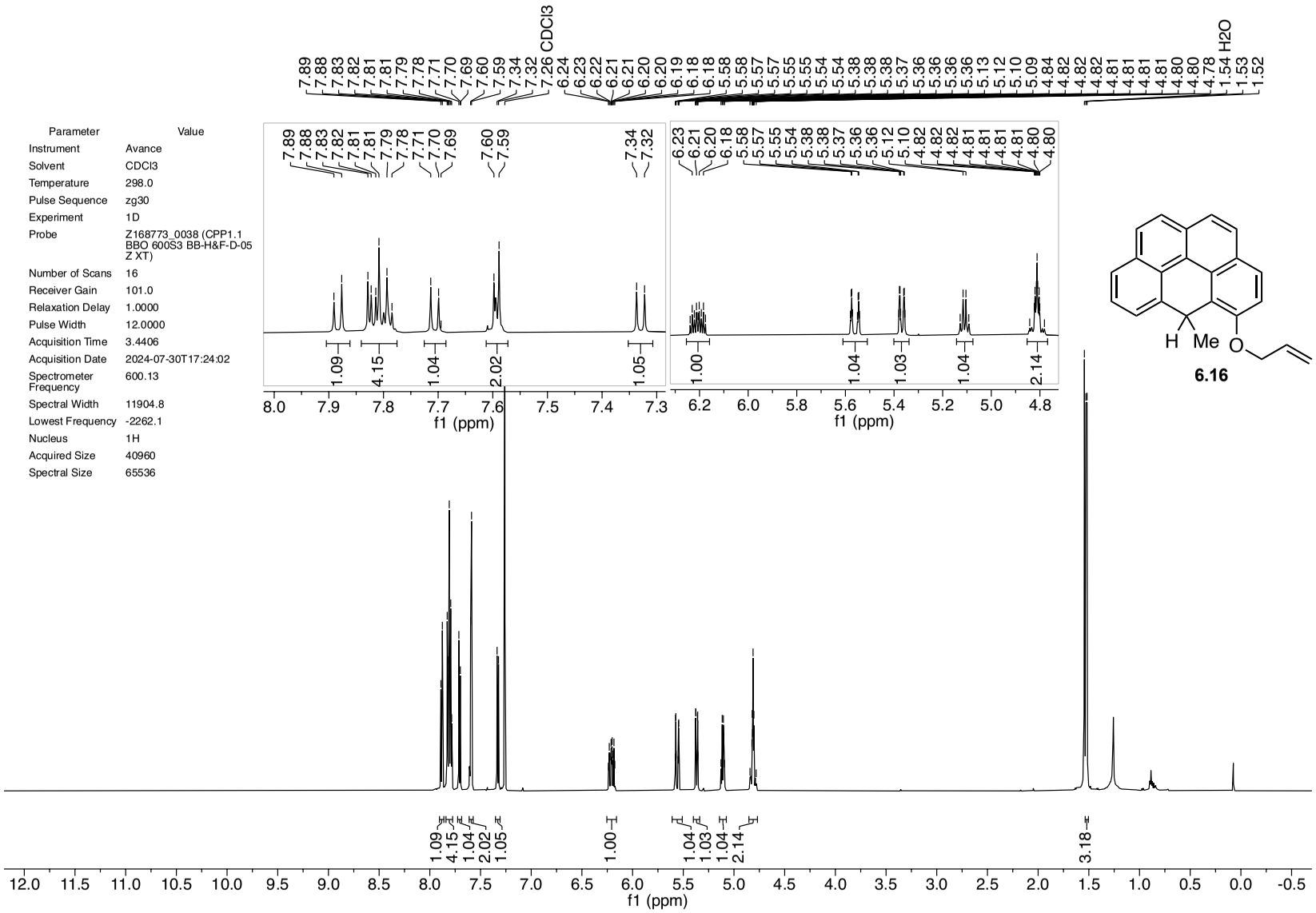
Parameter Value
Instrument Avance
Solvent CDCl3
Temperature 298.0
Pulse Sequence zg30
Experiment 1D
Probe Z168773_0038 (CPP1.1 BBO 600S3 BB-H&F-D-05 Z XT)
Number of Scans 16
Receiver Gain 101.0
Relaxation Delay 1.0000
Pulse Width 12.0000
Acquisition Time 3.4406
Acquisition Date 2024-07-30T17:24:02
Spectrometer Frequency 600.13
Spectral Width 11904.8
Lowest Frequency -2262.1
Nucleus 1H
Acquired Size 40960
Spectral Size 65536
CDCl3
H2O
H Me O
6.16
f1 (ppm)

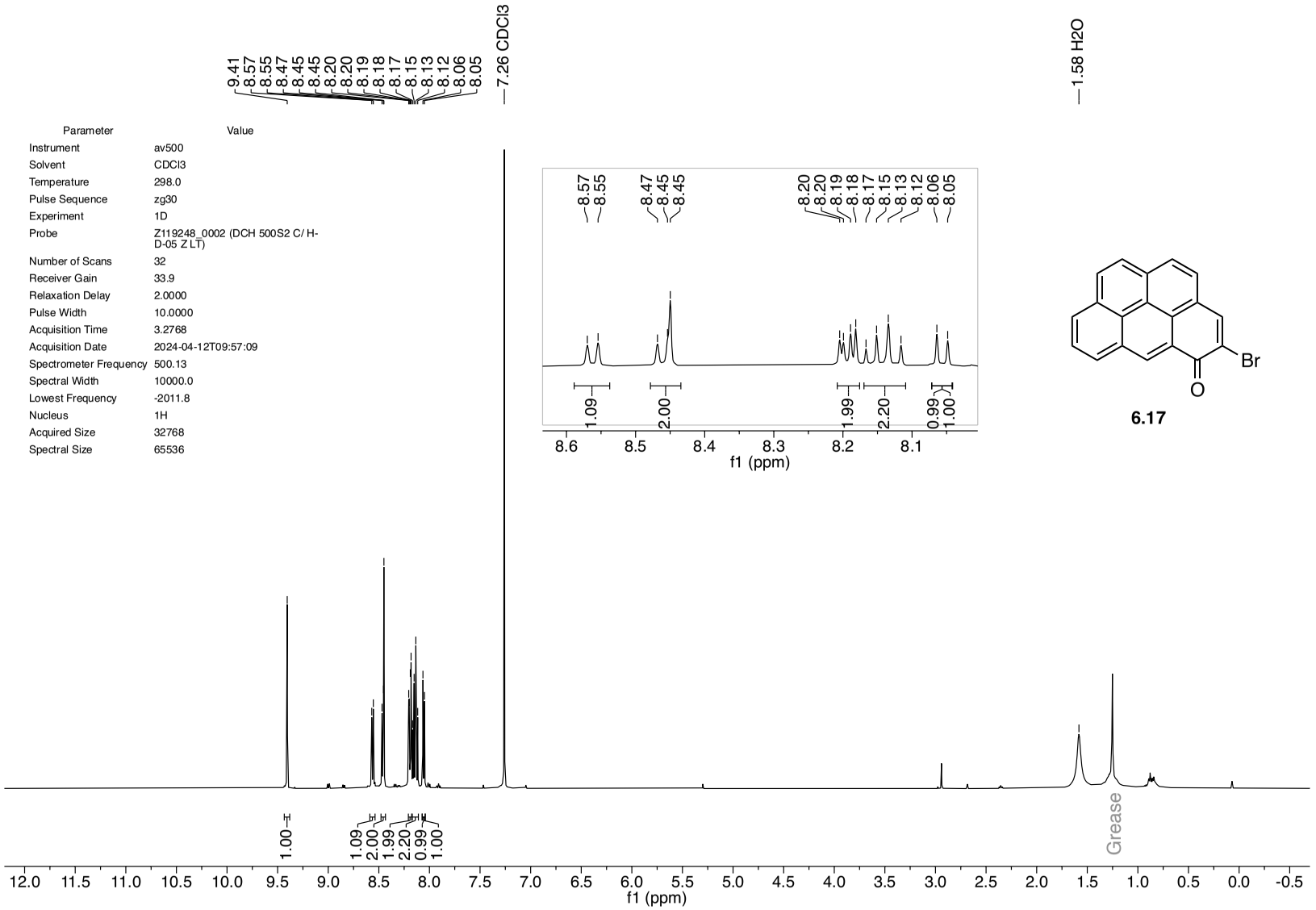
9.41
8.57
8.55
8.47
8.45
8.45
8.20
8.19
8.18
8.17
8.15
8.13
8.12
8.06
8.05
7.26 CDCl3
1.58 H2O
Parameter Value
Instrument av500
Solvent CDCl3
Temperature 298.0
Pulse Sequence zg30
Experiment 1D
Probe Z119248_0002 (DCH 500S2 C/ H-D-05 Z LT)
Number of Scans 32
Receiver Gain 33.9
Relaxation Delay 2.0000
Pulse Width 10.0000
Acquisition Time 3.2768
Acquisition Date 2024-04-12T09:57:09
Spectrometer Frequency 500.13
Spectral Width 10000.0
Lowest Frequency -2011.8
Nucleus 1H
Acquired Size 32768
Spectral Size 65536
1.09
2.00
1.99
2.20
0.99
1.00
f1 (ppm)
Br
O
6.17
Grease

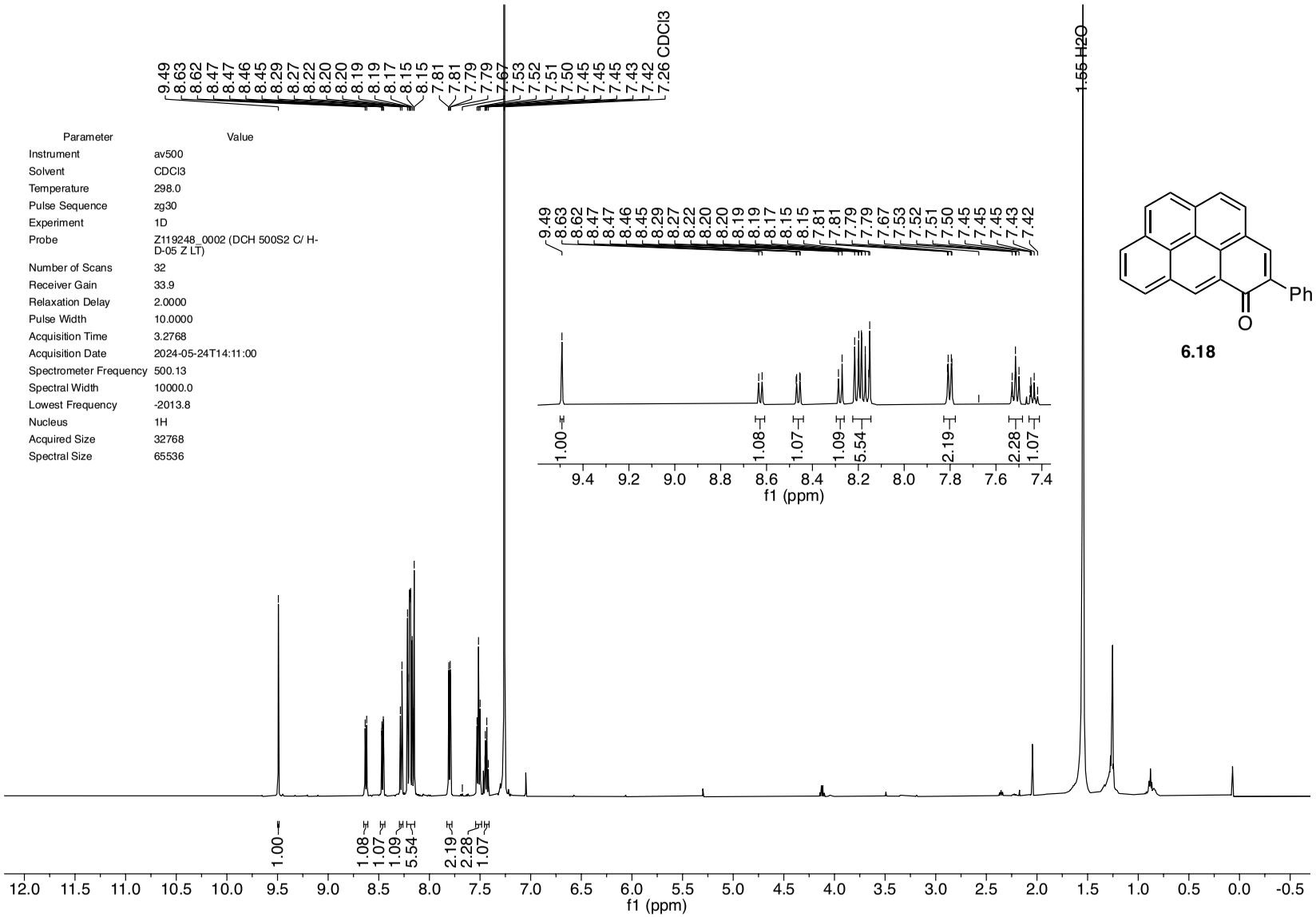
9.49
8.63
8.62
8.47
8.47
8.46
8.45
8.29
8.27
8.22
8.20
8.20
8.19
8.19
8.17
8.15
8.15
7.81
7.81
7.79
7.79
7.67
7.53
7.52
7.51
7.50
7.45
7.45
7.45
7.43
7.42
7.26 CDCl3
1.55 H2O
Parameter Value
Instrument av500
Solvent CDCl3
Temperature 298.0
Pulse Sequence zg30
Experiment 1D
Probe Z119248_0002 (DCH 500S2 C/ H-D-05 Z LT)
Number of Scans 32
Receiver Gain 33.9
Relaxation Delay 2.0000
Pulse Width 10.0000
Acquisition Time 3.2768
Acquisition Date 2024-05-24T14:11:00
Spectrometer Frequency 500.13
Spectral Width 10000.0
Lowest Frequency -2013.8
Nucleus 1H
Acquired Size 32768
Spectral Size 65536
1.00
1.08
1.07
1.09
5.54
2.19
2.28
1.07
f1 (ppm)
Ph
O
6.18

6.5.6 ^{13}C NMR specta

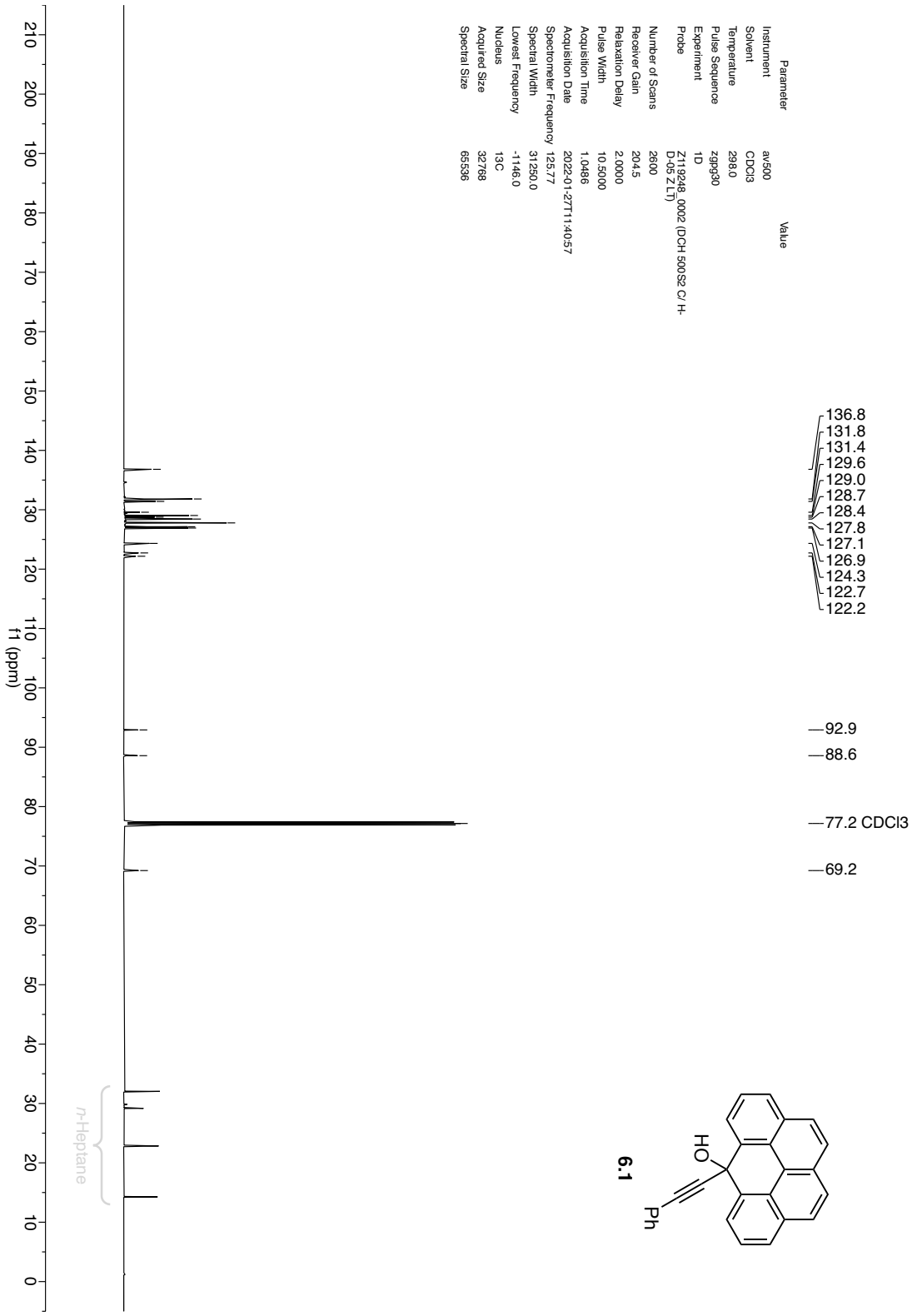

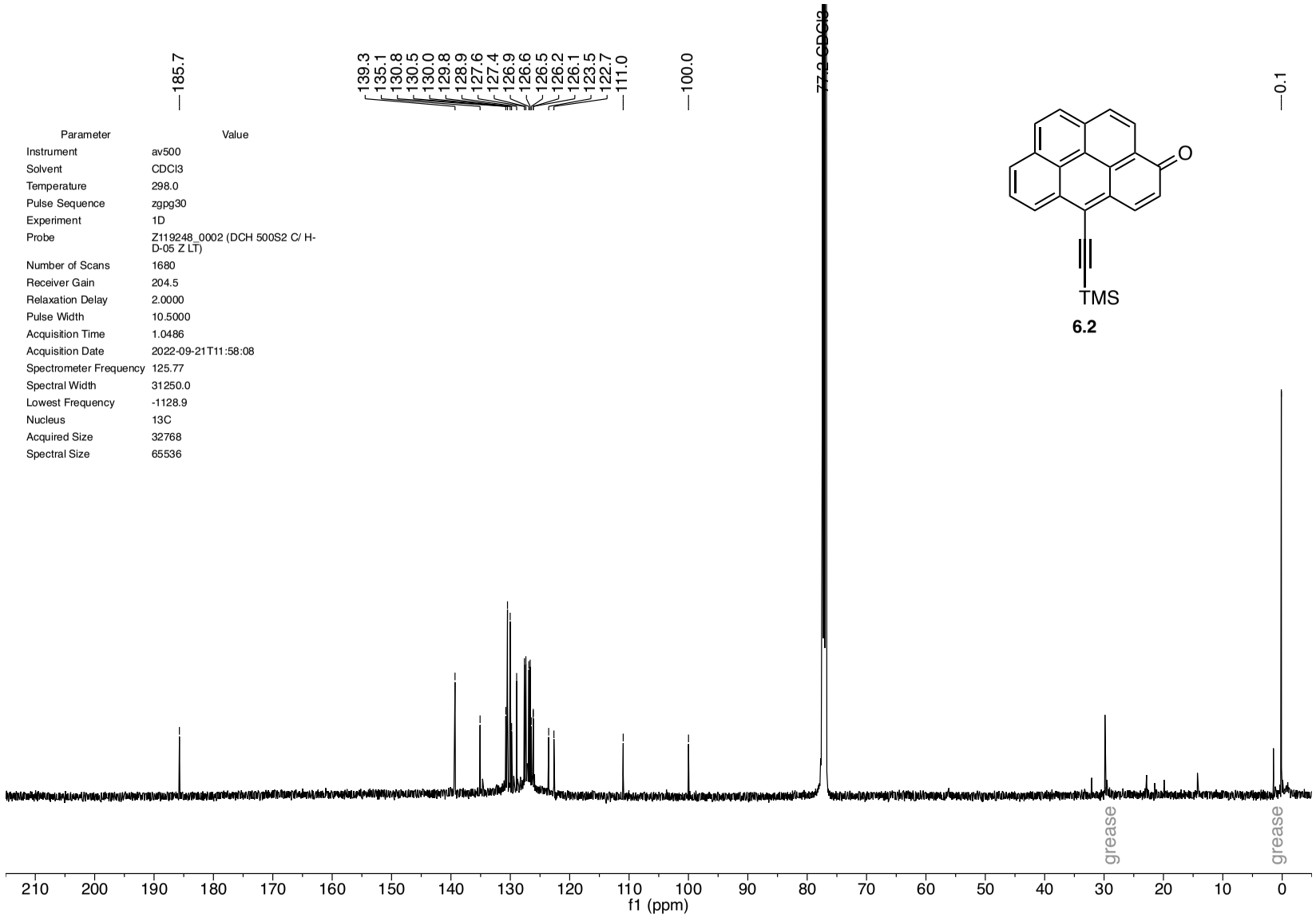
185.7
139.3
135.1
130.8
130.5
130.0
129.8
128.9
127.6
127.4
126.9
126.6
126.5
126.2
126.1
123.5
122.7
111.0
100.0
77.0 CDCl3
0.1
Parameter Value
Instrument av500
Solvent CDCl3
Temperature 298.0
Pulse Sequence zgpg30
Experiment 1D
Probe Z119248_0002 (DCH 500S2 C/ H-D-05 Z LT)
Number of Scans 1680
Receiver Gain 204.5
Relaxation Delay 2.0000
Pulse Width 10.5000
Acquisition Time 1.0486
Acquisition Date 2022-09-21T11:58:08
Spectrometer Frequency 125.77
Spectral Width 31250.0
Lowest Frequency -1128.9
Nucleus 13C
Acquired Size 32768
Spectral Size 65536
O
TMS
6.2
grease
grease
210 200 190 180 170 160 150 140 130 120 110 100 90 80 70 60 50 40 30 20 10 0
f1 (ppm)

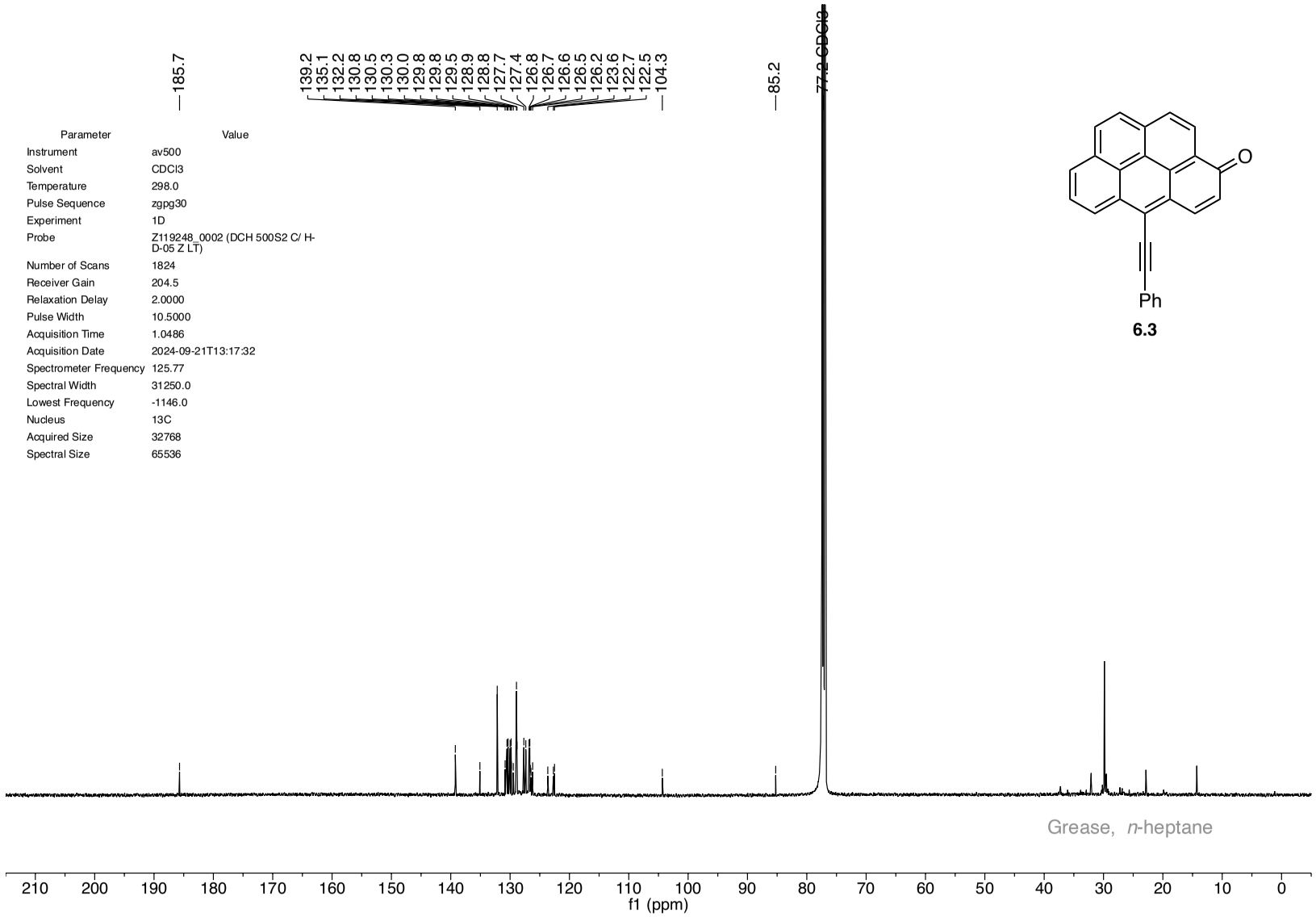

Parameter	Value
Instrument	av500
Solvent	CDCl3
Temperature	298.0
Pulse Sequence	zgpg30
Experiment	1D
Probe	Z119248_0002 (DCH 500S2 C/ H-D-05 Z LT)
Number of Scans	1824
Receiver Gain	204.5
Relaxation Delay	2.0000
Pulse Width	10.5000
Acquisition Time	1.0486
Acquisition Date	2024-09-21T13:17:32
Spectrometer Frequency	125.77
Spectral Width	31250.0
Lowest Frequency	-1146.0
Nucleus	13C
Acquired Size	32768
Spectral Size	65536

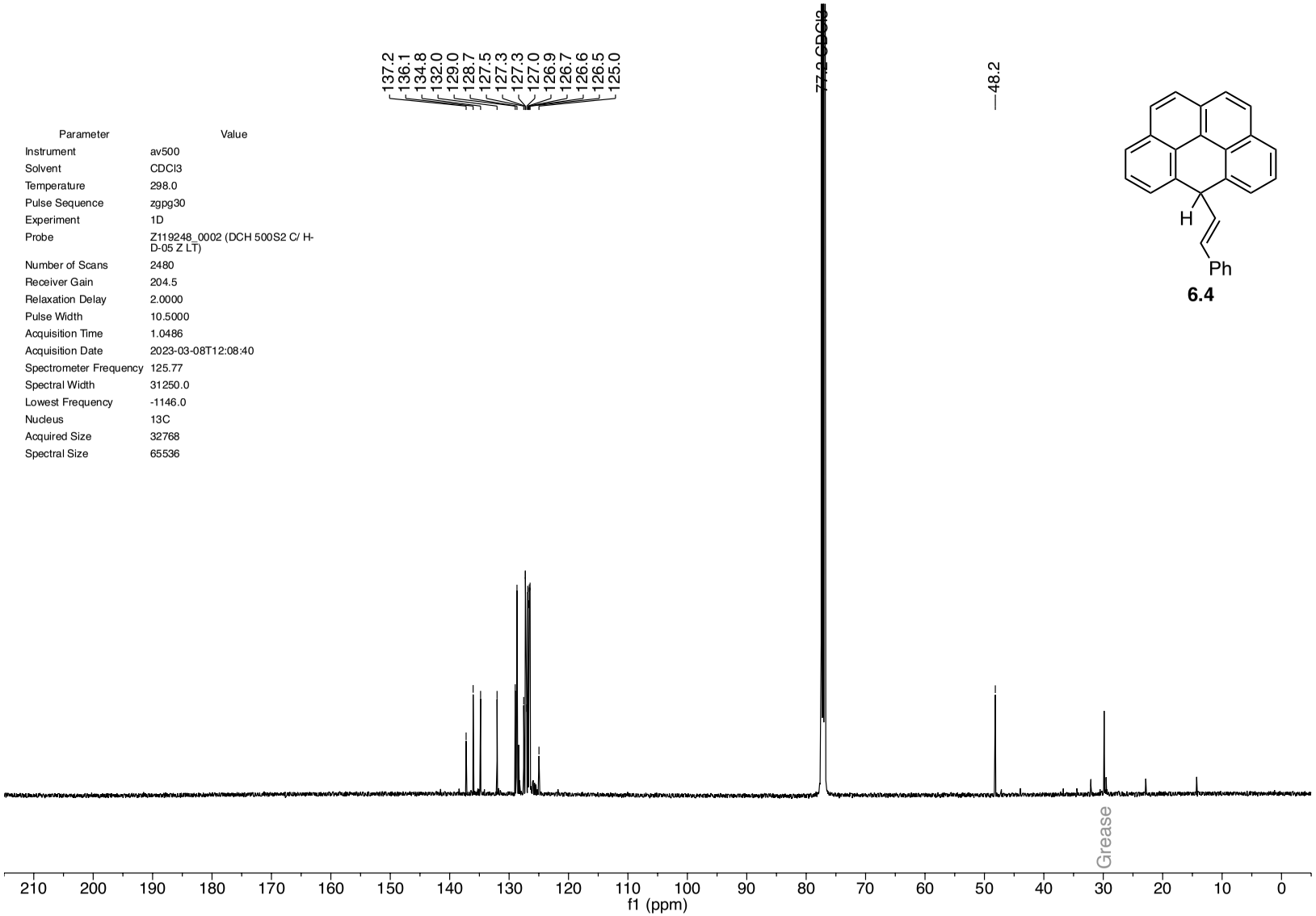

Parameter	Value
Instrument	av500
Solvent	CDCl3
Temperature	298.0
Pulse Sequence	zgpg30
Experiment	1D
Probe	Z119248_0002 (DCH 500S2 C/ H-D-05 Z LT)
Number of Scans	2480
Receiver Gain	204.5
Relaxation Delay	2.0000
Pulse Width	10.5000
Acquisition Time	1.0486
Acquisition Date	2023-03-08T12:08:40
Spectrometer Frequency	125.77
Spectral Width	31250.0
Lowest Frequency	-1146.0
Nucleus	13C
Acquired Size	32768
Spectral Size	65536

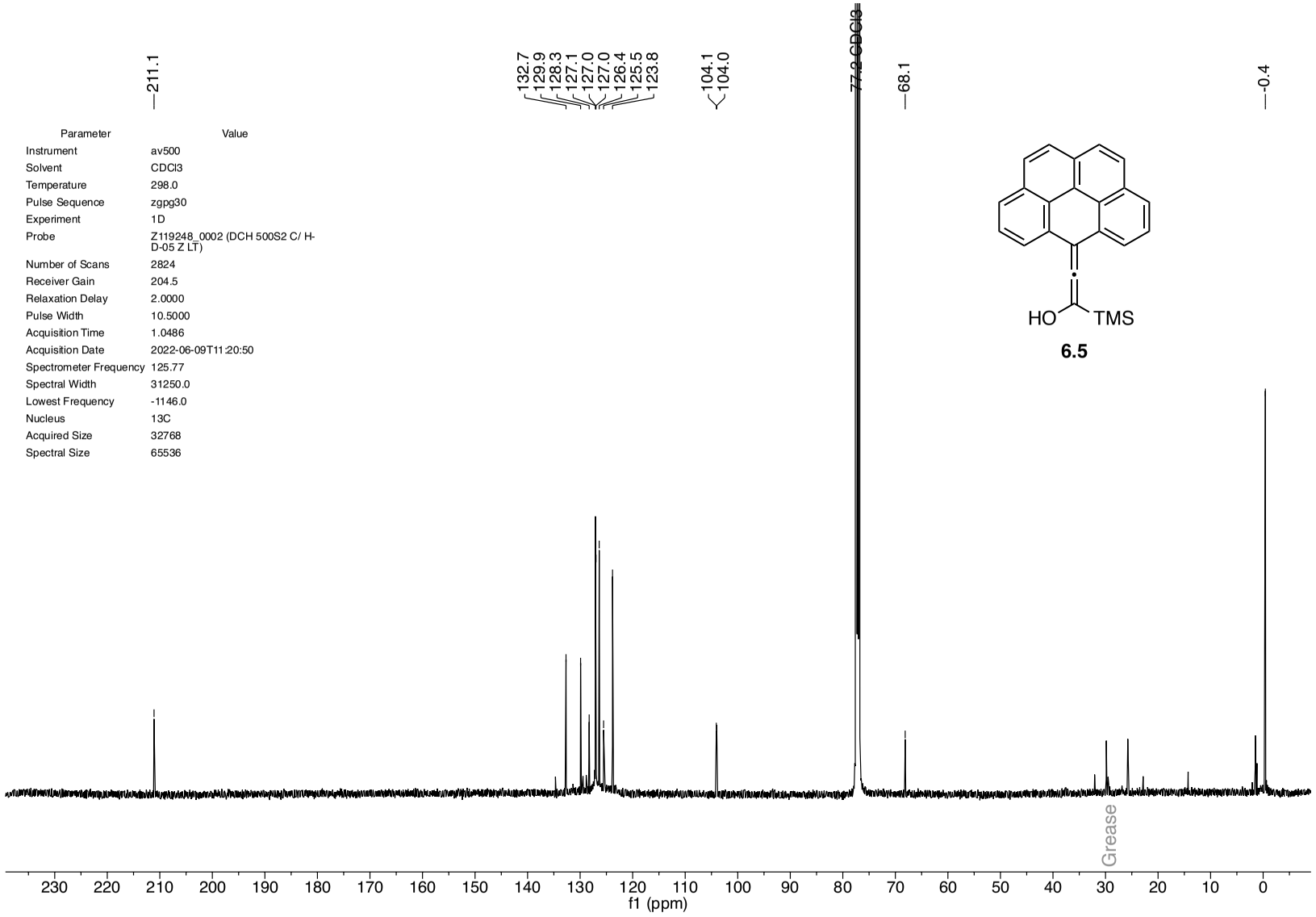
211.1
132.7
129.9
128.3
127.1
127.0
127.0
126.4
125.5
123.8
104.1
104.0
77.2 CDCl3
68.1
-0.4
Parameter Value
Instrument av500
Solvent CDCl3
Temperature 298.0
Pulse Sequence zgpg30
Experiment 1D
Probe Z119248_0002 (DCH 500S2 C/ H-D-05 Z LT)
Number of Scans 2824
Receiver Gain 204.5
Relaxation Delay 2.0000
Pulse Width 10.5000
Acquisition Time 1.0486
Acquisition Date 2022-06-09T11:20:50
Spectrometer Frequency 125.77
Spectral Width 31250.0
Lowest Frequency -1146.0
Nucleus 13C
Acquired Size 32768
Spectral Size 65536
HO
TMS
6.5
Grease
230 220 210 200 190 180 170 160 150 140 130 120 110 100 90 80 70 60 50 40 30 20 10 0
f1 (ppm)

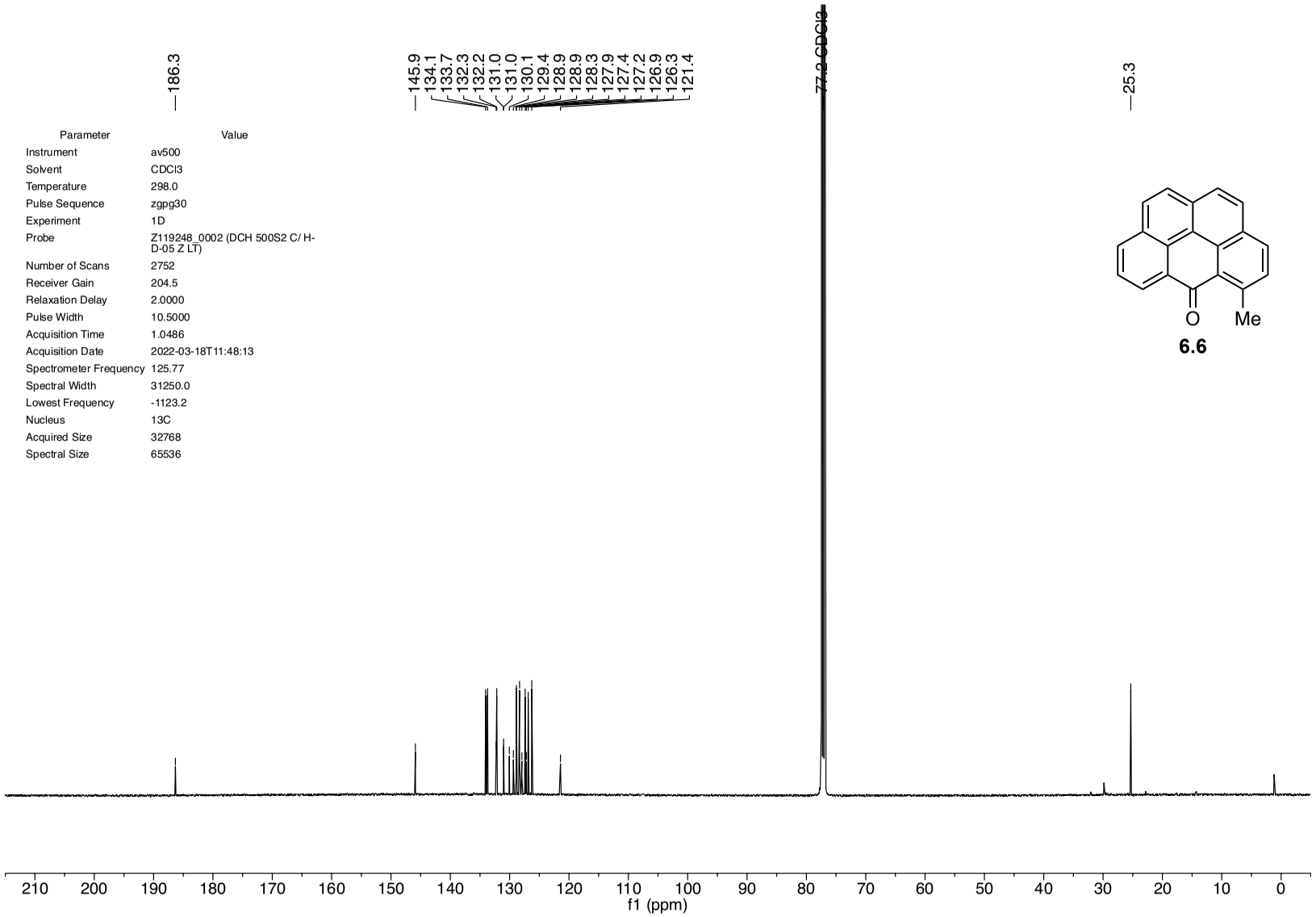
186.3
145.9
134.1
133.7
132.3
132.2
131.0
131.0
130.1
129.4
128.9
128.9
128.3
127.9
127.4
127.2
126.9
126.3
121.4
77.2 CDCl3
25.3
Parameter Value
Instrument av500
Solvent CDCl3
Temperature 298.0
Pulse Sequence zgpg30
Experiment 1D
Probe Z119248_0002 (DCH 500S2 C/ H-D-05 Z LT)
Number of Scans 2752
Receiver Gain 204.5
Relaxation Delay 2.0000
Pulse Width 10.5000
Acquisition Time 1.0486
Acquisition Date 2022-03-18T11:48:13
Spectrometer Frequency 125.77
Spectral Width 31250.0
Lowest Frequency -1123.2
Nucleus 13C
Acquired Size 32768
Spectral Size 65536
O
Me
6.6
210 200 190 180 170 160 150 140 130 120 110 100 90 80 70 60 50 40 30 20 10 0
f1 (ppm)

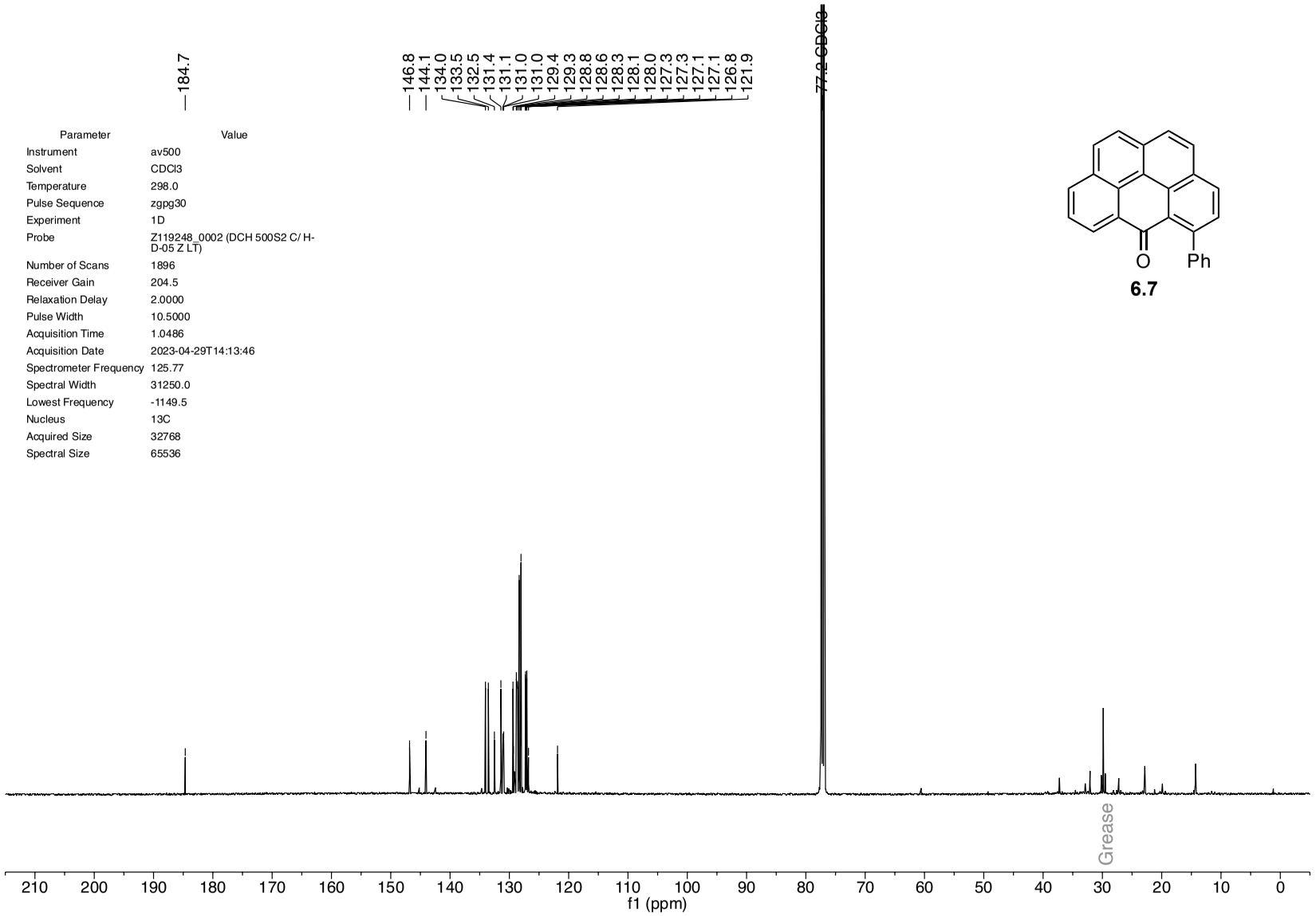

Parameter	Value
Instrument	av500
Solvent	CDCl3
Temperature	298.0
Pulse Sequence	zgpg30
Experiment	1D
Probe	Z119248_0002 (DCH 500S2 C/ H-D-05 Z LT)
Number of Scans	1896
Receiver Gain	204.5
Relaxation Delay	2.0000
Pulse Width	10.5000
Acquisition Time	1.0486
Acquisition Date	2023-04-29T14:13:46
Spectrometer Frequency	125.77
Spectral Width	31250.0
Lowest Frequency	-1149.5
Nucleus	13C
Acquired Size	32768
Spectral Size	65536

6.7

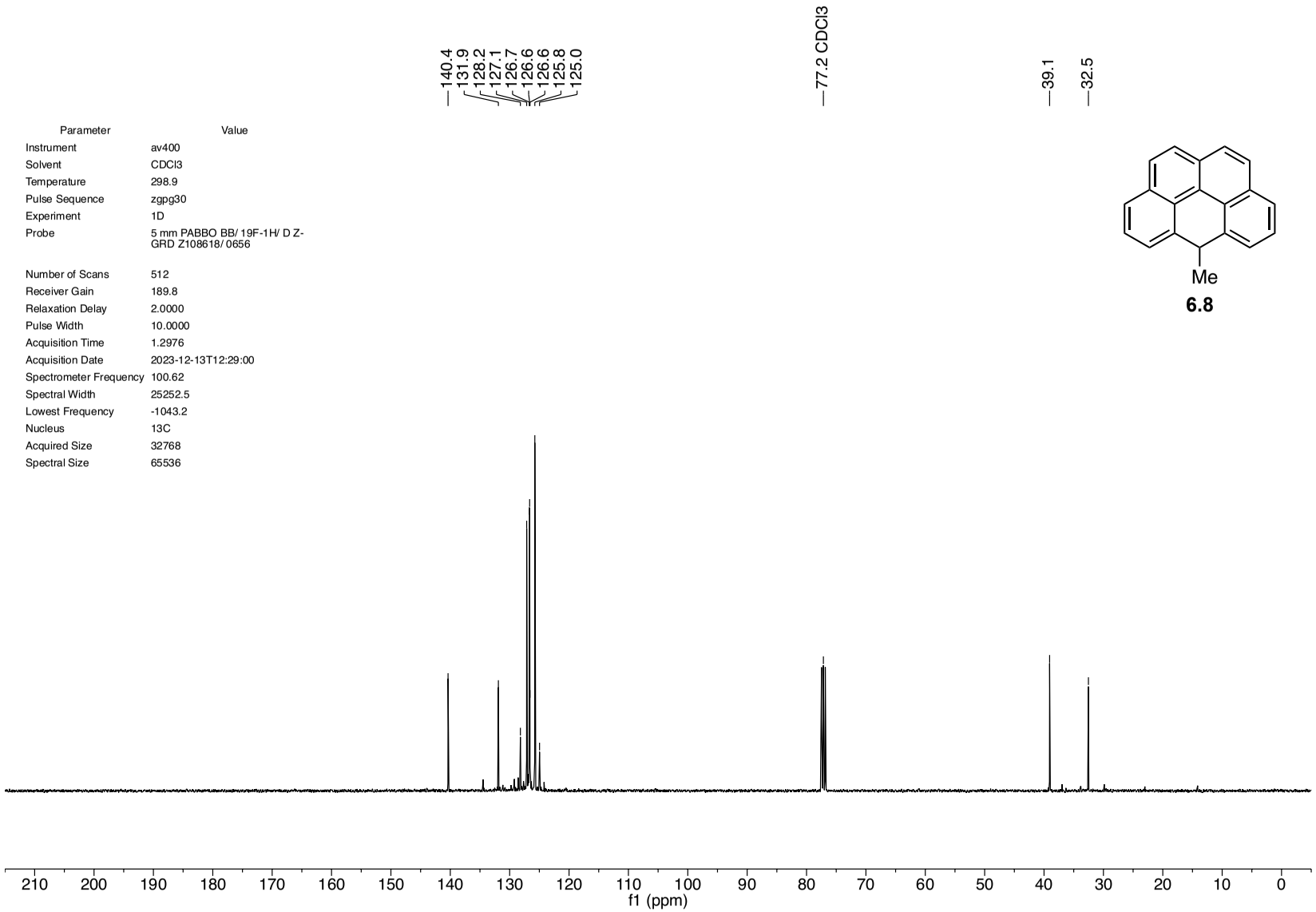
140.4
131.9
128.2
127.1
126.7
126.6
126.6
125.8
125.0
77.2 CDCl3
39.1
32.5
Me
6.8
Parameter Value
Instrument av400
Solvent CDCl3
Temperature 298.9
Pulse Sequence zgpg30
Experiment 1D
Probe 5 mm PABBO BB/ 19F-1H/ D Z-GRD Z108618/ 0656
Number of Scans 512
Receiver Gain 189.8
Relaxation Delay 2.0000
Pulse Width 10.0000
Acquisition Time 1.2976
Acquisition Date 2023-12-13T12:29:00
Spectrometer Frequency 100.62
Spectral Width 25252.5
Lowest Frequency -1043.2
Nucleus 13C
Acquired Size 32768
Spectral Size 65536
210 200 190 180 170 160 150 140 130 120 110 100 90 80 70 60 50 40 30 20 10 0
f1 (ppm)

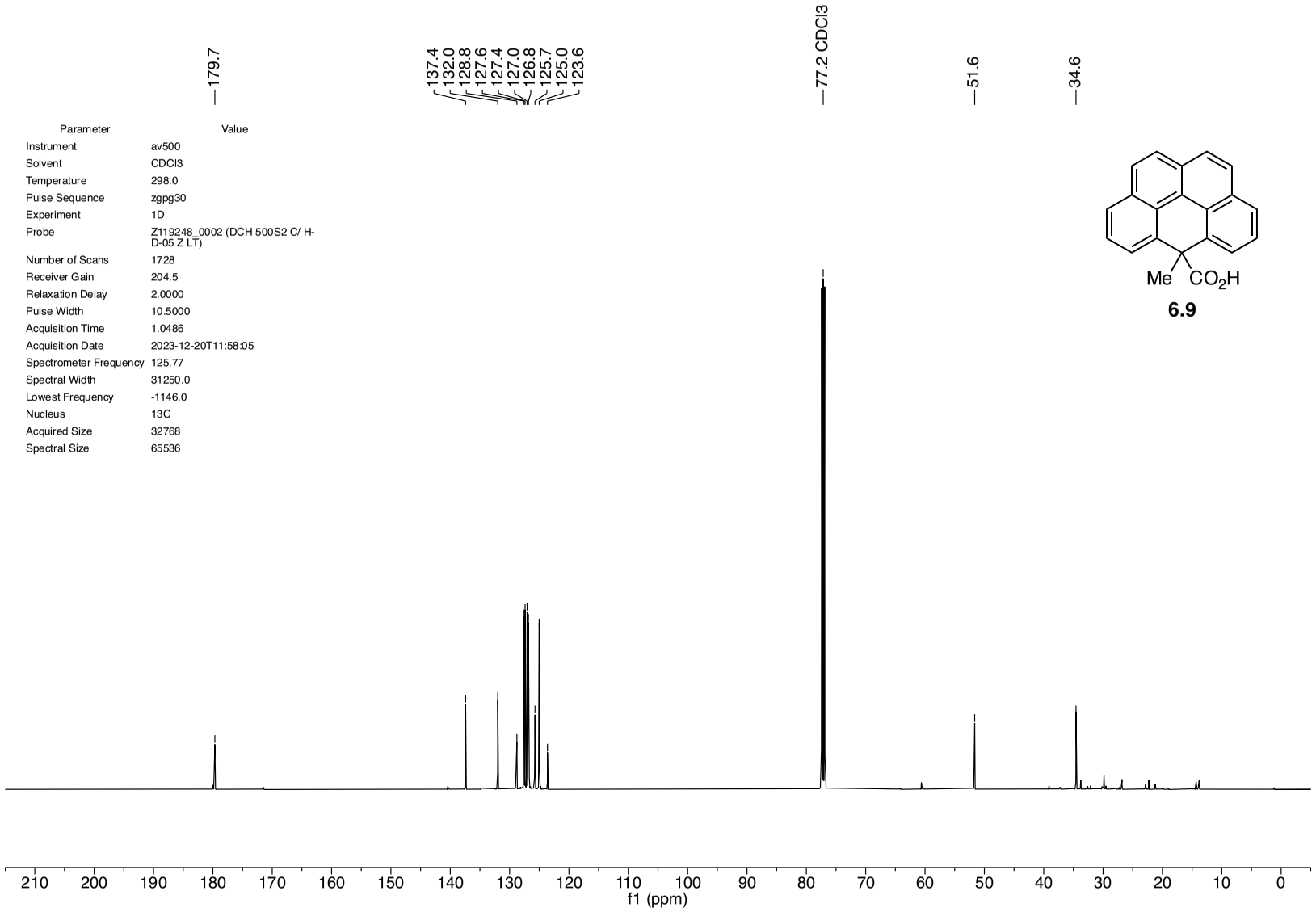
179.7
137.4
132.0
128.8
127.6
127.4
127.0
126.8
125.7
125.0
123.6
77.2 CDCl3
51.6
34.6
Parameter Value
Instrument av500
Solvent CDCl3
Temperature 298.0
Pulse Sequence zgpg30
Experiment 1D
Probe Z119248_0002 (DCH 500S2 C/ H-D-05 Z LT)
Number of Scans 1728
Receiver Gain 204.5
Relaxation Delay 2.0000
Pulse Width 10.5000
Acquisition Time 1.0486
Acquisition Date 2023-12-20T11:58:05
Spectrometer Frequency 125.77
Spectral Width 31250.0
Lowest Frequency -1146.0
Nucleus 13C
Acquired Size 32768
Spectral Size 65536
Me
CO2H
6.9
210 200 190 180 170 160 150 140 130 120 110 100 90 80 70 60 50 40 30 20 10 0
f1 (ppm)

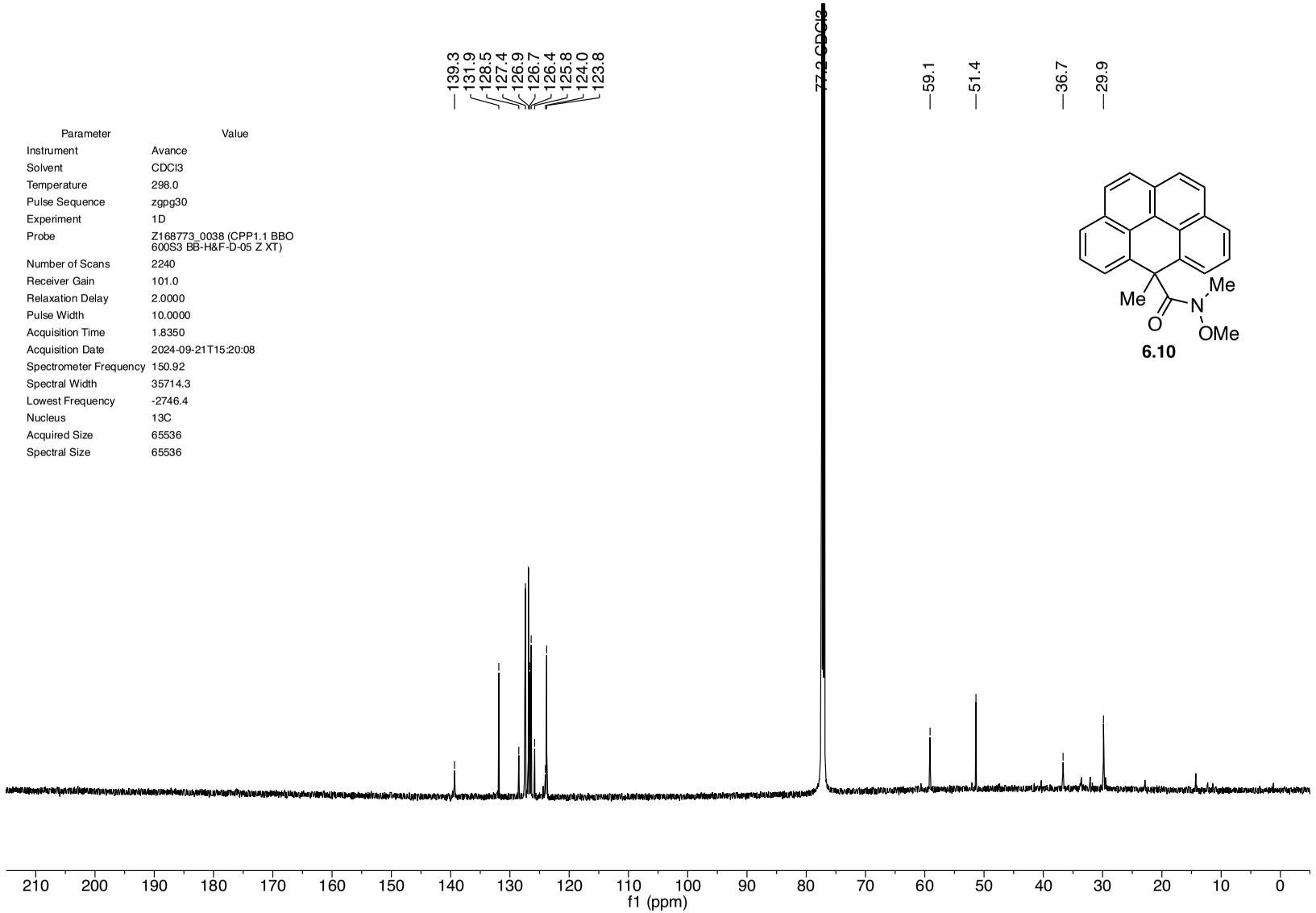

Parameter	Value
Instrument	Avance
Solvent	CDCl3
Temperature	298.0
Pulse Sequence	zgpg30
Experiment	1D
Probe	Z168773_0038 (CPP1.1 BBO 600S3 BB-H&F-D-05 Z XT)
Number of Scans	2240
Receiver Gain	101.0
Relaxation Delay	2.0000
Pulse Width	10.0000
Acquisition Time	1.8350
Acquisition Date	2024-09-21T15:20:08
Spectrometer Frequency	150.92
Spectral Width	35714.3
Lowest Frequency	-2746.4
Nucleus	13C
Acquired Size	65536
Spectral Size	65536

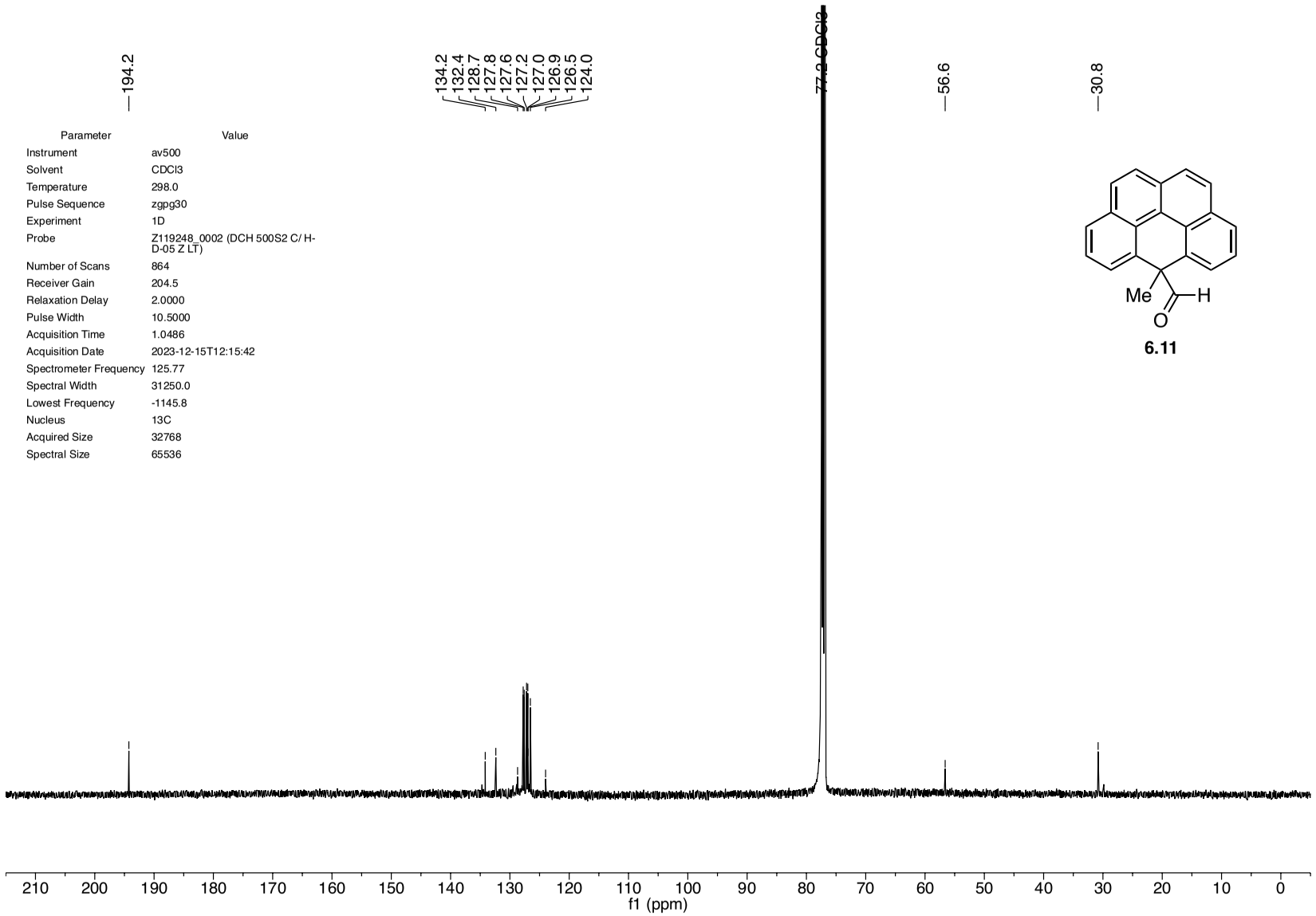
194.2
134.2
132.4
128.7
127.8
127.6
127.2
127.0
126.9
126.5
124.0
77.3 CDCl3
56.6
30.8
Parameter Value
Instrument av500
Solvent CDCl3
Temperature 298.0
Pulse Sequence zgpg30
Experiment 1D
Probe Z119248_0002 (DCH 500S2 C/ H-D-05 Z LT)
Number of Scans 864
Receiver Gain 204.5
Relaxation Delay 2.0000
Pulse Width 10.5000
Acquisition Time 1.0486
Acquisition Date 2023-12-15T12:15:42
Spectrometer Frequency 125.77
Spectral Width 31250.0
Lowest Frequency -1145.8
Nucleus 13C
Acquired Size 32768
Spectral Size 65536
Me
H
O
6.11
210 200 190 180 170 160 150 140 130 120 110 100 90 80 70 60 50 40 30 20 10 0
f1 (ppm)

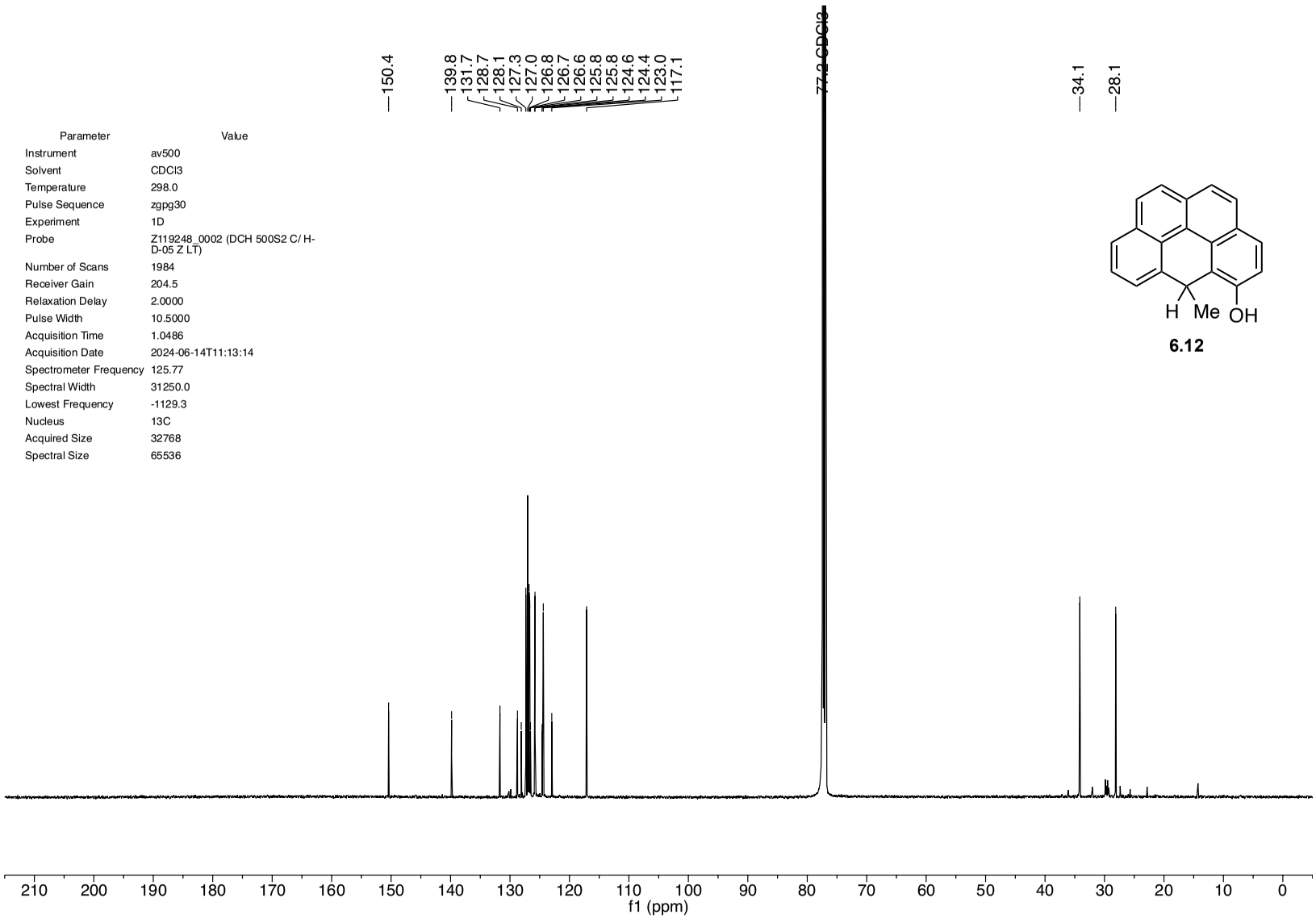

Parameter	Value
Instrument	av500
Solvent	CDCl3
Temperature	298.0
Pulse Sequence	zgpg30
Experiment	1D
Probe	Z119248_0002 (DCH 500S2 C/ H-D-05 Z LT)
Number of Scans	1984
Receiver Gain	204.5
Relaxation Delay	2.0000
Pulse Width	10.5000
Acquisition Time	1.0486
Acquisition Date	2024-06-14T11:13:14
Spectrometer Frequency	125.77
Spectral Width	31250.0
Lowest Frequency	-1129.3
Nucleus	13C
Acquired Size	32768
Spectral Size	65536

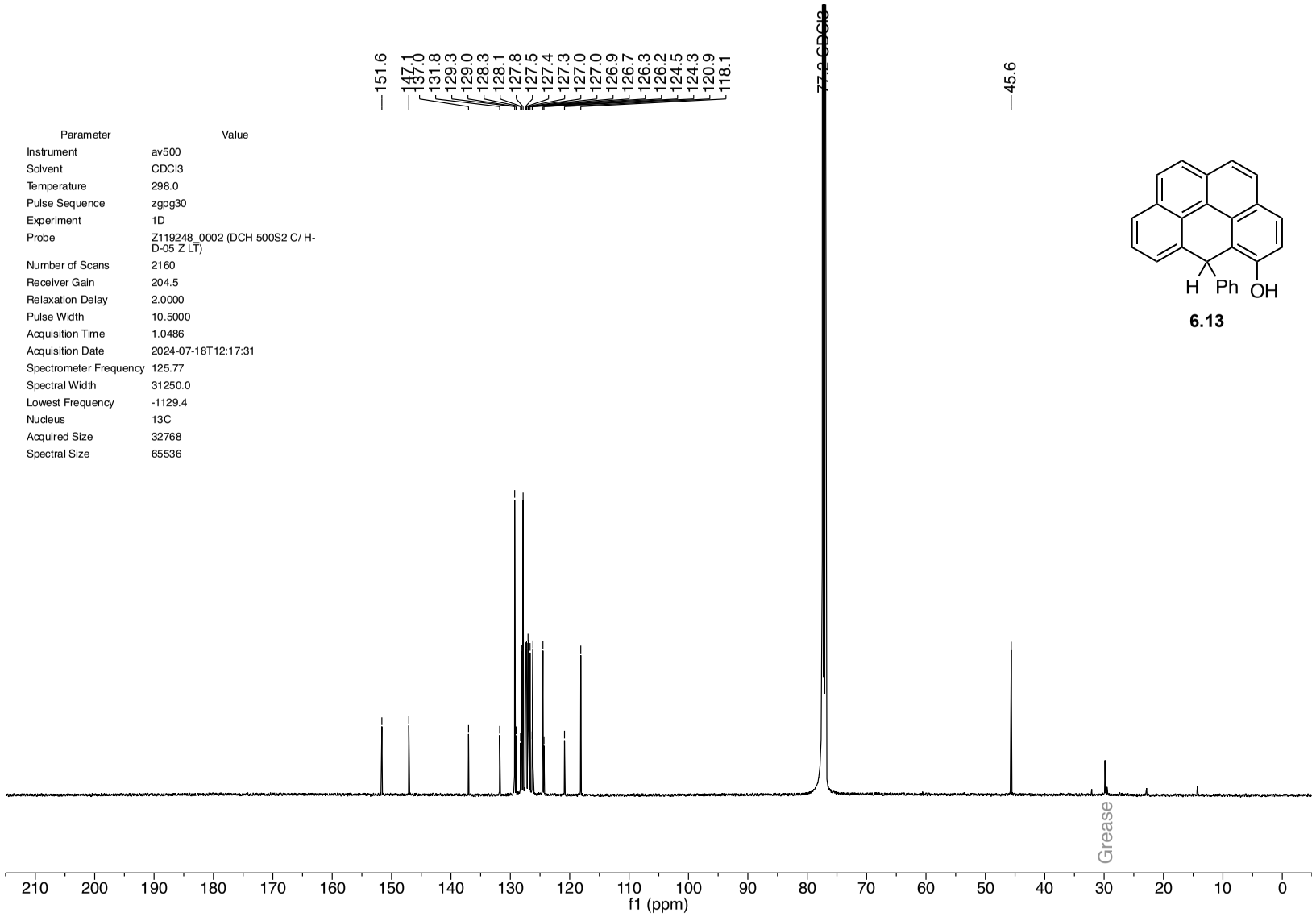

Parameter	Value
Instrument	av500
Solvent	CDCl3
Temperature	298.0
Pulse Sequence	zgpg30
Experiment	1D
Probe	Z119248_0002 (DCH 500S2 C/ H-D-05 Z LT)
Number of Scans	2160
Receiver Gain	204.5
Relaxation Delay	2.0000
Pulse Width	10.5000
Acquisition Time	1.0486
Acquisition Date	2024-07-18T12:17:31
Spectrometer Frequency	125.77
Spectral Width	31250.0
Lowest Frequency	-1129.4
Nucleus	13C
Acquired Size	32768
Spectral Size	65536

6.13

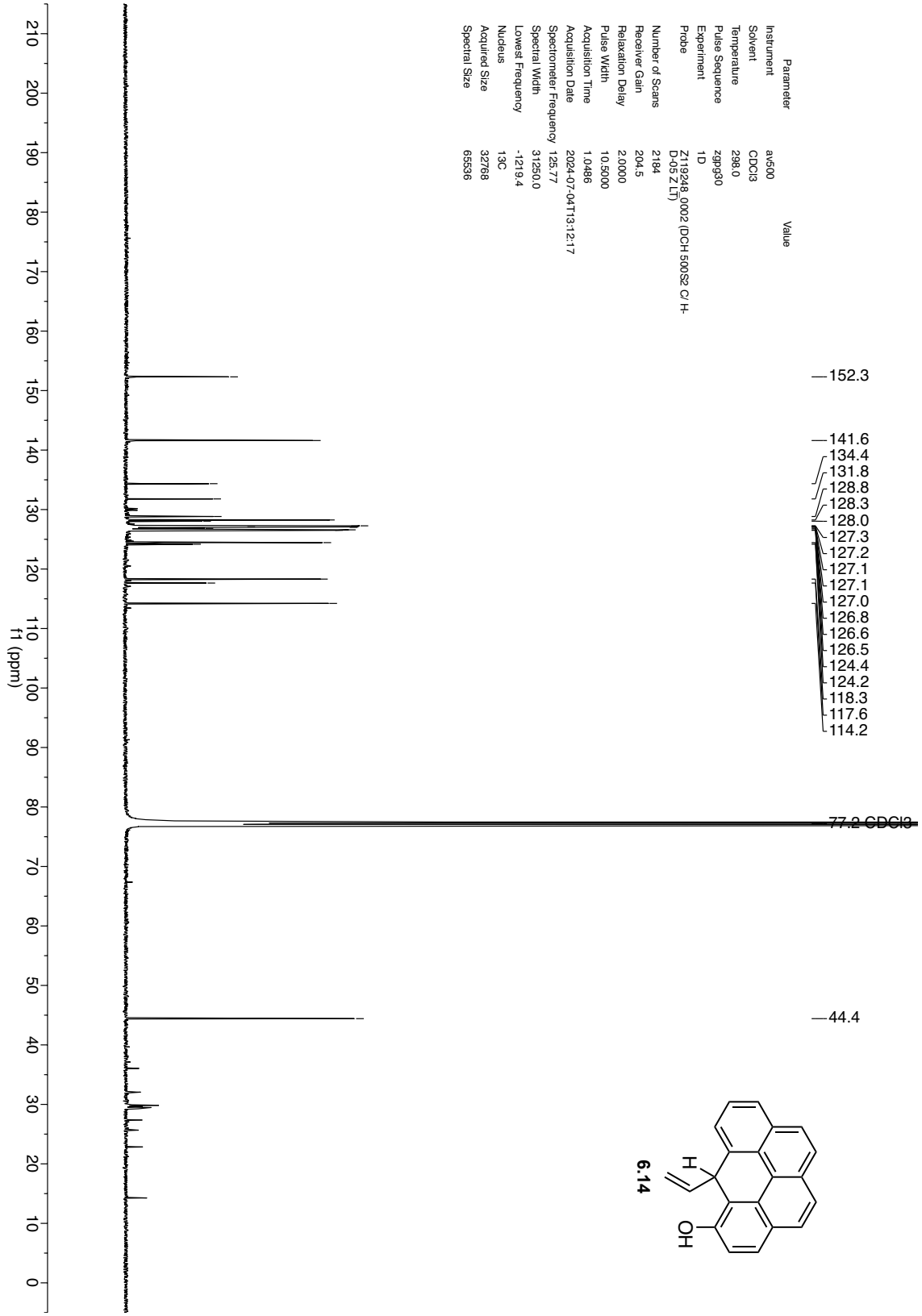
Parameter Value
Instrument av500
Solvent CDCl3
Temperature 298.0
Pulse Sequence zgpg30
Experiment 1D
Probe Z119248_0002 (DCH 500S2 C/ H-D-05 Z LT)
Number of Scans 2184
Receiver Gain 204.5
Relaxation Delay 2.0000
Pulse Width 10.5000
Acquisition Time 1.0486
Acquisition Date 2024-07-04T13:12:17
Spectrometer Frequency 125.77
Spectral Width 31250.0
Lowest Frequency -1219.4
Nucleus 13C
Acquired Size 32768
Spectral Size 65536
152.3
141.6
134.4
131.8
128.8
128.3
128.0
127.3
127.2
127.1
127.1
127.0
126.8
126.6
126.5
124.4
124.2
118.3
117.6
114.2
77.2 CDCl3
44.4
f1 (ppm)
6.14
H
OH

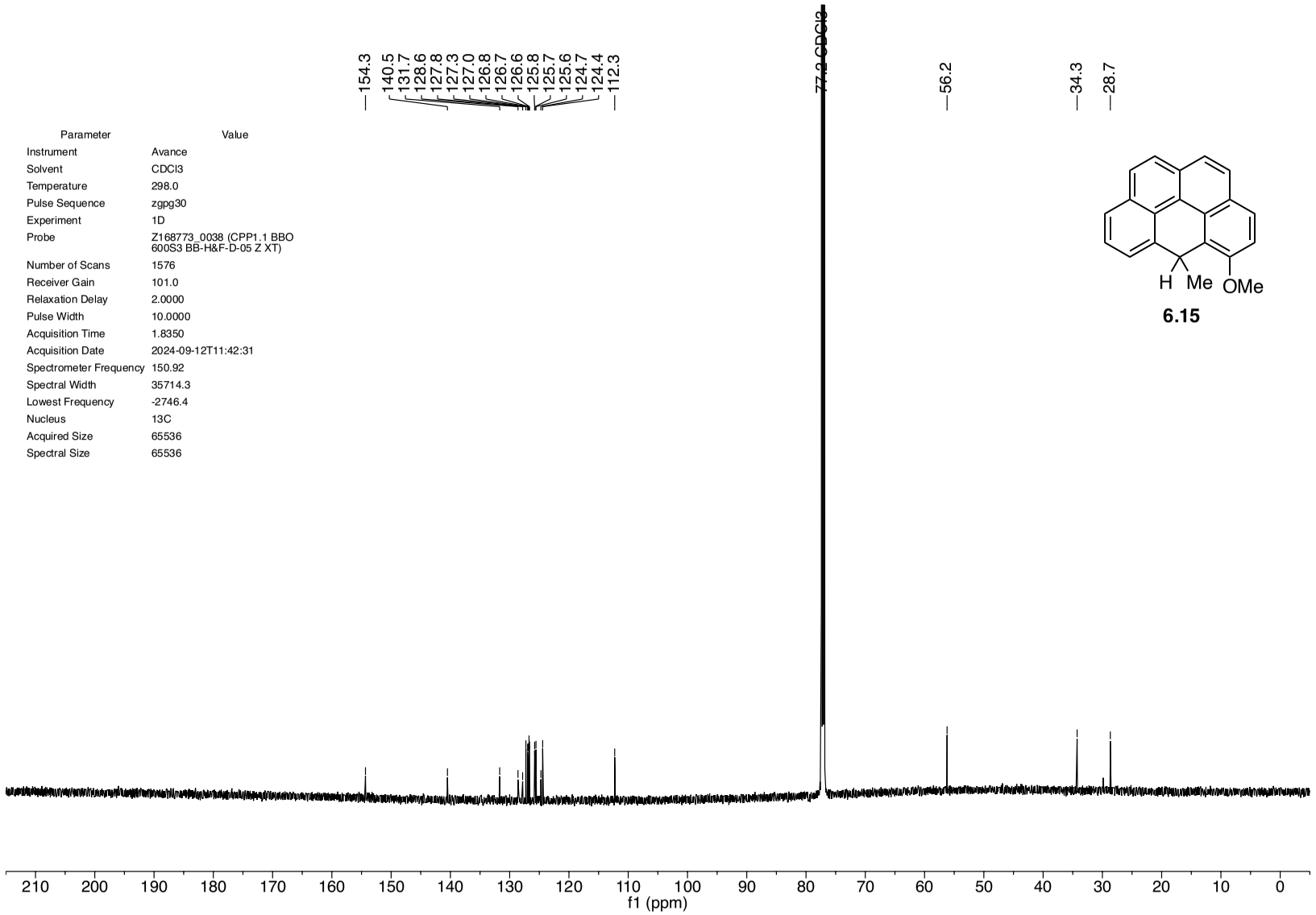
154.3
140.5
131.7
128.6
127.8
127.3
127.0
126.8
126.7
126.6
125.8
125.7
125.6
124.7
124.4
112.3
77.2 CDCl3
56.2
34.3
28.7
Parameter Value
Instrument Avance
Solvent CDCl3
Temperature 298.0
Pulse Sequence zgpg30
Experiment 1D
Probe Z168773_0038 (CPP1.1 BBO 600S3 BB-H&F-D-05 Z XT)
Number of Scans 1576
Receiver Gain 101.0
Relaxation Delay 2.0000
Pulse Width 10.0000
Acquisition Time 1.8350
Acquisition Date 2024-09-12T11:42:31
Spectrometer Frequency 150.92
Spectral Width 35714.3
Lowest Frequency -2746.4
Nucleus 13C
Acquired Size 65536
Spectral Size 65536
H Me OMe
6.15
210 200 190 180 170 160 150 140 130 120 110 100 90 80 70 60 50 40 30 20 10 0
f1 (ppm)

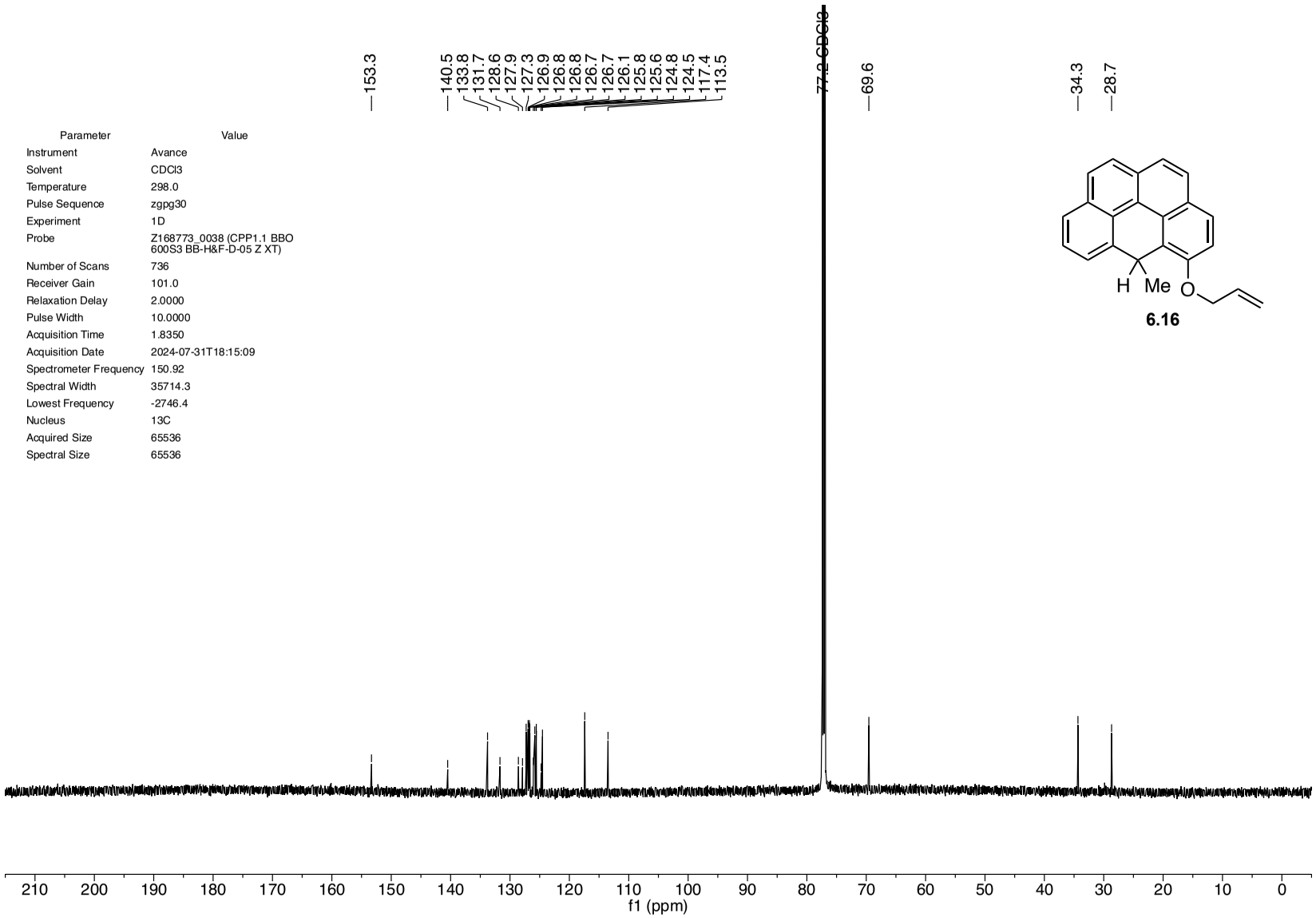
153.3
140.5
133.8
131.7
128.6
127.9
127.3
126.9
126.8
126.8
126.7
126.7
126.1
125.8
125.6
124.8
124.5
117.4
113.5
77.2 CDCl3
69.6
34.3
28.7
Parameter Value
Instrument Avance
Solvent CDCl3
Temperature 298.0
Pulse Sequence zgpg30
Experiment 1D
Probe Z168773_0038 (CPP1.1 BBO 600S3 BB-H&F-D-05 Z XT)
Number of Scans 736
Receiver Gain 101.0
Relaxation Delay 2.0000
Pulse Width 10.0000
Acquisition Time 1.8350
Acquisition Date 2024-07-31T18:15:09
Spectrometer Frequency 150.92
Spectral Width 35714.3
Lowest Frequency -2746.4
Nucleus 13C
Acquired Size 65536
Spectral Size 65536
H
Me
O
6.16
210 200 190 180 170 160 150 140 130 120 110 100 90 80 70 60 50 40 30 20 10 0
f1 (ppm)

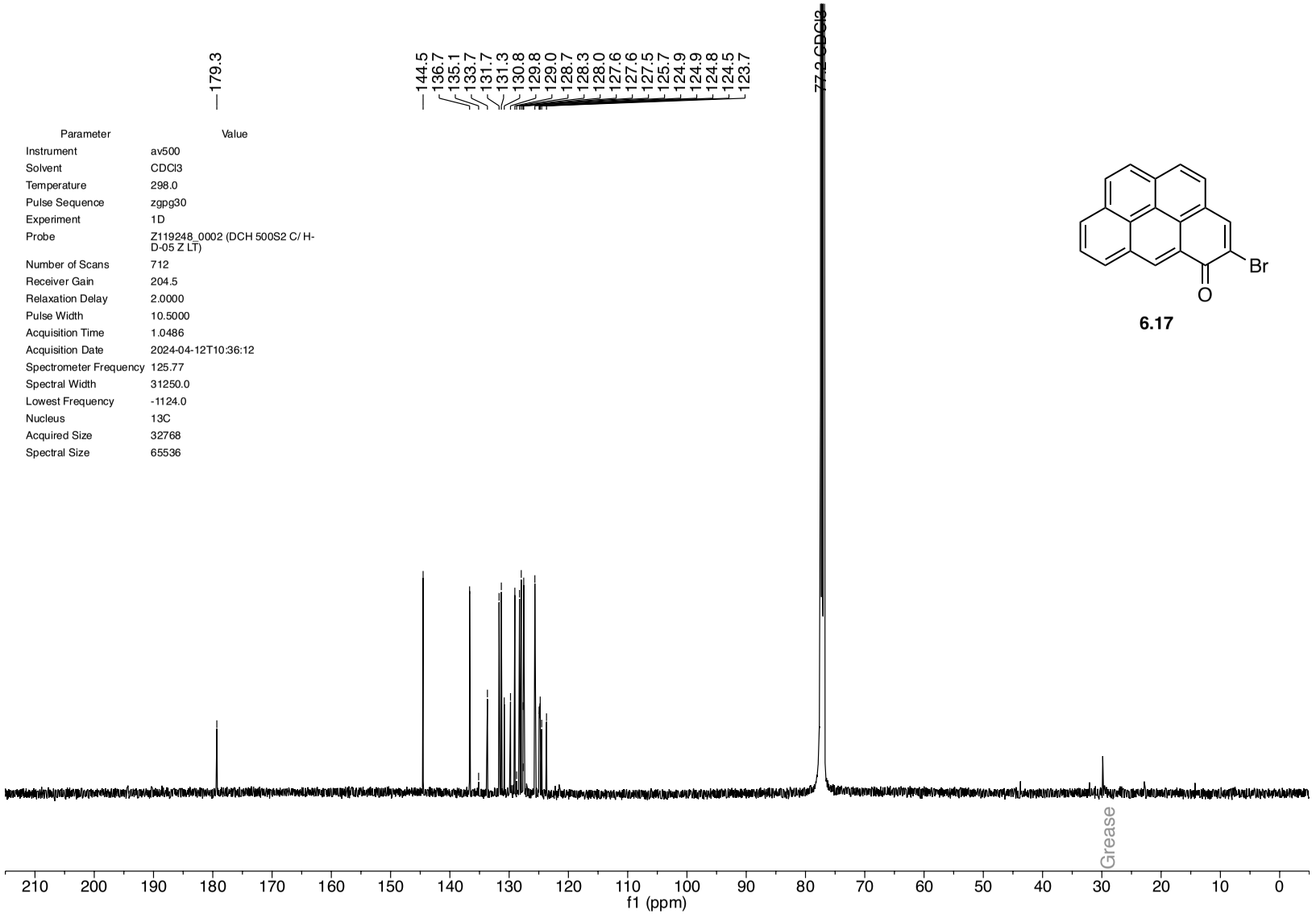

Parameter	Value
Instrument	av500
Solvent	CDCl3
Temperature	298.0
Pulse Sequence	zgpg30
Experiment	1D
Probe	Z119248_0002 (DCH 500S2 C/ H-D-05 Z LT)
Number of Scans	712
Receiver Gain	204.5
Relaxation Delay	2.0000
Pulse Width	10.5000
Acquisition Time	1.0486
Acquisition Date	2024-04-12T10:36:12
Spectrometer Frequency	125.77
Spectral Width	31250.0
Lowest Frequency	-1124.0
Nucleus	13C
Acquired Size	32768
Spectral Size	65536

6.17

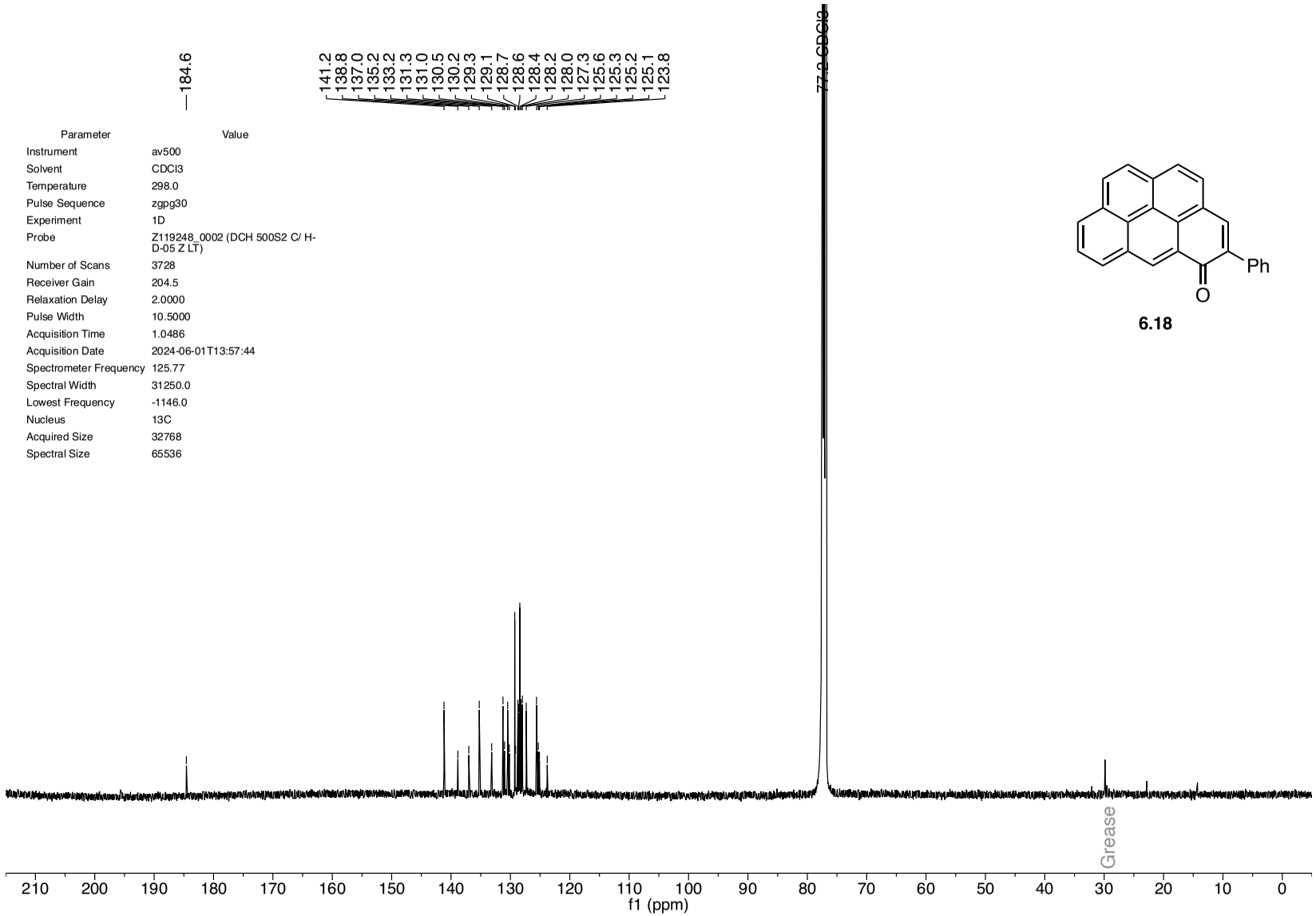

Parameter	Value
Instrument	av500
Solvent	CDCl3
Temperature	298.0
Pulse Sequence	zgpg30
Experiment	1D
Probe	Z119248_0002 (DCH 500S2 C/ H-D-05 Z LT)
Number of Scans	3728
Receiver Gain	204.5
Relaxation Delay	2.0000
Pulse Width	10.5000
Acquisition Time	1.0486
Acquisition Date	2024-06-01T13:57:44
Spectrometer Frequency	125.77
Spectral Width	31250.0
Lowest Frequency	-1146.0
Nucleus	13C
Acquired Size	32768
Spectral Size	65536

6.18

6.5.7 2-D NMR spectra

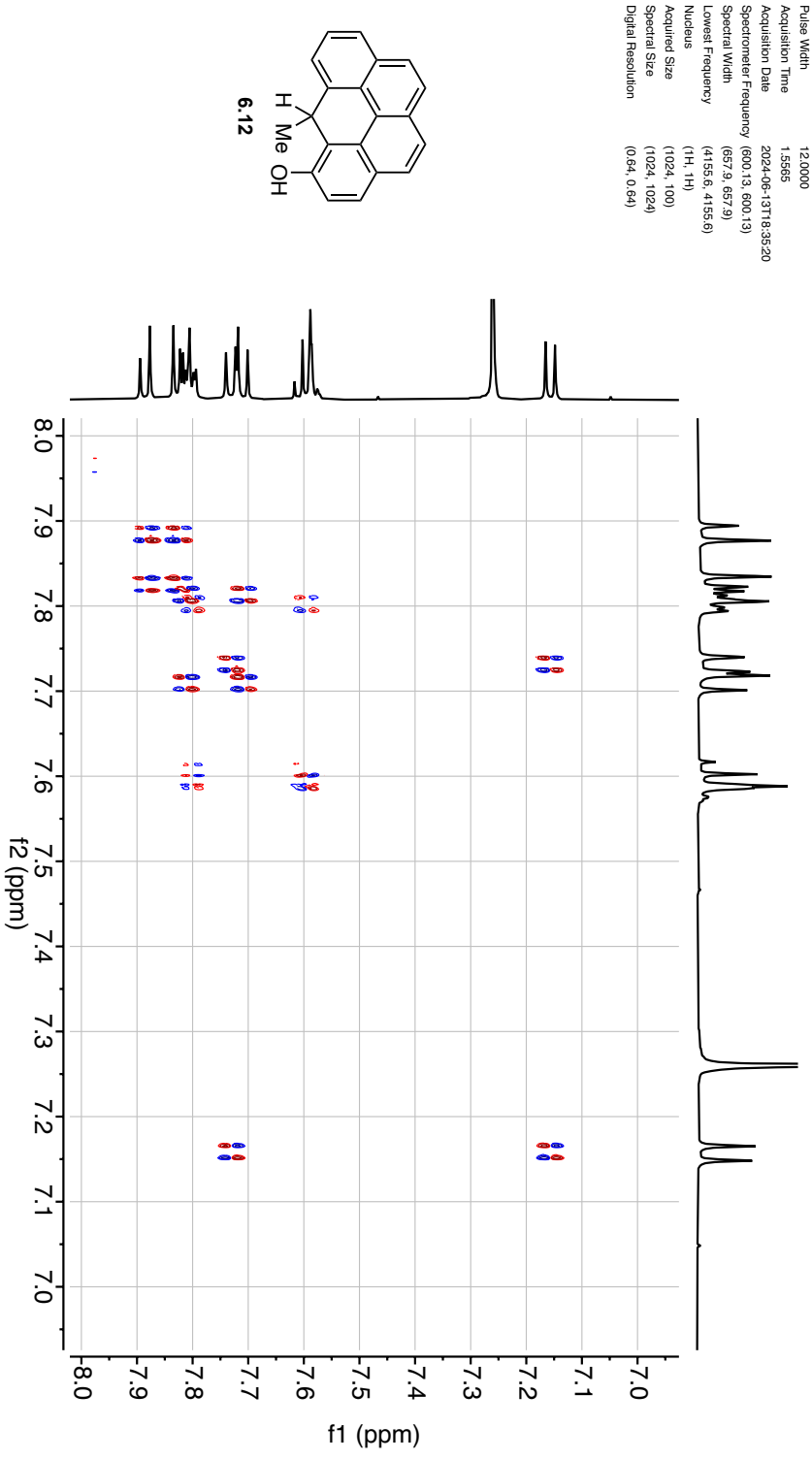

Parameter	Value
Instrument	Avance
Solvent	CDCl3
Temperature	298.0
Pulse Sequence	noesygpph
Experiment	NOESY
Probe	Z168773_0038 (CPP1.1 BBO 600S3 BB-H&F-D-05 Z XT)
Number of Scans	2
Receiver Gain	101.0
Relaxation Delay	2.0000
Pulse Width	12.0000
Acquisition Time	0.2458
Acquisition Date	2024-06-25T18:47:04
Spectrometer Frequency	(600.13, 600.13)
Spectral Width	(4166.7, 4166.7)
Lowest Frequency	(601.6, 601.8)
Nucleus	(1H, 1H)
Acquired Size	(1024, 166)
Spectral Size	(1024, 1024)
Digital Resolution	(4.07, 4.07)

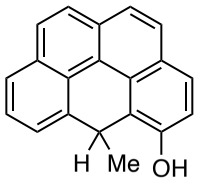

6.12

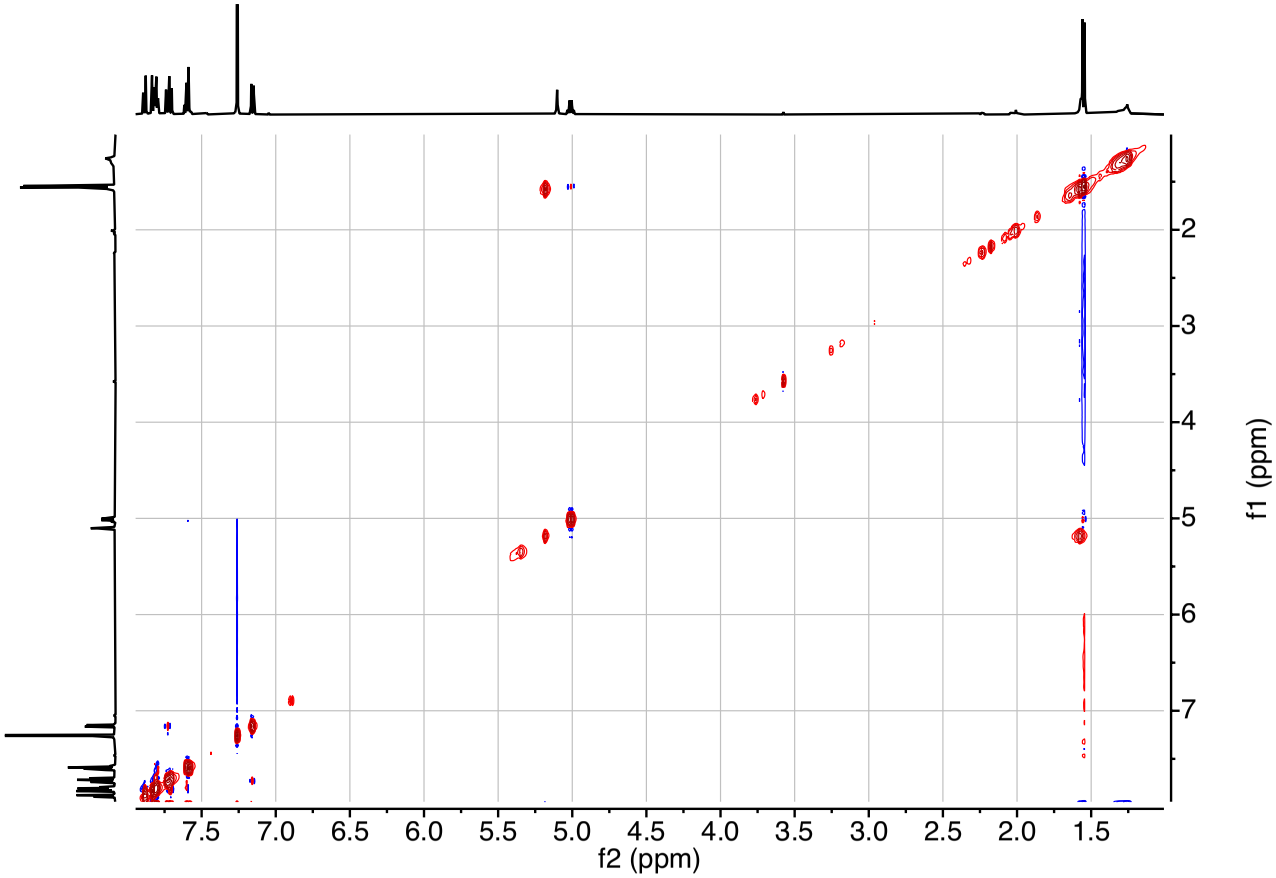

Parameter	Value
Instrument	av500
Solvent	CDCl3
Temperature	298.0
Pulse Sequence	cosygpmfphpp
Experiment	COSY
Probe	Z119248_0002 (DCH 500S2 C/ H-D-05 Z LT)
Number of Scans	2
Receiver Gain	30.1
Relaxation Delay	2.0000
Pulse Width	10.0000
Acquisition Time	0.4096
Acquisition Date	2024-04-18T11:28:55
Spectrometer Frequency	(500.13, 500.13)
Spectral Width	(2500.0, 2501.3)
Lowest Frequency	(3236.1, 3224.1)
Nucleus	(1H, 1H)
Acquired Size	(1024, 256)
Spectral Size	(1024, 1024)
Digital Resolution	(2.44, 2.44)

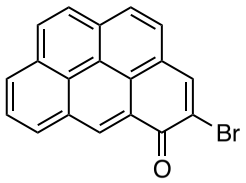

6.17

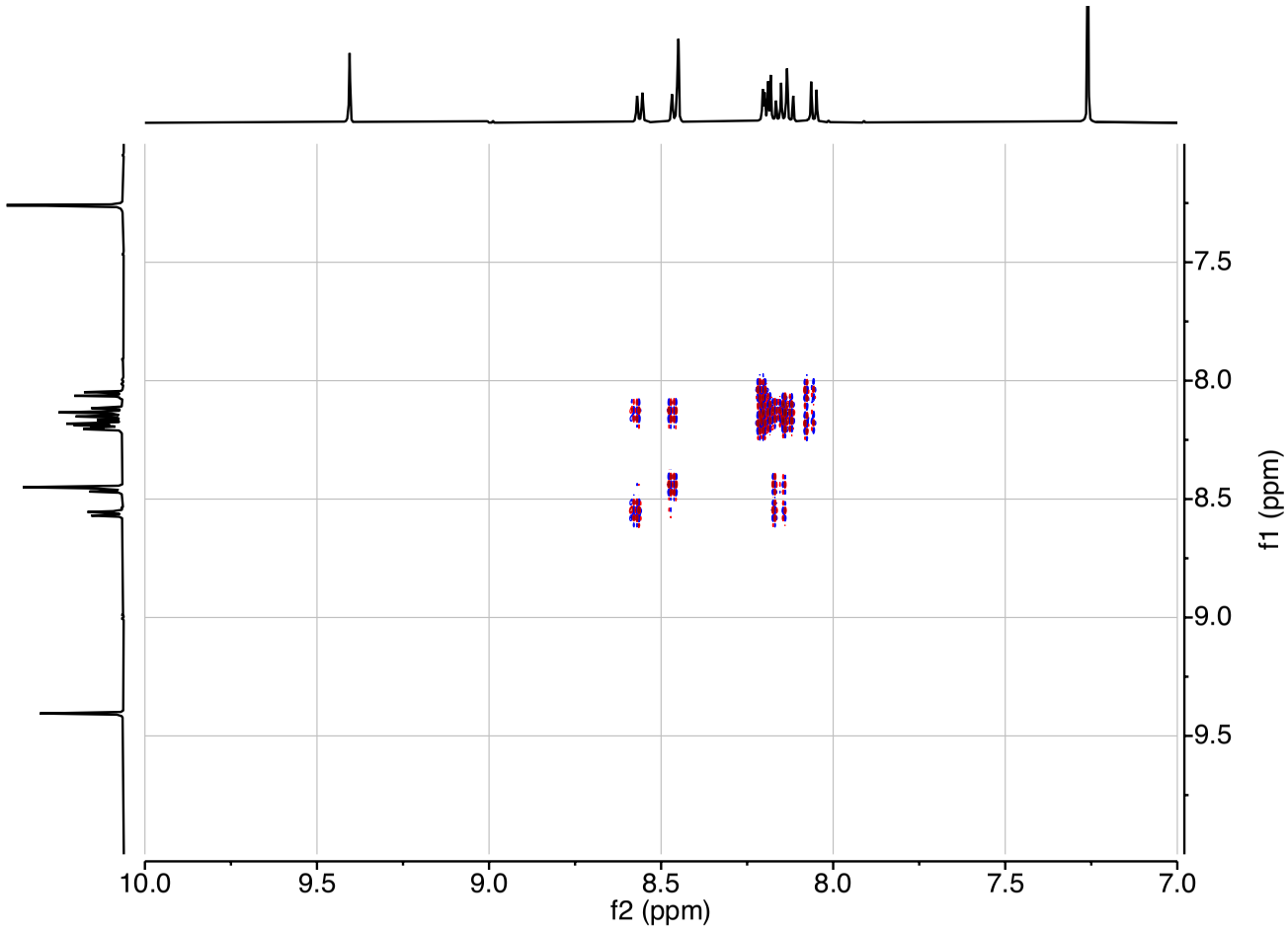

Parameter	Value
Instrument	Avance
Solvent	CDCl3
Temperature	298.0
Pulse Sequence	noesygpph
Experiment	NOESY
Probe	Z168773_0038 (CPP1.1 BBO 600S3 BB-H&F-D-05 Z XT)
Number of Scans	2
Receiver Gain	101.0
Relaxation Delay	2.0000
Pulse Width	12.0000
Acquisition Time	0.3400
Acquisition Date	2024-04-17T17:47:47
Spectrometer Frequency	(600.14, 600.14)
Spectral Width	(3012.0, 3000.7)
Lowest Frequency	(3880.4, 3877.0)
Nucleus	(1H, 1H)
Acquired Size	(1024, 256)
Spectral Size	(1024, 1024)
Digital Resolution	(2.94, 2.93)

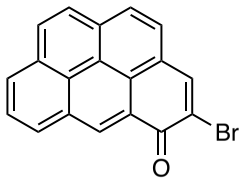

6.17

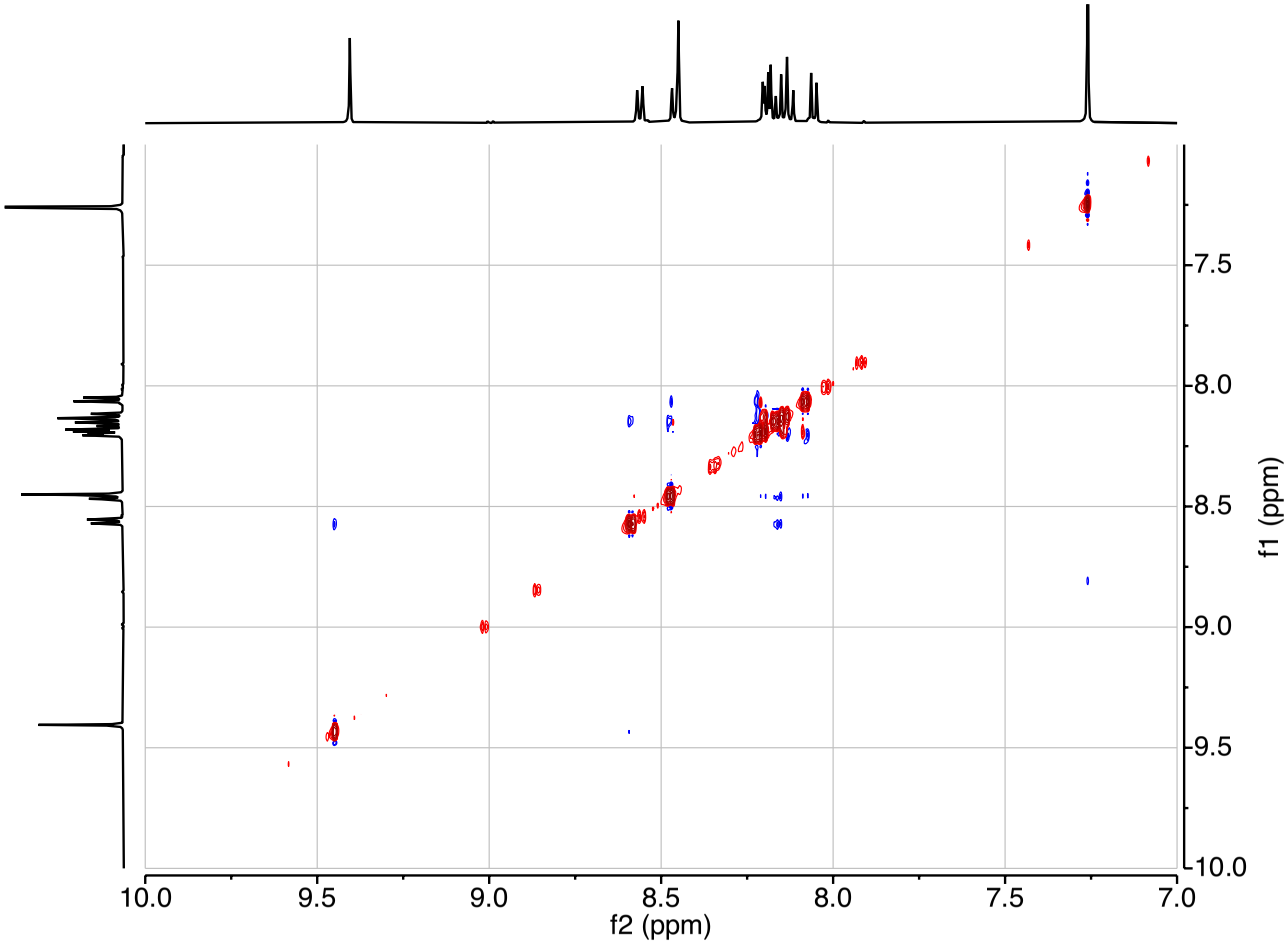

6.5.8 Absorption spectra

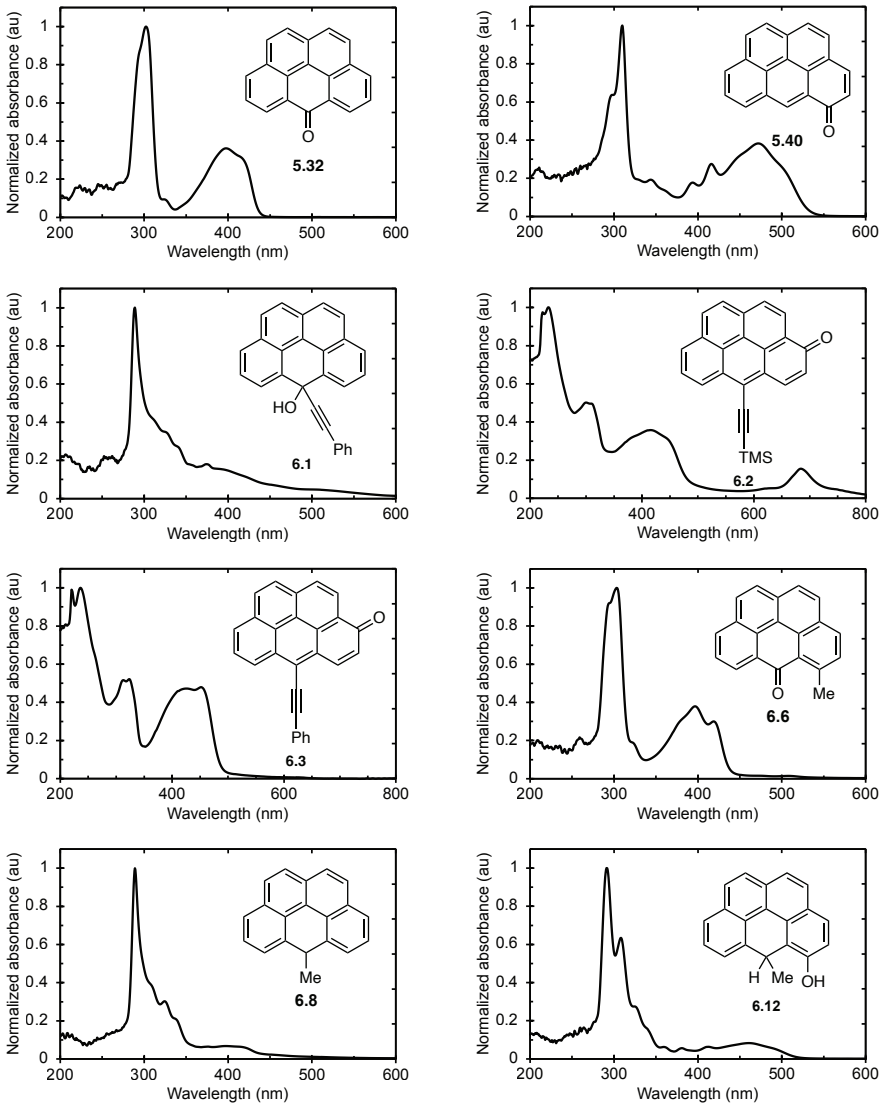

Measurements were taken in CH_2Cl_2 at concentrations with non-normalized absorbance values < 1 au in a 1-cm cuvette.

6.5.9 Computational methods and data

All calculations were performed with Spartan Student v. 9.0.2 molecular modeling software. The gas phase geometries were optimized with ωB97X-D functional and 6-31G(D) basis set.

6*H*-benzo[*cd*]pyren-6-one (5.32) Geometry data; gas phase
Method: ωB97X-D
Basis set: 6-31G(D)
Total energy: -805.059356 hartrees
Cartesian Coordinates (Å):

	Atom	x	y	z
1	C C1	2.4609356	0.0000000	-0.6194773
2	C C4	2.4739322	0.0000000	2.1859608
3	C C2	3.6752881	0.0000000	0.0994256
4	C C6	1.2402327	0.0000000	0.0962924
5	C C5	1.2654586	0.0000000	1.5130685
6	C C3	3.6838965	0.0000000	1.4781664
7	H H2	2.4579955	0.0000000	3.2711476
8	H H3	4.6111795	0.0000000	-0.4537589
9	H H6	4.6255279	0.0000000	2.0179819
10	C C7	0.0000000	0.0000000	-0.6205981
11	C C8	0.0000000	0.0000000	-2.0211011
12	C C9	1.2467697	0.0000000	-2.7222473
13	C C10	2.4281956	0.0000000	-2.0501865
14	H H9	1.2320255	0.0000000	-3.8087384
15	H H10	3.3698024	0.0000000	-2.5927027
16	C C11	-1.2467697	0.0000000	-2.7222473
17	C C12	-2.4281956	0.0000000	-2.0501865
18	C C13	-2.4609356	0.0000000	-0.6194773
19	C C14	-1.2402327	0.0000000	0.0962924
20	H H11	-1.2320255	0.0000000	-3.8087384
21	H H12	-3.3698024	0.0000000	-2.5927027
22	C C15	-1.2654586	0.0000000	1.5130685
23	C C16	-2.4739322	0.0000000	2.1859608
24	C C17	-3.6838965	0.0000000	1.4781664
25	C C18	-3.6752881	0.0000000	0.0994256
26	H H16	-2.4579955	0.0000000	3.2711476
27	H H17	-4.6255279	0.0000000	2.0179819
28	H H18	-4.6111795	0.0000000	-0.4537589
29	C C19	0.0000000	0.0000000	2.2948578
30	O O1	0.0000000	0.0000000	3.5169770

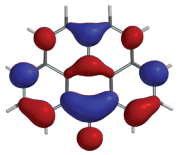

6*H*-benzo[*cd*]pyren-6-one
5.32

Mulliken localization of Molecular Orbitals (in percent) for LUMO of **5.32**:

	LUMO
	-0.7 (ev)
--	-----
C1	0.18
C4	8.21
C2	10.00
C6	0.94
C5	5.40
C3	1.97
H2	0.00
H3	0.00
H6	0.00
C7	5.25
C8	6.04
C9	0.92
C10	5.63
H9	0.00
H10	0.00
C11	0.92
C12	5.63
C13	0.18
C14	0.94
H11	0.00
H12	0.00
C15	5.40
C16	8.21
C17	1.97
C18	10.00
H16	0.00
H17	0.00
H18	0.00
C19	11.12
O1	11.06

5*H*-benzo[*cd*]pyren-5-one (5.40) Geometry data; gas phase
Method: ωB97X-D
Basis set: 6-31G(D)
Total energy: -805.044643 hartrees
Cartesian Coordinates (Å):

	Atom	x	y	z
1	C C1	0.1085591	0.0000000	2.5460585
2	C C4	-2.6438391	0.0000000	1.9646377
3	C C2	-0.8438882	0.0000000	3.5705260
4	C C6	-0.3341426	0.0000000	1.1984086
5	C C5	-1.7245020	0.0000000	0.9070252
6	C C3	-2.2052452	0.0000000	3.2821113
7	H H2	-3.7071974	0.0000000	1.7416175
8	H H3	-0.5090564	0.0000000	4.6046546
9	H H6	-2.9273183	0.0000000	4.0924629
10	C C7	-2.1424185	0.0000000	-0.4620799
11	C C8	-1.2425616	0.0000000	-1.4850021
12	C C9	0.1698324	0.0000000	-1.2069882
13	C C10	0.6149800	0.0000000	0.1352571
14	H H7	-3.2021301	0.0000000	-0.7043547
15	C C11	2.0055693	0.0000000	0.4221728
16	C C12	2.9169027	0.0000000	-0.6431127
17	C C13	2.4730624	0.0000000	-1.9550891
18	C C14	1.1061101	0.0000000	-2.2559496
19	H H12	3.9823691	0.0000000	-0.4303200
20	H H13	3.1938896	0.0000000	-2.7686690
21	C C15	1.5242439	0.0000000	2.8084438
22	H H5	1.8571902	0.0000000	3.8428490
23	C C16	2.4259635	0.0000000	1.7980760
24	H H10	3.4915178	0.0000000	2.0111290
25	C C17	0.6216738	0.0000000	-3.6273438
26	H H9	1.3662607	0.0000000	-4.4207203
27	C C18	-0.6887290	0.0000000	-3.9362338
28	H H14	-1.0369845	0.0000000	-4.9637701
29	C C20	-1.7287814	0.0000000	-2.8953458
30	O O1	-2.9213301	0.0000000	-3.1704511

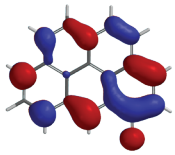

5*H*-benzo[*cd*]pyren-5-one
5.40

Mulliken localization of Molecular Orbitals (in percent) for LUMO of **5.40**:

	LUMO
	-1.0 (ev)
--	-----
C1	0.96
C4	8.66
C2	9.87
C6	0.84
C5	1.72
C3	0.29
H2	0.00
H3	0.00
H6	0.00
C7	14.53
C8	4.32
C9	2.33
C10	0.09
H7	0.00
C11	5.91
C12	3.70
C13	2.75
C14	5.62
H12	0.00
H13	0.00
C15	5.18
H5	0.00
C16	2.01
H10	0.00
C17	8.51
H9	0.00
C18	6.34
H14	0.00
C20	7.37
O1	9.00

6.5.10 Crystallographic information

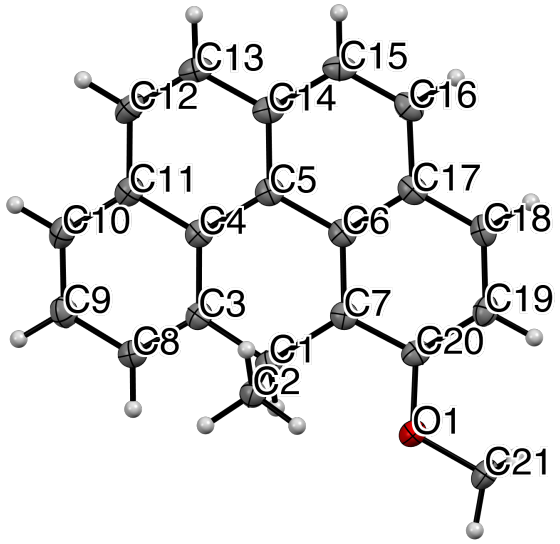

Table S1. Crystal data and structure refinement for 6.15.

CCDC number	2408380
Empirical formula	$C_{21}H_{16}O$
Formula weight	284.34
Temperature [K]	100(2)
Crystal system	orthorhombic
Space group (number)	$Pna2_1$ (33)
a [Å]	21.2459(9)
b [Å]	13.0033(5)
c [Å]	5.0323(2)
α [°]	90
β [°]	90
γ [°]	90
Volume [Å^3]	1390.26(10)
Z	4
ρ_{calc} [gcm^{-3}]	1.358
μ [mm^{-1}]	0.634
F(000)	600
Crystal size [mm^3]	0.057×0.096×0.181
Crystal colour	colorless
Crystal shape	block
Radiation	CuK_α (λ=1.54178 Å)
2θ range [°]	7.97 to 133.44 (0.84 Å)
Index ranges	$-25 \le h \le 25$ $-15 \le k \le 15$ $-5 \le l \le 5$
Reflections collected	17425
Independent reflections	2421

	R_{int} = 0.0507
	R_{sigma} = 0.0269
Completeness to θ = 66.721°	100.0 %
Data / Restraints / Parameters	2421 / 1 / 202
Absorption correction T_{min}/T_{max} (method)	0.6523 / 0.7528 (multi-scan)
Goodness-of-fit on F^2	1.055
Final R indexes	R_1 = 0.0313
[$I \geq 2\sigma(I)$]	wR_2 = 0.0813
Final R indexes	R_1 = 0.0349
[all data]	wR_2 = 0.0832
Largest peak/hole [eÅ^{-3}]	0.15/−0.12
Extinction coefficient	0.0017(5)
Flack X parameter	0.29(18)

Table S2. Atomic coordinates and U_{eq} [Å^2] for **17**. U_{eq} is defined as 1/3 of the trace of the orthogonalized U_{ij} tensor.

Atom	***x***	***y***	***z***	U_{eq}
O1	0.28168(7)	0.16948(12)	0.9172(3)	0.0246(4)
C1	0.39049(11)	0.15543(16)	0.6253(5)	0.0213(5)
H1	0.394332	0.139321	0.818938	0.026
C2	0.36348(10)	0.05994(17)	0.4816(5)	0.0242(5)
H2A	0.359386	0.074611	0.291360	0.036
H2B	0.322026	0.043303	0.555384	0.036
H2C	0.391924	0.001432	0.507007	0.036
C3	0.45557(10)	0.17626(16)	0.5158(5)	0.0208(5)
C4	0.46431(11)	0.25258(17)	0.3192(5)	0.0201(5)
C5	0.41491(11)	0.32340(16)	0.2537(4)	0.0203(5)
C6	0.35679(10)	0.32208(17)	0.4012(4)	0.0203(5)
C7	0.34531(10)	0.24457(16)	0.5927(5)	0.0202(5)
C8	0.50542(11)	0.11601(17)	0.5929(5)	0.0243(5)
H8	0.499694	0.066250	0.729030	0.029
C9	0.56493(11)	0.12702(18)	0.4730(5)	0.0271(5)
H9	0.599235	0.085781	0.530464	0.033
C10	0.57329(11)	0.19738(18)	0.2730(5)	0.0273(6)
H10	0.613102	0.202638	0.188099	0.033
C11	0.52385(11)	0.26170(17)	0.1920(5)	0.0231(5)
C12	0.53082(11)	0.33636(17)	−0.0153(5)	0.0268(5)
H12	0.569620	0.340628	−0.108558	0.032
C13	0.48353(11)	0.40072(18)	−0.0811(5)	0.0250(5)
H13	0.489252	0.448115	−0.222730	0.030
C14	0.42487(11)	0.39884(18)	0.0588(4)	0.0225(5)
C15	0.37762(11)	0.47466(17)	0.0103(5)	0.0240(5)
H15	0.384015	0.524748	−0.124476	0.029
C16	0.32361(11)	0.47589(17)	0.1549(5)	0.0249(5)
H16	0.293238	0.528024	0.122470	0.030
C17	0.31156(11)	0.40024(17)	0.3551(5)	0.0223(5)
C18	0.25621(11)	0.40058(17)	0.5066(5)	0.0235(5)
H18	0.225653	0.452725	0.477558	0.028
C19	0.24539(11)	0.32650(17)	0.6971(5)	0.0236(5)
H19	0.207973	0.328470	0.800298	0.028
C20	0.28970(10)	0.24824(17)	0.7381(5)	0.0214(5)

C21	0.22753(11)	0.17370(18)	1.0832(5)	0.0254(5)
H21A	0.189513	0.169728	0.973400	0.038
H21B	0.227521	0.238487	1.182721	0.038
H21C	0.228254	0.115806	1.207849	0.038

Table S3. Anisotropic displacement parameters [Å^2] for es2kh. The anisotropic displacement factor exponent takes the form: $-2\pi^2[\, h^2(a^*)^2U_{11} + k^2(b^*)^2U_{22} + \ldots + 2hka^*b^*U_{12}\,]$

Atom	U_{11}	U_{22}	U_{33}	U_{23}	U_{13}	U_{12}
O1	0.0239(8)	0.0270(8)	0.0229(9)	0.0027(7)	0.0049(7)	0.0010(7)
C1	0.0234(12)	0.0228(10)	0.0176(11)	0.0014(10)	0.0014(10)	−0.0009(9)
C2	0.0224(11)	0.0232(11)	0.0269(12)	0.0000(10)	0.0027(11)	0.0003(9)
C3	0.0231(11)	0.0223(10)	0.0169(12)	−0.0036(10)	−0.0004(10)	−0.0007(9)
C4	0.0214(11)	0.0212(10)	0.0178(11)	−0.0042(10)	−0.0018(9)	−0.0033(9)
C5	0.0228(11)	0.0215(10)	0.0167(12)	−0.0043(9)	−0.0033(9)	−0.0032(9)
C6	0.0218(12)	0.0218(11)	0.0173(12)	−0.0031(10)	−0.0039(9)	−0.0012(9)
C7	0.0206(11)	0.0217(11)	0.0182(11)	−0.0031(10)	−0.0035(10)	−0.0020(9)
C8	0.0256(12)	0.0240(11)	0.0233(12)	0.0008(10)	0.0005(10)	−0.0012(9)
C9	0.0223(11)	0.0269(11)	0.0321(13)	−0.0005(11)	−0.0021(11)	0.0014(9)
C10	0.0215(12)	0.0293(12)	0.0310(15)	−0.0041(11)	0.0053(11)	−0.0022(10)
C11	0.0231(11)	0.0233(11)	0.0228(12)	−0.0057(10)	0.0014(10)	−0.0051(9)
C12	0.0244(11)	0.0298(12)	0.0261(13)	−0.0023(12)	0.0055(11)	−0.0081(10)
C13	0.0320(13)	0.0244(11)	0.0187(12)	0.0003(10)	0.0007(10)	−0.0083(10)
C14	0.0258(12)	0.0239(11)	0.0179(12)	−0.0011(9)	−0.0036(10)	−0.0057(9)
C15	0.0312(12)	0.0227(11)	0.0183(12)	0.0013(10)	−0.0051(10)	−0.0058(9)
C16	0.0263(12)	0.0233(11)	0.0252(13)	−0.0010(10)	−0.0068(10)	0.0013(9)
C17	0.0248(12)	0.0211(11)	0.0210(12)	−0.0036(10)	−0.0061(10)	−0.0008(9)
C18	0.0226(11)	0.0241(11)	0.0238(12)	−0.0054(11)	−0.0034(10)	0.0026(9)
C19	0.0210(12)	0.0293(12)	0.0205(13)	−0.0037(10)	0.0006(10)	0.0001(9)
C20	0.0225(11)	0.0251(11)	0.0167(12)	−0.0009(10)	−0.0016(10)	−0.0031(9)
C21	0.0217(11)	0.0309(12)	0.0236(12)	−0.0014(11)	0.0062(10)	−0.0015(9)

Table S4. Bond lengths and angles for **6.15**

Atom–Atom	**Length [Å]**
O1–C20	1.375(3)
O1–C21	1.423(3)
C1–C3	1.513(3)
C1–C7	1.514(3)
C1–C2	1.547(3)
C3–C8	1.373(3)
C3–C4	1.414(3)
C4–C11	1.423(3)
C4–C5	1.435(3)
C5–C14	1.403(3)
C5–C6	1.441(3)
C6–C7	1.416(3)
C6–C17	1.418(3)
C7–C20	1.390(3)
C8–C9	1.408(3)
C9–C10	1.372(3)
C10–C11	1.403(3)
C11–C12	1.433(3)

C12–C13	1.349(3)
C13–C14	1.432(3)
C14–C15	1.428(3)
C15–C16	1.359(3)
C16–C17	1.431(3)
C17–C18	1.402(3)
C18–C19	1.378(3)
C19–C20	1.402(3)
Atom–Atom–Atom	**Angle [°]**
C20–O1–C21	117.16(17)
C3–C1–C7	113.76(18)
C3–C1–C2	108.20(18)
C7–C1–C2	109.19(18)
C8–C3–C4	119.8(2)
C8–C3–C1	120.0(2)
C4–C3–C1	120.0(2)
C3–C4–C11	119.4(2)
C3–C4–C5	121.0(2)
C11–C4–C5	119.6(2)
C14–C5–C4	119.9(2)
C14–C5–C6	119.8(2)
C4–C5–C6	120.1(2)
C7–C6–C17	120.3(2)
C7–C6–C5	120.5(2)
C17–C6–C5	119.2(2)
C20–C7–C6	118.70(19)
C20–C7–C1	120.5(2)
C6–C7–C1	120.64(19)
C3–C8–C9	120.9(2)
C10–C9–C8	119.9(2)
C9–C10–C11	120.9(2)
C10–C11–C4	119.0(2)
C10–C11–C12	122.5(2)
C4–C11–C12	118.4(2)
C13–C12–C11	121.5(2)
C12–C13–C14	121.2(2)
C5–C14–C15	119.7(2)
C5–C14–C13	119.1(2)
C15–C14–C13	121.1(2)
C16–C15–C14	120.7(2)
C15–C16–C17	121.3(2)
C18–C17–C6	118.8(2)
C18–C17–C16	122.1(2)
C6–C17–C16	119.1(2)
C19–C18–C17	121.1(2)
C18–C19–C20	119.9(2)
O1–C20–C7	115.14(19)
O1–C20–C19	123.6(2)
C7–C20–C19	121.2(2)

6.6 References

(1) Wu, J. Polycyclic Aromatic Compounds for Organic Field-Effect Transistors: Molecular Design and Syntheses. *Curr. Org. Chem.* **2007**, *11*, 1220–1240.

(2) Gong, Y.; Zhan, X.; Li, Q.; Li, Z. Progress of Pyrene-Based Organic Semiconductor in Organic Field Effect Transistors. *Sci. China Chem.* **2016**, *59*, 1623–1631.

(3) Tao, S.; Peng, Z.; Zhang, X.; Wang, P.; Lee, C. S.; Lee, S. T. Highly Efficient Non-Doped Blue Organic Light-Emitting Diodes Based on Fluorene Derivatives with High Thermal Stability. Adv. Funct. Mater. **2005**, *15*, 1716–1721.

(4) Zhang, Y.; Galoppini, E. Organic Polyaromatic Hydrocarbons as Sensitizing Model Dyes for Semiconductor Nanoparticles. *ChemSusChem* **2010**, *3*, 410–428.

(5) Francesconi, O.; Ienco, A.; Papi, F.; Dolce, M.; Catastini, A.; Nativi, C.; Roelens, S. A Sulfonated Tweezer-Shaped Receptor Selectively Recognizes Caffeine in Water. *J. Org. Chem.* **2022**, *87*, 2662–2667.

(6) Sheridan, R. E.; Whitlock, H. W. Concave Functionality: Design of a Phenol Sticky Host. *J. Am. Chem. Soc.* **1986**, *108*, 7120–7121.

(7) Kim, S. K.; Lim, J. M.; Pradhan, T.; Jung, H. S.; Lynch, V. M.; Kim, J. S.; Kim, D.; Sessler, J. L. Self-Association and Nitroaromatic-Induced Deaggregation of Pyrene Substituted Pyridine Amides. *J. Am. Chem. Soc*. **2014**, *136*, 495–505.

(8) (a) Hirshfeld, F. L.; Sandler, S.; Schmidt, G. M. J. 398. The Structure of Overcrowded Aromatic Compounds. Part VI. The Crystal Structure of Benzo[*c*]Phenanthrene and of 1,12-Dimethylbenzo[*c*]Phenanthrene. *J. Chem. Soc.* **1963**, 2108. (b) Valentine, A. J. S.; Mazziotti, D. A. Theoretical Prediction of the Structures and Energies of Olympicene and its Isomers. *J. Phys. Chem. A* **2013**, *117*, 9746−9752.

(9) Reid, D. H.; Bonthrone, W. 1109. Conjugated Cyclic Hydrocarbons. Part VIII. The Benzo[*cd*]Pyrenium Cation: Synthesis and Reactivity. *J. Chem. Soc* **1965**, 5920.

(10) Berger, R. J. F.; Fuchter, M. J.; Krossing, I.; Rzepa, H. S.; Schaefer, J.; Scherer, H. Gold(I) Mediated Rearrangement of [7]-Helicene to Give a Benzo[*cd*]Pyrenium Cation Embedded in a Chiral Framework. *Chem. Commun.* **2014**, *50*, 5251–5253.

(11) Murata, I.; Yamamoto, K.; Hara, O. The Chemistry of Phenalenium System XVII. Benzo[*cd*]Pyrenyl Anion. *Tetrahedron Lett.* **1974**, *15*, 2047–2048.

(12) Streitwieser, A.; Word, J. M.; Guibe, F.; Wright, J. S. Carbon Acidity. 62. Equilibrium Acidities of Some Phenalene Hydrocarbons: SCF-.Pi. MO Correlation. *J. Org. Chem.* **1981**, *46*, 2588–2589.

(13) Nowakowski, J. On the Assignment of Proton Hyperfine Splitting Constants in Benzo[*cd*]Pyrenyl. *Chem. Phys. Lett.* **1972**, *13*, 589–591.

(14) Reddoch, A. H.; Paskovich, D. H. The EPR Spectrum of Benzo[*cd*]Pyrenyl. *Chem. Phys. Lett.* **1969**, *3*, 351–352.

(15) Xiang, Q.; Ye, L.; Ma, L.; Sun, Z. The Olympicenyl Radical and Its Derivatives. *ChemPlusChem* **2024**, *89*, e202300571.

(16) Mistry, A.; Moreton, B.; Schuler, B.; Mohn, F.; Meyer, G.; Gross, L.; Williams, A.; Scott, P.; Costantini, G.; Fox, D. J. The Synthesis and STM/AFM Imaging of "Olympicene" Benzo[*cd*]Pyrenes. *Chem. Eur. J.* **2015**, *21*, 2011–2018.

(17) Xiang, Q.; Guo, J.; Xu, J.; Ding, S.; Li, Z.; Li, G.; Phan, H.; Gu, Y.; Dang, Y.; Xu, Z.; Gong, Z.; Hu, W.; Zeng, Z.; Wu, J.; Sun, Z. Stable Olympicenyl Radicals and Their π-Dimers. *J. Am. Chem. Soc.* **2020**, *142*, 11022–11031.

(18) Wang, P.; Xiang, Q.; Tian, M.; Tao, S.; Xu, Z.; Guo, Y.; Hu, W.; Sun, Z. Spin-Distribution-Directed Regioselective Substitution Strategy for Highly Stable Olympicenyl Radicals. *Angew. Chem. Int. Ed.* **2023**, *62*, e202313257.

(19) Spörler, S.; Strinitz, F.; Rodehutskors, P.; Müller, L.; Waterloo, A. R.; Dürr, M.; Hübner, E.; Ivanović-Burmazović, I.; Tykwinski, R. R.; Burzlaff, N. Carbon-Rich Cyclopentadienyl Ruthenium Allenylidene Complexes. *New. J. Chem.* **2016**, *40*, 6127–6134.

(20) Kumar, S.; Ho, M. T.; Tao, Y. T. Unsymmetrically Extended Polyfused Aromatics Embedding Coronene and Perylene Frameworks: Syntheses and Properties. *Org. Lett.* **2016**, *18*, 200–203.

(21) Xu, X.; He, G.; Xu, X.; Wu, Z.; Cai, T. Investigation of the Electrochemical Oxidation of 2,3′-Bisindolylmethanes in Positive-Ion Electrospray Ionization Mass Spectrometry. *RSC Adv.* **2019**, *9*, 10727–10732.

(22) Okoročenkova, J.; Filgas, J.; Khan, N. M.; Slavíček, P.; Klán, P. Thermal Truncation of Heptamethine Cyanine Dyes. *J. Am. Chem. Soc.* **2024**, *146*, 19768–19781.

(23) Strinitz, F.; Tucher, J.; Januszewski, J. A.; Waterloo, A. R.; Stegner, P.; Förtsch, S.; Hübner, E.; Tykwinski, R. R.; Burzlaff, N. Carbon-Rich Ruthenium Allenylidene Complexes Bearing Heteroscorpionate Ligands. *Organometallics* **2014**, *33*, 5129–5144.

(24) Marshall, J. L.; Lehnherr, D.; Lindner, B. D.; Tykwinski, R. R. Reductive Aromatization/Dearomatization and Elimination Reactions to Access Conjugated Polycyclic Hydrocarbons, Heteroacenes, and Cumulenes. *ChemPlusChem* **2017**, *82*, 967–1001.

(25) Lehnherr, D.; Hallani, R.; McDonald, R.; Anthony, J. E.; Tykwinski, R. R. Synthesis and Properties of Isomerically Pure Anthrabisbenzothiophenes. *Org. Lett.* **2012**, *14*, 62–65.

(26) Banide, E. V.; Molloy, B. C.; Ortin, Y.; Müller-Bunz, H.; McGlinchey, M. J. From Allenes to Tetracenes: A Synthetic and Structural Study of Silyl- and Halo-Allenes and their Dimers. *Eur. J. Org. Chem.* **2007**, 2611–2622.

(27) Qiu, S.; Zhang, Y.; Huang, X.; Bao, L.; Hong, Y.; Zeng, Z.; Wu, J. 9-Ethynylfluoroenyl Radicals: Regioselective Dimerization and Post Ring-Cyclization Reactions. *Org. Lett.* **2016**, *18*, 6018–6021.

(28) West, R.; Gornowicz, G. A. Polylithium Compounds. V. Polylithium Compounds from Phenylpropynes and Their Polysilicon Derivatives. *J. Am. Chem. Soc.* **1971**, *93*, 1720–1724.

(29) Debeaux, M.; Brandhorst, K.; Jones, P. G.; Hopf, H.; Grunenberg, J.; Kowalsky, W.; Johannes, H. H. A Stable Enol from a 6-Substituted Benzanthrone and its Unexpected Behaviour under Acidic Conditions. *Beilstein J. Org. Chem.* **2009**, *5*, 1–10.

(30) Zhang, X.; Li, J.; Qu, H.; Chi, C.; Wu, J. Fused Bispentacenequinone and its Unexpected Michael Addition. *Org. Lett.* **2010**, *12*, 3946–3949.

(31) Ribar, P.; Valenta, L.; Šolomek, T.; Juríček, M. Rules of Nucleophilic Additions to Zigzag Nanographene Diones. *Angew. Chem. Int. Ed.* **2021**, *60*, 13521–13528.

(32) Carey, F. A.; Sundberg, R. J. Advanced Organic Chemistry Part B: Reactions and Synthesis, 5th ed.; Springer US: Boston, MA, 2007.

(33) Reus, C.; Lechner, M. P.; Schulze, M.; Lungerich, D.; Diner, C.; Gruber, M.; Stryker, J. M.; Hampel, F.; Jux, N.; Tykwinski, R. R. Unexpected Michael Additions on the Way to

2.3,8.9-Dibenzanthanthrenes with Interesting Structural Properties. *Chem. Eur. J.* **2016**, *22*, 9097–9101.

(34) Li, Y.; Huang, K. W.; Sun, Z.; Webster, R. D.; Zeng, Z.; Zeng, W.; Chi, C.; Furukawa, K.; Wu, J. A Kinetically Blocked 1,14:11,12-Dibenzopentacene: A Persistent Triplet Diradical of a Non-Kekulé Polycyclic Benzenoid Hydrocarbon. *Chem. Sci.* **2014**, *5*, 1908–1914.

(35) Hara, O.; Yamamoto, K.; Murata, I. The Chemistry of Phenalenium Systems. XXXI. The Synthesis, Dimerization, and Trapping of 6-Methylenebenzo[*cd*]Pyrene. *Bull. Chem. Soc. Jpn.* **1980**, *53*, 2036–2039.

(36) Stokes, B. J.; Cai, X.; Amsbaugh, R. V.; Drake, L. J.; Kotamraju, R. M. A.; Licauco, N. J. C. Tert -Butoxide-Mediated Protodeformylative Decarbonylation of α-Quaternary Homobenzaldehydes. *SynOpen* **2023**, *8*, 47–50.

(37) Guo, Y.; Ding, S.; Zhang, N.; Xu, Z.; Wu, S.; Hu, J.; Xiang, Q.; Li, Z. Y.; Chen, X.; Sato, S.; Wu, J.; Sun, Z. π-Extended Doublet Open-Shell Graphene Fragments Exhibiting One-Dimensional Chain Stacking. *J. Am. Chem. Soc.* **2022**, *144*, 2095–2100.

(38) Zong, C.; Zhu, X.; Xu, Z.; Zhang, L.; Xu, J.; Guo, J.; Xiang, Q.; Zeng, Z.; Hu, W.; Wu, J.; Li, R.; Sun, Z. Isomeric Dibenzoheptazethrenes for Air-Stable Organic Field-Effect Transistors. *Angew. Chem. Int. Ed.* **2021**, *60*, 16230–16236.

(39) Arnbjerg, J.; Paterson, M. J.; Nielsen, C. B.; Jørgensen, M.; Christiansen, O.; Ogilby, P. R. One- and Two-Photon Photosensitized Singlet Oxygen Production: Characterization of Aromatic Ketones as Sensitizer Standards. *J. Phys. Chem. A* **2007**, *111*, 5756–5767.

(40) Bregnhøj, M.; Ogilby, P. R. Two-Photon Excitation of Neat Aerated Solvents with Visible Light Produces Singlet Oxygen. *J. Phys. Chem. A* **2019**, *123*, 7567–7575.

(41) da Silva, E. F. F.; Pimenta, F. M.; Pedersen, B. W.; Blaikie, F. H.; Bosio, G. N.; Breitenbach, T.; Westberg, M.; Bregnhøj, M.; Etzerodt, M.; Arnaut, L. G.; Ogilby, P. R. Intracellular Singlet Oxygen Photosensitizers: On the Road to Solving the Problems of Sensitizer Degradation, Bleaching and Relocalization. *Integr. Biol.* **2016**, *8*, 177–193.

(42) Sandoval-Altamirano, C.; Berrios, E.; Morales, J.; Silva, C.; Gunther, G. Phenalenone Derivatives: The Voyage from Photosensitizers to Push-Pull Fluorescent Molecules. *J. Photochem. Photobiol., A* **2023**, *439*, 114587.

(43) Maļeckis, A.; Cvetinska, M.; Griškjāns, E.; Dmitrijevs, K.; Traskovskis, K.; Belyakov, S.; Kirilova, E. Benzanthrone Sulfides: Synthesis, Solvatochromism Characterization and Analysis of Experimental Photophysical Parameters and Theoretical Calculations. *Dyes Pigm.* **2023**, *219*, 111599.

(44) Thomas, A.; Kirilova, E. M.; Nagesh, B. V.; Manohara, S. R.; Siddlingeshwar, B.; Belyakov, S. V. Synthesis, Solvatochromism and DFT Study of Pyridine Substituted Benzanthrone with ICT Characteristi. *J. Mol. Struct.* **2022**, 1262, 132971.

(45) Shivraj; Siddlingeshwar, B.; Kirilova, E. M.; Belyakov, S. V.; Divakar, D. D.; Alkheraif, A. A. Photophysical Properties of Benzanthrone Derivatives: Effect of Substituent, Solvent Polarity and Hydrogen Bonding. *Photochem. Photobiol. Sci.* **2018**, *17*, 453–464.

(46) Fernandez de la Mora, J.; Van Berkel, G. J.; Enke, C. G.; Cole, R. B.; Martinez-Sanchez, M.; Fenn, J. B. Electrochemical Processes in Electrospray Ionization Mass Spectrometry. *J. Mass Spectrom.* **2000**, *35*, 939–952.

(47) Chai, Y.; Sun, H.; Wan, J.; Pan, Y.; Sun, C. Hydride Abstraction in Positive-Ion Electrospray Interface: Oxidation of 1,4-Dihydropyridines in Electrospray Ionization Mass Spectrometry. *Analyst* **2011**, *136* (22), 4667–4669.

(48) Morgenthaler, J.; Rüchardt, C. New Hydrogen Transfer Catalysts. *Eur. J. Org. Chem.* **1999**, 2219–2230.

(49) Fieser, M. Fieser and Fieser's Reagents for Organic Synthesis; 1967; Vol. 1.

(50) Tsvetkov, N. P.; Gonzalez-Rodriguez, E.; Hughes, A.; dos Passos Gomes, G.; White, F. D.; Kuriakose, F.; Alabugin, I. V. Radical Alkyne Peri -Annulation Reactions for the Synthesis of Functionalized Phenalenes, Benzanthrenes, and Olympicene. *Angew. Chem. Int. Ed.* **2018**, *57*, 3651–3655.